

Synthesis of New Monomers for Semiconducting Polymers and Their Application in Organic Optoelectronic Devices

Dissertation

Zur Erlangung des Doktorgrades
der Mathematisch-Naturwissenschaftlichen Fakultät
der Christian-Albrechts-Universität zu Kiel

vorgelegt von

Sara Urrego-Riveros

Kiel 2019

Gedruckt bzw. veröffentlicht mit Unterstützung des Deutschen Akademischen Austauschdienstes (DAAD).

First referee: Prof. Dr. Anne Staubitz
Second referee: Prof. Dr. Anna McConnell
Date of oral examination: 22.08.2019
Approved for publication: 23.09.2019

gez. Prof. Dr. rer. nat. Frank Kempken, Dekan

The work described in the thesis was performed under the supervision of
Prof. Dr. Anne. Staubitz
Otto-Diels-Institute of Organic Chemistry, University of Kiel
Institute for Organic and Analytical Chemistry University of Bremen
from October 2013 to June 2019

I, the undersigned, Sara Urrego-Riveros, declare under penalty of perjury, this dissertation "Synthesis of New Monomers for Semiconducting Polymers and Their Application in Organic Optoelectronic Devices" is the result of my own work, apart from the advice of my supervisor Prof. Dr. Anne Staubitz. In those cases, in which other colleagues contributed to the results presented in this thesis, their and my own contributions are clarified at the beginning of the relevant chapter.

Apart from the included published papers (*Chapter 3.1.1.*: Urrego-Riveros, S.; Bremer, M.; Hoffmann, J.; Heitmann, A.; Reynaldo, T.; Buhl, J.; Gates, P. J.; Sönnichsen, F. D.; Hissler, M.; Gerken, M.; Staubitz, A., *Organic Chemistry Frontiers*. DOI: 10.1039/c9qo00947g; *Chapter 3.1.4.*: L.-Y. He, S. Urrego-Riveros, P. J. Gates, C. Näther, M. Brinkmann, V. Abetz, A. Staubitz, *Tetrahedron* **2015**, *71*, 5399-5406.; *Chapter 3.2.1.*: Urrego-Riveros, S.; Ramirez y Medina, I.; Hoffmann, J.; Heitmann, A.; Staubitz, A., *Chem. Eur. J.* **2018**, *24* (22), 5680-5696.; *Chapter 3.2.2.*: Urrego-Riveros, S.; Ramirez y Medina, I.-M.; Duvinage, D.; Lork, E.; Sönnichsen, F.; Staubitz, A., *Chem. Eur. J.*. DOI:10.1002/chem.201902255), no other part of the thesis has been published nor submitted for publishing.

The thesis has been prepared subject to the Rules of Good Scientific Practice of the German Research Foundation (DFG). It will be submitted exclusively for promotion at this point and it is my first doctoral attempt. Any of my academic degrees had been withdrawn from me.

Calw, 23.09.2019

Sara Urrego-Riveros

Esta tesis de doctorado se la dedico a mis amados padres, Luz Mary y Daniel María. Gracias a ustedes soy lo que soy.

Acknowledgements

I would like to take this opportunity to thank all the people that had been with me during my PhD journey. Thank you, god, for letting me finish this journey, not letting me fall and be with me every single moment of my life.

Thanks Prof. Dr. Anne Staubitz for accepting me in your group, teaching and guiding me on my PhD work. Thanks Anne, for your great and valuable support and helping me with every difficulty that came to me, not only in the scientific side but also in the personal one. Thanks for trusting in me more than I did on myself. Thanks for encouraging me to go to conferences and participating in the COST Short Term Scientific Mission in Rennes-France. I'm very lucky to know you and be part of a great research group.

To COLFUTURO-DAAD scholarship for funding me for four years. Without this funding, I could not come to Germany to learn very interesting topics and techniques, know such amazing people, have so many adventures and the opportunity to live in two different cities with all of the adversities that it brought. Thanks to the University of Bremen for having me as research assistant for three years.

Thanks Prof. Dr. Frank Sönnichsen for helping me on several chemistry discussions and letting always the door open to any question that I could have. I could not finish this thesis without the great support that you and the spectroscopy group gave to the Staubitz group for the NMR and MALDI measurement. Thanks Prof. Dr. Anne McConnell having agreed to be my second evaluator. Thanks also to Prof. Dr. Ulrich Lünning and Prof. Dr. Norbert Stock for being part of my evaluating committee and accepting my invitation without any hesitation.

A special thanks to Marion Höftmann, Holger Franzen and Gitta Kohlmeyer-Yilmaz team members of the NMR department, thanks for your big help measuring and processing all my samples. As well to Dr. Thomas Dülcks and Dorit Kemken for the mass spectrometry measurements in the group of Prof. Spiteller in the University of Bremen and Paul Gates from the University of Bristol. Thanks to Prof. Dr. Muriel Hissler and the members of her group in the University of Rennes – France for helping me with the Uv-Vis spectroscopy, fluorescence measurements and other discussions during my scientific stance. I really appreciate the help and trust given by Prof. Dr. Martina Gerken from the Institute of Electrical Engineering and Information Technology, for the construction of the OLEDs in the NanoLab in Kiel. Thanks to Markus Köpke, Mathias Bremer and Janek Buhl, members of the group for Integrated Systems and Photonics for your help in the fabrication and characterization of the OLEDs; and your constructive discussions.

I can't continue without showing my appreciation and gratitude to all the members of the Staubitz group during this period : Julian, Annika, Lu, Jan S., Matti, Lu, Stephan, Birk, Jonas, JOle, Nils, Yannik, Phil, Björn, Isabel, Nadi, Anni, Gernot, Sarah, Ruchi, Waldemar, Jan. M, Jasmin, Shuo, Clement, Melani and Souvik. No matter if I know you from the beginning of this journey, or if I know you since last year or if you have been away a long time ago, every single one of you taught me many scientific and personal things; and helped me to be a better person now. I could not be happier and more honoured to have had you as colleagues and friends, all of you left a big mark in my hearth. Thanks to my former lab mates Birk and Stephan for teaching me many lab tricks and techniques . Thank you, Isabel, Jasmin, Nadi and Ruchi for being my hands in the lab when I could not go. Thanks, Anni as well for the constructive talks and discussion in our office or in my beloved glovebox room. A very special thanks to my thesis's proof reviewers Annika, Yannik, Isabel, Jonas and Roman (You are not part of this selective group of chemists but you made a great help!!). I would not continue without thank to the Sönnichsen, Nachsheim, Beckmans and Gessing's groups for the help given with equipment or scientific discussions. To Mathias Lipfert, Daniel Duvoange and Marian Olaru, thanks guys for your help and company on the long days in the NMR.

My gratitude as well is showed to my friends, thanks to Mafe, Tatiana, Lu, Ameris and Edilene apart of the distance I think that anything had changed between us, you guys had been always in my hearth. Thanks to the family Meier to welcome me in your home and life. Thanks to my Aleja for being such a big support and a real good friend. I'm very lucky to have met you that day in the Bulevar in Bogotá and I know that our friendship now is more like a sisterhood that cannot break neither for the time nor the distance. Many many thanks to Anni and Isabel to be there in such difficult moments of my PhD journey and to do not let me down.

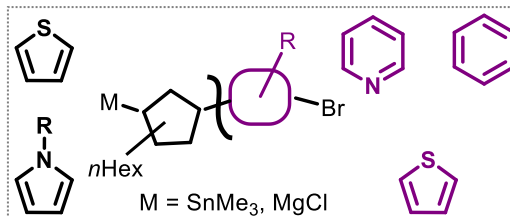
Vielen liebe Dank an meinen Boy ohne dich wäre ich heute nicht hier. Herzlichen Dank meine Liebe für deinen Rat und Unterstützung, die du mir gerade in den letzten Monaten gegeben hast, und dass du mir immer 100% vertraut und an mich geglaubt hast.

Y por último mil millones de gracias a las personas más importantes y valiosas de mi vida, mi familia Urrego-Riveros gracias simplemente por todo. Gracias papitos por darme esta vida tan maravillosa, por ser mis consejeros, mi soporte y motivación para salir adelante. A mi Petuti, Nico, Feli y Juani también les doy gracias por darme esa fuerza y soporte sin la cual no se en dónde estaría en este momento. Gracias por confiar en mí, darme tanto amor a parte del gran mar que nos separa pero que es tan grande que lo siento siempre en mi corazón. Gracias a ello he podido asumir este gran reto y alcanzar esta meta que he logrado.

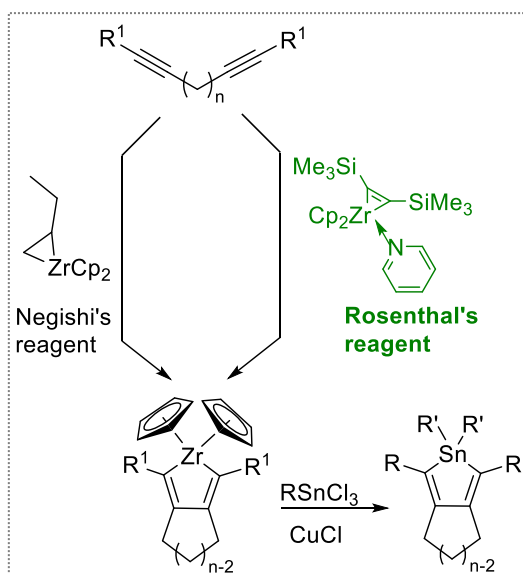
Abstract

Push-pull conjugated polymers, consisting of electron donating and withdrawing units gained increased attention because of their narrow band gap and their response to the light absorption and emission.

Accordingly, four monomers with an intrinsic push-pull effect were synthesized via a dually selective cross-coupling reaction under Stille conditions between two types of heterocycles. The dinucleophile type beared both a trimethyl stannyl



group and either a pinacol boronate (3-*n*-hexylthiophene) or a magnesium chloride group (N-derivate pyrrole). The dielectrophilic type consisted of iodo-bromo heterocycle derivates (phenyl, pyridine and thienyl). For these monomers, the presence of a remaining metal (pinacol boronate or magnesium chloride group) and bromine allowed further polymerizations under Suzuki-Miyaura or Kumada conditions. In the case of the thienyl-phenyl and thienyl-pyridine type monomer, oligomers were formed. Their electroluminescence was successfully demonstrated by the implementation into OLED devices.



Additionally, stannoles, which are tin analogues of cyclopentadienes, were studied as possible electron deficient systems in combination with thiophene derivates in organometallic push-pull monomers. The synthesis of stannoles is generally performed using the conditions of the well-known Fagan Nugent reaction of alkynes, where in the first step zirconacyclopentadienes are formed and secondly transmetalated with dichloro stannanes. This thesis focusses on the formation of zirconacyclopentadienes by comparing the synthetic reactions between Negishi's and

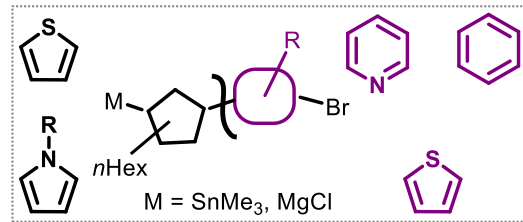
Rosenthal's reagent with several alkynes. The Rosenthal's reagent proved to give higher reaction rates as well as higher yields of zirconacyclopentadienes in those cases, in which functional groups as aryl-halides, trimethylstannyl and trimethylsilyl were present.

Lastly, first attempts of cross-coupling reactions between stannoles with nucleophilic substituents in 2- and 5-positions and thiophene electrophilic derivates were done to obtain dimers, trimers or polymers containing different ratios of stannole and thienyl units.

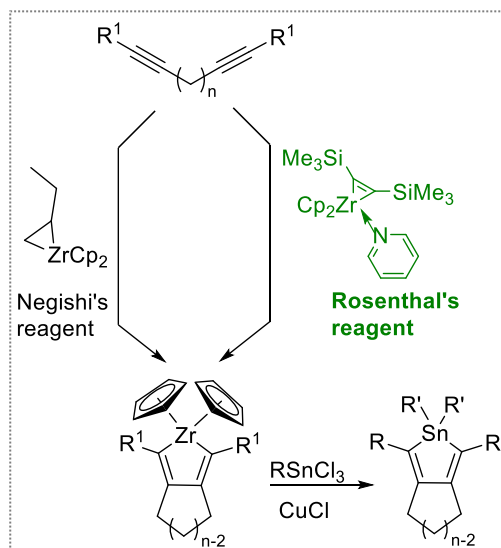
Zusammenfassung

Push-Pull-konjugierte Polymere, die aus Elektronendonator- und Elektronenakzeptoreinheiten bestehen, gewinnen aufgrund ihrer schmalen Bandlücke und ihrer Reaktion auf Lichtabsorption und -emission an Aufmerksamkeit.

Dementsprechend wurden vier Monomere mit einem intrinsischen Push-Pull-Effekt über eine zweifach selektive Kreuzkupplungsreaktion unter Stille-Bedingungen aus zwei Arten von



Heterozyklen synthetisiert. Der dinucleophile Typ wies sowohl eine Trimethylstannylgruppe als auch entweder ein Pinakolboronat- (3-n-Hexylthiophen) oder eine Magnesiumchloridgruppe (N-Derivatpyrrol) auf. Der dielektrophile Typ bestand aus Jod-Brom-Heterozyklusderivaten (Phenyl, Pyridin und Thienyl). Bei diesen Monomeren ermöglichte das Vorhandensein eines restlichen Metalls (Pinakolboronat- oder Magnesiumchloridgruppe) und Brom weitere Polymerisationen unter Suzuki-Miyaura- oder Kumada-Bedingungen. Im Falle eines Monomers vom Thienylphenyl- und Thienylpyridintyp wurden Oligomere gebildet. Ihre Elektrolumineszenz wurde durch die Implementierung in OLED-Geräte erfolgreich demonstriert.



Außerdem wurden Stannole, die Analoga von Cyclopentadienen sind, als mögliche Systeme mit Elektronenmangel in Kombination mit Thiophenderivaten in metallorganischen Push-Pull-Monomeren untersucht. Die Synthese von Stannolen wird im Allgemeinen unter den Bedingungen der bekannten Fagan-Nugent-Reaktion von Alkinen durchgeführt, wobei im ersten Schritt Zirkonacyclopentadiene gebildet werden und zweitens mit Dichlorstannanen transmetalliert werden. Diese Dissertation konzentriert sich auf die

Bildung von Zirkonacyclopentadienen durch den Vergleich der Synthesereaktionen zwischen Negishis und Rosenthals-Reagens mit mehreren Alkinen. Das Rosenthal-Reagens ergab höhere Reaktionsraten sowie höhere Ausbeuten an Zirkonacyclopentadien in solchen Fällen, in denen funktionelle Gruppen wie Arylhalogenide, Trimethylstannyl und Trimethylsilyl vorhanden waren. Schließlich wurden erste Versuche der Kreuzkupplungsreaktionen zwischen Stannolen mit nukleophilen Substituenten an 2- und 5-Position und elektrophilen Thiophen-Derivaten unternommen, um Dimere, Trimere oder Polymere mit unterschiedlichen Verhältnissen von Stannol- und Thienyleinheiten zu erhalten.

Abbreviations used in the Thesis

The following abbreviation list covers chapters 1-4 The experimental part described in chapter 5 has its own list of abbreviations.

AcOH	acetic acid
anhyd.	anhydrous
aq.	aqueous
a.u.	arbitrary units
br.	broad (IR)
Bpin	pinacol boronate group
Calcd.	calculated
COSY	correlated spectroscopy
Cp	cyclopentadienyl
DCM	dichloromethane
DSC	differential scanning calorimetry
DMF	<i>N,N</i> -dimethylformamide
DIPA	di/ <i>iso</i> propylamine
DMSO	dimethylsulfoxide
DEPT	distortionless enhancement by polarization transfer
d	doublet (NMR)
dd	doublet of doublets
EI	electron impact
ESI	electrospray ionization
eq.	equivalents
EtOAc	ethyl acetate
FPT	freeze-pump-thaw technique
GC-MS	gas chromatography-mass spectrometry
GPC	gel permeation chromatography
HMBC	heteronuclear multiple bond coherence
HSQC	heteronuclear single quantum coherence
HH	head-to-head coupling of 3-monosubstituted thiophenes
HT	head-to-tail coupling of 3-monosubstituted thiophenes
HRMS	high resolution mass spectrometry
HOMO	highest occupied molecular orbital
IR	infrared spectroscopy
<i>i</i> PrOBpin	<i>iso</i> propyl pinacol boronic ester
LUMO	lowest unoccupied molecular orbital

MS	mass spectrometry
MALDI	matrix-assisted laser desorption ionization mass spectrometry
MALDI-TOF-MS	matrix-assisted laser desorption ionization-time of flight mass spectrometry
m	medium (concerning the intensity) (IR)
M.p.	melting point
MeOH	methanol
μ W	microwave
m	multiplet (NMR)
M_n	number average molecular weight
NBS	<i>N</i> -bromosuccinimide
<i>n</i> BuLi	<i>n</i> -butyllithium
NIS	<i>N</i> -iodosuccinimide
NMR	nuclear magnetic resonance
OFET	organic field effect transistor
OLED	organic light emitting diode
OSC	organic solar cell
PEDOT:PSS	poly(3,4-ethylenedioxythiophene) with polystyrene sulfonate
P3HT	poly-3- <i>n</i> -hexylthiophene
\bar{D}	polydispersity index
R_f	retention factor
s	singlet (NMR)
SPS	solvent-purification system
s	strong (concerning the intensity IR)
TT	tail-to-tail coupling of 3-monosubstituted thiophenes
TD-DFT	time dependent density functional theory
THF	tetrahydrofuran
<i>t</i> BuLi	tert-butyllithium
TGA	thermogravimetry analysis
Tph	thiophene scaffold
TEA	triethylamine
t	triplet (NMR)
UV-vis	ultraviolet-visible spectroscopy
w	weak (IR)

A Guide to This Thesis

This thesis consists of 7 chapters. In chapter 1, a general introduction about organic semiconductors and optoelectronic devices is presented. Chapter 2 summarizes the objectives of this thesis and chapter 3 the results and discussion of it. Chapter 3 includes four publications. Each of these publications has its own introduction, experimental part, results and discussion section, conclusions and references.

In chapter 4, the general conclusions of the thesis are presented. Chapter 5 covers the experimental part of the chapter 3 including the “supporting information” from the publications. In chapter 6, annexes and a small glossary are presented. Finally, in chapter 7 all references used in the thesis are listed in addition to the ones of the manuscripts and publications.

The numeration of figures, schemes and structures starts with 1 for every manuscript and publication. To avoid numbering one structure from a manuscript (**M1** or **M2**) or publication (**P1** or **P2**) with two or more numbers in the course of this thesis, a nomenclature of type **MX-Y** or **PX-Y** was used. For example, in section 3.3 it was necessary to mention dinucleophile **13** from manuscript **1**, therefore the molecule was mentioned as **M1-13**.

There are four exceptions in this nomenclature to clarify. One is the Rosenthal's reagent, which is mentioned in **P2** (as molecule **38**) and **M2** (as molecule **9**). As it was synthesized in **M2**, the molecule is referred as **M2-9**. Other three exceptions are molecules **40**, **84** and **85** from **P2** which will not follow the nomenclature because they were only mentioned in in such publication, but their synthetic route was not described. In the thesis those molecules are numbered **51**, **52** and **53**.

Table of Contents

A Guide to This Thesis	xii
1. Introduction.....	1
1.1. Organic Semiconducting Materials	2
1.1.1. Conductivity.....	3
1.1.2. Morphology	4
1.1.3. Control of the Band Gap	5
1.2. Polythiophenes and Copolymers	6
1.2.1. Polythiophenes.....	6
1.2.2. Copolymers	8
1.2.3. Synthesis.....	9
1.3. Organometallic Semiconducting Materials: Metalloles.....	17
1.4. Organic Electronic Devices	18
1.4.2. Organic Light Emitting Diode (OLED)	18
1.4.3. Organic Solar Cell (OSC)	22
1.4.4. Organic Field Effect Transistor (OFET).....	22
2. Objectives	24
3. Results and Discussion.....	27
3.1. Results and Discussion. Synthesis of Monomers Under the Push-Pull Principle. Exploring their Reactivity in Polymerization Reactions.....	27
3.1.1. Conjugated Oligomers with Alternating Heterocycles from a Single Monomer: Synthesis and Demonstration of Electroluminescence	28
3.1.2. Reactivity of the Oligomer M1-O2	40
3.1.3. Synthesis of Poly-3-Hexylthiophene with a Dual Selectivity Approach	42
3.1.4. Synthesis of Poly (thiophene-alt-pyrrole) from a Difunctionalized Thienylpyrrole by Kumada Polycondensation.....	48
3.2. Results and Discussion Synthesis, Characterization and Reactivity of Stannoles....	57
3.2.1. Synthesis and Properties of Tin-Containing Conjugated Heterocycles.....	57
3.2.2. Negishi's Reagent Versus Rosenthal's Reagent in the Formation of Zirconacyclopentadienes.	76
3.2.3. Reactivity of Stannoles.....	90
4. Conclusions.....	107

5. Experimental Section	112
5.1. Experimental Section. Supporting Information Chapter 3.1.1	112
5.2. Experimental Section. Supporting Information Chapter 3.1.3	189
5.3. Experimental Section. Supporting Information Chapter 3.1.4	203
5.4. Experimental Section. Supporting Information Chapter 3.2.2	238
5.5. Experimental Section. Supporting Information Chapter 3.2.3	344
6. Appendix	383
7. References	395

1. Introduction

Inorganic semiconductors (mostly based on silicon, germanium and other materials as Gallium-Arsenide)^[1] revolutionized our daily life since the invention and commercialization of transistors in the middle of the last century.^[2] Nowadays, semiconductors are used in the vast majority of electronic devices such as diodes, integrated circuits, light-emitting diodes and photovoltaic devices.^[3]

Organic semiconductors on the other hand, came into focus of modern research as an alternative to their inorganic counterparts after the discovery of electroluminescence in anthracene in 1963,^[4] and description of conductivity of polyacetylene in 1980.^[5] They combine potentially similar optoelectronic properties to inorganic semiconductors with the advantage of easy accessibility, low costs of the starting materials, flexibility, synthetic versatility and easy processing.

After Shirakawa, MacDiarmid and Heeger, the founders of this area, were awarded with the Nobel Prize in 2000,^[6] organic semiconductors drew even more attention to organic electronics and their potential use for renewable energies. The devices fabricated with conductive polymers such as organic solar cells (OSC), organic light-emitting diodes (OLED) and organic field-effect transistors (OFET) became an alternative to the ones based on inorganic semiconductors because of the advantages of organic semiconductors mentioned above. Several companies and researchers around the world made efforts to develop new organic electronic devices. For example, the framework of Lyteus, Holst centre and Fraunhofer FEP, presented in 2018 the first 15-meter roll to roll OLED with a light output of 1000 cd/m² (Figure 1).^[7]

In the same year, the group of Chen from the Nakai University presented an organic solar cell which converts 17.3% of the sunlight energy into electricity.^[8] These results were a breakthrough in the field of organic photovoltaics, as such conversion efficiency is close to that of commercial silicon-based solar cells with efficiencies in the range of 18-22%.^[9]

Figure 1. Flexible and transparent 15 m roll to roll OLED Lyteus device. *Reproduced with permission from Lyteus and Holst Centre. Copyright Lyteus 2019.* ^[7]



1.1. Organic Semiconducting Materials

Semiconducting polymers consisting of organic materials are highly conjugated macromolecules with a high π -electron density.^[10] They exhibit interesting optoelectronic properties such as tuneable conductivity, light absorption and light emission.^[11] After the discovery of electroluminescent properties in small molecules like anthracene,^[4] the Nobel prize winner Shirakawa investigated polyacetylene as one of the first semiconducting polymers.^[6c] Afterwards, many other linear organic π -conjugated systems have been published as semiconducting materials.

Most of the organic semiconductors contain hydrocarbon units (e.g. polyparaphenylene vinylene (PPV), polyparaphenylene (PPP), ladder-type polyparaphenylene (LPPP)),^[12] sulfur (e.g. thiophene and thieno derivatives),^[13] nitrogen (e.g. pyrrole, pyridines and azo derivatives), oxygen (eg. furan derivatives)^[14] or more than one heteroelement (e.g. polyparaphenylene sulphide (PPS), polyethylene dioxythiophene (PEDOT)).^[13] Recently, semiconducting properties were discovered in metalloles, which are heterocyclic systems containing group 14 or 15 elements.^[15] Figure 2 shows examples of organic semiconducting materials.

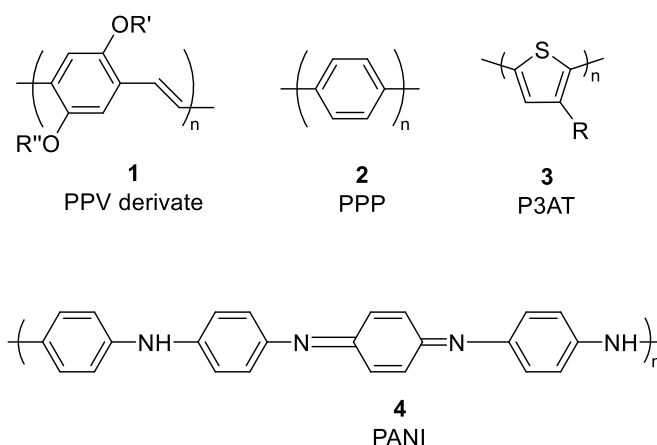


Figure 2. Examples of organic semiconducting materials for organic electronics. Alcoxy-substituted polyparaphenylene vinylene PPV **1**, polyparaphenylene (PPP) **2**; poly-(3-alkylthiophene) (P3AT) **3** and Polyaniline (PANI) **4**.

Organic semiconducting molecules can be classified depending of their molecular weight as small molecules, oligomers or polymers.^[10]

Small molecules are easy to synthesize, purify and characterize. Similar to the processing of their inorganic counterparts, films of small molecules organic semiconductors can be easily prepared by chemical vapor deposition.^[16] Polymers, on the other hand, are easily processable by solution techniques such as spin coating, ink injection printing or doctor blading.^[17] However, the scalability of the synthesis of polymers is challenging. As well the difficulty in the reproducibility of their morphology leads to different crystalline and non-

crystalline regions in the final material.^[10] Lastly, oligomers can be well-defined molecules and could behave like small molecules or polymers.^[18] Apart from the processability and the molecular weight, the conductivity, morphology and control of band gap are important factors to design new organic semiconducting materials and will be explained in detail in the following subchapters.^[19]

1.1.1. Conductivity

One important aspect in the understanding of the conductivity of π -conjugated systems with a continuous chain of carbon atoms is their electronic configuration.

In polymers the successive alternation of π -bonds along the backbone leads to an electron delocalization, which explains the mobility of charges along it. Each carbon atom in the conjugated pathway has a p-orbital perpendicular to the plane of conjugation, which takes the role of a π -band or valence band when they are successive accumulated. In the model of an infinitely long chain of trans-poly(acetylene), $(-\text{CH}-)_n$ a non-dimerized structure is suggested, where the carbon atoms along the chain are equidistant and where one unpaired electron per formula unit contributes to the valence band. With this, the valence band should be half-filled resulting in a metallic character. Peierls however suggested that this is not the case for semiconducting polymers, instead the alternation of single and double bonds forms a dimerized chain structure type $(-\text{CH}=\text{CH})_n$ with two carbons in the repeating unit is energetically more favourable. As a result of this Peierls distortion, the half-filled band is replaced by one full π -bonding and one empty π^* -antibonding band with an energy gap between them. Consequently, the proposed metallic character of the polymer changes into a semiconducting one.^[6a, 20]

Figure 3 shows the π -bonding band (black) and the π^* -antibonding band (red), with the role of valence and conductive bands respectively similar to what is known from the classical inorganic semiconductors.^[6a, 20b, 21] The highest occupied molecular orbital (HOMO) corresponds to a filled π -orbital in the valence band, while the lowest unoccupied molecular orbital (LUMO) to an empty π^* -orbital in the conductance band. The energy distance between the HOMO in the valence band and the LUMO in the conductive band is referred as energy band gap (E_g)*.^[22] The conductivity in semiconductors is proportional to the charge carrier's (electron and holes) concentration and mobility in their valence and conductive band.

* A more detailed description of the concept of band gap is given in the glossary at the end of the thesis.

In organic semiconductors the charge carriers (electron and holes) can be generated by thermal excitation, photoirradiation or external electrical fields.^[10, 21a, 23] There are internal factors (e.g. band gap, molecular packing or molecular weight) and external factors (e.g. temperature, pressure or electrical field) that can influence the concentration and mobility of the charge carriers in the organic semiconducting affecting its conductivity.

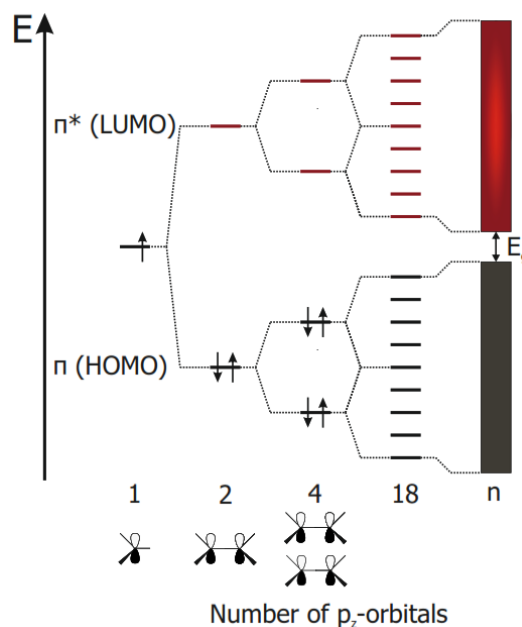


Figure 3. Schematic drawing of the accumulation of p_z orbitals forming the conductive and valence band in a semiconducting polymer. The energy distance between the HOMO and LUMO from the valence and conductive band is the band gap E_g .^[21b]

1.1.2. Morphology

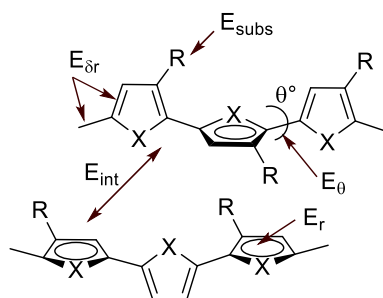
The morphology of the semiconducting materials influences the conductivity and the charge carrier mobilities. As the scattering of charge carriers in highly crystalline materials is reduced compared to in amorphous ones, the charge transport in such materials is higher. Small molecules, like the rubrene which is well known for its application in organic field transistors (OFETs),^[24] crystallize easily and have high mobilities of charge carriers.^[21a] In organic materials with high molecular weight, different crystalline domains can be observed which show different charge transport properties. In the case of the polymers, as for example poly-3-hexylthiophene (P3HT), during the crystallization process different regions of order can coexist.^[25] Most of the ordered regions are π -aggregates which are lowly order assemblies of chain sequences.^[26] A high interchain interaction exists in those aggregates resulting in a better transport of charges, allowing the application of P3HT in organic solar cells (OSC).^[27]

High mobilities of charges also means that the chance to have charge recombination is reduced. In OLEDs where recombination is desired, a certain disorder or even amorphousness in the semiconductor is beneficial.^[28] However, regions with certain order can as well coexist allowing the charges being transported from the electrodes to the disordered regions and the photons being emitted.^[21a] Examples of amorphous and disorder organic material are Polyphenylvinyl derivates or regio random-poly-3-hexylthiophene.

1.1.3. Control of the Band Gap

Due to the fact that the band gap influences the conductivity, carrier mobility, light absorption, light emission and other intrinsic properties of the materials, this factor is one of the most relevant to be studied. In fact, in 1997 Roncalli studied all energetic parameters that can contribute to the band gap in an organic semiconducting molecule, as they are: bond length alternation ($E_{\delta r}$), planarity related to the torsion angle (E_{θ}), resonance (E_r), substitution (E_{sub}) and energy related to the interchain coupling (E_{int}). (Figure 4).^[29] The results are summarized in the equation (1).

$$E_g = E_{\delta r} + E_{\theta} + E_r + E_{sub} + E_{int} \quad (1)$$



X= S, NH, CH=CH, O, Si, Ge, P, etc.

Figure 4. Description of the parameters which can affect the E_g .^[29]

Based on synthetic and theoretical approaches, it was studied how the contribution of each parameter may be altered to narrow the band gap.

The resonance energy can be decreased by aromatic compounds where a competition between π -electrons confinement in the ring and along the chain exists. To have a linear and effective conjugation the torsion angle should be the nearest to 0° .^[21a]

The energies of HOMO and LUMO can be modified depending on the substituents or functionalities in the molecule: When an electron donating group is attached, the HOMO energy increases. On the other hand, when an electron withdrawing group is added, the LUMO energy decreases.^[21a]

Finally, a quinoid like structure shows an appropriate alternation of double and single bounds, which makes the transport of electrons more effective (Figure 5). Additionally,

heteroatoms and side groups affect directly the n -electron confinement inside a ring tuning the properties of the semiconducting material.^[29-30]

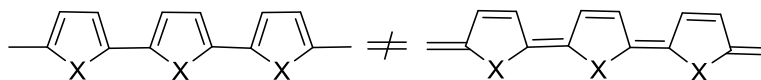


Figure 5. The quinoid like structure is more favourable to increase the conductivity of the semiconducting material than the aromatic one.

1.2. Polythiophenes and Copolymers

1.2.1. Polythiophenes

Thiophenes are the most common and best studied organic semiconducting materials.^[31] They exhibit high polarizability of the sulphur atom, and strong $S \cdots S$ and $S \cdots n$ intermolecular interactions, which allow a morphological stabilization (solid state packing) of the conjugated chain and a good charge carrier mobility.^[32] Because thiophene itself can be easily functionalized with a great variety of substituents, the electronic properties of the resulting polythiophenes can be easily tuned, for example with the aim of decreasing the band gap.^[33] Most of the studied thiophene containing polymers are monosubstituted in 3-position of the aromatic ring. The 2,5-poly-(3-substituted thiophene)s have narrow band gaps ($E_g < 3$ eV) and exhibit high solubility in common organic solvents, therefore they can be easily processed for the use in organic electronic devices.^[34]

Other thiophene assemblies are as well worth to mention due to the variation of the properties and applications; for example small molecules like fused thienothiophene **5** shows great applicability for OFETs, because its high carrier mobility for holes in the structure.^[35] On the other hand, poly-(3,4-disubstituted thiophene)s such as poly-(3,4-ethylenedioxythiophene) (PEDOT) (**6**) is a polymer with high conductivity ($\sigma = 500$ -700 S cm^{-1}) and high transparency. PEDOT is used commonly in a blend with polystyrene sulfonate in OSCs and OLEDs (Figure 6).^[31, 36]

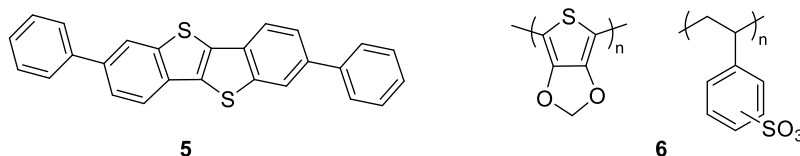


Figure 6. Fused thienothiophenes **5** for the use in OFETs and PEDOT:PSS **6** used as a hole layer for OSCs and OLEDs.

For polythiophenes that are monosubstituted in the 3-position of the ring, a certain nomenclature exists based on the way how the two rings are linked. A linkage from 2-position of the ring is called head of the ring (H) and a linkage from 5-position is called tail (T). The coupling reaction between two molecules of 3-substituted thiophenes can produce

three different dyads denominated HH, HT and TT. In the case that three molecules are connected to each other, four different triads can be formed, coupling consecutive dyads (HT-HT, HT-HH, TT-HH and TT-HT) (Figure 7). The triad configuration that allows the best π -conjugation is the HT-HT, in which the substituents on the thienyl moiety are highly organized with only a small steric hindrance effect and the rings are organized in a π -stacking structure with a low torsion angle. In that case, the mobility of electrons through the polymer increases.^[37] Polymers with high content of HT-HT connections (> 90%) are denominated regioregular. Polymers with a content of 20% in HH or TT defects are denominated regioirregular. The torsion angle between the rings in such case increases up to 30 ° disrupting the π -stacking and thereby decreasing the intermolecular conjugation. Finally, polymers with content below to 60% in HT connections are denominated random.

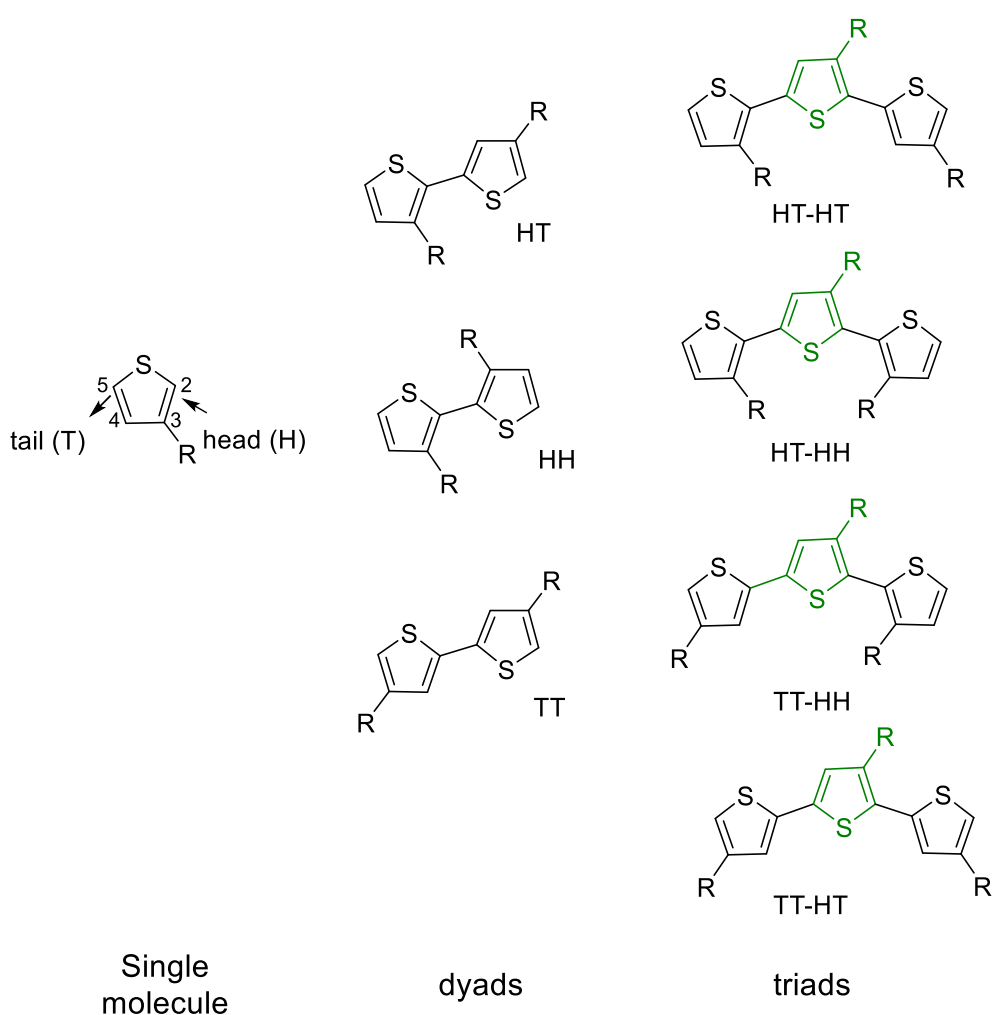


Figure 7. Isomers formed as product of the coupling reaction of 3-substituted thiophenes (single molecule, dyads and triads).^[31, 37]

The band gap of poly-3-alkylsubstituted thiophenes correlates with the absorption in the UV-vis region of the π - π^* transition. The higher the content of HT-HT in poly-(3-monosubstituted thiophene), the lower is their band gap. Therefore, a hypsochromic effect

occurs in regioirregular polymers (RIR) with higher content of HH or TT junctions, compared to regioregular P3HT (RR) with a high HT content (Figure 8).^[31, 38]

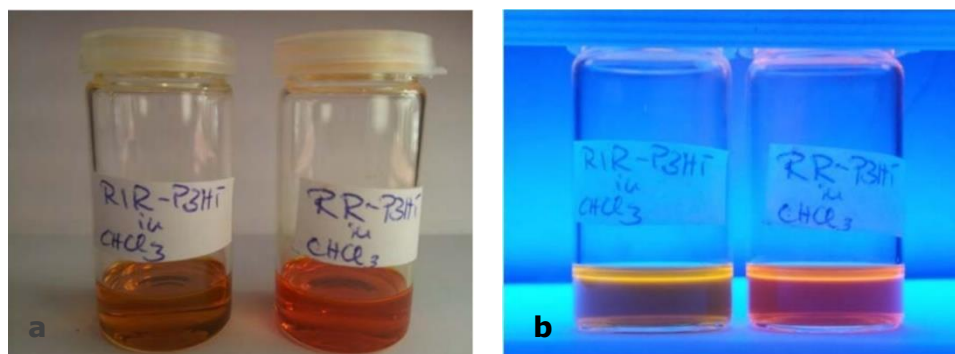


Figure 8. Images of two polymers of poly(3-hexylthiophene) (P3HT) regioirregular (RIR, with content of HH or TT) and regioregular (RR = >99 % content HT, solutions in chloroform): a) under visible light; b) Under irradiation $\lambda = 420$ nm. *Reproduced with permission of A.Heinrich, Copyright 2018.*^[38b]

1.2.2. Copolymers

The study of copolymers of thiophenes with other conjugated molecules is desirable as this can alter the properties of polythiophene like the band gap, interchain interactions and agglomeration.^[39] One possibility is the design of a push-pull system, placing a thienyl unit as an electron rich group adjacent to an electron deficient unit; e.g. another aryl group. (Figure 9).^[39a, 40]

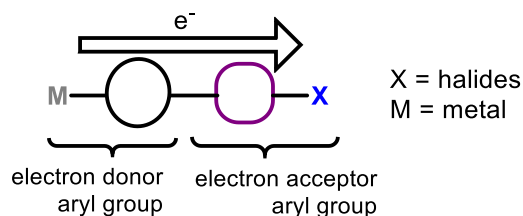


Figure 9. Design of semiconducting polymers using the push-pull principle.

In this system the electron rich group (π -donor) with an electron pair in their HOMO can donate electron density to the LUMO of an electron deficient group (π -acceptor) in the way that the band gap of the new molecule (D-A) is decreased (Figure 10).^[21a] In push-pull systems, non-radiative relaxation processes of the excitons, like vibrational relaxation, internal conversion or quenching of luminescence can be reduced.^[41] Considering the law of conservation of energy, the radiative transitions increase, which might improve the quantum yield as well.^[42]

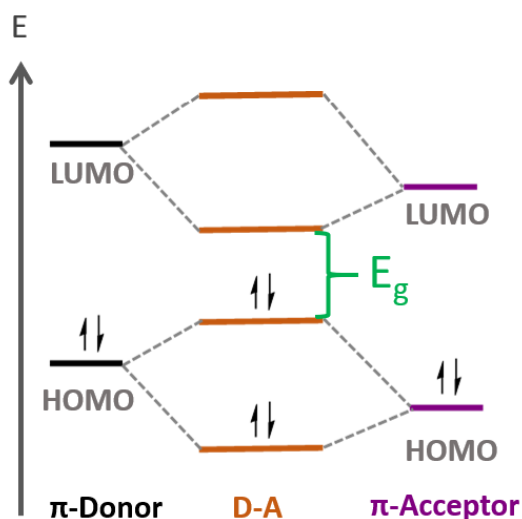


Figure 10. Influence of donor-acceptor in the molecular orbital of the D-A acceptor. The band gap of the new molecule D-A is lower than for each separated molecule.^[21a]

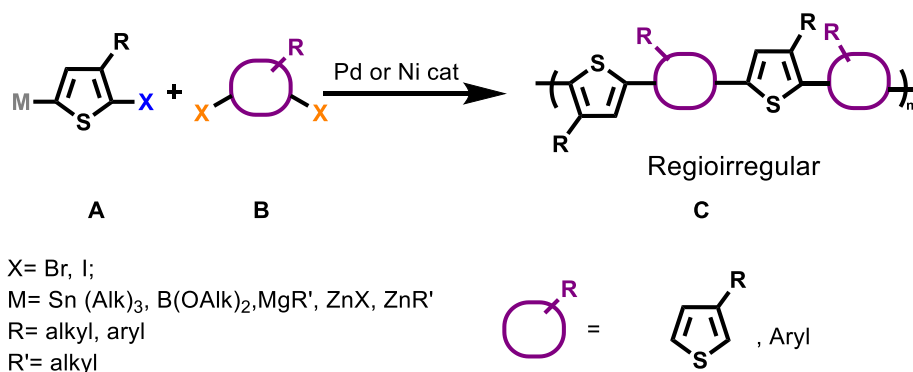
1.2.3. Synthesis

To produce regioregular polythiophenes with high content of HT-HT isomers and copolymers of thiophene with other conjugated molecules several synthetic routes have been proposed. Here, the most representative routes which are based on cross-coupling reactions using nickel or palladium catalysts are presented.

1.2.3.1. Cross Coupling Polymerization: Step-Growth Mechanism

In general, polythiophenes and their copolymers are synthesized via cross-coupling polycondensation techniques where an electrophilic monomer of the type X-Cycle-X (X = Br, I) **A** reacts with a nucleophilic monomer of type M-Cycle-M (M = Sn, B, Mg, Zn, Zr) **B** in the presence of a catalyst in general complexes of nickel or palladium (Scheme 1). The most commonly utilized cross-coupling reactions,^[43] based on the metal or semimetal of the nucleophilic monomer, are the Stille (Sn(Alk)₃),^[44]Rieke (ZnX),^[45] Suzuki (B(OAlk)₂)^[46] and Kumada (MgR) reaction.^[47]

Cross-coupling polymerization occurs in general via a step-growth mechanism,^[48] leading to polymers **C** with a high polydispersity index (\mathcal{D}) and a low molecular weight. In the case of poly-(3-monosubstituted thiophenes) the polymers are in general regiorregular.^[45a]



Scheme 1. Synthesis of poly-3-alkylthiophenes or copolymers of thiophene via cross-coupling polycondensation, proceeding via step-growth mechanism. Irregularities in the orientation of the side chains of polymers **c**, are observed.

Kinetic studies of these polymerizations showed that species of different sizes (e.g. monomers, trimers, tetramers and oligomers) are present during the reaction time and only at the very end of the reaction, close to reaching monomer conversion of 100%, polymers with high molecular weight are generated.^[40, 42b] In the polymerization of an equimolar mixture of two reagents (A and B), the relation between the degree of polymerization and conversion of the monomer is resumed in the Carothers's equation (2), where p is the extent of the reaction. As the degree of polymerization (X_n) is the ratio between the number-average molecular weight (M_n) and the molecular weight of the monomer M_o , the Carothers's equation can be rewritten to equation (3). The

Figure 11 is the graph resulting from the equation 3.^[49]

$$X_n = \frac{1}{(1-p)} \quad (2) \qquad M_n = \frac{M_o}{(1-p)} \quad (3)$$

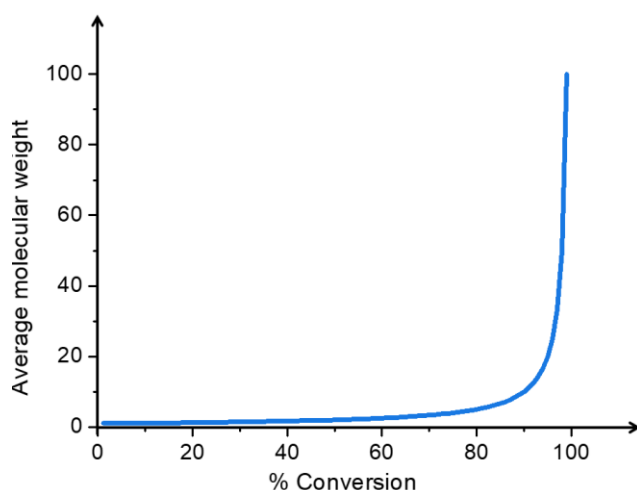


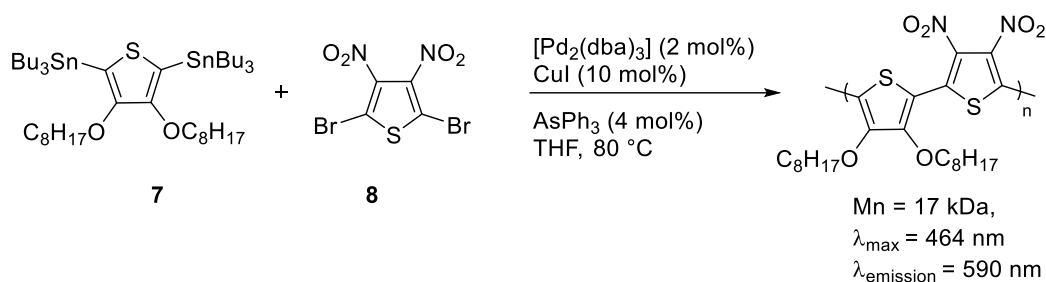
Figure 11. Relation between average molecular weight of polymers with the % of conversion of monomers $((1-p) \times 100\%)$ obtained in a step-growth mechanism polymerization. Under a high selectivity, with no side products and perfect stoichiometry reaction, polymers with high average molecular weight are formed after a very high reaction time.^[40, 42b]

In the case where an imbalance in the stoichiometric quantities of A or B or impurities in the polymerization reaction exist, the molecular weight of the polymer cannot be predicted using the Carothers's equation reaction. Instead it is necessary to take the stoichiometric ratio between the number of molecules of the reagents ($r = N_A/N_B$) into account. The degree

of polymerization and molecular weight are calculated with the equations 4 and 5 respectively.

$$X_n = \frac{1+r}{1+r-2rp} \quad (4) \quad M_n = M_o \left(\frac{1+r}{1+r-2rp} \right) \quad (5)$$

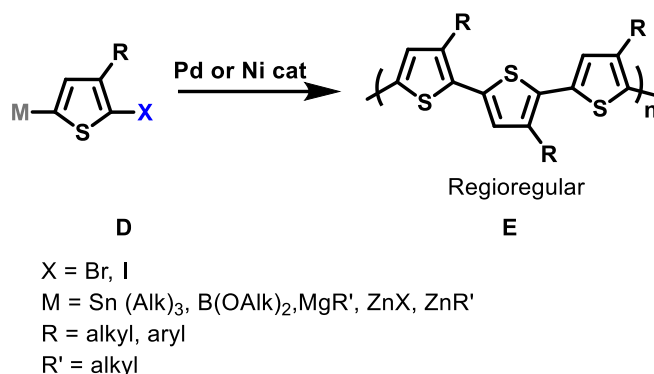
The low regioregularity in polythiophenes and high band gaps of polymers based on step-growth mechanism can be improved by the design of donor/acceptor (D/A) alternating polymers. With the correct selection of substituents in the D/A system steric interactions can be avoided and a coplanar configuration can be obtained extending the π -conjugation in the polymer. In combination with the zwitterionic character from D/A units, an intramolecular charge transfer is induced thereby the band gap is decreased. One example of a D/A system is the fully substituted polythiophene **9**, which has high molecular weight and low band gap. Its synthetic route is based on the step-growth polymerization between the donor monomer **7** with solubilizing alkoxy chains and the acceptor monomer **8** with nitro groups (Scheme 2).^[40]



Scheme 2. Synthesis of highly conjugated polythiophene **9** based on a step-growth polymerization.^[40]

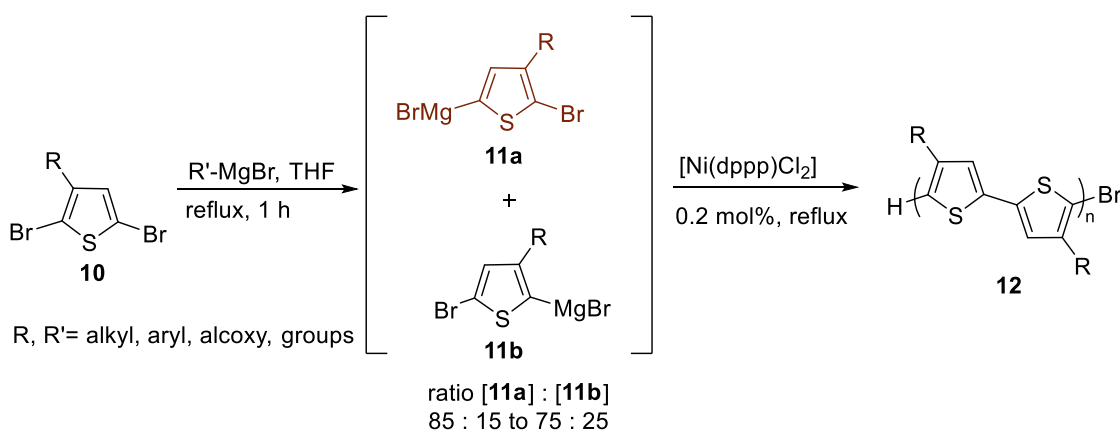
1.2.3.2. Catalyst-Transfer Condensation: Chain-Growth Polymerizations with Living Character

In order to synthesize highly regioregular polythiophenes **E**, a reaction has been developed, which starts with a monomer **D** that contains a metal in the 5 position (nucleophilic site) and a halogen in the 2 position (electrophilic site). The reaction is transition metal catalysed (Scheme 3). Depending on the metal functional groups, which act as nucleophile, different cross-coupling reaction conditions as Kumada,^[50] Suzuki,^[51] Stille^[52] or Rieke^[45b] can be used.



Scheme 3. Route of catalyst transfer condensation: from a single monomer **D** which contains both functionalities: electrophilic and nucleophilic polythiophenes **E** highly regioregular polymers are obtained.

One of the most common catalyst-transfer condensations is the Grignard metathesis method (GRIM) developed by McCullough and Yokoyama, which produces highly regioregular poly(3-substituted thiophene)s under moderate conditions at room temperature. The GRIM reaction starts with the reaction between 2,5-dibromo-3-substituted thiophene (**10**) with a Grignard reagent (R'-MgX), generating a mixture of two Grignard intermediaries (**11a** and **11b**) in a ratio between 85 to 75% for **11a** and 15 to 25% for **11b**. Afterwards, a metathesis between the Grignard intermediary **11a** and the Nickel-catalyst occurs leading to a C-C bond formation. Because electrophilic and nucleophilic motifs still remain, the reaction can proceed further in the same fashion towards the polymer **12** with high regioregularity (>99% HT) (Scheme 4).^[37, 50b]

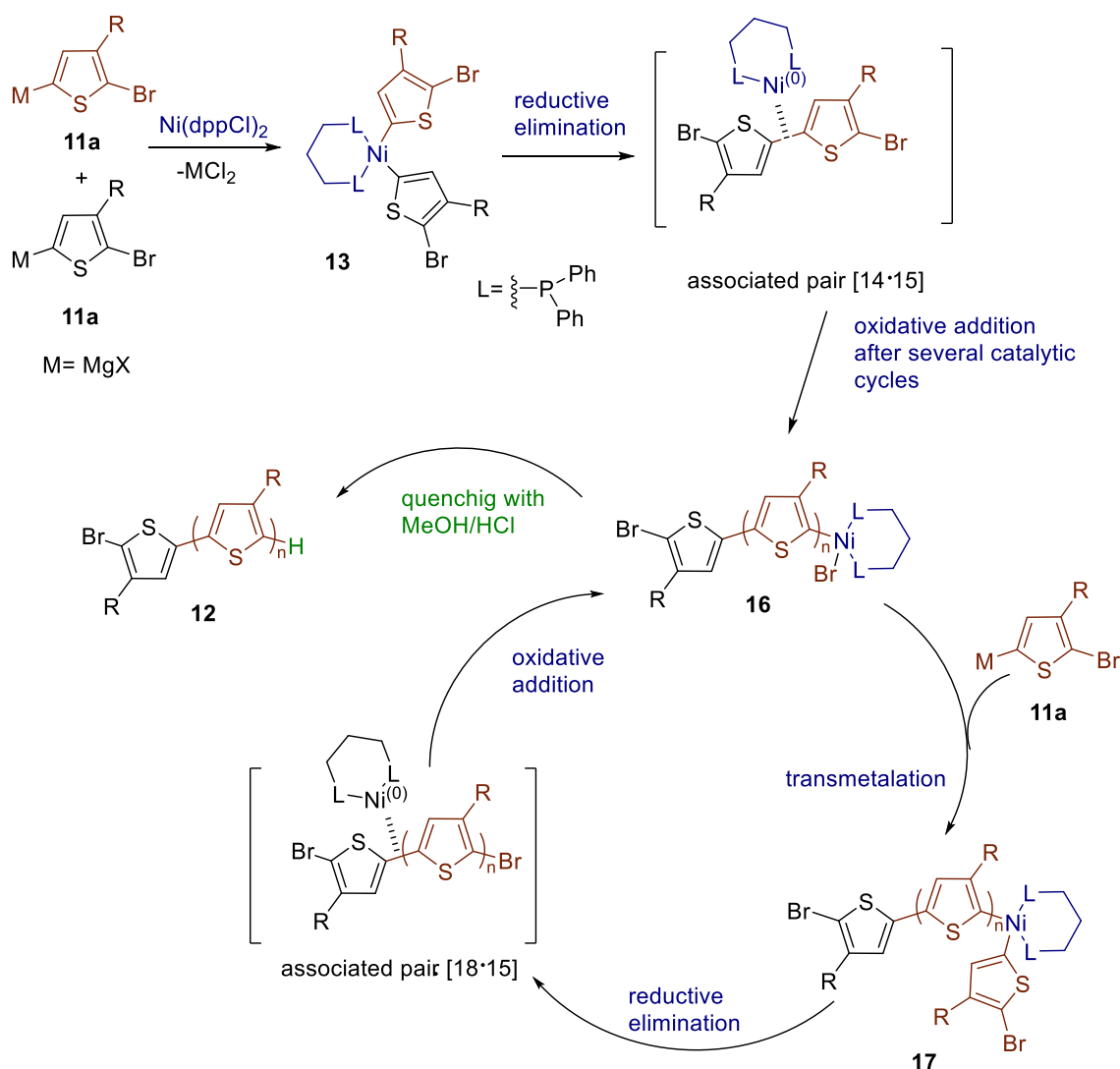


Scheme 4. Synthetic route of the GRIM method. The *in situ* generated Grignard compound **11a** reacts preferably with the nickel catalyst in a Grignard metathesis to generate P3HT **12** with high regioregularity (>99% HT).^[53]

In 2004, the McCullough group proposed that the polymerization of 3-substituted thiophenes, using nickel catalyst, under the GRIM condition proceeds via a chain-growth mechanism with a living character, producing polymers with high regioregularity (HT > 99%), high molecular weight ($M_n = 20$ kDa) and low polydispersity index ($\mathcal{D} = 1.2\text{-}1.4$).^[50a, 50c] In the case that the GRIM reaction is mediated with palladium catalyst, the polymerization proceeds via a step-growth mechanism (See behaviour of the M_n in

Figure 11).^[38c]

The explanation for the “living character” in the polymerization lies in the mechanism proposed by McCullough and co-workers (Scheme 5).^[50c] First, two equivalents from the most desirable intermediate **11a**, present in higher amount than **11b**, reacts with the catalyst [Ni(dppp)Cl₂] generating the bis-organonickel compound **13**. The reaction continues with a reductive elimination which produces the associated pair [**14·15**] of the bithiophene **14** (TT-coupling) and the Ni(0) complex **15**, which is stable during the reaction.^[54] The associated pair enters then in a cross-coupling reaction cycle, which starts with an oxidative addition between the dimer **14** and the Ni(0) complex **15** forming after several cycles the organonickel compound **16**, which contains a bromine motif. The cycle is followed by a transmetalation between the Nickel from compound **16** with the metal of **11a**, generating the new organonickel Ni(II) compound **17**. The next step is the formation of a new associated pair [**18·15**] by a reductive elimination. The cycle continues with either another oxidative addition step or with the quenching of the associated pair with a solution of HCl in methanol to produce poly-(3-substituted thiophene) **12** with Br/H end groups. As it was mentioned above, the GRIM method produces polymers with a high content of > 99% HT junctions. The one percentage left is due to the TT junction in the first dimer **14**.^[31]

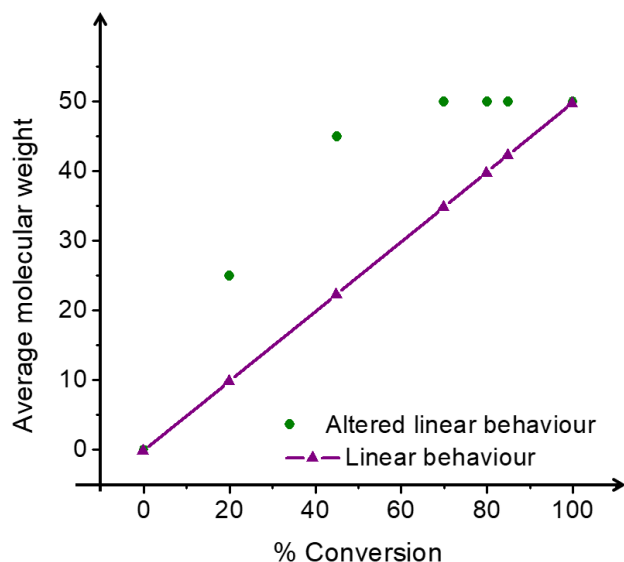


Scheme 5. Proposed mechanism for the GRIM method to produce high regioregular poly(3-substituted thiophene) **12**, based in a Nickel catalyst transfer condensation.^[50c]

The chain-growth mechanism of the polymerization can be explained by the strength of the associated pairs (**14·15**) and (**18·15**). When the interaction of such pairs is strong, an intramolecular oxidative addition step occurs, “moving” the Ni(0) species across the growing polymer until it arrives to the terminal chain. In that case after such a “ring walking”, the Ni from the catalyst remains associated with the growing chain, which is an important difference to other types of polycondensations.^[55] In the case of weak interactions of the associated pairs or too large dimensions of the monomers, the intramolecular oxidative addition can fail finishing the polymerization early.^[55]

The increasing molecular weight of the polymer with the monomer conversion is one indication for the living character of the polymerization (purple line from Figure 12) and depends on the molar ratio between the monomer and the nickel initiator (Equation 6).^[53] A second indicator is the continuous growing of the poly-(3-substituted thiophene) **12** after

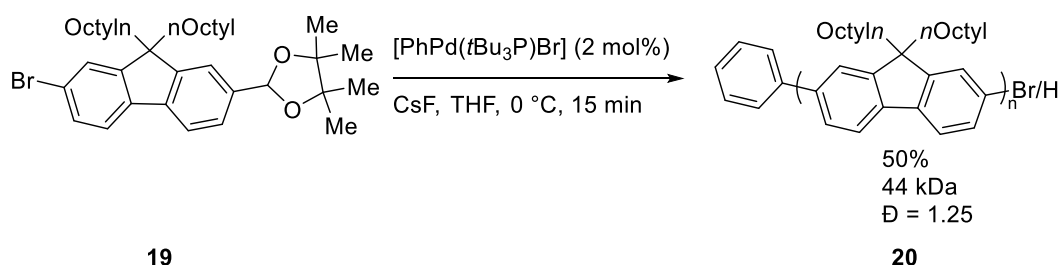
a second equivalent of the monomer **10** is added at the end of the polymerization. For this reason, it is possible to modify the end-capping of the resulted polymer using different Grignard reagents or monomers.^[53] Nevertheless, this linear behaviour can be altered in the case of a weak interaction of the catalyst with the growing polymer. In such cases for example, living-character can stop after 50% monomer conversion and the molecular remains unchanged after consuming all of the monomer (green dots from Figure 12).^[56]



$$M_n = \frac{M_o}{\% Ni\ cat.} \quad (6)$$

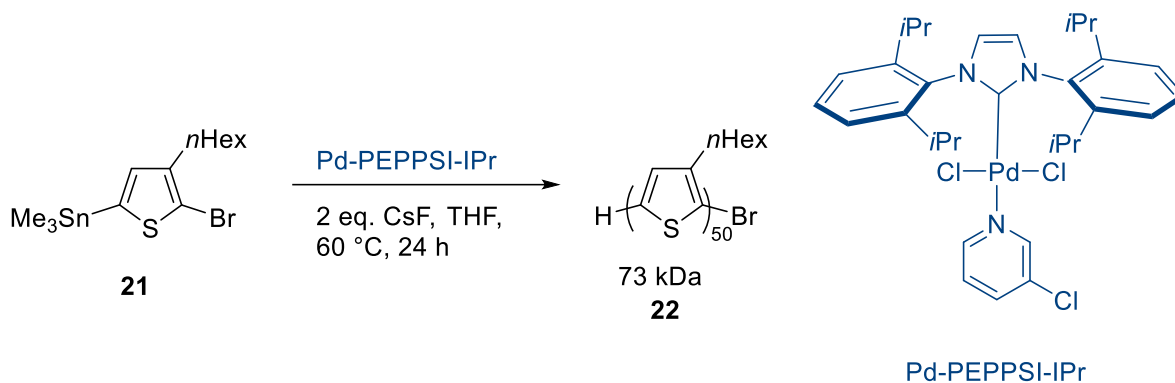
Figure 12. The purple triangles represent the average molecular weight obtained in a living growth polymerization, where a strong association between catalyst and the monomer exists. The green dots represent a disruption of the linearity due to a weak association between the catalyst and the monomer.^[56]

A living character, where polymers with high molecular weight and low \bar{D} are obtained, was observed as well in palladium catalysed reactions. In such a case of using $[\text{PhPd}(\text{tBu}_3\text{P})\text{Br}]$ as catalyst the phenyl groups acted as an initiator of the reaction and the end group of the polymer can be controlled with the addition of quenching species. One example is the Suzuki-polymerization of fluorene **19**, which bears a halogen and a pinacol boronate motif, producing the polymer **20** with Br or H end groups and a high molecular weight (Scheme 6).^[57]



Scheme 6. Effective Suzuki chain-growth polymerization with living character of the bifunctional fluorene **19**.^[57a]

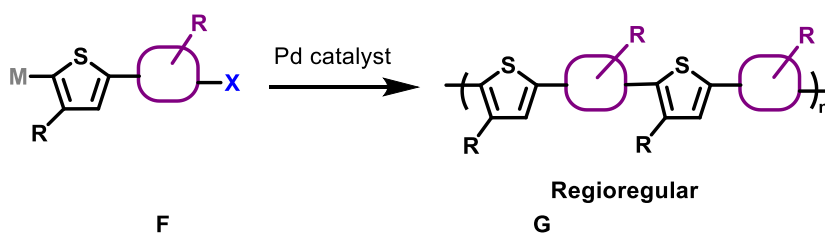
A more recent example (2015) is the Stille reaction from 2-bromo-3-hexyl-5-trimethylstannylthiophene (**21**) using a palladium N-heterocyclic carbene as catalyst to produce a high molecular weight P3HT (**22**) with 50 units (Scheme 7).^[52]



Scheme 7. Effective Stille chain-growth polymerization with living character to produce P3HT **22**.^[52]

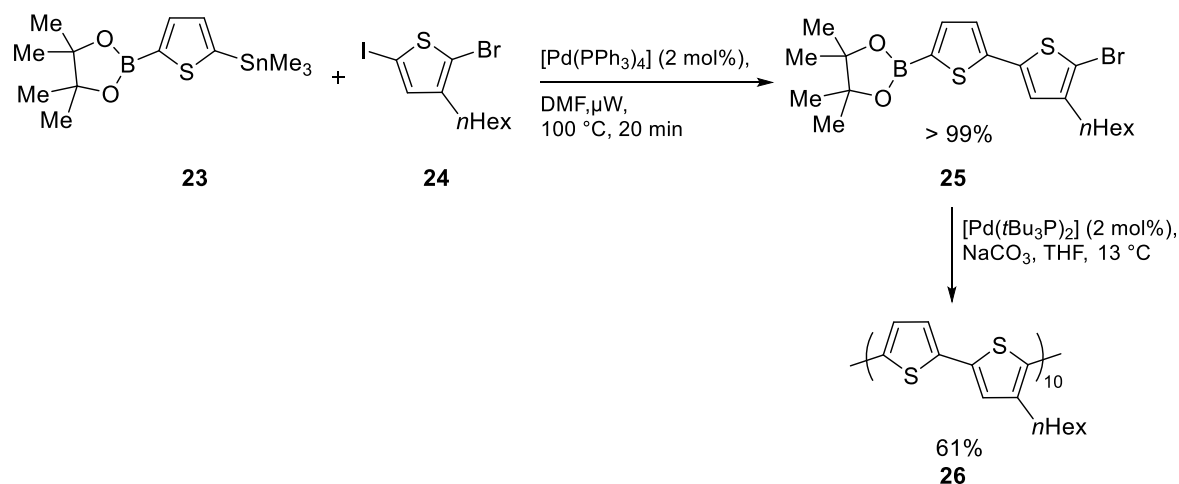
1.2.3.3. Dual Selectivity Cross-Coupling Reactions: Bi-Heterocycle Monomers

The concept of living polymerization with the advantage of combining two different building blocks in only one monomer **F** can be extended to produce copolymers with thiophenes and other heterocycles (Scheme 8). Such a monomer of the type M-Ar1-Ar2-X bears both an electrophilic and nucleophilic site and leads to regioregular polymers **G** with well-defined molecular weights (M_w) and narrow \mathcal{D} .^[50a, 58]



Scheme 8. Living polymerization synthetic path starting with bi-heterocycles monomers **F** to produce highly regioregular polymers or copolymers of thiophene **G**.

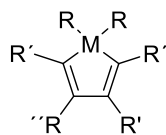
The synthesis of a bi-heterocyclic monomer type **F** that contains both electrophilic and nucleophilic functionalities via a dual selective cross-coupling reaction was introduced by Heinrich *et al.* in 2013.^[59] The work was based on a highly selective cross-coupling reaction between the dinucleophile **23**, which contained both a trimethylstannyl and pinacol boronate functional group, and a dielectrophile **24** (Scheme 9).^[60] They could show that the selectivity of the reaction depends on the leaving group of the electrophile (reactivity sequence: I > OTf > Br >> Cl) as well as on the catalyst and the other conditions.^[61] As iodine is the most reactive leaving group in electrophile **24**, a highly selective Stille cross-coupling occurs where the pinacol boronate stays unaffected. Also the heating under microwave irradiation plays an important role, as it decreases the reaction time and increases the yield of the reaction to produce the bi-heterocyclic **25**. The polymerization of **25** produced a polymer **26** with low molecular weight and low solubility due to the lack of a solubilizing alkyl chain in one of the thienyl unit.



Scheme 9. Synthetic path of the dually selective cross-coupling reaction between the dinucleophile **23** and **24** to obtain the bi-heterocyclic monomer **25** and further polymerization to produce **26**.^[59]

1.3. Organometallic Semiconducting Materials: Metalloles

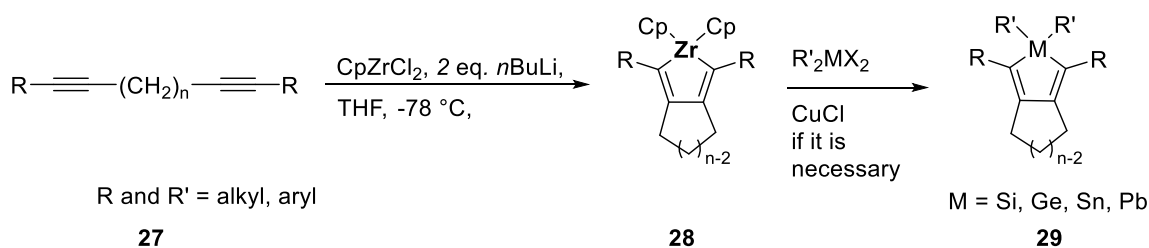
Metalloles are heteroles formed when a metal, for example a group 14 element, replaces the sp^3 -carbon atom of the cyclopentadiene (Figure 13). The properties of metalloles differ from the cyclopentadiene: they show an electron delocalization that includes the group 14 element, and in some of them the absorption undergoes a substantial bathochromic shift.^[62] These unusual characteristics have been exploited with great success for silicon containing heterocycles,^[63] which have been already discussed and used for applications as OSCs, LEDs^[15, 64] or OLEDs devices.^[63a] Germales and related germanium heterocycles are also receiving increased attention,^[65] but literature on stannoles is much scarcer. In chapter 3.2.1. an extended overview about the extent and type of electron delocalization, synthesis and characteristics of stannoles and polymers containing stannoles is discussed.^[66]



M = Si, Ge, Sn, Pb
R, R', R'' = Alkyl, Aryl groups

Figure 13. General structure of group 14 heteroles.

The most common method to prepare metalloles is based on a Fagan-Nugent reaction where a zirconacyclopentadiene **28** is formed from the reaction between the Negishi or the Rosenthal reagent with an acetylene derivate **27**, followed by a transmetalation with a group 14 element salt to produce metalloles **29** (Scheme 10).^[67] Furthermore other representative syntheses will be shown in chapter 3.2.1..



Scheme 10. General route for the preparation of metalloles under Fagan-Nugent conditions.

1.4. Organic Electronic Devices

In this thesis, two new polymers were synthesized and their use as light emitting layers in OLEDs will be presented (Chapter 3.1.1.). Therefore, the working principle and materials used in OLEDs will be described in detail. OSC and OFET are related semiconductor devices but because they were not fabricated, they will be only described briefly.

1.4.2. Organic Light Emitting Diode (OLED)

Light emitting diodes are devices based on the principle of the electroluminescence of a semiconducting material, converting electrical energy into light by the recombination of electron-hole pairs.^[18] In the configuration of the device, a layer of a semiconducting material called emitting layer is placed between a cathode and an anode where an external electrical current is applied. Organic light emitting diodes use organic semiconducting materials as emitting layer. The layer configuration of OLEDs is based on a substrate (glass or polyethylene), a transparent anode (usually indium tin oxide ITO), a hole transporting material, an emitting organic semiconducting material and a cathode (usually a mixture of Al/LiF^[68]) (Figure 14).^[69] The hole transporter material in general is a blend of poly-(3,4-ethylenedioxythiophene) with polystyrene sulfonate, well known as PEDOT:PSS.^[70]

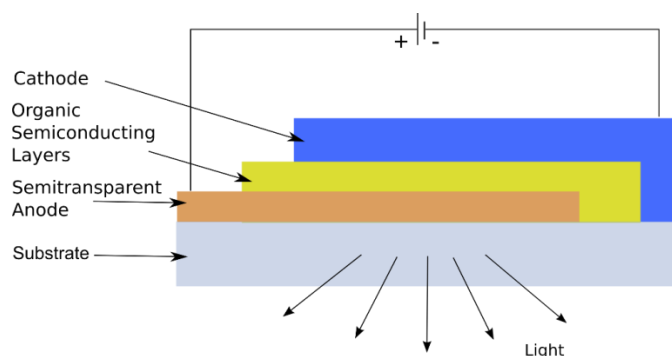


Figure 14. Layer configuration of an OLED.

a. Working Principle and Efficiency of OLEDs

The working principle of an OLED is based on the injection, migration and recombination of holes and electrons and the emission of photons.^[21a] The holes are injected from the anode which is typically ITO due to its transparency to visible light and their high work function (-4.7 eV). From there the holes migrate through the HTL (general PEDOT:PSS) to the emissive layer. Electrons on other hand are injected from the cathode typically made of a metal as Ca or Al due to their low work function (-2.5 to -3 eV). After migrating to the emissive layer, they form together with the holes so called excitons which are electron-hole pairs interacting with each other by their electrostatic fields. If this excited state decays by the recombination of the electron and hole, a photon can be emitted through the transparent substrate.^[21a, 71] Figure 15 describes the molecular orbital energy for each one of the layers.

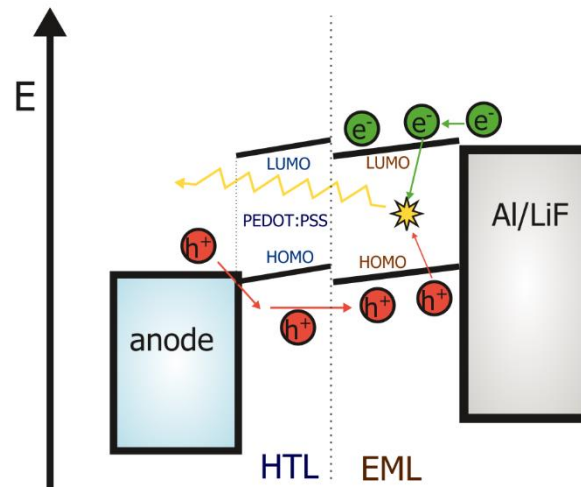


Figure 15. Energy level diagram and schematic work principle of an OLED based on the injection of holes from a high work function anode and electrons from a low work function cathode. Followed by their migration and recombination. Photons are emitted.

The efficiency of the OLEDs can be observed in different ways :

1. Internal and external efficiency (%): The internal electroluminescence efficiency of the OLEDs (η_{int}) is defined as the ratio of total photons emitted per electrons injected. Due the refraction index of the polymer (n) and orientations of the emissive layer, not all the photons released can be perceived by the human eye. Therefore, the measured efficiency which is defined as external quantum efficiency (η_{ext}), decreases with a factor of $2n^2$ in relation to the (η_{int}) (equation 7).^[18, 21a, 72]

$$\eta_{int} = \% \frac{\text{photons emitted}}{\text{electrons injected}}; \quad \eta_{int} = \eta_{ext} * 2n^2 \quad (7)$$

For the calculation of the η_{ext} , other factors should be considered as well. They are: the probability of charge recombination in the emissive layer (β), the probability to

produce emitting species (ρ_{ST}) and the fluorescence or phosphorescent quantum yield of the emissive material (ρ_{PL}). Therefore, the η_{ext} is calculated as well by the equation 8.

$$\eta_{ext} = \beta * \rho_{ST} * \rho_{PL} * \frac{\eta_{int}}{2n^2} \quad (8)$$

2. Power efficiency η_{pow} (W/W): represents the ratio of the output light power to input electrical power and is determined with the multiplication of η_{ext} by the ratio of photon energy (E_p in volts) and drive voltage (U in volts) (equation 9)

$$\eta_{pow} = \eta_{ext} * \frac{E_p}{U} \quad (9)$$

3. Energetic efficacy η_{Lum} (lm/W): considering that the human eye is more sensitive to light with different wavelengths, their response is standardized by the luminosity function (S) which has units of lm/W. The Luminous efficiency (η_{Lum}) of the OLED is obtained from the multiplication of the power efficiency and the luminosity function (S) (equation 10).^[18]

$$\eta_{Lum} = \eta_{pow} * S \quad (10)$$

4. Luminous efficacy L_e (cd/A): represents the ratio between the luminance (L in cd/m²) and the current density (A in A/m²) produced in the OLED (equation 11). It is worth to mention that luminance is as well a measurement of the efficiency of the devices. For example, looking directly to the sun has a L value of 10⁹ cd/m².^[72]

$$L_e = \frac{L}{A} \quad (11)$$

From the luminous efficacy it is possible to calculate the Energetic efficacy, considering that 1lm= cd*n and W= V*A (equation 12).

$$\eta_{Lum} = \frac{L_e * \pi}{V} \quad (12)$$

b. Organic Electroluminescent Materials (OEM)

The requirements of the organic electroluminescent materials (OEM) to be used as semiconductors in the emissive layer of OLEDs include : high quantum yields (defined as the number of emitted photons related to the number of absorbed photons of a compound), high color purity, ability to transport charges carriers (holes and electrons), high thermal stability, high stability against water and oxygen and formation of films without defects and crystalline sites.^[18, 71-72]

The color emitted from the OLED can be calculated from the optical band gap (E_g) of the OEM with the equation 13, where h is the Planck's constant, c is the speed of light and λ is the wavelength of the emitted radiation. [71] T

$$E_g = \frac{hc}{\lambda} = \frac{4.14 \times 10^{-15} \text{ eVs} * 3 \times 10^{17} \text{ nm/s}}{\lambda \text{ (nm)}} = \frac{1240 \text{ eV} * \text{ nm}}{\lambda \text{ (nm)}} \quad (13)$$

Table 1 summarizes the range of wavelength of light and optical band gaps of the OEM that is necessary to produce basic colors in OLEDs.[71] White emission OLEDs can be obtained by the mixture of all three colors or by combination of yellow and blue OEM.

Color	Wavelength λ (nm)	E_g (eV)
Red	610 - 760	1.63 - 2.0
Green	500 - 570	2.17 - 2.48
Blue	450 - 500	2.48 - 2.75

Table 1. Color obtained depending of wavelength of the photon emitted and bang gap of organic semiconductor.[71]

OEM can be small molecules (e.g. perylene, triphenylamine) as **30**, oligomers (e.g. oligothiophene, oligophenylene) as **31** or polymers (e.g. polyphenylene vinylene) as **32** which can have different emission wavelengths depending on the size of their band gap (Figure 16).[18] Molecules with blue emission are the most challenging to prepare because they need large E_g and high quantum yield but as well high mobilities of the charge carriers to ensure the high efficiency of the device. Example of blue emitter can be derivates of poly(para-phenylenes) as such as polymer **33**. [72]

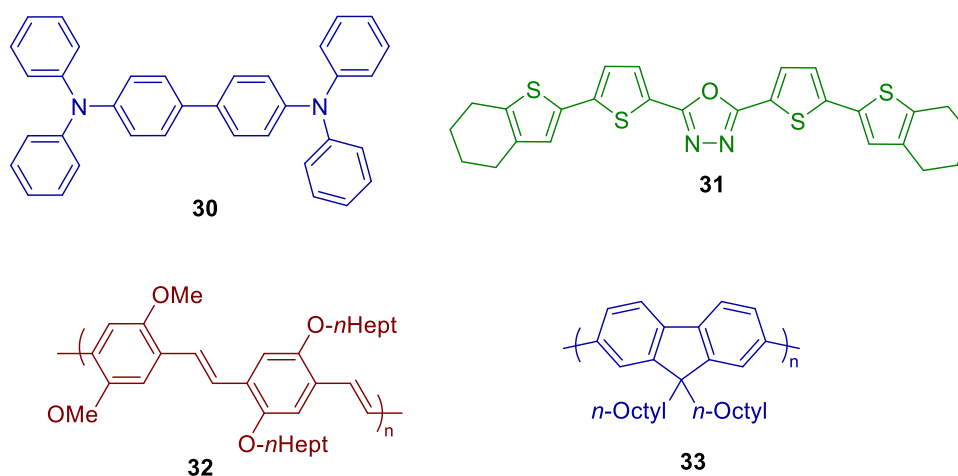


Figure 16. Examples of organic electroluminescent molecules with different size. The color represents the emission color of the materials. [18, 72]

1.4.3. Organic Solar Cell (OSC)

Solar cells are devices that convert the sunlight energy into electricity. In organic solar cells, the active layer, which absorbs the light, is based on a mixture of organic semiconducting materials which have electron donor (p-material) and electron acceptor (n-material) properties. Both components (small molecules or polymers) can be placed separately or as mixtures, which is then referred as a blend.^[20b] In the case that two polymers are mixed a bulk heterojunction is formed. The common layer configuration of an OSC type bulk heterojunction is based on a substrate, a transparent anode, a hole transport layer, an active layer and a cathode (Figure 17).^[27b]

The substrate consists either glass or polyethylene, depending of the final use of the OSC. The anode commonly consists of indium tin oxide (ITO). As a hole transporting layer, a blend of PEDOT:PSS is often used due to its high conductivity, improving the charge collection at the surface of the electrode. The donor material of the active layer can be P3HT^[73] or another hole-conductive polymer, whereas the acceptor material can be for example a derivative of buckminsterfullerene, phenyl-C61-butyric acid methyl ester (PCBM). Finally, Al or Ca metal with high work function are often used as cathode.

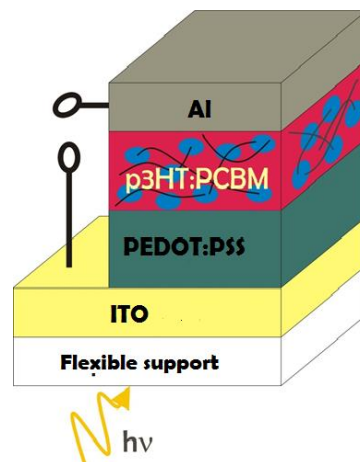


Figure 17. Layer configuration of a bulk heterojunction organic solar cell.

1.4.4. Organic Field Effect Transistor (OFET)

Field effect transistors (FET) are devices that can amplify or switch electrical signals using an electrical field. This can be done by modulating the conductance of a semiconducting channel by the application of a gate field. In organic field effect transistors (OFETs) an organic semiconductor is used. The typical configuration of an OFET consists of a gate electrode, a dielectric insulating layer and an organic semiconducting material which is

placed between the source and drain electrodes (Figure 18).^[31, 74] Depending of the type of the semiconductor, holes (p-channel) or electrons (n-channel) are accumulated between the channel and dielectric layer. In a n-channel OFET (Figure 18), when a voltage is applied between the source and drain ($V_{DS} > 0$) and the gate field is zero ($V_{GS} = 0$) the device is "OFF". The device is "ON" when a positive-source-gate bias is applied ($V_{GS} > 0$), generating an accumulation of electrons between the n-channel and the dielectric layers increasing the source-drain current.^[74]

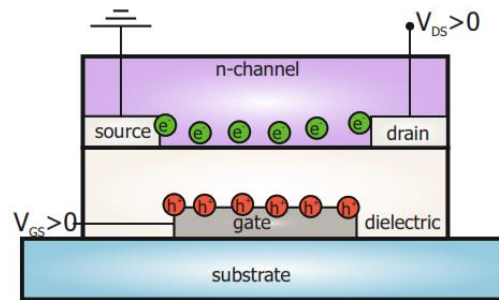
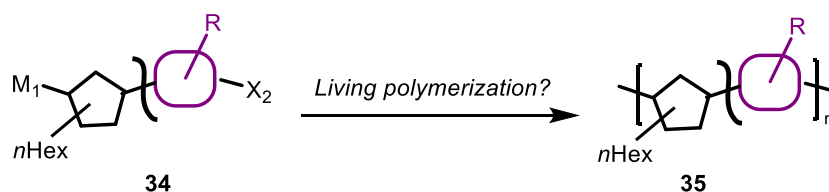


Figure 18. Layer configuration of n- channel OFET.^[31]

2. Objectives

2.1. Organic Semiconductors Based on the Push-Pull Principle

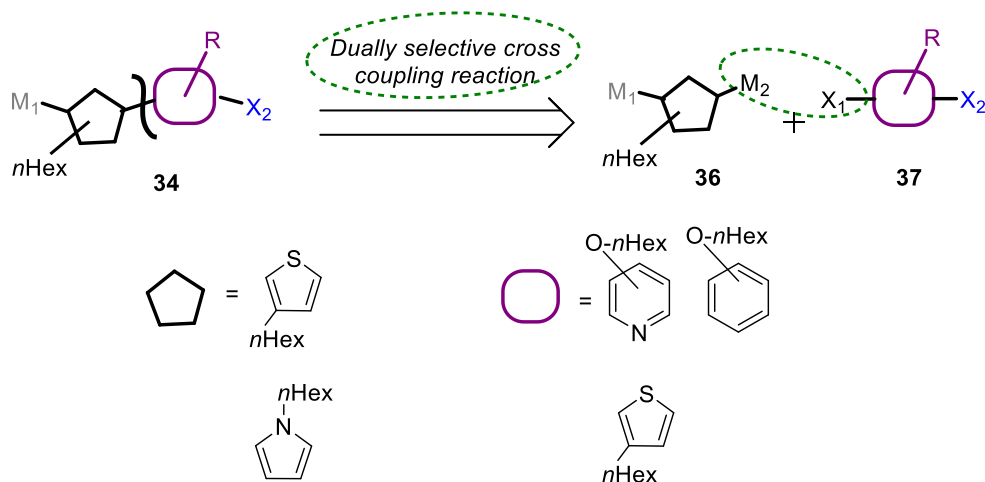
Semiconductor polymers that are mainly based on thiophenes have been used in the past years for different applications in organic electronic devices. Copolymers with thienyl units in combination with other systems (e.g. aromatic rings, heterocycles, alkenes or alkynes) are interesting because of the possibility of modifying the initial properties of polythiophenes and therefore tuning the optoelectronic properties. They could be prepared from donor- π -acceptor monomers, where a push-pull effect exists. In such systems thiophene is used as a push π -electron system and for example an aromatic system such as phenylene or pyridine as pull π -electron system.^[75] In the case that the copolymer includes a pyrrole unit, this one is used as a push π -electron and the thienyl unit as a pull π -electron system. Additionally, to have a donor- π -acceptor system, the monomer **34** is bi-functional, containing a nucleophilic (metal = M_1) and an electrophilic (halogen = X_2) motif. Monomer **34** may thus be used in living polymerization forming copolymers as **35** with potentially high molecular weight, high conjugation, high regioregularity and low \bar{D} (Scheme 11).



Scheme 11. General synthesis of polymers **35** from the chain-growth polymerization of monomers **34**.

The aim was to synthesize bi-functional monomers type **34** with thienyl, pyridine, phenyl and pyrrole groups based on a dually selective cross-coupling reaction, where one nucleophile (metal) from **36** reacts selectively with an electrophile (halogen) from **37** (Scheme 12).^[59] This strategy avoids costly and time-consuming protection group chemistry.

To obtain full insight into the properties of the polymers and to explore the possibility of applicability in devices, an in-depth characterization of the polymers is essential. Depending on the optoelectronic properties of the copolymers of type **35**, they may be used in organic electronic devices such as OLEDs.



Scheme 12. Retrosynthetic pathway of bi-functional monomers **34** based on dually selective cross-coupling reaction. Metal M_2 from the dinucleophile **36** reacts selectively with the halogen X_2 from the dielectrophile **37**.

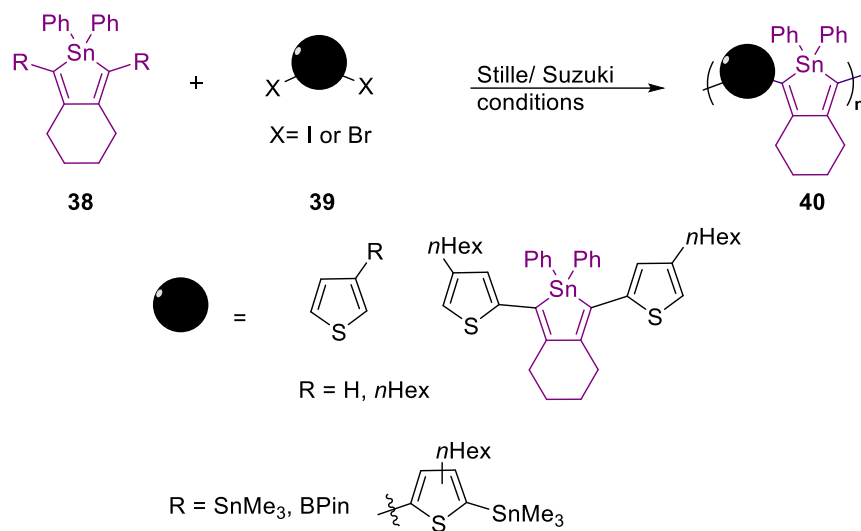
2.2. Stannoles : Organometallic Molecules

Stannoles are part of the class of 14 group element metalloles, where the tin replaces one carbon from the cyclopentadiene ring. Heavier group 14 element metalloles show a certain extent of electron delocalization due to $\sigma^*-\pi^*$ conjugation in the ring. This alone makes these compounds and their derivatives (oligomers and polymers) attractive molecules, both from a fundamental perspective but also based on their unusual optoelectronic properties. Such studies are mainly focused on siloles and germales, but on stannoles they are scarcer. This thesis should inspire progress in the area because stannoles have much to offer in term of novel fundamental insights into main group chemistry as well as potential for unusual functionality in optoelectronic devices.

One of the most common synthetic pathways to prepare stannoles is by the Fagan-Nugent transmetalation of zirconacyclopentadienes with a tin salt, as described above (Scheme 10). The formation of the zirconacyclopentadienes is based on the reduction of a diyne with "Cp₂Zr" species, whereby the most common sources of the "Cp₂Zr" species are Negishi's or Rosenthal's reagent. While some studies mention a preference for one or the other, a direct comparison of the reagent's similarities and differences of efficacies is not available yet. This thesis examines the differences between the two reagents when reacted with substituted dialkynes.

As it was observed with the first polymer containing three units of thiophene and one of stannole, reported by Linshoef *et al.*, the reaction between a stannole with two units of thienyl-iodo motif and the bis-trimethylstannyl-thiophene was possible. Such a system of thiophene-stannole shows a push-pull effect where the stannole acts as pull-electron system, due to the low-lying LUMO.^[66] The amount of thienyl units in such acceptor-donor system can affect the final optoelectronic properties. Therefore, cross-coupling reactions

between nucleophilic (**38**) and electrophilic (**39**) are tested to synthesize dimers, trimers or even polymers with thienyl and stannole rings in different ratios (**40**) (Scheme 13).



Scheme 13. Synthetic design to produce dimers, trimers or polymers containing stannole and thienyl rings in different ratios (3 : 1, 2 : 1; 1 : 1) and single polystannole.

3. Results and Discussion

3.1. Results and Discussion. Synthesis of Monomers Under the Push-Pull Principle. Exploring their Reactivity in Polymerization Reactions

This sub-chapter will cover the study of bi-functional monomers to be used in chain-growth polymerizations. Monomers of the type $M-Ar^1-Ar^2-X$ are push-pull systems, which bear both an electrophilic and nucleophilic site (Introduction-Scheme 8).^[50a, 58] This sub-chapter also includes studies of the kinetic growth of the products formed after their polymerization, and the optoelectronic and thermoanalytical characterization of such products.

Section 3.1.1. describes the polymerization of the monomers **M1-5** and **M1-6** by Suzuki cross-coupling and the potential use of the products of the polymerization in OLEDs. Section 3.1.2. describes a methylation experiment of the oligomer **M1-O2**. Section 3.1.3. describes the Suzuki reaction of the monomer **46** to produce P3HT and Section 3.1.4. the synthesis and Kumada polymerization of the monomer **P1-7** (Figure 19).

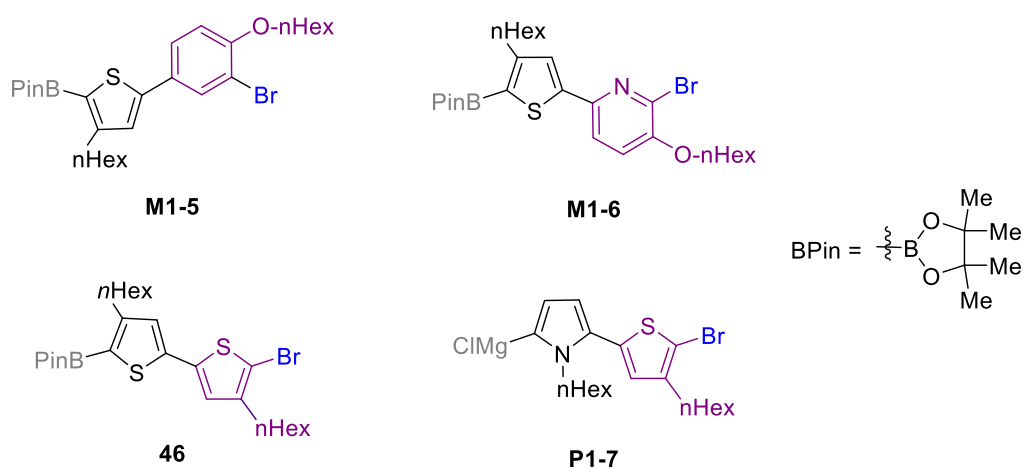


Figure 19. Summary of the monomers prepared under the push-pull concept in this thesis and explained in sub-chapter 3.1.. The pinacol boronate is labelled as BPin.

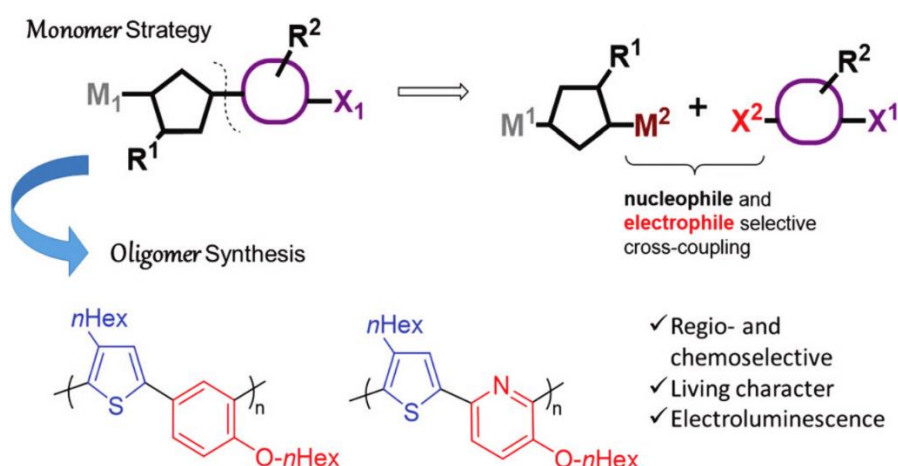
3.1.1. Conjugated Oligomers with Alternating Heterocycles from a Single Monomer: Synthesis and Demonstration of Electroluminescence

Full paper

Urrego-Riveros, S.; Bremer, M.; Hoffmann, J.; Heitmann, A.; Reynaldo, T.; Buhl, J.; Gates, P. J.; Sönnichsen, F. D.; Hissler, M.; Gerken, M.; Staubitz, A., *Organic Chemistry Frontiers*. DOI: 10.1039/c9qo00947g.

Abstract

Conjugated oligomers based on two different heterocycles are typically prepared by step growth polycondensation cross-coupling methods from two monomers $X\text{-Cycle}^1\text{-X}$ and $M\text{-Cycle}^2\text{-M}$ with no control of the regioselectivity. In this work, we used a new synthetic strategy that involves an extremely chemoselective reaction of a dielectrophilic compound, $X^1\text{-Cycle}^1\text{-X}^2$, with a dinucleophilic component, $M^1\text{-Cycle}^2\text{-M}^2$, under Stille conditions. The resulting monomers, $X^1\text{-Cycle}^1\text{-Cycle}^2\text{-M}^2$ are di-heterocyclic push pull monomers that still contain a nucleophilic site (boronic acid) and electrophilic site (bromide) and are set up for a controlled polymerization under Suzuki conditions. In this way, two semiconducting oligomers, based on thiophene / benzene and thiophene / pyridine motifs were synthesized. Both oligomers were characterized in terms of their, thermal, electrochemical, absorption, emission and electroluminescence properties.



TOC graphic. A synthetic strategy for push-pull oligomers is based on a nucleophile and electrophile selective synthesis of the corresponding monomers

Scientific contribution to this manuscript

In this project I synthesized the starting materials (**11**, **12**, **13**), both monomers (**5**, **6**) and the two oligomers (**O1**, **O2**). Dr. Anne Heitmann prepared compounds **15**, **16**, **18** and **19**. I performed the structural characterization of all synthesized compounds. GPC, TGA and DSC measurements were conducted by me in the Institute for Organic and Analytical Chemistry at Bremen University. Furthermore, I accomplished the optoelectronic characterization of the oligomers in the Institut des Sciences Chimiques de Rennes in Rennes University, under the supervision of Thibault Reynaldo and Prof. Dr. Muriel Hissler. Dr. Mathias Bremer and me prepared the OLED's and together with Janek Buhl their characterization in the Institute of Electrical and Information Engineering in the group from Prof. Dr. Martina Gerken from Kiel University. Jonas Hoffmann performed the DFT calculations. The manuscript was written by me and Prof. Dr. Staubitz. The rest of the authors proofread it.

RESEARCH ARTICLE

Conjugated oligomers with alternating heterocycles from a single monomer: synthesis and demonstration of electroluminescence†

Cite this: DOI: 10.1039/c9qo00947g

Sara Urrego-Riveros,^{a,b,c} Matthias Bremer,^d Jonas Hoffmann,^{ib} ^{a,b,e}
 Anne Heitmann,^{a,b} Thibault Reynaldo,^e Janek Buhl,^d Paul J. Gates,^{ib} ^f
 Frank D. Sönnichsen,^{ib} ^c Muriel Hissler,^e Martina Gerken^{ib} ^d and
 Anne Staubitz^{ib} ^{*a,b,c}

Conjugated oligomers based on two different heterocycles are typically prepared by step growth polycondensation cross-coupling methods from two monomers **X-Cycle¹-X** and **M-Cycle²-M** with no control of the regioselectivity. In this work, we used a new synthetic strategy that involves an extremely chemoselective reaction of a dielectrophilic compound, **X¹-Cycle¹-X²**, with a dinucleophilic component, **M¹-Cycle²-M²**, under Stille conditions. The resulting monomers, **X¹-Cycle¹-Cycle²-M²** are di-heterocyclic push pull monomers that still contain a nucleophilic site (boronic acid) and electrophilic site (bromide) and are set up for a controlled polymerization under Suzuki conditions. In this way, two semiconducting oligomers, based on thiophene/benzene and thiophene/pyridine motifs were synthesized. Both oligomers were characterized in terms of their thermal, electrochemical, absorption, emission and electroluminescence properties.

Received 27th July 2019,
 Accepted 13th September 2019
 DOI: 10.1039/c9qo00947g
 rsc.li/frontiers-organic

Introduction

Organic semiconductors are promising functional materials for applications in electronic devices such as light emitting diodes (OLED's), field effect transistors (OFET's) or photovoltaic solar cells.^{1–9} For example, oligo and polythiophenes have been widely used as semiconductors due to their electron rich character, high conductivity (>10⁵ S cm⁻¹)¹⁰ and band gaps (*E_g*) ranging between 1 and 3 eV.^{11,12} Many polythiophenes show a high aggregation in solid-state leading to high charge mobilities.^{13,14} However this aggregation can lead to non-radiative decay pathways, such as intersystem crossing or internal conversion into the ground state, which decreases the

quantum yield of oligo- and poly-thiophenes and limits their utilization in OLEDs.^{11,15}

To overcome these limitations to be utilized in OLEDs, first of all, the aggregation in the solid state can be suppressed. This can be achieved by designing specific copolymers of thiophenes with other conjugated molecules, to prevent interchain interactions.^{15,16} Tuning the band gap can be achieved by combining different heterocycles in the polymer chain; a push-pull system can be generated by placing an electron rich group; e.g. a thiophene unit adjacent to an electron deficient unit; e.g. another aryl group (Fig. 1). Typically, this leads to a bathochromic shift in the absorption.^{12,15} However, the quantum yield may be decreased, depending on the strength of the dipoles. The push-pull combination decreases the mobility of the excitons and prevents them from quenching. In addition, non-radiative decay processes of excitons can be avoided.^{17,18}

^aInstitute for Organic and Analytical Chemistry, University of Bremen, Leobener Str.7 NW2C, 28359 Bremen, Germany. E-mail: Staubitz@uni-bremen.de

^bUniversity of Bremen, MAPEX Center for Materials and Processes, Bibliothekstr. 1, 28359 Bremen, Germany

^cOtto-Diels-Institute for Organic Chemistry, University of Kiel, Otto-Hahn-Platz 4, 24098 Kiel, Germany

^dInstitute of Electrical Engineering and Information Technology, University of Kiel, Kaiserstr.2, 24143 Kiel, Germany

^eInstitut des Sciences Chimiques de Rennes, UMR 6226, CNRS-Université de Rennes 1, Campus de Beaulieu, 35042 Rennes Cedex, France

^fSchool of Chemistry, University of Bristol, Cantock's Close, Bristol BS8 1TS, UK

†Electronic supplementary information (ESI) available. See DOI: 10.1039/c9qo00947g

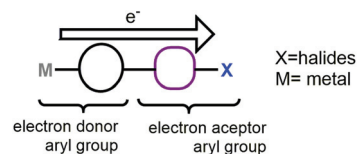


Fig. 1 Design of semiconducting polymers using the push-pull principle.

One of the most common methods to produce such copolymers is based on the step-growth polymerization between two different co-monomers **A** and **B**. In such a reaction, monomer **A** would have two electrophilic sites for cross-coupling (halides, pseudohalides), whereas monomer **B** would have two nucleophilic sites (organotin, boronic acids, boronic esters, organozinc groups for example (Scheme 1a)).^{12,18} The polymers **C** produced by this method can be expected to have a high dispersity (\mathcal{D}) and a low regioregularity.

A second method is based on the chain-growth polymerization developed by McCullough and Yokozawa. The mechanism involves a catalyst-transfer condensation using a single monomer **D**, which contains an electrophilic and nucleophilic site (Scheme 1b).^{19–21} With this breakthrough concept, it was possible, in the case of poly(3-alkylthiophenes), to obtain good molecular weights (M_n), a very high regioregularity >98%, and a low dispersity; in addition, the nature of the end groups of the polymers **E** could be controlled.²² Even alternating copolymers have been obtained by this method, although in that case, only one heterocycle contained a solubilizing group, thus reducing problems of torsional defects.²³ A third, novel method is based on the C–H arylation of monomers of type **F** to produce homopolymers type **E** (Scheme 1c).^{24–26} The C–H bond is activated by using a catalytic system formed between a Pd, or Ni catalyst, a ligand and a base (e.g. Hermann's catalyst- Cs_2CO_3 ,^{25,27} $\text{NiCl}_2\text{-dppf}/(\text{TMP})_2\text{Mg}\cdot 2\text{LiBr}$ ²⁸ or $\text{Pd}(\text{OAc})_2\text{-pivalic acid}$ ²⁷). This method holds much promise and can be extended to heteropolymers of the type AB.^{26,29}

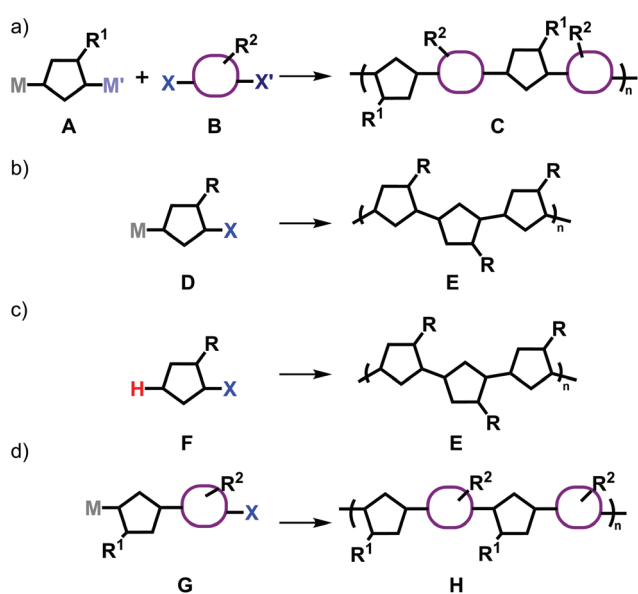
The aim of this work was to combine the concept of living polymerization with the advantage of combining two different

building blocks in only one monomer. Therefore, monomers **G** of type **M–Ar–Ar–X** were designed that bear both an electrophilic and nucleophilic site allowing to obtain polymer **H** (Scheme 1d).^{19,30}

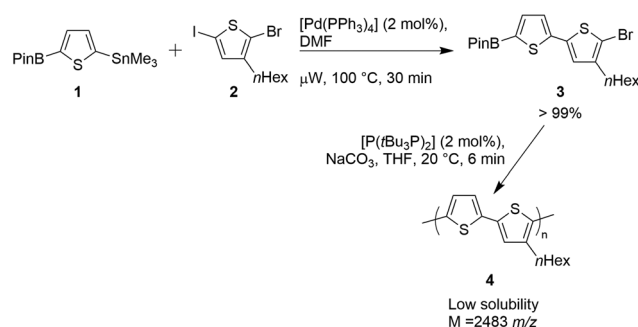
Recently, we published a monomer, which was the product of a dually nucleophilic–electrophilic selective cross-coupling reaction.³¹ Therein, monomer **3** was prepared to contain two different units of thiophene; a key strategic synthetic element was that dinucleophile **1** and dielectrophile **2** reacted extremely chemo specifically (Scheme 2): only the iodo- and the trisubstituted functional groups cross-coupled. However, the polymer **4** that was obtained showed a very low solubility and could only be used as a proof-of-concept. It was impossible to analyze it by solution-state NMR and the optoelectronic properties could not be measured. However by MALDI-MS, an oligomer with a mass of 2483 m/z was detected,³¹ which was very promising and led us to pursue the concept of monomer formation by dually electrophile and nucleophile selective reactions for monomers that would lead to soluble polymers or oligomers. In this context, the work of Zhang and Hong should be mentioned, who at the same time as ourselves followed a similar strategy for the synthesis of a polyarene.³²

In this work, we report a dually nucleophilic–electrophilic selective cross-coupling reaction to prepare two monomers, **5** and **6** type **G** (**M–Ar–Ar–X**). The monomers **5** and **6** were designed using the concept of the push–pull principle, having an aryl or pyridine (**6**) moiety as an electron acceptor group.¹⁸ This part of the molecule was designed as the di-electrophilic part, whereas the thiophene moiety was designed as the electron-rich di-nucleophilic part. In order to improve the solubility of the monomers, a hexyl chain was installed at the thiophene unit and a hexyloxychain on the six-membered aromatic ring (Fig. 2). The oligomers **O1** and **O2** were then obtained by a Suzuki cross-coupling living polymerization.

In addition to the synthesis, we report on the structural, optical and thermal characteristics of the obtained oligomers **O1** and **O2**. First electroluminescence tests were performed to assess these materials as potential emission layers in OLEDs.



Scheme 1 Types of polymerization (a) step-growth polymerization between **A** and **B** molecules (b) living polymerization from one type of heterocycle **D**. (c) Direct arylation polymerization from the monomer **F** (d) living polymerization of copolymers from di-heterocyclic monomers **G** (this work).



Scheme 2 Synthetic way to obtain a polymer based on a single monomer type **M–Ar–Ar–X**.³¹

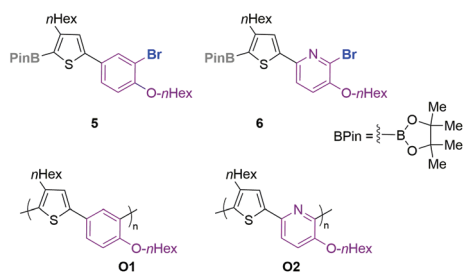


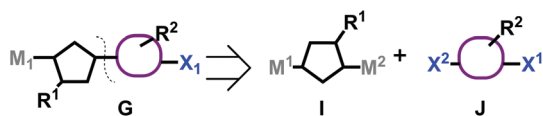
Fig. 2 Newly prepared push pull monomers **5** and **6** and oligomers **O1** and **O2**.

Results and discussion

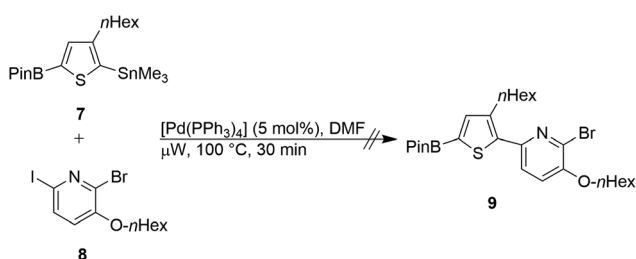
Synthesis of the monomers

The retrosynthetic analysis explains the high selectivity, which is required to obtain the monomer type **G** (Scheme 3): it is vital that in the dinucleophile **I**, only metal M^2 reacts and in dielectrophile **J**, only halogen X^2 . Any reaction of M^1 or X^1 would lead to slightly different monomers that would be inseparable from the desired ones and, moreover, there would be no regioselectivity with respect to the solubilizing side groups R^1 and R^2 .

The dinucleophile **7** was prepared as reported in the literature.³¹ The first attempt to prepare the monomer **9** was a selective Stille cross-coupling reaction between the dinucleophile **7** and the dielectrophile **8** (Scheme 4), in a similar way to how monomer **3** was obtained (Scheme 2). However, no product was formed either with conventional or under microwave conditions. One reason might be the steric hindrance of the hexyl chain that prevents the Stille reaction between the iodo-group of **8** and the trimethylstannyl group of **7**, although electronic reasons might play a role. McCullough *et al.* showed that 3-hexylthiophene monomers react much more readily if the M functional group is in 5-position and the X functional group in



Scheme 3 Retrosynthetic pathway to obtain the desired monomers type **G**.



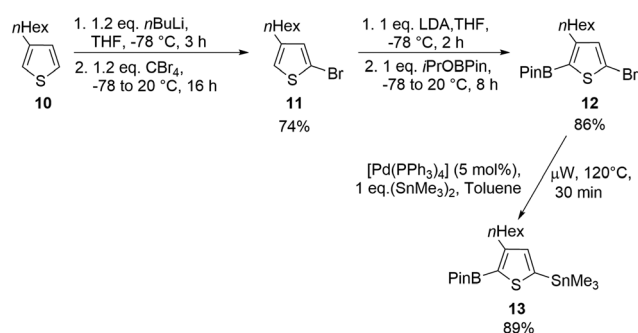
Scheme 4 Synthetic pathway to obtain monomer **9**.³¹

2-position. They argue that the transmetalation step is favorable if the M functional group is in a less steric hindered position relative to the catalyst center of the growing polymer.^{33–35}

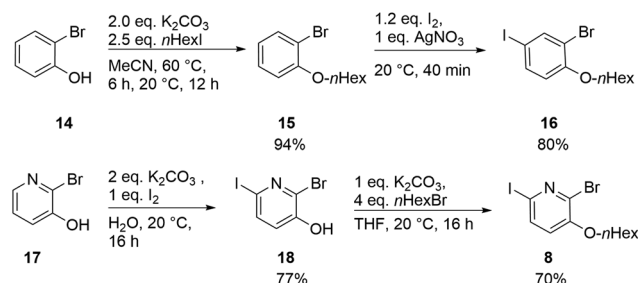
Therefore, the dinucleophile had to be redesigned. Thus, dinucleophile **13** was prepared (Scheme 5). The synthetic pathway involved a site-selective lithiation reaction of 3-hexylthiophene (**10**) in 5-position, followed by quenching with CBr_4 to obtain 2-bromo-4-hexylthiophene (**11**).³⁶ Site-selective deprotonation followed by a lithium-boron exchange led to mononucleophile **12**. In a final step, a selective Stille–Kelly coupling reaction of **12**,³⁷ with $(SnMe_3)_2$, Pd(0) under microwave heating led to the novel dinucleophile **13** in a yield of 89%.

For the Stille cross-coupling reaction, two dielectrophiles **16** and **19** were also required. The synthesis of the dielectrophile **16** started from the commercially available 2-bromophenol (**14**), which was subjected to a Williamson etherification with 1-iodohexane and led to **15** in a yield of 94%.³⁸ Then, a solvent-free iodination of 1-bromo-2-(n-hexyloxy)benzene (**15**) was carried out to give the 1-bromo-2-(hexyloxy)benzene-5-iodobenzene (**16**) in 80% yield (Scheme 6).³⁹ The synthesis of dielectrophile **8** started from 2-bromopyridine-3-ol (**17**), which was subjected to an iodination reaction to yield the iodo-pyridine derivate **18** in 77%. Compound **18** was then used in an alkylation reaction with 1-bromohexane to yield the dielectrophile **8** in 70% (Scheme 6).⁴⁰

The dinucleophile **13** and dielectrophiles **16** and **8**, respectively, were subjected to a Stille cross-coupling reaction under



Scheme 5 Synthetic pathway to form the dinucleophile **13**.

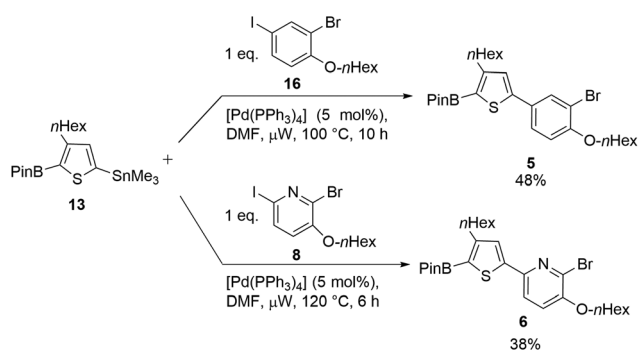


Scheme 6 Synthetic path to obtain the dielectrophiles **16** and **8**.

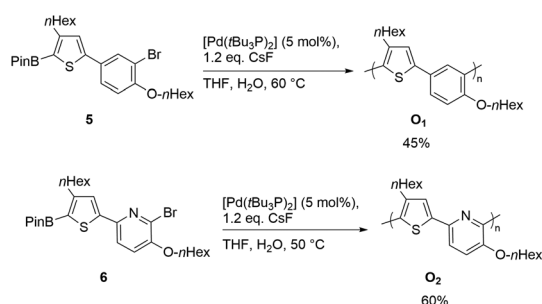
microwave conditions leading selectively to the monomers **5** and **6** (Scheme 7).^{31,41} The high selectivity of the reaction can be explained by the use of dinucleophile **13**, as the reaction occurred selectively between the iodo and trimethyl tin group. There is less steric hindrance for the tin functional group compared to the boronic ester, and Suzuki-reactions would require an additional base. In addition, the C–I bonds in **16** and **8** are much weaker than the C–Br bonds.

Synthesis of oligomers **O1** and **O2**

Polycondensation Suzuki reactions of the monomers **5** and **6** were tested with two catalysts, ([Pd(*t*Bu₃P)₂] and [Pd(dppf)Cl₂]) (see in ESI Tables SI-3 and SI-4†). From these, [Pd(*t*Bu₃P)₂] emerged as the best system and it was used in the polymerization reactions for both monomers, which were heated at 60 and 50 °C respectively (Scheme 8).⁴² The crude products were precipitated from the reaction mixture with a solution of HCl in methanol (1 M) and washed several times with methanol by Soxhlet extractions. The products were soluble in chloroform. Oligomer **O1** was obtained in a yield of 46% (*M_n* = 1.56 kDa, *D* = 1.12, GPC calibrated against polystyrene) and **O2** in a yield of 60% (*M_n* = 5.39 kDa, *D* = 1.83), respectively. It was found by MALDI-TOF mass spectrometry that for both polymers, the end groups were H and Br (see in ESI, Fig. S1–2 for **O1** and S1–9 for **O2** †).



Scheme 7 Synthetic pathway to form the monomers **5** and **6** in a Stille cross-coupling reaction between dinucleophile **13** and dielectrophiles **16** and **8**, respectively.



Scheme 8 Syntheses of the oligomers **O1** and **O2**.

Analysis of the oligomerization of oligomers **O1** and **O2**

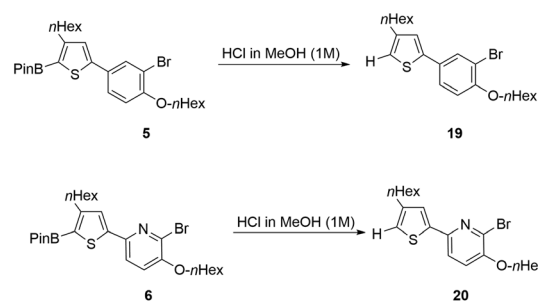
To evaluate the type of kinetics of polymer chain formation, reaction monitoring studies of the polymerization were performed. Samples from the reaction mixture were taken in the course of 24 h for **O1** and 27 h for **O2**. Each sample was quenched with a solution of HCl in methanol 1 M straight after removal from the reaction, extracted with DCM and split in two for measurements of GPC and ¹H NMR spectroscopy. The percentage of conversion for each sample, was calculated relative to the protonated products **19** and **20** that are formed by protonolysis (Scheme 9). The plots of % conversion vs. time and % conversion vs. *M_n* and *M_n*/*M_w* are depicted in Fig. 3 for **O2**. The conversion was calculated with respect to the consumption of product **20** observed by ¹H NMR spectra and from the UV-Vis/elugram areas visualized in the 2D plots from the GPC measurements (see ESI†).

The oligomer appeared to grow approximately linearly in length during the first 9 h, reaching 60% conversion and a *M_n* = 1.40 kDa. Then, in the period from 9 h to 28 h, only very little growth in length took place, but a conversion of eventually 100% product was reached. This observation may be interpreted that the reaction had a living character until a conversion of 60%. A similar behavior could be observed for **O1**: after 8 h, the conversion reached 40%, growing sharply until 92% in the following 16 h (see the ESI for Fig. S1–21–23†).

It needs to be pointed out that although the formal classification of the polymerization kinetics is chain growth, the linear region of the quasi-living character is relatively limited, presumably because the catalyst diffuses from the growing chain more quickly than a new monomer is reacted with it.^{19,43} This can be attributed to the sterically relatively congested site of cross-coupling (with adjacent alkyl and alkoxy groups).

Optical and electrochemical characterization

In order to establish structure/properties relationships, the optical (UV-Vis absorption and fluorescence) and electrochemical properties of **O1** and **O2** were studied in CH₂Cl₂. The two oligomers **O1** and **O2** presented a broadband in the absorption spectrum (Fig. 4). The absorption maximum observed for **O2** (*λ_{max}* = 387 nm) was bathochromically-shifted compared to the absorption maximum of **O1** (*λ_{max}* = 318 nm)



Scheme 9 Compounds **5** and **6** were transformed into the products **19** and **20**, respectively, by treating them with HCl/MeOH (1 M).

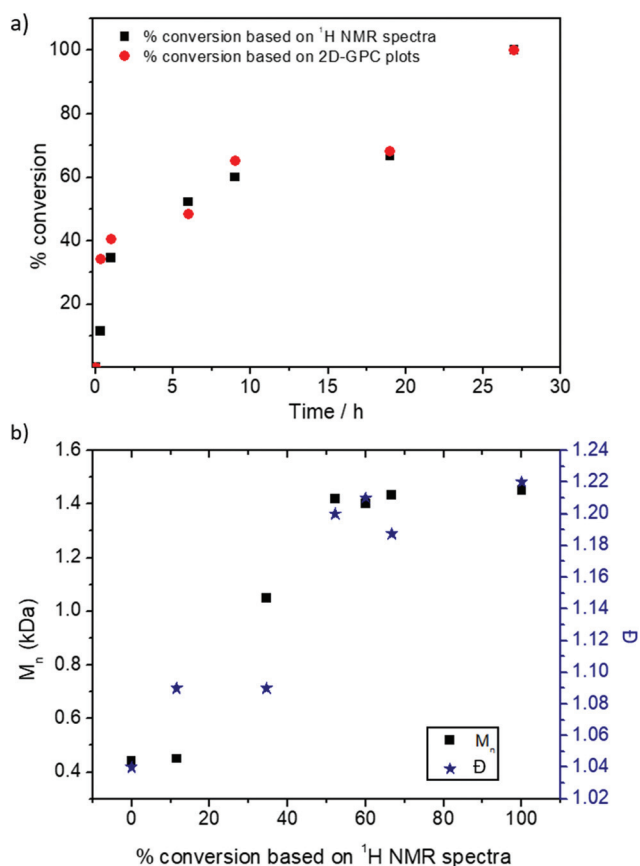


Fig. 3 Plots of (a) % conversion vs. time. Calculated by the two detectors (¹H and 2D-plots GPC) and (b) M_n and D vs. % conversion calculated by ¹H NMR; for the polymerization of **6** with 5 mol% of $[Pd(tBu_3P)_2]$, 1.2 eq. CsF in THF at 50 °C. The conversion was calculated relative to compound **20** (product from the quenching process with HCl/MeOH) based on ¹H NMR spectra and 2D-GPC plots.

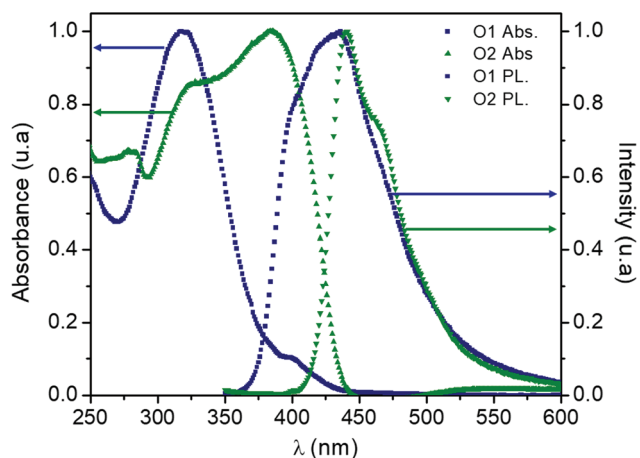


Fig. 4 Normalized absorption spectra (abs.) and PL spectra of **O1** and **O2** ($\lambda_{exc} = 340$ nm) in dichloromethane.

suggesting a higher extended π -conjugation in **O2** due to a certain charge transfer character of π - π^* transition of the thiophene-pyridine motif. A similar trend was observed for the

fluorescence of the oligomers. Oligomers **O1** and **O2** showed fluorescence around 435 nm with a small red-shift for the derivative **O2** ($\Delta\lambda = 5$ nm). The fluorescence quantum yields measured *versus* quinine sulfate were moderate in solution (10%, **O1** and 28%, **O2**, Table 1). Excitation spectra also confirmed the observations made for the UV-Vis absorption of oligomers **O1** and **O2** (see Fig. SI-3 and SI-10[†]). The optoelectronic properties from both oligomers in comparison with a 4-unit oligomer of thiophene (in chloroform solution: $\lambda_{max} = 372$ nm,⁴⁴ $\lambda_{PL} = 494$ nm,⁴⁴ $\Phi = 0.09$ (ref. 44) and $E_g^{optical} = 3.33$ eV (ref. 45)), shows that a combination with a stronger acceptor than thiophene (pyridyl group in **O2**) leads indeed to a higher bathochromic shift. However, although a phenyl group is also an acceptor with respect to thiophene,¹⁸ λ_{max} of **O1** is hypsochromically shifted, likely due to torsional defects arising from the six-membered ring that are not sufficiently counterbalanced by an acceptor property that is lower than that of a pyridyl ring. The photoluminescence is most strongly shifted in the oligomer of oligo-3-hexylthiophene.

The redox properties of oligomers **O1** and **O2** were investigated by cyclic voltammetry (CH_2Cl_2 , 0.2 M, Bu_4NPF_6 , $\nu = 200$ mV s⁻¹, Table 1). All compounds showed a quasi-reversible oxidation wave at relatively low potential. Compound **O1** displayed an oxidation wave at around +0.48 V (*vs.* Fc^+/Fc) while **O2** was slightly easier to oxidize ($E_{ox} = +0.47$ V *vs.* Fc^+/Fc). These electrochemical characterizations indicated that the highest occupied molecular orbital (HOMO) was energetically destabilized for oligomer **O2** compared to the HOMO of **O1** (Table 1).⁴⁶ The reduction potentials, which are attributed to the energy of the lowest unoccupied molecular orbital (LUMO) and therefore to the π^* band, were not possible to detect because the potentials were out of the electrochemical window (Fig. SI-4 for **O1** and SI-14 for **O2** [†] respectively). Hence, the reduction potential (LUMO) for both oligomers were estimated using the HOMO and optical energy gap values.

Such a difference in the optoelectronic behavior between the oligomers **O1** and **O2** can be related to the enhanced donor-acceptor effect in **O2**, because of the higher π acceptance of the pyridine compared to the benzene in **O1**.¹⁸

Table 1 Optical and electrochemical properties of the oligomers **O1** and **O2**

Compound	Φ^a/λ_{PL} (nm)	E_g (eV) exp ^b /calc. ^f	E_{Ox}^c (V)	E_{HOMO} (eV) exp ^d /calc. ^f	E_{LUMO} (eV) Exp ^e /calc. ^f
O1	0.10/432	3.17/3.95	+0.48	-5.87/-5.17	-2.70/-1.22
O2	0.28/442	2.77/3.54	+0.47	-5.86/-5.11	-3.09/-1.57

^a The quantum yield was calculated using a solution of quinine sulfate (1 M in H_2SO_4) with a Φ of 0.54. ^b Optical band gap. ^c Obtained from the cyclic voltogram of a solution of the oligomer in DCM (1×10^{-3} M) with Bu_4NPF_6 (0.2 M in DCM) as electrolyte.⁴⁶ ^d The energy from the HOMO was calculated with the equation: $E_{HOMO} = -(E_{onset\ ox.} vs. Fc^+/Fc + 5.39)$ eV.⁴⁶ ^e The energy from the LUMO was calculated with the equation $E_{LUMO} = -(E_g - E_{HOMO})$.⁴⁶ ^f Calculated using TD-DFT based on the trimers.

Computational studies

These experimental observations were further supported by time-dependent density functional theory (TD-DFT) studies in the gas phase. To simplify this computational study, the calculations were carried out on two simplified monomer structures **S1** and **S2**, and the corresponding dimers and trimers (Fig. 5).

TD-DFT calculations confirmed that trimer **S2-3** had a narrower energy gap (see Table 1) between the calculated HOMO and LUMO (3.54 eV) compared to **S1-3** (3.95 eV) Fig. 6. Besides, the HOMO levels in both trimers were similar (−5.17 eV vs. −5.11 eV), the LUMO is more stabilized in the case of **S2-3** than in **S1-3** (−1.57 eV vs. −1.22 eV). To explain this phenomenon and further estimate the effect of either the phenyl or pyridine ring on the respective thiophene unit, the bond length alternation (BLA) for both systems were calculated.

By comparing the double and single bond lengths in π -conjugated linear polymers, BLA values can indicate if the ground state is more likely to form a quinoid-like or an aromatic structure.⁴⁷ Since **S1** and **S2** are asymmetric, the BLA calculations were done by only taking the inner thiophene bonds into account. Shorter BLA values of the flanked thiophene in **S2-3** (maximum 0.045 Å) in comparison to **S1-3** (maximum 0.052 Å, Table SI-15†), and a shorter central carbon bond between the thiophene and phenyl/pyridine of **S2-3** (1.467 Å vs. 1.472 Å) indicate that the quinoidal structure is more likely

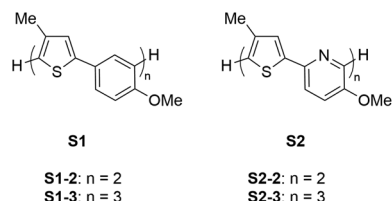


Fig. 5 Monomers, dimers and trimers proposed for computational studies. The hexyl chains from the monomers **5** and **6** were replaced by methyl groups in **S1** and **S2** respectively, to reduce computational time. Further the end groups were replaced by a proton as the most neutral substituent.

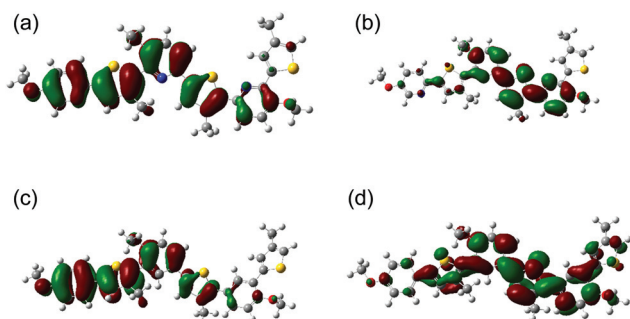


Fig. 6 Molecular orbitals (displayed with an isovalue of 0.02) of trimer **S1-3**: HOMO (a) and LUMO (b) and of trimer **S2-3-3**: HOMO (c) and LUMO (d).

formed in **S2-3** and explains the stabilization of its LUMO by fortified delocalization of π -electrons.

Thermal behavior of **O1** and **O2**

The thermal stability of the polymers was studied by thermogravimetric analysis under N_2 at a heating rate of 10 K min^{-1} in a range from 25–600 °C. **O1** lost 59% of weight at 406 °C (onset temperature). **O2** showed two segments of weight loss: first 4% weight loss at 221 °C (onset temperature), probably due to traces of volatiles in the sample; and 50% weight loss at 405 °C (onset temperature), directly related to the loss of the alkoxy and alkyl chains.

The DSC thermograms indicated a glass transition temperature of −7.1 °C for **O1** and of 25 °C for **O2**.

Electroluminescence experiments

The oligomers **O1** and **O2** were tested as emissive layer between electrodes in single-layer OLED devices, to prove their electroluminescent properties. The configurations of the devices were ITO/PEDOT:PSS/**O1** or **O2**/LiF/Al. The electroluminescence spectra of both devices (Fig. 7) resemble the PL spectra of compounds **O1** and **O2** but they are red shifted (Fig. 4 and 7; for **O1** shifted from 432 to 533 nm and for **O2** from 442 to 593 nm). These EL spectra are obtained with high applied voltages of 7.7 V and 10.7 V (corresponding to 1 cd m^{-2}), respectively. At this voltage, the luminescence of **O1** started to level, indicating an instability of the compound. **O2**, albeit with a lower luminescence, did not show such a decomposition. Furthermore, a luminance of 2.5 and 0.8 cd m^{-2} was achieved at ca. 10 V, respectively and the external quantum yields are quite low presumably due to unbalanced carrier injection and/or transport.

Effectively, the energy level between the ITO/PEDOT:PSS-anode and the oligomers did not match well (with an energy difference of 0.66 eV for **O2** and 0.67 eV for **O1**, Fig. 8). The current densities are high, suggesting that charge carriers

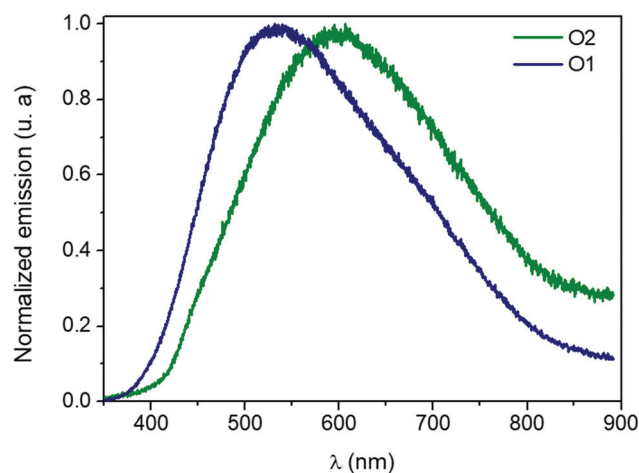


Fig. 7 Electroluminescence spectra for the OLED-type devices using **O1** and **O2** as emissive layer.

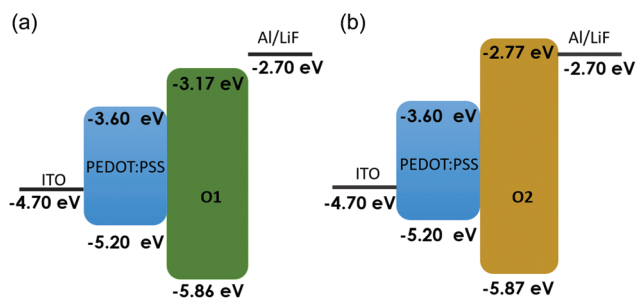


Fig. 8 Schematic diagrams of the energy levels of the OLEDs using the oligomers (a) **O1** and (b) **O2** as emissive layers.

move thought the device without many emissive recombination events (see Fig. SI-28 and Table SI-7†). This may be caused by a carrier injection imbalance or a dominant non-radiate recombination in a different layer. Therefore, in order to explore the full potential of oligomers **O1** and **O2**, an optimization of the device is required, which is beyond the scope of this study and the object of further investigations.

Experimental part

All the synthesis and characterization of the starting materials and polymers are given in the ESI.†

Characterization of the OLED-type devices

The *I-V* characterization of the OLED-type devices was performed with a Keithley 2400 Source Measurement Unit, a calibrated photodiode and an Avantes AvaSpec-2048 USB spectrometer.

OLED-type device fabrication

ITO coated glass substrates were cleaned in an ultrasonic bath of acetone and isopropanol for 15 min each. Subsequently, they were dried under a nitrogen stream, heated to 160 °C for 10 min and then cleaned with an oxygen plasma with 300 W for 3 min. 200 μL of a PEDOT:PSS solution were spin-coated onto the substrates (3500 rpm for 60 s). The samples were then transferred into a glovebox and annealed at 150 °C for 5 min. Afterwards, they were cooled down to 50 °C over 2 min. A solution of the polymers either in toluene or chloroform was prepared with a concentration of 10 mg mL⁻¹. 180 μL of the polymer solution were spin coated (500 rpm for 5 s, and 1000 rpm for 60 s) on the PEDOT:PSS layer and the samples were annealed at 70 °C. Finally, a layer of LiF (1 nm) and Al (200 nm) were deposited by thermal evaporation.

Conclusions

Monomers based on the push pull principle were synthesized using a highly chemo selective Stille reaction between a dinucleophile, containing pyridinyl **5**, or aryl groups **6**, and a dielectrophile, which contained a thiophene moiety. Based on

those monomers (**5** and **6**), two oligomers **O1** and **O2** were synthesized using a Suzuki polymerization reaction. Studies analyzing the dependence of molecular weight on conversion showed that the monomers **5** and **6** may grow in a living fashion, at least until a certain point, 60% and 40% respectively, to obtain the oligomers **O1** and **O2**. After this point, the catalyst presumably dissociates from the chain. **O1** and **O2** showed optical band gaps in solution with values of 3.17 eV and 2.77 eV; and quantum yields of 10% and 28% respectively. Due to those optoelectronic properties, simple devices to test for electroluminescence with the configuration ITO/PEDOT:PSS/**O1** or **O2**/LiF/Al were fabricated. The devices showed a turn on voltage of 4.3 and 4.6 V demonstrating the electroluminescent character from the oligomers **O1** and **O2**.

Conflicts of interest

There are no conflicts to declare.

Acknowledgements

S. U. R. thanks the German Academic Exchange Service (DAAD) and the Colfuturo Fund for a Ph. D. scholarship. Grant number: A/13/72356. M. B. and M. G. acknowledge financial support by the ERC within the project “PhotoSmart” (Starting Grant Agreement 307800).

This research has been supported by the Institutional Strategy of the University of Bremen, funded by the German Excellence Initiative.

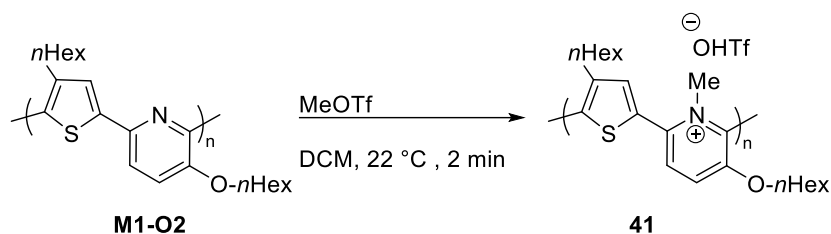
Notes and references

- 1 K. Müllen and G. Wegner, *Electronic Materials: The Oligomer Approach*, Wiley-VCH, Weinheim, 1998.
- 2 T. A. Skotheim and J. Reynolds, *Handbook of Conducting Polymers*, CRC, Boca-Raton, Fla, 2007.
- 3 K. Müllen and U. Scherf, *Organic Light Emitting Devices: Synthesis, Properties and Applications*, Wiley-VCH, Weinheim, 2006.
- 4 S. Scholz, D. Kondakov, B. Lüssem and K. Leo, *Chem. Rev.*, 2015, **115**, 8449–8503.
- 5 A. C. Grimsdale, K. Leok Chan, R. E. Martin, P. G. Jokisz and A. B. Holmes, *Chem. Rev.*, 2009, **109**, 897–1091.
- 6 M. Grätzel, *Inorg. Chem.*, 2005, **44**, 6841–6851.
- 7 A. Hagfeldt, G. Boschloo, L. Sun, L. Kloo and H. Pettersson, *Chem. Rev.*, 2010, **110**, 6595–6663.
- 8 Y.-J. Cheng, S.-H. Yang and C.-S. Hsu, *Chem. Rev.*, 2009, **109**, 5868–5923.
- 9 H. Sirringhaus, *Adv. Mater.*, 2014, **26**, 1319–1335.
- 10 R. D. McCullough and R. D. Lowe, *J. Chem. Soc., Chem. Commun.*, 1992, 70–72, DOI: 10.1039/C39920000070.
- 11 M. R. Andersson, O. Thomas, W. Mammo, M. Svensson, M. Theander and O. Inganäs, *J. Mater. Chem.*, 1999, **9**, 1933–1940.

- 1 12 Q. T. Zhang and J. M. Tour, *J. Am. Chem. Soc.*, 1998, **120**, 5355–5362.
- 13 R. D. McCullough, P. C. Ewbank and R. S. Loewe, *J. Am. Chem. Soc.*, 1997, **119**, 633–634.
- 5 14 B. S. Ong, W. Yiliang and L. Ping, *Proc. IEEE*, 2005, **93**, 1412–1419.
- 15 15 I. F. Perepichka, D. F. Perepichka, H. Meng and F. Wudl, *Adv. Mater.*, 2005, **17**, 2281–2305.
- 10 16 J. Hollinger, A. A. Jahnke, N. Coombs and D. S. Seferos, *J. Am. Chem. Soc.*, 2010, **132**, 8546.
- 17 P. L. Burn, A. B. Holmes, A. Kraft, D. D. C. Bradley, A. R. Brown, R. H. Friend and R. W. Gymer, *Nature*, 1992, **356**, 47.
- 15 18 T. Yamamoto, Z.-h. Zhou, T. Kanbara, M. Shimura, K. Kizu, T. Maruyama, Y. Nakamura, T. Fukuda, B.-L. Lee, N. Ooba, S. Tomaru, T. Kurihara, T. Kaino, K. Kubota and S. Sasaki, *J. Am. Chem. Soc.*, 1996, **118**, 10389–10399.
- 19 E. E. Sheina, J. S. Liu, M. C. Iovu, D. W. Laird and R. D. McCullough, *Macromolecules*, 2004, **37**, 3526–3528.
- 20 20 A. Yokoyama, R. Miyakoshi and T. Yokozawa, *Macromolecules*, 2004, **37**, 1169–1171.
- 21 I. Osaka and R. D. McCullough, *Acc. Chem. Res.*, 2008, **41**, 1202–1214.
- 25 22 T. Yokozawa, Y. Nanashima, H. Kohno, R. Suzuki, M. Nojima and Y. Ohta, *Pure Appl. Chem.*, 2013, **85**, 573–587.
- 23 S. Govaerts, P. Verstappen, H. Penxten, M. Defour, B. Van Mele, L. Lutsen, D. Vanderzande and W. Maes, *Macromolecules*, 2016, **49**, 6411–6419.
- 30 24 M. Sévignon, J. Papillon, E. Schulz and M. Lemaire, *Tetrahedron Lett.*, 1999, **40**, 5873–5876.
- 35 25 Q. Wang, R. Takita, Y. Kikuzaki and F. Ozawa, *J. Am. Chem. Soc.*, 2010, **132**, 11420–11421.
- 26 K. Okamoto, J. Zhang, J. B. Housekeeper, S. R. Marder and C. K. Luscombe, *Macromolecules*, 2013, **46**, 8059–8078.
- 27 M. Lafrance and K. Fagnou, *J. Am. Chem. Soc.*, 2006, **128**, 16496–16497.
- 40 28 S. Tamba, S. Mitsuda, F. Tanaka, A. Sugie and A. Mori, *Organometallics*, 2012, **31**, 2263–2267.
- 29 R. Matsidik, J. Martin, S. Schmidt, J. Obermayer, F. Lombeck, F. Nübling, H. Komber, D. Fazzi and M. Sommer, *J. Org. Chem.*, 2015, **80**, 980–987.
- 30 Y. Tokita, M. Katoh, Y. Ohta and T. Yokozawa, *Chem. – Eur. J.*, 2016, **22**, 17436–17444.
- 31 A. C. J. Heinrich, B. Thiedemann, P. J. Gates and A. Staubitz, *Org. Lett.*, 2013, **15**, 4666–4669.
- 5 32 H.-H. Zhang, Y.-X. Zhu, W. Wang, J. Zhu, P. V. Bonnesen and K. Hong, *Polym. Chem.*, 2018, **9**, 3342–3346.
- 33 R. S. Loewe and R. D. McCullough, *Chem. Mater.*, 2000, **12**, 3214–3221.
- 34 R. S. Loewe, P. C. Ewbank, J. S. Liu, L. Zhai and R. D. McCullough, *Macromolecules*, 2001, **34**, 4324–4333.
- 10 35 A. Kiriy, V. Senkovskyy and M. Sommer, *Macromol. Rapid Commun.*, 2011, **32**, 1503–1517.
- 36 A. A. El-Shehaw, N. I. Abdo, A. A. El-Barbary and J.-S. Lee, *Tetrahedron Lett.*, 2010, **51**, 4526–4529.
- 15 37 T. Ross Kelly, Q. Li and V. Bhushan, *Tetrahedron Lett.*, 1990, **31**, 161–164.
- 38 J. Y. Hwang, L. A. Arnold, F. Zhu, A. Kosinski, T. J. Mangano, V. Setola, B. L. Roth and R. K. Guy, *J. Med. Chem.*, 2009, **52**, 3892–3901.
- 20 39 M. S. Yusubov, E. N. Tveryakova, E. A. Krasnokutskaya, I. A. Perederyna and V. V. Zhdankin, *Synth. Commun.*, 2007, **37**, 1259–1265.
- 40 A. K. Parhi, A. Xiang, J. D. Bauman, D. Patel, R. S. Vijayan, K. Das, E. Arnold and E. J. Lavoie, *Bioorg. Med. Chem.*, 2013, **21**, 6435–6446.
- 25 41 J. Linshoef, A. C. J. Heinrich, S. A. W. Segler, P. J. Gates and A. Staubitz, *Org. Lett.*, 2012, **14**, 5644–5647.
- 42 H. Noguchi, K. Hojo and M. Sugimoto, *J. Am. Chem. Soc.*, 2007, **129**, 758–759.
- 30 43 A similar deviation from linearity has been observed for high monomer to catalyst loadings in ref. 19. Other researchers also report a high dependence on the catalyst whether and how much linearity is observed in this type of plot: M.-P. Van Den Eede, J. De Winter, P. Gerbaux and G. Koeckelberghs, *Macromolecules*, 2018, **51**, 9043–9051.
- 35 44 S. Gondo, Y. Goto and M. Era, *Mol. Cryst. Liq. Cryst.*, 2007, **470**, 353–358.
- 45 D. Khlaifia, C. P. Ewels, F. Massuyeau, M. Chemek, E. Faulques, J.-L. Duvail and K. Alimi, *RSC Adv.*, 2016, **6**, 56174–56182.
- 40 46 C. M. Cardona, W. Li, A. E. Kaifer, D. Stockdale and G. C. Bazan, *Adv. Mater.*, 2011, **23**, 2367–2371.
- 47 J. L. Brédas, *J. Chem. Phys.*, 1985, **82**, 3808–3811.
- 45

3.1.2. Reactivity of the Oligomer **M1-O2**

Due to the presence of the pyridine ring in **M1-O2** it is possible that a reaction at the nitrogen can occur. A methylation of **M1-O2** using MeOTf to produce an expected methylated compound **41** was investigated by optical characterization (Scheme 14).



Scheme 14. Methylation route of **M1-O2**.

24 additions of a solution of MeOTf in DCM (8.0 μL , 0.095 M, 7.57×10^{-7} mmol) were made to a solution of **M1-O2** (1.12×10^{-5} M) and NBu_4PF_6 (0.095 M) in DCM (3.0 mL, 3.4×10^{-8} mol). After each addition the absorption spectrum was recorded (Figure 20a). Figure 20b depicts the spectrum of the mixture after the addition of 72, 80, 176 and 184 μL , where the formation of two different compounds was visible.

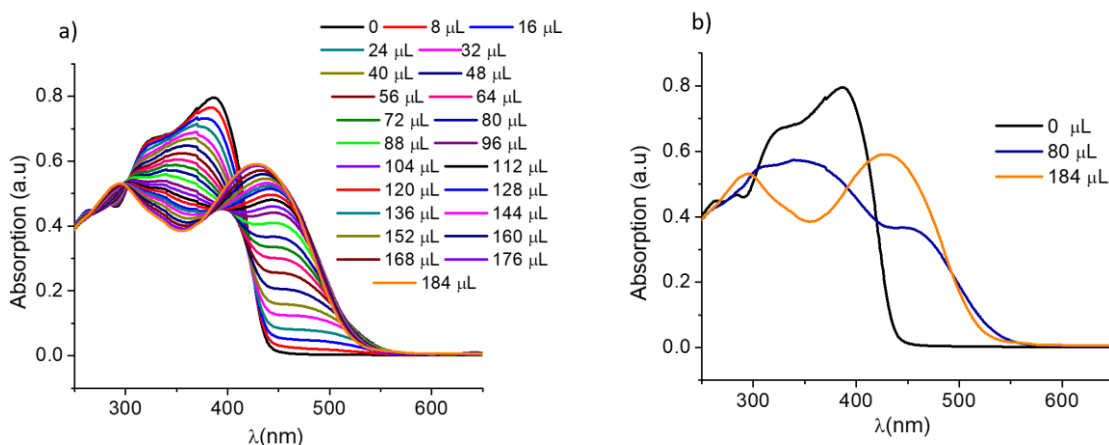


Figure 20. a) Absorption spectrum of the methylation reaction of the oligomer **M1-O2** b) Absorption spectrum after the addition of 7.2, 8.0, 17.6 and 18.4 μL of MeOTf (0.095 M) in dichloromethane.

In the emission spectra it was observed that the emission wavelength of **M1-O2** at 440 nm was decreased after every addition of MeOTf and a broad band with a maxima at 596 nm with lower intensity started to appear (Figure 20). After each addition, the emission for the new species formed is lower with respect to the starting material (Figure 22).

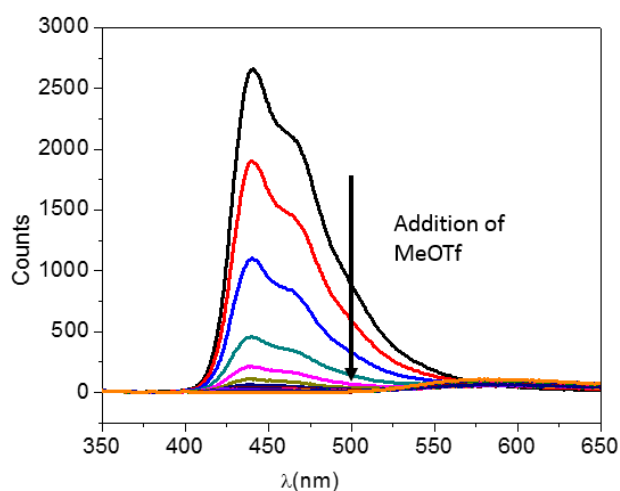


Figure 21. Emission spectrum from the methylation reaction of **M1-O2**.

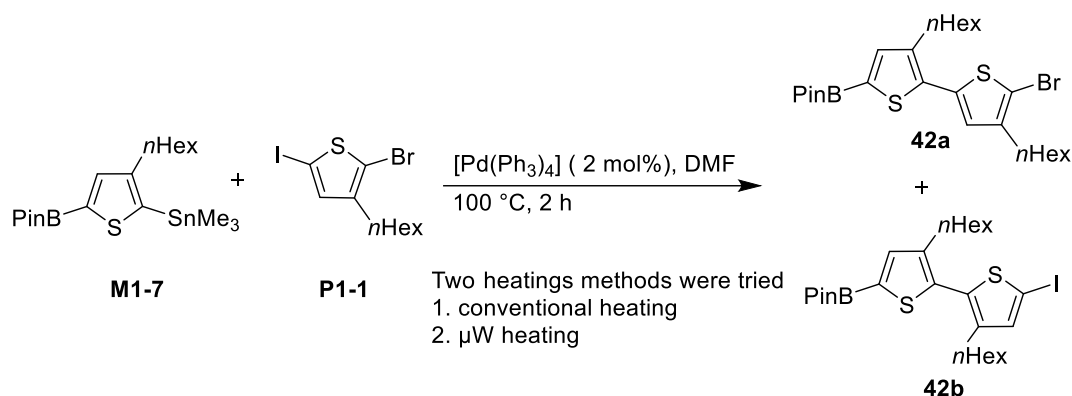


Figure 22. Picture of the fluorescence behavior of the DCM solution of the oligomer **M1-O2** and the two compounds formed by the methylation of the oligomer ($\lambda_{exc} = 366$ nm).

The new species formed seemed to be more electron deficient than the starting material **M1-O2**, reinforcing the charge transfer between the methyl-pyridine and the thienyl ring, which may explain the absence of fluorescence. Further structural characterization of each of the compounds is required to confirm their identification during the methylation of the oligomer.

3.1.3. Synthesis of Poly-3-Hexylthiophene with a Dual Selectivity Approach

The first attempt to synthesize the bi-functional monomer (**42**), precursor of P3HT via the dually selectivity approach, was by the Stille reaction between the dinucleophile **M1-7** and the dielectrophile **P1-1** (Scheme 15).^[76]



Scheme 15. Stille reaction between **M1-7** and **P1-1** produced a 50:50 mixture of bi-functional monomers **42a** and **42b**.

From the reaction described in the Scheme 15 a mixture of regioisomers of bi-functional monomers **42a** and **42b** was formed, irrespectively of if that the reaction was heated under conventional or under microwave conditions. By observation of the proton from the thienyl motifs by ^1H NMR, it was possible to identify that the mixture shows a content of 50% of each bi-functional monomer (Figure 23).

As it was discussed before in the section 3.1.1., due to the high steric effect from the hexyl-chain on the 3-position of the thiophene in the dinucleophile ring, the reaction between the trimethylstannyl group in the 2-position of **M1-7** and the iodine group in the 5-position of **P1-1** was unselective to the desirable product.

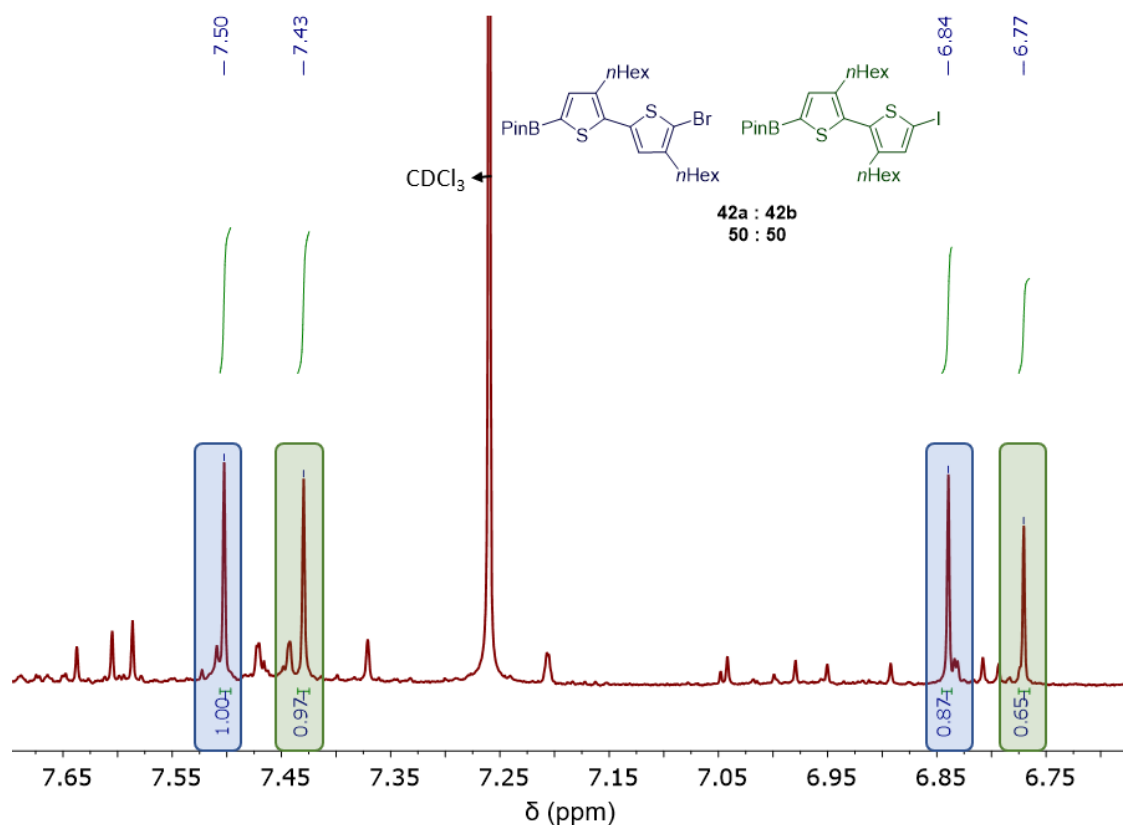
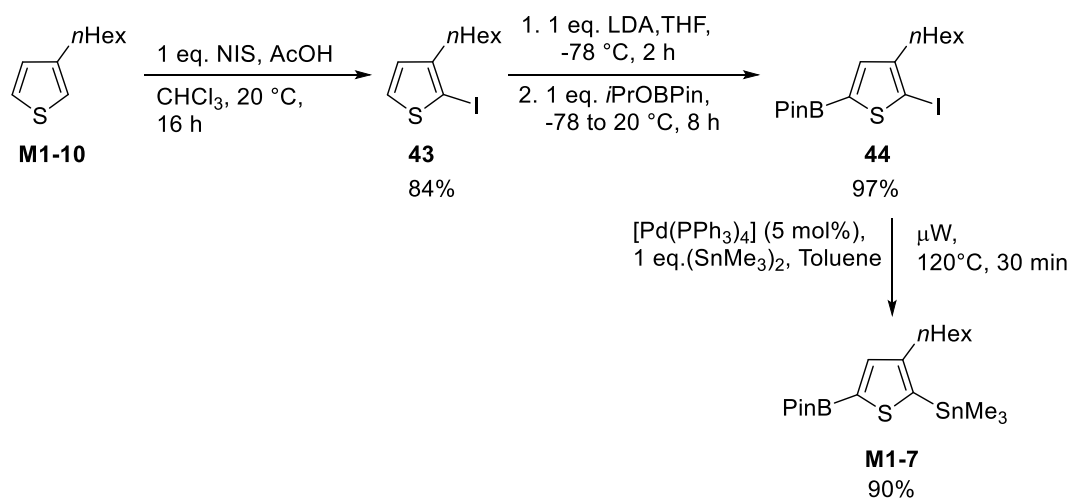


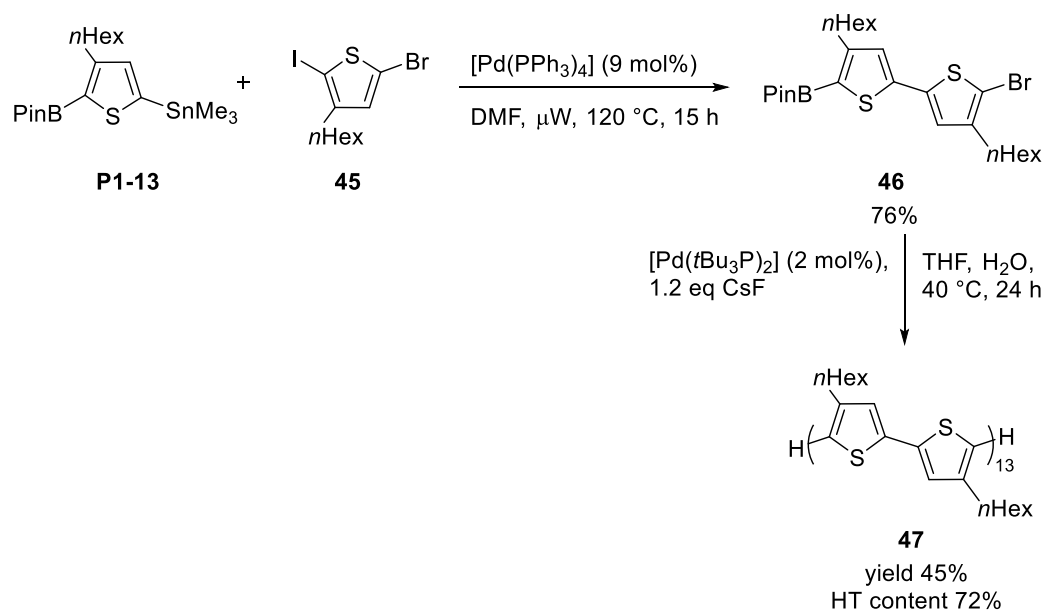
Figure 23. ^1H NMR spectrum from the Stille product between the dinucleophile **M1-7** and **P1-1**. A regioisomer mixture of two bi-functional thiophene monomers **42a** and **42b** was obtained.

The synthetic route towards dinucleophile **M1-7** was initiated by the iodination of 3-*n*-hexylthiophene (**M1-10**) with NIS to afford the 2-iodo-3-*n*-hexylthiophene (**43**) in a yield of 84%,^[77] followed by a lithiation, after which a lithium-boron exchange was performed to obtain the mononucleophile **44** in a yield of 97%.^[59] In a final step, a selective Stille-Kelly coupling reaction of **44** with $(\text{SnMe}_3)_2$ and $[\text{Pd}(\text{PPh}_3)_4]$ as catalyst, under microwave heating at 100 °C led to the dinucleophile **M1-7** in a yield of 90% (Scheme 16).



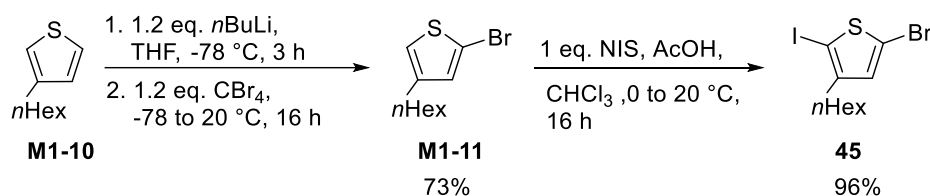
Scheme 16. Synthetic pathway towards the dinucleophile **M1-7**.

The second attempt to produce the bi-functional thiophene precursor **46** of P3HT was based on the dually selective cross-coupling reaction between the dielectrophile **45** and the dinucleophile **M1-13** (Scheme 17). This reaction was performed successfully under microwave heating at 120 °C with a yield of 76%. Furthermore, a Suzuki-Miyaura reaction of **46** proceeded using $[\text{Pd}(\text{tBu}_3\text{P})_2]$ as catalyst and CsF as salt for the acceleration of the transmetalation step in the catalytic cycle. The reaction was heated at 40 °C leading to P3HT (**47**) in a yield of 45% with a HT content of 72%.



Scheme 17. Synthetic route for the synthesis of P3HT (**47**) from a dimer formed under the conditions of a dual selectivity cross-coupling.

The dielectrophile **45** was synthesized starting with a regioselective lithiation reaction of 3-*n*-hexylthiophene (**M1-10**), followed by the quenching with CBr_4 to form the 4-Bromo-2-*n*-hexylthiophene (**M1-11**). The reaction followed with an iodination reaction with NIS, acetic acid and chloroform to form the dielectrophile (Scheme 18).



Scheme 18. Synthetic route for the synthesis of the dielectrophile **45**.

The polymer **47** was soluble in common solvents as chloroform, dichloromethane and THF which allowed its further optoelectronic characterization. With the analysis of the ¹H NMR spectrum of P3HT, it was possible to observe its regioregularity because the chemical shifts of the α -methylene protons of the hexyl chain of the thienyl ring vary depending on the type of couplings. The HT coupling is represented by a peak at 2.8 ppm and the HH coupling

is represented by a broad peak at 2.60 ppm.^[31] The peak corresponding to the TT coupling is usually overlapping with the HH one. In the ¹H NMR spectrum of P3HT (**47**) both methylene peaks were observed in a ratio of 76% of HT couplings (Figure 24).

Furthermore, considering that in a chain living polymerization only one TT coupling is obtained within the polymer chain, the end groups from the polymerization can be analyzed from the TT peak. If the P3HT has two different end groups, the TT peak (about 2.6 ppm) will split into two triplets.^[53] After the quenching process of the polymer **47** with a solution of HCl in methanol, one multiplet (doublet of doubles dd) was observed at 2.60 ppm. As it was reported by Iovu *et al.* one triplet with this chemical shift, indicates that the end groups of P3HT are protons.^[53]

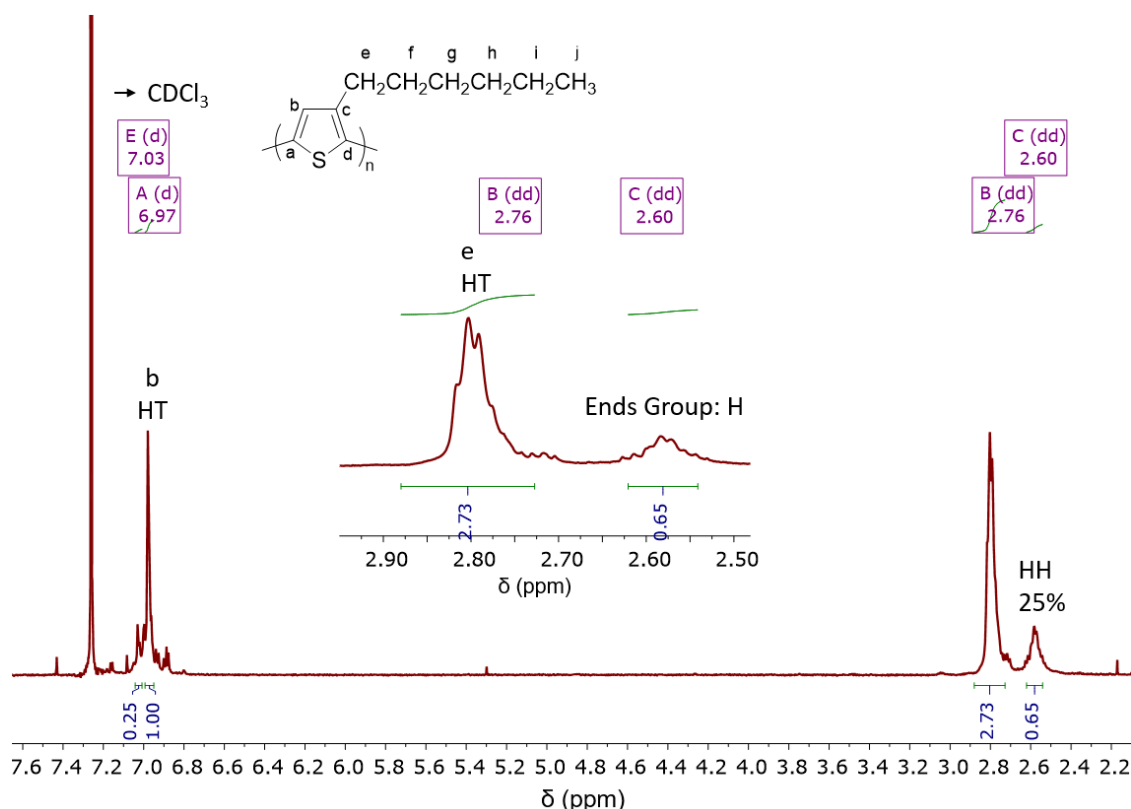


Figure 24. ¹H NMR spectrum from the P3HT (**47**). The %HT couplings and end groups are shown.

From GPC measurements using conventional calibration with polystyrene standards, the calculated molecular weight was 4.56 kDa which corresponds to a degree of polymerization of 13 monomer units. In addition, the polymer had a \bar{D} of 2.5.

Kinetic studies were performed to analyze the type of growth mechanism in the same way as for the oligomers **M1-O1** and **M1-O2** in chapter 3.1.1. A mixture of monomer **46** with [Pd(*t*Bu₃P)₂], CsF, water and THF was heated to 40 °C and samples were taken in defined intervals over the course of 24 h. Each sample was quenched with a solution of 1.0 M solution of HCl in methanol, extracted with DCM and split into two batches for measurements of GPC and ¹H NMR. Table 2 summarizes the molecular weights (M_n and M_w)

and \bar{D} , obtained by GPC analysis. Only few increases of the molecular weight with the time was observed and the \bar{D} 's remained lower than 2.6. The conversion from the monomer to the polymer was only possible to trace until 60% by ^1H NMR analysis (Figure 25). Without a complete conversion of the monomer, it was not possible to plot the graph of conversion vs M_n and \bar{D} for determining the type of growth mechanism for the polymerization.

Time (h)	M_n (Da)	M_w (Da)	\bar{D}
0.0	513.84	650.44	1.27
0.2	728.17	1628.20	2.24
0.5	861.21	1859.00	2.16
1.0	869.19	1858.30	2.14
2.0	864.14	1903.40	2.20
3.0	856.36	1915.90	2.24
6.0	894.32	2018.60	2.26
24.0	809.50	2073.40	2.56

Table 2. M_n , M_w and \bar{D} determined by GPC of the products obtained in the kinetic control of the polymerization of **46**.

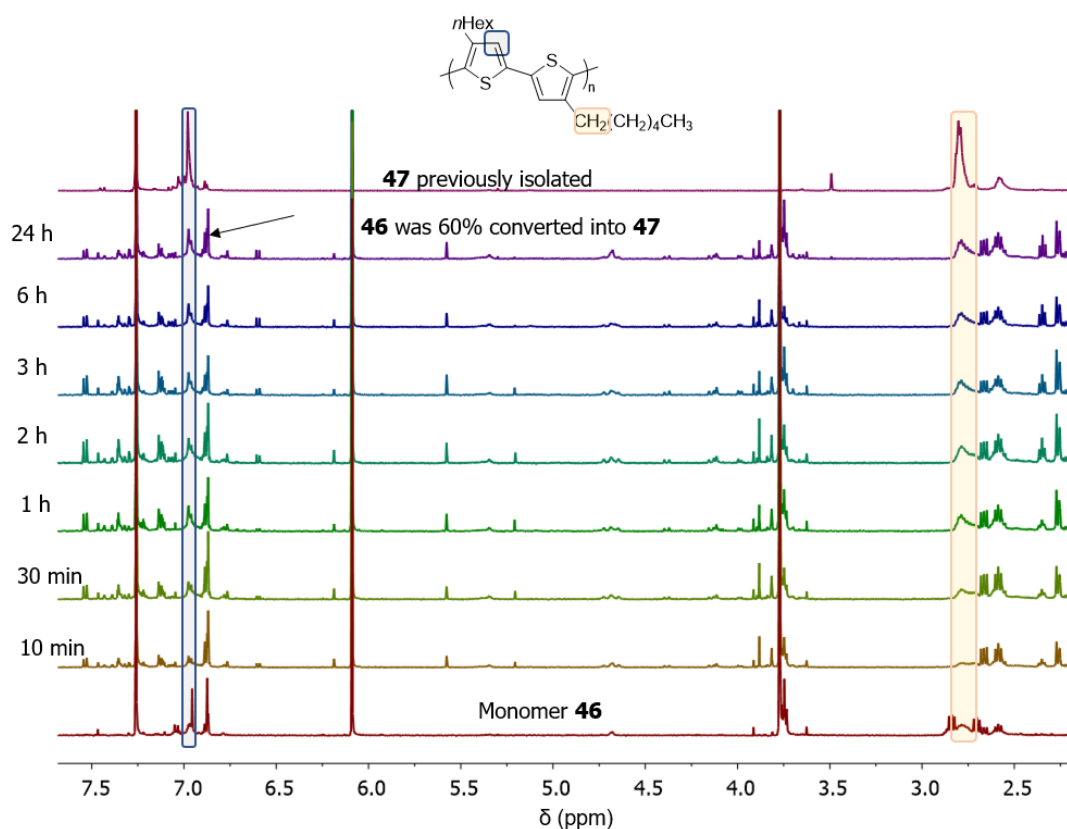


Figure 25. ^1H NMR spectra (recorded at 300 K, 500 MHz in CDCl_3) of the kinetic control for the polymerization of **46** to produce **47**, 1,3,5-trimethoxybenzene was used as standard.

When the samples were irradiated ($\lambda = 366$ nm), a reaction time dependant change of emission color could be observed, which was a good indication for the conversion from monomer to the polymer (Figure 26).



Figure 26. Picture of the fluorescence behaviour of the kinetic samples of the polymerization of **46** ($\lambda_{\text{exc}} = 366$ nm).

In the Figure 25 and Figure 26 a trend for the polymerization could be observed, where the monomer is consumed through the time and converted into the polymer. However, the Φ values summarized in the Table 2 are very high compared to expected values (< 2.0 for living polymerization) and the conversion was only 60% after 24 h. One explanation for the uncomplete conversion in the transferred catalyst polycondensation reaction could be the weak interaction of the associated pair formed by the catalyst and the growing polymer (Scheme 5).^[55a] To improve these results a variation of the reaction conditions as type of solvent, salt and especially the catalyst would be necessary.

3.1.4. Synthesis of Poly (thiophene-alt-pyrrole) from a Difunctionalized Thiénylpyrrole by Kumada Polycondensation"

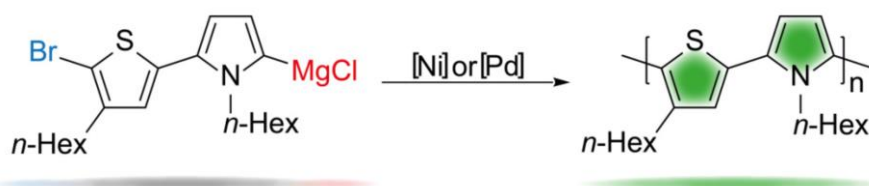
Full paper

Lu-Ying He, Sara Urrego-Riveros, Paul J. Gates, Christian Näther, Maren Brinkmann, Volker Abetz and Anne Staubitz. *Tetrahedron* **2015**, 71 (33), 5399-5406. Collaboration project

Reprinted with permission from Elsevier.(©)

Abstract

A difunctional thiénylpyrrole monomer with a bromide on the thiényl moiety and a magnesium halide on the pyrrole moiety was prepared via chemo-selective magnesium-iodine exchange. Based on this monomer p-conjugated alternating poly(thiophene-*alt*-pyrrole) PTP was synthesized via nickel and palladium catalysed Kumada polycondensation. The optical and thermal properties of this polymer have been investigated and suggested a wide band gap polymer with a very low T_g for such materials



TOC graphic. Kumada polymerization path to obtain poly(thiophene-*alt*-pyrrole).

Scientific contribution to this paper

In this collaboration project I synthesized the starting materials (**1,3,4,11**) and proofread the paper. All other experiments and work were done by the other authors.



Contents lists available at ScienceDirect

Tetrahedron

journal homepage: www.elsevier.com/locate/tet



Synthesis of poly(thiophene-*alt*-pyrrole) from a difunctionalized thienylpyrrole by Kumada polycondensation



Lu-Ying He^a, Sara Urrego-Riveros^a, Paul J. Gates^b, Christian Näther^c,
Maren Brinkmann^d, Volker Abetz^{d,e}, Anne Staubitz^{a,*}

^a Otto Diels-Institute for Organic Chemistry, University of Kiel, Otto-Hahn-Platz 4, D-24098 Kiel, Germany

^b School of Chemistry, University of Bristol, Cantock's Close, Bristol BS8 1TS, UK

^c Institute for Inorganic Chemistry, University of Kiel, Otto-Hahn-Platz 6, D-24098 Kiel, Germany

^d Helmholtz-Zentrum Geesthacht, Institute of Polymer Research, Max-Planck-Str. 1, D-21502 Geesthacht, Germany

^e Institute of Physical Chemistry, University of Hamburg, Grindelallee 117, D-20146 Hamburg, Germany

ARTICLE INFO

Article history:

Received 22 March 2015

Received in revised form 19 May 2015

Accepted 25 May 2015

Available online 2 June 2015

Keywords:

Thiophene

Pyrrole

Alternating copolymers

Kumada polycondensation

Step-growth polymerization

ABSTRACT

A difunctional thienylpyrrole monomer with a bromide on the thienyl moiety and a magnesium halide on the pyrrole moiety was prepared via chemo-selective magnesium–iodine exchange. Based on this monomer, a π -conjugated alternating poly(thiophene-*alt*-pyrrole) **PTP** was synthesized via nickel and palladium catalyzed Kumada polycondensation. The optical and thermal properties of this polymer have been investigated and suggested a wide band gap polymer, with a very low T_g for such polymers.

© 2015 Elsevier Ltd. All rights reserved.

1. Introduction

Conjugated polymers have attracted extensive attention because of their potential industrial applications, due to their unique semiconducting and optoelectronic properties.^{1–3} Among the conjugated polymers, polythiophenes and polypyrroles are centrally important and have been widely investigated as potential materials for organic electronics.^{4–8} The properties of polythiophene and polypyrrole are different: polypyrrole has a larger band gap (ca. 3 eV⁹ compared to ca. 2 eV for polythiophene¹⁰), resulting in a relatively low conductivity;^{11,12} and has a lower oxidation potential,^{13,14} which makes it highly reactive toward oxygen. As the copolymerization of the monomer containing several distinct units can lead to an interesting combination of the properties observed in the corresponding homopolymers,^{15–18} it is interesting to obtain copolymers that contain both heterocycles simultaneously. Cava and co-worker described that the poly(thienylpyrrole) showed tailored electroactive properties.¹⁹

Copolymers of thiophene and pyrrole have mainly been prepared via electrochemical polymerization of 2,5-di(thiophen-2-yl)-

1*H*-pyrrole derivatives.^{20–30} However, this method may lead to significant branching and regioirregular polymers. In addition, organometallic polycondensations have recently been employed to obtain copolymers via a bis(trimethylstannyl)thiophene monomer and a dibromo pyrrole monomer.^{31–33} However, the polymers obtained by the Stille polycondensation had a very low molecular weight. There was no report on preparing poly(thiophene-*alt*-pyrrole) via a single monomer, which contains a metal functional group and a halogen group. However, this kind of monomer is highly desirable as it has the potential to proceed via a quasi-living chain growth mechanism.^{34–43} Herein, we report the highly chemo-selective synthesis of difunctional thienylpyrrole monomer containing a metal functional group and a bromo group. Based on the monomer, π -conjugated alternating poly(thienylpyrrole) was prepared via palladium catalyzed Kumada polycondensation.

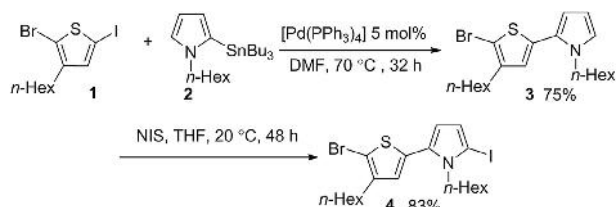
2. Results and discussion

2.1. Synthesis of the pre-monomer 4

The precursor monomer **4** was synthesized by an electrophile-selective Stille cross-coupling⁴⁴ between the 2-bromo-3-hexyl-5-iodothiophene **1** and the tributyltin substituted pyrrole **2**, followed

* Corresponding author. Tel.: +49 431 880 3697; fax: +49 431 880 1558; e-mail address: astaubitz@oc.uni-kiel.de (A. Staubitz).

by iodination of the pyrrole unit with an excess *N*-iodosuccinimide (NIS) in a yield of 62% over two steps (Scheme 1). Although we initially planned to use **3** directly as a monomer precursor by lithiation through deprotonation as a lithiated monomer or followed by lithium–metal exchange if required, several metallation experiments using lithium diisopropylamide (LDA), and 1-lithio-2,2,6,6-tetramethyl-piperidine (LTMP) failed (For details see in the SD).



Scheme 1. Synthesis of precursor monomer **4**.

A more reliable route seemed to be the lithiation of **4** by iodine–lithium exchange using different alkyl lithium reagents such as *n*-BuLi, *t*-BuLi or MeLi under different conditions (Table 1) (For details see the SD). In order to analyze the success of the lithiation procedure, the lithiated heterocycles were quenched with MeI, which could be easily identified by gas chromatography–mass spectrometry (GC–MS) and ¹H NMR spectroscopy. However, lithiation and quenching with MeI did not give the product 2-(5-bromo-4-hexylthiophen-2-yl)-1-hexyl-5-methyl-1H-pyrrole; on the contrary, 2-bromo-1-hexyl-5-(4-hexyl-5-methylthiophen-2-yl)-1H-pyrrole **5** was obtained as main product. This suggests a ‘halogen dance reaction’,⁴⁵ in which the initial iodo–lithium exchange on the pyrrole moiety was followed by bromination from the brominated thiophene moiety. This observation is unusual because in hexylthiophene, a bromide substituent is much more favored in the 2 position adjacent to the *n*-hexyl group, but metallation is favored in the 5 position (which in **4** is blocked by the pyrrole).^{46–48} In addition, *n*-BuLi and *t*-BuLi (entries 1–3) also gave another byproduct 1-hexyl-2-(4-hexyl-5-methylthiophen-2-yl)-5-iodo-1H-pyrrole **6**. This is a consequence of a bromo–lithium exchange without a halogen dance. Although MeLi just gave trace amount of **6** (entry 4), other unidentified compounds were shown from the NMR (For details see in the SD).

Table 1
Lithiation of precursor monomer **4**

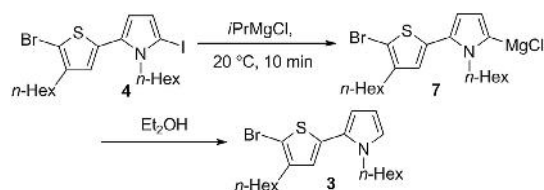
Entry	Lithium reagents	Solvents	T (°C)	Ratio ^a 5:6
1	<i>n</i> -BuLi	THF	–78	6:1
2	<i>n</i> -BuLi	THF	–100	10:1
3	<i>t</i> -BuLi	Me-THF	–129	0.5:1
4	MeLi	THF	–78	>99:1 ^b

^a Estimated by ¹H NMR spectroscopy and identified by GC–MS.

^b A trace amount of compound **6** was detected only by GC–MS.

2.2. Synthesis of the Grignard type monomer **7**

Surprisingly then, the Grignard-type monomer **7** could be synthesized by treating the precursor monomer **4** with 1 equiv of *i*PrMgCl at 20 °C for 10 min via a fast magnesium–iodine exchange reaction (100% yield based on analytical GC with analysis of the protonated species **3** (Scheme 2)). The metallation occurred selectively at the α -position of the thiophene, leaving the aryl bromide intact.



Scheme 2. Synthesis of Grignard-type monomer **7** by magnesium–iodine exchange.

2.3. Synthesis of poly(thiophene-*alt*-pyrrole) (PTP) with **7**

Based on the Grignard-type monomer **7**, polymerization was carried out firstly by the addition of 2 mol % of [Ni(dppp)Cl₂] at 20 °C for 24 h. These conditions are well established for the synthesis of well-defined poly(3-hexylthiophene) by Kumada catalyst-transfer condensation polymerization.^{34,35} However, the yield was only 65% and the molecular weight of the polymer ($M_n=3.9$ kDa, $M_w/M_n=1.5$, GPC calibrated against polystyrene) was also quite low. Analysis of the polymer by MALDI-TOF revealed a series of peaks suggesting an isopropyl end group (Fig. 1A). This could arise from quenching the metallated monomer by isopropyl iodide, which is the product from the previous magnesium–iodine exchange. In view of the fact that this reaction was not observed without a transition metal catalyst, also it is more likely that this end group arises as a cross-coupling product. This problem has been reported for other polymers, such as poly(9,9-dioctylfluorene).⁴⁹ In that case, the use of the magnesium complex [tBuMgCl·LiCl·15-crown-5] as the metallating species prevented any further substitution most likely because the *tert*-butyl cation is more stable compared to the isopropyl cation. Treatment of **4** with 1 equiv of [tBuMgCl·LiCl·15-crown-5] at 20 °C for 10 min in THF gave **7** (100% yield based on analytical GC–MS with analysis of the protonated species **3**). The polymerization was then carried out by adding of 2 mol % of [Ni(dppp)Cl₂] to the reaction mixture. After 24 h at 20 °C the polymer was obtained in a yield of 43% ($M_n=6.3$ kDa, $M_w/M_n=1.5$, with a conversion of 99%). The MALDI-TOF MS spectra of the oligomer showed no evidence for a *tert*-butyl end group, with H/H, H/Br and Br/Br being the major end groups (Fig. 1B). The obtained Br/Br terminated polymer was presumably as a result of the dissociation of the associated Ni⁰-arene π complexes according to the proposed mechanism by Yokozawa^{50–53} and McCullough.^{54,55} Although preventing the quenching reaction of polymerization, the relatively high polydispersity and only moderate yield led us to analyze further reaction conditions.

Palladium catalysts are generally less reactive than nickel catalysts for Kumada coupling with alkyl halides. In this instance, we decided to use [Pd(*t*Bu₃P)₂] as catalyst as it has been shown to be a suitable catalyst for chain growth polymerization of alternating copolymers based on Stille or Suzuki coupling reactions.⁴³ Although inefficient at 20 °C, (Table 2, entry 1) this catalyst was more efficient at 50 °C. The reaction was performed in the ethereal solvents MTBE, DME, THF, and dioxane (Table 2, entries 2–5). In all cases, polymeric products were obtained. The highest molecular weight polymer was obtained by using MTBE as solvent (Table 2, entry 3) with a weight average molecular weight of $M_n=7700$. However, in all cases, the polymers’ polydispersities were relatively high between 1.5 and 1.6 and molecular weights stayed below the expected molecular weights. For a controlled living polymerization process, PDIs would be expected to be lower with molecular weights matching calculated weights. To increase the rate of polymerization, the reaction in 4 mL of MTBE was conducted under microwave irradiation at 50 °C for 6.5 h. The conversion was 100% and 94% of the polymer was obtained with a higher molecular weight than under thermal conditions ($M_n=13.2$ kDa, $M_w/M_n=2.2$) (Table 2, entry 6). Different catalysts loadings (1, 2, 5 mol %) were

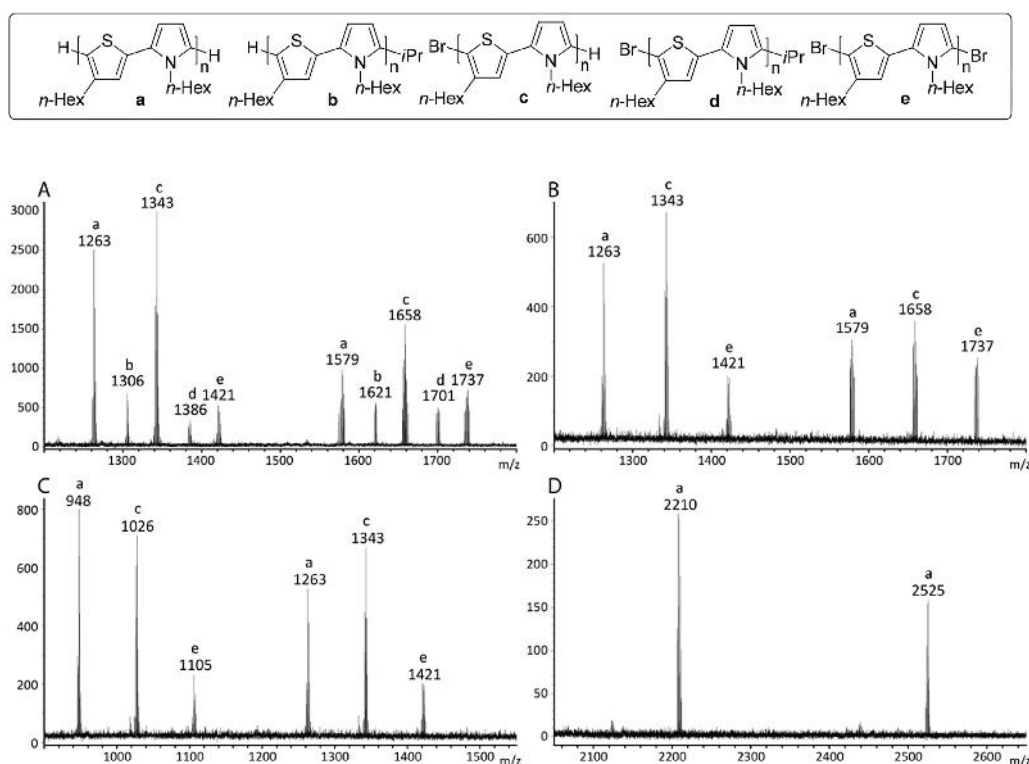
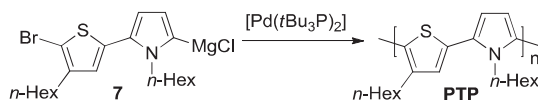


Fig. 1. MALDI-TOF MS spectra of the poly(pyrrole-*alt*-thiophene): (A) polymer synthesized with *i*PrMgCl and [Ni(dppp)Cl₂]; (B) polymer synthesized with *t*BuMgCl, LiCl, 15-crown-5 and [Ni(dppp)Cl₂]; (C) polymer synthesized with *i*PrMgCl and [Pd(*t*Bu₃P)₂] (Table 1, entry 6); (D) polymer synthesized with [*i*PrMgCl·LiCl] and [Pd(*t*Bu₃P)₂] (Table 1, entry 10).

Table 2

Polymerization of **7** with various ether solvents and different catalyst loadings^a



Entry	Cat. loading [mol %]	Solvent	T (°C)	Time (h)	Yield (%)	M_n^b	M_w/M_n^b	Expected M_n^c
1	2	MTBE	20	24	—	—	—	15,700
2	2	MTBE	50	18	91	7700	1.6	15,700
3	2	DME	50	18	38	4000	1.5	15,700
4	2	THF	50	18	49	5000	1.6	15,700
5	2	Dioxane	50	18	73	5600	1.6	15,700
6	2	MTBE	50 (MW)	6.5	94	13,200	2.2	15,700
7	1	MTBE	50 (MW)	5	14	1700	1.4	31,500
8	2	MTBE	50 (MW)	5	27	2100	1.4	15,750
9	5	MTBE	50 (MW)	5	97	17,800	2.8	6300
10	5	MTBE/LiCl	50 (MW)	5	99	29,500	4.6	6300

^a The polymerizations were carried out by treatment of **4** with 1.0 equiv of *i*PrMgCl at 20 °C for 10 min to form **7**, followed by addition of [Pd(*t*Bu₃P)₂].

^b Estimated by GPC calibrated against a polystyrene standard (eluent: CHCl₃, 1 mL/min).

^c If the polymerization was a quasi-living chain-growth polymerization.

also investigated for the polymerization catalyzed by [Pd(*t*Bu₃P)₂] at 50 °C for 5 h under microwave irradiation (Table 1, entry 7–9), 5 mol % of [Pd(*t*Bu₃P)₂] afforded the longest polymer chain ($M_n=17.8$ kDa, $M_w/M_n=2.9$). In general, higher catalyst loadings gave higher yields and polymers with higher molecular weights, but also with increased polydispersities (M_w/M_n), which is counter indicative of a quasi-living chain growth polymerization. The polymers synthesized with [Pd(*t*Bu₃P)₂] also had H/H, H/Br and Br/Br end groups (Fig. 1C), which proves the polymerization process did not undergo the quenching with isopropyl iodide. However, the dissociation of the associated Pd⁰-arene π complexes occurred, which could lead to the Br/Br terminated polymer. Stefan and co-workers reported the palladium-mediated polymerization of 2-

bromo-5-chloromagnesio-3-hexylthiophene proceeded by a step-growth mechanism and with lower regioirregularity as various side reactions of dissociated Pd(0) catalyst.⁵⁶ It has been shown the addition of LiCl to Kumada catalyst transfer polycondensation could have beneficial effects on the chain-growth polymerization characteristics of aryl-Grignard monomers.^{36,41} Bielawski and co-workers reported the addition of LiCl led to controlled chain-growth polymerization of 2-(4-bromo-2,5-bis(2-ethylhexyloxy)phenyl)-5-chloromagnesio-thiophene to afford poly(thiophene-*alt*-*p*-phenylene).⁴¹ However, in our case, LiCl did not show this effect; on the contrary, the M_w/M_n (4.6) value was much higher with much bigger M_n (29,500) (Table 2, entry 10). The polymer had only H/H as the main end group in the presence of LiCl (Fig. 1D).

5402

L.-Y. He et al. / Tetrahedron 71 (2015) 5399–5406

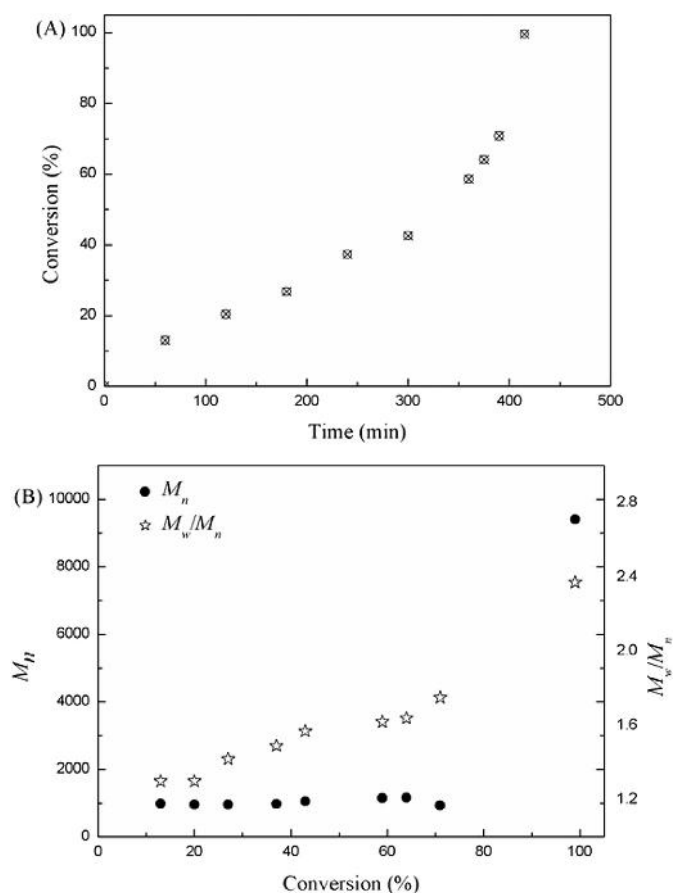


Fig. 2. Conversion versus time (A), and M_n and M_w/M_n vs. conversion (B) plots for the polymerization of **7** with 2 mol % of $[\text{Pd}(\text{tBu}_3\text{P})_2]$ in MTBE ($[\text{4}]_0=0.1$ mol/L) at 50 °C under microwave conditions. The conversion was defined as amount of compound **3** (from the quenching of a sample with ethanol) and determined by GC using naphthalene as internal calibration standard.

Based on these results, the best reaction conditions for the polymerization of **7** was 2 mol % of $[\text{Pd}(\text{tBu}_3\text{P})_2]$ in MTBE as the solvent at 50 °C for 6.5 h under microwave irradiation.

The conversion versus time plot (Fig. 2A) shows that the polymerization of **7** catalyzed by 2 mol % of $[\text{Pd}(\text{tBu}_3\text{P})_2]$ in 5 mL of MTBE at 50 °C under microwave conditions went smoothly in the first 390 min, up to a conversion of about 70%. However, after 390 min, the apparent conversion increased sharply and reached 100% in 25 min. The M_n and M_w/M_n values of the crude **PTP** (without purification by precipitation and fractionation) at each conversion in this polymerization were analyzed by GPC to evaluate the polymerization in detail. The M_n values did not increase in proportion to the conversion, and the M_n increased sharply toward the end of the reaction. Both of these observations suggest a step-growth polymerization. The M_w/M_n values of the collected polymer samples increased along with the consumption of monomer.

2.4. Optical properties of PTP

The polymer samples were analyzed with respect to their absorption properties and their photoluminescence spectra (Fig. 3, a representative example of a polymer prepared under the conditions of Table 2, entry 6). The absorption spectra of **4** in diethyl ether solution showed a maximum peak at 306 nm. The absorption peaks of the polymers **PTP** (Table 2, entries 6, 9–10) in diethyl ether solution were all observed at ca. 348 nm, largely irrespective of the chain length obtained. If the polymers were processed as a film

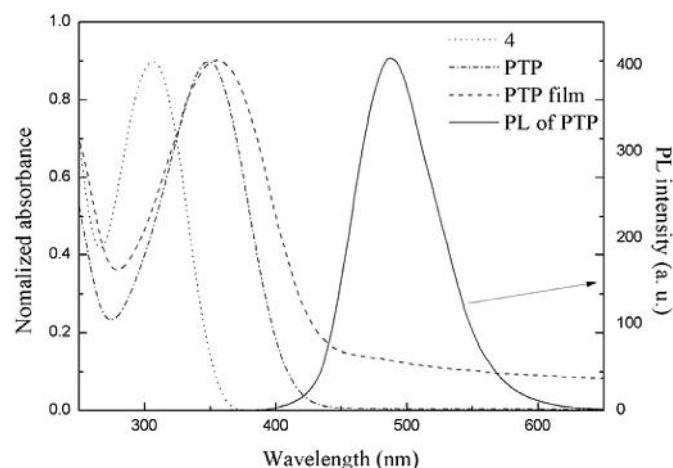


Fig. 3. UV-vis spectra of **4** and **PTP** in diethyl ether and as a film, PL spectra ($\lambda_{\text{exc}}=348$ nm) of **PTP** in diethyl ether.

prepared by spin-coating, the absorption peaks were all at ca. 354 nm. The absorption bands of the polymer **PTP** in both solution and processed as a film were relatively narrow compared to regioregular poly(3-alkylthiophene) (**rr-P3AT**) ($\lambda_{\text{max}} \approx 450$ nm).⁴⁸ This may be attributed to the effect of steric interactions of neighboring *n*-hexyl groups that reduce the conjugation length of the polymers. In fact, DFT calculations suggest a torsion angle between the planes of the two heterocycles of ca. -143° in the *anti*-conformation of thiophene and pyrrole and 46° for the *syn*-conformation. These values are similar in the tetramers in all possible conformations (see SD). Irrespective of the chain length obtained (Table 2, entries 6, 9 and 10), the ether solutions of **PTP** all give a bright-green fluorescence with the maximum emission wavelength of ca. 487 nm, corresponding to the onset of π - π^* transition of the electronic absorption spectra, which is at significantly higher energy than for the **rr-P3AT** ($\lambda_{\text{max}} \approx 570$ nm).⁴⁸

2.5. Thermal behavior of the polymer PTP

The thermal stability of the polymers was studied by thermogravimetric analysis (TGA) under N_2 at a heating rate of 4 °C/min (Fig. 4). A representative example of a polymer prepared under the conditions of Table 2, entry 6 showed a 2% weight loss at 201 °C and a 38% weight loss at 451 °C. The first mass loss might be traced back to the removal of volatile species from the polymer, whereas the

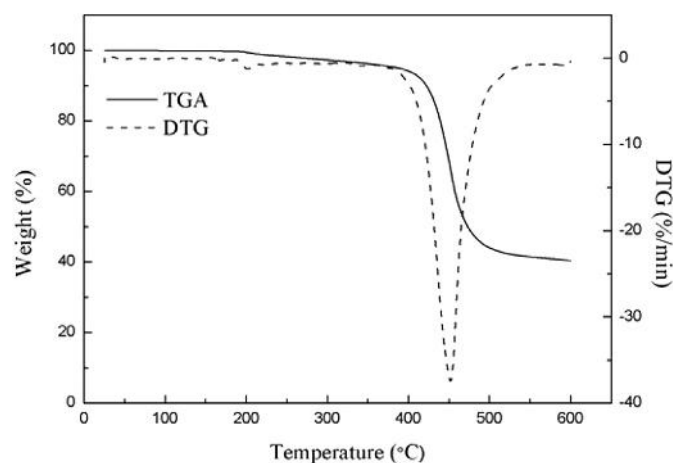


Fig. 4. TGA and DTG curves of **PTP**.

second mass loss can be due to the decomposition of the polymer. On the other hand, a DSC thermogram suggested a glass transition temperature at ca. $-14\text{ }^{\circ}\text{C}$ (see SD), which is quite low comparing to other semiconducting polymers. This lower transition temperature may be caused by the torsion between thiophene and pyrrole, which renders the material very flexible.

3. Conclusions

A difunctional thienylpyrrole monomer containing a magnesium group and a bromo group was synthesized via a chemo-selective halogen-magnesium exchange. All halogen lithium exchange reactions on the dihalogenated starting material (with bromide on the thiophenyl moiety and iodide on the pyrrole moiety) proved unselective, leading to halogen dance or quenching with the alkyl halide that forms *in situ*. By using a magnesiated monomer, alternating copolymers **PTP** containing 3-alkylthiophene and *N*-alkylpyrrole were prepared by palladium catalyzed Kumada polycondensation. The molecular weights were high and a moderate polydispersity was found. The M_n vs. conversion plot indicated that the polymerization proceeded via a step-growth mechanism, presumably due to the dissociation of the associated Pd^0 -arene π complexes. The absorption bands of the polymer **PTP** in both solution and processed as a film were relatively very narrow due to the effect of steric interactions of neighboring *n*-hexyl groups that reduce the conjugation length of the polymers. This study highlights the difficulties for introducing pyrroles into semiconducting polymers. It points out optimal reaction conditions for the selective metallation of pyrroles in spite of the presence of competing thiophenes. The optical and thermal properties suggest a wide band gap polymer, with a very low T_g for such materials.

4. Experimental section

4.1. General methods and materials

All syntheses were carried out using standard Schlenk techniques or in glovebox under a dry and inert nitrogen atmosphere unless stated otherwise. Glassware and NMR-tubes were dried in an oven at $200\text{ }^{\circ}\text{C}$ for at least 2 h prior to use. Reaction vessels were heated under vacuum and purged with nitrogen three times before adding reagents.

All solvents that were used for reactions were used freshly distilled after refluxing for several hours over the specified drying agent under nitrogen and were stored in a J. Young's tube. If no drying agent is noted, the solvents were used for chromatography only and distilled for purification purposes.

4.2. Instruments and measurements

^1H NMR and ^{13}C NMR spectra were recorded at 300 K. ^1H NMR spectra were recorded on a Bruker DRX 500 (500 MHz) spectrometer. ^{13}C NMR spectra were recorded on a Bruker DRX 500 (125 MHz) spectrometer. All ^1H NMR and ^{13}C NMR spectra were referenced against the residual solvent peak. The exact assignment of the peaks was proved by ^1H , ^{13}C DEPT and two-dimensional NMR spectroscopy such as ^1H COSY, ^{13}C HSQC or $^1\text{H}/^{13}\text{C}$ HMBC when possible.

IR spectra were recorded on a Perkin Elmer Paragon 1000 FT-IR spectrometer with a A531-G Golden-Gate-ATR-unit. Ultra High resolution EI mass spectra were run on a VG Analytical Autospec apparatus. MALDI-MS analyses were performed using Bruker Daltonics UltrafleXtreme 2. The analyte (DCM, 1 mg/ml) was pre-mixed with the Dithranol matrix (MeOH, 10 mg/ml) in a 1:1 (v/v) ratio immediately prior to analysis. UV/Vis spectra were recorded

on a Perkin Elmer Lambda14 spectrometer. Luminescence spectra were recorded on a Perkin Elmer LS55 spectrometer.

M_n and M_w were determined on a Viscotek GPCmax VE2001, equipped with a Viscotek VE3580 RI detector (columns: ViscotekLT5000L 300×7.8 mm and LT4000L 300×7.8 mm).

The DTA-TG measurements were performed in Al_2O_3 crucibles using a Netzsch STA-409CD instrument. All measurements were performed under N_2 and were corrected for buoyancy and current effects. The instruments were calibrated using standard reference material, DSC investigations were performed with the DSC 204/1/F from Netzsch and the DSC 1 Star System with STARe Excellence Software from Mettler-Toledo AG. The measurements were performed in Al pans and the instruments were calibrated using standard reference materials.

GC-MS analysis was performed on a Hewlett Packard 5890A gas chromatograph, equipped with a Hewlett Packard 5972A mass selective detector and an Agilent Technologies dimethylpolysiloxane column (19091S-931E, nominal length 15 m, 0.25 mm diameter, 0.25 μm grain size).

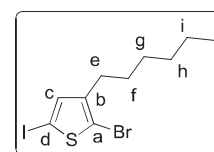
GC analysis was performed on an Agilent Technologies 6890N gas chromatograph, equipped with an Agilent Technologies 7683 Series Injector, an Agilent Technologies (5 %-phenyl)-methylpolysiloxane column (19091J-413, nominal length 30 m, 0.32 mm diameter, 0.25 μm grain size) and a flame ionization detector (FID).

Reactions under microwave irradiation were carried out using a Biotage[®] Initiator+SP Wave synthesis system, with continuous irradiation power from 0 to 300 W (Organic Synthesis Mode). The temperature was measured with an external IR sensor during microwave heating. All reactions were carried out in 5 mL oven-dried Biotage microwave vials sealed with an aluminum/Teflon[®] crimp top, which can be exposed to a maximum of $250\text{ }^{\circ}\text{C}$ and 20 bar internal pressure.

For chromatographic purifications, silica gel (Macherey-Nagel Inc., grain size 0.040–0.063 mm) was used. Thin layer chromatography was performed using pre-coated plates from Macherey-Nagel Inc., ALUGRAM[®]Xtra SIL G/UV254. Chromatographic purification for compounds (**3**, **4**, **5**, **6**, **8**) were carried out using an InterchimPuriflash 430 system, where cartridges by Interchim (silica HC, grain size 50 μm , 40 g, 80 g or 120 g) were used.

4.3. Synthesis

4.3.1. 2-Bromo-3-hexyl-5-iodothiophene (**1**).

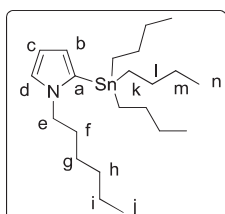


2-Bromo-3-hexyl-5-iodothiophene was prepared similarly to a method described by Koeckelberghs and co-workers⁵⁷ and was modified as follows: 2-bromo-3-hexylthiophene (5.00 g, 20.2 mmol) (For the synthetic procedure and analytic data see in the SD) was dissolved in a mixture of chloroform (100 mL) and acetic acid (50 mL) and shielded from light under an air atmosphere. Then, *N*-iodosuccinimide (6.75 g, 30.0 mmol) was added in one portion. The reaction was stirred for 16 h at $20\text{ }^{\circ}\text{C}$. The solution was poured into water (100 mL) and the water phase was extracted with *n*-hexane (3×100 mL). The combined organic phases were washed with aqueous NaOH (2 M, 1×500 mL), water (2×200 mL), brine (1×100 mL) and were dried over MgSO_4 . After the solvent was removed in vacuo, the crude product was purified by Kugelrohr distillation ($110\text{ }^{\circ}\text{C}$, 1.7×10^{-1} mbar) to get 6.8 g (89%, lit.⁵⁷ 78%) of the product as yellow oil.

^1H NMR (500 MHz, CDCl_3): δ =6.96 (s, 1H, H-c), 2.52 (t, 3J =7.6 Hz, 2H, H-e), 1.59–1.50 (m, 2H, H-f), 1.37–1.24 (m, 6H, H-g, h, i), 0.89 (t,

$^3J=6.7$ Hz, 3H, H-j) ppm. ^{13}C NMR (126 MHz, CDCl_3): $\delta=144.3$ (C-b), 138.0 (C-c), 111.7 (C-a), 71.0 (C-d), 31.6, 29.6, 29.2, 28.8 (C-e, f, g, h), 22.6 (C-i), 14.1 (C-j) ppm. HRMS (EI-sector) m/z : $[\text{M}]^+$ Calcd for $[\text{C}_{10}\text{H}_{14}\text{BrIS}]^+$ 371.9044; Found 371.9032. IR (ATR): $\tilde{\nu}=2953$ (m), 2923 (s), 2854 (s), 1534 (w), 1456 (m), 1403 (m), 1377 (w), 1275 (w), 1261 (w), 1191 (w), 1095 (w), 995 (s), 909 (w), 826 (s), 750 (s), 724 (m), 694 (w), 650 (w), 578 (w), 470 (s) cm^{-1} .

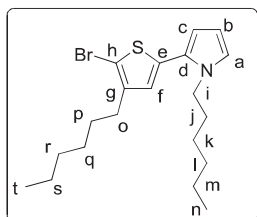
4.3.2. 1-Hexyl-2-(tributylstannyl)-1H-pyrrole (2).



n-Butyllithium (12.48 mL, 31.20 mmol, 2.50 M in hexanes) was added to a stirred solution of *N,N,N',N'*-tetramethyl-ethane-1,2-diamine (4.710 g, 31.20 mmol) in *n*-hexane (90 mL) at 0 °C within 5 min. The reaction mixture was stirred for 1 h at 0 °C. *N*-(*n*-hexyl)-pyrrole (3.620 g, 24.00 mmol) (For the synthetic procedure and analytic data see in the SD) was added dropwise to the solution at this temperature over the course of 10 min. The reaction mixture was allowed to warm up to 20 °C and stirred for 18 h. The reaction mixture was cooled back to 0 °C and tri-*n*-butyltin chloride (10.28 g, 36.00 mmol) was added dropwise over the course of 20 min and warm up to 20 °C and stirred for another 8 h. Then the reaction was quenched with saturated NH_4Cl aqueous solution (50 mL). The aqueous layer was extracted with *n*-hexane (3×50 mL) and the combined organic phases were washed with water (3×100 mL). The organic phase was dried over MgSO_4 and the solvent was removed in vacuo. The crude product was filtered over silica gel (which was pretreated by stirring it in a 5% Et_3N in *n*-hexane solution to deactivate it). After removal of the solvent, the mixture was purified by bridge distillation (190 °C, 5 mbar) to receive 9.7 g (91%) of colorless oil.

^1H NMR (500 MHz, CDCl_3): $\delta=6.90$ (t, $^3J=1.9$ Hz, 1H, H-d), 6.32–6.15 (m, 2H, H-b, c), 3.83 (t, $^3J=7.6$ Hz, 2H, H-e), 1.77–1.71 (m, 2H, H-f), 1.55–1.49 (m, 6H, H-k), 1.36–1.28 (m, 12H, H-g, h, i, l), 1.06–1.02 (m, 6H, H-m), 0.90 (t, $^3J=7.3$ Hz, 12H, H-j, n) ppm. ^{13}C NMR (126 MHz, CDCl_3): $\delta=131.6$ (C-a), 123.9 (C-d), 118.6 (C-b/c), 108.5 (C-b/c), 51.5 (C-e), 32.4, 31.6 (C-f, g), 29.1 (C-k), 27.3, 26.7, 22.5 (C-h, i, l), 13.9, 13.6 (C-j, n), 10.3 (C-m) ppm. ^{119}Sn NMR (187 MHz, CDCl_3): $\delta=-64.0$ ppm. HRMS (EI-sector) m/z : $[\text{M}]^+$ Calcd for $[\text{C}_{22}\text{H}_{43}\text{NSn}]^+$ 441.2434; Found 441.2418. IR (ATR): $\tilde{\nu}=2955$ (m), 2925 (s), 2854 (m), 1510 (w), 1462 (m), 1417 (w), 1376 (w), 1282 (m), 1072 (m), 1001 (w), 960 (w), 864 (w), 765 (m), 749 (m), 710 (s), 690 (m), 665 (m), 613 (w), 596 (m), 504 (m) cm^{-1} .

4.3.3. 2-(5-Bromo-4-hexylthiophen-2-yl)-1-hexyl-1H-pyrrole (3).

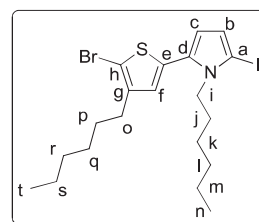


$[\text{Pd}(\text{PPh}_3)_4]$ (866 mg, 750 μmol) was added to a solution of 1-hexyl-2-(tributylstannyl)-1H-pyrrole (6.60 g, 15.0 mmol) and 2-bromo-3-hexyl-5-iodothiophene (5.60 g, 15.0 mmol) in DMF (60 mL) at 20 °C. The reaction mixture was stirred at 70 °C for 32 h

and then poured into water (100 mL). The aqueous layer was extracted with diethyl ether (3×50 mL) and the combined organic phase was washed with water (3×80 mL) before drying over MgSO_4 . The volatiles were removed in vacuo. The crude product was purified by column chromatography over silica gel (*n*-hexane/DCM 14:1, $R_f=0.51$) to obtain 4.50 g (76%) of a yellow oil.

^1H NMR (500 MHz, CDCl_3): $\delta=6.73$ (t, $^3J=2.2$ Hz, 1H, H-a), 6.67 (s, 1H, H-f), 6.23 (dd, $^3J=3.6$ Hz, $^4J=1.7$ Hz, 1H, H-c), 6.14 (t, $^3J=3.2$ Hz, 1H, H-b), 3.94 (t, $^3J=7.5$ Hz, 2H, H-i), 2.55 (t, $^3J=7.5$ Hz, 2H, H-o), 1.72–1.66 (m, 2H, H-j), 1.62–1.56 (m, 2H, H-p), 1.38–1.22 (m, 12H, H-k, l, m, q, r, s), 0.91–0.84 (m, 6H, H-n, t) ppm. ^{13}C NMR (126 MHz, CDCl_3): $\delta=142.2$ (C-g), 134.6 (C-e), 126.5 (C-f), 125.8 (C-d), 122.9 (C-a), 110.4 (C-c), 107.9 (C-b), 107.7 (C-h), 47.5 (C-i), 31.7, 31.5, 31.4 (C-j, k, l), 29.7, 29.6 (C-o, p), 28.9, 26.4, 22.6, 22.5 (C-m, q, r, s), 14.1, 14.0 (C-n, t) ppm. HRMS (EI-sector) m/z : $[\text{M}]^+$ Calcd for $[\text{C}_{20}\text{H}_{30}\text{BrNS}]^+$ 395.1282; Found 395.1275. IR (ATR): $\tilde{\nu}=2955$ (m), 2925 (s), 2854 (m), 1573 (w), 1525 (w), 1457 (m), 1432 (m), 1408 (w), 1377 (w), 1291 (m), 1195 (m), 1113 (w), 1071 (m), 1032 (w), 1002 (w), 835 (m), 783 (m), 750 (m), 710 (s), 643 (w), 612 (m), 584 (w), 497 (w), 478 (w) cm^{-1} .

4.3.4. 2-(5-Bromo-4-hexylthiophen-2-yl)-1-hexyl-5-iodo-1H-pyrrole (4).



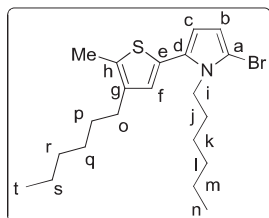
N-Iodo-succinimide (896 mg, 4.00 mmol) was added in one portion to a stirred solution of 2-(5-bromo-4-hexylthiophen-2-yl)-1-hexyl-1H-pyrrole (794 mg, 2.00 mmol) in THF (15 mL) at 20 °C. The reaction was stirred at 20 °C for 48 h. The reaction mixture was quenched with and aqueous solution of $\text{Na}_2\text{S}_2\text{O}_3$ (1 M, 10 mL) and the organic phase was extracted with diethyl ether (3×15 mL) before drying it over MgSO_4 . The solvent was removed in vacuo. The crude product was purified by column chromatography over silica gel (*n*-hexane, $R_f=0.64$) to give 866 mg (83%) of a yellow oil.

^1H NMR (500 MHz, CDCl_3): $\delta=6.78$ (s, 1H, H-f), 6.33 (d, $^3J=3.8$ Hz, 1H, H-c), 6.23 (d, $^3J=3.8$ Hz, 1H, H-b), 4.02 (t, $^3J=7.8$ Hz, 2H, H-i), 2.59 (t, $^3J=7.5$ Hz, 2H, H-o), 1.64–1.57 (m, 4H, H-j, p), 1.38–1.21 (m, 12H, H-k, l, m, q, r, s), 0.91–0.86 (m, 6H, H-n, t) ppm. ^{13}C NMR (126 MHz, CDCl_3): $\delta=143.7$ (C-g), 135.8 (C-e), 129.6 (C-d), 128.5 (C-f), 119.8 (C-c), 114.1 (C-b), 109.3 (C-h), 72.8 (C-a), 49.0 (C-i), 32.8, 32.4, 32.1 (C-j, k, l), 30.8, 30.4, 29.8 (C-o, p, q), 27.1 (C-m), 23.7, 23.5 (C-r, s), 14.4, 14.3 (C-n, t) ppm. HRMS (EI-sector) m/z : $[\text{M}]^+$ Calcd for $[\text{C}_{20}\text{H}_{29}\text{BrINS}]^+$ 521.0249; Found 521.0238. IR (ATR): $\tilde{\nu}=2954$ (s), 2924 (s), 2854 (s), 1573 (w), 1521 (w), 1455 (s), 1402 (s), 1375 (m), 1288 (m), 1199 (m), 1102 (w), 1035 (w), 1002 (w), 967 (w), 867 (w), 839 (m), 754 (s), 725 (m), 661 (w), 584 (w), 475 (w) cm^{-1} .

4.3.5. Typical procedure of lithiation of precursor monomer 4. 4 (261 mg, 0.50 mmol) was added in one portion to THF (15 mL) and the solution was cooled to -78 °C. *n*-BuLi (0.2 mL, 0.50 mmol, 2.5 M in hexanes) was added dropwise to the solution over the course of 1 min and stirred for 10 min. Then MeI (426 mg, 0.2 mL, 3 mmol) was added in one portion and stirred for 2 h at -78 °C. The reaction was quenched with water (5 mL) and the aqueous phase was extracted with ether (2×15 mL). The combined organic phase was dried over MgSO_4 . The solvent was removed in vacuo and the crude

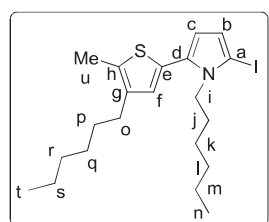
product was checked by GC–MS and NMR. The isolated products are shown as follows.

4.3.6. 2-Bromo-1-hexyl-5-(4-hexyl-5-methylthiophen-2-yl)-1H-pyrrole (5).



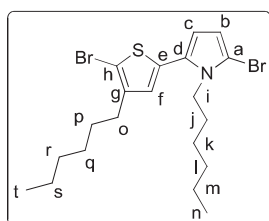
^1H NMR (500 MHz, MeOD): δ =6.72 (s, 1H, H-f), 6.14 (d, 3J =3.8 Hz, 1H, H-b/c), 6.11 (d, 3J =3.8 Hz, 1H, H-b/c), 4.05–3.95 (m, 2H, H-i), 2.53 (t, 3J =7.5 Hz, 2H, H-o), 2.34 (s, 3H, H-u), 1.65–1.54 (m, 4H, H-j, p), 1.38–1.19 (m, 12H, H-k, l, m, q, r, s), 0.93–0.83 (m, 6H, H-n, t) ppm. ^{13}C NMR (126 MHz, MeOD): δ =139.8 (C-g), 133.7 (C-h), 131.1 (C-e), 129.3 (C-a/d), 129.2 (C-f), 111.6(C-b/c), 111.4 (C-b/c), 103.7 (C-a/d), 46.9 (C-i), 31.8 (C-j/p), 31.6 (C-j/p), 29.0 (C-o), 32.9, 32.4, 30.0, 27.1, 23.7, 23.6 (C-k, l, m, q, r, s), 14.4, 14.3 (C-t, n), 12.7 (C-u) ppm. HRMS (EI-sector) m/z : $[\text{M}]^+$ Calcd for $[\text{C}_{21}\text{H}_{32}\text{BrNS}]^+$ 409.1339; Found 409.1442. IR (ATR): $\tilde{\nu}$ =2954 (s), 2924 (s), 2855 (s), 1458 (s), 1428 (m), 1402 (w), 1377 (m), 1289 (m), 1194 (m), 1158 (w), 1109 (w), 1030 (w), 961 (w), 892 (w), 839 (m), 750 (vs) cm^{-1} .

4.3.7. 1-Hexyl-2-(4-hexyl-5-methylthiophen-2-yl)-5-iodo-1H-pyrrole (6).



^1H NMR (500 MHz, MeOD): δ =6.70 (s, 1H, H-f), 6.29 (d, 3J =3.7 Hz, 1H, H-b/c), 6.16 (d, 3J =3.7 Hz, 1H, H-b/c), 4.03–3.98 (m, 2H, H-i), 2.53 (t, 3J =7.5 Hz, 2H, H-o), 2.34 (s, 3H, H-u), 1.65–1.53 (m, 4H, H-j, p), 1.38–1.19 (m, 12H, H-k, l, m, q, r, s), 0.93–0.83 (m, 6H, H-n, t) ppm. ^{13}C NMR (126 MHz, MeOD): δ =139.7 (C-g), 133.9 (C-h), 131.1 (C-d/e), 131.1 (C-d/e), 129.2 (C-f), 119.5 (C-b/c), 113.2(C-b/c), 71.2 (C-a), 49.0 (C-i),⁵⁸ 32.1 (C-j/p), 31.6 (C-j/p), 29.0 (C-o), 32.9, 32.4, 30.0, 27.1, 23.7, 23.6 (C-k, l, m, q, r, s), 14.4, 14.3 (C-t, n), 12.7 (C-u) ppm. HRMS (EI-sector) m/z : $[\text{M}]^+$ Calcd for $[\text{C}_{21}\text{H}_{32}\text{INS}]^+$ 457.1300; Found 457.1292. IR (ATR): $\tilde{\nu}$ =2954 (s), 2924 (s), 2855 (s), 1458 (s), 1420 (m), 1396 (w), 1376 (m), 1289 (m), 1194 (m), 1158 (w), 1102 (w), 1030 (w), 961 (w), 889 (w), 839 (m), 752(vs) cm^{-1} .

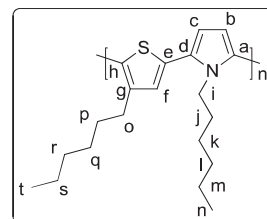
4.3.8. 2-Bromo-5-(5-bromo-4-hexylthiophen-2-yl)-1-hexyl-1H-pyrrole (8).



^1H NMR (500 MHz, MeOD): δ =6.80 (s, 1H, H-f), 6.22 (d, 3J =3.8 Hz, 1H, H-b/c), 6.16 (d, 3J =3.8 Hz, 1H, H-b/c), 4.06–4.01 (m, 2H, H-i), 2.63–2.56 (2H, H-o), 1.67–1.57 (m, 4H, H-j, p), 1.41–1.20 (m, 12H, H-k, l, m, q, r, s), 0.94–0.84 (m, 6H, H-n, t) ppm. ^{13}C NMR

(126 MHz, MeOD): δ =143.8 (C-g), 135.8 (C-e), 128.5 (C-f), 127.9 (C-d), 112.4 (C-b/c), 112.0 (C-b/c), 109.0 (C-h), 105.0 (C-a), 46.9 (C-i), 32.8, 32.4, 31.8, 30.8, 30.4, 29.9, 27.1, 23.7, 23.6 (C-j, k, l, m, o, p, q, r, s), 14.4, 14.3 (C-t, n) ppm. HRMS (EI-sector) m/z : $[\text{M}]^+$ Calcd for $[\text{C}_{20}\text{H}_{29}\text{Br}_2\text{NS}]^+$ 473.0388; Found 473.0411. IR (ATR): $\tilde{\nu}$ =2955 (s), 2925 (s), 2856 (s), 1577 (w), 1524 (w), 1461 (s), 1411 (m), 1378 (w), 1290 (m), 1202 (m), 1111 (w), 1034 (w), 971 (w), 869 (w), 839 (m), 751(vs) cm^{-1} .

4.3.9. General procedure for polymerization of 7.



In a microwave vial, *i*PrMgCl (0.25 mL, 2.00 M in THF, 0.50 mmol) was added dropwise to a solution of precursor monomer 4 (261 mg, 0.50 mmol) in dry MTBE (3.0 mL) via a Hamilton syringe in the glove box at 20 °C over the course of 1 min. After stirring the reaction mixture for 10 min at 20 °C, a solution of $[\text{Pd}(\text{tBu}_3\text{P})_2]$ (5.11 mg, 10.0 μmol) in MTBE (1.0 mL) was added to the reaction mixture. The reaction mixture was heated up to 50 °C under microwave irradiation and stirred for 5 h. Then the reaction mixture was quenched with H_2O (10 mL) and the aqueous phase was extracted with diethyl ether (2 \times 20 mL). The combined organic layer was washed with brine (1 \times 20 mL) and dried with MgSO_4 . The volatiles were removed in vacuo to give the crude product. This was dissolved in diethyl ether (0.5 mL) and the solution was added dropwise into methanol (200 mL) with vigorous stirring to remove the low molecular weight compounds. The precipitated polymer was extracted by Soxhlet extractor with MeOH (200 mL) for 5 h. For removal from the Soxhlet extractor, the solid polymer was refluxed by diethyl ether (100 mL). The volatiles were removed in vacuo and product was dried under reduced pressure for 16 h give the polymer as orange to red–brown viscous solid.

^1H NMR (600 MHz, CDCl_3): δ =6.97 (s, 1H, H-f), 6.41 (d, 3J =3.6 Hz, 1H, H-b/c), 6.26 (d, 3J =3.6 Hz, 1H, H-b/c), 4.17–3.92 (m, 2H, H-i), 2.66–2.46 (m, 2H, H-o), 1.64–1.51 (m, 4H, H-j, p), 1.35–1.09 (m, 12H, H-k, l, m, q, r, s), 0.88 (t, 3J =6.8 Hz, 3H, H-n/t), 0.81 (t, 3J =7.1 Hz, 3H, H-n/t) ppm. ^{13}C NMR (150 MHz, CDCl_3): δ =142.8 (C-g), 134.9 (C-e), 128.1 (C-a/d), 127.6 (C-h), 126.7 (C-a/d), 126.3 (C-f), 112.0 (C-b/c), 110.0 (C-b/c), 45.3 (C-i), 31.7 (C-k/l/m/q/r/s), 31.2 (C-k/l/m/q/r/s), 31.0 (C-j/p), 30.7 (C-j/p), 29.1 (C-o), 29.1 (C-k/l/m/q/r/s), 26.3 (C-k/l/m/q/r/s), 22.6 (C-k/l/m/q/r/s), 22.4 (C-k/l/m/q/r/s), 14.1 (C-n/t), 13.9 (C-n/t) ppm. IR (ATR): $\tilde{\nu}$ =2953 (s), 2923 (s), 2854 (s), 1458 (s), 1402 (m), 1376 (m), 1308 (m), 1193 (m), 1033 (m), 873 (w), 839 (m), 762 (m), 723 (m), 684 (w), 637 (w), 567 (w) cm^{-1} .

4.3.10. Procedure for the kinetics study. In a microwave vial, *i*PrMgCl (0.25 mL, 2.00 M in THF, 0.50 mmol) was added dropwise to a solution of precursor monomer 4 (261 mg, 0.50 mmol) and naphthalene (64.1 mg, 0.50 mmol, used as an internal standard for GC analysis to analyze the conversion) in dry MTBE (3.0 mL) via a Hamilton syringe in the glove box at 20 °C over the course of 1 min. After stirring the reaction mixture for 10 min at 20 °C, a solution of $[\text{Pd}(\text{tBu}_3\text{P})_2]$ (5.11 mg, 10.0 μmol) in MTBE (2.0 mL) was added to the reaction mixture. After the 60 min, 120 min, 180 min, 240 min, 300 min, 360 min, 375 min, 390 min, 415 min, 440 min, a sample (0.3 mL) was taken out of the reaction mixture. 0.1 mL of the solution was quenched with 2 droplets of ethanol. The quenched solution was diluted with 3 mL of THF, 2 mL of the solution was filtered with a syringe filter (0.45 μm) and used for GC

analysis. The other 0.2 mL of reaction mixture was quenched with ethanol (1 mL) and diluted with Et₂O (4 mL) and water (2 mL). After shaking the vial, the layers were separated. The organic phase was dried over MgSO₄ and filtered with a syringe filter (0.45 μm). Half of the solvent was removed in vacuo, diluted in chloroform (HPCL grade, 2 mL) and used for GPC analysis. The other half of the solvent was removed in vacuo, diluted in deuterated benzene for NMR analysis.

Acknowledgements

L.-Y. H. thanks the China Scholarship Council (CSC) for a Ph. D. scholarship and Prof. Zheng-Guo Zhang's and Prof. Xiao-Ming Fang's support for her work. S. U.-R. thanks the German Academic Exchange Service (DAAD) and the Colfuturo Fund for a Ph. D. scholarship. Grant number: A/13/72356 (DAAD).

Supplementary data

Supplementary data associated with this article can be found in the online version, at <http://dx.doi.org/10.1016/j.tet.2015.05.091>.

References and notes

- Muccini, M. *Nat. Mater.* **2006**, *5*, 605–613.
- O'Neill, M.; Kelly, S. M. *Adv. Mater.* **2011**, *23*, 566–584.
- Wang, C. L.; Dong, H. L.; Hu, W. P.; Liu, Y. Q.; Zhu, D. B. *Chem. Rev.* **2012**, *112*, 2208–2267.
- Roncali, J. *Chem. Rev.* **1992**, *92*, 711–738.
- Ong, B. S.; Wu, Y. L.; Liu, P.; Gardner, S. J. *Am. Chem. Soc.* **2004**, *126*, 3378–3379.
- Perepichka, I. F.; Perepichka, D. F.; Meng, H.; Wudl, F. *Adv. Mater.* **2005**, *17*, 2281–2305.
- Ramanavicius, A.; Ramanaviciene, A.; Malinauskas, A. *Electrochim. Acta* **2006**, *51*, 6025–6037.
- Takagi, S.; Makuta, S.; Veamatahau, A.; Otsuka, Y.; Tachibana, Y. *J. Mater. Chem.* **2012**, *22*, 22181–22189.
- Ford, W. K.; Duke, C. B.; Salaneck, W. R. *J. Chem. Phys.* **1982**, *77*, 5030–5039.
- Chung, T. C.; Kaufman, J. H.; Heeger, A. J.; Wudl, F. *Phys. Rev. B* **1984**, *30*, 702–710.
- Bakhshi, A. K.; Ladik, J.; Seel, M. *Phys. Rev. B* **1987**, *35*, 704–712.
- Ullah, H.; Shah, A. U. A.; Bilal, S.; Ayub, K. *J. Phys. Chem. C* **2014**, *118*, 17819–17830.
- Diaz, A. F.; Castillo, J. I. *J. Chem. Soc., Chem. Commun.* **1980**, 397–398.
- Diaz, A. F.; Crowley, J.; Bargon, J.; Gardini, G. P.; Torrance, J. B. *J. Electroanal. Chem.* **1981**, *121*, 355–361.
- Svensson, M.; Zhang, F. L.; Veenstra, S. C.; Verhees, W. J. H.; Hummelen, J. C.; Kroon, J. M.; Inganas, O.; Andersson, M. R. *Adv. Mater.* **2003**, *15*, 988–991.
- Bundgaard, E.; Krebs, F. C. *Sol. Energy Mater. Sol. Cells* **2007**, *91*, 954–985.
- Li, Y. N.; Ding, J. F.; Day, M.; Tao, Y.; Lu, J. P.; D'iorio, M. *Chem. Mater.* **2004**, *16*, 2165–2173.
- Blouin, N.; Michaud, A.; Gendron, D.; Wakim, S.; Blair, E.; Neagu-Plesu, R.; Belletete, M.; Durocher, G.; Tao, Y.; Leclerc, M. *J. Am. Chem. Soc.* **2008**, *130*, 732–742.
- Parakka, J. P.; Chacko, A. P.; Nikles, D. E.; Wang, P.; Hasegawa, S.; Maruyama, Y.; Metzger, R. M.; Cava, M. P. *Macromolecules* **1996**, *29*, 1928–1933.
- Varis, S.; Ak, M.; Tanyeli, C.; Akhmedov, I. M.; Toppare, L. *Eur. Polym. J.* **2006**, *42*, 2352–2360.
- Yigitsoy, B.; Varis, S.; Tanyeli, C.; Akhmedov, I. M.; Toppare, L. *Thin Solid Films* **2007**, *515*, 3898–3904.
- Celik, B.; Celik, I.; Dolas, H.; Gorcay, H.; Sahin, Y.; Sarac, A. S.; Pekmez, K. *React. Funct. Polym.* **2014**, *83*, 107–112.
- El'shina, T. S.; Sosnin, E. A.; Shklyayeva, E. V.; Abashev, G. G. *Russ. J. Gen. Chem.* **2013**, *83*, 726–730.
- Abashev, G. G.; Bushueva, A. Y.; Shklyayeva, E. V. *Chem. Heterocycl. Compd.* **2011**, *47*, 130–154.
- Chang, K. H.; Wang, H. P.; Wu, T. Y.; Sun, I. W. *Electrochim. Acta* **2014**, *119*, 225–235.
- Just, P. E.; Chane-Ching, K. I.; Lacaze, P. C. *Tetrahedron* **2002**, *58*, 3467–3472.
- Kim, Y. H.; Hwang, J.; Son, J. I.; Shim, Y. B. *Synth. Met.* **2010**, *160*, 413–418.
- Ferraris, J. P.; Andrus, R. G.; Hrcir, D. C. *J. Chem. Soc., Chem. Commun.* **1989**, 1318–1320.
- Rockel, H.; Huber, J.; Gleiter, R.; Schuhmann, W. *Adv. Mater.* **1994**, *6*, 568–571.
- Niziorskimann, R. E.; Scordiliskelley, C.; Liu, T. L.; Cava, M. P.; Carlin, R. T. *J. Am. Chem. Soc.* **1993**, *115*, 887–891.
- Yamamoto, T.; Yoshizawa, M.; Mahmut, A.; Abe, M.; Kuroda, S.; Imase, T.; Sasaki, S. *J. Polym. Sci. Part B Polym. Chem.* **2005**, *43*, 6223–6232.
- Yamashita, R.; Koizumi, T.; Sasaki, S.; Yamamoto, T. *Polym. J.* **2007**, *39*, 1202–1206.
- Yamamoto, T.; Yamashita, R. *Polym. J.* **2008**, *40*, 775–778.
- Mccullough, R. D.; Lowe, R. D. *J. Chem. Soc., Chem. Commun.* **1992**, 70–72.
- Yokoyama, A.; Miyakoshi, R.; Yokozawa, T. *Macromolecules* **2004**, *37*, 1169–1171.
- Miyakoshi, R.; Shimono, K.; Yokoyama, A.; Yokozawa, T. *J. Am. Chem. Soc.* **2006**, *128*, 16012–16013.
- Nanashima, Y.; Yokoyama, A.; Yokozawa, T. *Macromolecules* **2012**, *45*, 2609–2613.
- Sui, A. G.; Shi, X. C.; Wu, S. P.; Tian, H. K.; Geng, Y. H.; Wang, F. S. *Macromolecules* **2012**, *45*, 5436–5443.
- Wu, S. P.; Sun, Y. Q.; Huang, L.; Wang, J. W.; Zhou, Y. H.; Geng, Y. H.; Wang, F. S. *Macromolecules* **2010**, *43*, 4438–4440.
- Locke, J. R.; McNeil, A. J. *Macromolecules* **2010**, *43*, 8709–8710.
- Ono, R. J.; Kang, S. S.; Bielawski, C. W. *Macromolecules* **2012**, *45*, 2321–2326.
- Palermo, E. F.; McNeil, A. J. *Macromolecules* **2012**, *45*, 5948–5955.
- Kang, S. S.; Ono, R. J.; Bielawski, C. W. *J. Am. Chem. Soc.* **2013**, *135*, 4984–4987.
- Heinrich, A. C. J.; Thiedemann, B.; Gates, P. J.; Staubitz, A. *Org. Lett.* **2013**, *15*, 4666–4669.
- Schnurch, M.; Spina, M.; Khan, A. F.; Mihovilovic, M. D.; Stanetty, P. *Chem. Soc. Rev.* **2007**, *36*, 1046–1057.
- Hoffmann, K. J.; Carlsen, P. H. J. *Synth. Commun.* **1999**, *29*, 1607–1610.
- Wang, C. G.; Benz, M. E.; Legoff, E.; Schindler, J. L.; Allbrittonthomas, J.; Kannewurf, C. R.; Kanatzidis, M. G. *Chem. Mater.* **1994**, *6*, 401–411.
- Chen, T. A.; Wu, X. M.; Rieke, R. D. *J. Am. Chem. Soc.* **1995**, *117*, 233–244.
- Stefan, M. C.; Javier, A. E.; Osaka, I.; McCullough, R. D. *Macromolecules* **2009**, *42*, 30–32.
- Yokozawa, T.; Yokoyama, A. *Chem. Rev.* **2009**, *109*, 5595–5619.
- Yokoyama, A.; Yokozawa, T. *Macromolecules* **2007**, *40*, 4093–4101.
- Adachi, I.; Miyakoshi, R.; Yokoyama, A.; Yokozawa, T. *Macromolecules* **2006**, *39*, 7793–7795.
- Miyakoshi, R.; Yokoyama, A.; Yokozawa, T. *J. Am. Chem. Soc.* **2005**, *127*, 17542–17547.
- Osaka, I.; McCullough, R. D. *Acc. Chem. Res.* **2008**, *41*, 1202–1214.
- Iovu, M. C.; Sheina, E. E.; Gil, R. R.; McCullough, R. D. *Macromolecules* **2005**, *38*, 8649–8656.
- Bhatt, M. P.; Magurudeniya, H. D.; Sista, P.; Sheina, E. E.; Jeffries-EL, M.; Janesko, B. G.; McCullough, R. D.; Stefan, M. C. *J. Mater. Chem. A* **2013**, *1*, 12841–12849.
- Smeets, A.; Van den Bergh, K.; De Winter, J.; Gerbaux, P.; Verbiest, T.; Koeckelberghs, G. *Macromolecules* **2009**, *42*, 7638–7641.
- The peak is overlapping with the solvent peak

3.2. Results and Discussion. Synthesis, Characterization and Reactivity of Stannoles

This sub-chapter covers the topic stannoles as a motif in semiconducting polymers. The section 3.2.1. resumes the concept of stannoles itself taking into account the history, electron delocalization, common methods of synthesis, reactivity and optoelectronic properties.

The section 3.2.2. describes the synthesis and reaction control of zirconacyclopentadienes which are synthons of stannoles.

Finally, in the section 3.2.3. the reactivity of stannoles in cross-coupling reactions to produce monomers, dimers or polymers containing stannole and thienyl units under different ratio is described.

3.2.1. Synthesis and Properties of Tin-Containing Conjugated Heterocycles

Concept article

Sara Urrego-Riveros, Isabel-Maria Ramirez y Medina, Jonas Hoffmann, Anne Heitmann, Anne Staubitz, *Chem. Eur. J.* **2018**, *24* (22), 5680-5696.

Reprinted with permission from WILEY-VCH.(c)

Abstract

Heterocycles that contain tin can be aromatic in a similar sense to classical carbon aromatic heterocycles such as benzene, but such examples are rare. However, due to the low-lying σ^* -orbitals of the tin-substituent bond in stannoles they are capable of $\sigma^* - \pi^*$ conjugation in a way that is exclusive to heavier element containing heterocycles. This makes stannoles very interesting alternatives for purely organic heterocycles in materials applications, in which optoelectronic properties are of interest. This concept article will highlight the synthesis, reactivity and physical properties of stannoles and the related fluorenostannoles. At first, a brief introduction on different types of tin containing heterocycles is presented, followed by a discussion on different approaches to prepare stannoles, their reactivity and their physical properties. In addition, the first stannole-containing polymer will be reviewed.

Scientific contribution to this paper

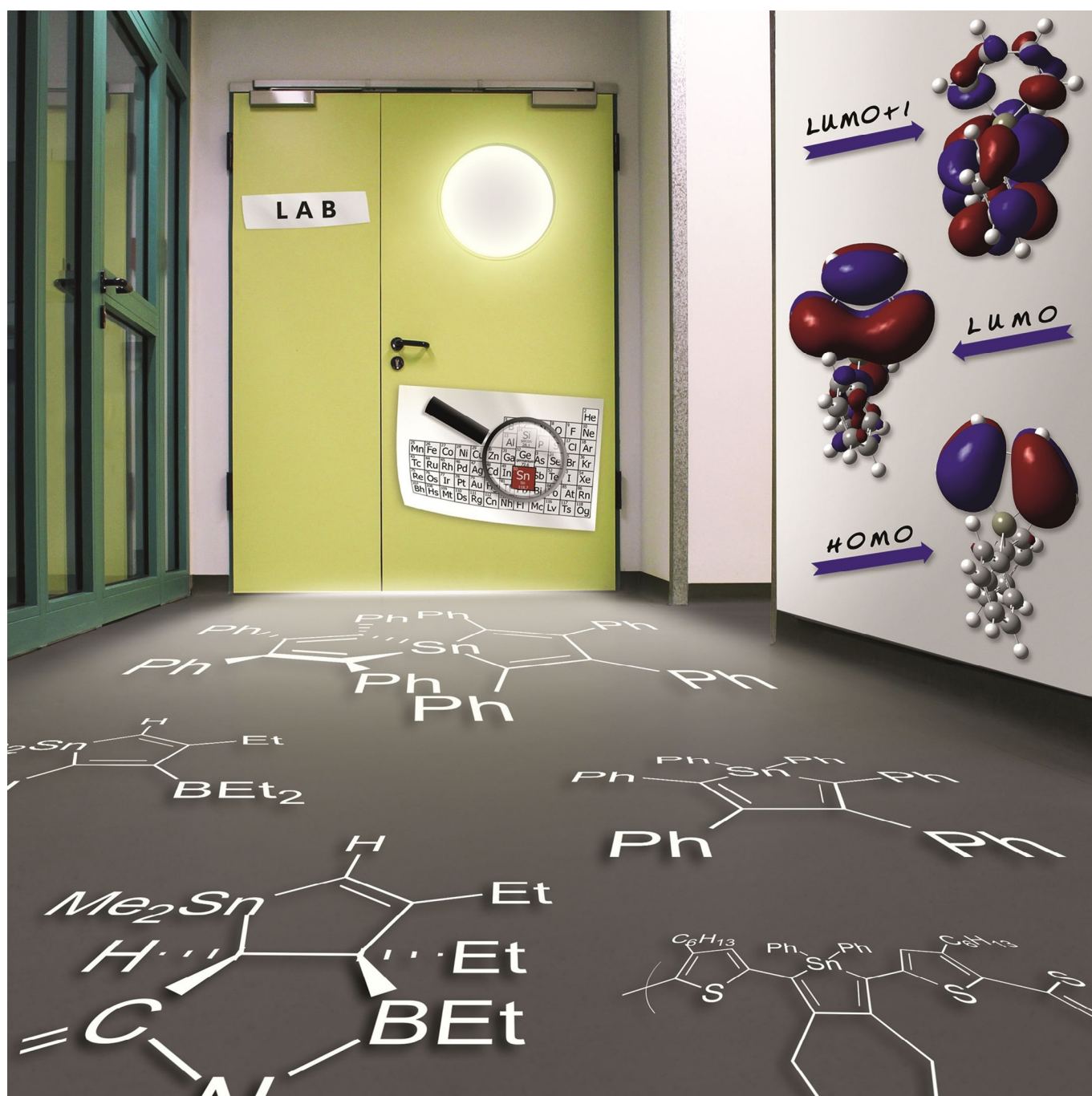
This concept article is a literature collection related to the electron delocalization, reactivity and properties of stannoles. Most of the literature research was done by me. Prof. Dr. Anne Staubitz and I wrote and reviewed 80% of the paper. The missing 20% were done by the other co-authors: Isabel-M. Ramirez y Medina, Jonas Hoffmann and Dr. Anne Heitmann. All Schemes and Figures were drawn by me. The proposed frontispiece was designed for all the authors with the hint of Olga Schreiner from the Dezernat für IT | medientechnische Infrastruktur und zentrale Dienste (Dez 5), Bremen University.

Conjugated Tin Structures

Syntheses and Properties of Tin-Containing Conjugated Heterocycles

Sara Urrego-Riveros,^[a, b] Isabel-Maria Ramirez y Medina,^[a, b] Jonas Hoffmann,^[a, b]
Anne Heitmann,^[a, b] and Anne Staubitz*^[a, b]

Dedicated to Professor Bernd Wrackmeyer



Abstract: Heterocycles that contain tin atoms can be aromatic in a similar sense to well-known aromatic compounds such as benzene or thiophene, but such examples are rare. However, due to the low-lying σ^* -orbitals of the tin-substituent bond in stannoles, they are capable of σ^* - π^* conjugation in a way that is exclusive to heavier element containing heterocycles. This makes stannoles very interesting alternatives for purely organic heterocycles in material applications, in which optoelectronic properties are of interest. This Concept article will highlight the synthesis, reactivity and physical properties of stannoles and related fluorenostannoles. At first, a brief introduction to different types of tin-containing heterocycles is presented, followed by a discussion on different approaches to prepare stannoles, their reactivity and their physical properties. In addition, the first stannole-containing polymer will be reviewed.

Introduction

Cyclopentadienes are cyclic dienes that exhibit distinctive physical and chemical properties that can be attributed to their nonaromatic character: They absorb UV light (absorption maximum λ_{max} between 235 and 261 nm in alcoholic solvents with a molar extinction coefficient (ϵ) between 7.2 and $1.7 \times 10^3 \text{ L mol}^{-1} \text{ cm}^{-1}$),^[1] they readily undergo Diels–Alder reactions (in fact, they dimerize to the dicyclopentadiene at room temperature) and they are easily deprotonated ($\text{p}K_{\text{a}}=16.0$ in water, but can be up to $\text{p}K_{\text{a}}=26.0$ for substituted or anellated cyclopentadienes)^[2] to give the aromatic cyclopentadienyl anions. However, if the sp^3 -carbon is replaced by a heavier group 14 element, the properties change substantially: Such compounds show a certain degree of electron delocalization and the absorption wavelengths undergo a substantial bathochromic shift. The unusual characteristics have been exploited with great success for Si-containing heterocycles,^[3] which are already discussed and used for applications in organic solar cells (OSC),^[4] and organic electroluminescent devices.^[3a,5] Germales and related germanium-containing heterocycles are also receiving increased attention.^[6] However, the literature on stannoles is more scarce.

In this Concept article, we focus on tin-containing heterocycles, in particular stannoles and closely related systems. After a

discussion of the nature of the electron delocalization in such molecules, the various synthetic routes leading to these heterocycles will be shown followed by a report on current knowledge concerning the functionalization of these heterocycles. Finally, their spectroscopic and optoelectronic properties will be described and potential applications of stannoles in polymers will be discussed.

Aromaticity of Tin-Containing Heterocycles

The Hückel rule is one of the oldest and perhaps still the most reliable rule to predict aromaticity. It states that a planar cyclic system exhibits aromaticity if it contains $[4n+2]\pi$ electrons in conjugated molecular orbitals. For tin analogues of all-carbon aromatic cycles, this is not easily achieved; heavier main group elements show an inherent, substantial reluctance to form double bonds. Although double and triple bonds of heavier alkene and alkyne analogues of group 13–group 16 elements have been reported, the geometry of such molecules is often not equivalent to their carbon analogues: Instead of a planar geometry of the bonds at the atom that partakes in multiple bonds, pyramidalization is typical.^[7] In addition, the stability of compounds with multiple bonds between heavier elements is much lower than that of the all-carbon analogues: In the case of distannyne systems (RSnSnR), the group R has to be sterically demanding to provide kinetic protection of the SnSn triple bond.^[8] Therefore, heavier group 14 analogues of benzene are structurally and electronically intriguing—in the few cases that do exist: The unsubstituted monosilabenzene C_5SiH_6 ^[9] as well as the 1,4-disilabenzene $\text{C}_4\text{Si}_2\text{H}_6$ ^[10] could be isolated under matrix isolation conditions at 10 K. The IR and UV/Vis spectroscopic analysis suggested an aromatic character with a substantial red shift of the spectra that increased from the mono- to the disilabenzene. Interestingly, 1,4-disilabenzene can be formed (albeit not isolated) from 1,4-disila(Dewar-benzene), which is more stable than the aromatic valence isomer.^[11] With kinetic protection by large groups, a stable silabenzene could even be isolated.^[12] Polycyclic aromatic rings with C–Si replacement have also been reported; the substituent on silicon is always sterically encumbered.^[13] The substituted hexasilabenzene **1**, a silicon analogue of benzene, with chair shape geometry has been reported to be thermally stable at 100°C , with a “dismutational aromaticity” and three resonance forms (Figure 1).^[14]

However, a similar aromatic compound could not be observed for tin. A reaction between RSnH_3 , **2** and carbene **3** (Scheme 1; $\text{R}=2,4,6$ -triisopropylphenyl=trip) produced ini-

[a] S. Urrego-Riveros, I.-M. Ramirez y Medina, J. Hoffmann, Dr. A. Heitmann, Prof. Dr. A. Staubitz
Institute for Organic and Analytical Chemistry, University of Bremen
Leobener Str.7 NW2C, 28359 Bremen (Germany)

[b] S. Urrego-Riveros, I.-M. Ramirez y Medina, J. Hoffmann, Dr. A. Heitmann, Prof. Dr. A. Staubitz
MAPEX Center for Materials and Processes, University of Bremen
Bibliothekstraße 1, 28359 Bremen (Germany)
E-mail: staubitz@uni-bremen.de

DOI The ORCID numbers for the authors of this article can be found under <https://doi.org/10.1002/chem.201703533>.

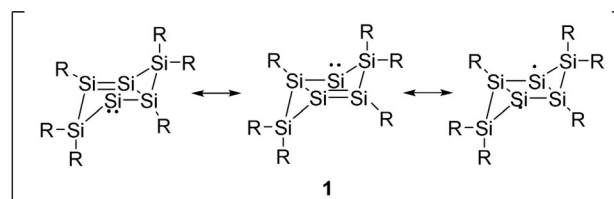
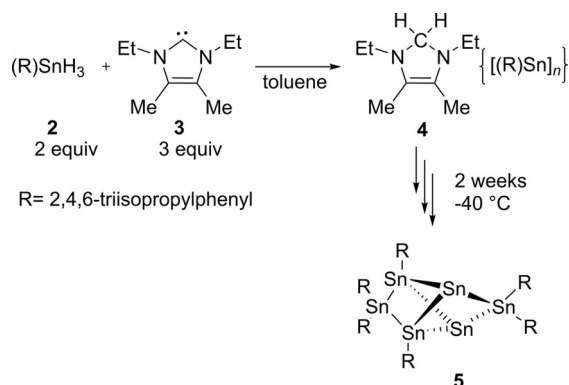


Figure 1. Resonance forms of the hexasilabenzene **1** ($\text{R}=2,4,6$ -triisopropylphenyl).^[14a]



Scheme 1. Reaction path to the formation of the nonaromatic cluster **5**.^[15]

tially complex **4**, but after some days at $-40\text{ }^{\circ}\text{C}$, crystals of cluster **5** were observed.^[15] This cluster is likely to be the global energy minimum, with a bonding propellane structure, similar to their isoelectronic silicon analogue and mixed heavier homologues $\text{E}_2\text{Si}_4(\text{trip})_6$ ($\text{E} = \text{Ge}, \text{Sn}$).^[16] Therefore, despite the stoichiometry of **5**, R_6Sn_6 that at first glance might suggest aromaticity, **5** is nonaromatic. It should be mentioned in this context that a hexasilaprismane, R_6Si_6 has been synthesized and isolated; but the UV/Vis maximum at $\lambda_{\text{max}} = 241\text{ nm}$ does not suggest aromatic character.^[17]

For compounds in which only one atom in an otherwise all aromatic carbon skeleton is replaced by a tin atom, the issue with energetically unfavorable formation of π -bonds involving tin atoms also exists. Due to the comparatively large tin atom and long carbon-tin bonds,^[18] a geometric distortion of the ring out of the plane results. This in turn reduces the stability that can be gained through resonance effects. It is therefore unsurprising that only very few tin containing compounds that are aromatic in the classical sense have been prepared to date.

The criteria that have been used to define if a compound is aromatic are numerous. For example, a strong downfield shift of ^1H NMR signals of protons of an aromatic ring compared to proton-shifts of double bonds can be used. This fact is complemented by computational data such as a negative value of the nucleus-independent chemical shift (NICS),^[19] calculations of the anisotropy of the induced ring current to chemical reactivity and the experimental aromatic stabilization energy (ASE).^[5] Further aspects are structural: for aromatic compounds an equalization of bond lengths is expected that can be proven by X-ray crystallography (XRD) or other spectroscopic methods.^[20] However, even the less stringent concepts of aromaticity have been much expanded in recent years; three-dimensional aromatic systems^[21] have been described as well as six-membered rings in chair conformation (see Si_6R_6 above).^[14a] Main group chemistry in particular has played a major role in the expansion of such concepts.

Aromaticity has become a question of perspective because there are many examples that fulfill some but not all criteria for aromaticity. For example, heavier elements may distort bond length equalization but still allow electron delocalization and depending on how one rates the importance of these two criteria, the degree of aromaticity may become debatable.

Heteroles with higher group 14 elements provide an entirely different type of aromaticity: aromaticity by $\sigma^*-\pi^*$ conjugation. Because this phenomenon is of such central importance to stannoles, the concept will be described in more detail here; for a more in-depth discussion with a focus on aromaticity see the definitive review of Lee et al.^[20]

$\sigma^*-\pi^*$ conjugation

Structurally, stannoles are similar to other cyclopentadiene congeners with group 14 elements. Their rings are essentially planar, but the geometry around the heteroatom can be described as a distorted tetrahedron, with an endocyclic bond angle of about $83\text{--}94\text{ }^{\circ}$ for stannoles. This forces a parallel arrangement between the π^* -orbitals inside the diene ring and the σ^* -orbitals of the $\text{Sn}-\text{R}$ bonds. By effectively mixing the HOMO of the diene system with the σ^* -orbitals, $\sigma^*-\pi^*$ conjugation occurs that lowers the energy level of the LUMO, while leaving the HOMO almost unchanged (Figure 2).^[5,22] Using standard DFT calculations, this can be seen by analyzing the LUMO (which corresponds to the π^* -orbital of the diene system) and the LUMO + 1 (which corresponds to the σ^* -orbital). The distances between the ring carbon atoms and the group 14 atoms become longer with heavier atoms (Figure 3). Therefore, the interaction between the σ^* - and the π^* -orbitals is lower in stannoles than in siloles or germales.^[22]

Another complementary way of describing the electronic character of stannoles has been proposed by Ottosson and co-workers.^[23] In this work, the Hückel aromatic character of the ground state and the Baird aromatic character in the lowest π^* singlet and triplet states are taken into consideration.^[24] The T_1

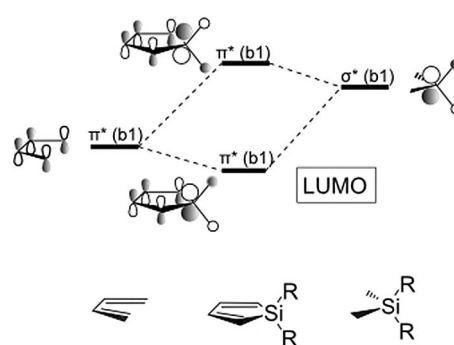


Figure 2. Orbital correlation diagram of the $\sigma^*-\pi^*$ conjugation in the LUMO of 1,1-disubstituted silole. Adapted with permission from reference [25]. Copyright (1996) The Chemical Society of Japan.

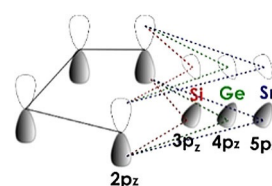


Figure 3. Schematic drawing of the change in $\sigma^*-\pi^*$ conjugation as a function of Si, Ge and Sn. Adapted with permission from reference [22]. Copyright (1998) American Chemical Society.

state has been calculated to be lower in energy than the S_1 state. For siloles, three resonance forms can be described (Figure 4). In the first, **A**, a positive charge is delocalized in the ring and a corresponding negative charge on the substituent

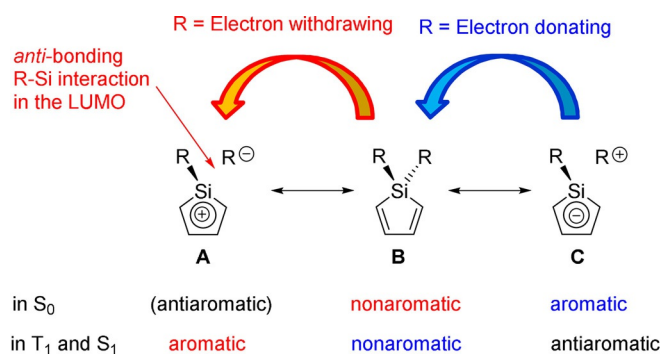


Figure 4. Different mesomeric forms of siloles in ground and excited states. Adapted with permission from reference [23].

on the silicon atom. This arrangement is antiaromatic in the ground state, but according to Baird's rule aromatic in the excited state. The cyclopentadienyl structure **B** is nonaromatic in both ground- and excited states. However, in the mesomeric form **C** with a negative charge delocalized in the ring and a cationic substituent on the silicon atom, the ground state is aromatic and the excited state antiaromatic (Figure 4). If the substituents on the silicon atom are electron donating, the ground state S_0 has some aromatic character, whereas the excited T_1 state is nonaromatic to even slightly antiaromatic. Thus, the HOMO is stabilized and the LUMO destabilized leading to higher energy gaps. With electron-withdrawing groups, the ground state is nonaromatic, the S_1 slightly antiaromatic, and the T_1 state slightly aromatic, dominating the transition. Therefore, in this case, the excited T_1 state is stabilized by Baird aromaticity leading to a lower LUMO level compared to the case with electron-donating groups. Thus, it should be possible to tune the HOMO–LUMO gap by varying the substituents on group 14 atoms. Although calculations exist for Si, this has not yet been performed for stannoles and experimental evidence is yet to be provided. This study highlights that if one speaks of “aromaticity” in the context of stannoles, it is of a different type than the Hückel aromaticity and the term “ σ^* – π^* conjugation” is to be preferred.

However, it is likely that electronic influences of substituents on the Sn atom or the ring are not the only parameter by which the HOMO–LUMO gap of stannoles can be tuned. Also, the geometry of the molecule plays a role. Again, in the case of stannoles, there is still no analysis. An insight might be transferrable from related siloles. In the case of siloles, it was shown that bisiloles show both substantial torsion angles between the planes of the heterocycles, but they also folded against one another (Figure 5).^[25]

This geometrical distortion perturbs an efficient conjugation across the two connected butadiene motifs, thus leading to a higher π^* -orbital than in a hypothetical coplanar case. This in turn increases the σ^* – π^* conjugation within one ring. The re-

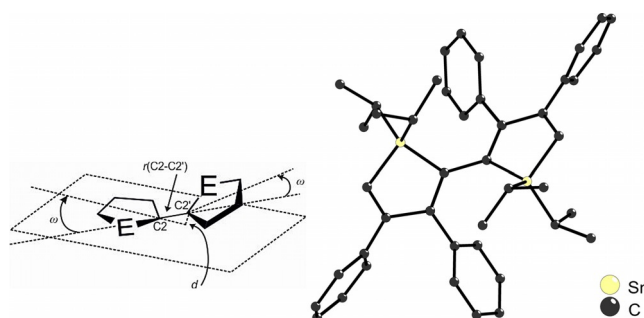


Figure 5. General description of the torsion angle of bisiloles. Adapted with permission from reference [25]. Copyright (1996) Chemical Society of Japan. Crystal structure of the 1,1,1',1'-tetraisopropyl-3,3',4,4'-tetraphenyl-2,2'-bisilole.^[26]

duction potential of siloles is about 0.5 V lower than that of the carbon analogue, whereas for corresponding bicyclic systems, the difference is about 0.4 V, reflecting the lowered LUMOs for silanoles.

Organotin heterocycles obeying the Hückel rule

The smallest hypothetical aromatic tin cycle analogue of the cyclopropenium cation (2π -electrons) is the stannacyclopropene cation **6** (Figure 6).^[27] As a proof of its aromaticity, the aromatic stabilization energies were studied by different computational

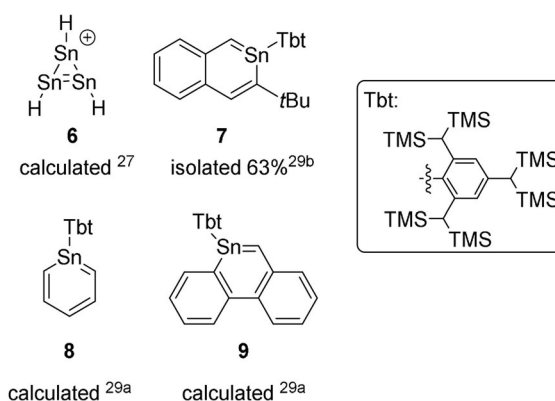


Figure 6. Examples of aromatic organotin heterocycles obeying the Hückel rule.

methods such as energy decomposition analysis (EDA) or block-localized wavefunctions (BLW). Furthermore, this compound had a calculated NICS value of around -8.55 ^[27] which suggests a strong aromatic character (for comparison, the NICS value for benzene is -9.70).^[28] However, this compound or any substituted congener has not been synthesized to date. Whenever Hückel aromatic organotin heterocycles were synthesized to date, they had to be stabilized by bulky substituents or when they are incorporated in bi- or tricycles **7** (isolated; **8** and **9** calculated because they were unstable at room temperature; Figure 6).^[20,29]

The 2-stannanaphthalene **7** is the only example that was isolated in which a tin atom replaces a carbon atom exactly anal-

ogously to the aromatic bicycle naphthalene.^[29b] Other benzene analogues, for example the Tbt-stannabenzene **8** and the 9-Tbt-9-stannaphenanthrene **9** readily undergo [4+2] and [2+2] dimerizations at room temperature.^[29a]

The stability of compound **7** results from a combination of bulky substituents on the tin atom and the adjacent carbon atom. The C–C bond lengths of the 2-stannanaphthalene ring **7** are between 1.356 and 1.443 Å. This intermediate length between single and C=C double bond indicates a delocalization of the π electrons. Furthermore, X-ray crystallography showed a trigonal planar geometry around the tin atom. The experimental chemical shifts observed with ^1H and ^{13}C NMR spectroscopy were also a strong indication of the aromatic character of these compounds [$\delta(^1\text{H})=7.05\text{--}9.28$ ppm, $\delta(^{13}\text{C})=120\text{--}170$ ppm]. The ^{119}Sn NMR shift [$\delta(^{119}\text{Sn})=264$ ppm] is associated with a low coordinated tin atom, the valence electrons of which contribute to the resonance inside the ring. The most intense Raman signal of 2-stannanaphthalene **7** was found at 1331 cm^{-1} and results from a planar skeletal vibration; which is similar to the signals of the aromatic compounds naphthalene (1382 cm^{-1}), 2-silanaphthalene (1368 cm^{-1}) and 2-germanaphthalene (1360 cm^{-1}).^[29b]

Classification of stannoles

The concept of metalloles as heavy congeners of the cyclopentadiene was introduced in 1959 by Leavitt and co-workers.^[30] Since then, four classes of stannoles have been studied: unfunctionalized stannoles (I), functionalized stannoles in which the tin atom bears functional groups (II), functionalized stannoles in which one carbon atom of the stannole ring bears functional groups (III), and as closely related structures to the annelated analogues, the 9-stannafluorenes (IV) (Figure 7).^[31] In what we define as unfunctionalized stannoles, all substituents are either alkyl, or aryl groups, or a proton. In the stannafluorenes, the tin atom is without exception in the 9-position. As C-functionalized stannoles, we define stannoles that contain

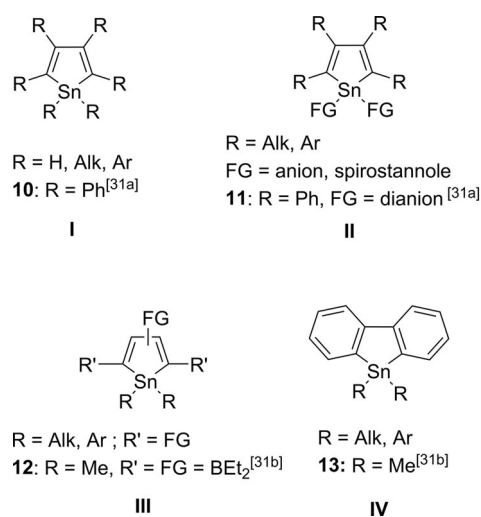


Figure 7. Four different basic classes of stannoles with an example for each class.

substituents other than aryl, alkyl or H on the carbon atom of the ring, or in the wider periphery on a carbon atom. Sn-functionalized stannoles bear substituents other than aryl, alkyl, or H on the tin atom.

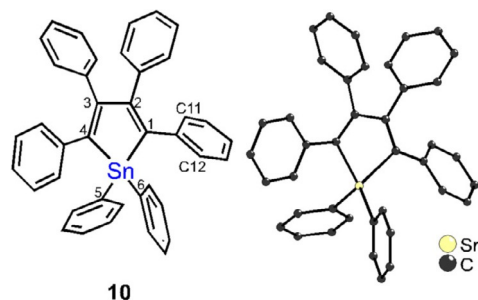


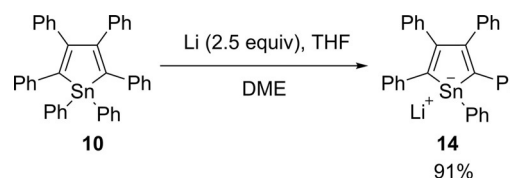
Figure 8. Representation and crystal structure of hexaphenylstannole **10**. The torsion angle Sn–C1–C11–C12 is 1.2° . Adapted with permission from reference [32]. Copyright (1999) American Chemical Society.

Neutral stannoles

The typical geometry of stannoles was revealed with a single X-ray crystallographic analysis of hexaphenylstannole **10** (Figure 8).^[32] One of the phenyl rings on a ring carbon atom adjacent to tin (C11) is coplanar with respect to the metallole ring, whereas the other phenyl groups are twisted out of the plane for steric reasons. In the case of the two phenyl rings in the 1 and 4 positions, the torsional angles are 1.2° and 47° , respectively. The distance between Sn–C1 is 2.126 \AA , between C1–C2 1.352 \AA , and between C2–C3 it is 1.511 \AA . The bond lengths for Sn–C5 and Sn–C6 are both 2.125 \AA ; this is very similar to the Sn–C1 and Sn–C4 bond distance. However, ^{13}C NMR shift values of $153\text{--}125$ ppm (compared to (*E,E*)-1,2,3,4-tetra-phenylbutadiene of $145\text{--}126$ ppm) and a maximum of the UV absorption spectrum of 355 nm suggests some $\sigma^*-\pi^*$ -conjugation.^[32]

Stannole salts

To obtain the stannole monoanion **14**, the reaction with elemental lithium could be halted at the stage of mono-lithiation, when **10** was allowed to react with only 2.5 equivalents of lithium (Scheme 2).^[33] Crystallization of **14** in the presence of 12-crown-4 salts, improved the X-ray data of the monoanion. The crystal structure of the salt of **14** (Figure 9) showed no interaction between the Sn and Li (distance between the atoms: 6.5 \AA) in comparison with the dianion **11** (distance: 2.77 \AA , see



Scheme 2. Formation of the stannole monoanion **14**. DME = (1,2-dimethoxyethane).^[33b]

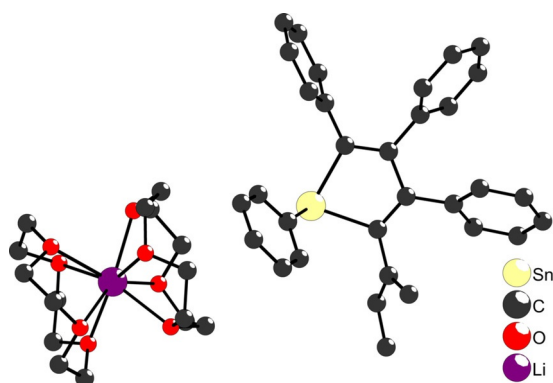
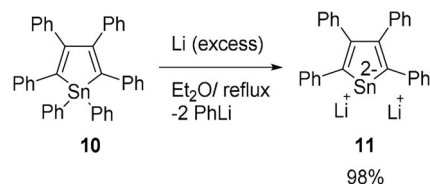


Figure 9. Crystal structure of the salt **14** $[\text{Ph}_5\text{C}_4\text{Sn}][\text{Li}^+(12\text{-crown-}4)_2]$.^[33b]

below). The stannolate ring and the lithium cation are separated by coordinating solvent molecules. In addition, contrary to the equal C–C bond distances of **14** hinting at substantial electron delocalization, the salt of **14** showed a 1,3-butadiene character with significant alternation of the C–C bond distances (C1–C2 1.36 Å, C2–C3 1.493 Å, C3–C4 1.364 Å). The monoanion **14** therefore appears to be nonaromatic.^[33b]

A study of the stannole dianion **11** by Saito and co-workers revealed a Hückel-like aromaticity of dianionic stannoles. This dianion could be prepared by reductive cleavage of the exocyclic Sn–C bonds with an excess of lithium (Scheme 3).^[31a] The



Scheme 3. Synthetic route to obtain the stannole dianion **11**.^[31a]

structure of dianion **11** was comparable to the cyclopentadiene monoanion, containing 6 π -electrons; however, the stannole monoanion was not structurally equivalent to the cyclopentadiene anion. The stannole dianion **11** has a planar structure with almost equal C–C bond distances within the ring (C1–C2 1.422, C2–C3 1.442, C3–C4 1.446 Å), suggesting a considerable aromatic delocalization of the negative charges (Figure 10a). When the crystal structure of **11** (Figure 10a) is compared with the cyclopentadienyl lithium **15** (Figure 10b),^[34] the Sn–Li bond lengths (2.770 Å) in **11** and the C–Li bonds in **15** (C1–Li 2.335, C2–Li 2.331, C3–Li 2.293, C4–Li 2.275 and C5–Li 2.301 Å) differ due to the size of the tin atom. However, the bond lengths inside the rings were similar, in which they were least influenced by the tetravalent atom. In the case of the cyclopentadiene derivative **15**, the bonds inside the ring are C1–C2 1.413, C2–C3 1.414, C3–C4 1.413, and C4–C5 1.413 Å. In addition, the analysis of the ^7Li NMR signal of **11** ($\delta = -4.36$ ppm in C_6D_6) showed the high shielding effect of the diatropic ring current from the 6 π -electron system and is comparable to the ^7Li NMR signal in **15** (-8.37 ppm in $[\text{D}_8]\text{THF}$).^[35]

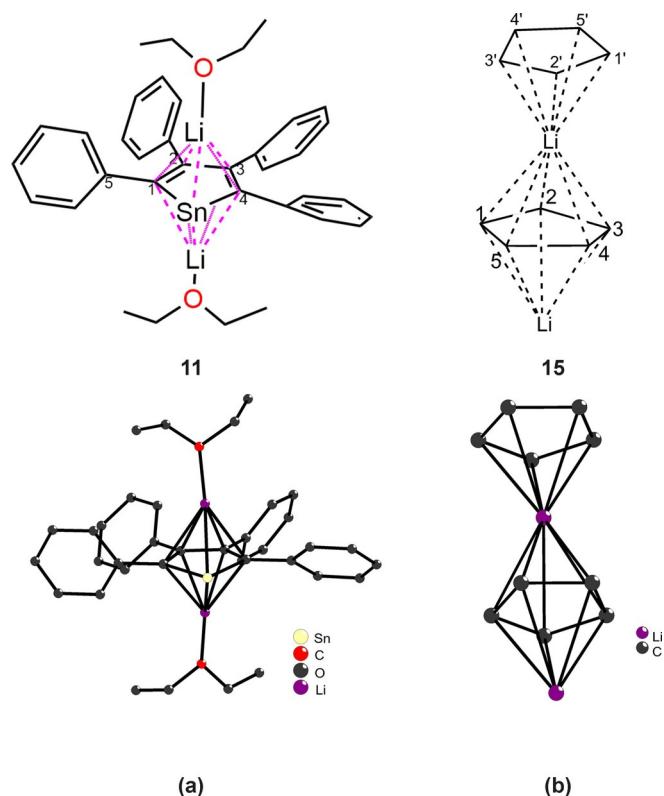


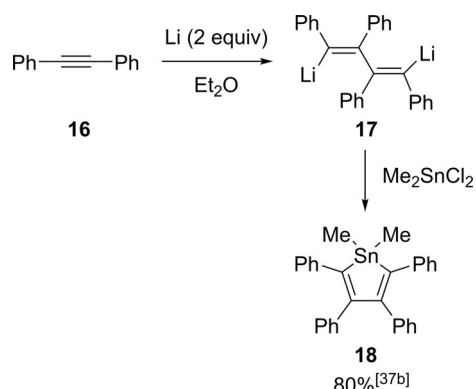
Figure 10. Representation and crystal structure from the dilithium stannole dianion **11** (a)^[36] and the cyclopentadienyl lithium **15** (b).^[34]

Comparing the ^{119}Sn NMR signal in CDCl_3 for **11** ($\delta = 163.3$ ppm) and for **14** ($\delta = -88$ ppm), dianion **11**^[36] shows a much higher aromatic character (compared with compound **7**).^[29b] Finally, a NICS value of -5.96 ppm, points to a certain aromatic character of **11**.^[31a] What this suggests is that the energy gain achieved by aromatization by deprotonating a cyclopentadiene is substantial; hence the dianion is aromatic. In contrast, aromatization is less energetically beneficial in case of a stannole anion; this is most likely caused by difficulties of orbital overlap between the π -system of the dienyl motif and the lone pair of the tin atom due to size and energy differences.

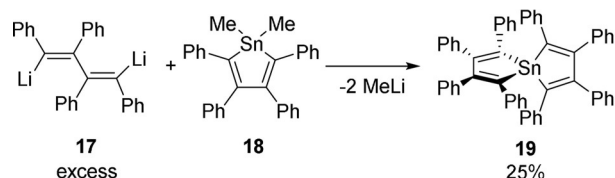
Synthesis

Unfunctionalized stannoles (type I)

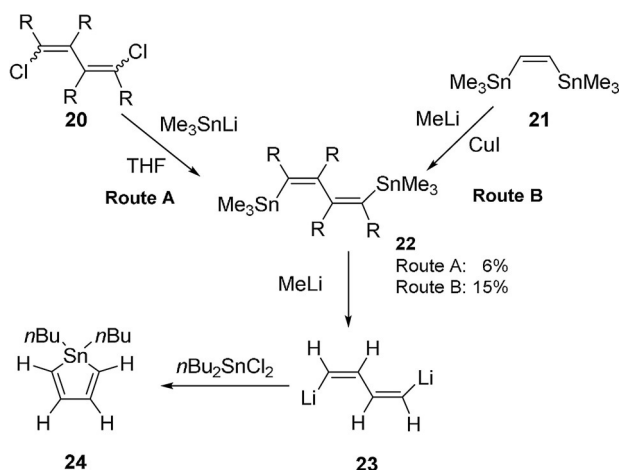
We use the term “unfunctionalized” stannoles to indicate that all substituents on the carbon atoms or the tin atom are either alkyl or aryl groups or H. To date, these constitute the majority of compounds in the class of stannoles. The synthesis of stannoles can be performed by three different routes: the first method to produce stannoles of type I was introduced by Braye and Hübel.^[37] It is based on a transmetalation reaction of 1,1-dilithio-1,2,3,4-tetraphenyl-1,3-butadiene (**17**) with dialkyl or diaryltin dichlorides to produce stannole **18**. The formation of **17** is based on reductive coupling of diphenylacetylene **16** with elemental lithium (Scheme 4). When the transmetalation



Scheme 4. Synthetic route to obtain the tetraphenyl-substituted stannole **18**, a stannole of type I.^[37a,b]



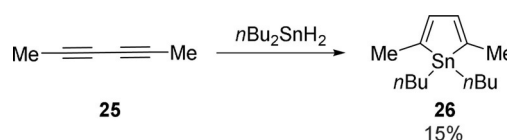
Scheme 5. Synthetic route for the preparation of spirobistannole **19**.^[38]



Scheme 6. Synthetic pathway to stannoles of type I, proposed by Ashe.^[39]

was performed with an excess of compound **17** relative to stannole **18** the octaphenyl 1,1'-spirobistannole **19** was obtained (Scheme 5).^[38]

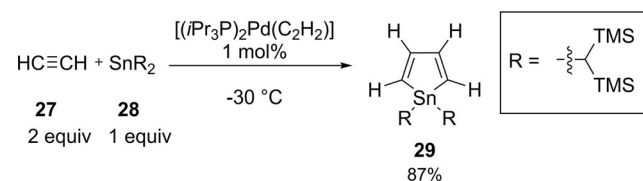
A second well-known method is the route described by Ashe and co-workers to obtain stannoles as **24**, using (1Z,3Z)-1,4-dithio-1,3-butadiene (**23**) as starting material (Scheme 6). Although the key step afforded yields between 25 and 70%, the problematic step in this route was the selective synthesis of the bis(trimethylstannyl)-1,3-butadiene **22**. When the isomeric mixture of 1,4-dichloro-1,3-butadiene **20** was allowed to react with an excess of (trimethylstannyl)-lithium in THF at -78°C (route **A**), only 6% of **22** was found in an isomeric mix-



Scheme 7. Synthetic route for the first stannole **26** that had only two substituents on the carbon scaffold.^[40]

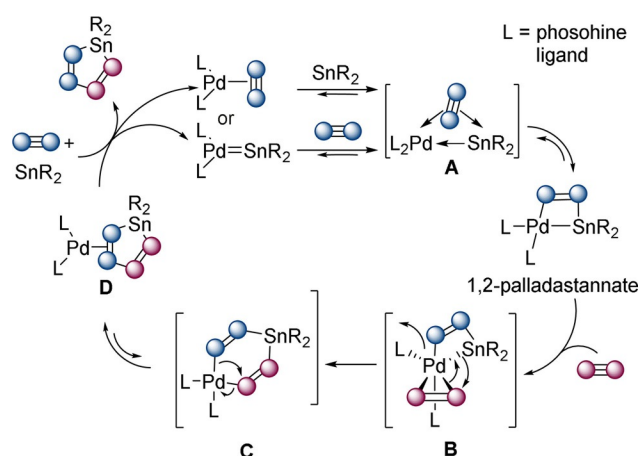
ture, which proved to be difficult to separate. The alternative reaction between (*Z*)-1,2-bis(trimethylstannyl)ethene (**21**) with MeLi and CuI (route **B**) led to **22** with a yield of only 15%.^[39] In addition, Ashe et al. developed another method to synthesize stannoles that are not fully C-substituted as in molecule **26**.^[40] This synthetic concept was based on the dihydrostannation of 2,4-hexadiyne (**25**) using dibutyltin dihydride (Scheme 7). However, the yield did not exceed 15%. **26** was the only compound which was produced by this route.^[40,41]

Pörschke and co-workers developed another method, which was based on the reaction of ethylene gas **27** with an excess of a tin analogue of a carbene: stannylene SnR_2 **28** (Scheme 8).



Scheme 8. Synthetic route for the synthesis of carbon unsubstituted stannole **29**.^[42]

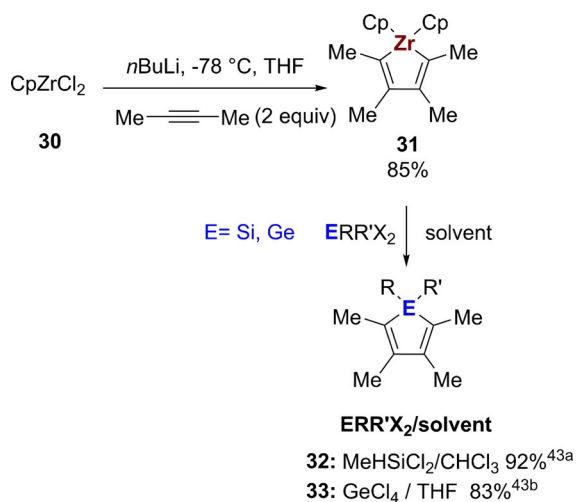
In a [2+2+1] cycloaddition reaction at -30°C utilizing a $[\text{Pd}^0]$ catalyst with bulky, monodentate ligands, stannole **29** could be obtained in an excellent yield.^[42] The mechanism of this reaction was intensely studied (Scheme 9). The palladium-catalyzed [2+2+1] cycloaddition reaction of ethyne and the stannylene starts with the formation of the labile adduct **A** from Pd^0 , SnR_2 and C_2H_2 . This adduct is converted to the corresponding 1,2-palladastannate which is the key intermediate in the cycle. The cycle proceeds with the insertion of the ethyne into



Scheme 9. Palladium-catalyzed cycle for the synthesis of stannole **29**.^[42]

the Pd–Sn bond producing an activated complex **B**. As the ethyne is coplanar with the Pd–Sn bond, it causes a ring enlargement leading to the intermediate **C**. In a following step, a nucleophilic reaction between two vinyl ligands occurs, displacing the Pd atom. Thereby Pd^{II} is reduced to Pd⁰ and the stannole is formed coordinated as a ligand. In a final step, intermediate **D** reacts with the ethyne leading to the stannole and to the complex Pd-ethyne, or a palladium-stannylene complex, which re-enter the cycle.^[42]

Fagan et al. developed a route most commonly used today. This route involves a metallacycle transfer from zirconacyclopentadiene derivatives such as **31** to main group halides. Under such conditions siloles as **32** and germoles as **33** were produced with high yields (Scheme 10).^[43] The simplicity of the synthesis to obtain zirconium derivatives makes this pathway



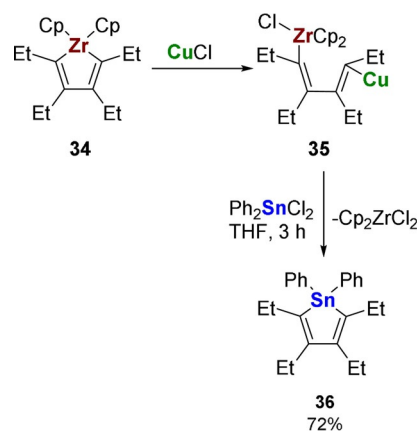
Scheme 10. General Fagan–Nugent reaction to synthesize silole **32** and germole **33**.

potentially much more convenient than the previously described routes.^[43b]

However, initially stannoles prepared under these conditions, could only be obtained in poor yields and the reaction times were between one and two days. A breakthrough was achieved in 1998, when Takahashi and co-workers added a copper(I) salt in catalytic amount to the reaction mixture of the zirconocene **34**. Scheme 11 shows the formation of the proposed intermediate **35**. A Cu–Sn transmetallation, with diphenyltin chloride and a further intramolecular cyclisation reaction of Sn–Cl with the second Zr–C bond led to stannole **36**. With these improved conditions, the reaction rates and yields of the reaction increased dramatically. With this modification, the yields typically range between 70 and 90%.^[43a,44]

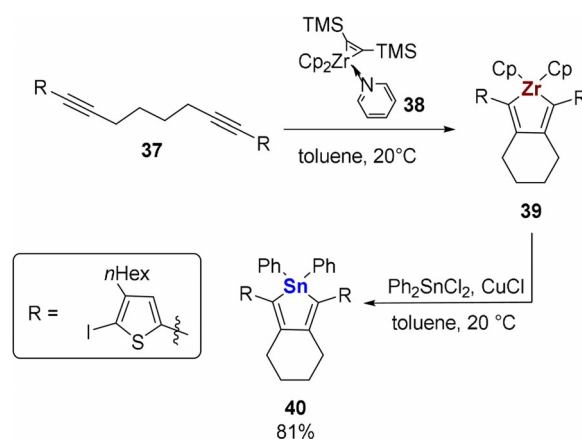
Functionalized stannoles of type II

To obtain functionalized stannoles of type II, the selection of the type of “Cp₂Zr” species is very important.^[45] The reaction between *n*BuLi and CpZrCl₂ produces the “Cp₂ZrC₄H₈” species which is called the Negishi reagent.^[46] This is the most



Scheme 11. An example of a transmetalation reaction from the zirconacyclopentadiene derivative **34** to prepare stannole **36**.^[44a]

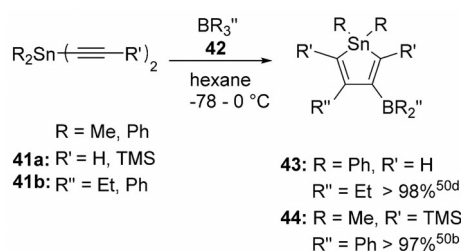
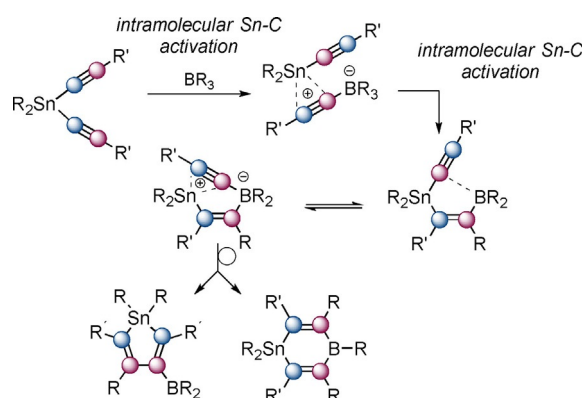
common reagent for the synthesis of zirconocenes such as **31**, which can serve as reagent to prepare unfunctionalized stannoles (e.g., **36**). However, the use of the Negishi reagent might be expected to cause problems with different functional groups in the starting material, for instance halogen groups. An alternative to this is Rosenthal’s pyridine stabilized bis(trimethylsilyl) acetylene complex **38**.^[47] Initial results suggest that the functional group tolerance is much more improved;^[48] see for example the formation of zirconocene **39** from the 1,8-ocadyne (**37**), which bears halide functionalized thiophenyl substituents (Scheme 12). Further transmetalation of **39** produced the stannole **40**.^[49]



Scheme 12. Example of the use of Rosenthal’s zirconocene **38** to obtain the stannole **40**.^[49]

Functionalized stannoles of type III

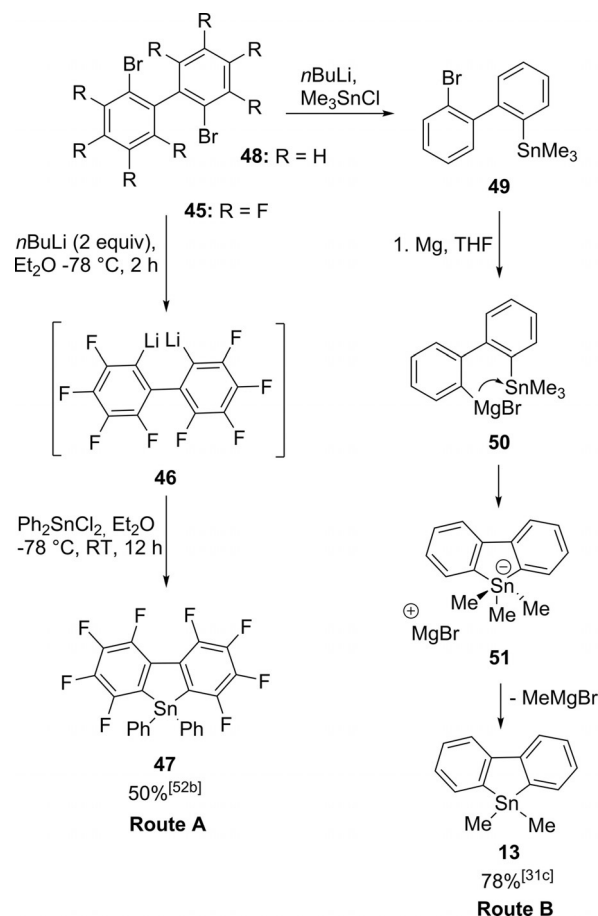
Wrackmeyer and co-workers developed a method based on a 1,1-carboboration of activated tin diacetylides **41** by electrophilic triorganoboranes **42** to prepare stannole derivatives of type II, **43**, **44** (Scheme 13).^[31b,50] Due to the high reactivity of the Sn–C(sp) bonds, the reaction takes place under relatively mild conditions. Furthermore, the isolation and structural analysis of intermediates was possible and a plausible mechanism

Scheme 13. General synthesis for Wrackmeyer-type stannoles.^[50b,d]Scheme 14. Mechanism of the 1,1-carboboration to obtain stannoles.^[51]

could be proposed. It proceeds through a two-step pathway (Scheme 14).^[51] Initially, an intramolecular activation of one of the Sn–C≡ bonds triggered by the Lewis acidic borane and a 1,1-carboboration occurs. Due to the favorable stereochemistry in a next step, the second Sn–C≡ bond is activated intramolecularly. Then a migration of the alkyne group from the tin atom to boron takes place forming a zwitterionic intermediate. In a final step, a rearrangement reaction either leads to the stanole (1,1-vinylboration) or to the stanna-4-bora-cyclohexa-2,5-diene (transfer of R). Which product is mainly formed depends on kinetic and electronic effects as well as steric repulsion.

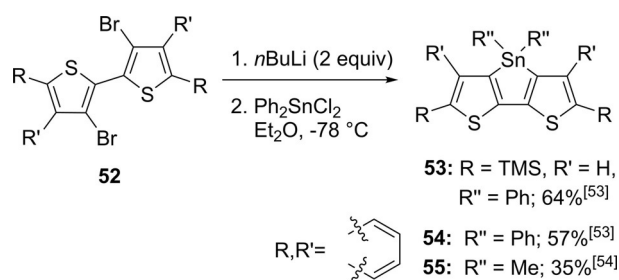
Stannafluorenes and dithienostannoles of type IV

Stannafluorenes (IV) can be synthesized by two routes (Scheme 15): route **A** is based on the lithiation of 2,2'-dibromo-octafluorobiphenyl **45** to produce the fluorinated dilithiobiphenyl **46**. Subsequent condensation with diphenyltin dichloride as an electrophile produces the dithienostannole **47**.^[52] Route **B**, on the other hand, is based on a Grignard reaction. The synthetic sequence starts from the (2'-bromo-[1,1'-biphenyl]-2-yl)trimethylstannane (**49**), which is converted to the Grignard reagent **50**. Next, in an intramolecular rearrangement reaction the carbon–magnesium bond reacts with the trimethyltin group. The formation of the intermediate **51** is favorable due to the geometric arrangement of the biphenyl system in which the two phenyl rings are no longer twisted against each other. In a final dissociation reaction, methylmag-

Scheme 15. Synthetic route for stannafluorenes **47**,^[52b] and **13**.^[31c]

nesium bromide and stanole **13** are formed in a respectable yield of 75%.^[31c,53]

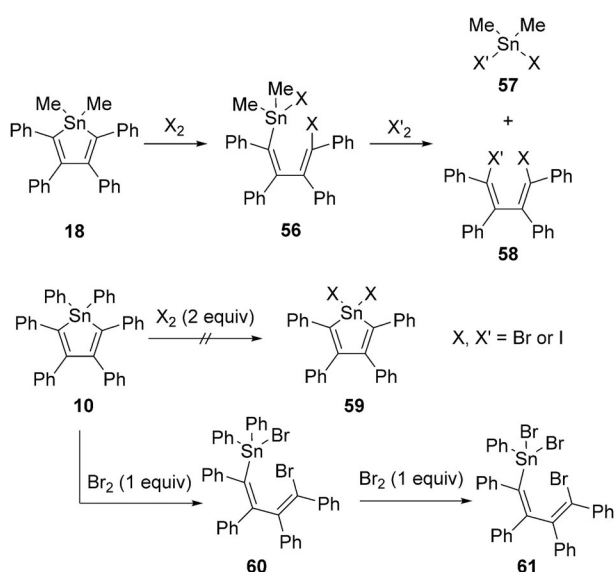
Dithienostannoles **53–55** are interesting in terms of their optoelectronic properties. Due to their planar tricyclic structure, the conjugation between the tin σ^* and the bithiophene π^* orbitals lower the LUMO energy, similar to stanholes of type I. Their synthesis (Scheme 16) follows a similar route compared to route **A** (Scheme 15).^[53,54] Physical chemical properties will be described below.

Scheme 16. Synthesis of dithienostannoles.^[53,54]

Reactivity

Halogenation of classical stanноles

Stannoles that are halogenated on the tin atom offer easy access to further substitution and functionalization. The first halogenation using elemental halogens was reported with 1,1-dimethyl-2,3,4,5-tetraphenylstannole (**18**) which led initially to an asymmetric oxidative ring cleavage (Scheme 17).^[55] This



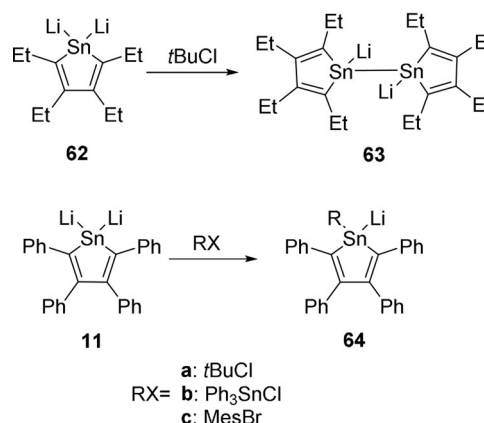
Scheme 17. Direct halogenation of stanноles with elemental halogens.^[55–57]

could then be followed by a second halogenation leading to the dihalogenated *Z,Z*-butadiene derivative **58** and the dimethyltin dihalide **57**, although the products were only identified using elemental analysis. In 1981, Zuckerman and co-workers reported a different reactivity pattern with the dihalogenation of 1,1-dialkyl-2,3,4,5-tetraphenylstannoles on the exocyclic phenyltin bond using bromine or iodine. The identification of the structure was based on Mössbauer and IR spectra. Although their structural analysis implied retention of the stanноle ring as opposed to cleavage, the assignment seemed reasonable at the time, because it was well known that halogens cleave the Sn–C bond in R_4Sn compounds, with a decreasing reactivity in the series $R = \text{aromatic rings} > \text{vinyl groups} > \text{alkyl groups}$.^[56] However, in 2001, Saito and co-workers reinvestigated this halogenation and found that this Sn-phenyl substituted stanноle was also cleaved at the ring.^[57] By performing the reaction with one or two equivalents of the halogen, they found the same reactivity as had been reported in the very first publication.^[55] Because this last study used NMR spectroscopy and single X-ray crystallography, these results are conclusive although the mechanism has not been demonstrated (homolytic vs. heterolytic cleavage of the halogen molecule, concerted or stepwise). Indeed, Zuckerman mentioned bromobenzene as a side product of the bromination, which is further evidence for the second oxidation step.

In all cases, with the first equivalent of X_2 , a Sn–C bond of the cycle is cleaved oxidatively. This process can then be followed by further degradation with either cleavage of the vinyl substituent from Sn (**58**) or halogenative cleavage of an aromatic substituent (**61**).

Reactions of stanноle salts

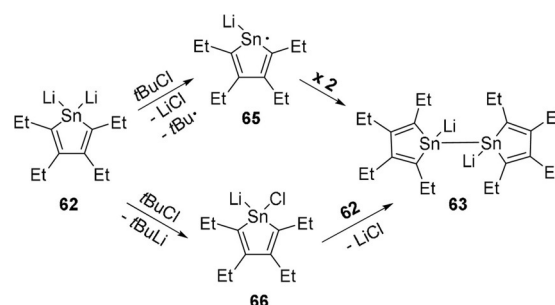
Depending on the steric environment around the tin atoms, the reactivity can vary for stanноle dianions. When the dilithiostannole **62** reacted with *tert*-butyl chloride, this reaction led to the corresponding bis(1,1'-dilithiobistannole) **63** (Scheme 18).^[36,58] Contrary to this result, when dilithiostannole



Scheme 18. Reactivity of dilithiostannoles (**62** and **11**) with bulky reagents.^[36,58]

11 reacted with *tert*-butyl chloride and other bulky halides, it underwent monosubstitution producing **64**. The evidence for **64b** and **64c** could only be observed by NMR spectroscopy. Isolation of the complexes was not possible.^[33a,36]

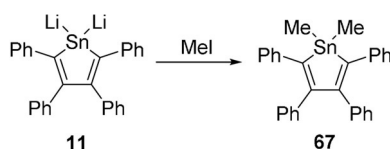
The reaction mechanism of the formation of **63** has not been elucidated yet, but two plausible possibilities have been proposed (Scheme 19).^[58] In the first one, a Sn-centered radical **65** would be formed that could then dimerize to give **63**. The second pathway involves a nucleophilic attack of **62** on *tert*-butyl chloride giving **66**, this one in turn would react with **62** again, also by nucleophilic substitution to yield the product **63**. In the case of the reaction of the dilithiostannole **11** with



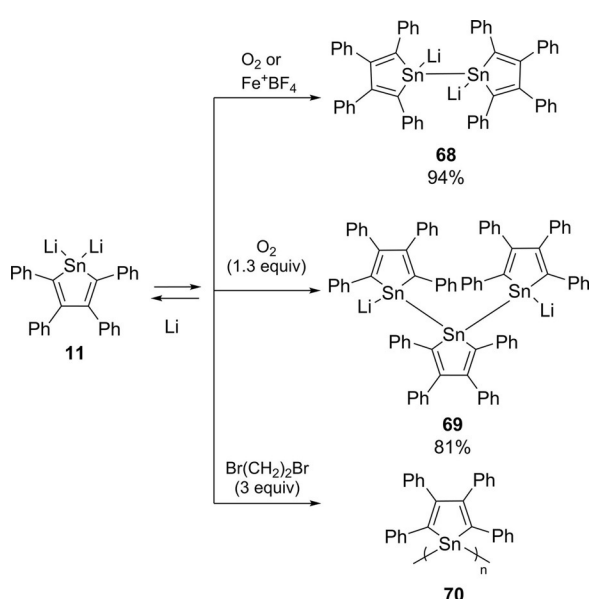
Scheme 19. Plausible mechanisms for the formation of **63**. Adapted with permission from reference [58]. Copyright (2010) The Chemical Society of Japan.

methyl iodide, a double substitution at the tin atom took place, forming 1,1-dimethylstannole **67** (Scheme 20).^[36] If **11** was reacted with different quantities of oxidizing agents, it afforded 1,2-dilithiobistannoles **68**, 1,3-dilithiostannoles **69** and the unstable poly(1,1-stannole) **70** (Scheme 21).^[59]

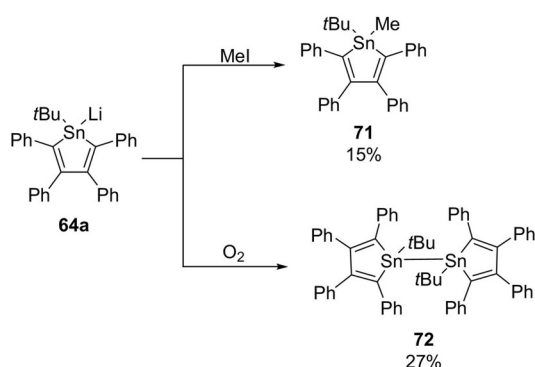
The *Sn-tert-butyl-Sn-lithiostannole* **64a** can react with MeI to produce **71** or, if it is exposed to air, 1,1-bistannoles **72** (Scheme 22).^[33a] When the stannole monoanion **14** reacted with 1,6-dibromohexane, bis(stannole) **73** was formed in which the two rings are connected by an alkyl chain (Scheme 23); this is contrary to the reaction of the dianionic stannole **11**. However when **14** was exposed to air, the dimer **74** was produced similar to the formation of **72**.^[33a]



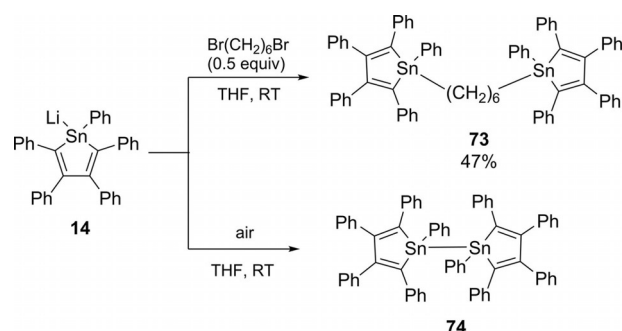
Scheme 20. Substitution reaction of the dilithiostannole **11** with MeI.^[56]



Scheme 21. Reactions of the dilithiostannole **11** with oxidizing agents.^[59]



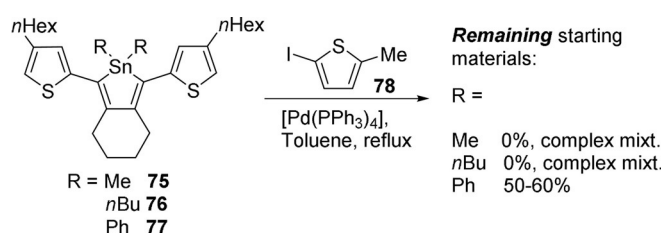
Scheme 22. Reaction of lithiostannole **64a** with MeI or air.^[33a]



Scheme 23. Reaction of the monoanion of stannole **14** with oxidants.^[33a]

Reactions of functionalized stannoles of type II

To show the importance of stabilizing groups on the Sn center in the stannole ring, investigations into reactions under cross coupling conditions with different stannoles (**75–77**) and 2-iodo-5-methylthiophene (**78**) were performed by our group (Scheme 24).^[49] When the substituents on the tin atom were only alkyl groups, NMR studies revealed that almost no starting

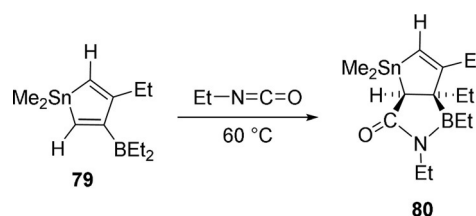


Scheme 24. Cross coupling reactions of stannoles **75–77**.^[49]

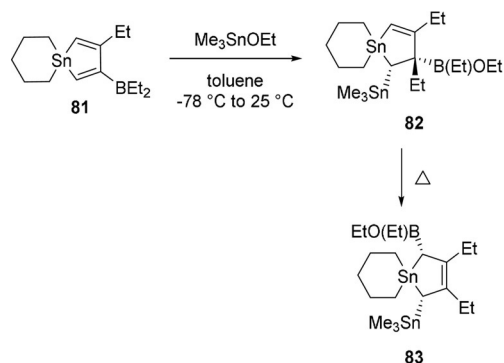
material of stannoles **75** or **76** was present in the complex reaction mixture (>99% had reacted): The Sn center in the ring could easily react. By comparison, with stannole **77**, only 40 to 50% was consumed. Thus sterically hindering phenyl groups at the Sn atom led to a higher kinetic stability.

Reactions of functionalized stannoles of type III

Compounds of type III contain a functional group on the stannole ring; to date, just a few examples of such stannoles exist. If this functional group is a boron atom, which is electrophilic, further transformations with nucleophilic centers are possible. One example was the reaction between **79** and isocyanatoethane (Scheme 25). In this reaction, the nitrogen and carbonyl carbon acted as nucleophilic and electrophilic centers, respec-



Scheme 25. Reaction of stannole **79** with isocyanates.^[50d]



Scheme 26. Reaction of the spiro-stannole **81** with trimethyltin ethoxide.^[50a]

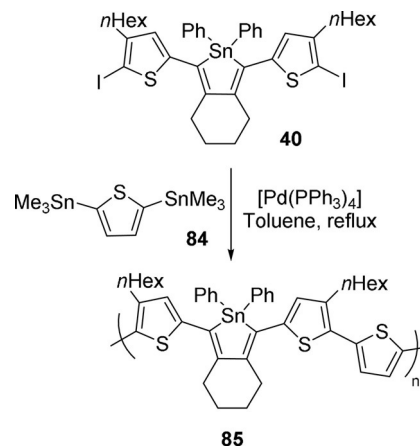
tively. The nitrogen could attack the boron, thus functioning as a nucleophile; one of the alkyl chains on boron then migrated to the adjacent carbon, rendering the β -carbon in the stannole ring a nucleophile that could attack the carbonyl group, giving the 1-stannacyclopent-2-ene derivative **80**.^[50d]

Another example was the reaction of the spiro tin compound **81** with the ambiphilic reagent trimethyltin ethoxide (Scheme 26). The ethoxy group reacted with the boryl group. At the same time, a 1,2-shift of one ethyl group from the boron center to the carbon took place. The spiro compound **82** that was formed under heating conditions underwent an irreversible allylic rearrangement of the boryl group affording the spiro tin compound **83** with a 3-stannole unit.^[50a]

Stannoles in polymers

To harvest the potential of optoelectronic properties of stan- noles, processing is a very important aspect. Polymers can be easily spin-coated and are often able to form stable polymer films. Moreover, if the stannole was to be incorporated in a fully conjugated backbone, a π -system that is more extended than that of the monomer might result, leading to further bathochromic shifts. Such polymers are typically accessed by cross-coupling polymerization reactions. However, in the case of a stannole containing monomer, this approach presented a substantial challenge; it had to be considered that not only $R_3Sn-Ar-SnR_3$ groups of the co-monomer would react, but also that the stannole ring might open. Indeed, for stannafluorenes, this type of reaction has already been successfully employed to produce triphenylene (see section on stannafluorenes below).^[53] To overcome this issue, a highly nucleophile selective cross-coupling reaction had to be performed that would not only leave the stannole intact, but would also be highly effective because the length of a polymer using step growth polycondensation methods depends on the conversion of the polymerization reaction (Carothers equation).^[48, 60]

A thiophene flanked stannole monomer with peripheral iodide functional groups **40** as an electrophilic component and a bis(ditrimethyltin) thiophene **84** as the nucleophilic monomer allowed the successful preparation of the polymer **85** using a Stille cross-coupling reaction (Scheme 27).^[49] The dark purple polymer had a relatively high molecular weight of $M_w =$

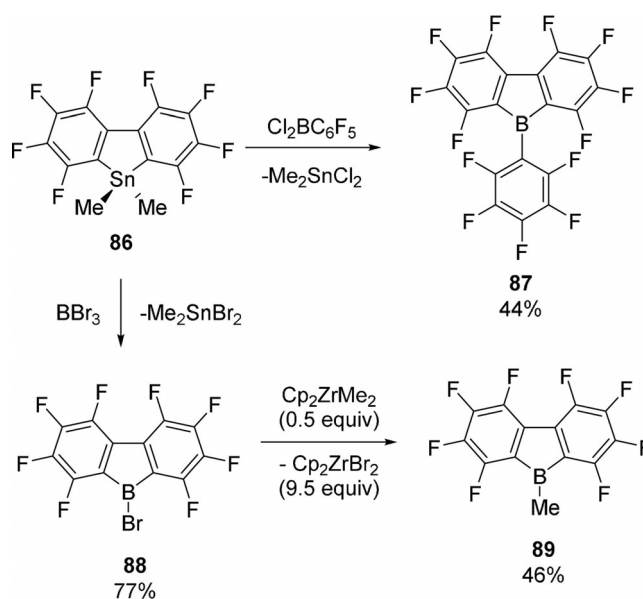


Scheme 27. Selective Stille cross-coupling reaction of stannole **40** to afford polymer **85**.^[49]

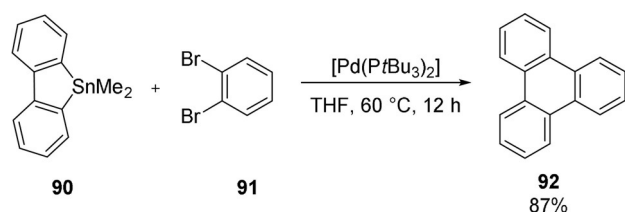
17.0 kDa (gel permeation chromatography standard calibration against polystyrene), which demonstrates the very high selectivity of the reaction even under harsh conditions, that is, refluxing toluene. For the optoelectronic properties of this polymer, see below.

Reactions of stannafluorenes of type IV

Because tin can be easily transmetallated to boron, relatively stable organotin heterocycles can be used as convenient precursors for borafuorenes. 9-Stannafluorene **86** was used in the boron–tin exchange reaction to prepare a new 9-borafuorene **87**.^[61] The product **88** from the reaction between **86** and BBr_3 can be methylated with $Cp_2Zr(Me)_2$ to produce **89** (Scheme 28). Both 9-borafuorenes can be used as Lewis acids in the activation of metallocenes for olefin polymerization processes.



Scheme 28. Synthetic route for the synthesis of 9-borafuorenes **87** and **89**.^[61]



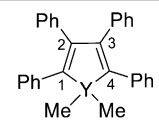
Scheme 29. Example of the use of a stannafluorene **90** for the preparation of triphenylene **92**.^[53]

In stannafluorenes, the two aromatic submotifs can almost be viewed as independent aromatic systems. From this perspective, the tin atom is comparable to a standard nucleophilic functional group of the type ArSnR_3 . Using this concept, a double cross-coupling reaction of stannafluorene **90** with dibromobenzene (**91**) has been used to perform an aromatic anelation and triphenylene **92** was formed (Scheme 29).^[53] Further work using this strategy followed.^[62]

Physicochemical Properties

In general, tetra phenyl dimethylcyclopentadiene **93** and its silicon, germanium and tin analogues exhibit almost C_{2v} symmetry, at least in solution. Therefore, the ^{13}C NMR shifts of C1/C4 and C2/C3 are similar. In the case of Si, Ge and Sn as metal atoms in heteroles, the C2 and C3 atom are increasingly more deshielded and the corresponding signals can be found as downfield-shifted signals (Table 1). Although the trend is also

Table 1. NMR data of several heteroles of group 14 elements.

Compound	$\text{Y}^{[a]}$			
		$\delta(^{13}\text{C})$: C1,C4 [ppm]	$\delta(^{13}\text{C})$: C2,C3 [ppm]	$\delta(^{13}\text{C})$: Me [ppm]
93 ^[b]	C	152.34	140.16	22.19
94 ^[c]	Si	153.90	141.80	−3.90
95 ^[c]	Ge	151.20	143.90	−2.54
18 ^[c]	Sn	153.57	144.91	−7.75

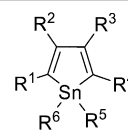
[a] Measured in CDCl_3 . [b] See reference [63]. [c] See reference [32].

observed for C1 and C4, germoles are an exception. The ^{13}C atoms of the methyl carbons experience more shielding, the heavier the group 14 element, with germoles exhibiting again a slightly smaller effect than expected. The difference between the shift for the methyl carbon of the cyclopentadiene **93** (22.19 ppm)^[63] and the silanole **94** (−3.90 ppm)^[32] is by far the largest.

For stannoles, the coupling of ^{13}C atoms with ^{117}Sn and ^{119}Sn isotopes is significant. For compound **18**, the $J_{\text{Sn-C}}$ coupling values depend on the magnitude of coupling. For the coupling of the tin atom with the neighboring C1 or C4 atoms, values of $^1J(^{119}\text{Sn}-^{13}\text{C})=209$ Hz and $^1J(^{117}\text{Sn}-^{13}\text{C})=119$ Hz could be ob-

served. Tin/carbon spin coupling towards the methyl substituents shows values of $^1J(^{119}\text{Sn}-^{13}\text{C})=166$ Hz and $^1J(^{117}\text{Sn}-^{13}\text{C})=159$ Hz. $^2J_{\text{Sn-C}}$ values for the coupling of the tin atom with C2 and C3 atoms are smaller with $^2J(^{119/117}\text{Sn}-^{13}\text{C})=41$ Hz.^[32] In general, the carbon atoms of the stannole ring have ^{13}C NMR shifts ranging from 120 to 175 ppm. C2/C3 carbon atoms are the most deshielded inside the ring. The ^{119}Sn NMR signals of common stannoles can range from about 20 ppm to −90 ppm. Due to the distortion in type I stannoles, such as in **10** and **18**, a weak π -interaction with the phenyl ring is observed. This leads to a decrease of electron density in stannoles and a higher chemical shift of the resulting carbon atoms in the ^{13}C NMR spectrum. A change from an aromatic to an alkylic substituent at the tin atom leads to a downfield shift in the ^{119}Sn NMR spectrum (from −88.0 for **10** to −52.0 for **18**)^[31a,64] (Table 2).

Table 2. NMR data of stannoles type I.

Compound			$\delta(^{119}\text{Sn})$	$\delta(^{13}\text{C})$	$\delta(^{13}\text{C})$
	$\text{R}^{1,2,3,4}$	$\text{R}^{5,6}$	[ppm]	C1,C4 [ppm]	C2,C3 [ppm]
10 ^[a,d]	Ph	Ph	−88.0	143.00	155.00
18 ^[b,e]	Ph	Me	−52.0	144.91	153.57
24 ^[a,f]	H	<i>n</i> Bu	− ^[i]	131.60	145.60
29 ^[c,g]	H	$\text{CH}(\text{SiMe}_3)_2$	− ^[i]	137.50	144.80
96 ^[a,h]	TMS	Ph	−3.0	145.09	168.80

[a] Measured in CDCl_3 . [b] Combined data set. [c] Measured in $[\text{D}_8]\text{THF}$. [d] See reference [31a]. [e] See references [32,65]. [f] See reference [39]. [g] See reference [42]. [h] See reference [66]. [i] Not measured.

For stannoles **24** and **29**, which have unsubstituted positions on the ring, the protons showed ^1H NMR shifts between 7.15–6.50 ppm (Figure 11).^[39,42] If alkyl groups are attached to the tin

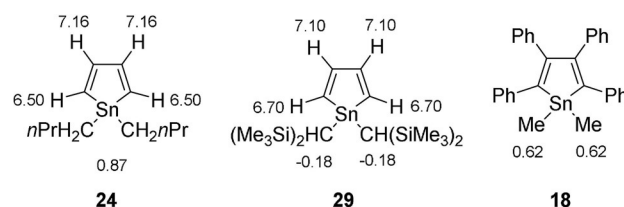
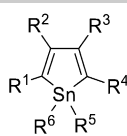


Figure 11. ^1H NMR chemical shifts of stannoles **24**, **29** and **18**.

atom of a stannole, as in **24** (Bu) or **18** (Me), their methylene, or methyl protons, respectively, were shielded and displayed shifts in the range of $\delta(^1\text{H})=0.87$ – 0.62 ppm. In the case of stannole **29**, the methine proton of the bis(trimethylsilyl)-methylene moiety was observed at −0.18 ppm. Due to shielding effects, the respective ^{13}C NMR shifts of the methyl carbon atom tend to be negative, for example, −7.75 ppm in the methyl group of **18**.

Table 3. NMR data of stannoles type II.


Compound	R ^{1,4}	R ^{2,3}	R ^{5,6}	$\delta(^{119}\text{Sn})$ [ppm]	$\delta(^{13}\text{C})$ C1,C4 [ppm]	$\delta(^{13}\text{C})$ C2,C3 [ppm]
14 ^[a,d]	Ph	Ph, Li		-28.6	176.47	133.46
11 ^[b,e]	Ph	Li, Li		163.3	183.68	150.47
97 ^[c,f]	TMS	Ph	Li, Li	446.4	182.38	146.23

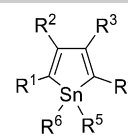
[a] Measured in THF/C₆D₆. [b] Measured in Et₂O/C₆D₆. [c] Measured in C₆D₆. [d] See reference [33a]. [e] See reference [31a]. [f] See reference [66].

For type II stannoles, a high diversity of NMR shifts was observed. In particular, the ¹¹⁹Sn NMR shifts give an idea about the electronic neighborhood of the tin atom (Table 3). For the mono- and dilithiated phenyl substituted stannoles **14** and **11** ¹¹⁹Sn NMR shifts of -28.6 ppm and 163.3 ppm were observed.^[31a,33a] In comparison to stannole **10**, which has a ¹¹⁹Sn NMR shift of -88.0 ppm, the shifts of the stannole monoanion **14** and dianion **11** were observed downfield. This very strong downfield shift (163.3 ppm) of **11** was attributed to the resonance stabilization of a delocalized stannylene structure. With forming the lithium salts, the most deshielded carbon atom was now the one which was directly attached to the tin atom: $\delta(^{13}\text{C})$ for C1,C4 in **14** was observed at 176.47 ppm and for the dilithiated stannole **11**, a shift of 183.68 ppm was observed.

An abnormally high ¹¹⁹Sn NMR spectroscopic shift was observed for compound **97** with 446.4 ppm, which was highly shifted from its starting material **96** with a ¹¹⁹Sn NMR shift of -3.0 ppm.^[66] This was explained by the extended interaction of the butadiene LUMO and the 5p orbital of the tin atom forming a stannylene. Thus, the LUMO is stabilized by silyl substituents at C1 and C4.^[66] The ¹³C NMR shifts of C1 and C4 from compound **11** and **97** were found to be nearly the same (183.68 ppm vs. 182.38 ppm), but their ¹¹⁹Sn NMR shift differed (163.3 ppm vs. 446.4 ppm).

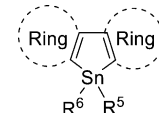
The boron-functionalized stannoles **79** and **81** showed a downfield shift of the C2 and C3 atoms in the ¹³C NMR spectrum. Due to the quadrupole effect of the boron atom adjacent to the C2 atom, the signal showed a significant broadening. The ¹H NMR shifts of the aromatic protons occurred in the aromatic region, for example, for **79** 6.07 ppm (Table 4).^[67] The increased shielding in the ¹¹⁹Sn NMR spectrum from **81** to **79** (by approximately 41 ppm) was caused by the integration of the tin atom in a six-membered ring, whereas the ¹³C NMR shifts of the stannole carbon atoms remained nearly the same.^[50a,b]

Depending on the chemical environment the most downfield shift of the ¹¹⁹Sn NMR signal can be found for type IV stannoles, for example, dithienostannoles ($\delta(^{119}\text{Sn})$) for **54** was -153.50 ppm and for **55** -145.72 ppm; Table 5).^[54] In the form of the lithium salts, such as in compound **98**, the ¹¹⁹NMR shift can reach values up to -210.60 ppm (Table 5).^[68] Due to the addition of electron density coming from the phenyl/thio-

Table 4. NMR data of stannoles type III.


Compound	R ^{1,4}	R ^{2,3}	R ^{5,6}	$\delta(^{119}\text{Sn})$ [ppm]	$\delta(^{13}\text{C})$ C1,C4 [ppm]	$\delta(^{13}\text{C})$ C2,C3 [ppm]
79 ^[a,b]	H	BEt ₂ /Et	Me	19.1	127.6, 120.8	177.0, 164.5
81 ^[b,c]	H	BEt ₂ /Et	-(CH ₂) ₅ -	-21.7	126.6, 119.5	175.0, 162.4

[a] Measured in CH₂Cl₂/C₆D₆. [c] Measured in [D₈]toluene. [b] See reference [67]. [c] See reference [50a].

Table 5. NMR data of stannoles of type IV.


Compound	Ring	R ^{2,3}	$\delta(^{119}\text{Sn})$ [ppm]	$\delta(^{13}\text{C})$ C1,C4 [ppm]	$\delta(^{13}\text{C})$ C2,C3 [ppm]
13 ^[a,c]	benzo	Me	-30.95	140.81	148.15
54 ^[a,d]	thieno	Ph	-153.50	- ^[f]	- ^[f]
55 ^[a,d]	thieno	Me	-145.72	- ^[f]	- ^[f]
98 ^[b,e]	thieno	Ph, Li	-210.60	- ^[f]	- ^[f]

[a] Measured in CDCl₃. [b] Measured in DME with [D₆]acetone. [c] See reference [31c]. [d] See reference [54]. [e] See reference [68]. [f] Not reported.

phene rings, the incorporation of the tin atom in fluorene **13** or dithieno substituents results in an increased shielding effect.^[31c]

In general, the infrared spectra of siloles, germanoles and stannoles show nearly the same absorption bands. A shift towards higher wavenumbers of the symmetrical methyl $\tilde{\nu}(\text{C}-\text{H})$ vibration in the case of molecules **94**, **95** and **18**, which correlates with the mass of the central metal atom could be observed. The values of these vibration bands are 2958/2898 cm⁻¹ for **94** 2976/2906 cm⁻¹ for **95** and 2990/2921 cm⁻¹ for stannole **18**.^[32] One of the most important IR signals in stannoles is the stretching band of the C=C bond with a range between 1560 and 1600 cm⁻¹. Antisymmetric and symmetric aromatic C-H stretching absorption bands appear between 3080 and 3010 cm⁻¹.^[32]

Stannoles of type **40** are both suitable for electron impact (EI) ionization and electrospray ionization (ESI) mass spectrometry. With both methods, molecule ions ($[M]^+$ for EI ionization and $[M+H]^+$ for ESI) can typically be detected with typical isotope distribution for tin. A typical fragmentation pattern is the loss of the SnR₂ fragment.^[49]

Optoelectronic properties

As explained previously, stannoles have a low-lying LUMO in comparison to their carbon cyclopentadiene analogues. This

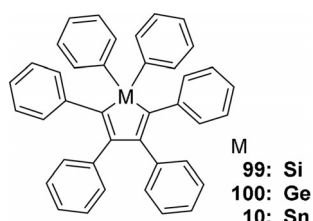


Figure 12. Hexaphenylmetalloles with heavier group 14 elements.

leads to an unusual broad and long-wavelength absorption compared to the carbon analogues. For metalloles $R_2MC_4Ph_4$ with $R=Me$ or Ph and $M=Si, Ge, Sn$, the luminescence has also been studied (Figure 12).^[32] After irradiation, an intermediate state is reached that in the case of $R=Ph$ is the emissive state. It appears that R_2M affects the vibronic states of the molecule and for Me_2Sn quenches luminescence entirely. In the case of stannoles, it is instructive to compare their optoelectronic properties with other heavier element cyclopentadiene analogues (Si, Ge).^[22,69] Theoretical studies on heavier group 14 metalloles ($M=Si, Ge, Sn$) showed that the HOMO–LUMO gap increases slightly in the order $99 < 100 < 10$ from 3.58 to 3.73 eV. This phenomenon could be observed because of the already mentioned lower $\sigma^*-\pi^*$ interaction as a consequence of the longer C–M bond (see section on $\sigma^*-\pi^*$ conjugation).^[69] Comparisons of their absorption spectra show that the absorption maximum is bathochromically shifted in the order $10 < 100 < 99$ from 379 to 405 nm theoretically and from 355 to 360 nm experimentally. In general, all showed the unusual broad absorption maximum. Although **10** and **99** have similar emission maxima (549 nm and 547 nm theoretically 494 nm and 496 nm exp.), the maximum of **100** is slightly hypsochromically shifted to 529 nm (experimentally 486 nm).^[70]

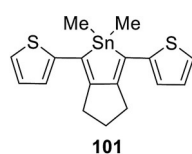


Figure 13. Stannole **101** with thienyl substituents.^[22]

If stannoles contain π -conjugated substituents connected to carbon atoms of the ring, their optoelectronic properties can change dramatically, most often further reducing the HOMO–LUMO gap.^[71] In the case of stannole **101** (Figure 13), the interaction between the σ^* orbital and the π^* orbital is increased for Sn compared to Ge and Si because the σ^* level becomes closer to the π^* orbital level

from the thienyl groups and the structure becomes more planar. The absorption spectra showed two peaks at 406 and 430 nm; and the fluorescence spectra one peak at 479 nm ($\Phi_f = 0.495 \times 10^{-2}$).^[22]

The stannafluorene **47** showed a wide HOMO–LUMO gap (3.95 eV), and a low lying LUMO (–2.60 eV). However the solid state study showed that these molecules were aligned in two nearly parallel directions blocking the π fluorene–fluorene cofacial packing. 2,7-Di(phenylethynyl)hexafluorostannafluorene (**102**), on the other hand, exhibited a unidirectional π -stacking, which may enhance charge transport (Figure 14). With a band gap of 3.2 eV and a LUMO of –2.8 eV, the stannafluorene **102**

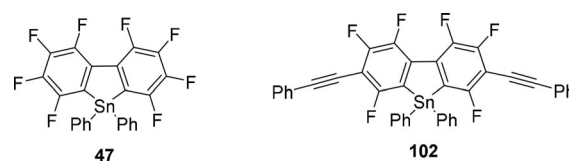


Figure 14. Stannafluorenes **47** and **102**.^[52b]

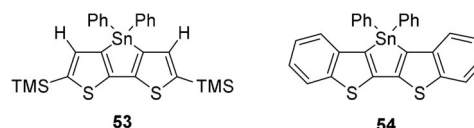


Figure 15. Dithienostannoles **53** and **54**.^[54]

might be used as a n-type semiconducting material in organic electronics.^[52b]

Further dithienostannoles **53** and **54** were investigated in terms of their optical properties and crystal structures supported by quantum chemical calculations (Figure 15). Compound **53** exhibited a low intensity emission in solution ($\lambda_{em,max} = 410$ nm, $\Phi_f = 0.009$), a slightly higher emission intensity in the solid state ($\lambda_{em,max} = 411$ nm, $\Phi_f = 0.028$) and a high emission intensity in the crystalline state ($\lambda_{em,max} = 422$ nm, $\Phi_f = 0.556$). The bathochromic shift of the emission maximum and the higher fluorescence quantum yield is attributed to crystallization-enhanced emission. Compound **54** showed a slightly different behavior in solution and in the crystal state; the maximum of emission was observed at 431 and 454 nm, respectively, whereas the quantum yield of **53** in solution was higher than in the crystal state ($\Phi_f = 0.296$ and $\Phi_f = 0.214$).^[54]

When a stannole was incorporated into the backbone of a polymer **85**,^[49] the absorption in solution was drastically bathochromically shifted ($\lambda_{abs,max}$ 536 nm) compared to the starting material **40** ($\lambda_{abs,max}$ 441 nm; Figure 16). The absorption of the thin films of the polymer (Figure 17) was shifted even more ($\lambda_{abs,max}$ 536 nm), which may be explained by the increased coplanarity of the thiophene–stannole rings in solid state. This enhances the π -conjugation through the material and the poly-

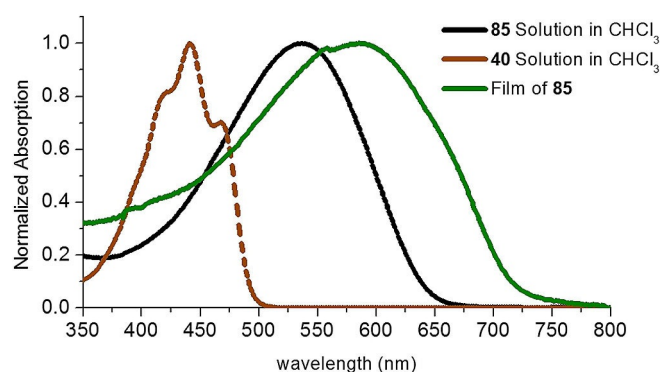


Figure 16. UV/Vis spectra of the monomer **40** and the polymer **85** in chloroform and as a thin film. Adapted from reference [49].



Figure 17. Film of the polymer **85**.^[49]

mer **85** may be used as semiconductor in organic electronics (Figure 17).^[49,71]

As known for group 14 heteroles, stannoles exhibit aggregation-induced emission (AIE).^[72] Although siloles display intense AIE effects, the effect is much less pronounced in germoles and stannoles. Stannoles show the longest emission wavelength in comparison with siloles and germoles but are less efficient in terms of fluorescence quantum yields. This has been attributed to the heavy atom effect. Stannoles **18** and **10** exhibit fluorescence quantum yields in the aggregated state of 0.4 and 0.10%, respectively, which is only 10-fold higher than in solution (0.04 and 0.010%, respectively). In comparison, the luminescence quantum yield of silole **94** increased from 0.11% in solution to 16% by AIE. The optoelectronic properties of stannoles and stannafluorenes are quite different from that of their lower homologs and they represent very interesting systems to study. The scarcity of the data reported to date demonstrates that much more research in this area is needed.

Summary

Stannoles can be defined as cyclopentadiene analogues with some electron-delocalization behavior despite a tetravalent group 14 element in the ring. For this, two different models, $\pi^*-\sigma^*$ conjugation and the Ottosson valence structure model are discussed and backed up by several experimental techniques (XRD, NMR, IR and NICS). Although this is unusual and a direct consequence of tin being a heavy atom, classical Hückel aromaticity can also occur, but in the stannole dianion and not in the monoanion.

The compound class of stannoles and the related fluoreno-stannoles can be sorted into four main types of stannoles, depending on their structure and functionalization. Typical synthetic routes with their advantages and pitfalls are assessed and compared. We highlight areas of research in which only little is known and in which we hope to inspire further research from the community. Not only improved yields are desirable in many cases, but also the exploration of new reactivities, especially for functionalized stannoles. So far, in a highly selective synthesis a stable stannole based polymer with a very high absorption and film forming properties has been produced.

The optoelectronic properties of stannoles are unusual; often they show broad absorption bands in UV/Vis spectroscopy and are bathochromically shifted compared to carbon analogues. Aggregation-induced emission is a common feature, although quantum yields are lower than for lower homologs of

tin. To give the practitioner useful guidelines, typical analytical properties have been reviewed. However, the most interesting properties are the absorption characteristics of these materials because they may pave the way for future potential applications as well as unusual discoveries in fundamental main group chemistry.

Acknowledgements

S.U.R. thanks the German Academic Exchange Service (DAAD) and the Colfuturo Fund for a Ph.D. scholarship. Grant number: A/13/72356. This research has been supported by the Institutional Strategy of the University of Bremen, funded by the German Excellence Initiative.

Conflict of interest

The authors declare no conflict of interest.

Keywords: aromaticity · heterocycles · optoelectronic properties · stannoles · tin

- [1] For the unsubstituted cyclopentadiene, see: a) R. W. Holder, J. P. Daub, W. E. Baker, R. H. Gilbert, N. A. Graf, *J. Org. Chem.* **1982**, *47*, 1445–1451; b) for the 2,3,4,5-tetraphenylcyclopentadiene, which is closely related to many of the stannoles presented here, λ_{\max} in an alcoholic solvent is 328 nm, the molar extinction coefficient and the pK_a have not been described: W.-T. Gong, X.-C. Li, G.-L. Ning, Y. Lin, *J. Chem. Res.* **2004**, *2004*, 444–444.
- [2] a) A. Streitwieser, L. L. Nebenzahl, *J. Am. Chem. Soc.* **1976**, *98*, 2188–2190; b) F. G. Bordwell, M. J. Bausch, *J. Am. Chem. Soc.* **1983**, *105*, 6188–6189.
- [3] a) S. Yamaguchi, K. Tamao, *Dalton Trans.* **1998**, 3693–3702; b) G. W. Parshall, *Organometallics* **1987**, *6*, 687–692.
- [4] J. Jagur-Grodzinski, *Polym. Adv. Technol.* **2002**, *13*, 615–625.
- [5] M. Hissler, P. W. Dyer, R. Réau, *Coord. Chem. Rev.* **2003**, *244*, 1–44.
- [6] B. L. Lucht, M. A. Buretea, T. D. Tilley, *Organometallics* **2000**, *19*, 3469–3475.
- [7] a) P. P. Power, *Chem. Rev.* **1999**, *99*, 3463–3504; b) E. Rivard, P. P. Power, *Inorg. Chem.* **2007**, *46*, 10047–10064.
- [8] a) A. D. Phillips, R. J. Wright, M. M. Olmstead, P. P. Power, *J. Am. Chem. Soc.* **2002**, *124*, 5930–5931; b) L. Pu, A. D. Phillips, A. F. Richards, M. Stender, R. S. Simons, M. M. Olmstead, P. P. Power, *J. Am. Chem. Soc.* **2003**, *125*, 11626–11636.
- [9] G. Maier, G. Mihm, H. P. Reisenauer, *Chem. Ber.* **1982**, *115*, 801–803.
- [10] G. Maier, K. Schöttler, H. P. Reisenauer, *Tetrahedron Lett.* **1985**, *26*, 4079–4082.
- [11] a) Y. Kabe, K. Ohkubo, H. Ishikawa, W. Ando, *J. Am. Chem. Soc.* **2000**, *122*, 3775–3776; b) N. Nakata, T. Oikawa, T. Matsumoto, Y. Kabe, A. Sekiguchi, *Organometallics* **2005**, *24*, 3368–3370.
- [12] K. Wakita, N. Tokitoh, R. Okazaki, N. Takagi, S. Nagase, *J. Am. Chem. Soc.* **2000**, *122*, 5648–5649.
- [13] For example see: a) N. Tokitoh, K. Wakita, R. Okazaki, S. Nagase, P. von Ragué Schleyer, H. Jiao, *J. Am. Chem. Soc.* **1997**, *119*, 6951–6952; b) N. Takeda, A. Shinohara, N. Tokitoh, *Organometallics* **2002**, *21*, 256–258; c) N. Takeda, A. Shinohara, N. Tokitoh, *Organometallics* **2002**, *21*, 4024–4026.
- [14] a) K. Abersfelder, A. J. P. White, H. S. Rzepa, D. Scheschkewitz, *Science* **2010**, *327*, 564–566; b) C. Gerdes, T. Müller, *Angew. Chem. Int. Ed.* **2010**, *49*, 4860–4862; *Angew. Chem.* **2010**, *122*, 4978–4981.
- [15] C. P. Sindlinger, L. Wesemann, *Chem. Sci.* **2014**, *5*, 2739–2746.
- [16] a) D. Kratzert, D. Leusser, J. J. Holstein, B. Dittrich, K. Abersfelder, D. Scheschkewitz, D. Stalke, *Angew. Chem. Int. Ed.* **2013**, *52*, 4478–4482; *Angew. Chem.* **2013**, *125*, 4574–4578; b) K. Abersfelder, A. J. P. White,

- R. J. F. Berger, H. S. Rzepa, D. Scheschkewitz, *Angew. Chem. Int. Ed.* **2011**, *50*, 7936–7939; *Angew. Chem.* **2011**, *123*, 8082–8086; c) A. Jana, V. Huch, M. Repisky, R. J. F. Berger, D. Scheschkewitz, *Angew. Chem. Int. Ed.* **2014**, *53*, 3514–3518; *Angew. Chem.* **2014**, *126*, 3583–3588.
- [17] A. Sekiguchi, T. Yatabe, C. Kabuto, H. Sakurai, *J. Am. Chem. Soc.* **1993**, *115*, 5853–5854.
- [18] M. F. Lappert, J. B. Pedley, J. Simpson, T. R. Spalding, *J. Organomet. Chem.* **1971**, *29*, 195–208.
- [19] P. von Ragué Schleyer, M. Manoharan, Z.-X. Wang, B. Kiran, H. Jiao, R. Puchta, N. J. R. van Eikema Hommes, *Org. Lett.* **2001**, *3*, 2465–2468.
- [20] V. Y. Lee, A. Sekiguchi, *Angew. Chem. Int. Ed.* **2007**, *46*, 6596–6620; *Angew. Chem.* **2007**, *119*, 6716–6740.
- [21] a) Y. Morita, A. Ueda, in *Fragments of Fullerenes and Carbon Nanotubes*, Wiley, **2011**, pp. 95–134; b) M. Bühl, A. Hirsch, *Chem. Rev.* **2001**, *101*, 1153–1184.
- [22] S. Yamaguchi, Y. Itami, K. Tamao, *Organometallics* **1998**, *17*, 4910–4916.
- [23] K. Jorner, R. Emanuelsson, C. Dahlstrand, H. Tong, A. V. Denisova, H. Ottosson, *Chem. Eur. J.* **2014**, *20*, 9295–9303.
- [24] a) N. C. Baird, *J. Am. Chem. Soc.* **1972**, *94*, 4941–4948; b) P. W. Fowler, E. Steiner, L. W. Jenneskens, *Chem. Phys. Lett.* **2003**, *371*, 719–723; c) F. Feixas, J. Vandenbussche, P. Bultinck, E. Matito, M. Sola, *Phys. Chem. Chem. Phys.* **2011**, *13*, 20690–20703; d) H. Ottosson, *Nat. Chem.* **2012**, *4*, 969–971.
- [25] S. Yamaguchi, K. Tamao, *Bull. Chem. Soc. Jpn.* **1996**, *69*, 2327–2334.
- [26] K. Tamao, S. Yamaguchi, M. Shiro, *J. Am. Chem. Soc.* **1994**, *116*, 11715–11722.
- [27] I. Fernández, M. Duvall, J. I-Chia Wu, P. v. R. Schleyer, G. Frenking, *Chem. Eur. J.* **2011**, *17*, 2215–2224.
- [28] P. v. R. Schleyer, C. Maerker, A. Dransfeld, H. Jiao, N. J. R. v. E. Hommes, *J. Am. Chem. Soc.* **1996**, *118*, 6317–6318.
- [29] a) Y. Mizuhata, N. Noda, N. Tokitoh, *Organometallics* **2010**, *29*, 4781–4784; b) Y. Mizuhata, T. Sasamori, N. Takeda, N. Tokitoh, *J. Am. Chem. Soc.* **2006**, *128*, 1050–1051.
- [30] F. C. Leavitt, T. A. Manuel, F. Johnson, *J. Am. Chem. Soc.* **1959**, *81*, 3163–3164.
- [31] a) M. Saito, R. Haga, M. Yoshioka, K. Ishimura, S. Nagase, *Angew. Chem. Int. Ed.* **2005**, *44*, 6553–6556; *Angew. Chem.* **2005**, *117*, 6711–6714; b) B. Wrackmeyer, S. Kundler, R. Boese, *Chem. Ber.* **1993**, *126*, 1361–1370; c) G. P. M. van Klink, H. J. R. de Boer, G. Schat, O. S. Akkerman, F. Bickelhaupt, A. L. Spek, *Organometallics* **2002**, *21*, 2119–2135.
- [32] J. Ferman, J. P. Kakareka, W. T. Klooster, J. L. Mullin, J. Quattrucci, J. S. Ricci, H. J. Tracy, W. J. Vining, S. Wallace, *Inorg. Chem.* **1999**, *38*, 2464–2472.
- [33] a) R. Haga, M. Saito, M. Yoshioka, *Eur. J. Inorg. Chem.* **2007**, 1297–1306; b) M. Saito, T. Kuwabara, K. Ishimura, S. Nagase, *Bull. Chem. Soc. Jpn.* **2010**, *83*, 825–827.
- [34] R. E. Dinnebier, U. Behrens, F. Olbrich, *Organometallics* **1997**, *16*, 3855–3858.
- [35] R. H. Cox, H. W. Terry, L. W. Harrison, *J. Am. Chem. Soc.* **1971**, *93*, 3297–3298.
- [36] M. Saito, *Coord. Chem. Rev.* **2012**, *256*, 627–636.
- [37] a) E. H. Bray, W. Hübel, I. Caplier, *J. Am. Chem. Soc.* **1961**, *83*, 4406–4413; b) J. J. Eisch, J. E. Galle, S. Kozima, *J. Am. Chem. Soc.* **1986**, *108*, 379–385; c) J. Dubac, A. Laporterie, G. Manuel, *Chem. Rev.* **1990**, *90*, 215–263.
- [38] J. G. Zavistoski, J. J. Zuckerman, *J. Org. Chem.* **1969**, *34*, 4197–4199.
- [39] A. J. Ashe, S. Mahmoud, *Organometallics* **1988**, *7*, 1878–1880.
- [40] A. J. Ashe III, T. R. Diephouse, *J. Organomet. Chem.* **1980**, *202*, C95–C98.
- [41] A. J. Ashe, L. L. Lohr, S. M. Al-Taweel, *Organometallics* **1991**, *10*, 2424–2431.
- [42] J. Krause, K.-J. Haack, K.-R. Pörschke, B. Gabor, R. Goddard, C. Pluta, K. Seevogel, *J. Am. Chem. Soc.* **1996**, *118*, 804–821.
- [43] a) X. Yan, C. Xi, *Acc. Chem. Res.* **2015**, *48*, 935–946; b) P. J. Fagan, W. A. Nugent, J. C. Calabrese, *J. Am. Chem. Soc.* **1994**, *116*, 1880–1889.
- [44] a) Y. Ura, L. Yanzhong, X. Zhenfeng, T. Takahashi, *Tetrahedron Lett.* **1998**, *39*, 2787–2790; b) T. Takahashi, W.-H. Sun, Y. Liu, K. Nakajima, M. Kotora, *Organometallics* **1998**, *17*, 3841–3843.
- [45] C. Fan, W. E. Piers, M. Parvez, *Angew. Chem. Int. Ed.* **2009**, *48*, 2955–2958; *Angew. Chem.* **2009**, *121*, 2999–3002.
- [46] E. Negishi, S. J. Holmes, J. M. Tour, J. A. Miller, F. E. Cederbaum, D. R. Swanson, T. Takahashi, *J. Am. Chem. Soc.* **1989**, *111*, 3336–3346.
- [47] a) U. Rosenthal, A. Ohff, M. Michalik, H. Görls, V. V. Burlakov, V. B. Shur, *Angew. Chem. Int. Ed. Engl.* **1993**, *32*, 1193–1195; *Angew. Chem.* **1993**, *105*, 1228–1230; b) J. Linshoef, *Synlett* **2014**, *25*, 2671–2672.
- [48] J. Linshoef, A. C. J. Heinrich, S. A. W. Segler, P. J. Gates, A. Staubitz, *Org. Lett.* **2012**, *14*, 5644–5647.
- [49] J. Linshoef, E. J. Baum, A. Hussain, P. J. Gates, C. Näther, A. Staubitz, *Angew. Chem. Int. Ed.* **2014**, *53*, 12916–12920; *Angew. Chem.* **2014**, *126*, 13130–13134.
- [50] a) B. Wrackmeyer, U. Klaus, W. Milius, E. Klaus, T. Schaller, *J. Organomet. Chem.* **1996**, *517*, 235–242; b) B. Wrackmeyer, P. Thoma, S. Marx, T. Bauer, R. Kempe, *Eur. J. Inorg. Chem.* **2014**, 2103–2112; c) G. Kehr, G. Erker, *Chem. Commun.* **2012**, *48*, 1839–1850; d) B. Wrackmeyer, P. Thoma, R. Kempe, *Eur. J. Inorg. Chem.* **2009**, 1469–1476.
- [51] B. Wrackmeyer, E. Khan, *Eur. J. Inorg. Chem.* **2016**, 300–312.
- [52] a) S. C. Cohen, A. G. Massey, *J. Organomet. Chem.* **1967**, *10*, 471–481; b) K. Geramita, J. McBee, T. D. Tilley, *J. Org. Chem.* **2009**, *74*, 820–829.
- [53] I. Nagao, M. Shimizu, T. Hiyama, *Angew. Chem. Int. Ed.* **2009**, *48*, 7573–7576; *Angew. Chem.* **2009**, *121*, 7709–7712.
- [54] D. Tanaka, J. Ohshita, Y. Ooyama, N. Kobayashi, H. Higashimura, T. Nakanishi, Y. Hasegawa, *Organometallics* **2013**, *32*, 4136–4141.
- [55] H. H. Freedman, *J. Org. Chem.* **1962**, *27*, 2298–2303.
- [56] W. A. Gustavson, L. M. Principe, W. Z. M. Rhee, J. J. Zuckerman, *J. Am. Chem. Soc.* **1981**, *103*, 4126–4131.
- [57] M. Saito, R. Haga, M. Yoshioka, *Heteroat. Chem.* **2001**, *12*, 349–353.
- [58] M. Saito, T. Kuwabara, C. Kambayashi, M. Yoshioka, K. Ishimura, S. Nagase, *Chem. Lett.* **2010**, *39*, 700–701.
- [59] R. Haga, M. Saito, M. Yoshioka, *Chem. Eur. J.* **2008**, *14*, 4068–4073.
- [60] A. C. J. Heinrich, B. Thiedemann, P. J. Gates, A. Staubitz, *Org. Lett.* **2013**, *15*, 4666–4669.
- [61] P. A. Chase, W. E. Piers, B. O. Patrick, *J. Am. Chem. Soc.* **2000**, *122*, 12911–12912.
- [62] a) B. Kumar, C. E. Strasser, B. T. King, *J. Org. Chem.* **2012**, *77*, 311–316; b) M. Shimizu, T. Hiyama, *Eur. J. Org. Chem.* **2013**, 8069–8081.
- [63] S. H. Li, L. C. Li, C. H. Xu, *Chin. Chem. Lett.* **2012**, *23*, 69–72.
- [64] J. M. Fox, T. J. Katz, S. Van Elshocht, T. Verbiest, M. Kauranen, A. Persoons, T. Thongpanchang, T. Krauss, L. Brus, *J. Am. Chem. Soc.* **1999**, *121*, 3453–3459.
- [65] P. G. Harrison, S. E. Ulrich, J. J. Zuckerman, *J. Am. Chem. Soc.* **1971**, *93*, 5398–5402.
- [66] T. Kuwabara, J.-D. Guo, S. Nagase, M. Minoura, R. H. Herber, M. Saito, *Organometallics* **2014**, *33*, 2910–2913.
- [67] L. Killian, B. Wrackmeyer, *J. Organomet. Chem.* **1977**, *132*, 213–221.
- [68] M. Saito, M. Shiratake, T. Tajima, J. D. Guo, S. Nagase, *J. Organomet. Chem.* **2009**, *694*, 4056–4061.
- [69] N. Y.-L. Deng Chun-Mei, Peng Qian, Shuai Zhi-Gang, *Acta Phys.-Chim. Sin.* **2010**, *26*, 1051–1058.
- [70] H. J. Tracy, J. L. Mullin, W. T. Klooster, J. A. Martin, J. Haug, S. Wallace, I. Rudloe, K. Watts, *Inorg. Chem.* **2005**, *44*, 2003–2011.
- [71] A. M. Priegert, B. W. Rawe, S. C. Serin, D. P. Gates, *Chem. Soc. Rev.* **2016**, *45*, 922–953.
- [72] J. Mei, N. L. C. Leung, R. T. K. Kwok, J. W. Y. Lam, B. Z. Tang, *Chem. Rev.* **2015**, *115*, 11718–11940.

Manuscript received: July 28, 2017

Accepted manuscript online: September 14, 2017

Version of record online: January 31, 2018

3.2.2. Negishi's Reagent Versus Rosenthal's Reagent in the Formation of Zirconacyclopentadienes.

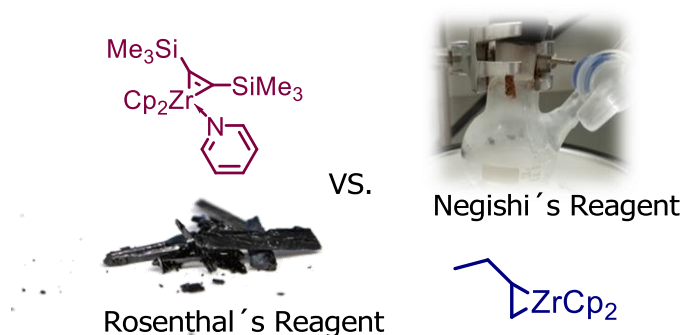
Full paper

Urrego-Riveros, S.; Ramirez y Medina, I.-M.; Duvinage, D.; Lork, E.; Sönnichsen, F.; Staubitz, A., Chem. Eur. J.. doi:10.1002/chem.201902255

Reprinted with permission from WILEY-VCH.(c)

Abstract

Zirconacyclopentadienes are versatile precursors for a large number of heteroles that are accessible by Zr-element exchange reactions. The vast majority of reports describe their preparation by the use of Negishi's reagent, which is a species that is formed *in situ*. The zirconacyclopentadiene is then formed by the addition of one equivalent of a diyne or two equivalents of a monoyne moiety to this Negishi species. Another route involves Rosenthal's reagent ($\text{Cp}_2\text{Zr}(\text{py})\text{Me}_3\text{SiC}\equiv\text{CSiMe}_3$), which then reacts with a diyne or monoyne moiety. In this work, the efficiency of both routes was compared in terms of reaction time, stability of the product in the reaction mixture and yield. The synthetic implications of using both routes are evaluated. Novel zirconacyclopentadienes were synthesized, characterized directly from the reaction mixture and crystal structures could be obtained in most cases.



TOC graphic. In this study, two " Cp_2Zr " sources, the Negishi's and the Rosenthal's reagent were compared with respect to yield, reaction time and product stability. In total, twelve compounds with different substituents were used for the reductive coupling by these zirconium sources.

Scientific contribution to this paper.

The first authorship of this collaboration project, written as manuscript is shared with my colleague Isabel-M. Ramirez y Medina. The synthesis of the starting materials **10a** and **10b** were carried by me and from the starting materials **10c-10j** were carried by Isabel-M. Ramirez y Medina. The synthesis and reaction controls from the zirconacyclopentadienes **11a-11f** were carried by both and from the compounds **11g-11l** by my colleague. The writing part was done in equally way. Prof. Dr. Anne Staubitz proofread this manuscript and gave us experimental hints. Prof. Dr. Frank D. Sönnichsen collaborate with the NMR experiments and proofread the paper as well. Daniel Duvinage and Dr. Enno Lork carried out the X-Ray crystal measurements for the compounds **11d, 11f, 11h, 11i,11k** and **11l**.

Metallacycles | *Hot Paper*
Negishi's Reagent Versus Rosenthal's Reagent in the Formation of Zirconacyclopentadienes

 Sara Urrego-Riveros,^{+, [a]} Isabel-Maria Ramirez y Medina,^{+, [a]} Daniel Duvinage,^[b] Enno Lork,^[b] Frank D. Sönnichsen,^[c] and Anne Staubitz^{*, [a]}

Abstract: Zirconacyclopentadienes are versatile precursors for a large number of heteroles, which are accessible by Zr-element exchange reactions. The vast majority of reports describe their preparation by the use of Negishi's reagent, which is a species that is formed in situ. The zirconacyclopentadiene is then formed by the addition of one equivalent of a diyne or two equivalents of a monoyne moiety to this Negishi species. Another route involves Rosenthal's reagent

(Cp₂Zr(py)Me₃SiC≡CSiMe₃), which then reacts with a diyne or monoyne moiety. In this work, the efficiency of both routes was compared in terms of reaction time, stability of the product in the reaction mixture, and yield. The synthetic implications of using both routes are evaluated. Novel zirconacyclopentadienes were synthesized, characterized directly from the reaction mixture, and crystal structures could be obtained in most cases.

Introduction

Heteroles are five-membered cycles derived from cyclopentadiene or its derivatives. In these molecules, the sp³ carbon is replaced by a heteroatom. They have become very important during the past few decades in the areas of biology,^[1] materials science,^[2] and medicinal chemistry.^[5]

The most common of these heterocycles are aromatic (e.g., thiophene, pyrrole, or furan),^[3] although others are formally anti-aromatic (e.g., boroles).^[4] Some are non-aromatic with other forms of conjugations such as σ*–π* conjugation, which is exclusive to heavier element containing heterocycles (for example, group 14 metalloces).^[5]

There are many established routes for the synthesis of these classical aromatic heteroles,^[6] but the breakthrough to access

the non-classical non- or anti-aromatic congeners was achieved by the use of zirconacyclopentadienes or other metallacyclopentadienes^[7] as precursor molecules.^[8] In zirconacyclopentadienes, the sp³ atom of a cyclopentadiene is replaced by a Zr atom with further ligands saturating the coordination sphere of the zirconium. These ligands are Cp rings in most cases. Starting with a zirconacyclopentadiene (e.g., **1 a**), many metalloces can be synthesized, in which group 14 elements (E = Si, Ge, Sn, Pb) or other main group elements are introduced into the cycle by transmetalation reactions.^[5a,9] Moreover, zirconacyclopentadienes show other synthetic uses (Scheme 1). For example, if the zirconacyclopentadiene core (e.g., **1 b**) is part of a large polyaromatic system, protonation with HCl gives dienes such as compound **3**, which are otherwise difficult to access.^[10] Furthermore, if zirconacyclopentadienes are included in polymeric systems (e.g., **1 c**), they can be converted into stable aromatic building blocks as in polymer **4**.^[11]

Zirconacyclopentadienes **1** are typically formed by a reductive coupling of alkynes **5** by the zirconocene species "Cp₂Zr" **8** (Scheme 2).^[12] Such zirconacyclopentadienes can be also synthesized by the reaction of two monoynes with the active zirconocene species **8**.

In general, there are different methods to form this "Cp₂Zr" species from reagents that are mixtures of Cp₂ZrCl₂/Na, Cp₂ZrCl₂/Mg, or Cp₂ZrCl₂/Ln.^[9c] Further reagents are Takahashi's ("Cp₂ZrEt₂"),^[13] Negishi's ("Cp₂ZrBu₂"),^[14] and Rosenthal's reagent (Cp₂Zr(py)Me₃SiC≡CSiMe₃).^[15] However, the vast majority of reports describe the formation of the active "Cp₂Zr" species by using either of the latter two methods.

The synthesis of zirconacyclopentadienes via Negishi's reagent includes an in situ formed Zr reagent, coordinated by THF, which is not stable for long times at room temperature and which can be not isolated in pure form.^[12,14,16] The reaction between Cp₂ZrCl₂ (**6**) and two equivalents of *n*BuLi yields the

[a] S. Urrego-Riveros,⁺ I.-M. Ramirez y Medina,⁺ Prof. Dr. A. Staubitz
Institute for Organic and Analytical Chemistry/MAPEX Center for
Materials and Processes, University of Bremen
Leobener Str. 7/Bibliothekstr. 1, 28359 Bremen (Germany)
E-mail: staubitz@uni-bremen.de

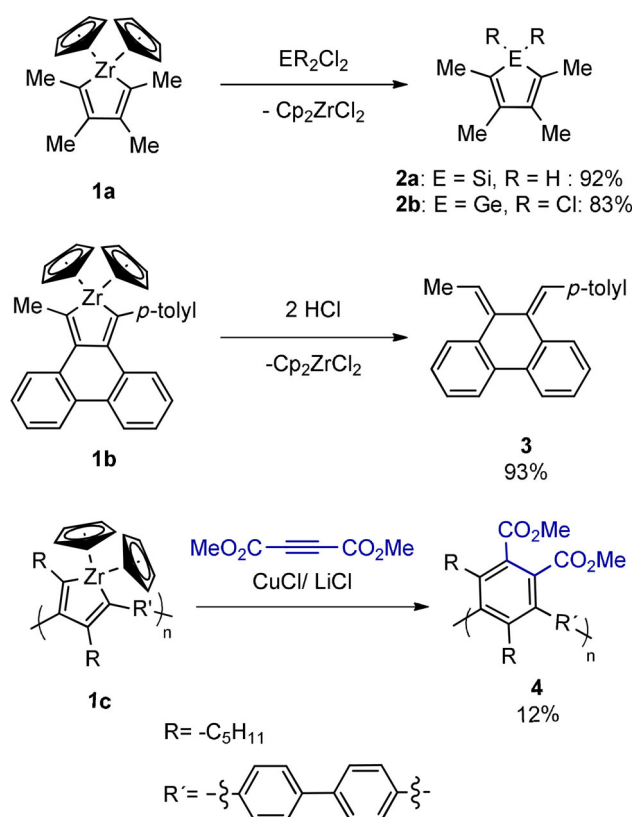
[b] D. Duvinage, Dr. E. Lork
Institute for Inorganic Chemistry and Crystallography/
MAPEX Center for Materials and Processes, University of Bremen
Leobener Str. 7/Bibliothekstr. 1, 28359 Bremen (Germany)

[c] F. D. Sönnichsen
Otto-Diels-Institute for Organic Chemistry, University of Kiel
Otto-Hahn-Platz 4, 24098 Kiel (Germany)

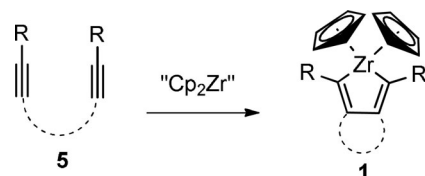
[*] These authors contributed equally to this work.

Supporting Information and the ORCID identification number(s) for the author(s) of this article can be found under:
<https://doi.org/10.1002/chem.201902255>.

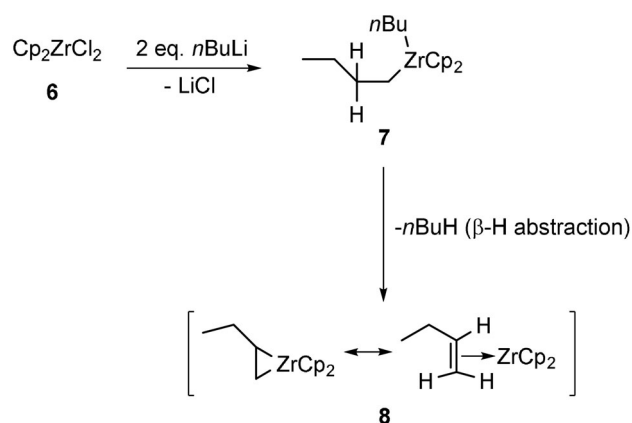
© 2019 The Authors. Published by Wiley-VCH Verlag GmbH & Co. KGaA. This is an open access article under the terms of Creative Commons Attribution NonCommercial-NoDerivs License, which permits use and distribution in any medium, provided the original work is properly cited, the use is non-commercial and no modifications or adaptations are made.



Scheme 1. Transformation of zirconacyclopentadienes into metalloles and extended diene systems.^[9b-d] Use of polyzirconacyclopentadienes for the synthesis of stable polymers.^[10-11]



Scheme 2. General synthesis of zirconacyclopentadienes of type 1.



Scheme 3. Formation of the "Cp₂Zr" Negishi's reagent **8**.^[12]

intermediate **7** and insoluble LiCl (Scheme 3). The zirconocene **7** then decomposes into *n*-butane and a number of active

species collectively labelled as "Cp₂Zr" (**8**),^[17] which is Negishi's reagent. The advantages of using this reagent include the use of relatively cheap precursors, time-saving in situ handling of the precursor reagents, and the high reactivity of the Negishi species. However, the latter may turn into a disadvantage when the dialkynes bear functional groups such as aromatic rings with halogen atoms. In a side reaction, these can undergo halogen-lithium exchange reactions if the concentration of *n*BuLi is not exactly known and an excess is used. Also, the tolerance towards other functional groups and heterocycles as substituents is often not given.^[10b] Finally, the reaction conditions limit the choice of solvent, because Cp₂ZrCl₂ (**6**) is insoluble in non-polar solvents such as *n*-pentane or *n*-hexane.^[10b]

Another possibility for the formation of zirconacyclopentadienes is the use of Rosenthal's reagent **9** (Figure 1).^[15, 18] The synthesis of Rosenthal's zirconocene is based on the substitution of THF by pyridine of the complex Cp₂Zr(THF)Me₃SiC≡CSiMe₃. Rosenthal and co-workers exchanged THF with pyridine because the zirconocene complex of THF is not as stable as with pyridine in solution and in pure form. There are two ways to prepare such a complex: one is based on the reduction of Cp₂ZrCl₂ with magnesium in the presence of bis(trimethylsilyl)acetylene in THF at room temperature (in a yield of 66%).^[15b] An improved method is based on the formation of the complex via Negishi's conditions (Scheme 3), elaborated by Tilley and co-workers (in a yield of 85%).

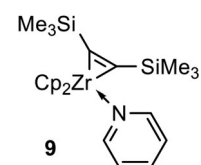


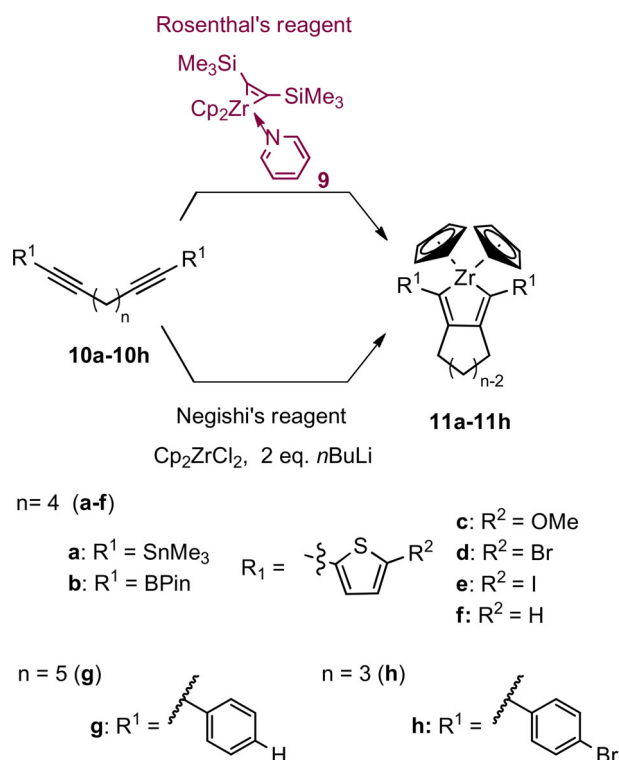
Figure 1. Structure of the Rosenthal's reagent **9**.

The "Cp₂Zr" species, stabilized by a pyridine and a bis(trimethylsilyl)acetylene ligand, is a thermally stable compound that can be easily crystallized and stored under inert conditions.^[10b, 19]

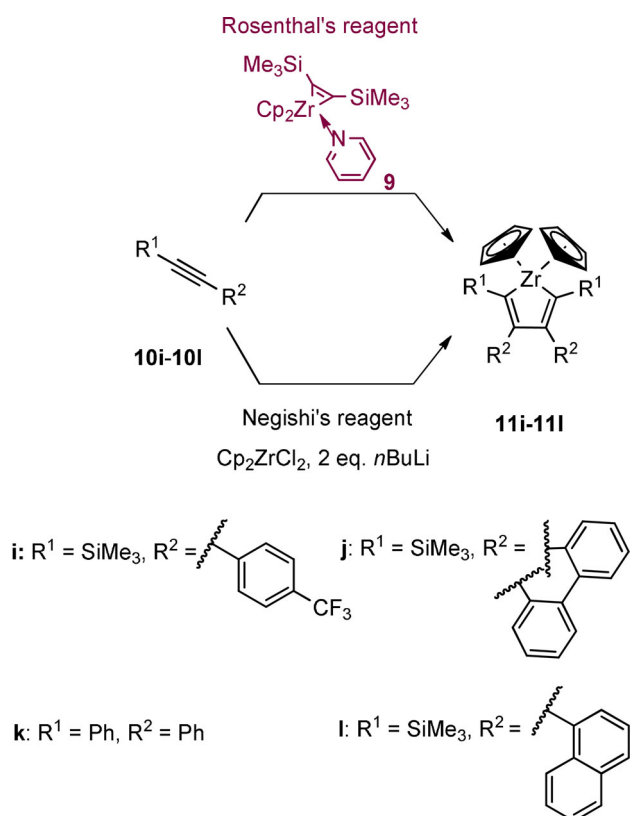
This means that for further syntheses with the Rosenthal reagent, much milder reaction conditions will be given to form further metalloles in general; some examples for the synthesis of functionalized metalloles already exist.^[20] The great solubility in different solvents including non-polar ones renders this reagent particularly useful for applications in macrocyclic and polymer chemistry, but mostly non-coordinating solvents are used in the literature. Furthermore, only volatile byproducts (pyridine and bis(trimethylsilyl)acetylene) are formed during the reaction and can be therefore easily removed compared with LiCl.^[10b, 18a, 21]

However, a direct, quantitative, and practicability comparison between the two reagents has not been made so far. The aim of this work was to investigate the exact differences between the use of two sources of "Cp₂Zr" in the preparation of zirconacyclopentadienes **11a–11h** starting with eight dialkynes **10a–10h** (Scheme 4) and zirconacyclopentadienes **11i–11l** from four alkynes **10i–10l** (Scheme 5).^[22] A particular focus was the compatibility of the reagents with the alkynes that are functionalized.

In the case of the dialkynes **10a** and **10b**, the use of Negishi's reagent for the formation of the zirconacyclopentadienes has already been documented; the isolated yields are



Scheme 4. Synthetic path to form the zirconacyclopentadienes **11a-11h** by using two different sources of “ Cp_2Zr ” and eight types of dialkynes **10a-10h**.



Scheme 5. Synthetic path to form the zirconacyclopentadienes **11i-11l** by using two different sources of “ Cp_2Zr ” and four alkynes **10i-10l**.

55% for zirconacyclopentadiene **11a**^[23] and 48% for compound **11b**.^[9d] They are included in this study as benchmarks.

Results and Discussion

The “Results and Discussion” part of the synthesis of the alkynes can be found as a part of the Supporting Information.

Synthesis of zirconacyclopentadienes: Monitoring of reaction progress by ^1H NMR spectroscopy

Reaction of the diynes and monoynes **10a-10l**, respectively, with the “ Cp_2Zr ” species, derived either from Negishi’s or Rosenthal’s reagent, should lead to the formation of the zirconacyclopentadienes **11a-11l** (Scheme 4 and Scheme 5). The progress of the reactions under both conditions was followed by ^1H NMR spectroscopy by using naphthalene as an internal standard for quantification.

In the case of Negishi’s reagent, the reactive “ Cp_2Zr ” species was formed by adding $n\text{BuLi}$ to a solution of zirconocene dichloride in THF at -78°C . The time started with the addition of the solution of the respective alkynes **10a-10l** in THF. The cooling bath was then removed, allowing the reaction to reach room temperature (ca. 22°C in our laboratories, see the Supporting Information for details). A defined sample was taken out after 10 min, 30 min, 1 h, 3 h, and 22 h, and the solvent was removed immediately under reduced pressure at 22°C . Then, naphthalene in C_6D_6 as an internal standard was added in equimolar proportions for the ^1H NMR measurements.

The formation of the zirconacyclopentadiene **11a** via this route was confirmed as reported in the literature,^[23] after 30 min of reaction, the product was formed with a yield of 85%. The ^1H NMR spectrum showed a resonance at 6.00 ppm, which was indicative for the cyclopentadienyl groups (Cp) of zirconacyclopentadiene **11a** (Figure 2). Such a downfield shift of the Cp signal in the ^1H NMR spectrum in comparison to the chemical shift of these protons of the starting material (Cp_2ZrCl_2 , C_6D_6): $\delta = 5.88$ ppm) suggests zirconacyclopentadiene ring formation, because the shift is affected by the C–C double bonds inside the zirconacyclopentadiene.

However, over 22 h, the Cp signal shifted from 6.00 ppm to 6.04 ppm and the methylene groups were not as well defined as before, which may indicate that the product was not stable in the reaction mixture.

In the case of zirconacyclopentadiene **11b** with BPin moieties attached, 20% yield was observed after 10 min of reaction; after 3 h the yield increased to 58%. However, after 22 h, the zirconacyclopentadiene decomposed (for the corresponding ^1H NMR spectra see Figure S61 in the Supporting Information).

For the reaction of Negishi’s reagent and the dialkynes **10c-10f** with thiophene moieties, quite a different outcome was observed. In the case of the reaction of diyne **10c**, the zirconacyclopentadiene **11c** was formed after 10 min with a yield of 15%, but after 30 min the yield decreased to 9% and after 1 h to 2% (Figure 3). After 3 h of reaction, the product appeared to be entirely decomposed to the starting material **10c**, indicating that the zirconacyclopentadiene **11c** was unstable

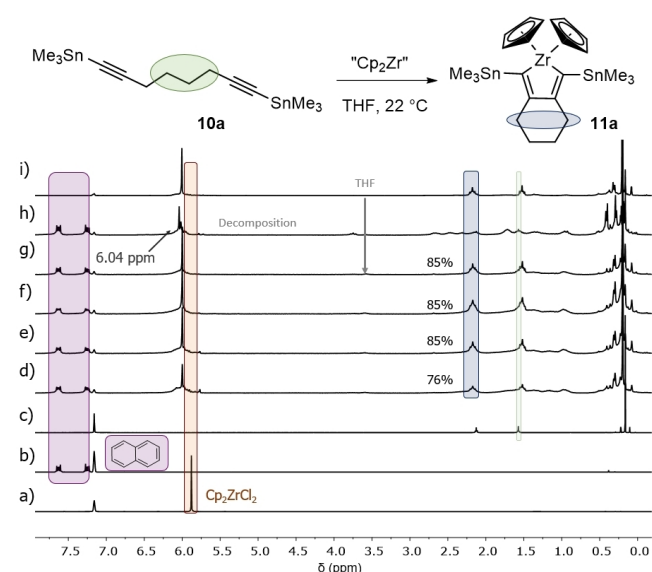


Figure 2. ^1H NMR spectra (recorded at 300 K, 200 MHz in C_6D_6) of the reaction monitoring for the synthesis of zirconacyclopentadiene **11a** (Negishi's reagent) with naphthalene as standard (1 equiv). a) Starting material Cp_2ZrCl_2 , b) naphthalene, c) starting material **10a** at $t=0$ min. Reaction monitoring after d) $t=10$ min, e) $t=30$ min, f) $t=1$ h, g) $t=3$ h, and h) $t=22$ h. i) Zirconacyclopentadiene **11a** previously isolated.^[23]

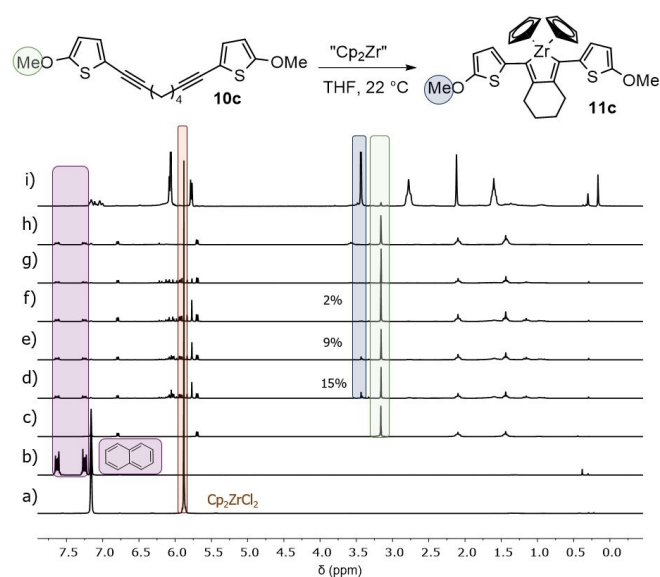


Figure 3. ^1H NMR spectra (recorded at 300 K, 200 MHz in C_6D_6) of the reaction monitoring for the synthesis of zirconacyclopentadiene **11c** (Negishi's reagent) with naphthalene as standard (1 equiv). a) Starting material Cp_2ZrCl_2 , b) naphthalene, c) starting material **10c**. Reaction monitoring after d) $t=10$ min, e) $t=30$ min, f) $t=1$ h, g) $t=3$ h, and h) $t=22$ h. i) Zirconacyclopentadiene **11c** that was previously isolated.

under the conditions of this synthetic route. This finding was confirmed by integration of the peak corresponding to the methoxy group compared with the standard, which indicated that 98% of the starting material was present in the reaction mixture at 3 h.

For the formation of the zirconacyclopentadienes **11d** and **11f** by the reaction of the Negishi's reagent and diynes **10d**

or **10f**, respectively, something similar could be observed. After 10 min reaction time, 26% was generated for compound **11d** and 82% for **11f**. After 30 min, the yield increased to 28% for **11d** whereas for **11f**, it decreased to 80%. The yield decreased after 1 h to 21% for **11d** and after 3 h to 65% for **11f**. After 22 h, the signals present were attributed to the starting materials **10d** and **10f** and decomposition of the zirconium part into different structures^[16] was observed; a spectrum of different Cp signals appeared in the ^1H NMR spectra (see Figures S63 and S66 in the Supporting Information). The zirconacyclopentadiene **11e** was not formed at any time of the reaction, just starting material **10e** and decomposition of the zirconium reagent was observed throughout the reaction monitoring by ^1H NMR spectroscopy (see Figure S64 in the Supporting Information).

However, if bis(trimethylsilyl)acetylene (BTMSA) is first added to the Negishi's reagent followed by the diene **10e**, it could be observed that the zirconacyclopentadiene **11e** was formed in a yield of 41% after 60 min. Still, after 22 h, the zirconacyclopentadiene **11e** was decomposed again (Figure 4). The difference in both reactions of diene **10e** with Negishi's reagent was the BTMSA, which seemed to be the crucial factor determining whether the product **11e** can be formed or not.

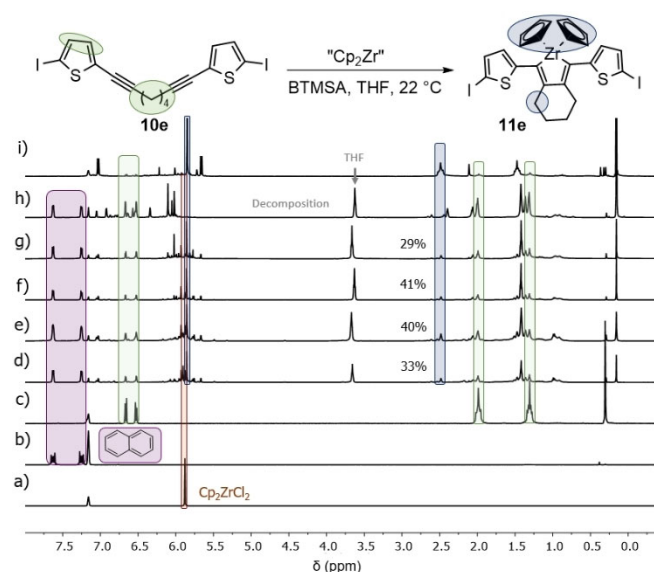


Figure 4. ^1H NMR spectra (recorded at 300 K, 600 MHz in C_6D_6) of the reaction monitoring of the formation of zirconacyclopentadiene **11e** at 22 °C with naphthalene as an internal standard. a) Starting material Cp_2ZrCl_2 , b) naphthalene, c) starting material **10e** at $t=0$ min. Reaction monitoring after d) $t=10$ min, e) $t=30$ min, f) $t=1$ h, g) $t=3$ h, and h) $t=22$ h. i) Zirconacyclopentadiene **11e** previously isolated.

In the case of the reaction of Negishi's reagent with the starting materials **10h** and **10k**, their respective zirconacyclopentadienes **11h** and **11k** were formed with high yields of 99% and 97% after 10 min, respectively (see Figures S67 and S70 in the Supporting Information). Contrary to previous results, both were still stable within the reaction mixture after 22 h with yields of 99% and 70%. For the conversion of the al-

kynes **10i**, **10j**, and **10l** into the zirconacyclopentadienes **11i**, **11j**, and **11l**, the yield rose to 94%, 88%, and 80% after 10 min, 10 min, and 30 min, respectively, but decreased after 22 h to 67%, 65%, and 26% (see Figures S68, S69, and S71 in the Supporting Information). This means that these particular zirconacyclopentadienes were insufficiently stable within the reaction mixture over time: care would need to be taken to terminate the reaction with the appropriate Zr exchange at an optimal reaction time.^[24]

The yield of zirconacyclopentadiene **11g** could not be determined by ¹H NMR measurements (monitoring of reaction progress by ¹H NMR spectroscopy), because this compound could not be completely redissolved after isolation. The compound instead formed gel-like needles with the NMR solvents. Therefore, the yield of the zirconacyclopentadiene **11g** had to be determined after complete isolation after 3 h from the reaction mixture. It could be successfully synthesized with a yield of 88% (purity 90%). A long ¹H NMR measurement and HR-MS confirmed the identity of the product.

Thus, Negishi's reagent proved to be incompatible with all compounds that bear thiophenyl motifs. In general, the synthesis was successful with yields between 28% and 98% for all other zirconacyclopentadienes.

The reactions with Rosenthal's reagent were placed inside a glovebox under a nitrogen atmosphere. To a solution of Rosenthal's zirconocene **9** in toluene, the alkynes **10a–l**, respectively, were added as a solution in toluene. After removing the solvent of each sample for the reaction monitoring, naphthalene in C₆D₆ as an internal standard was added in equimolar proportions and the reactions were monitored immediately by ¹H NMR spectroscopy. Rosenthal's reagent is mostly used in non-coordinating solvents (*n*-pentane, *n*-hexane, toluene, or benzene) in the literature, a reason for which could be that the original zirconium complex undergoes ligand-exchange reactions and might be less stable again. Also, for further transmetalation reactions, which can be done by one-pot reaction, it is often desired to have non-coordinating solvents. Therefore, toluene was used as the solvent, but two further experiments in THF were also conducted.

Figure 5 shows the progress of the formation of the zirconacyclopentadiene **11a**. After 10 min, a signal at 6.00 ppm appears, which can be assigned to the Cp protons of the desired zirconacyclopentadiene, whereas the Cp signals at 5.44 ppm of the Rosenthal's reagent disappear. Contrary to the synthesis with the Negishi reagent, the product was still stable after 22 h.

The transformation of the alkynes **10b–l** in toluene to their respective zirconacyclopentadienes **11b–l** proceeded in the same manner and were completed in all cases after 10 min; the products were stable for more than 22 h with yields ranging from 83% to 99% (For the ¹H NMR spectra of the reaction monitoring of the zirconacyclopentadienes **11b–l**, see the Supporting Information). In the cases of the zirconacyclopentadienes **11i** and **11l**, the yield dropped from 97% and 95% to 83% and 90%, respectively, after 22 h (see Figures S82 and S85 in the Supporting Information). It appears that these two compounds might undergo a reversion of the cyclization as was

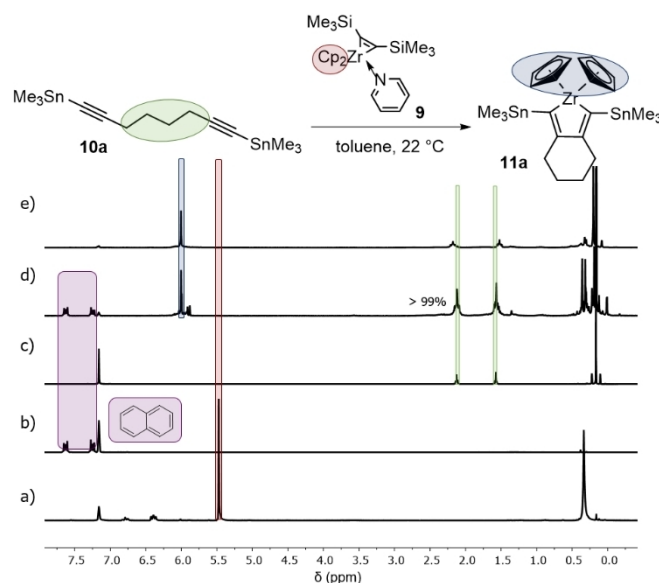


Figure 5. ¹H NMR spectra (recorded at 300 K, 200 MHz in C₆D₆) of the reaction monitoring of the formation of zirconacyclopentadiene **11a** at 22 °C with naphthalene as an internal standard. a) Rosenthal's reagent **9**, b) naphthalene, c) starting material **10a**, d) monitoring after 10 min. e) Zirconacyclopentadiene **11a**.^[23]

observed in most of the synthesis examples under the Negishi conditions. Zirconacyclopentadiene **11g** could be obtained with a yield of 91% (purity 92%) after 3 h of reaction time after complete isolation from the reaction mixture. Because of the solubility problems, the identity was determined again with a long ¹H NMR measurement and a HR-MS measurement. Zirconacyclopentadienes **11d** and **11h** were also synthesized by using Rosenthal's reagent in THF. The yield for both reactions was >99% after 10 min, but after 22 h dropped to 63% and 83%, respectively. After 22 h, both ¹H NMR spectra showed again signals of the alkyne starting materials **10d** and **10h**, thus, the zirconium complex is not quite as stable as in toluene. This might arise because the coordinating THF in excess can induce the reverse reaction.

To investigate the stability of the zirconacyclopentadienes in solution in the presence of lithium chloride (which is a byproduct of the Negishi reagent), isolated zirconacyclopentadiene **11e** was stirred in a mixture of LiCl in toluene for 22 h and defined samples were taken after 10 min, 30 min, 60 min, 180 min, and 22 h. It was observed that a precipitate formed and, after 22 h, the zirconacyclopentadiene **11e** was completely decomposed (Figure 6).

Table 1 summarizes the ¹H NMR signals of the Cp groups and the analytical yields of all zirconacyclopentadienes obtained with both routes.

In general, it seems that for longer reaction times, the Rosenthal reagent is more stable in solution than the Negishi reagent. This is most likely due to the stabilizing ligands (bis(trimethylsilyl)acetylene and pyridine). This might be also explained by the slower and lower conversion for five (**11a–11e**) of the examples, because a certain amount of the active "Cp₂Zr" species might decompose before it can undergo the

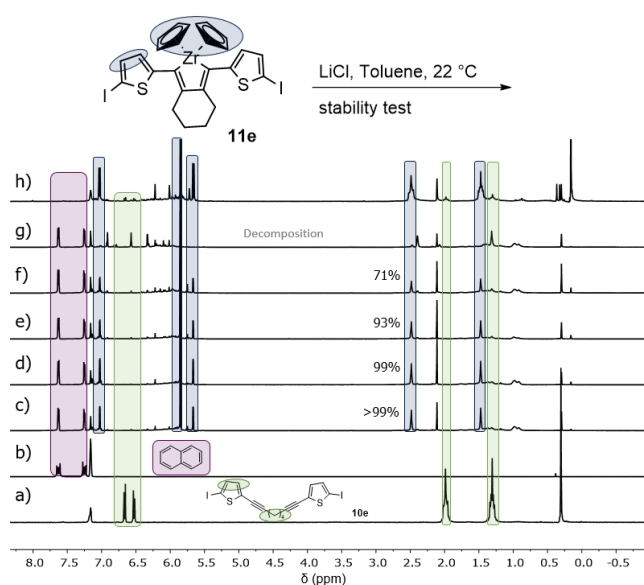


Figure 6. ^1H NMR spectra (recorded at 300 K, 600 MHz in C_6D_6) of the reaction monitoring of the stability test of zirconacyclopentadiene **11e** with naphthalene as standard (1 equiv). a) Naphthalene, b) starting material **10e**. Reaction monitoring after c) 10 min, d) 30 min, e) 1 h, f) 3 h, g) 22 h, and h) isolated zirconacyclopentadiene **11e**.

cyclization reaction. The extra experiment of Negishi's reagent with diyne **10e**, where BTMSA was added beforehand, shows also that stabilizing ligands are important for the prevention of decomposition of the active zirconium species and the formation of the zirconacyclopentadienes. For the other seven (**11f–11l**) examples, the conversion with the Negishi reagent was nearly as fast and high-yielding as with Rosenthal's reagent (Table 1).

An important fact to recognize is also that the zirconacyclopentadienes (**11a–11f**) were more stable over time (monitoring until 22 h) under the mild Rosenthal conditions than under the harsher Negishi conditions. In the six examples **11a–11f**, the product was completely decomposed under Negishi's conditions. However, in the case of the compounds **11h–11l**, with less reactive motifs such as phenyl groups or trimethylsilyl groups, the stability under the Negishi conditions was almost equal; the remaining yields after 22 h were higher than 26%. The maximum conversion for all reactions with Rosenthal's reagent were nearly quantitative after only 10 min and the remaining yields were higher than 83% (toluene) and 63% (THF).

For each of the two reagents, it could be observed that the conversion for all alkynes was different. One reason for this could be the stability of the alkyne complex of the Zr species in general. The formation of the zirconacyclopentadiene is an equilibrium reaction, which means for some of the alkynes the equilibrium might be on the side of the alkyne complex, but for some it might be on the side of the starting material. This can be seen by the fact that the maximal conversion for all the alkynes is different for the reaction with Rosenthal's reagent and the same is also for the route with Negishi's reagent. This observation may be explained by the different binding behav-

ior of the alkynes to the zirconium, which means the yield of the zirconacyclopentadiene should be higher for a good-binding alkyne. For the reaction with Negishi's reagent, this can be seen more extremely in terms of yields (Table 1, maximum conversion and remaining yield after 22 h) than for the reaction with Rosenthal's reagent owing to the fact that there are stabilizing ligands such as pyridine and/or bis(trimethylsilyl)acetylene from Rosenthal's reagent remaining in the solution. Therefore, in the equilibrium, there are stable starting materials and products. In the case of the Negishi reagent, the starting material is unstable; thus, if the reverse reaction occurs, decomposition of the alkyne complex cannot be prevented. Because of the decomposition of the active " Cp_2Zr " species over time, the yield decreases and new zirconacyclopentadiene cannot be formed.

The visible formation of a solid after 22 h in all of the reactions with Negishi's reagent might result from LiCl slowly precipitating; however, it could also be a result of the decomposition of the " Cp_2Zr " species and the reversibility of the cyclization reaction to the starting materials.^[19] Another point in terms of decomposition of the zirconacyclopentadienes under Negishi's conditions could be the LiCl in the solution. Zirconacyclopentadiene **11e**, which performed worst with Negishi's reagent, was tested for its stability. In a mixture of LiCl and pure zirconacyclopentadiene **11e** in toluene, we observed indeed that LiCl can induce decomposition. It appears again that the stability of the alkyne complex in the reaction mixture is crucial, because in the study with Negishi's reagent, the zirconacyclopentadiene did not decompose in all cases. The choice of solvent also clearly has an effect on the overall stability, which can be seen from the reactions with Rosenthal's reagent in THF.

In addition, comparing both methods, the handling of the Rosenthal's reagent was much easier compared with Negishi's reagent; especially when exact stoichiometry is needed. On the one hand, it was sufficient to prepare merely one stock solution for several reactions without the need for lower temperatures for the formation of such zirconacyclopentadienes. The in situ formation of Negishi's reagent, on the other hand, requires lower temperatures and therefore temperature controls to prevent the reagent from decomposing.^[16]

Additionally, air stability tests were conducted for all products and can be found as a part of the Supporting Information.

Structures in the solid state

The molecular structures of **11d**, **11f**, and **11h–11l** are shown in Figure 7 (and are also part of the Supporting Information) and confirm the identity of the compounds. Single crystals were obtained from a saturated toluene solution. Selected bond lengths and angles of all structures can be found as a part of the Supporting Information (Tables S6–8). In all compounds, the Zr atom is incorporated into almost planar five-membered central rings (e.g., $\text{Zr}(1)\text{-C}(1)\text{-C}(2)\text{-C}(7)$ is $8.3(2)^\circ$ for **11d**). In all cases where the zirconacyclopentadiene ring bears aryl groups in the 2- and 5-positions, these groups are twisted to the plane (e.g., $\text{Zr}(1)\text{-C}(1)\text{-C}(10)\text{-C}(11)$ is $-23.0(3)^\circ$ for **11d**).

Table 1. Summary of ^1H NMR signals of the Cp rings in C_6D_6 and the highest conversion [%] for the zirconacyclopentadienes **11 a–l** synthesized by using the Rosenthal or Negishi reagents.

Entry	Product	^1H δ_{Cp} [ppm]	Max. conversion [%] ^[a] in toluene	Rosenthal		Max. conversion [%] ^[a]	Negishi	
				t [min]	Remaining yield after 22 h [%]		t [min]	Remaining yield after 22 h [%]
1	11 a	6.00	>99	10	>99	85	10	0
2	11 b	6.37	97	10	97	56	180	0
3	11 c	6.05	98	10	96	15	30	0
4	11 d	5.84	91 (>99% in THF)	10	88 (63% in THF)	28	30	0
5	11 e	5.85	>99	10	>99	0 (41% with BTMSA)	–(60 min)	0
6	11 f	6.00	93	10	93	83	10	0
7	11 g	5.93	91	180 ^[b]	–	88	180 ^[c]	–
8	11 h	5.70	>99 (>99% in THF)	10	>99 (83% in THF)	98	10	98
9	11 i	6.09	97	10	90	94	10	67
10	11 j	5.94	96	10	96	88	10	65
11	11 k	6.01	>99	10	>99	97	10	70
12	11 l	6.35	95	10	83	80	30	26

[a] The conversion was calculated based on the consumption of the starting material. [b] Yield obtained after complete isolation of the product after 3 h. [c] Yield obtained after complete isolation of the product after 3 h.

In the compounds **11 i–11 l**, the aryl groups in the 3- and 4-positions of the zirconacyclopentadiene ring are almost completely twisted with respect to the plane (e.g., $\text{C}(1)\text{--C}(2)\text{--C}(20)\text{--C}(21)$ is $83.36(2)^\circ$ for **11 l**), whereas the annulated six- or five-membered rings in that position show puckered confirmations.

Conclusions

In summary, it could be observed that the use of Rosenthal's reagent was much more efficient for the synthesis of zirconacyclopentadienes in most of the cases with respect to yield, stability of the zirconacyclopentadiene, and reaction time

when compared with Negishi's reagent. More particularly, our study has shown the high importance of stabilizing ligands in the reaction mixture. In addition to reliably producing high yields, Rosenthal's reagent is very functional group tolerant; but in general, it was shown that halides also do not react under Negishi's conditions, when *n*BuLi is titrated and used in exact amounts. However, the advantages of using Negishi's reagent include using relatively cheap precursors, time-saving in situ handling of the precursor reagents, and a highly reactive species. But, overall, Rosenthal's zirconocene is a thermally stable reagent that can be prepared with great convenience.

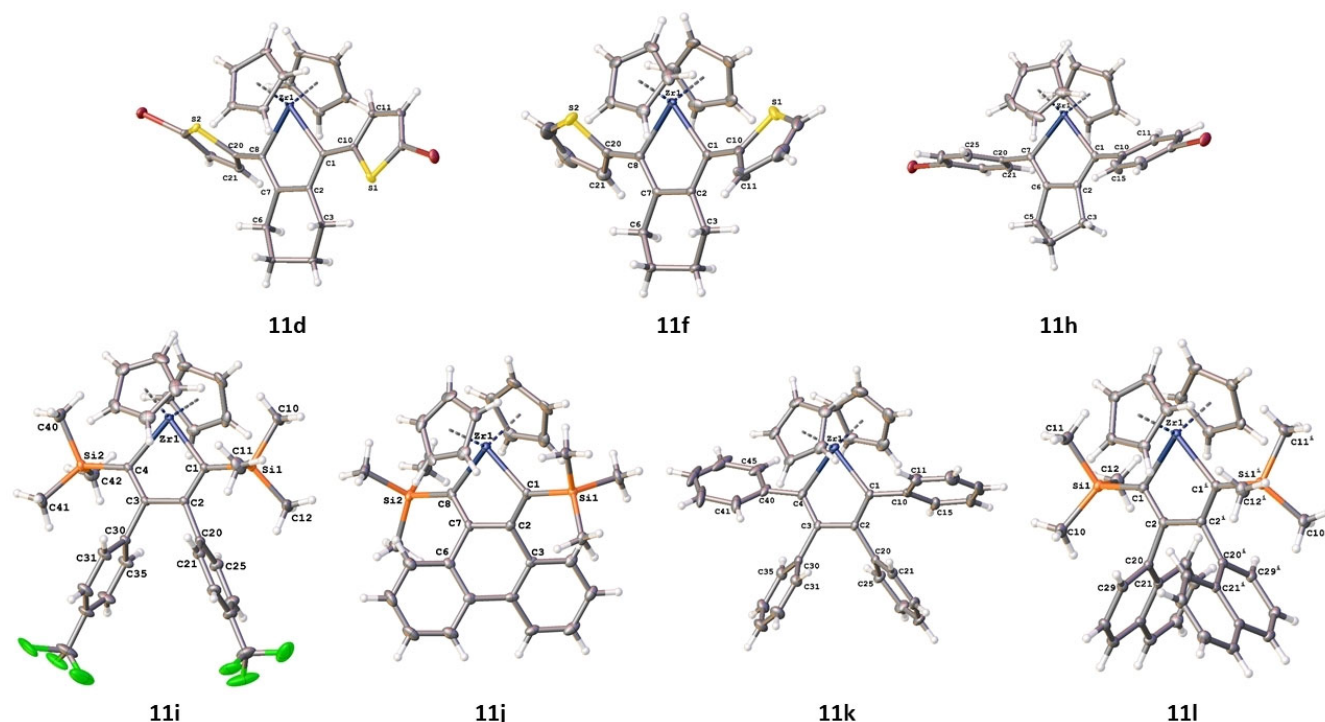


Figure 7. Molecular structures of **11 d**, **11 f**, **11 h–11 l** showing 50% probability ellipsoids and the crystallographic numbering scheme. Only the major parts of the disordered molecule of **11 f** are shown for clarity. For **11 h**, only one independent molecule is shown. Only the major parts of the disordered molecule of **11 i** are shown for clarity.

Experimental Section

General methods and materials

All reactions were carried out by using standard Schlenk techniques under a dry, inert nitrogen or argon atmosphere unless noted otherwise. Some reactions were performed inside a nitrogen-filled glovebox from Inert, Innovative Technology, Inc. (<0.1 ppm O₂ and <0.1 ppm H₂O).

All dry solvents were taken from the solvent purification system (SPS), degassed by freeze–pump–thaw cycles and stored under a nitrogen atmosphere unless noted otherwise. All chemicals were commercially available and were used without further purification unless noted otherwise. *n*BuLi was titrated by the Lin and Paquette method^[25] for exact concentrations.

Analytical instruments

¹H NMR, ¹³C{¹H} NMR, ¹¹B{¹H} NMR, ¹¹⁹Sn{¹H} NMR, ¹⁹F NMR, and ²⁹Si{¹H} NMR spectra were recorded with a Bruker Avance Neo 500, Bruker Avance Neo 600, or Bruker DPX-200 spectrometer at 300 K. All ¹H NMR and ¹³C{¹H} NMR were referenced against the solvent residual proton signals (¹H), or the solvent itself (¹³C). The reference for the ¹¹⁹Sn{¹H} NMR spectra was calculated based on the ¹H NMR spectrum of TMS. ¹¹B{¹H} NMR and ¹⁹F NMR spectra were referenced against BF₃·Et₂O in CDCl₃. ²⁹Si{¹H} NMR spectra were referenced against TMS in CDCl₃. All chemical shifts (δ) are given in parts per million (ppm) and all coupling constants (*J*) in Hz. Electron impact (EI) ionization mass spectra were obtained with the double focusing mass spectrometer MAT 95+ or MAT 8200 from FINNIGAN mat. Samples were measured by direct inlet or indirect inlet methods with a source temperature of 200 °C. The ionization

energy of the electron impact ionization was 70 eV. All signals were reported with the quotient from mass to charge (*m/z*).

Crystallography

Intensity data of **11 d**, **11 f**, **11 h–11 l** were collected with a Bruker Venture D8 diffractometer at 100 K with MoK_α (0.7107 Å) radiation. All structures were solved by intrinsic phasing and refined based on *F*² by use of the SHELX^[26] program package as implemented in OLex21.2.^[27] All non-hydrogen atoms were refined by using anisotropic displacement parameters. Hydrogen atoms attached to carbon atoms were included in geometrically calculated positions by using a riding model. Crystal and refinement data are collected in Tables S3–5 in the Supporting Information.

A rotational disorder was resolved for the thiophene groups of compound **11 f**. The refinement led to a split atom model for each group with refined occupancies of 76:24 and 53:47, respectively. Compound **11 h** comprises two crystallographically independent conformers. The fluorine atoms of the two CF₃ groups of compound **11 i** were disordered and were refined with split occupancies of 71:29 and 57:43, respectively. The C–F distances were restrained to be equal. Compound **11 k** crystallized with one molecule of toluene per asymmetric unit. The toluene solvate molecule was disordered over two positions with split occupancies of 65:35. Compound **11 l** crystallized with a half molecule in the asymmetric unit. The Zr atom is located on the Wyckoff position 4e of space group C2/*c*.

CCDC 1900225, 1900228, 1900226, 1915992, 1900380, 1900227 (**11 d**, **11 h**, **11 i**, **11 j**, **11 k**, **11 l**, respectively) contain the supplementary crystallographic data for this paper. These data are provided free of charge by The Cambridge Crystallographic Data Centre.

General procedure for the synthesis of the zirconacyclopentadienes (11 a–l)

An equimolar solution of Rosenthal's reagent (**9**) and alkyne (**10 a–l**) in toluene was stirred at 22 °C for 10 min. The solvent was removed under inert conditions. After filtration over Celite, the final product was afforded.

Bis(*h*⁵-cyclopentadienyl)-1,3-bis(trimethylstannyl)-4,5,6,7-tetrahydro-2*H*-benzo[*c*]zirconacyclopentadiene **11 a: **10 a** (100 mg, 230 μmol), Rosenthal's reagent (109 mg, 230 μmol), toluene (5 mL), 22 °C, yield: 141 mg, 94%. ¹H NMR (500 MHz, C₆D₆): δ = 6.00 (s, 10H, Cp), 2.22–2.15 (m, 4H, c), 1.57–1.50 (m, 4H, d), 0.20 ppm (d, ³J_{Sn-H} = 24 Hz, 18H, e); ¹³C{¹H} NMR (126 MHz, C₆D₆): δ = 206.1 (a), 150.7 (b), 111.4 (Cp), 38.7 (c), 23.1 (d), –6.7 ppm (e; ¹J_{Sn-C} = 146 Hz); ¹¹⁹Sn{¹H} NMR (187 MHz, CDCl₃): δ = –81.3 ppm; HR-MS (EI, C₂₄H₃₆Sn₂Zr): *m/z* calcd: 653.99153; found: 653.99188 (*R* = 10000); MS (EI, 70 eV, direct inlet, 200 °C): *m/z* (% relative intensity) = 654 (5) [*M*]⁺, 155 [*M*–C₁₂H₁₂]⁺, (100).**

Bis(*h*⁵-cyclopentadienyl)-1,3-bis(4,4,5,5-tetramethyl-1,3,2-dioxaborolan-2-yl)-4,5,6,7-tetrahydro-2*H*-benzo[*c*]zirconacyclopentadiene **11 b: **10 b** (100 mg, 280 μmol), Rosenthal's reagent (132 mg, 280 μmol), toluene (5 mL), 22 °C, yield: 151 mg, 93%. ¹H NMR (500 MHz, C₆D₆): δ = 6.37 (s, 10H, Cp), 2.59–2.54 (m, 4H, c), 1.65–1.58 (m, 4H, d), 1.10 ppm (s, 24H, f); ¹³C{¹H} NMR (126 MHz, C₆D₆): δ = 147.0 (b), 111.7 (Cp), 81.5 (e), 35.4 (c), 24.9 (f), 23.5 (d) ppm; ¹²⁸B NMR (160 MHz, C₆D₆): δ = 30.9 ppm; HR-MS (EI, C₃₀H₄₂–¹⁰¹B₂O₄⁹⁰Zr): *m/z* calcd: 577.23471; found: 577.23484 (*R* = 10000); MS (EI, 70 eV, direct inlet, 200 °C): *m/z* (% relative intensity) = 578 (13) [*M*]⁺, 83 (100).**

Bis(*h*⁵-cyclopentadienyl)-1,3-bis(5-methoxythiophen-2-yl)-4,5,6,7-tetrahydro-2*H*-benzo[*c*]zirconacyclopentadiene **11 c: **10 c** (150 mg, 454 μmol), Rosenthal's reagent (213 mg, 454 μmol), toluene (6 mL), 22 °C, yield: 233 mg, 93%. ¹H NMR (500 MHz, C₆D₆): δ = 6.07 (d, ³J = 3.8 Hz, 2H, g), 6.05 (s, 10H, Cp), 5.77 (d, ³J = 3.7 Hz, 2H, f), 3.44 (s, 6H, i), 2.80–2.74 (m, 4H, c), 1.63–1.57 ppm (m, 2H, d); ¹³C{¹H} NMR (126 MHz, C₆D₆): δ = 177.9 (a), 165.7 (h), 141.3 (b), 136.8 (e), 119.9 (f), 112.1 (Cp), 104.1 (g), 59.7 (i), 30.7 (c), 24.4 ppm (d); HR-MS (EI, C₂₈H₂₈O₂S₂⁹⁰Zr): *m/z* calcd: 550.05723; found: 550.05796 (*R* = 10000); MS (EI, 70 eV, direct inlet, 200 °C): *m/z* (% relative intensity) = 550 (74) [*M*]⁺, 220 (100) [Cp₂Zr]⁺.**

Bis(*h*⁵-cyclopentadienyl)-1,3-bis(5-bromothiophen-2-yl)-4,5,6,7-tetrahydro-2*H*-benzo[*c*]zirconacyclopentadiene **11 d: **10 d** (150 mg, 352 μmol), Rosenthal's reagent (166 mg, 352 μmol), toluene (6 mL), 22 °C, yield: 210 mg, 93%. ¹H NMR (600 MHz, C₆D₆): δ = 6.82 (d, ³J = 3.8 Hz, 2H, g), 5.84 (s, 10H, Cp), 5.69 (d, ³J = 3.8 Hz, 1H, f), 2.49 (m, 4H, c), 1.50–1.46 ppm (m, 4H, d); ¹³C{¹H} NMR (126 MHz, C₆D₆): δ = 177.0 (a), 151.8 (e), 143.0 (b), 130.2 (g), 121.8 (f), 112.3 (Cp), 109.4 (h), 30.1 (c), 23.8 ppm (d); HR-MS (EI, C₂₆H₂₂⁷⁹Br₂S₂⁹⁰Zr): *m/z* calcd: 645.85712; found: 645.85714 (*R* = 10000); MS (EI, 70 eV, direct inlet, 200 °C): *m/z* (% relative intensity) = 646 (38) [*M*]⁺, 301 (100).**

Bis(*h*⁵-cyclopentadienyl)-1,3-bis(5-iodothiophen-2-yl)-4,5,6,7-tetrahydro-2*H*-benzo[*c*]zirconacyclopentadiene **11 e: **10 e** (150 mg, 287 μmol), Rosenthal's reagent (137 mg, 287 μmol), toluene (6 mL), 22 °C, yield: 194 mg, 91%. ¹H NMR (500 MHz, C₆D₆): δ = 7.03 (d, ³J = 3.7 Hz, 2H, g), 5.85 (s, 10H, Cp), 5.66 (d, ³J = 3.7 Hz, 2H, f), 2.52–2.45 (m, 4H, c), 1.50–1.45 ppm (m, 4H, d); ¹³C{¹H} NMR (126 MHz, C₆D₆): δ = 176.9 (a), 156.1 (e), 142.8 (b), 137.1 (g), 129.1 (f), 112.1 (Cp), 70.0 (h), 29.9 (c), 23.6 ppm (d); HR-MS (EI, C₂₆H₂₂I₂S₂⁹⁰Zr): *m/z* calcd: 741.82939; found: 741.82934 (*R* = 10000); MS (EI, 70 eV, direct inlet, 200 °C): *m/z* (% relative intensity) = 742 (44) [*M*]⁺, 347 (100).**

Bis(*h*⁵-cyclopentadienyl)-1,3-di(thiophen-2-yl)-4,5,6,7-tetrahydro-2*H*-benzo[*c*]zirconacyclopentadiene **11 f: **10 f** (150 mg, 555 μmol), Rosenthal's reagent (261 mg, 555 μmol), toluene (6 mL), 22 °C, yield: 259 mg, 95%. ¹H NMR (500.1 MHz, C₆D₆): δ = 6.96 (dd, ³J = 5.2 Hz, ⁴J = 1.0 Hz, 2H, h), 6.90 (dd, ³J = 5.2, 3.5 Hz, 2H, g), 6.21 (dd, ³J = 3.5 Hz, ⁴J = 1.0 Hz, 2H, f), 6.00 (s, 10H, Cp), 2.70–2.64 (m, 2H, c), 1.57–1.54 ppm (m, 2H, d); ¹³C{¹H} NMR (126 MHz, C₆D₆): δ = 177.9 (a), 150.3 (e), 142.4 (b), 127.3 (g), 123.0 (h), 121.4 (f), 112.2 (Cp), 30.1 (c), 24.0 ppm (d); HR-MS (EI, C₂₆H₂₄S₂⁹⁰Zr): *m/z* calcd: 490.03610; found: 490.03669 (*R* = 10000); MS (EI, 70 eV, direct inlet, 200 °C): *m/z* (% relative intensity) = 490 (19) [*M*]⁺, 220 (100) [Cp₂Zr]⁺.**

Bis(*h*⁵-cyclopentadienyl)-1,3-(diphenyl)-2,4,5,6,7,8-hexahydrocyclohepta[*c*]zirconacyclopentadiene **11 g: **10 g** (150 mg, 551 μmol), Rosenthal's reagent (259 mg, 552 μmol), toluene (6 mL), 22 °C, yield: 248 mg, 91%, 92% purity. ¹H NMR (500 MHz, C₆D₆): δ = 7.42–7.23 (m, 4H, g, g'), 7.09–6.95 (m, 6H, h, h', i), 5.93 (s, 10H, Cp), 2.38–2.31 (m, 4H, c), 1.61–1.50 ppm (m, 6H, d, e); ¹³C{¹H} NMR (126 MHz, C₆D₆): δ = 189.3 (a), 149.6 (b), 137.9 (f), 128.6 (g, g'), 126.3, 123.3 (h, h, l'), 112.2 (Cp), 31.6 (c), 31.1 ppm (d, e); HR-MS (EI, C₃₁H₃₀⁹⁰Zr): *m/z* calcd: 492.13891; found: 492.13982 (*R* = 10000); MS (EI, 70 eV, direct inlet, 200 °C): *m/z* (% relative intensity) = 492 (8) [*M*]⁺, 220 (100) [Cp₂Zr]⁺.**

Bis(*h*⁵-cyclopentadienyl)-1,3-bis(4-bromophenyl)-2,4,5,6-tetrahydrocyclopenta[*c*]zirconacyclopentadiene **11 h: **10 h** (150 mg, 373 μmol), Rosenthal's reagent (176 mg, 373 μmol), toluene (6 mL), 22 °C, yield: 223 mg, 96%. ¹H NMR (600 MHz, C₆D₆): δ = 7.49–7.44 (m, 4H, g, g'), 6.80–6.74 (m, 4H, f, f'), 5.70 (s, 10H, Cp), 2.33 (t, ³J = 7.1 Hz, 4H, c), 1.26 ppm (p, ³J = 7.1 Hz, 2H, d); ¹³C{¹H} NMR (151 MHz, C₆D₆): δ = 182.2 (a), 149.0 (b), 131.7 (g, g'), 128.0 (f, f'), 126.2 (e), 117.8 (h), 110.4 (Cp), 35.6 (c), 22.5 ppm (d); HR-MS (EI, C₂₉H₂₄^{79/80}Br₂⁹⁰Zr): *m/z* calcd: 621.92728; found: 621.92652 (*R* = 10000); MS (EI, 70 eV, direct inlet, 200 °C): *m/z* (% relative intensity) = 620 (69) [*M*]⁺, 220 (100) [Cp₂Zr]⁺.**

Bis(*h*⁵-cyclopentadienyl)-3,4-bis(4-(trifluoromethyl)phenyl)-2,5-bis(trimethylsilyl)zirconacyclopentadiene **11 i: **10 i** (150 mg, 650 μmol), Rosenthal's reagent (146 mg, 310 μmol), toluene (6 mL), 22 °C, yield: 206 mg, 94%. ¹H NMR (600 MHz, C₆D₆): δ = 7.10 (d, ³J = 7.8 Hz, 4H, e, e'), 6.48 (d, ³J = 7.98 Hz, 4H, d, d'), 6.08 (s, 10H, Cp), –0.28 ppm (s, 18H, SiMe₃); ¹³C{¹H} NMR (151 MHz, C₆D₆): δ = 206.3 (a), 149.4 (c), 148.2 (b), 130.2 (d, d'), 127.5 (q, ²J_{C-F} = 32.2 Hz, f), ²⁹Si{¹H} NMR (99 MHz, C₆D₆): δ = –62.1 ppm; ²⁹Si{¹H} NMR (99 MHz, C₆D₆): δ = –14.9 ppm; MS (EI, 70 eV, direct inlet, 200 °C): compound shows no molecule ion.**

Bis(*h*⁵-cyclopentadienyl)-1,3-bis(trimethylsilyl)-2*H*-phenanthro[9,10-*c*]zirconacyclopentadiene **11 j: **10 j** (122 mg, 352 μmol), Rosenthal's reagent (166 mg, 352 μmol), toluene (3 mL), 22 °C, yield: 192 mg, 96%. ¹H NMR (600 MHz, C₆D₆): δ = 7.60 (dd, ³J = 7.6 Hz, ⁴J = 1.3 Hz, 2H, e), 7.51 (dd, ³J = 7.6 Hz, ⁴J = 1.3 Hz, h), 7.14 (td, ³J = 7.6 Hz, ⁴J = 1.3 Hz, 2H, f), 7.07 (td, ³J = 7.6 Hz, ⁴J = 1.3 Hz, 2H, g), 5.94 (s, 10H, Cp), 0.21 ppm (s, 18H, SiMe₃); ¹³C{¹H} NMR (151 MHz, C₆D₆): δ = 208.9 (a), 137.5 (b), 136.2 (c or d), 133.7 (d or c), 129.7 (h), 128.8 (f), 126.9 (g), 123.7 (e), 110.2 (Cp), 3.8 ppm (SiMe₃); HR-MS (EI, C₃₂H₃₆²⁸Si₂⁹⁰Zr): *m/z* calcd: 566.13971; found: 566.13966 (*R* = 10000); MS (EI, 70 eV, direct inlet, 200 °C): *m/z* (% relative intensity) = 566 (5) [*M*]⁺, 220 (100) [Cp₂Zr]⁺.**

Bis(*h*⁵-cyclopentadienyl)-2,3,4,5-tetraphenylzirconacyclopentadiene **11 k: **10 k** (150 mg, 842 μmol), Rosenthal's reagent (198 mg, 421 μmol), toluene (6 mL), 22 °C, yield: 231 mg, 95%. ¹H NMR (500 MHz, C₆D₆): δ = 7.06–7.01 (m, 4H, i, i'), 7.00–6.93 (m, 4H, d, d'), 6.86–6.82 (m, 4H, e, e'), 6.82–6.79 (m, 2H, j), 6.76–6.71 (m, 2H, f), 6.71–6.66 (m, 4H, h, h'), 6.01 ppm (s, 10H, Cp); ¹³C{¹H} NMR (126 MHz, C₆D₆): δ = 194.8 (a), 148.6 (g), 142.8 (b), 141.7 (c), 131.3 (i,**

i'), 128.3 (h, h'), 127.7 (d, d'), 127.2 (e, e'), 125.1 (f), 123.4 (j), 112.3 ppm (Cp); HR-MS (EI, C₃₈H₃₀⁹⁰Zr); *m/z* calcd: 576.13891; found: 576.13987 (*R* = 10000); MS (EI, 70 eV, direct inlet, 200 °C): *m/z* (% relative intensity) = 576 (18) [M]⁺, 220 (100) [Cp₂Zr]⁺.

Bis(*h*⁵-cyclopentadienyl)-3,4-di(naphthalen-1-yl)-2,5-bis(trimethylsilyl)zirconacyclopentadiene 11i: 101 (150 mg, 669 μmol), Rosenthal's reagent (158 mg, 335 μmol), toluene (6 mL), 22 °C, yield: 202 mg, 90%. ¹H NMR (600 MHz, C₆D₆): δ = 8.32 (dq, ³*J* = 8.4 Hz, ⁴*J* = 0.9 Hz, 2H, k), 7.46 (ddd, ³*J* = 8.4 Hz, ³*J* = 6.8 Hz, ⁴*J* = 1.3 Hz, 2H, j), 7.38 (ddt, ³*J* = 8.1 Hz, ⁴*J* = 1.2 Hz, 0.6 Hz, 2H, h), 7.21 (ddd, ³*J* = 8.1 Hz, ³*J* = 6.8 Hz, ⁴*J* = 1.3 Hz, 2H, i), 7.02 (d, ³*J* = 8.1 Hz, 2H, f), 6.84 (dd, ³*J* = 7.0 Hz, ⁴*J* = 1.3 Hz, 2H, d), 6.59 (dd, ³*J* = 8.2 Hz, ³*J* = 7.0 Hz, 2H, e), 6.34 (s, 10H, Cp), -0.39 ppm (m, 18H, SiMe₃); ¹³C{¹H} NMR (151 MHz, C₆D₆): δ = 207.7 (a), 150.0 (b), 142.6 (c), 133.4 (l), 132.8 (g), 128.0 (h), 126.8 (k), 126.0 (d), 125.8 (f), 124.8 (j), 124.6 (i), 124.0 (e), 111.1 (Cp), 2.1 ppm (SiMe₃); ²⁹Si{¹H} NMR (99 MHz, C₆D₆): δ = -14.9 ppm; MS (EI, 70 eV, direct inlet, 200 °C): compound shows no molecule ion.

Monitoring of reaction progress of the zirconacyclopentadienes (11 a–l) by ¹H NMR spectroscopy

Procedure for Negishi's conditions: example 11 a

To a solution of Cp₂ZrCl₂ (67.7 mg, 231 μmol) in THF (2.0 mL) at -78 °C, *n*-butyllithium (180 μL, 463 μmol; 2.59 M in hexanes) was added dropwise over the course of 1 min. The reaction mixture was stirred at -78 °C for 1 h and a solution of **10 a** (100 mg, 231 μmol) in THF (1.0 mL) was added. The cooling bath was removed, and the reaction's time started to run. A sample (0.30 mL, 14 μmol) was taken after 10 min, 30 min, 1 h, 3 h, and 22 h and the solvent was removed immediately under inert conditions. Naphthalene in C₆D₆ was added (0.2 mL, 0.06 M, 14 μmol) to the sample and used as an internal standard. The reaction progress was analyzed by ¹H NMR spectroscopic measurements of each sample.

Procedure for Rosenthal's condition: example 11 a

In a GB, a solution of **9** (109 mg, 230 μmol) and **10 a** (100 mg, 230 μmol) in toluene (5 mL) was stirred at 22 °C. A sample of the reaction (0.3 mL, 14 μmol) was taken after 10 min, 30 min, 1 h, 3 h, and 22 h and the solvent was removed immediately under inert conditions. Naphthalene in C₆D₆ was added (0.2 mL, 0.06 M, 14 μmol) to the sample and used as an internal standard. The reaction progress was analyzed by ¹H NMR spectroscopic measurements of each sample.

More detailed reaction monitoring conditions of both routes for the zirconacyclopentadienes **11 b–l** can be found in the Supporting Information.

Acknowledgments

S.U.-R. thanks the German Academic Exchange Service (DAAD) and the Colfuturo Foundation for a PhD scholarship, grant number A/13/72356. This research has been supported by the Institutional Strategy of the University of Bremen, funded by the German Excellence Initiative.

Conflict of interest

The authors declare no conflict of interest.

Keywords: metallocycles · Negishi's reagent · Rosenthal's reagent · substituent effects · zirconium

- [1] A. W. Trautwein, R. D. Süßmuth, G. Jung, *Bioorg. Med. Chem. Lett.* **1998**, 8, 2381–2384.
- [2] a) C. Wang, H. Dong, W. Hu, Y. Liu, D. Zhu, *Chem. Rev.* **2012**, 112, 2208–2267; b) A. Facchetti, *Chem. Mater.* **2011**, 23, 733–758; c) Y. Matano, H. Ohkubo, T. Miyata, Y. Watanabe, Y. Hayashi, T. Umeyama, H. Imahori, *Eur. J. Inorg. Chem.* **2014**, 1620–1624.
- [3] K. E. Horner, P. B. Karadakov, *J. Org. Chem.* **2013**, 78, 8037–8043.
- [4] a) J. O. C. Jimenez-Halla, E. Matito, M. Solà, H. Braunschweig, C. Hörl, I. Kruppenmacher, J. Wahler, *Dalton Trans.* **2015**, 44, 6740–6747; b) A. Iida, S. Yamaguchi, *J. Am. Chem. Soc.* **2011**, 133, 6952–6955.
- [5] a) S. Yamaguchi, Y. Itami, K. Tamao, *Organometallics* **1998**, 17, 4910–4916; b) B. Goldfuss, P. v. R. Schleyer, *Organometallics* **1997**, 16, 1543–1552; c) M. Saito, M. Sakaguchi, T. Tajima, K. Ishimura, S. Nagase, *Phosphorus Sulfur Silicon Relat. Elem.* **2010**, 185, 1068–1076.
- [6] a) S. Khaghaninejad, M. M. Heravi, in *Advanced Heterocyclic Chemistry Vol. 111* (Ed.: A. R. Katritzky), Academic Press, Waltham, **2014**, pp. 95–146; b) A. J. Ashe, L. L. Lohr, S. M. Al-Taweel, *Organometallics* **1991**, 10, 2424–2431; c) G. Mross, E. Holtz, P. Langer, *J. Org. Chem.* **2006**, 71, 8045–8049.
- [7] a) Y. Zhang, L. Liu, T. Chen, Z. Huang, W.-X. Zhang, Z. Xi, *Organometallics* **2019**, 38, 2174–2178; b) J. Wei, L. Liu, M. Zhan, L. Xu, W.-X. Zhang, Z. Xi, *Angew. Chem. Int. Ed.* **2014**, 53, 5634–5638; *Angew. Chem.* **2014**, 126, 5740–5744.
- [8] a) J. Dubac, A. Laporterie, G. Manuel, *Chem. Rev.* **1990**, 90, 215–263; b) W. Ma, C. Yu, T. Chen, L. Xu, W.-X. Zhang, Z. Xi, *Chem. Soc. Rev.* **2017**, 46, 1160–1192; c) L. Liu, W. Geng, Q. Yang, W.-X. Zhang, Z. Xi, *Organometallics* **2015**, 34, 4198–4201.
- [9] a) Z. Xi, R. Hara, T. Takahashi, *J. Org. Chem.* **1995**, 60, 4444–4448; b) P. J. Fagan, W. A. Nugent, *J. Am. Chem. Soc.* **1988**, 110, 2310–2312; c) X. Yan, C. Xi, *Acc. Chem. Res.* **2015**, 48, 935–946; d) G. He, L. Kang, W. Torres Delgado, O. Shynkaruk, M. J. Ferguson, R. McDonald, E. Rivard, *J. Am. Chem. Soc.* **2013**, 135, 5360–5363; e) I.-M. Ramirez y Medina, M. Rohdenburg, F. Mostaghimi, S. Grabowsky, P. Swiderek, J. Beckmann, J. Hoffmann, V. Dorcet, M. Hissler, A. Staubitz, *Inorg. Chem.* **2018**, 57, 12562–12575; f) Z. Dong, C. R. W. Reinhold, M. Schmidtman, T. Müller, *Organometallics* **2018**, 37, 4736–4743; g) P. Tholen, Z. Dong, M. Schmidtman, L. Albers, T. Müller, *Angew. Chem. Int. Ed.* **2018**, 57, 13319–13324; *Angew. Chem.* **2018**, 130, 13503–13508.
- [10] a) G. R. Kiel, M. S. Ziegler, T. Tilley, *Angew. Chem. Int. Ed.* **2017**, 56, 4839–4844; *Angew. Chem.* **2017**, 129, 4917–4922; b) J. R. Nitschke, S. Zürcher, T. D. Tilley, *J. Am. Chem. Soc.* **2000**, 122, 10345–10352.
- [11] S. S. H. Mao, T. D. Tilley, *Macromolecules* **1997**, 30, 5566–5569.
- [12] E. Negishi, S. J. Holmes, J. M. Tour, J. A. Miller, F. E. Cederbaum, D. R. Swanson, T. Takahashi, *J. Am. Chem. Soc.* **1989**, 111, 3336–3346.
- [13] T. Takahashi, M. Kageyama, V. Denisov, R. Hara, E. Negishi, *Tetrahedron Lett.* **1993**, 34, 687–690.
- [14] E. Negishi, F. E. Cederbaum, T. Takahashi, *Tetrahedron Lett.* **1986**, 27, 2829–2832.
- [15] a) U. Rosenthal, A. Ohff, M. Michalik, H. Görls, V. V. Burlakov, V. B. Shur, *Angew. Chem. Int. Ed. Engl.* **1993**, 32, 1193–1195; *Angew. Chem.* **1993**, 105, 1228–1230; b) U. Rosenthal, A. Ohff, W. Baumann, A. Tillack, H. Görls, V. V. Burlakov, V. B. Shur, *Zeitschr. Anorg. Allg. Chem.* **1995**, 621, 77–83.
- [16] V. K. Dioumaev, J. F. Harrod, *Organometallics* **1997**, 16, 1452–1464.
- [17] V. K. Dioumaev, J. F. Harrod, *Organometallics* **1997**, 16, 2798–2807.
- [18] a) J. Linshoef, *Synlett* **2014**, 25, 2671–2672; b) U. Rosenthal, *Angew. Chem. Int. Ed.* **2018**, 57, 14718–14735; *Angew. Chem.* **2018**, 130, 14932–14950.
- [19] A. D. Miller, J. L. McBee, T. D. Tilley, *J. Am. Chem. Soc.* **2008**, 130, 4992–4999.
- [20] a) J. Linshoef, E. J. Baum, A. Hussain, P. J. Gates, C. Näther, A. Staubitz, *Angew. Chem. Int. Ed.* **2014**, 53, 12916–12920; *Angew. Chem.* **2014**, 126, 13130–13134; b) S. Urrego-Riveros, I. M. Ramirez y Medina, J. Hoffmann, A. Heitmann, A. Staubitz, *Chem. Eur. J.* **2018**, 24, 5680–5696.
- [21] U. Rosenthal, *Eur. J. Inorg. Chem.* **2019**, 895–919.

- [22] Y. Ura, L. Yanzhong, Z. Xi, T. Takahashi, *Tetrahedron Lett.* **1998**, *39*, 2787–2790.
- [23] K. Oouchi, M. Mitani, M. Hayakawa, T. Yamada, T. Mukaiyama, *J. Organomet. Chem.* **1996**, *516*, 111–114.
- [24] a) B. Jiang, T. D. Tilley, *J. Am. Chem. Soc.* **1999**, *121*, 9744–9745; b) B. L. Lucht, M. A. Buretea, T. D. Tilley, *Organometallics* **2000**, *19*, 3469–3475.
- [25] H.-S. Lin, L. A. Paquette, *Synth. Commun.* **1994**, *24*, 2503–2506.
- [26] a) G. Sheldrick, *Acta Crystallogr. Sect. A* **2008**, *64*, 112–122; b) L. Farrugia, *J. Appl. Crystallogr.* **1999**, *32*, 837–838.
- [27] O. V. Dolomanov, L. J. Bourhis, R. J. Gildea, J. A. K. Howard, H. Puschmann, *J. Appl. Crystallogr.* **2009**, *42*, 339–341.
- [28] The signal from the carbon atom bond to boron was not visible owing to the high quadrupole moment of the boron nucleus.
- [29] The signal is overlapping with the solvent signal.

Manuscript received: May 16, 2019

Accepted manuscript online: July 25, 2019

Version of record online: ■ ■ ■ ■, 0000

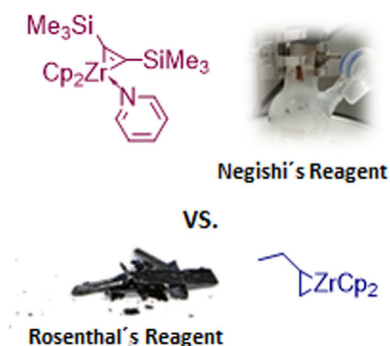
FULL PAPER

Metallacycles

 S. Urrego-Riveros, I.-M. Ramirez y Medina,
D. Duvinage, E. Lork, F. D. Sönnichsen,
A. Staubitz*

■■ - ■■

  Negishi's Reagent Versus Rosenthal's
Reagent in the Formation of
Zirconacyclopentadienes

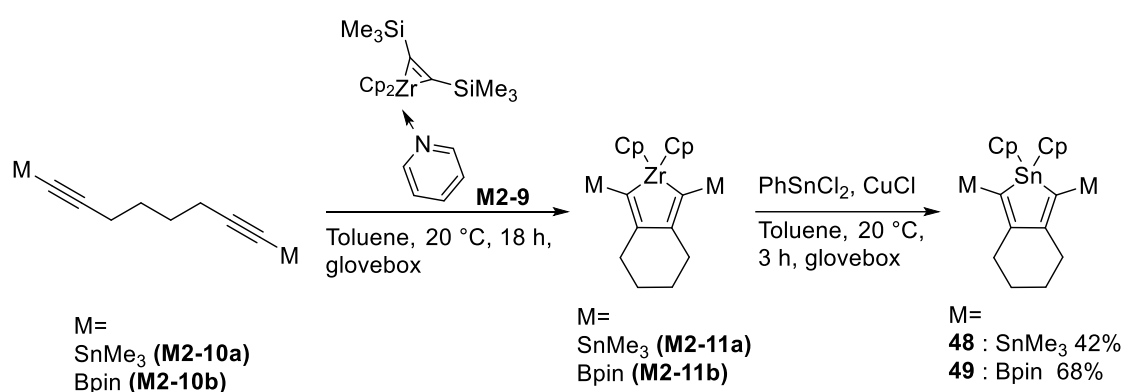


Negishi vs. Rosenthal: Two "Cp₂Zr" sources, the Negishi and the Rosenthal reagents, were compared with respect to yield, reaction, time, and product stability. In total, twelve compounds with different substituents were used for the reductive coupling by these zirconium sources.

3.2.3. Reactivity of Stannoles

3.2.3.1. Synthesis and Characterization of Stannoles with Nucleophilic Motifs in 2- and 5-Position

Two novel stannoles **48** and **49** bearing trimethylstannyl and pinacol boronate groups respectively, in the 2- and 5-position of the ring, were prepared to be used as nucleophilic species in cross-coupling reactions testing the reactivity of stannoles. Both were obtained by a transmetalation from the zirconacyclopentadienes **M2-11a** and **M2-11b** in a Fagan-Nugent reaction with yields of 42% and 68% for **48** and **49** respectively (Scheme 19). The zirconacyclopentadienes **M2-11a** and **M2-11b** were formed in a cyclization reaction of dialkynes **M2-10a** and **M2-10b** with the active "Cp₂Zr" species of the Rosenthal's reagent.



Scheme 19. Synthetic path of stannoles **48** and **49** from Fagan-Nugent reaction from zirconacyclopentadienes **M2-11a** and **M2-11b** respectively.

The characterization by ¹¹⁹Sn NMR showed that the chemical shift of the tin in the cycle of **48** was -35.28 ppm, and for **49** the shift was -34.67 ppm, which is similar to values in other stannoles.^[62b, 78] The ¹¹⁹Sn shift of the trimethylstannyl group in **48** (δ Sn = -47.72 ppm) was comparable to the ones of the silole **50** and germole **51** congeners. For **50** and **51** the two ¹¹⁹Sn shifts of the trimethylstannyl group are in the range from -40.8 to -50.1 ppm (Figure 27).^[79]

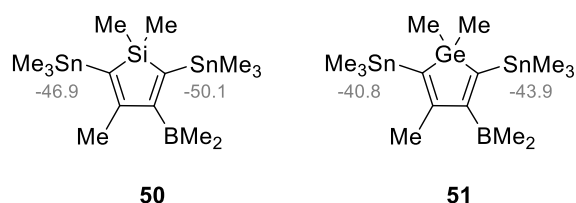


Figure 27. Silole **50** and germole **51** like the stannole **48** with their respective ¹¹⁹Sn chemical shifts.

The crystal structure confirmed the formation of the stannoles. The endocyclic angle (C8-Sn-C1) is similar with 85.07 °for **48** and 84.28 °for **49** suggesting that the arrangement of

the tin atom lays in a distorted tetrahedral environment comparable to other stannoles.^[62b, 78] As well the long bonds Sn-C1 (2.137 for **48** and 2.1361 Å for **49**) and Sn-C8 (2.132 for **48** and 2.133 Å for **49**) within the stannole ring are large as it is expected for the big atom size of the tin, in comparison with the bond Si-C in siloles (1.887).^[62a]

The stannole **48** crystallizes in an orthorhombic system, space group $Pc2_1$, $Z' = 3$. One of the molecules in the asymmetric unit is shown in Figure 28 with atom numbering scheme. The phenyl group attached to the stannole ring is disordered in two molecules within the asymmetric unit. Within a molecule, though all the three tin atoms are in tetrahedral coordination, the bond angle distributions are different in case of the Sn within stannole ring (85.19 °), compared to the terminal trimethylstannyl groups (116.2 °) (Table 10 in Chapter 5.5). The crystal structure is stabilized by various weak dispersive interactions (C–H... π , C–H...Sn, H...H). (Table 11 and Table 12 in Chapter 5.5. and Figure 29).

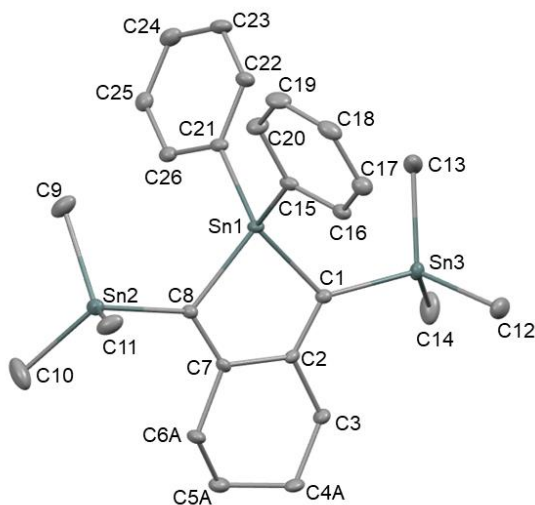


Figure 28. The asymmetric unit of **49** with 30% probability ellipsoids ; atom numbering scheme is shown. The H atoms have been omitted for clarity.

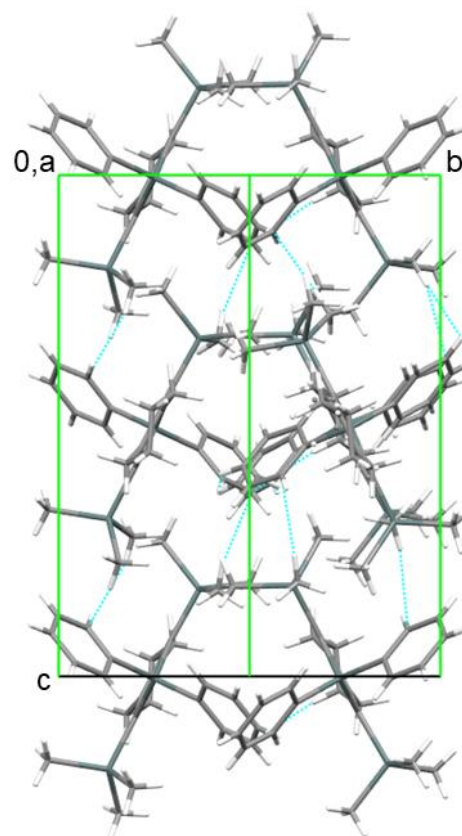


Figure 29. The crystal packing of **49** is viewed perpendicular to a axis, the structure is stabilized by various C–H... π and H...H interactions. (The green lines, parallel to c , are the 2_1 screw axis.)

The stannole **49** crystallizes in a monoclinic system, space group $P2_1/c$, $Z' = 1$. The asymmetric unit is shown in Figure 30 with atom numbering scheme. One of the $\text{BO}_2(\text{CH}_3)_2$ group attached to the

central stannole ring is disordered. The crystal structure was stabilized by various weak dispersive interactions ($C-H\cdots O$, $C-H\cdots\pi$, $H\cdots H$) (Figure 31 and Figure 32).

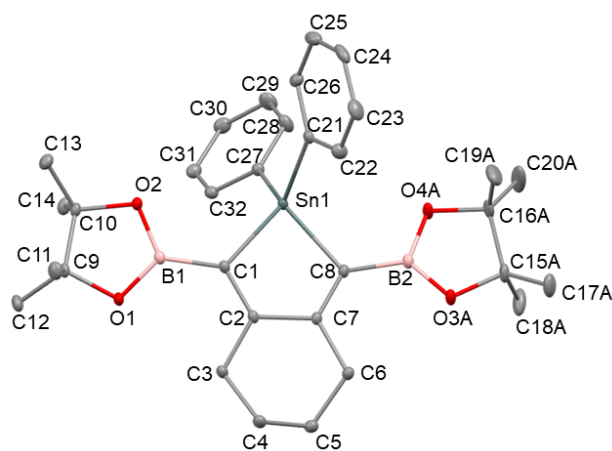


Figure 30. The asymmetric unit of **49** with 30% probability ellipsoids; the major component of the disordered part is shown along with atom numbering scheme. The H atoms have been omitted for clarity.

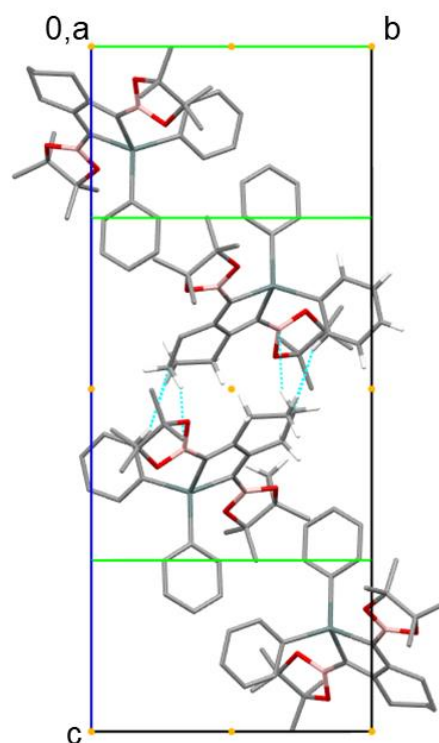


Figure 31. The two molecules of **49** related by inversion center (yellow dots) are stabilized by intermolecular $C-H\cdots\pi$ (BO2 unit) and $H\cdots H$ dispersive interactions between phenyl and C6H8 ring, viewed perpendicular to a axis. (The green lines, parallel to b , are the 2-fold axis.)

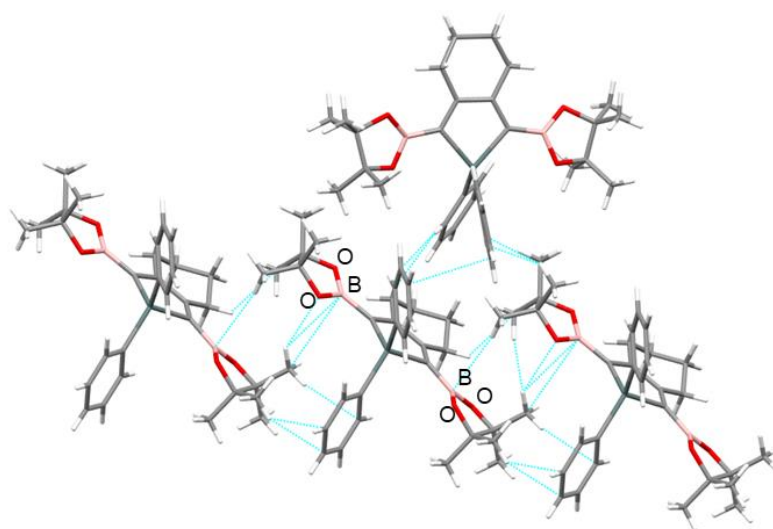


Figure 32. The molecules of **49** are held together by various intermolecular weak $C-H\cdots\pi$ and $C-H\cdots O$ interactions.

For **48** it was possible to calculate the HOMO and LUMO orbitals (Figure 33). As for other stannoles, the tin atom from the stannole group is involved in the LUMO and not involved in the HOMO, which explains the $\sigma^*-\pi^*$ conjugation inside the ring. The calculations for **49** were not done during the time of this thesis.²

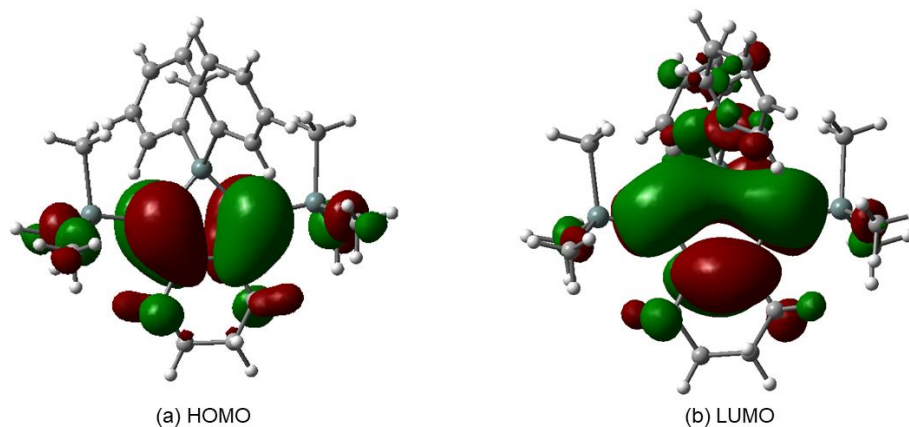


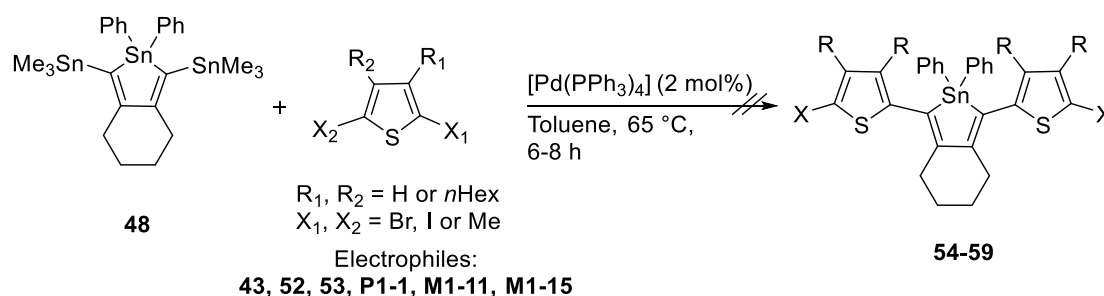
Figure 33. Isosurfaces representations and energy values of the (a) HOMO, (b) LUMO for **48** (Contour level = 0.03, blue positive, red negative.) HOMO, LUMO of **48**; $E(\text{HOMO}) = -0.21141$ a.u.; $E(\text{LUMO}) = -0.05385$ a.u. $\Delta E(\text{LUMO-HOMO}) = 0.1575$ a.u., 4.29 eV. (gas phase optimized geometry, at b3lyp/LanL2DZ, GD3BJ dispersion).

3.2.3.2. Cross-Coupling Reactions

The aim was to analyse the reactivity of **48** and **49** in cross coupling reactions.

For the stannole **49** Stille cross-coupling reactions with several electrophiles (commercial and previously synthesized) were tested (Scheme 20). The Table 4 summarizes the di-electrophiles used and expected products.

For any of the reactions an analysable product could be observed because of the challenging purification and the formation of different side by-products.



Scheme 20. Stille cross-coupling reaction of stannole **48** with several electrophiles.

² The X-Ray crystal measurements and calculations were performed by Dr. Rumpa Pal from the group of Prof. Grabowsky in the University of Bremen.

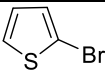
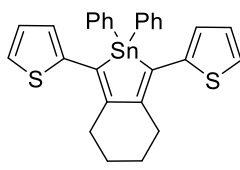
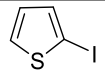
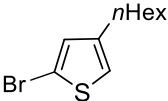
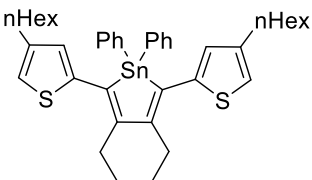
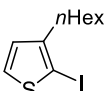
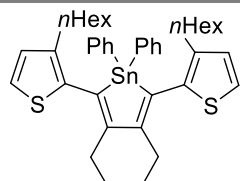
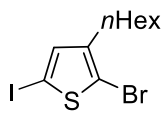
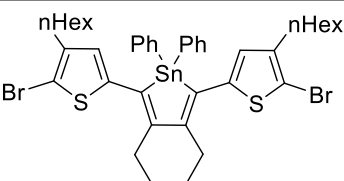
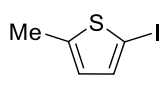
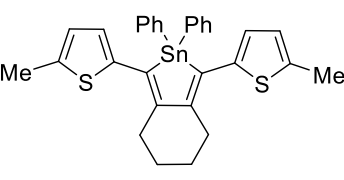
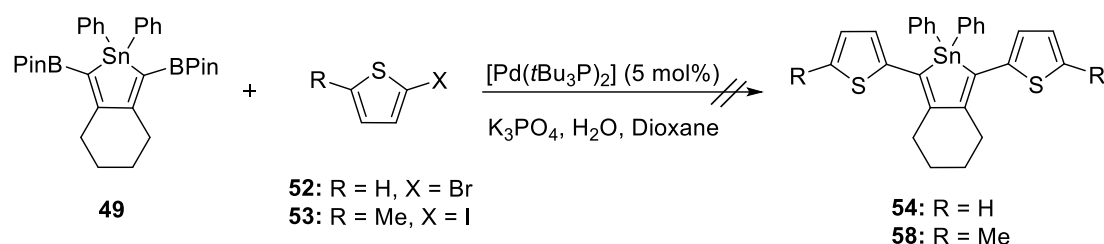
Entry	Electrophile	Expected product
1	 52	 54
2	 M1-15	
3	 M1-11	 55
4	 43	 56
5	 P1-11	 57
6	 53	 58

Table 3. Electrophiles used in the Stille reaction with the stannole **48** and expected products.

In the case of using the stannole **49** in Suzuki-Miyaura cross-coupling reactions, two reactions were tested using two different electrophiles (**52** and **53**) (Scheme 21). The products **54** and **58** were soluble in common solvents such as DCM and chloroform. However, it was not possible to obtain a clean ^1H NMR spectrum, in which the signatory proton signals of the thiophene were distinguishable. For future work, the optimization of this reaction should be studied by controlling various conditions such as type of catalyst, solvent, amount of water, type of salt and temperature. As motivation for continuing this research, similar conditions reactions were observed in group 15 element containing heterocycles. Rivards, *et al.* for example, used tellurophene **59** and selenophene **60** (Figure

34) in a Suzuki-Miyaura reaction with 2,5-diiodo-3-hexylthiophene producing polymers with high yields.^[80]



Scheme 21. Suzuki-Miyaura cross-coupling reaction of stannole **49** with electrophiles **52** and **53**.

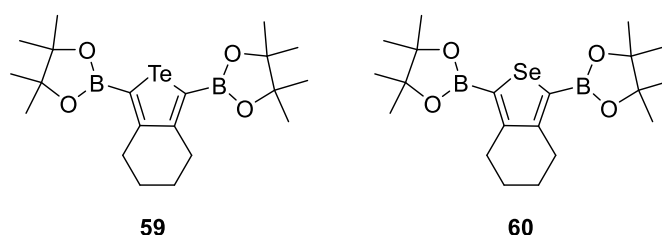
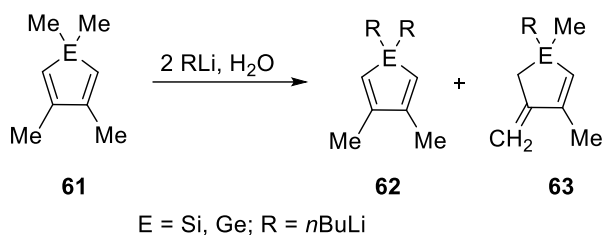


Figure 34. Similar tellurophene **59** and selenophene **60** to the stannole **49**.

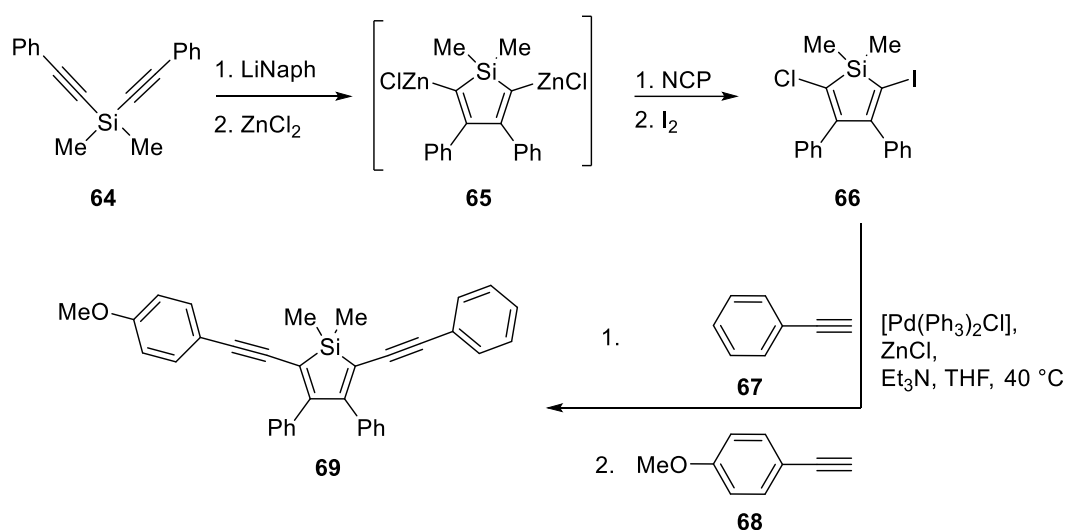
Under Suzuki-Miyaura and Stille cross-coupling conditions, it was not successful to form the new C-C bond between the 2,5-dinucleophilestannoles **48** and **49** with different electrophiles (Scheme 20 and Scheme 21). One explanation for the difficulties in the reactivity could be the high steric hindrance by the cyclobutene in the 3- and 4-position and the phenyl groups at the tin from the ring.^[66] In the literature, there are reports suggesting that the reactivity of stannoles is based on their substituents on the ring or directly on the tin atom.^[66] In this case, it is important to compare stannoles with more intensively investigated metalloles for example siloles. For instance, the reactivity in the 2,5-trimethyltin substituted siloles is low, which can be an indication that stannole **48** shows similar properties (Scheme 20).^[81] The Suzuki-Miyaura reaction of siloles with boronic acid as substituents and dibutyl chains in the silicon atom was reported to be successful.^[81c] As it was not in the case of the stannole **49** the studies can be directed as for example in the use of a stronger base to improve the reaction.^[82]

As well it is important to remark that under certain conditions as for example in lithiations, stannoles as other metalloles **61**, can suffer isomerization obtaining a mixture of isomers **62** and **63** (Scheme 22).^[83] Therefore it is possible that in the case of the cross-coupling reactions of the stannoles **48** and **49**, isomers were formed which makes the identification of the products that challenging.



Scheme 22. Isomerization of metalloles as **61** under lithiation conditions, producing a mixture of isomers **62** and **63**.

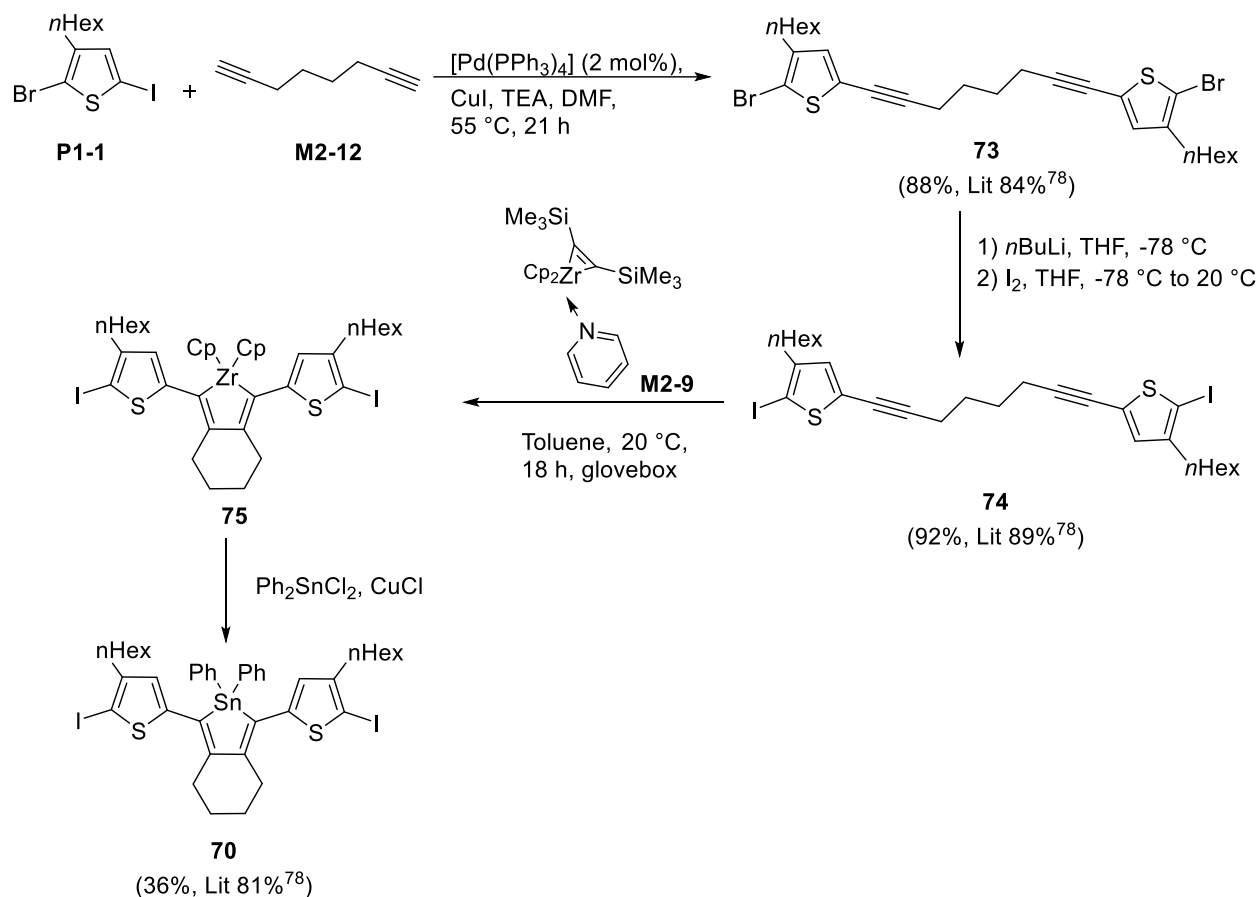
Cross-coupling reactions directly at the 2- and 5-position in siloles are possible. For example, the halogenated silole **66** was used as electrophile in a Negishi coupling with two acetylene derivatives (**67** and **68**) to form the silole derivative **69** (Scheme 23).^[84] The 2,5-halogenated silole **66** was formed from the initial cyclization of the silicon diyne derivative **64** with lithium naphthalenide, followed by the quenching with ZnCl to form dizincated silole **65** and a subsequent halogenation. Even that the conditions from Scheme 23 can be used for stannoles it is necessary to keep in mind that the reactivity of stannoles and siloles cannot be transferred completely because of the atom size difference between both atoms and the high stability of the Si-C (1.88 Å) bond in siloles.^[62a, 83, 85]



Scheme 23. Successful Negishi cross-coupling reactions of the dihalogenated siloles **66** to form siloles derivatives as **69**.^[84]

3.2.3.3. Polymers Containing Thienyl and Stannole Rings in Different Ratios

Thiophene and its derivatives belong to the most studied molecules in the field of semiconducting polymers. Recently, it has been found out that thiophenes as substituents in the 2- and 5-position of the stannoles can tailor the optoelectronic properties of the stannoles.^[62b] In addition, the combination of stannole with thiophene form a push-pull system where the stannole acts as electron pull motif, due to the low energy LUMO, decreasing the band gap of the formed molecule. Polymers containing stannole and thienyl



Scheme 25. Synthetic path to obtain stannole **70**.

In order to optimize the synthesis of the polymer **72** with high molecular weight and low polydispersity the ratio of both starting materials **70** and **71** were varied.^[87] The reason of this variation is to study the compensation of possible impurities that can influence the performance of the polymerization. The Carother's equation (eq. 5) indicates for such type of polymerization that every change in the stoichiometric ratio between the monomers will represent a change in the molecular weight and \mathcal{D} of the polymer.^[49]

For the experiments the ratio of the monomer **70** was varied from 1.00 to 1.15 equivalents remaining the monomer **71** constant in 1.00 equivalents. Two catalysts were screened as well: $[\text{Pd}(t\text{Bu}_3\text{P})_2]$ and $[\text{Pd}(\text{PPh}_3)_4]$. ^1H NMR measurements were done to identify the polymer in every sample. GPC measurements were used to calculate the molecular weight and polydispersity, using chloroform as solvent. In THF, another usual GPC solvent, the polymer got decomposed. Table 4 summarizes the obtained results of the experiments. It was observed that the best reaction conditions are using 1.05 eq. of **70** as electrophile and $[\text{Pd}(\text{PPh}_3)_4]$ as catalyst. In this case the polymer formed has higher molecular weight ($M_n = 3.94 \text{ kDa}$) lower polydispersity (1.72) and lower energy absorption compared to the other experiments. The NMR analysis shows that the formation of the polymer is satisfactory in the experiments 2-6 (Figure 35).

Entrance	Ratio 70 : 71	catalyst 5 mol%	Mn(kDa)	Đ	λ_{\max} (nm) in DCM
1	1.00 : 1.00	[Pd(<i>t</i> -Bu ₃ P) ₂]	1.99	2.35	501
2	1.05 : 1.00	[Pd(<i>t</i> -Bu ₃ P) ₂]	3.26	1.80	509
3	1.10 : 1.00	[Pd(<i>t</i> -Bu ₃ P) ₂]	2.91	1.79	495
4	1.15 : 1.00	[Pd(<i>t</i> -Bu ₃ P) ₂]	3.29	1.69	501
5	1.00 : 1.00	[Pd(PPh ₃) ₄]	3.31	1.70	516
6	1.05 : 1.00	[Pd(PPh ₃) ₄]	3.94	1.72	533
7	1.10 : 1.00	[Pd(PPh ₃) ₄]	3.70	1.64	514
8	1.15 : 1.00	[Pd(PPh ₃) ₄]	2.82	1.59	511

Table 4. Results from the ratio screening between the monomers **70** and **71**, using two catalysts.

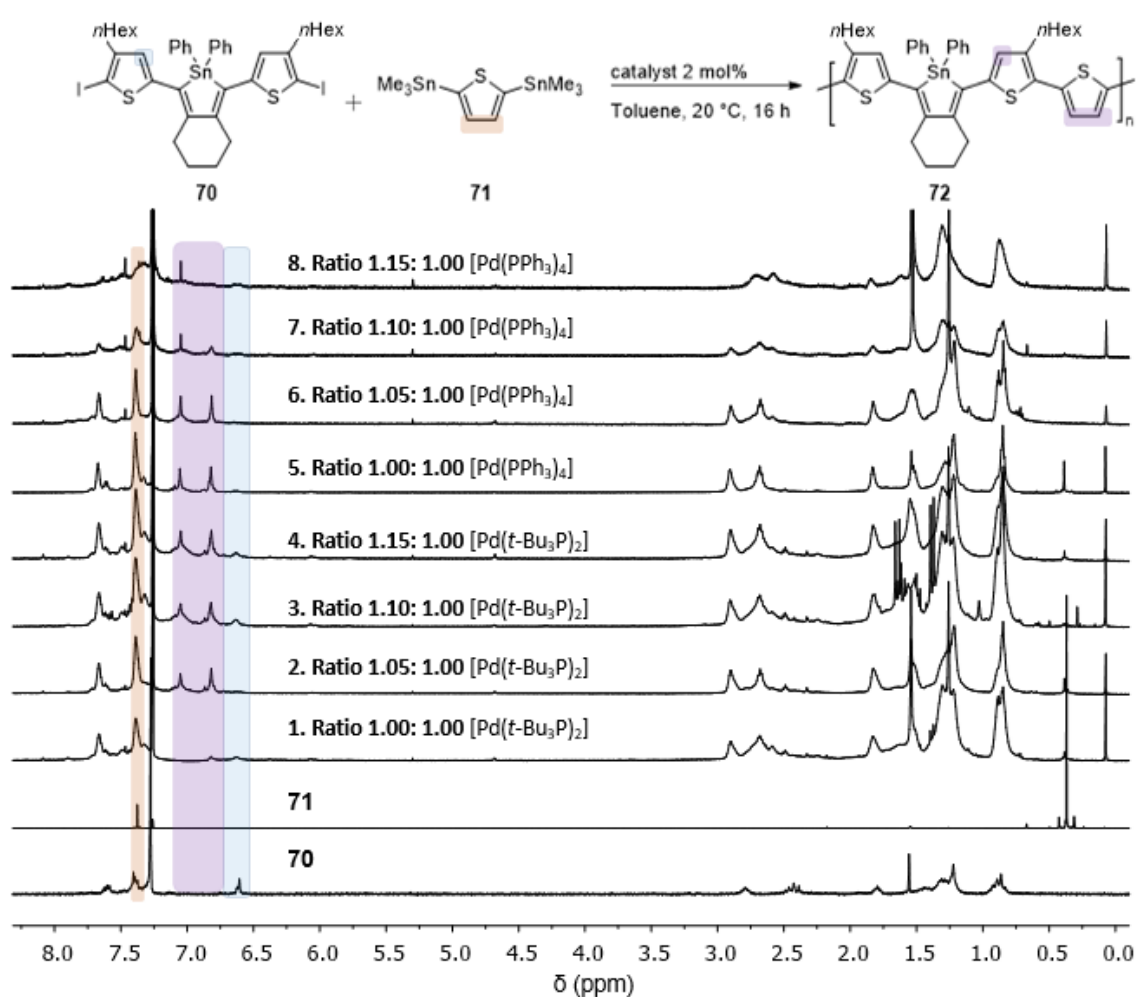


Figure 35. ¹H NMR spectra comparison of the experiment of polymerization to form **72** with different catalyst and ratio between starting materials **70** and **71**.

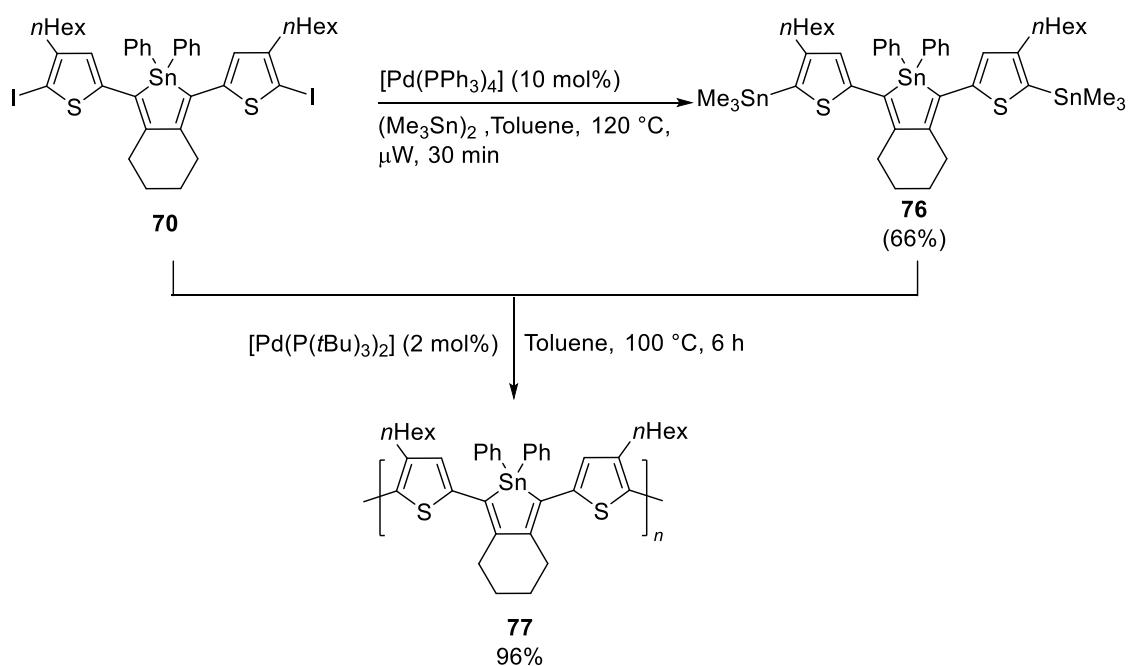
In the original publication the Stille polymerization of the monomers **70** and **71** in a ratio 1:1 was heated under normal conditions (Scheme 24); a new experiment, heating by microwave conditions was performed confirming the selectivity in the formation of the desirable polymer.

With microwave irradiation, the time of the reaction decreased from 16 h to 4 h giving polymers with similar \bar{D} (2.35) and smaller in size (M_n of 3.82 kDa, M_w of 9.0 kDa) than the reported by Linsoeft *et al.* (M_n of 6.8 kDa and \bar{D} of 2.5).^[78] With this result it is confirmed that the use of microwave irradiation decreases the reaction time and forms the desired product with high selectivity. However this result together with the ones from the entry 5 of the Table 4 does not show a reproducibility regarding the reported results showing that the reaction is very fickle and the optimization is challenging.

As the ratio and the choice of catalyst seems to have an important impact on the results, further investigation bears a lot of potential in optimizing the reaction, obtaining higher molecular weights and lower polydispersity compared the original publication. With the help of the microwave this can be proceeded in a less time-consuming way.

Polymers with Thienyl and Stannole Moieties with a Ratio of 2 : 1

The synthetic route proposed to form the polymer **77** with a ratio thienyl : stannole 2 : 1 was based on a Stille cross-coupling reaction between the stannoles **70** and **76** (Scheme 26). The stannole **76** was prepared by the exchange of the iodo motif from the monomer **70** by trimethylstannyl functional groups in a yield of 66%.^[86, 88]



Scheme 26. Reaction conditions to obtain polymer with ratio thienyl to stannole 2:1 **77**.

The reaction for the formation of **77** was followed by thin layer chromatography (TLC) and ^1H NMR spectroscopy. After 5 h of heating at 100 °C no starting material was observed. The crude product was washed with methanol by Soxhlet extraction over two days. After changing the solvent to chloroform and removing the volatiles, red solid material of compound **77** was obtained. The molecular weight of the product of **77** was calculated by GPC using conventional calibration and had a M_n of 1.30 kDa and a \bar{D} of 1.41, suggesting two repeating units. The ^1H NMR spectrum confirmed the formation of broad signals with chemical shifts like in the polymer **72**, where two thiophenes have hexyl chain in the 3-position (Figure 36). The broad peak in the thiophene area at 6.84 ppm lays in between the peaks of the starting material **70** (6.60 ppm) and **76** (6.60 ppm) confirming the presence of a new proton in the thiophene region in **77**.

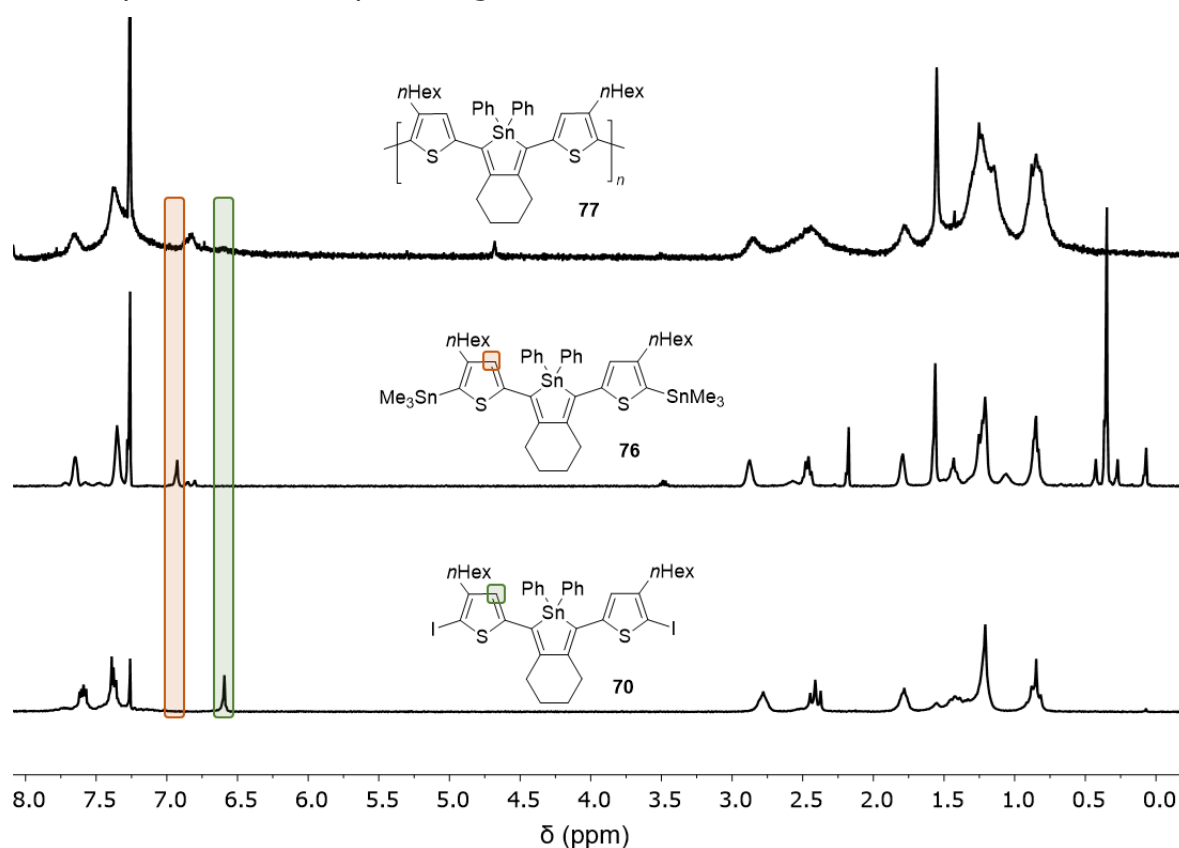
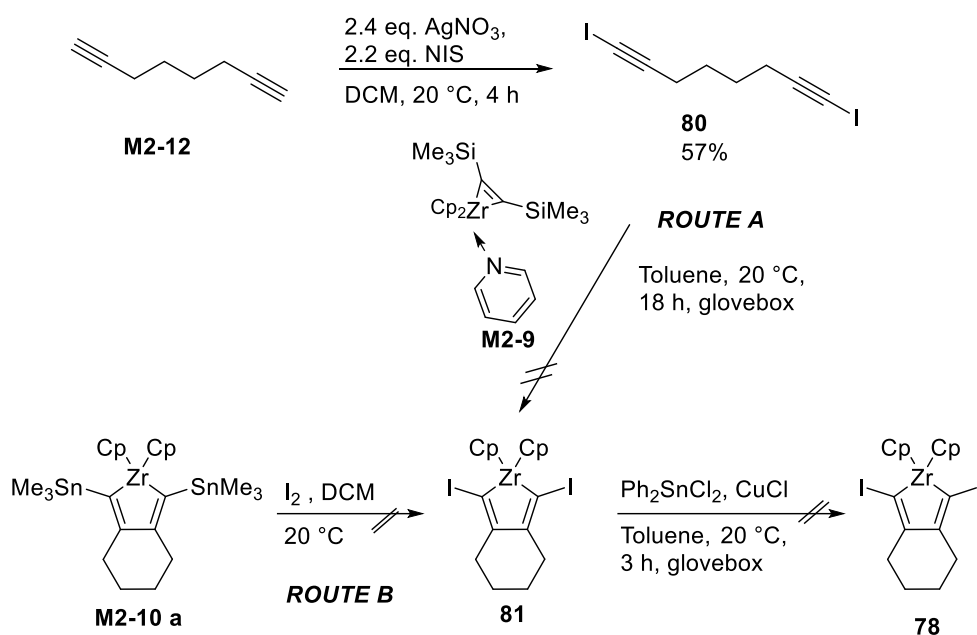


Figure 36. Comparison of ^1H NMR spectra of the starting materials **70** and **76** with the dimer **77**. In the orange box the tracing of the proton from the thienyl ring of the starting material **76** and the green box the proton from the starting material **70** can be observed.

The UV-vis spectrum shows that the dimer **77** has a slight hypsochromic effect ($\lambda_{\text{max}} = 436$ nm) compared to the starting materials (λ_{max} **70** = 440 nm and λ_{max} **76** = 439 nm). The shape of the spectrum is broad, as it is expected for conjugated materials (Figure 37).



Scheme 28. Synthetic routes proposed to obtain the dihalogenated stannole **78**.

While the precursor **80** was successfully synthesized via a silver nitrate catalysed halogenation of 1,7-octadiyne (**M2-12**) with a yield of 57%,^[89] the following reaction to produce the intermediate **81** was not. The route *B* was as well unsuccessful. For the synthetic routes *A* and *B* the ring of the zirconacyclopentadiene **81** opened forming the iodinated by-products **82** and **83** respectively (Figure 38). The by-products and decomposition of the zirconium reagent were identified by the analysis of the ¹H NMR spectrum (Figure 39 and Figure 40). The ring-opening was observed in literature when zirconacyclopentadienes reacted with iodine.^[90]

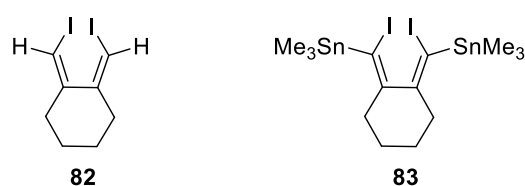


Figure 38. (1*Z*,2*Z*)-1,2-bis(iodomethylene)cyclohexane (**82**) and (1*Z*,2*Z*)-1,2-bis(iodo(trimethylstannyl)methylene)cyclohexane (**83**) formed as by-product in the attempt to produce the zirconacyclopentadiene **81**.

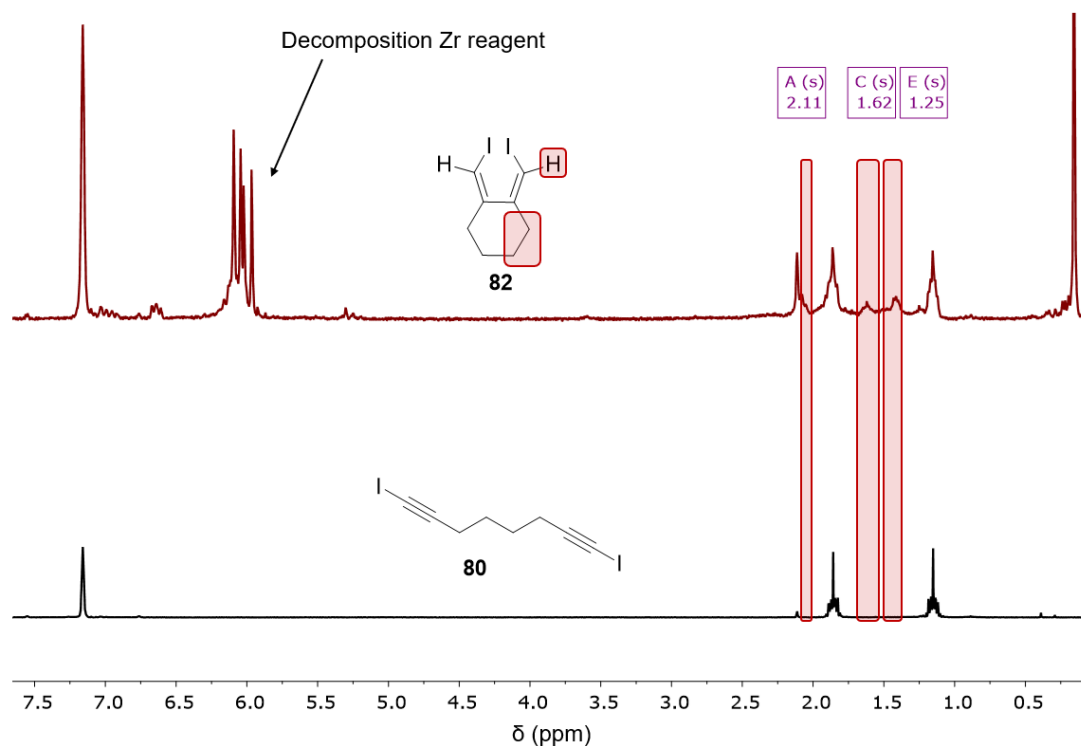


Figure 39. Comparison between the ^1H NMR spectrum from the starting material **82** and the by-product **82** formed in the route *A* in the attempt to form the zirconacyclopentadiene **81**. The boxes highlight the protons from the product.

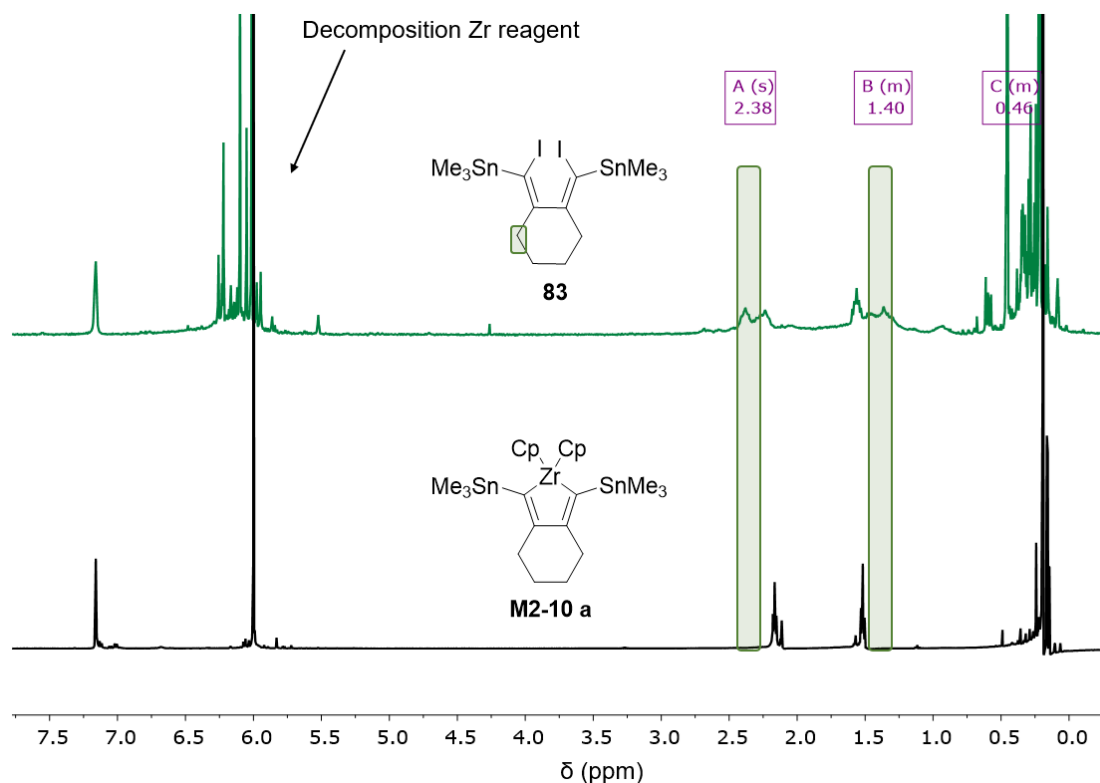
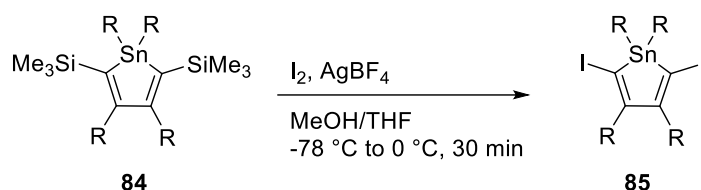


Figure 40. Comparison between the ^1H NMR spectrum from the starting material **M2-10a** and the by-product **83** formed in the route *B* in the attempt to form the zirconacyclopentadiene **81**. The boxes highlight the protons from the product.

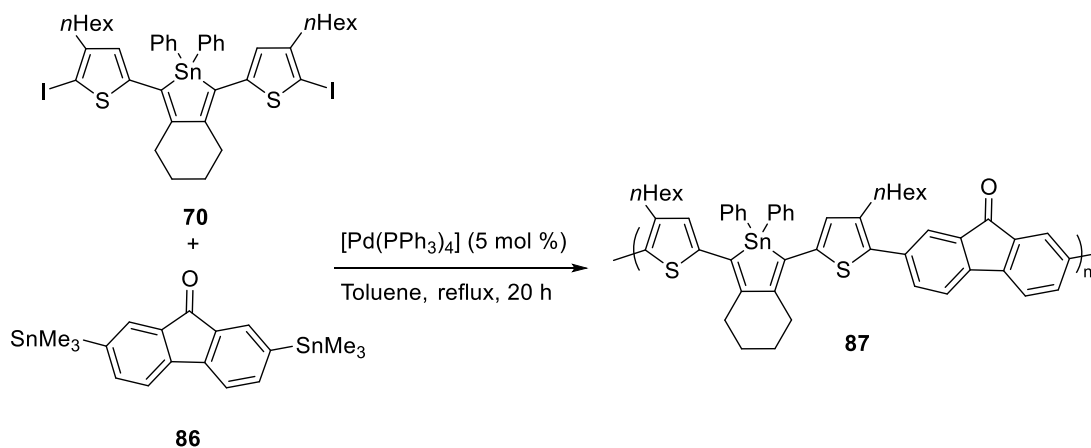
3.2.3.4 Outlook

The optimization in the formation of the dihalogenated stannole **78** opens the possibility to obtain pure 2,5-distannole (Scheme 27). One solution for its formation could be starting with the disilylated stannole like **84**, proceeding with a further iodination in presence of a silver salt. The result of this reaction could be the desirable dihalogenated stannole **85** (Scheme 29), as it was observed previously in siloles.^[91] In such case it would be beneficial if the R group, especially the substituents of the tin, are small (e.g. methyl or butyl chains) facilitating the reaction.



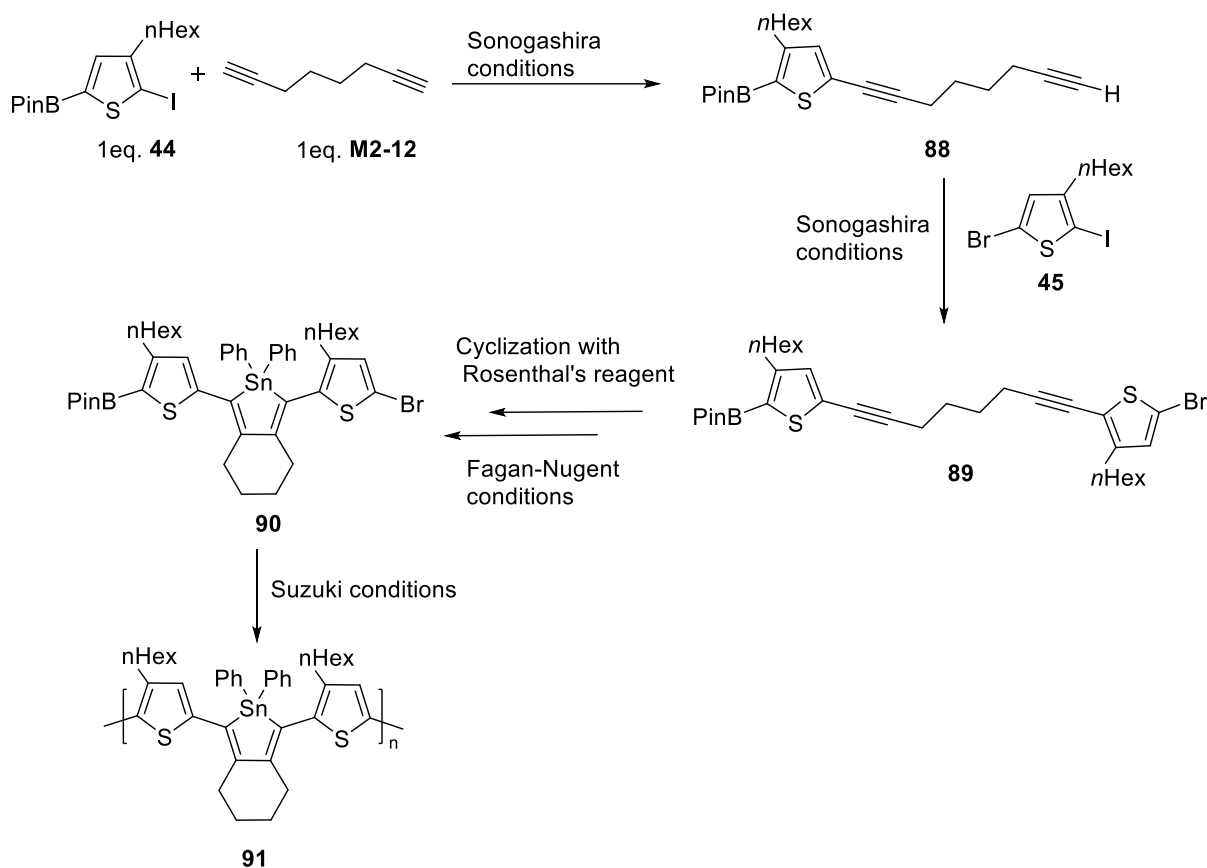
Scheme 29. Proposed synthetic route from the iododesilylation of **84** with iodine and a silver salt to obtain the desirable dihalogenated stannole **85**. Adapted from the literature, where diiodo siloles similar to **48** reacted satisfactory in cross-coupling reactions.^[91]

Isabel-M. Ramirez and Dr. Nadi Eleya obtained a polymer containing stannole **87**. They were successful in the Stille cross-coupling polymerization between the stannole **70** and the fluorene with trimethylstannyl motif **86** (Scheme 30). The polymer could be analyzed by ¹H NMR because any remaining signal from the starting materials was observed. Nevertheless, further characterizations are necessary to confirm the structure and properties of the polymer. In such coupling the tin from the stannole stays intact as it was observed before by Linshöft *et al.*^[78] This results together with the results obtained from the polymer **77** with the ratio thienyl to stannole of 2:1, shows two ways to synthesize polymers containing stannoles. In both cases it was convenient that the stannoles hold substituents in the 2- and 5-position as thiophene with reactive groups, such as iodo in **70** and trimethylstannyl group in **76**.



Scheme 30. Synthesis of the polymer containing stannole and fluorene **87** developed by Isabel M. Ramírez and Dr. Nadi Eleya. *Personal communication approved by the respective authors.*

In future work aimed at including stannoles in polymers, the bi-functional monomer concept, where the same starting material has an electrophile and nucleophile group, can be used as shown in chapter 3.1.. In that case the monomer **90** with pinacol boronate and bromide moieties should be synthesized using as starting materials compounds synthesized in this thesis **44**, **45** and **M2-12** (Scheme 31). From this monomer, under Suzuki-Miyaura conditions a polymer **91** may be obtained.



Scheme 31. Synthesis pathway proposed for polymer containing stannole and thiophene rings **88**.

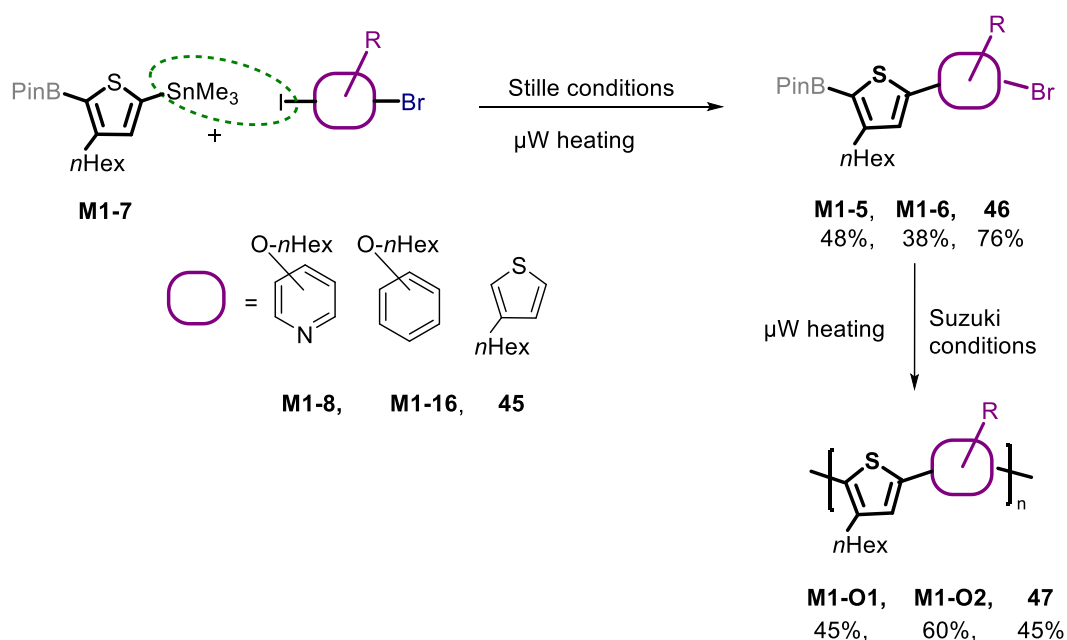
4. Conclusions

The main aim of this thesis was the synthesis of organic and organometallic monomers for the synthesis of semiconducting polymers. The organic monomers were based on the concept of push-pull systems where thiophene constituted the electron rich units whereas thienyl, pyridine or phenyl units were the electron deficient moieties. Other system in which a pyrrole unit constituted the electron rich unit was investigated.

As well the possibility of including stannole unit into organometallic monomers and furthermore into polymers was studied. Furthermore, the reaction conditions to form zirconacyclopentadienes, synthons of stannoles were explored.

Organic Semiconductors Based on the Push-Pull Principle

Three of the organic monomers were synthesized using a dually selective reaction. The trimethylstannyl group from a dinucleophile containing 3-hexythiophene and pinacol boronate (**M1-7**) reacted highly selectively in a Stille reaction, under microwave heating, with the iodo from a dielectrophile containing thienyl, pyridine or phenyl motif (green dashed line in Scheme 32). The formed monomers contain pinacol boronate and bromide moieties, which allow a further Suzuki-Miyaura cross-coupling reaction to form polymers or oligomers (Scheme 32).

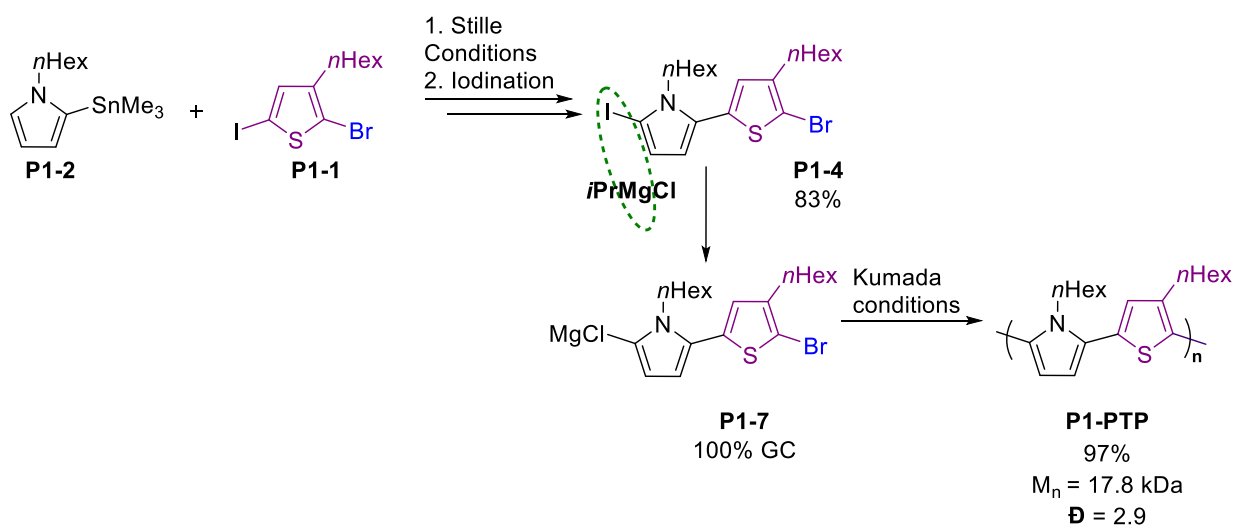


Scheme 32. Synthetic route to produce monomers **M1-5**, **M1-6** and **46** based on the push-pull principle. Furthermore, Oligomers **M1-O1**, **M1-O2** and P3HT (**47**) where formed through a polycondensation.

In the case of the monomers thienyl-phenyl (**M1-5**) and thienyl-pyridine (**M1-6**) kinetic studies of the polymerization showed a living growth behaviour in the first hours of reaction.

However, the oligomers obtained have low molecular weight which is not expected in such kind of growth mechanism. Therefore, changes in the conditions of the kinetic studies and furthermore of the polymerization reaction could confirm the living growth character for the polymerization of the monomers **M1-5** and **M1-6**. In that way polymers with higher molecular weight and lower polydispersity should be produced. Changes in the conditions for the polycondensation of the monomer **46**, as well can be applied to produce P3HT. The electroluminescence of the oligomers **M1-O1** and **M1-O2** was successfully demonstrated by the implementation into OLED devices. Nevertheless, the devices have potential to further optimizations.

The monomer **P1-7**, where the pyrrole unit constituted the electron rich unit and the thiophene the electron deficient unit, contains a magnesium and a bromo group. It was synthesized by a chemoselective iodo-magnesium exchange from the dielectrophile precursor **P1-4** (green dashed lines in Scheme 33). The formation of the copolymer (thiophene-alt-pyrrole) **P1-PTP** was successfully prepared by a palladium catalysed Kumada polycondensation from the monomer **P1-7**. The polymerization proceeded via a step-growth mechanism (Scheme 33).



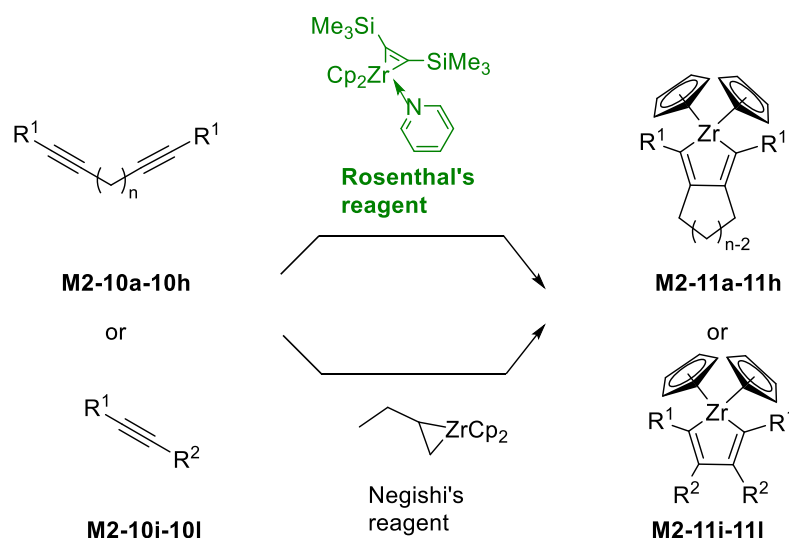
Scheme 33. Synthetic route used for the synthesis of the monomer **P1-7** based on a push-pull principle and its polymerization under Kumada conditions.

Stannoles as an interesting concept

This thesis gave an important input in the concept of stannoles as organometallic motif in semiconducting polymers. With the concept article directed to stannoles, their synthesis, structural and optoelectronic properties, it was possible to provide a general overview of this class of compounds.

Synthesis of Zirconacyclopentadienes using Rosenthal's reagent

In the study of zirconacyclopentadienes, synthons of the stannoles, the selection of the "Cp₂Zr" source was very important for the zirconium cyclization of acetylenes. In this thesis 12 starting materials (**M2-10 a-l**) including diacetylenes and acetylenes were tried under two reaction conditions using Rosenthal's and Negishi's reagents (Scheme 34). The Negishi's reagent is broadly studied and used frequently in literature; however, the facile manipulation of the Rosenthal's reagent makes it more adequate for the formation of this synthons, despite the type of starting material.



Scheme 34. General synthetic path to form the zirconacyclopentadienes **M2-11a-11l** using two different sources of "Cp₂Zr" and twelve types of alkynes **M2-10a-10l**.

Reactivity of Stannoles

Two new stannoles **48** and **49** were synthesized and completely characterized (Figure 41). With trimethylstannyl and pinacol boronate groups cross-coupling reactions on the 2- and 5-positions of a stannole ring were attempted.

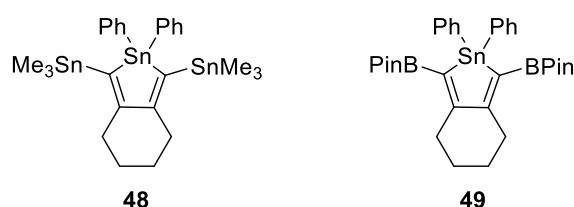
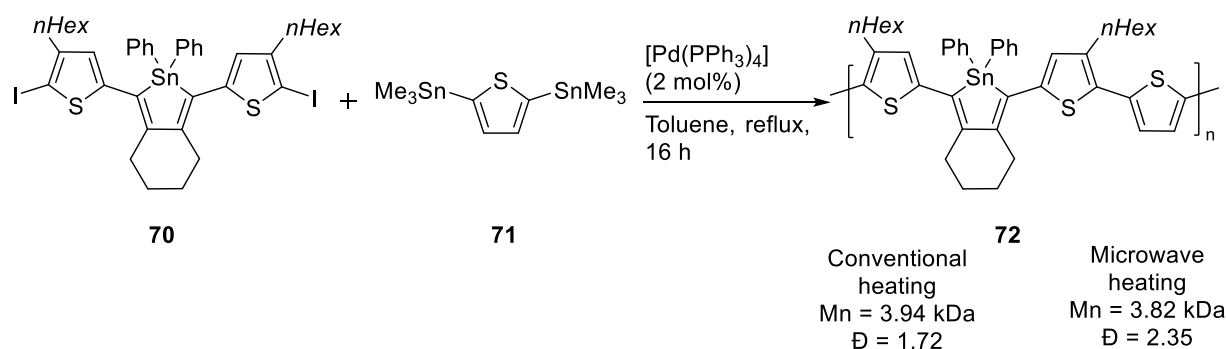


Figure 41. Two new stannoles **48** and **49** synthesized during the PhD studies.

However, the formation of a C-C bond on the 2- and 5-position from the stannole ring is very difficult to obtain. In such case the cross-coupling reactions used in the synthesis of monomers, dimers or polymers containing stannoles and thienyl rings will need further optimizations. Reaction conditions as type and amount of catalyst, solvent, temperature,

type of heating can be tested for this purpose. If the new molecules are synthesized adequately the study of the optoelectronic properties in stannoles can be continued. Another solution can be the use of other reagent groups as for example halogens in the 2- and 5-position of the stannole ring.

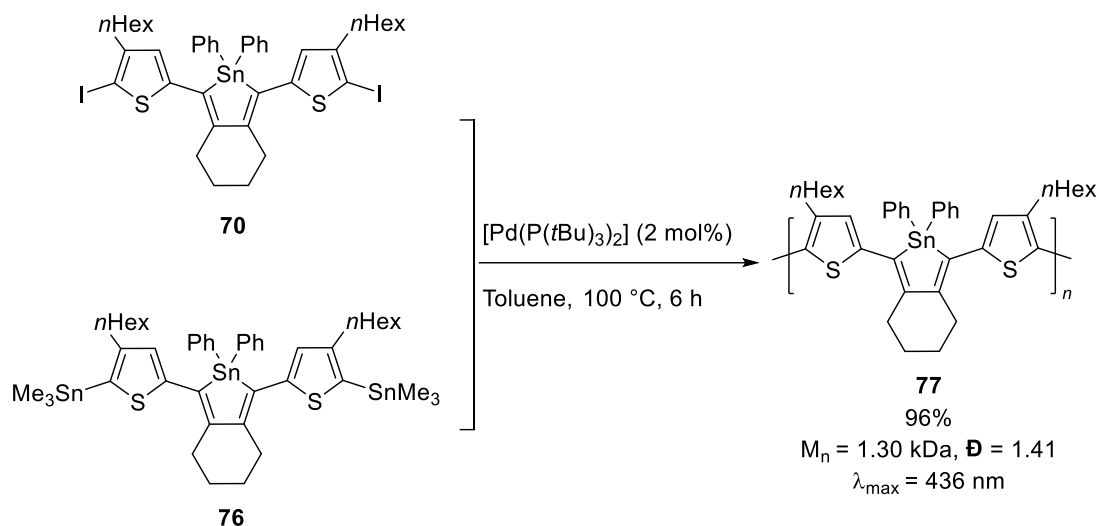
The optimization of the synthesis conditions of the stannole containing polymer **72** was attempted by changing the ratio between the monomers and using two types of heating. By differing the ratio between the monomers **70** : **71** from 1.00 : 1.00 as it was reported in literature to 1.05 : 1.00 the molecular weight improved from 3.31 to 3.91 kDa. Irrespective of both types of heating the λ_{\max} (nm) in DCM was 533 nm ($E_g = 1.91$ eV) (Scheme 35), indicating that the polymer remained with a low E_g (*Lit.* λ_{\max} (CHCl₃) = 536 nm, $E_g = 1.89$ eV).^[78] A big advantage from the microwave heating conditions is the reduction of time from 16 to 4 h, which makes further studies less time consuming. However, the molecular weight and \bar{D} from **72** under both heating types (3.94 kDa and 3.82 kDa for conventional and microwave respectively) were lower compared to the published results ($M_n = 6.8$ kDa and \bar{D} of 2.5). This concludes that the reaction is very fickle and the optimization to obtain higher molecular weight is not easy.



Scheme 35. Synthetic route used to obtain polymer **72** under two types of heating different results on the molecular weight and \bar{D} were observed.

The polymer **77** with a ratio thienyl to stannole of 2:1 was synthesized under Suzuki conditions (Scheme 36). Comparing the maximum UV-Vis absorption of **77** ($\lambda_{\max} = 436$ nm) with the one from polymer **72** the effect of one additional thienyl ring in the optoelectronic properties is observable by a lower E_g .

Further optimization of the reaction conditions for the synthesis and characterization of **77** is needed to confirm such result.



Scheme 36. Synthetic route used to obtain polymer with ratio thienyl to stannole 2:1 **77**.

Furthermore, exploring the conditions for cross-coupling reactions of the stannoles **48** and **49** could open the possibility to be used in polymerizations to obtain polymers containing thienyl and stannole in a ratio 1 : 1 , with other type of substituents on the rings or using another type of aromatic ring.

5. Experimental Section

5.1. Experimental Section. Supporting Information Chapter 3.1.1.

Supporting Information

Conjugated Oligomers with Alternating Heterocycles from a Single Monomer: Synthesis and Demonstration of Electroluminescence

Sara Urrego-Riveros,^{a,b} Matthias Bremer,^c Jonas Hoffmann,^{a,b,d} Anne Heitmann,^{a,b} Thibault Reynaldo,^d Janek Buhl,^c Paul J. Gates,^e Frank D. Sönnichsen,^f Muriel Hissler,^d Martina Gerken,^c Anne Staubitz^{a,b,†}

^a Institute for Organic and Analytical Chemistry, University of Bremen, Leobener Str.7, 28359 Bremen, Germany.

^b University of Bremen, MAPEX Center for Materials and Processes, Bibliothekstr.1, 28359 Bremen, Germany

^c Institute of Electrical Engineering and Information Technology, University of Kiel, Kaiserstr.2, 24143 Kiel, Germany.

^d Institut des Sciences Chimiques de Rennes, UMR 6226, CNRS-Université de Rennes 1, Campus de Beaulieu, 35042 Rennes Cedex, France.

^e School of Chemistry, University of Bristol, Cantock's Close, Bristol BS8 1TS, UK

^f Otto-Diels-Institute for Organic Chemistry, University of Kiel, Otto-Hahn-Platz 4, 24098 Kiel, Germany

[†]E-Mail: staubitz@uni-bremen.de

Table of Contents

General Considerations	3
Syntheses	11
Reaction Monitoring	32
OLED-like Device Fabrication	42
NMR Spectra	45
DFT Calculations	61
Literature	75

General Considerations

Abbreviations

aq	aqueous
ATR	attenuated total reflectance
br	broad (IR)
calcd.	calculated
δ	chemical shift in parts per million
COSY	correlated spectroscopy
DCM	dichloromethane
DSC	differential scanning calorimetry
DIPA	<i>N,N</i> -diisopropylamine
DMF	<i>N,N</i> -dimethylformamide
\bar{D}	dispersity
DEPT	distortionless enhancement by polarization transfer
d	doublet (NMR)
EI	electron impact
ESI	electrospray ionization
EtOAc	ethyl acetate
ϵ	extinction coefficient
GPC	gel permeation chromatography
GB	glovebox
HMBC	heteronuclear multiple bond coherence

HSQC	heteronuclear single quantum coherence
HOMO	highest occupied molecular orbital
HR-MS	high resolution mass spectrometry
ITO	indium tin oxide
IR	infrared spectroscopy
<i>i</i> PrOBpin	<i>isopropyl pinacol boronic ester</i>
LUMO	lowest unoccupied molecular orbital
MALDI-TOF MS	matrix-assisted laser desorption ionization time-of-flight mass spectrometry
λ_{\max}	maximum absorption wavelength
m	medium (IR)
mp	melting point
MeOH	methanol
MeOTf	methyl trifluoromethanesulfonate
m	multiplet (NMR)
<i>n</i> BuLi	<i>n</i> -butyllithium
NICS	nuclear independent chemical shift
NMR	nuclear magnetic resonance
ppm	parts per million
Ph	phenyl group
PL	photoluminescence
λ_{PL}	photoluminescence emission wavelength

PEDOT:PSS	poly(3,4-ethylenedioxythiophene) with polystyrene sulfonate
D	dispersity
OLED	Organic light emitting diode
RI	refraction index detector (GPC)
R	resolution (mass spectrometry)
R _f	retention factor
s	singlet (NMR)
SPS	solvent purification system
s	strong (IR)
THF	tetrahydrofuran
TMS	tetramethylsilane
TLC	thin layer chromatography
TGA	thermogravimetric analysis
TD-DFT	time dependent density functional theory
t	triplet (NMR)
Uv-vis	ultraviolet visible spectroscopy
w	weak (IR)

Chemicals and Solvents

All reactions were carried out using standard Schlenk techniques under a dry, inert nitrogen or argon atmosphere unless noted otherwise. Some reactions were performed in a nitrogen filled glovebox from Inert, Innovative Technology, Inc. Company (< 0.1 ppm O₂ and < 0.1 ppm H₂O). All dry solvents were taken from the solvent purification system (SPS), degassed by freeze-

pump-thaw cycles and stored under a nitrogen atmosphere unless noted otherwise. All chemicals were commercially available and were used without further purification unless noted otherwise.

Reagent	Supplier	Purity	Comments
Aluminum	Kurt J. Lesker	99.99%	
Acetonitrile	Sigma Aldrich	≥ 99.8%	
Ammonium chloride	Carl Roth	≥ 99.5%	
2-Bromophenol	ABCR	98%	
2-Bromopyridine-3-ol	Alfa Aesar	99%	
<i>n</i> BuLi	Acros Organics	N. A.	2.5 M or 1.6 M in hexanes
Carbon tetrabromide	Sigma Aldrich	99%	
<i>n</i> -Bromohexane	ABCR	97%	Degassed prior to use
Celite (SiO ₂)	Macherey Nagel		
Cesium fluoride	ABCR	99.9% (metal basis)	
DIPA	Sigma Aldrich	≥ 99.5%	Degassed prior to use
(SnMe ₃) ₂	ABCR GmbH	99%	
3- <i>n</i> -Hexylthiophene	TCI	> 98%	
Iodine	Applichem	Pure Ph. Eur.	
Iodohexane	Acros Organics Inc.	98	
<i>p</i> ROBpin	Hoffman-La Roche	>95%	Degassed prior to use
ITO	Präzisions-Glas-Optik GmbH	Conductivity: 170 Ω, film thickness = 110 nm, Glass substrate thickness = 1.1 mm, η = 1.95	
LiF	Sigma Aldrich	99.99%	
NIS			
Magnesium sulfate	Grüssing	99%	

MeOTf	Chempur	96%	
Potassium carbonate	VWR Chemicals	≥ 99.5%	
PEDOT:PSS	Sigma Aldrich	2.8 wt % dispersion in water	Low- conductive grade
[Pd(PPh ₃) ₄]	TCI	> 97%	Stored in a freezer in a GB
[Pd(P(<i>t</i> Bu) ₃) ₂]	TCI	> 98%	Stored in a freezer in a GB
[Pd(dppf)Cl ₂]	Sigma Aldrich	n.a.	
Silver nitrate	ABCR GmbH	99%	
Sodium carbonate	VWR Chemicals	N.a.	ACS, Reag. Ph. Eur.
Sodium hydrogen carbonate	VWR Chemicals	N.a.	ACS, Reag. Ph. Eur.
Sodium chloride	Grüssing	99%	ACS, Reag. Ph. Eur.
Sodium sulfate	VWR Chemicals	N.a.	ACS, Reag. Ph. Eur.
Sodium thiosulfate	Grüssing	97%	
Tetrabutylammonium hexa-fluorophosphate.	Sigma Aldrich	≥ 99.0%	
1,3,5-trimethoxybenzene	ABCR	98%	

Table SI- 1. List of suppliers and of the purity of the chemicals used in this work.

Solvent	Comments
Acetic acid	Alfa Aesar, 99+%
Chloroform	VWR Chemicals; ACS, Reag. Ph. Eur.
Chloroform deuterated	Eurisotop
Dichloromethane	VWR Chemicals; for HPLC; dry from the SPS
Diethyl ether	VWR Chemicals; for HPLC; dry, distilled from sodium / benzophenone
<i>N,N</i> -Dimethylformamide	Extra dry from Acros Organics; 99.8%
Ethyl acetate	VWR Chemicals; ACS, Reag. Ph. Eur.
<i>n</i> -Hexane	VWR Chemicals; ACS, Reag. Ph. Eur.
Hydrochloric acid	VWR Chemicals; ACS, Reag. Ph. Eur.
Methanol	VWR Chemicals; ACS, Reag. Ph. Eur.
Tetrahydrofuran	VWR Chemicals; for HPLC; dry from the SPS and degassed
Toluene	VWR Chemicals; for HPLC; dry, from the SPS and degassed

Table SI- 2. List of suppliers and purity of used solvents.

Analyses

^1H NMR, $^{13}\text{C}\{^1\text{H}\}$ NMR, $^{11}\text{B}\{^1\text{H}\}$ NMR and $^{119}\text{Sn}\{^1\text{H}\}$ NMR spectra were recorded on a Bruker Avance Neo 500 (for isolated compounds and reaction monitoring experiments) All ^1H NMR and $^{13}\text{C}\{^1\text{H}\}$ NMR were referenced against the solvent residual proton signals (^1H), or the solvent itself (^{13}C). $^{119}\text{Sn}\{^1\text{H}\}$ NMR spectra were calculated based on the ^1H NMR spectrum of TMS. $^{11}\text{B}\{^1\text{H}\}$ NMR spectra were referenced against $\text{BF}_3 \cdot \text{Et}_2\text{O}$ in CDCl_3 . All chemical shifts δ are given in parts per million (ppm) and all coupling constants J in Hz. The exact elucidation of the compounds was proved by ^1H , ^{13}C DEPT and two-dimensional NMR spectroscopy such as ^1H COSY, $^{13}\text{C}\{^1\text{H}\}$ HSQC or $^1\text{H}/^{13}\text{C}\{^1\text{H}\}$ HMBC when possible.

Electron impact (EI) ionization mass spectra were recorded on the double focusing mass spectrometer MAT 95+ or MAT 8200 from FINNIGAN mat. Samples were measured by direct inlet or indirect inlet method with a source temperature of 200° C. The ionization energy of the electron impact ionization was 70 eV. All signals were reported with the quotient from mass to charge m/z . Accurate masses were determined via the peak-matching method. The resolution

(R) of the peak-matching performance was 10 000. The calculated isotopic distribution for each ion agreed with experimental values.

High-resolution accurate-mass electrospray ionization (ESI) spectra were recorded on a Bruker Daltonics microTOF II mass spectrometer. High resolution accurate-mass MALDI mass spectra and MALDI MS analysis of the oligomers **O1** and **O2** were recorded on a Bruker Daltonics ultrafleXtreme TOF/TOF mass spectrometer using graphite as the matrix.

IR spectra were recorded on a NICOLET Thermo IS10 SCIENTIFIC IR spectrometer with a diamond-ATR-unit. The resolution was 4 cm⁻¹. Relative intensities of the IR bands were described by s = strong, m = medium or w = weak.

All melting points were measured with a BÜCHI Melting Point M-560 using a heating ramp of 5 K / min.

Thin layer chromatography (TLC) was carried out on aluminum plates coated with silica gel 60 F₂₅₄ with a layer thickness of 0.2 mm from Fluka or Macherey-Nagel. All bands were detected by using a fluorescent lamp (254 nm and 366 nm). Column chromatography was carried out by using the column machine PuriFlash 4250 from Interchim. Silica gel columns of the type PF-15SiHP-F0012, PF-15SiHP-F0025, PF-50SiHP-JP-F0080, PF-50SiHP-JP-F0120, and PF-50SiHP-JP-F0220 were used. The injection of the sample was made via dry load. The column material of the dry load was Celite 503 from Macherey-Nagel.

The molecular weight and molecular weight distribution of all synthesized polymers were determined using a PSS GPC/SEC system 1260/1290. The system was equipped with three PSS-SDV high combination columns (styrene-divinylbenzene copolymer network) with a molecular range from 100-3000 kDa, a refractive index detector (SECurity RID Article Nr. 404-0106), a diode array detector (SECurity DAD Article Nr. 404-0110), a viscometer detector (DVD 1260 Article Nr. 404-0025) and a Light Scattering Detector with 3D spectra option (SECcurity Multichrom SLD 1000 Article Nr. 404-0196). The columns were heated at 35 °C with a column thermostat (SECcurity TCC6000). THF (HPLC grade without stabilizer) was used as an eluent. The measurements were recorded at 35° C under an eluent flow of 1 mL/min. The apparatus was calibrated using polystyrene standards (PSS) under a conventional calibration.

The electrochemical studies were carried out under argon using an Eco Chemie Autolab PGSTAT 30 potentiostat for cyclic voltammetry with the three-electrode configuration: the working electrode was a platinum disk; the reference electrode was a saturated calomel electrode and the counter-electrode was a platinum wire. All potentials were

internally referenced to the ferrocene / ferrocenium couple. For the measurements, concentrations of 10^{-3} M of the electroactive species were used in freshly distilled and degassed dichloromethane and 0.2 M tetrabutylammonium hexafluorophosphate as the electrolyte.

Uv-vis measurements were recorded on a Jasco spectrometer model V-630, with dichloromethane as a solvent. Extinction coefficients were deduced from Uv-vis spectra measured at six different concentrations for each oligomer. The concentration was calculated based on the molecular weights calculated by MALDI measurements.

The solid state Uv-vis spectra of **O2** were recorded with a resolution of 0.1 nm on a UV-2700v- from Shimadzu with a double monochromator.

Fluorescence measurements were recorded on a Photon Technology International spectrometer with a lamp power supply LPS-220B, Motor Driver MD-5020 and 1 Photomultiplier 814. Dichloromethane was used as a solvent.

TGA measurements were performed on a Mettler Toledo DSC 3/TGA + STAR system using aluminum crucibles and under a flow of nitrogen of 20 mL/min with a temperature ramp of 10 K/min.

DSC measurements were performed on a Mettler Toledo DSC 3+ STAR system using aluminum pans, under nitrogen atmosphere and a temperature ramp of 10 K/min.

Microwave Apparatus

All microwave irradiation reactions were carried out on a Biotage® Initiator+ SP Wave synthesis system, with continuous irradiation power from 0 to 300 W. All reactions were carried out in 5 or 20 mL oven-dried Biotage microwave vials sealed with an aluminum/Teflon® crimp top, which can be exposed to a maximum of 250 °C and 20 bar internal pressure. The reaction temperature was measured by an IR sensor on the outer surface of the process vial.

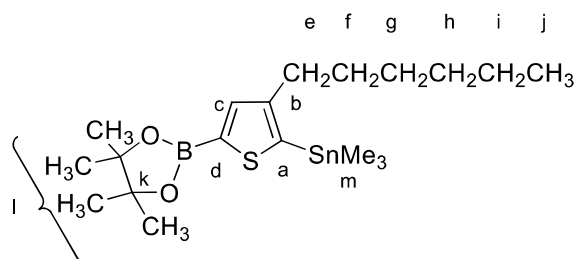
Characterizations of the OLED-type devices

The I-V characterization of the OLEDs was performed with Keithley 2400 Source measurement unit, a calibrated photodiode and an Avantes AvaSpec-2048 USB spectrometer.

The absorption spectra of the OLED-type devices were recorded on a PerkinElmer Lambda 650 spectrometer and. the photoluminescence spectra were recorded on an Avantes AvaSpec-2048 USB spectrometer.

Syntheses

(3-Hexyl-5-(4,4,5,5-tetramethyl-1,3,2-dioxaborolan-2-yl)thiophen-2-yl)trimethylstannane (7)



This procedure was adapted from the literature.^[1]

In a GB, a solution of 2-(4-hexyl-5-iodothiophen-2-yl)-4,4,5,5-tetramethyl-1,3,2-dioxaborolane (848 mg, 2.02 mmol), [Pd(PPh₃)₄] (120 mg, 0.10 mmol, 5 mol%), and (SnMe₃)₂ (737 mg, 2.24 mmol) in toluene (5 mL) was transferred in a microwave vial. The mixture was heated to 120 °C in a microwave apparatus for 30 min. After allowing the mixture to cool to ambient temperature, water (10 mL) was added to the reaction mixture and it was extracted with DCM (3 x 15 mL) and washed with brine (2 x 10 mL). The combined organic layers were dried over MgSO₄, filtered, and the solvent was removed *in vacuo*. The residue was diluted in *n*-hexane (10 mL) and filtered over celite. The volatiles were removed *in vacuo* to afford an orange oil in a yield of 850 mg (92%, 1.86 mmol).

¹H NMR (500 MHz, CDCl₃) δ = 7.61 (s, 1H, c), 2.62 (dd, ³J = 10.6, 5.0 Hz, 2H, e), 1.67 – 1.54 (m, 2H, f), 1.32 – 1.28 (m, 18H, g/h/i/l), 0.94 – 0.83 (m, 3H, j), 0.37 (s, 9H, m) ppm.

¹³C{¹H} NMR (126 MHz, CDCl₃) δ = 152.3 (b), 141.2 (a), 138.9 (c), 83.9 (k), 32.3 (f), 31.9 (e), 32.2, 31.7, 29.5, 22.7 (g/h/i/l), 24.9 (k), 14.2 (j), -7.9 (l) ppm.¹

¹¹⁹Sn{¹H} NMR (187 MHz, CDCl₃): δ = -35.70 ppm.

¹¹B{¹H} NMR (160 MHz, CDCl₃): δ = 28.71 ppm.

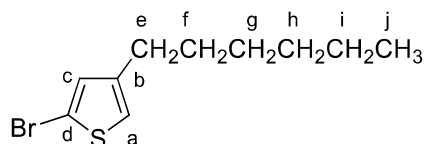
IR (ATR): ν = 2977 (w), 2926 (m), 1526 (m), 1123 (m), 1369 (m), 1322 (s), 1267 (m), 1142 (s), 982 (m), 853 (s), 771 (s), 6.65 (s), 529 (s) cm⁻¹.

HR-MS (EI, C₁₉H₃₅BO₂¹¹⁹SnS): *m/z* calcd. 458.14725, found 458.14685 (R = 10000).

¹ Carbon d was could not be identified, because of the quadrupole moment from the adjacent boron atom.

MS (EI, 70 eV, direct inlet, 200 °C): m/z (% relative intensity) = 458.2 (4) $[M]^+$, 443 (100) $[M-CH_3]^+$.

4-Bromo-2-*n*-hexylthiophene (11)



This procedure was adapted from the literature.^[2]

In a Schlenk flask, a solution of 3-*n*-hexylthiophene (5.01 g, 29.2 mmol) in THF (40 mL) was cooled to -78 °C and *n*BuLi (22.3 mL, 1.6 M in hexanes, 35.7 mmol) was added dropwise over 20 min. The solution was stirred for 3 h and this temperature. A solution of CBr₄ (11.8 g, 35.6 mmol) in THF (16 mL) was added with a syringe pump (rate = 1 mL / min) to the orange-brown suspension and the reaction was allowed to reach ambient temperature (ca. 20 °C) and it was stirred for 16 h. The reaction was quenched with water (100 mL) and the mixture was extracted with DCM (4 x 100 mL) and brine (2 x 50 mL). The combined organic layers were dried over MgSO₄, filtered, and the solvent was removed *in vacuo*. The product was purified by Kugelrohr distillation (70 °C, 9.0 x 10⁻² mbar) to afford a yellow oil in a yield of 5.35 g (74%, 21.7 mmol).

¹H NMR (500 MHz, CDCl₃): δ = 6.88 (d, ³J = 1.7 Hz, 1H, c), 6.80 (dt, ³J = 1.7, 0.9 Hz, 1H, a), 2.57 - 2.51 (m, 2H, e), 1.60 - 1.53 (m, 2H, f), 1.35 - 1.26 (m, 6H, g/h/i), 0.89 (dd, ³J = 9.3, 4.5 Hz, 3H, j).

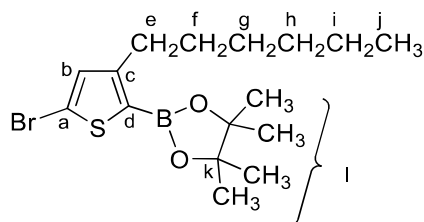
¹³C{¹H} NMR (126 MHz, CDCl₃): δ = 142.8 (d), 129.9 (c), 120.2 (a), 110.4 (b), 29.1 (f), 29.05 (e), 30.5, 27.7, 21.5 (g/h/i), 12.9 (j).

IR (ATR): ν = 2955 (m), 2925 (s), 2855 (s), 1760 (w), 1539 (w), 1457 (m), 1412 (m), 1194 (w), 1275 (w), 1126 (m), 982 (m), 921 (w), 829 (s), 727 (s), 640 (m), 577 (w), 456 (w) cm⁻¹.

HR-MS (EI, C₁₀H₁₅⁷⁹BrS): m/z calcd. 246.0081, found 246.0078 (R = 10000).

MS (EI, 70 eV, direct inlet, 200 °C): m/z (% relative intensity) = 245.9 (22) $[M]^+$, 248.0 (34) $[M+2]^+$, 177.9 (100) $[M+2-C_5H_{11}]^+$, 175.9 (77) $[M-C_5H_{11}]^+$.

2-(5-Bromo-3-*n*-hexylthiophene-2-yl)-4,4,5,5-tetramethyl-1,3,2-dioxaborolane (**12**)



This procedure was adapted from the literature.^[3]

In a Schlenk flask, a solution of DIPA (1.04 g, 10.3 mmol) in THF (33 mL) was cooled to -78 °C and *n*BuLi (4.0 mL, 2.6 M in hexanes, 10.3 mmol) was added dropwise over 20 min. The mixture was warmed to 0 °C over the course of 30 min, cooled to -78°C and stirred for 5 min. A solution of **4** (2.54 g, 10.3 mmol) in THF (33 mL) was added with a syringe pump over the course of 20 min (rate = 0.5 mL / min) and the mixture was stirred for 1 h at this temperature. A solution of *t*PrOBPin (1.82 g, 9.78 mmol) in THF (5 mL) was added with a syringe pump (rate = 1 mL / min) to the orange-green suspension. The reaction mixture was allowed to reach ambient temperature and was stirred for further 16 h. Afterwards the reaction was quenched with methanol (100 mL) and all volatiles were removed *in vacuo*. The residue was diluted in DCM (50 mL) and washed with water (2 x 100 mL), brine (2 x 100 mL) and dried over MgSO₄. After filtration, the volatiles were removed *in vacuo* and the mixture was purified by flash chromatography (*n*-hexane : EtOAc, 9: 1; R_f = 0.20) to afford an orange oil in a yield of 3.23 g (86%, 8.83 mmol).

¹H NMR (500 MHz, CDCl₃): δ = 6.94 (s, 1H, b), 2.85 - 2.77 (m, 2H, e), 1.59 - 1.50 (m, 2H, f), 1.33 - 1.27 (m, 18H, g/h/i/l), 0.88 (dd, ³J = 9.5, 4.5 Hz, 3H, j) ppm.

¹³C{¹H} NMR (126 MHz, CDCl₃): δ = 155.1(c), 133.0 (b), 118.01 (a), 83.6 (k), 31.4 (f), 30.2 (e), 28.7, 24.6, 22.5 (g/h/i), 31.5 (l), 14.0 (j) ppm.²

¹¹B{¹H} NMR (160 MHz, CDCl₃): δ = 28.40 ppm.

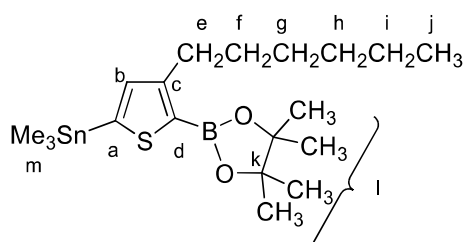
IR (ATR): $\tilde{\nu}$ = 2978 (w), 2956 (w), 2926 (m), 2857 (w), 1755 (w), 1534 (m), 1427 (s), 1370 (m), 1336 (s), 1304 (s), 1270 (m), 1140 (s), 1097(w), 1040 (s), 957 (m), 853 (s), 668 (w), 645 (m), 578 (m), 520 (w) cm⁻¹.

HR-MS (EI, C₁₈H₂₇¹¹B⁷⁹BrO₂S): *m/z* calcd. 373.1006, found 373.1006 (R = 10000).

² Carbon d could not be identified because of the quadrupole moment from the adjacent boron atom.

MS (EI, 70 eV, direct inlet, 200 °C): m/z (% relative intensity) = 373.10 (17) $[M]^+$, 259.19 (100) $[M-C_8H_{19}]^+$.

(4-Hexyl-5-(4,4,5,5-tetramethyl-1,3,2-dioxaborolan-2-yl)thiophen-2-yl)trimethylstannane (13)



In a GB, a solution of **5** (752 mg, 2.02 mmol), $[Pd(PPh_3)_4]$ (116 mg, 0.10 mmol, 5 mol%), and $(SnMe_3)_2$ (661 mg, 2.02 mmol) in toluene (5 mL) was transferred in a microwave vial. The mixture was heated to 120 °C in a microwave apparatus for 30 min. After allowing the mixture to cool to ambient temperature, water (10 mL) was added to the reaction mixture and it was extracted with DCM (3 x 15 mL) and brine (2 x 10 mL). The combined organic layers were dried over $MgSO_4$, filtered, and the solvent was removed *in vacuo*. The residue was diluted in *n*-hexane (10 mL) and filtered over celite. The volatiles were removed *in vacuo* to afford an orange oil in a yield of 830 mg (89%, 1.80 mmol).

1H NMR (500 MHz, $CDCl_3$): δ = 7.09 (s, 1H, a), 2.92 – 2.87 (m, 2H, e), 1.64 – 1.53 (m, 2H, f), 1.37 – 1.28 (m, 18H, g/h/i/l), 0.89 (t, $^3J = 7.0$ Hz, 3H, j), 0.35 (s, 9H, m) ppm.

$^{13}C\{^1H\}$ NMR (126 MHz, $CDCl_3$) δ = 155.6 (c), 145.3 (a), 138.6 (b), 83.6 (i), 32.1 (f), 29.3 (e), 31.8, 30.1, 22.8, 24.63 (l), 14.28 (j), -8.19 (m) ppm.³

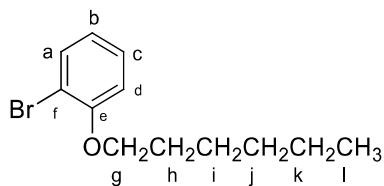
$^{119}Sn\{^1H\}$ NMR (187 MHz, $CDCl_3$): δ = -28.40 ppm.

$^{11}B\{^1H\}$ NMR (160 MHz, $CDCl_3$): δ = 28.91 ppm.

IR (ATR): $\tilde{\nu}$ = 2977(w), 2956(w), 2924(m), 2856(w), 1523 (w), 1425 (s), 1370 (m), 1327 (s), 1270 (m), 1192(w), 1141 (s), 1041 (m), 953 (w), 855 (m), 770(s), 695 (m), 647 (m), 531 (s), 512 (m) cm^{-1} .

ESI-MS ($[M+Na]$, $C_{19}H_{35}^{11}BO_2Na^{119}SnS$): m/z = Calcd. 481.1374 ; found 481.1370.

³ It was not possible to identify carbon d because the quadrupole moment of the adjacent boron atom.

1-Bromo-2-(*n*-hexyloxy)benzene (15)

This procedure was adapted from the literature.^[4]

To a solution of 2-bromophenol (2.80 g, 16.2 mmol) in acetonitrile (50 mL), K_2CO_3 (4.47 g, 32.4 mmol) and *n*-iodohexane (3.11 mL, 17.3 mmol) were added. The reaction mixture was stirred at 60 °C for 6 h and for 12 h at 20 °C. The reaction mixture was poured into water (70 mL). The aqueous phase was extracted with EtOAc (3 x 70 mL). The organic phase was washed with water (70 mL) and brine (70 mL). It was dried over Na_2SO_4 , filtered and the filtrate concentrated under reduced pressure. The crude product was purified by column chromatography (*n*-pentane : EtOAc, 50 : 1; $R_f = 0.75$) to afford a colorless oil in a yield of 3.92 g (94%, 15.2 mmol).

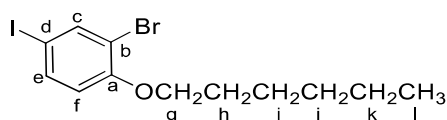
$^1\text{H NMR}$ (500 MHz, CDCl_3): $\delta = 7.53$ (dd, $^3J = 7.9$ Hz, $^4J = 1.6$ Hz, 1H, a), 7.23 (ddd, $^3J = 8.2$, 7.9 Hz, $^4J = 1.6$ Hz 1H, c), 6.88 (dd, $^3J = 8.2$ Hz, $^4J = 1.6$ Hz, d), 6.84 – 6.79 (m, 1H, b), 4.02 (t, $^3J = 6.5$ Hz, 2H, g), 1.87 – 1.80 (m, 2H, h), 1.51 (ddd, $^3J = 15.2$, 7.2 Hz, $^4J = 4.7$ Hz, 2H, i), 1.39 – 1.33 (m, 4H, j/k), 0.96 – 0.89 (m, 3H, l) ppm.

$^{13}\text{C}\{^1\text{H}\}$ NMR (126 MHz, CDCl_3) $\delta = 155.9$ (e), 133.7 (a), 128.8 (c), 122.0 (b), 113.07(d), 112.7 (f), 69.6 (g), 29.5 (h), 26.1 (i), 31.9, 23.0 (j/k), 14.4 (l) ppm.

IR (ATR): $\tilde{\nu} = 2928$ (w), 1586 (w), 1466 (m), 1442 (m), 1275 (s), 1246 (s), 1126 (w), 1050 (s), 1030 (s), 743 (s), 665 (m) cm^{-1} .

HR-MS (EI, $\text{C}_{12}\text{H}_{16}\text{O}^{79}\text{Br}$): m/z calcd. 256.04573, found. 256.04554 ($R = 10000$).

MS (EI, 70 eV, indirect inlet, 200 °C): m/z (% relative intensity) = 256 (100) $[\text{M}]^+$.

1-Bromo-2-(*n*-hexyloxy)-5-iodobenzene (16)

This procedure was adapted from the literature.^[5]

A mixture of I_2 (3.39 g, 13.3 mmol) and AgNO_3 (1.73 g, 10.3 mmol) was gently blended in an agate mortar for 1 min, and then **10** (2.62 g, 17.3 mmol) was added. The resulting

homogeneous mixture was additionally ground for 10 min, and then after a 2-min break, the grinding was continued for an additional 1 or 1.5 h, until the mixture had a light yellow bright color. The resulting mixture was extracted with diethyl ether (2 x 100 mL), dried over MgSO₄ and filtered. The volatiles were removed *in vacuo*. The product was purified by Kugelrohr distillation (140 °C, 2.7 x 10⁻¹ mbar) to afford a yellow solid in a yield of 3.13 g (80%, 8.15 mmol).

¹H NMR (500 MHz, CDCl₃): δ = 7.82 (d, ⁴J = 2.2 Hz, 1H, c), 7.51 (dd, ³J = 8.6 Hz, ⁴J = 2.2 Hz, 1H, e), 6.63 (d, ³J = 8.6 Hz, 1H, f), 3.99 (t, ³J = 6.5 Hz, 2H, g), 1.90 – 1.76 (m, 2H, h), 1.57 – 1.40 (m, 2H, i), 1.38 – 1.29 (m, 4H, j/k), 0.91 (t, ³J = 6.7 Hz, 3H, l) ppm.

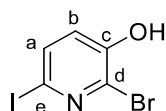
¹³C{¹H} NMR (126 MHz, CDCl₃) δ = 155.6 (a), 140.9 (c), 137.1 (e), 114.9 (f), 113.5 (b), 82.1 (d), 69.3 (g), 31.0, 22.5 (j/k), 28.9 (h), 25.6 (i), 14.0 (l) ppm.

IR (ATR): $\tilde{\nu}$ = 2925 (m), 2855 (m), 1573 (w), 1462 (s), 1377 (m), 1282(s), 1246 (s), 1152 (w), 1043 (s), 1014 (w), 813 (w), 799 (m), 687 (m), 629 (m), 544 (m) cm⁻¹.

HR-MS (EI, C₁₂H₁₆O⁷⁹BrI): *m/z* calcd. 381.9422, found 381.9429 (R = 10000).

MS (EI, 70 eV, direct inlet, 200 °C): *m/z* (% relative intensity) = 381.9 (55) [M]⁺, 384.9 (9) [M+2]⁺, 297.8 (100) [M-C₆H₁₃]⁺.

2-Bromo-6-iodo-3-pyridinol (18)



This procedure was adapted from the literature.^[6]

2-Bromopyridine-3-ol (5.00 g, 28.7 mmol) and K₂CO₃ (7.90 g, 57.5 mmol) were dissolved in water (66 mL) and I₂ (7.51 g, 29.6 mmol) was added. The reaction was stirred at 21 °C for 3 d. Excess iodine was reduced by addition of solid NaHSO₃. The pH of the solution was adjusted to -5-6 using glacial acetic acid. A solid formed during the process and was collected by filtration and dried *in vacuo* to afford a light gray solid in a yield of 8.03 g (93%, 26.8 mmol).

mp: 161.2 °C.

¹H NMR (500 MHz, CDCl₃): δ = 5.50 (OH), 7.0 (d, ³J = 8.2 Hz, 1H, a), 7.57 (d, ³J = 8.2 Hz, 1H, b) ppm.

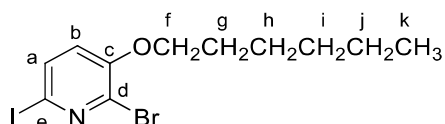
¹³C{¹H} NMR (126 MHz, CDCl₃) δ = 150.0 (e), 135.3 (d), 129.9 (c), 125.2 (a), 102.5 (b) ppm.

IR (ATR): $\tilde{\nu}$ = 3343.3 (br), 1654.0 (w), 1548 (m), 1462.2 (m), 1383.3 (s), 1287.9 (s), 1226 (s), 1132 (w), 1065 (s), 826.4 (m) cm^{-1} .

HR-MS (EI, $\text{C}_{15}\text{H}_{13}\text{O}^{79}\text{BrI}$): m/z calcd. 298.84344, found. 288.84344 ($R = 10000$).

MS (EI, 70 eV, direct inlet, 200 °C, $\text{C}_5\text{H}_3\text{O}^{79}\text{BrI}$): m/z (% relative intensity) = (299) (100) $[\text{M}]^+$.

2-Bromo-3-(hexyloxy)-6-iodopyridine (**8**)



This procedure was adapted from the literature.^[7]

To a solution of **18** (4.43 g, 14.8 mmol) in DMF (15 mL), K_2CO_3 (2.24 g, 16.2 mmol) was added, and the mixture was stirred for 30 min at 20 °C. To this mixture, *n*-bromohexane (9.26 g, 56.2 mmol) was added. The reaction mixture was stirred for 1.5 h at 100 °C. The reaction mixture was poured into ice water (70 mL) and extracted with EtOAc (3 x 70 mL). The organic phase was dried over MgSO_4 , filtered, and the volatiles were removed *in vacuo*. The product was purified by Kugelrohr distillation heating at 100 °C at 3.4×10^{-1} mbar to afford a yellow oil in a yield of 3.96 g (70%, 10.3 mmol).

^1H NMR (500 MHz, CDCl_3): δ = 7.56 (d, $^3J = 8.3$ Hz, 1H, a), 6.81 (d, $^3J = 8.3$ Hz, 1H, b), 4.00 (t, $^3J = 6.4$ Hz, 4H, f), 1.96 – 1.71 (m, 4H, g), 1.57 – 1.28 (m, 6H, h/i/j), 0.97 – 0.88 (m, 3H, k) ppm.

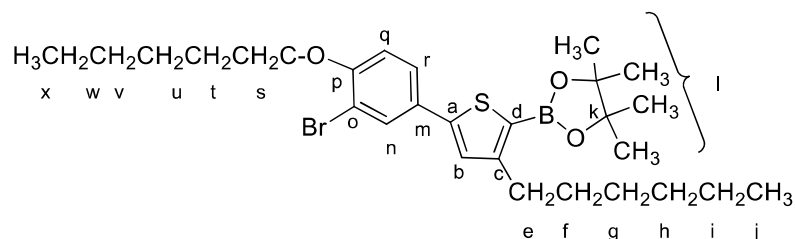
$^{13}\text{C}\{^1\text{H}\}$ NMR (126 MHz, CDCl_3) δ = 152.9 (c), 134.0 (a), 121.4 (d), 101.7 (e), 69.6 (f), 28.6 (g), 31.3, 25.4, 22.4 (h/i/j), 13.9 (k) ppm.

IR (ATR): $\tilde{\nu}$ = 2928 (w), 2857 (w), 1559 (w), 1417 (s), 1383 (m), 1347 (w), 1284 (s), 1228 (m), 1136 (w), 931 (w), 817 (m), 623 (m) cm^{-1} .

HR-MS (EI, $\text{C}_{11}\text{H}_{15}\text{NO}^{79}\text{BrI}$): m/z calcd. 382.9380, found 382.9382 ($R = 10000$).

MS (EI, 70 eV, direct inlet, 200 °C): m/z (% relative intensity) = 382:9 (43) $[\text{M}]^+$, 385.9 (17) $[\text{C}_{11}\text{H}_{15}\text{N}^{81}\text{BrI}]^+$, 298.8 (100) $[\text{M}-\text{C}_6\text{H}_{13}]^+$.

2-(5-(4-Bromo-3-(hexyloxy)phenyl)-3-hexylthiophen-2-yl)-4,4,5,5-tetramethyl-1,3,2-dioxaborolane (5)



In a GB, a mixture of **16** (444 mg, 1.16 mmol), **13** (500 mg, 1.09 mmol) and $[\text{Pd}(\text{PPh}_3)_4]$ (31 mg, 26 μmol , 2 mol%) in dry DMF (5 mL) was prepared in a microwave vial. The mixture was heated to 100 °C in a microwave apparatus for 12 h. After allowing the mixture to cool to ambient temperature (ca. 20 °C), water (5 mL) was added and the mixture was extracted with DCM (3 x 10 mL). The organic phase was washed with brine (3 x 5 mL) before drying the organic phase over MgSO_4 . After filtration, the volatiles were removed *in vacuo*. The mixture was purified by flash chromatography (*n*-hexane : EtOAc; 70 : 30; R_f : 0.20) to afford an orange oil in a yield of 421 mg (70%, 0.77 mmol).

^1H NMR (500 MHz, CDCl_3): δ = 7.82 (d, 3J = 2.3 Hz, 1H, n), 7.49 (dd, 3J = 8.6, 2.3 Hz, 1H, r), 7.12 (s, 1H, b), 6.86 (d, 3J = 8.6 Hz, 1H, q), 4.04 (t, 3J = 6.5 Hz, 2H, s), 2.90 – 2.80 (m, 2H, e), 1.84 (dt, 3J = 14.3, 6.5 Hz, 2H, t), 1.60 (dt, 3J = 7.5, 15.0 Hz, 2H, f), 1.53 – 1.48 (m, 2H, u), 1.39 – 1.22 (m, 22H, g/h/i/l/v/w), 0.97 – 0.86 (m, 6H, j/x) ppm.

$^{13}\text{C}\{^1\text{H}\}$ NMR (126 MHz, CDCl_3): δ = 155.9 (c), 155.3 (p), 148.2 (m), 130.9 (n), 128.6 (a), 126.2 (b), 126.2 (r), 113.3 (o), 112.7 (q), 83.7 (k), 69.5 (s), 31.6 (f), 30.6 (e), 29.1 (t), 25.9 (u), 31.8, 29.2, 24.9, 22.8 (g/h/i/l/v/w), 14.3, 14.2 (j/x) ppm.⁴

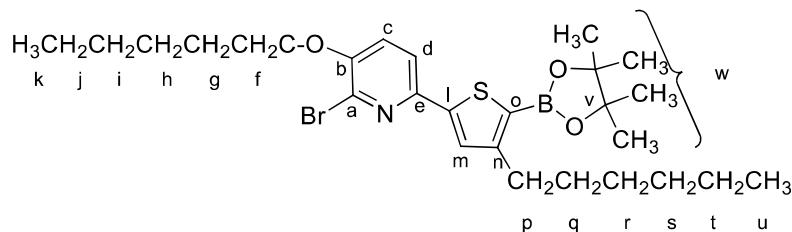
$^{11}\text{B}\{^1\text{H}\}$ NMR (160 MHz, CDCl_3): δ = 28.88 ppm.

IR (ATR): $\tilde{\nu}$ = 2954 (m), 2926 (m), 2857 (m), 1599(w), 1540 (m), 1501 (w), 1451 (s), 1371(m), 1338 (s), 1287 (s), 1254 (s), 1141 (s), 1047 (s), 958 (w), 855 (s), 807 (m), 669 (w), 609 (m), 579 (w) cm^{-1} .

ESI-MS($[\text{M}+\text{Na}]$, $\text{C}_{28}\text{H}_{42}^{11}\text{B}^{79}\text{BrNaO}_3\text{S}_2$): m/z = calc. 571.2024, found = 571.2028 (R = 10000).

⁴ It was not possible to identify carbon d because the quadrupole moment of the adjacent boron atom.

2-Bromo-6-(4-*n*-hexyl-5-(4,4,5,5-tetramethyl-1,3,2-dioxaborolan-2-yl)thiophen-2-yl)-3-(*n*-hexyloxy)pyridine (6)



In a GB, a mixture of **19** (418 mg, 1.09 mmol), **13** (500 mg, 1.09 mmol) and [Pd(PPh₃)₄] (25 g, 22 μmol, 2 mol%) in dry DMF (6 mL) was prepared in a microwave vial. The mixture was heated to 130 °C in a microwave apparatus for 6 h. After allowing the mixture to cool to ambient temperature (ca. 20 °C), water (5 mL) was added and extracted with DCM (3 x 10 mL). The organic phase was washed with brine (3 x 5 mL) before drying over MgSO₄. After filtration, the volatiles were removed *in vacuo*. The crude mixture was purified with flash chromatography (*n*-hexane : EtOAc, 70 : 30, R_f = 0.25) to afford an orange oil in a yield of 423 mg (70%, 770 μmol).

¹H NMR (500 MHz, CDCl₃): δ = 7.48 (d, ³J = 8.4 Hz, 1H, d), 7.47 (s, 1H, m), 7.09 (d, ³J = 8.4 Hz, 1H, c), 4.04 (t, ³J = 6.5 Hz, 2H, f), 2.87 – 2.82 (m, 2H, p), 1.89 – 1.81 (m, 2H, g), 1.61 – 1.58 (m, 2H, h), 1.54 – 1.48 (m, 2H, q), 1.38 – 1.35 (m, 2H, r), 1.35 – 1.31 (m, 18H, j, s/t/w), 1.31 – 1.29 (m, 2H, i), 0.91 – 0.90 (m, 3H, u), 0.88 (t, ³J = 6.9 Hz, 3H, k) ppm.

¹³C{¹H} NMR (126 MHz, CDCl₃): δ = 155.7 (n), 151.4 (b), 147.6 (l), 145.3 (e), 132.7 (a), 127.9 (m), 120.31 (c), 119.3 (d), 83.8 (v), 69.8 (f), 31.8 (i), 31.8 (r), 31.6 (h), 30.6 (p), 29.1 (g), 29.1/22.75/22.70 (j/s/t), 25.73 (q), 24.94 (w), 14.27 (k), 14.15 (u) ppm.⁵

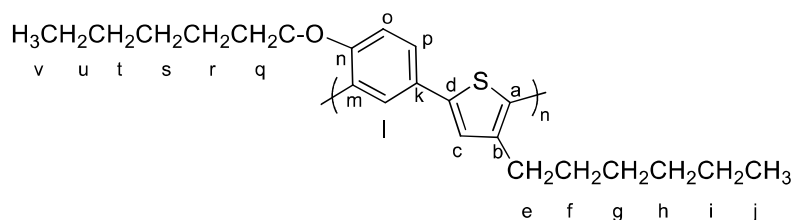
¹¹B{¹H} NMR (160 MHz, CDCl₃): δ = 29.25 ppm.

IR (ATR): $\tilde{\nu}$ = 2955 (m), 2925 (m), 2856 (m), 1526 (w), 1459 (s), 1426 (m), 1371 (m), 1337 (s), 1305 (m), 1270 (m), 1141 (s), 1045 (m), 959 (w), 854 (s), 830 (m), 668 (w), 647 (m), 578 (w), 517 (w) cm⁻¹.

ESI-MS ([M+Na], C₂₇H₄₁BBrNaO₃S₂): *m/z* = calcd. 572.1963 found 572.1981.

⁵It was not possible to identify carbon o because the quadrupole moment of the adjacent boron atom.

Poly(1,4-(3-hexyl)-thiophene-2,6-(3-hexyloxy)-phenylene) O1



Selection of the catalyst

In a Schlenk flask, **5** (69 mg, 13 μmol) was dissolved in THF (2 mL). A suspension of $[\text{Pd}(\text{tBu}_3\text{P})_2]$ or $[\text{Pd}(\text{dppf})\text{Cl}_2]$ 5 mol%, CsF (11 mg, 7 μmol) in degassed water (0.5 mL) and THF (1.5 mL) were added. The mixture was heated at 60 $^\circ\text{C}$ for 24 h under a nitrogen atmosphere. The crude mixture was quenched with a solution of HCl in methanol (1 M, 1 mL) to afford a sticky yellow oil. Water was added (5 mL) and the mixture was extracted with DCM (3 x 5 mL). The organic phase was washed with brine (3 x 5 mL) before being dried over MgSO_4 . After filtration, the volatiles were removed *in vacuo*. The crude product was purified by Soxhlet extraction. First, MeOH (50 mL) was used as solvent and the system was heated at 100 $^\circ\text{C}$ for 8 h. After oligomers and small molecules were removed, the solvent was changed to chloroform and the system was heated at 80 $^\circ\text{C}$ for 4 h.

Catalyst	Mass catalyst (mg)	M_n (kDa)	\bar{D}
$[\text{Pd}(\text{tBu}_3\text{P})_2]$	3	5.8	1.35
$[\text{Pd}(\text{dppf})\text{Cl}_2]$	5	2.4	1.34

Table SI- 3. GPC measurement results from the selection of the catalyst for the oligomerization of the monomer **5**. THF was used as eluent in a concentration of 1 mg/mL, at a flow rate of 1 mL/min. Calibrated against polystyrene standards using a conventional calibration method.

Oligomer synthesis

In a Schlenk flask, **5** (300 mg, 550 μmol) was dissolved in THF (2 mL). A suspension of $[\text{Pd}(\text{tBu}_3\text{P})_2]$ (28 mg, 55 μmol , 5 mol%), CsF (86 mg, 567 μmol) in degassed water (0.5 mL) and THF (1.5 mL) were added. The mixture was heated at 60 $^\circ\text{C}$ for 24 h under a nitrogen atmosphere. The crude mixture was quenched with a solution of HCl in methanol (1 M, 1 mL) to afford a sticky yellow oil. Water was added (5 mL) and the mixture was extracted with DCM

(3 x 10 mL). The organic phase was washed with brine (3 x 5 mL) before being dried over MgSO₄. After filtration, the volatiles were removed *in vacuo*. The crude product was purified by Soxhlet extraction. First, MeOH (200 mL) was used as solvent and the system was heated at 100 °C for 8 h. After oligomers and small molecules were removed, the solvent was changed to chloroform and the system was heated at 80 °C for 4 h. The volatiles were removed *in vacuo* to afford a sticky orange oil in a yield of 87.3 mg (46%).

¹H NMR (600 MHz, CDCl₃): δ = δ 7.59 (d, ³J = 2.1 Hz, 1H, l), 7.55 – 7.52 (m, 1H, p), 7.12 (m, 1H, c), 6.97 – 6.92 (m, 1H, o), 4.02 – 3.94 (m, 2H, q), 2.54 – 2.48 (m, 2H, e), 1.76 – 1.67 (m, 2H, r), 1.65 – 1.57 (m, 2H, f), 1.43 – 1.34 (m, 4H, g/s), 1.33 – 1.18 (m, 8H, h/i/t/u), 0.89 – 0.78 (m, 4H, j/v) ppm.

¹³C{¹H} NMR (126 MHz, CDCl₃): δ = 156.4 (n), 143.7 (d), 142.4 (a), 141.6 (b), 132.1 (k), 128.9 (p), 125.7 (o), 123.8 (c), 112.8 (l), 69.0 (q), 30.8 (f), 29.5 (e), 29.2 (r), 31.9 29.4, 25.8, 22.8 (g/h/i/s/t/u), 14.2 (j/v).

IR (ATR): $\tilde{\nu}$ = 2922 (m), 2854 (m), 1599(w), 1491 (m), 1464 (s), 1377 (w), 1248 (s), 1141 (m), 1016 (bm), 802(s), 724 (w) cm⁻¹.

λ_{\max} (DCM) = 318 nm.

ϵ (DCM) = 8.13 x 10³ L mol⁻¹ cm⁻¹. The extinction factor was calculated from solutions of **O1**, using the molecular weight calculated by GPC (1560 g/mol), in DCM with concentration / Absorption: 1.15 μ M / 0.013, 2.31 μ M / 0.021, 4.62 μ M / 0.043, 6.92 μ M / 0.060, 9.23 μ M / 0.080 and 11.5 μ M / 0.097.

λ_{PL} (DCM) = 432 nm.

M_n (GPC, conventional method) = 1.56 kDa.

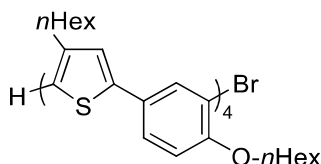
\bar{D} = 1.12.

MALDI (graphite): m/z = 1451

DP (based on M_n from GPC measurements) = 4.

DP (based on MALDI measurements) = 4.

Proposed structure with end groups based on MALDI analysis:



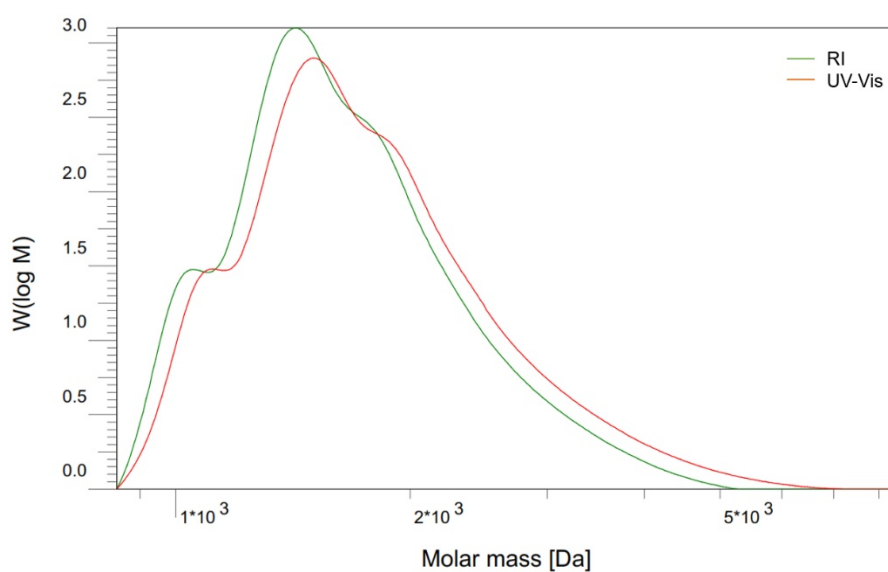


Figure SI- 1. GPC measurement result of **O1** using THF as eluent in a concentration of 1 mg/mL, at a flow rate of 1 mL/min. Calibrated against polystyrene standards using a conventional calibration method. Signals from the refraction index (RI) and Uv-vis detectors are shown.

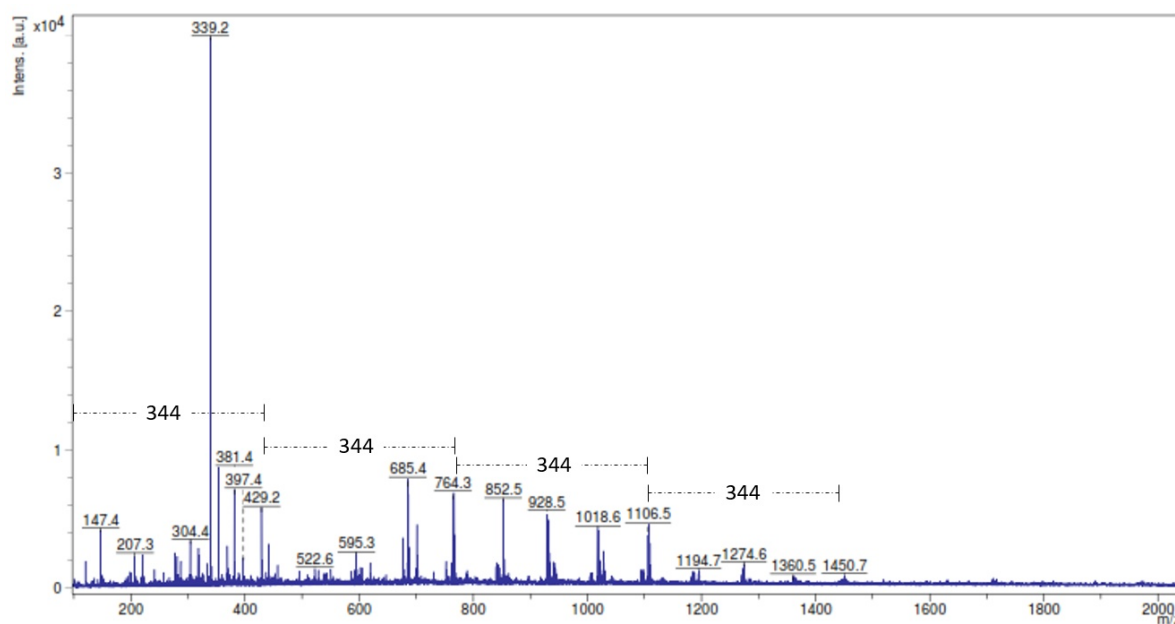


Figure SI- 2. MALDI (graphite) spectra of **O1**, with the mass of the repeating unit indicated in the picture.

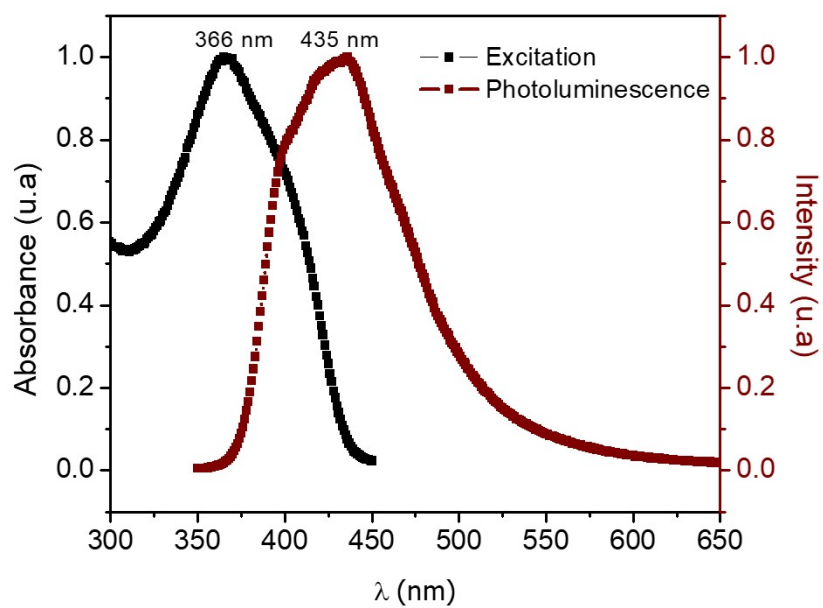


Figure SI- 3. Excitation and photoluminescence spectra ($\lambda_{\text{exc}} = 340$ nm) of a solution of **O1** in DCM (6.34×10^{-6} M).

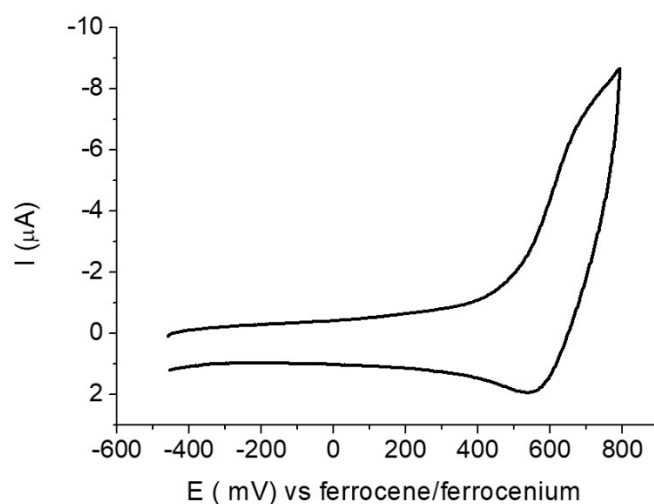


Figure SI- 4. Cyclic voltammogram of a solution of **O1** (1×10^{-3} M) using Bu_4NPF_6 as electrolyte in DCM (0.2 M).

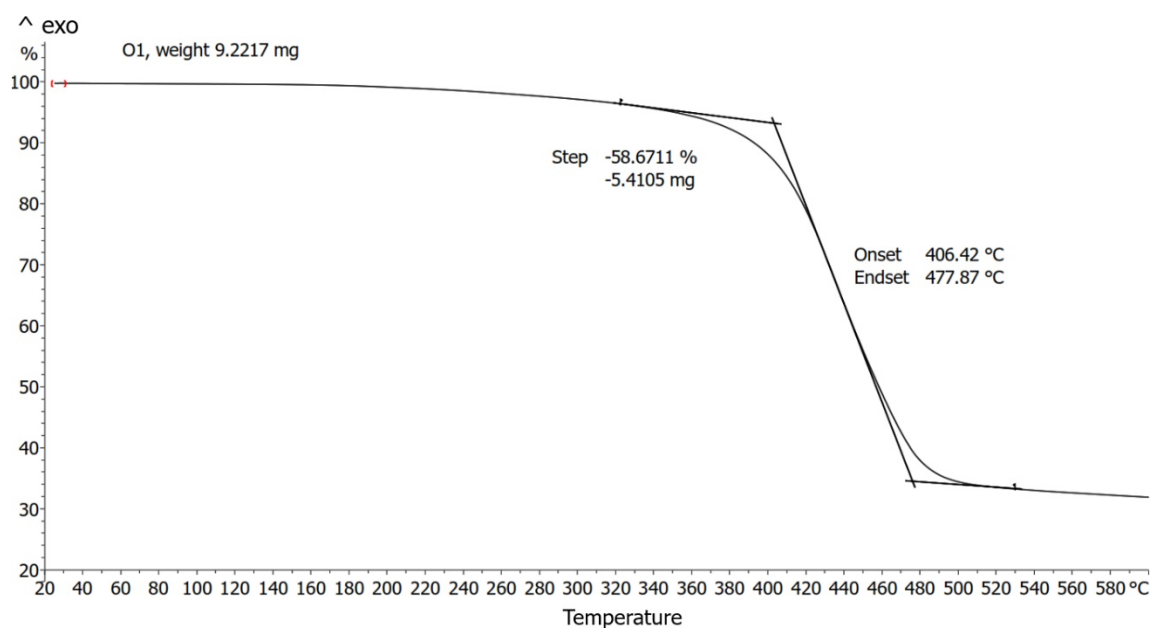


Figure SI- 5. TGA curve of **O1**. Heating rate 10 K/min, Al crucible, under a nitrogen gas flow of 20 mL/min.

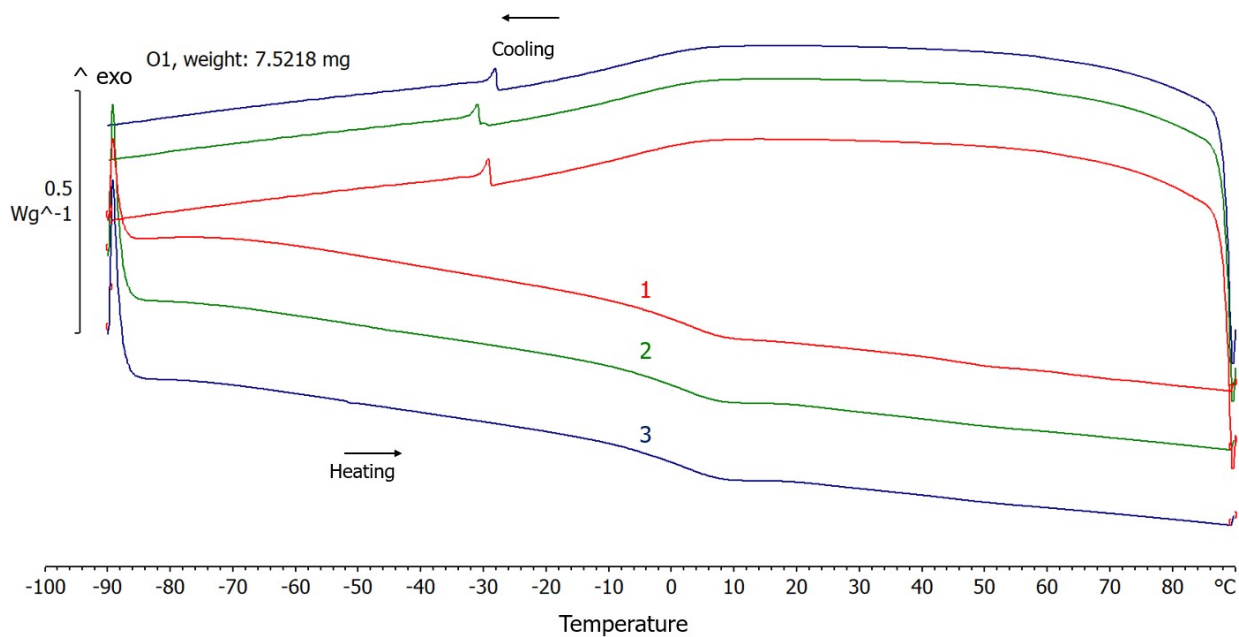


Figure SI- 6. DSC curve of **O1** Heating rate 10 K/min, Al crucible, 20 mL/min nitrogen gas, 3 cycles (-90 to +90 °C).

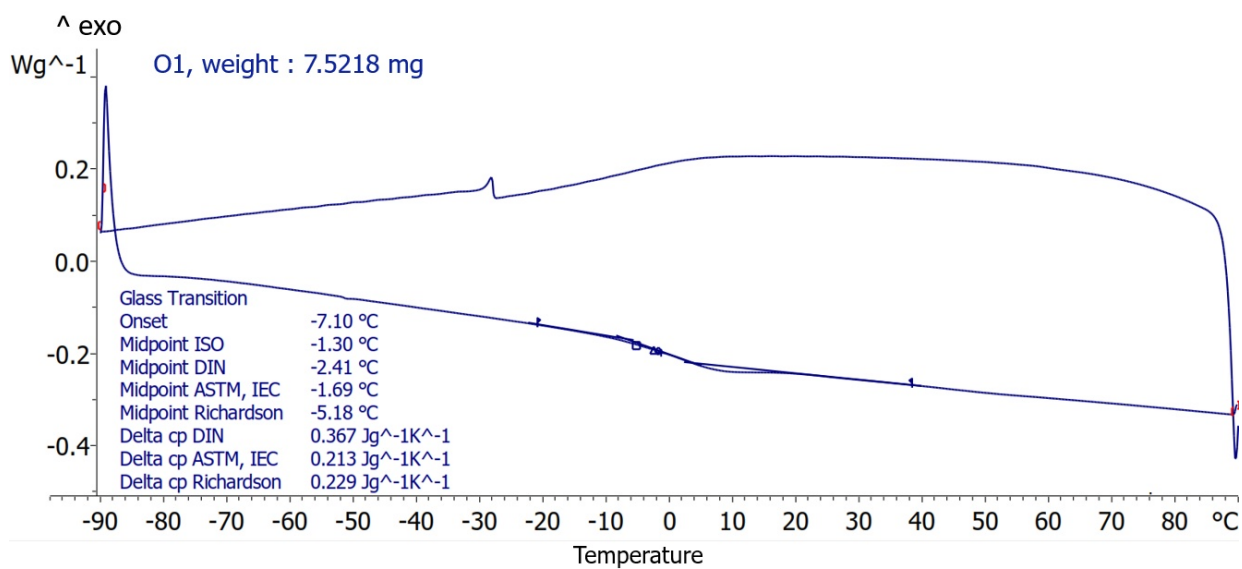
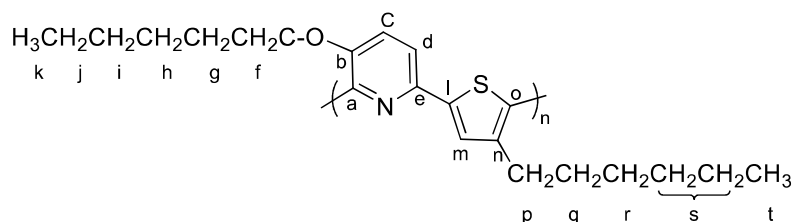


Figure SI- 7. DSC curve of **O1** Heating rate 10 K/min, Al crucible, 20 mL/min nitrogen gas, cycle 3 of 3 (-90 to +90 °C).

Poly(2,6-(3-*n*-hexyloxy)-pyridine-1,4-(3-*n*-hexyl)-thiophene) O2



Selection of the catalyst

In a Schlenk flask, **6** (55 mg, 10 μ mol) was dissolved in THF (2 mL). A suspension of $[\text{Pd}(\text{tBu}_3\text{P})_2]$ or $[\text{Pd}(\text{dppf})\text{Cl}_2]$ 5 mol%, CsF (20 mg, 13 μ mol) in degassed water (0.5 mL) and THF (1.5 mL) were added. The mixture was heated at 60 $^\circ\text{C}$ for 24 h under a nitrogen atmosphere. The crude mixture was quenched with a solution of HCl in methanol (1 M, 1 mL) to afford a sticky yellow oil. Water was added (5 mL) and the mixture was extracted with DCM (3 x 5 mL). The organic phase was washed with brine (3 x 5 mL) before being dried over MgSO_4 . After filtration, the volatiles were removed *in vacuo*. The crude product was purified by Soxhlet extraction. First, MeOH (100 mL) was used as solvent and the system was heated at 100 $^\circ\text{C}$ for 8 h. After oligomers and small molecules were removed, the solvent was changed to chloroform and the system was heated at 80 $^\circ\text{C}$ for 4 h.

Catalyst	Mass catalyst (mg)	M_n (kDa)	\bar{D}
$[\text{Pd}(\text{tBu}_3\text{P})_2]$	2	2.3	1.35
$[\text{Pd}(\text{dppf})\text{Cl}_2]$	3	2.3	1.48

Table SI- 4. GPC measurement results from the selection of the catalyst for the oligomerization of the monomer **6**. THF was used as eluent in a concentration of 1 mg/mL, at a flow rate of 1 mL/min. Calibrated against polystyrene standards using a conventional calibration method.

Oligomer synthesis

In a Schlenk flask, **6** (300 mg, 546 μ mol) was dissolved in THF (2 mL). A suspension of $[\text{Pd}(\text{tBu}_3\text{P})_2]$ (14 mg, 27 μ mmol, 5 mol%), CsF (108 mg, 710 μ mol) in degassed water (0.5 mL) and THF (1.5 mL) were added. The mixture was heated at 50 $^\circ\text{C}$ for 24 h under a nitrogen

atmosphere. The crude mixture was quenched with a solution of HCl in methanol (1 mL, 1 mmol, 1 M) to afford a greenish yellow solid. Water was added (5 mL) and the reaction mixture was extracted with DCM (3 x 10 mL) The organic phase was washed with brine (3 x 5 mL) before being dried over MgSO₄. After filtration, the volatiles were removed *in vacuo*. The crude product was purified by Soxhlet extraction. First MeOH (200 mL) was used as solvent and the system was heated at 100 °C for 8 h. After oligomers and small molecules were removed, the solvent was changed to chloroform (100 mL) and the system was heated at 80 °C for 4 h. The volatiles were removed *in vacuo* from the receiver flask to afford a greenish, fluorescent solid in a yield of 131 mg (70%).

¹H NMR (500 MHz, CDCl₃): δ= 7.51 (d, ³J = 8.4 Hz, 1H,c), 7.47 (s, 1H, m), 7.24 (d, ³J = 8.4 Hz, 1H, d), 4.13 – 3.94 (m, 2H, f), 3.11 – 2.99 (m, 2H, p), 1.94 – 1.81 (m, 2H, g), 1.80 – 1.67 (m, 2H, q), 1.58 – 1.41 (m, 4H, h/r), 1.41 – 1.14 (m, 12H, s/l/j), 0.88 – 0.70 (m, 6H, k/t) ppm.
¹³C{¹H} NMR (126 MHz, CDCl₃): 151.2 (b), 145.0 (e), 144.7 (l), 132.6 (a), 127.1 (c), 120.3 (d), 118.6 (m), 69.4 (f), 31.5 (q), 30.5 (p), 29.0 (g), 25.6 (h/r), 22.6, 29.5, 31.7, 31.9 (i/j/s/t), 14.0 (k/u) ppm.

IR (ATR): $\tilde{\nu}$ = 2921 (m), 2851 (m), 1565 (w), 1435 (s), 1379 (w), 1272 (m), 1130(m), 1071 (w), 816(m) cm⁻¹.

λ_{\max} (DCM) = 390 nm.

λ_{PL} (DCM) = 442 nm.

ϵ (DCM) = 7.10 × 10⁴ L mol⁻¹ cm⁻¹. The extinction factor was calculated from solutions of **O2**, using the molecular weight calculated by GPC (5390 g/mol), in DCM with concentration / Absorption : 0.13 μM / 0.014, 0.27 μM / 0.023, 0.54 μM / 0.043, 0.81 μM / 0.064, 1.09 μM / 0.087 and 1.36 μM / 0.096.

λ_{\max} (solid state) = 300 nm.

M_n (GPC, conventional method) = 5.39 kDa.

\bar{D} = 1.83.

MALDI (graphite) = *m/z*. 2059.

DP (based on GPC measurements) = 16.

DP (based on MALDI measurements) = 6.

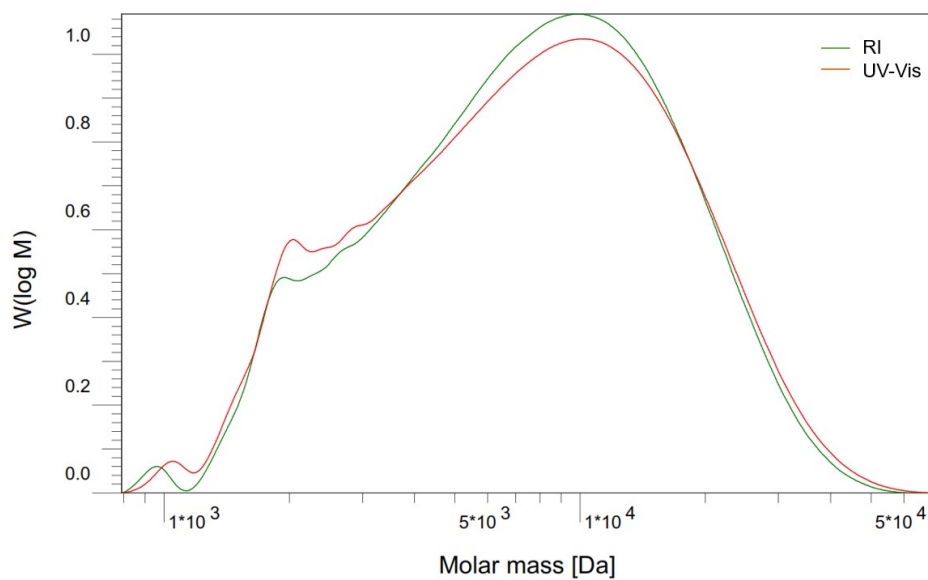
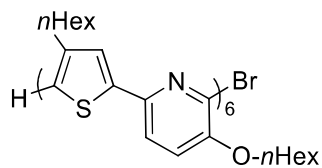
Proposed structure with end groups based on MALDI analysis

Figure SI- 8. GPC measurement result of **O2** using THF as eluent in a concentration of 1 mg/mL, at a flow rate of 1 mL/min. Calibrated against polystyrene standards using a conventional calibration method. Signals from the RI and Uv-vis detectors are shown.

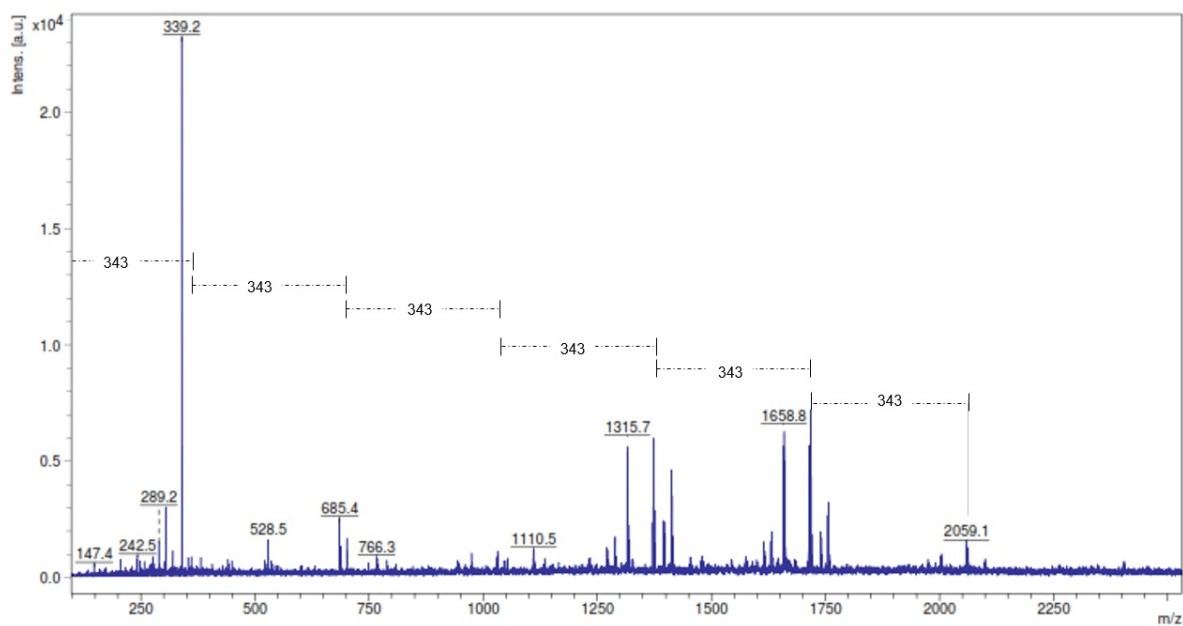


Figure SI- 9. MALDI (graphite) spectrometry of **O2**. With the mass of the repeating unit indicated in the picture.

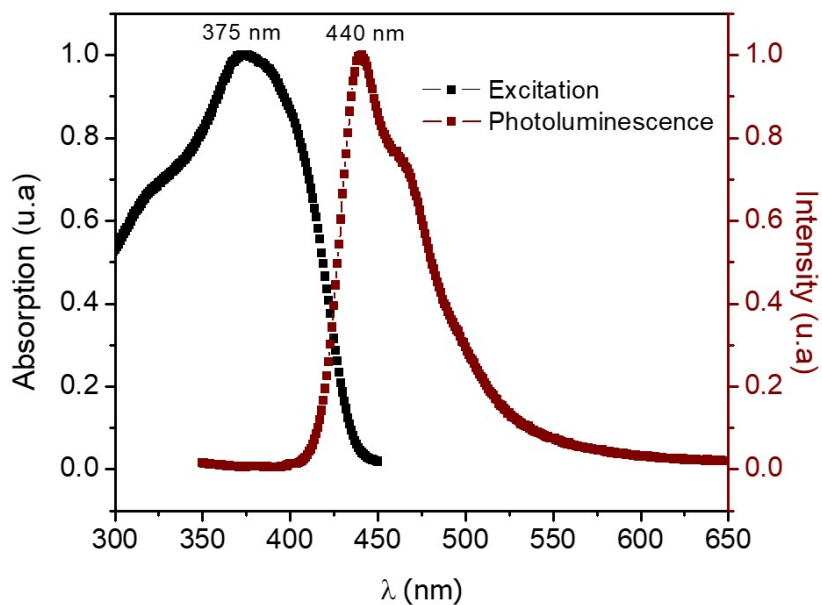


Figure SI- 10. Excitation and photoluminescence spectra ($\lambda_{exc} = 340$ nm) of a solution of **O2** in DCM (1.13×10^{-5} M).

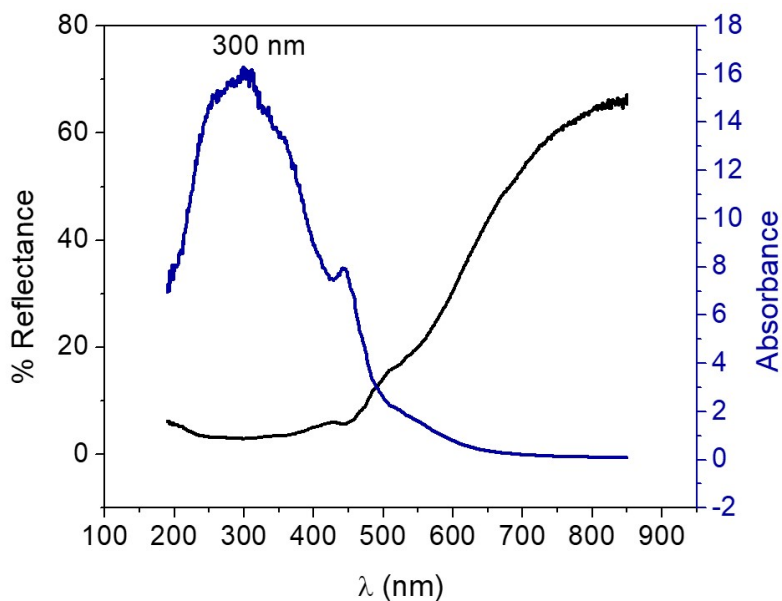


Figure SI- 11. Solid state absorption (blue) and reflection spectra (black) of **O2**.

With the reflectance spectrum it is possible to determine if the polymer has an indirect or direct band gap.

The expression proposed by Tauc, Davis and Mott it is used to calculate the band gap:^[8]

$$(h\nu\alpha)^{1/n} = A (h\nu - E_g) \quad (1)$$

where: h : Planck's constant, ν : frequency of vibration, α : absorption coefficient, E_g : band gap, A : proportional constant. The value of n denotes the nature of the sample transition. The most common ones are: $n = 1/2$ for direct allowed transition and $n = 2$ for indirect allowed transition.

The absorption coefficient α is proportional to the diffuse reflectance ($F(R_\infty)$) and the Tauc function (eq. 1) is converted into the Kubelka-Munk function (2).^[9]

$$(h\nu F(R_\infty))^{1/n} = A (h\nu - E_g) \quad (2)$$

Using expression 2, the Tauc graph was plotted using $n = 1/2$ and $n = 2$. The x intercept of the tangent from the point of inflection of the curve from the plot denotes the band gap E_g .

It is expected that the nearest band gap calculated with this plot with the one obtained from the Uv-vis spectra, predicts which type of transition the material has.

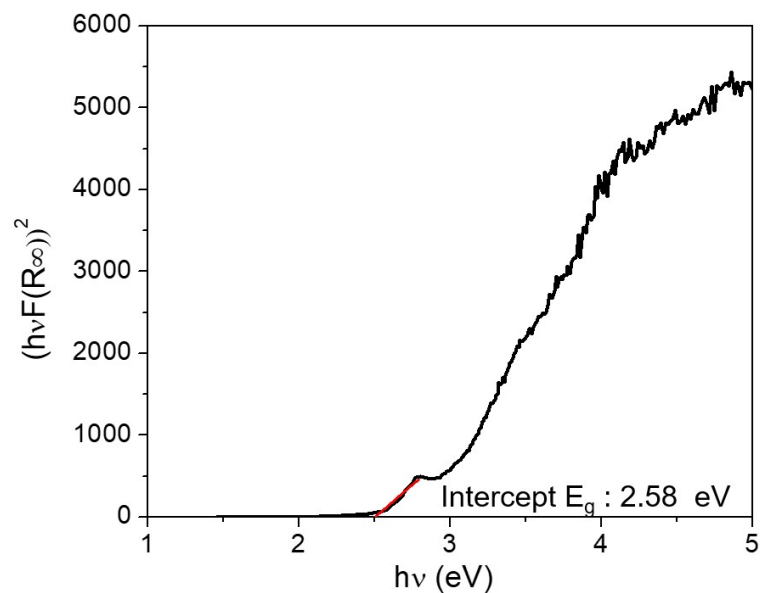


Figure SI- 12. Tauc plot of **O2** with $n = 1/2$ for direct transition.

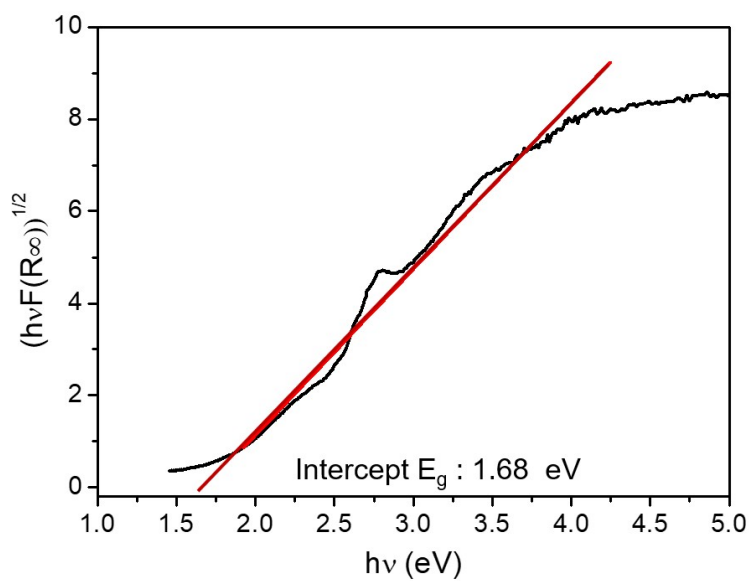


Figure SI- 13. Tauc plot of **O2** with $n = 2$ for an indirect transition.

Conclusion : **O2** showed an indirect allowed transition.

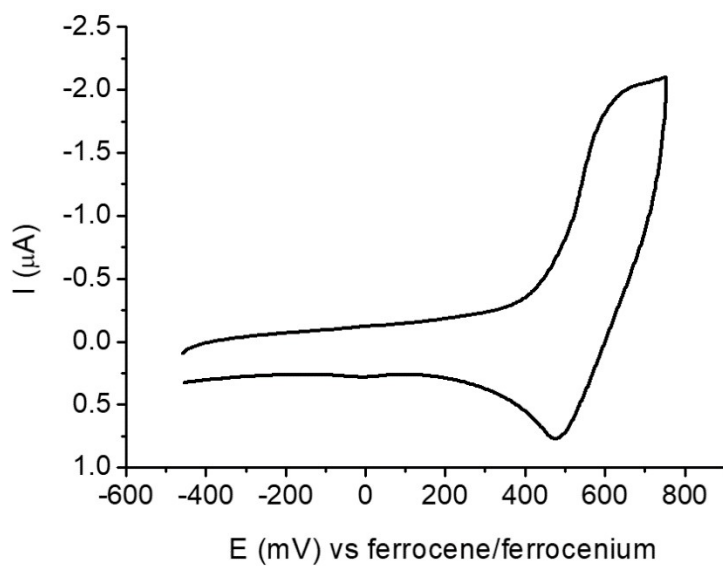


Figure SI- 14. Cyclic voltammogram of a solution of **O2** ($1 \times 10^{-3} \text{ M}$) using Bu_4NPF_6 as electrolyte in DCM (0.2 M).

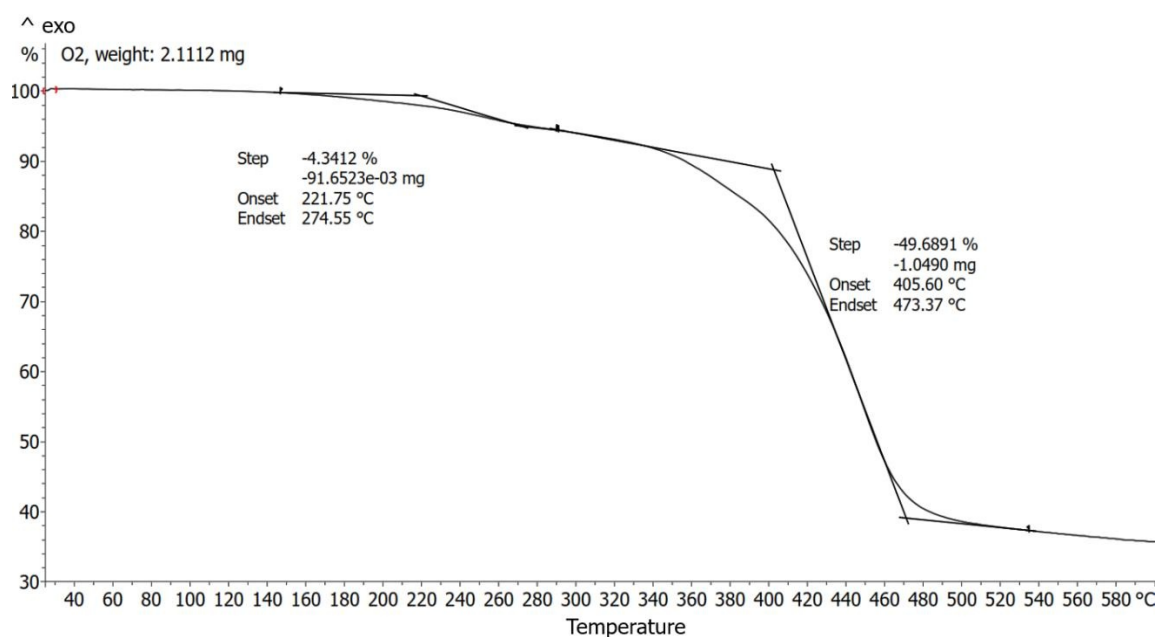


Figure SI- 15. TGA curve of **O2**. Heating rate 10 K/min, Al crucible, flow of 20 mL/min nitrogen gas.

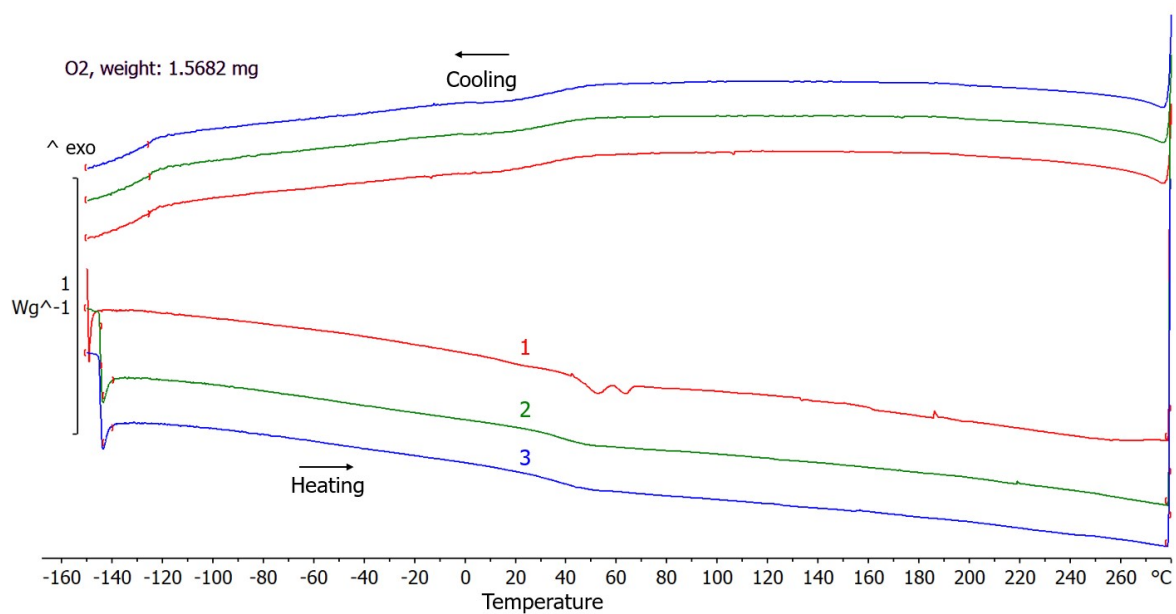


Figure SI- 16. DSC curve of **O2** Heating rate 10 K/min, Al crucible, flow of 20 mL/min nitrogen gas, 3 cycles (-150 to +250 °C).

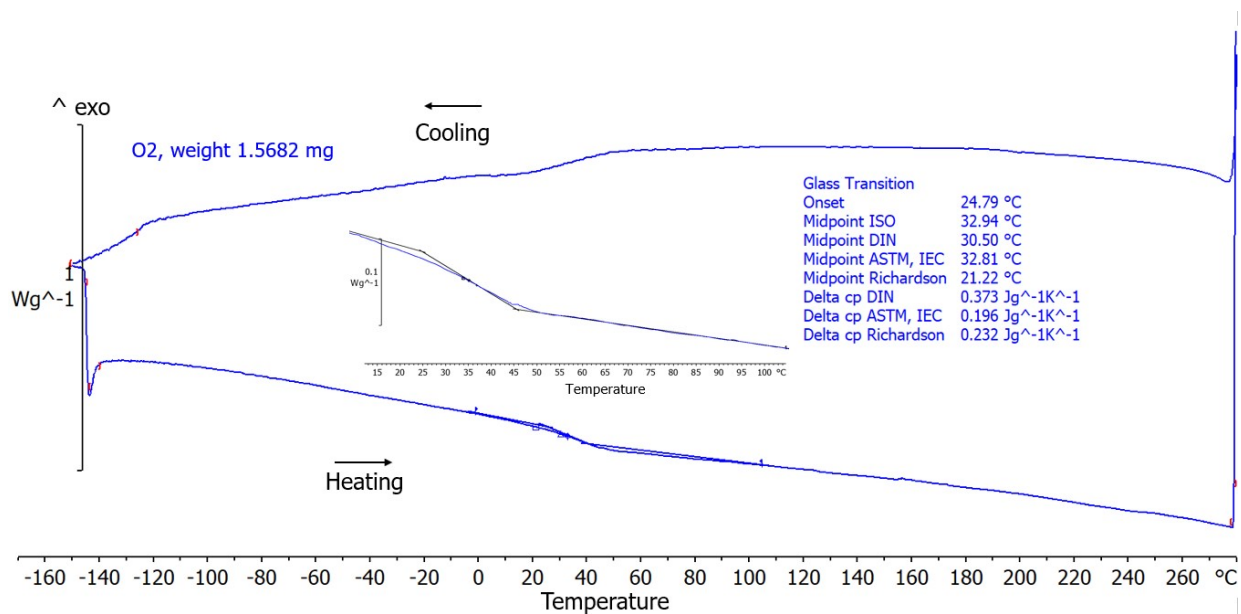


Figure SI- 17. DSC curve of **O₂** Heating rate 10 K/min, Al crucible, flow of 20 mL/min nitrogen gas, cycle 3 of 3 (-150 to +250 °C).

Reaction Monitoring

Poly(1,4-(3-*n*-hexyl)-thiophene-2,6-(3-*n*-hexyloxy)-phenylene) O1

In a Schlenk tube, a solution of **5** (103 mg, 180 μmol) and 1,3,5-trimethoxybenzene (33.8 mg, 200 μmol , used as internal standard) in THF (1 mL) was prepared and heated for 2 min at 60 °C. A first sample (0.2 mL) was taken out of from the reaction mixture (t_0). Immediately after, a suspension of $[\text{Pd}(\text{tBu}_3\text{P})_2]$ (4.6 mg, 9 μmol , 5 mol%), CsF (37 mg, 243 μmol), water (0.5 mL) and THF (stabilizer free, 1.5 mL) was added. After 1 h, 3 h, 6 h, 12 h and 24 h reaction time, a sample was taken out of the reaction mixture.

Every sample was quenched with a solution of HCl in MeOH (2.0 mL, 2 mmol, 1 M), then water (1 mL) was added and the mixture was extracted with DCM (2 x 3 mL). The organic phase was dried over MgSO_4 and filtered over a "mini column" (glass pipet filled with Celite. See Figure SI-18). The solution was split in two flasks and the solvents were removed *in vacuo*. Half of the sample was dissolved in THF for GPC analysis and the second one in CDCl_3 for ^1H NMR spectroscopic analysis.



Figure SI- 18. Picture from the filtration with the 'mini column' based on a glass pipet filled with Celite® and silica.

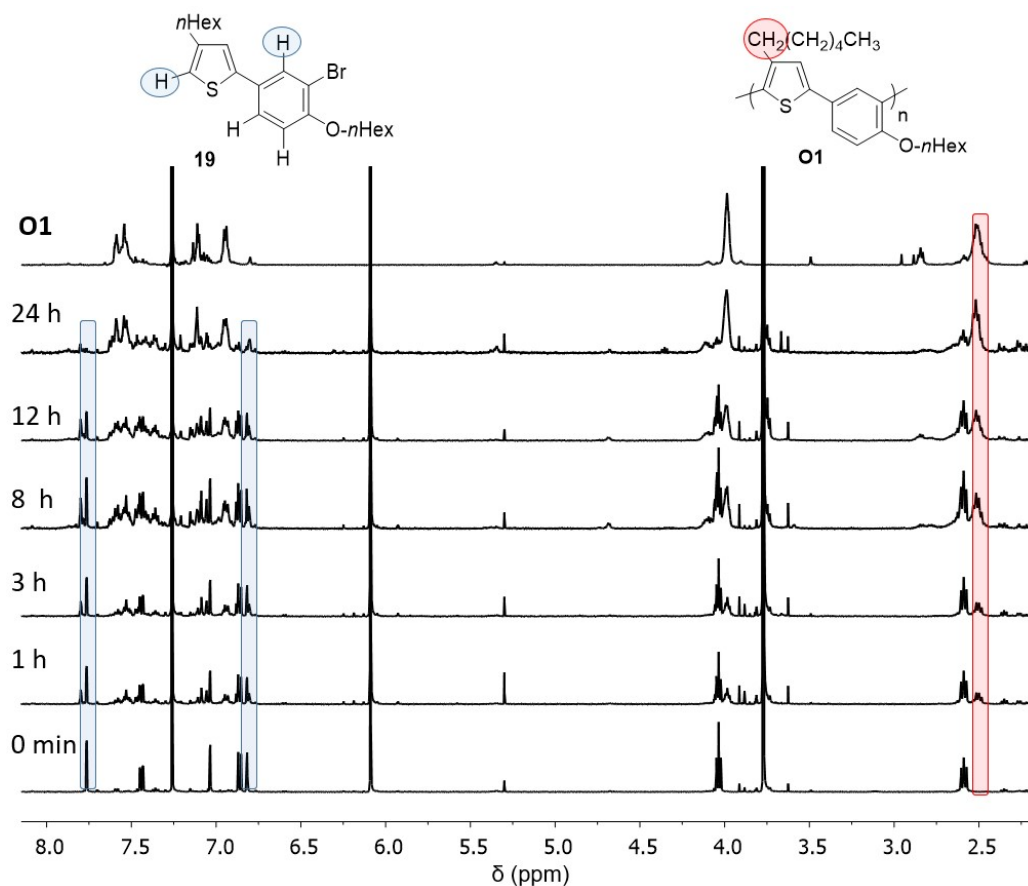


Figure SI- 19. ^1H NMR spectra (recorded at 300 K, 500 MHz in CDCl_3) of the reaction monitoring for the polymerization of **5** to produce **O1**, 1,3,5-trimethoxybenzene was used as standard. The conversion was based on the amount of compound **19** (product of the quenching of **5** with HCl/MeOH 1M).

Time (h)	% conversion	M_n (kDa)	M_w (kDa)	\bar{D}
0	0.0	0.44	0.44	1.01
1	15.0	0.99	1.06	1.07
3	16.4	1.00	1.09	1.08
8	40.5	1.50	1.65	1.10
12	37.4	1.50	1.68	1.12
24	91.6	1.58	2.60	1.65

Table SI- 5. Results from the reaction monitoring of **O1** : % conversion obtained from the ^1H NMR spectra (Figure SI-19); M_n , M_w and \bar{D} obtained from GPC measurements. The conversion was based on the amount of compound **19** (product of the quenching of **5** with HCl/MeOH 1M).

The growth behavior of **O1** was observable in the Uv-vis/elugram 2D-plot of the GPC samples (Figure SI-20). The spectra were recorded using the Win-GPC[®] software from the company PSS.

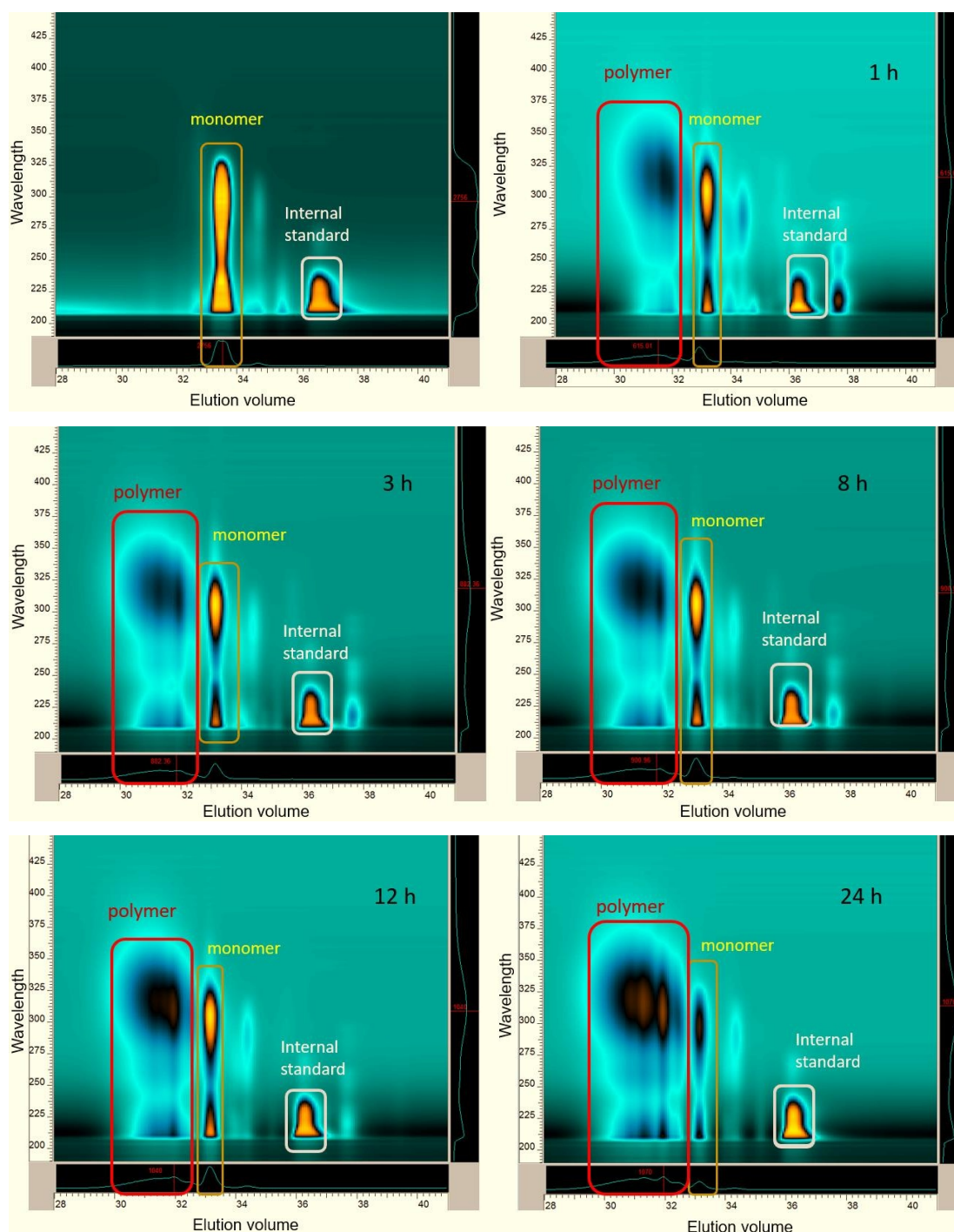


Figure SI- 20. Uv-vis spectra/ elugram 2D plots from the GPC measurements of the reaction monitoring of **O1**. The intensity (Z) of the yellow color is related to the concentration of internal standard, monomer and polymer in each sample.

The conversion of the monomer using the Uv-vis/ elution 2D-plot was based in the intensity (Z value) from the area corresponding to the monomer. The results of the time, % conversion (with respect disappearance of the monomer), M_n , M_w and \bar{D} for the polymerization of **5** are summarized in the Table SI-4.

Time (h)	% conversion	M_n (Da)	M_w (Da)	\bar{D}
0	0.0	0.44	0.44	1.01
1	36.7	0.99	1.06	1.07
3	48.7	1.00	1.09	1.08
8	51.3	1.50	1.65	1.10
12	62.0	1.50	1.68	1.12
24	100.0	1.58	2.60	1.65

Table SI- 6. Results from the reaction monitoring study of **01** : % conversion obtained from the Uv-vis/ elugram 2D- plot (Figure SI-20); M_n , M_w and \bar{D} obtained from GPC measurements.

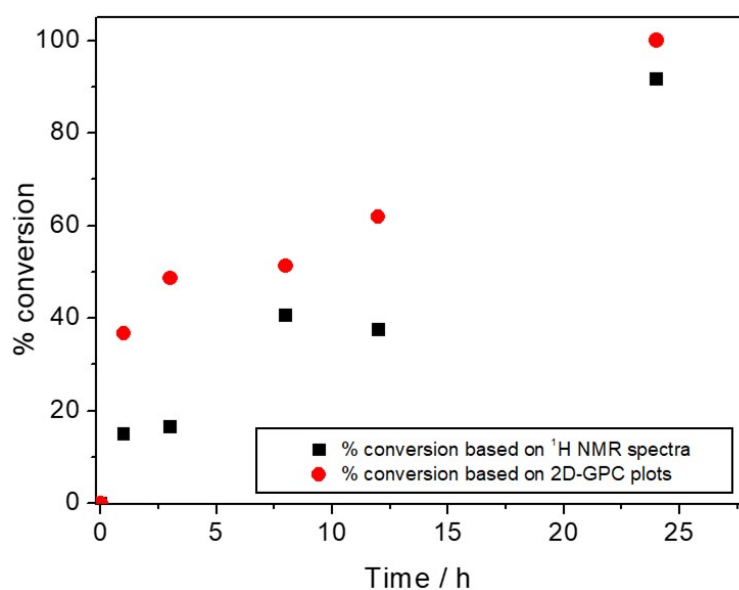


Figure SI- 21. Plots of % conversion vs. time. Calculated by the two detectors (^1H and 2D-plots GPC) for the polymerization of **5** with 5 mol% of $[\text{Pd}(\text{tBu}_3\text{P})_2]$, 1.2 eq. CsF in THF at 50 °C. The conversion was defined as amount of compound **19** consumed observed by the ^1H NMR spectra and 2D-GPC plots.

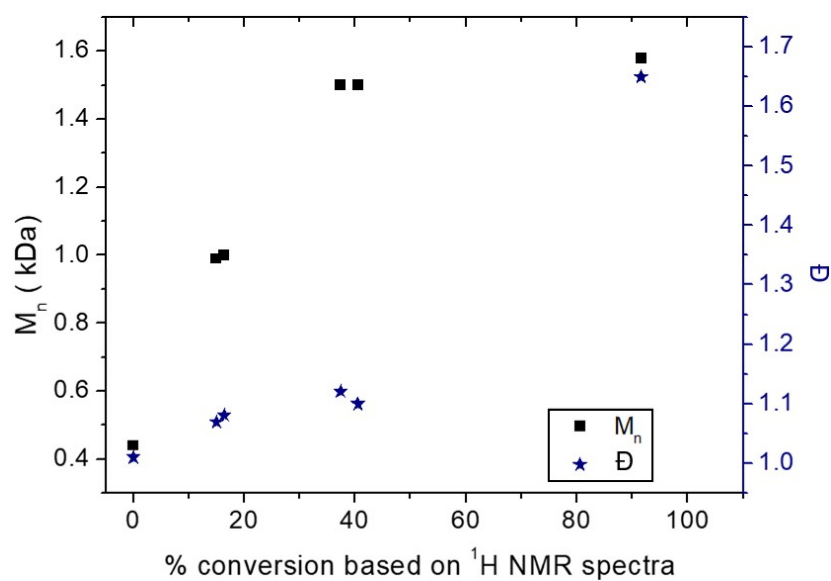


Figure SI- 22. Plot of the % conversion calculated by ^1H NMR spectra vs. M_n and \bar{D} for the polymerization of **5** with 5 mol% of $[\text{Pd}(\text{tBu}_3\text{P})_2]$, 1.2 eq. CsF in THF at 50 °C. The conversion was defined as amount of compound **19** consumed observed by the ^1H NMR spectra.

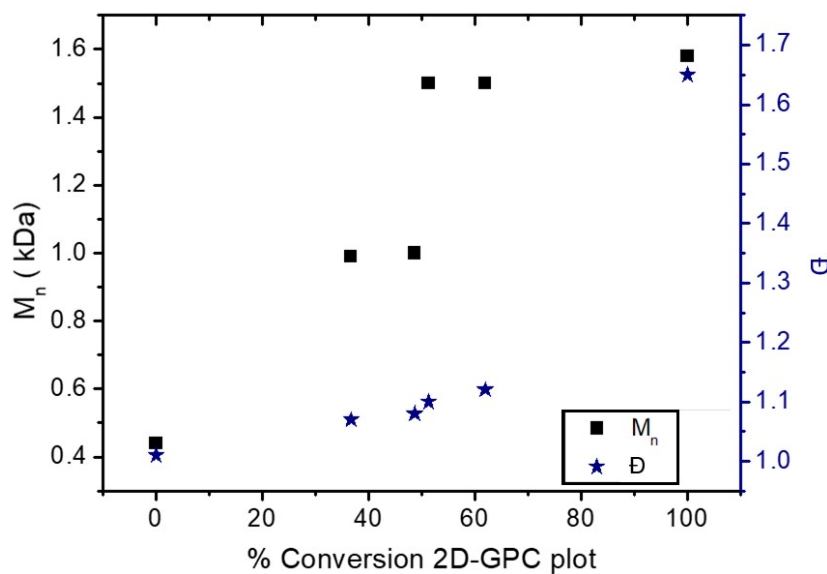


Figure SI- 23. Plot of % conversion calculated by 2D-GPC plot vs. M_n and \bar{D} for the polymerization of **5** with 5 mol% of $[\text{Pd}(\text{tBu}_3\text{P})_2]$, 1.2 eq. CsF in THF at 50 °C. The conversion was defined as amount of compound **19** consumed observed by the 2D-GPC plots.

Poly(2,6-(3-*n*-hexyloxy)-pyridine-1,4-(3-*n*-hexyl)-thiophene) O2

In a Schlenk tube, a solution of **6** (173 mg, 315 μmol) and 1,3,5-trimethoxybenzene (52.2 mg, 310 μmol , used as internal standard) in THF (1 mL) was prepared and heated for 2 min at 60 °C. A first sample (0.2 mL) was taken out of the reaction mixture (t_0). Immediately after, a suspension of $[\text{Pd}(\text{tBu}_3\text{P})_2]$ (7.9 mg, 15 μmol , 5 mol%), CsF (61 mg, 401 μmol), water (0.5 mL) and THF (stabilizer free, 1.5 mL) was added. After 1 h, 3 h, 6 h, 12 h and 24 h of reaction, a sample was taken from the reaction mixture.

Every sample was quenched with a solution of HCl in MeOH (2.0 mL, 2 mmol, 1 M), then water (1 mL) was added and the mixture was extracted with DCM (2 x 3 mL). The organic phase was dried over MgSO_4 and filtered over a 'mini column' (glass pipet filled with Celite® and silica. See Figure SI-18). The solution was split in two flasks and the solvents were removed *in vacuo*. Half of the sample was dissolved in THF for GPC analysis and the second one in CDCl_3 for ^1H NMR spectral analysis.

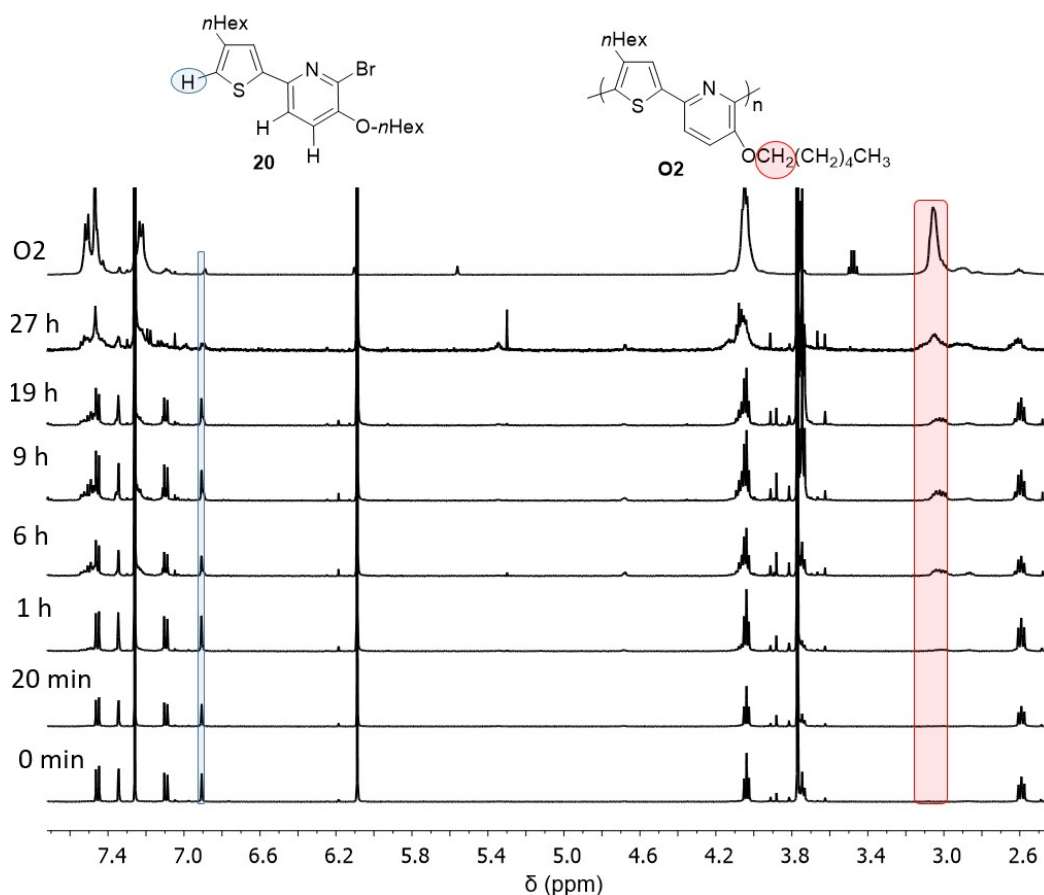
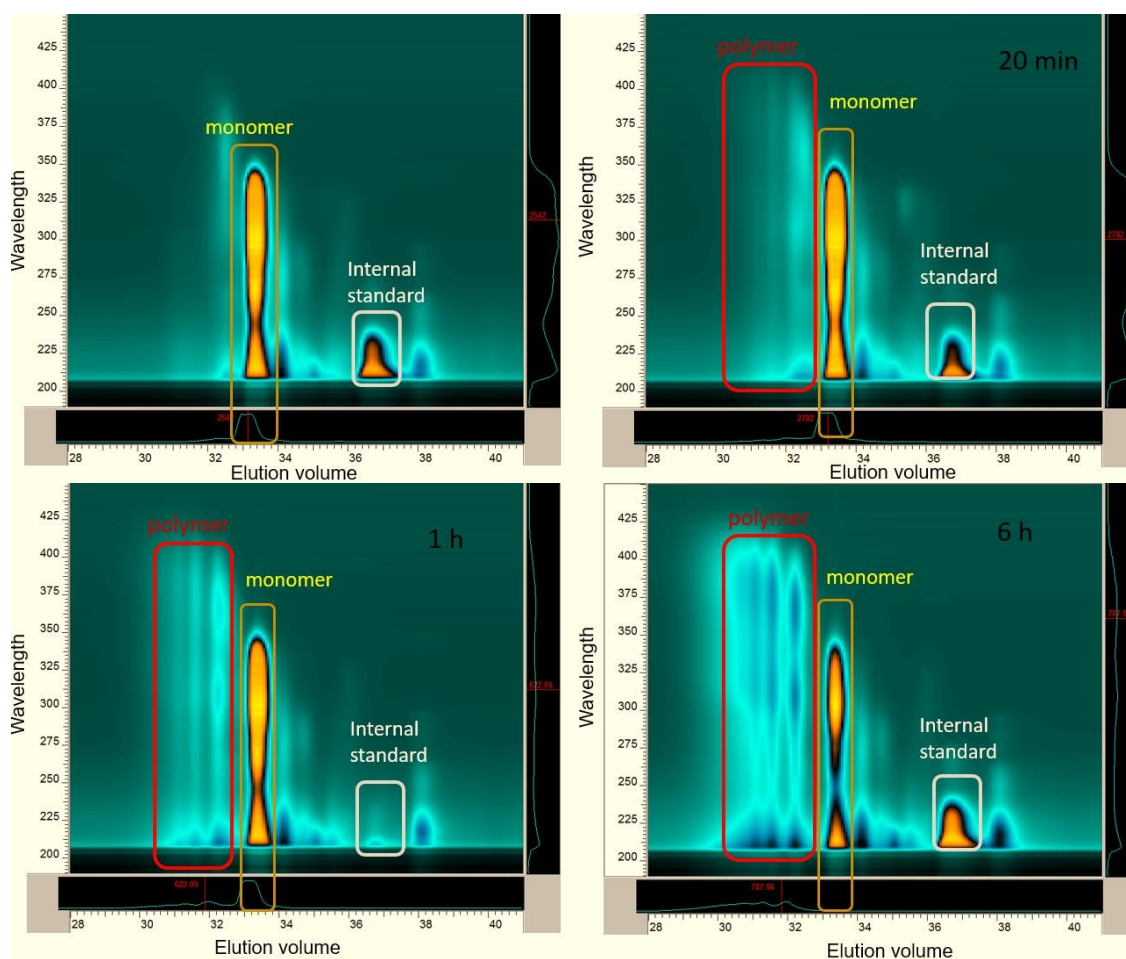


Figure SI- 24. ^1H NMR spectra (recorded at 300 K, 500 MHz in CDCl_3) of the reaction monitoring for the polymerization of **6** to produce **O2**, 1,3,5-trimethoxybenzene was used as standard. The conversion was based on the amount of compound **20** (product from the quenching of **6** in HCl/MeOH 1M).

Time (h)	% conversion	M_n (Da)	M_w (Da)	\bar{D}
0	0.0	441.3	457.7	1.04
1	34.6	1051.9	1144.8	1.09
6	52.2	1423.1	1706.1	1.20
9	60.0	1404.8	1703.1	1.21
19	66.7	1290.3	1500.9	1.16
27	100.0	1454.0	1770.1	1.22

Table SI- 7. Results from the reaction monitoring study of **O2**: % conversion obtained from the ^1H NMR spectra (Figure SI-24); M_n , M_w and \bar{D} obtained from GPC measurements. The conversion was based on the amount of compound **20** (product from the quenching of **6** in HCl/MeOH 1M).

The growth behavior of **O2** was observable in the Uv-vis/elugram 2D-plot of the GPC samples (Figure SI-25). The spectra were recorded using the Win-GPC[®] software from the company PSS.



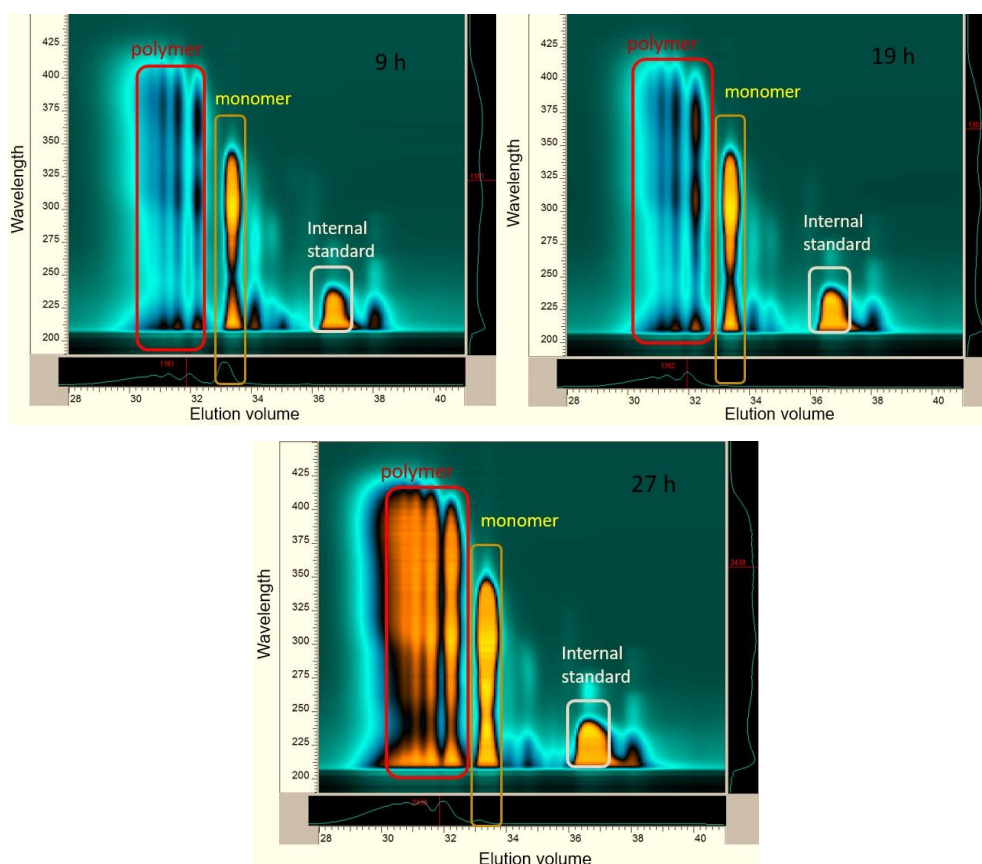


Figure SI- 25. Uv-vis spectra/ elugram 2D plots from the GPC measurements of the reaction monitoring of **O2**. The intensity (Z) of the yellow color is related to the concentration of internal standard, monomer and polymer in each sample.

The conversion of the monomer using the Uv-vis/ elution 2D-plot was based in the intensity (Z value) from the area corresponding to the monomer. The results of the time, % conversion (with respect disappearance of the monomer), M_n , M_w and \bar{D} for the polymerization of **6** are summarized in the Table SI-6.

Time (h)	% conversion	M_n (Da)	M_w (Da)	\bar{D}
0	0.0	0.44	0.46	1.04
0.33	34.3	0.45	0.49	1.09
1	40.4	1.05	1.14	1.09
6	48.3	1.42	1.71	1.20
9	65.0	1.40	1.70	1.21
19	68.1	1.29	1.50	1.16
27	100.0	1.45	1.77	1.22

Table SI- 8. Results from the reaction monitoring study of **O2**: % conversion obtained from the Uv-vis/ elugram 2D-plot (Figure SI-25); M_n , M_w and \bar{D} obtained from GPC measurements.

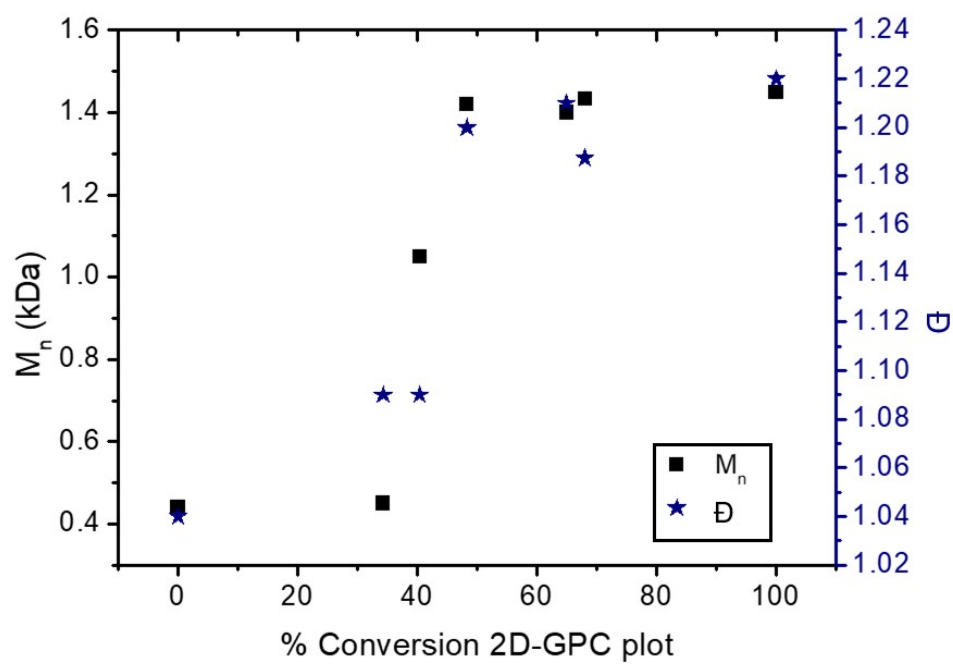
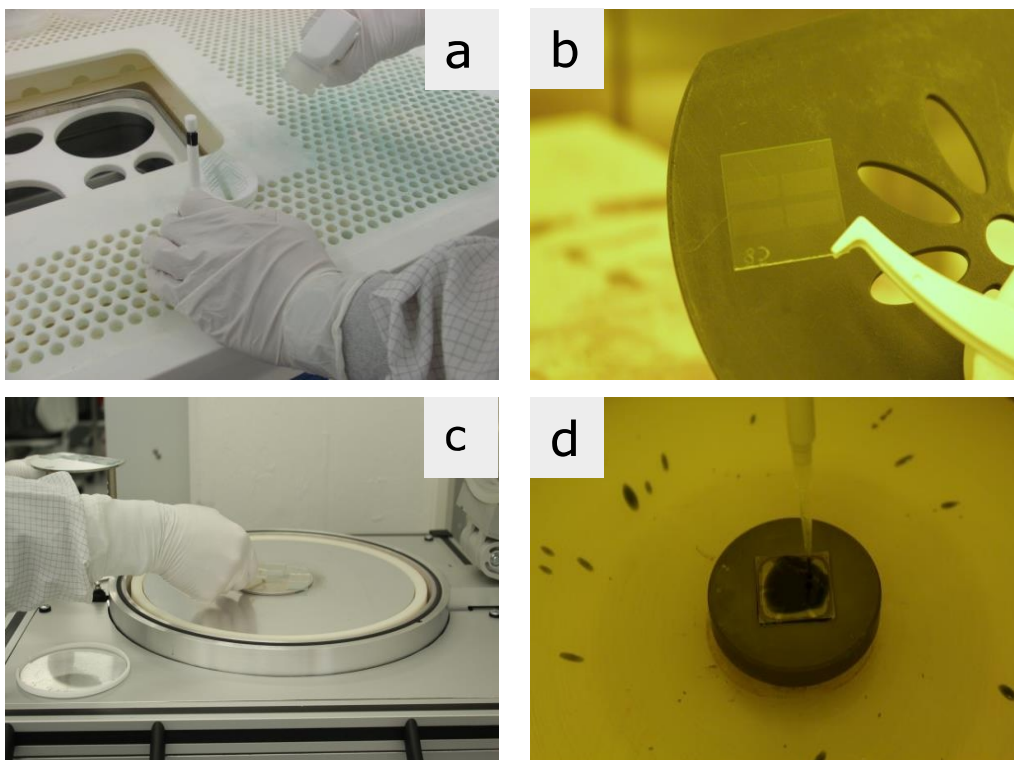


Figure SI- 26. Plot of the % conversion calculated by 2D-GPC plot vs M_n and Đ for the polymerization of **6** with 5 mol% of [Pd(t-Bu₃P)₂], 1.2 eq. CsF in THF at 50 °C. The conversion was calculated relative to compound **20** (product from the quenching process with HCl/MeOH) based on the 2D-GPC plots.

OLED-like Device Fabrication

ITO coated glass substrates were cleaned in an ultrasonic bath of acetone and isopropanol each for 15 min. Afterwards they were dried under a nitrogen stream, heated to 160 °C for 10 min and then cleaned with an oxygen plasma with 300 W for 3 min. 200 μL of a PEDOT: PSS water suspension were spin-coated onto the substrates (3500 rpm for 60 s). The samples were then transferred into a glovebox and annealed at 150 °C for 5 min. Afterwards, they were cooled down to 50 °C over the period of 2 h. A solution of the oligomers (**O1** or **O2**) in chloroform was prepared with a concentration of 10 mg/mL. 180 μL of the polymer solutions respectively were spin coated (500 rpm for 5 s, and 1000 rpm for 60 s) on the PEDOT:PSS layer and the samples were annealed at 70 °C for 2 h. Finally, a layer of LiF (1 nm) and Al (200 nm) were deposited by thermal evaporation.



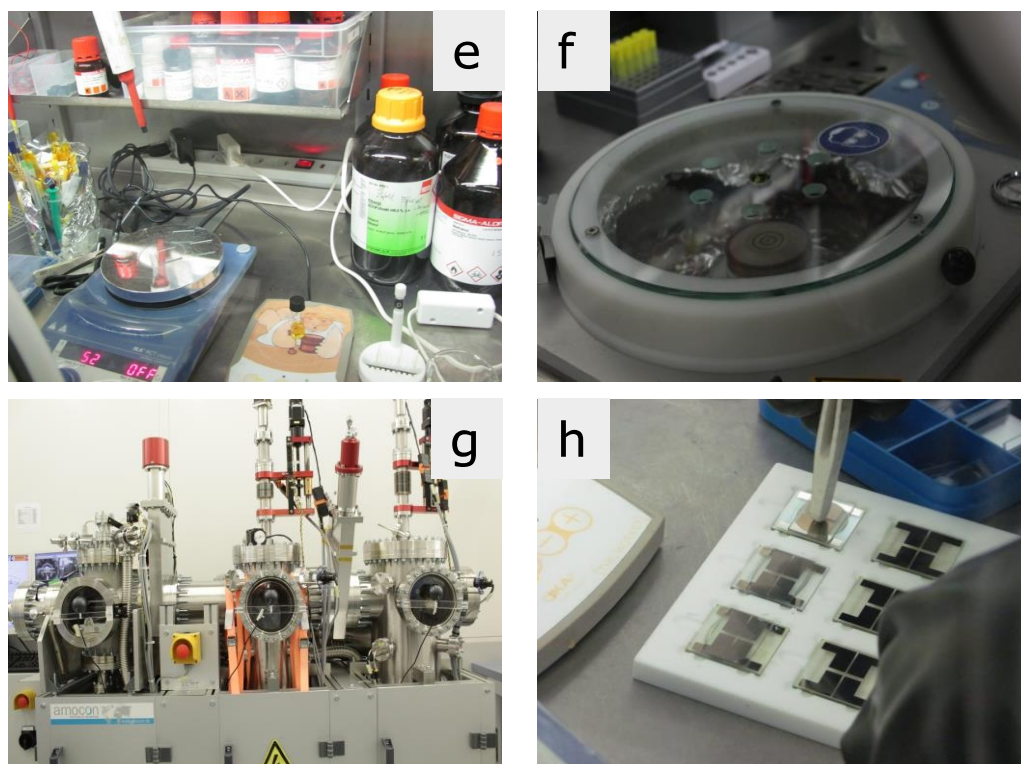


Figure SI- 27. Description of the OLED fabrication. a) Glass/ITO cleaning with acetone and isopropanol. b) Drying process of the glass/ITO. c) Glass/ITO cleaning with an oxygen plasma. d) Spin coating of a PEDOT:PSS solution over the glass/ITO. e) Annealing of the system (glass/ITO/PEDOT:PSS) inside a GB. f) Spin coating of a solution of the oligomers (**O1** or **O2**) in chloroform. g) Thermal evaporation of LiF and Al layers. h) OLED Encapsulation.

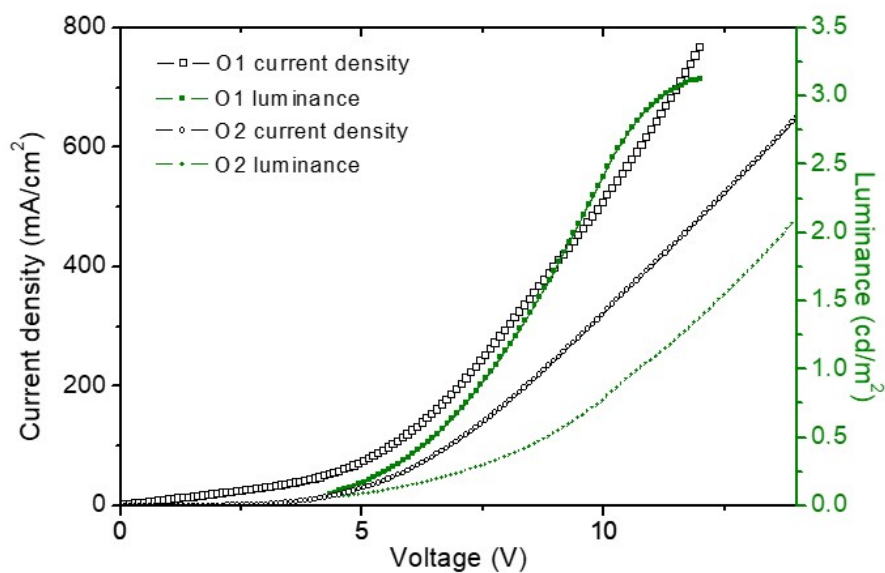


Figure SI- 28. Current density - voltage - luminance curves of the OLED-type devices with **O1** and **O2** as emissive layer.

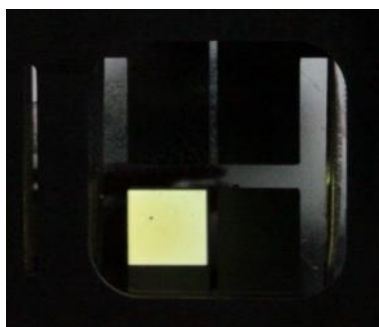


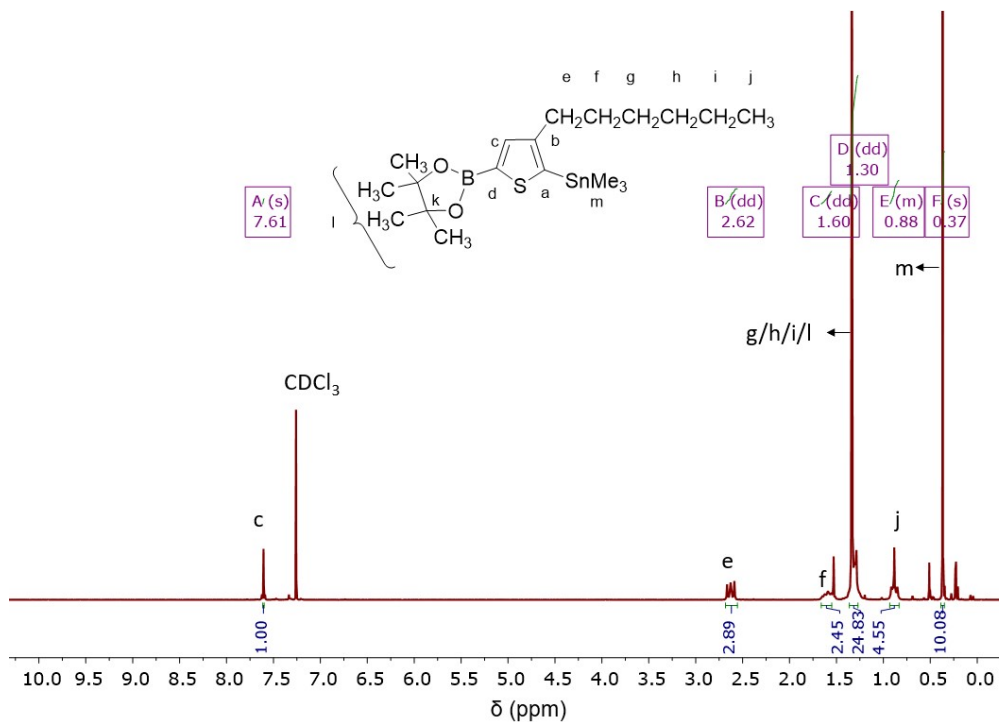
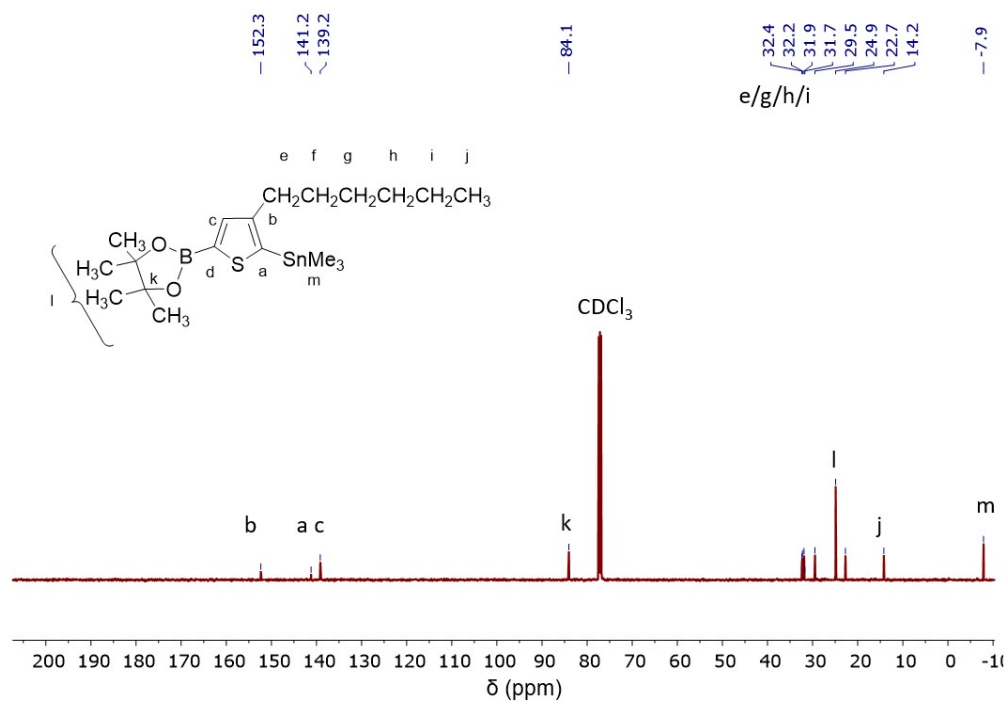
Figure SI- 29. Photo of the electroluminescence of the OLED-type device using **O2** as emissive layer. Exposure time: 1 s, which was visible to the human eye.

Device	Vol ^a (V)	EQE ^b (%)	CE ^b (cd/A)	PE ^b (lm/W)	CIE Color coordinates	Maximal brightness (cd/m ²) (@ mA/cm ²)
O1	7.7	3.4e ⁻⁴	4.7e ⁻⁴	1.5e ⁻⁴	0.351,0.385	3.1 (@ 750 mA/cm ²)
O2	10.7	2.6e ⁻⁴	2.6e ⁻⁴	0.8e ⁻⁴	0.379,0.381	2.1 (@ 650 mA/cm ²)

^a Voltage recorded at luminance of 1 cd/m², ^b EQE, CE and PE recorded at 500 mA/cm²

Table SI- 9. Electroluminescent performance of the OLED-type devices.

NMR Spectra

(3-Hexyl-5-(4,4,5,5-tetramethyl-1,3,2-dioxaborolan-2-yl)thiophen-2-yl)trimethylstannane (7)Figure SI- 30. ¹H NMR (500 MHz) spectrum of **7** in CDCl₃.Figure SI- 31. ¹³C{¹H} NMR (126 MHz) spectrum of **7** in CDCl₃.

4-Bromo-2-*n*-hexylthiophene (**11**)

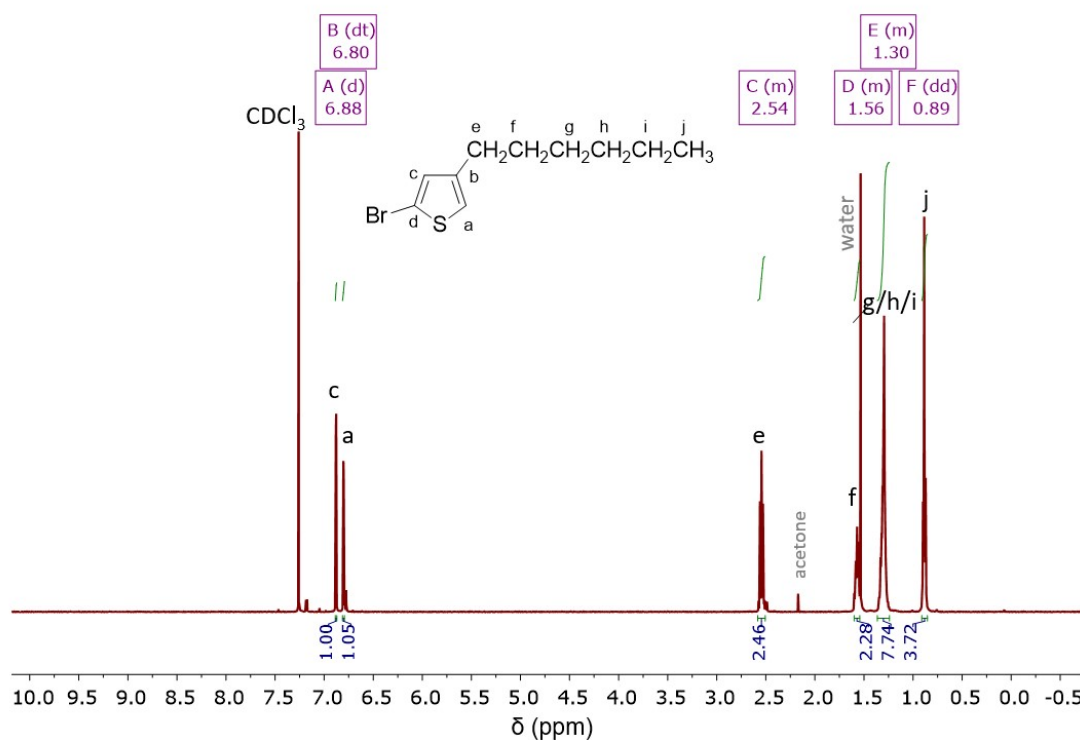


Figure SI- 32. ^1H NMR (500 MHz) spectrum of **11** in CDCl_3 .

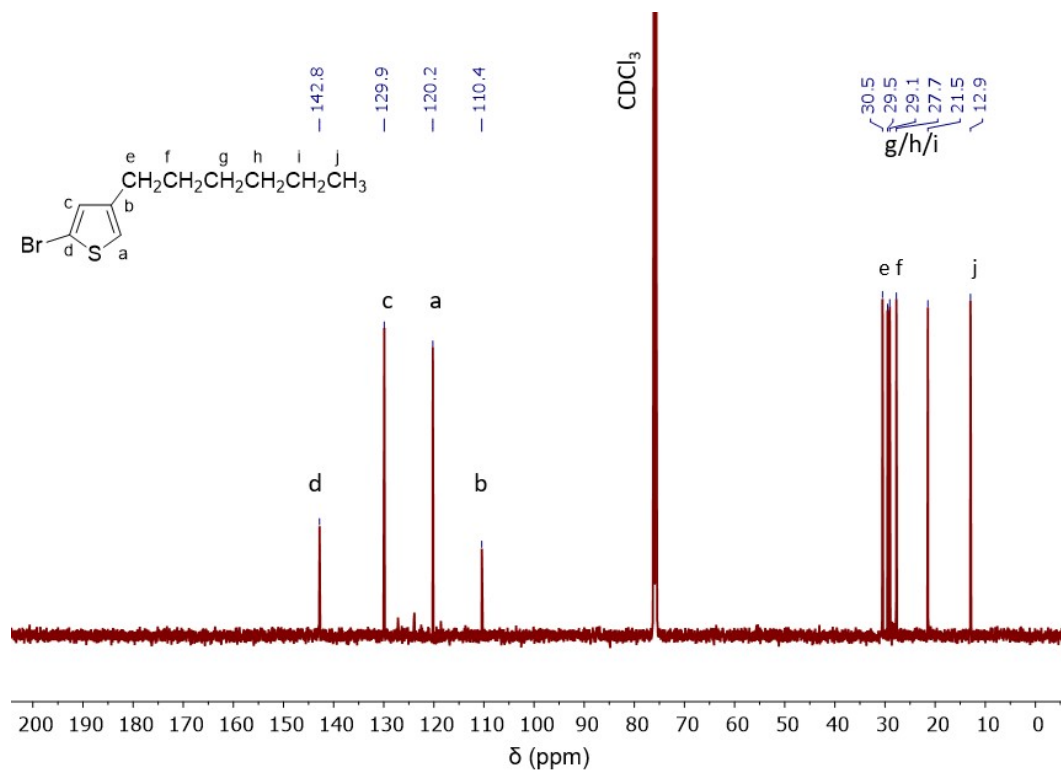
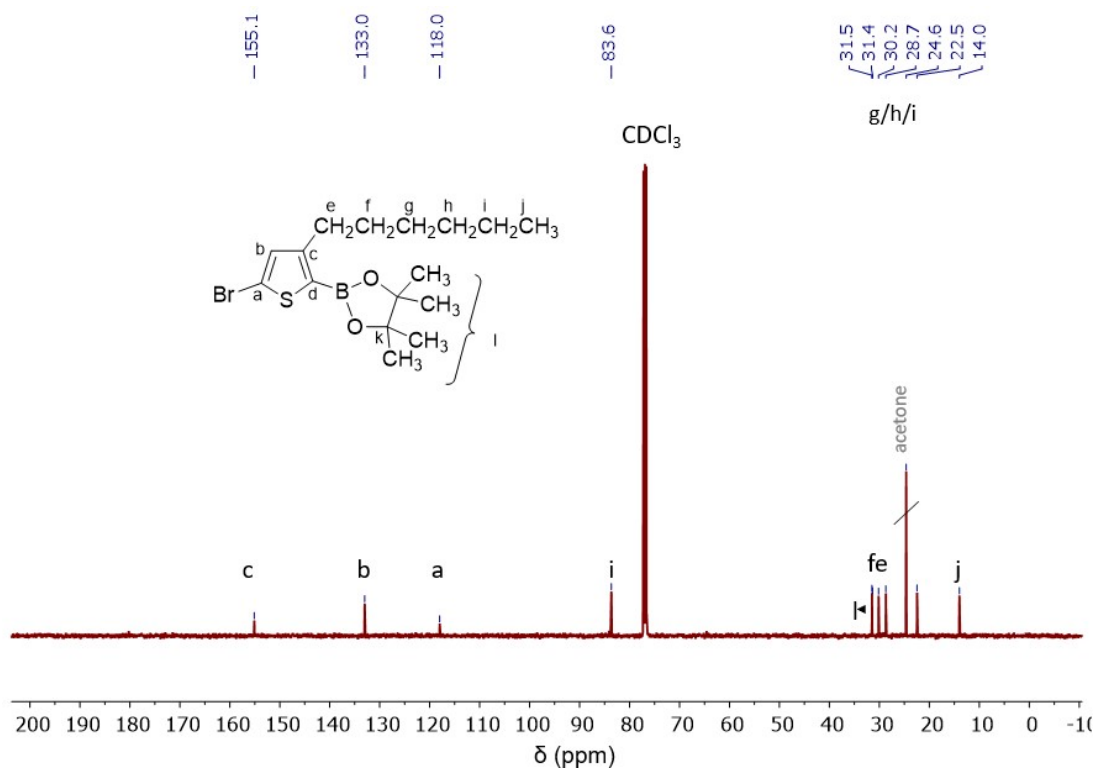
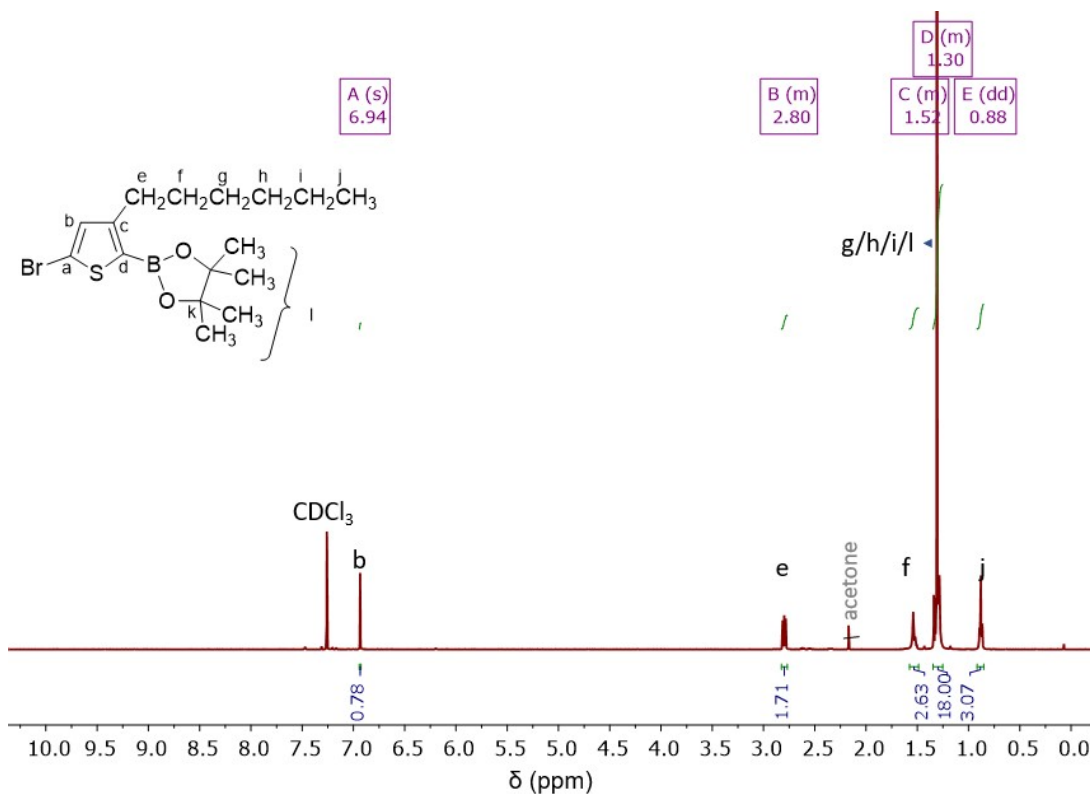


Figure SI- 33. $^{13}\text{C}\{^1\text{H}\}$ NMR (126 MHz) spectrum of **11** in CDCl_3 .

2-(5-Bromo-3-hexylthiophene-2-yl)-4,4,5,5-tetramethyl-1,3,2-dioxaborolane (12)


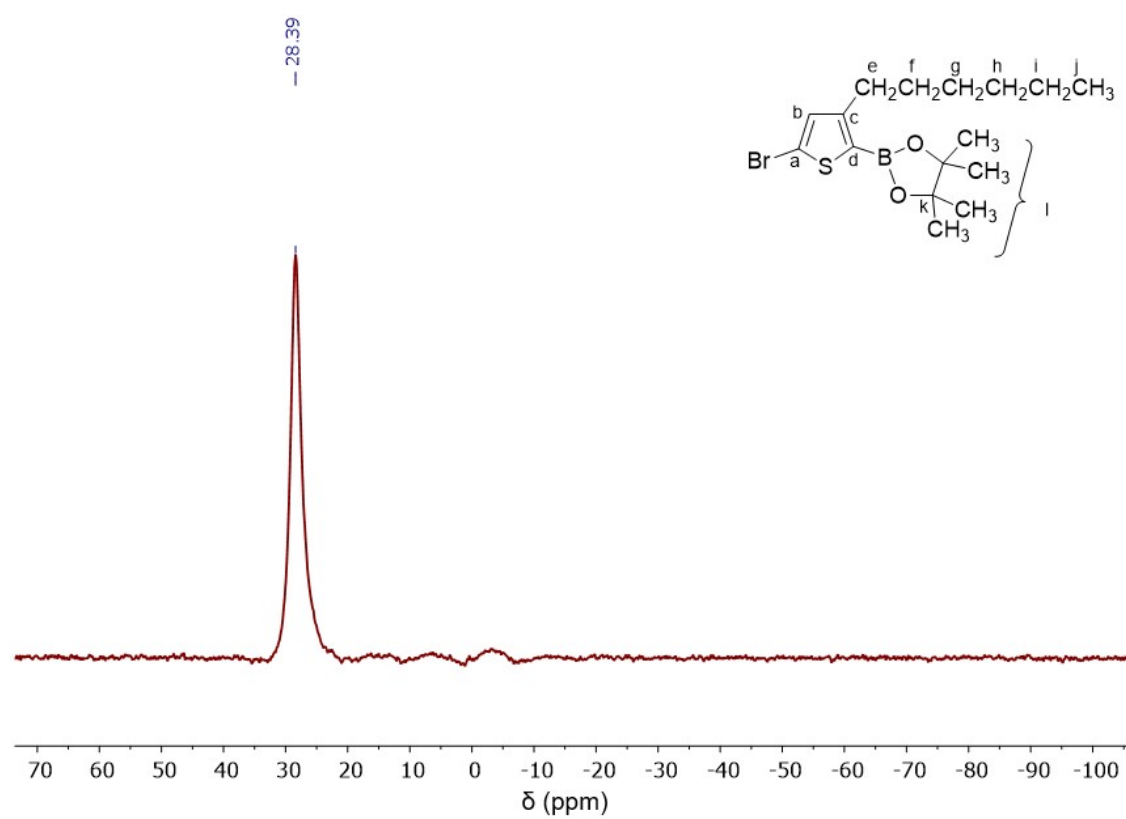
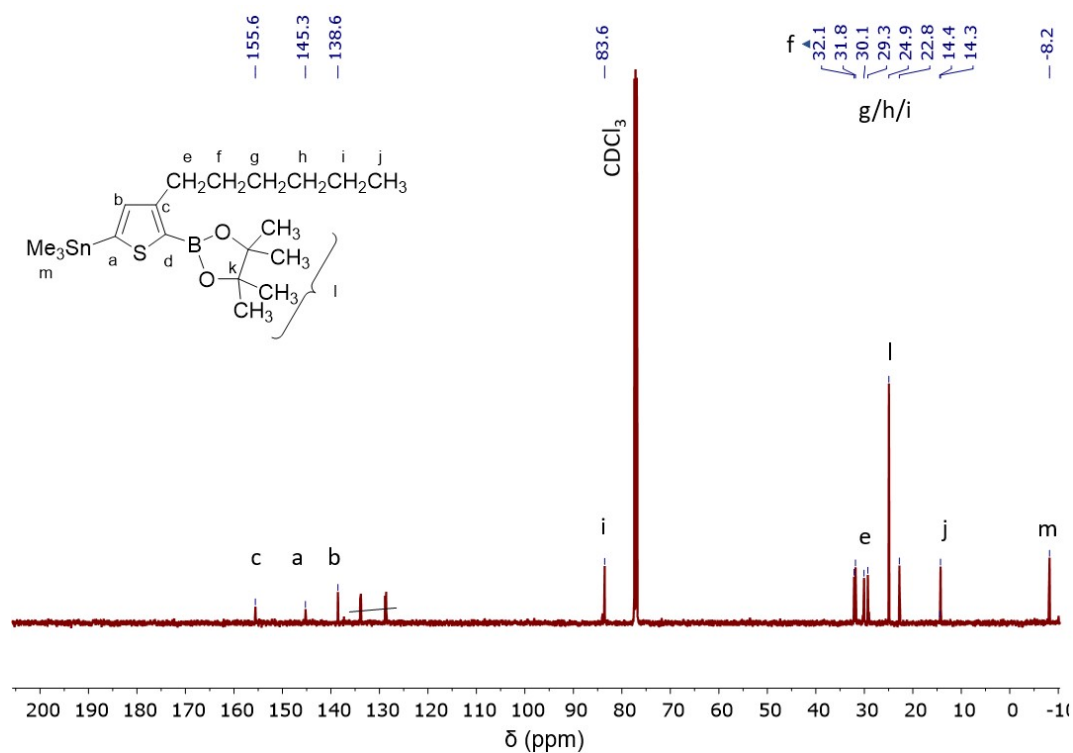
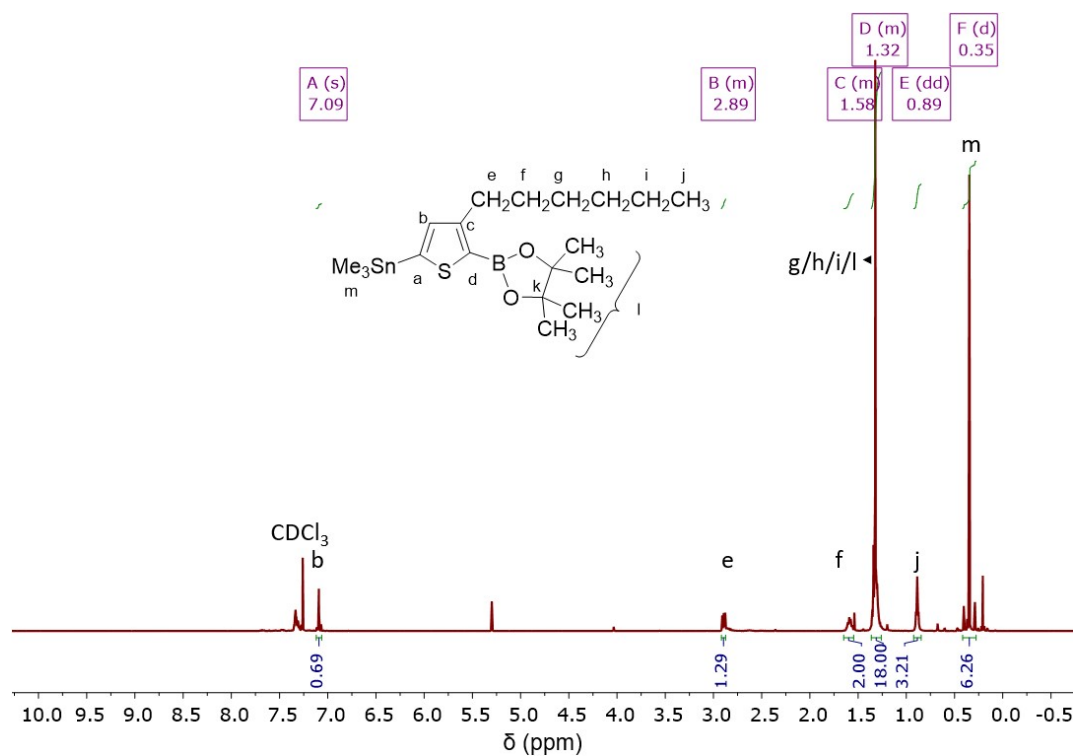


Figure SI- 36. $^{11}\text{B}\{^1\text{H}\}$ NMR (160 MHz) spectrum of **12** in CDCl_3 .

(4-Hexyl-5-(4,4,5,5-tetramethyl-1,3,2-dioxaborolan-2-yl)thiophen-2-yl)trimethylstannane (13)



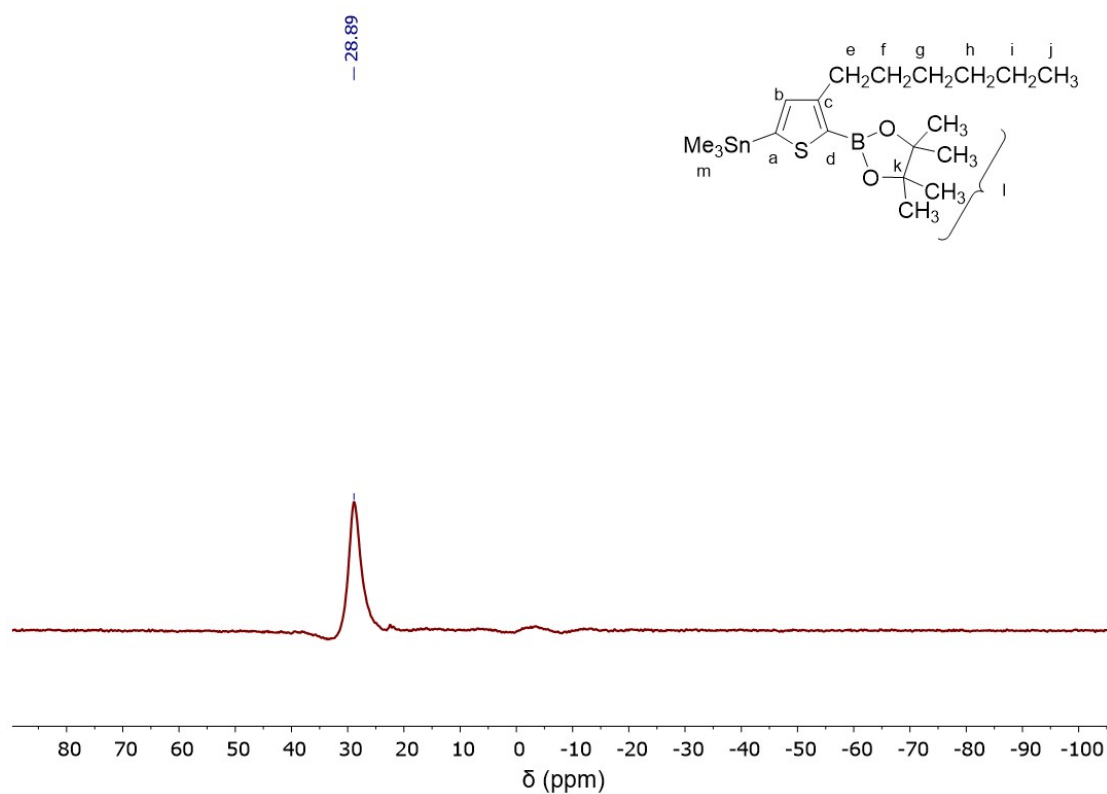


Figure SI- 39. $^{11}\text{B}\{^1\text{H}\}$ NMR (160 MHz) spectrum of **13** in CDCl_3 .

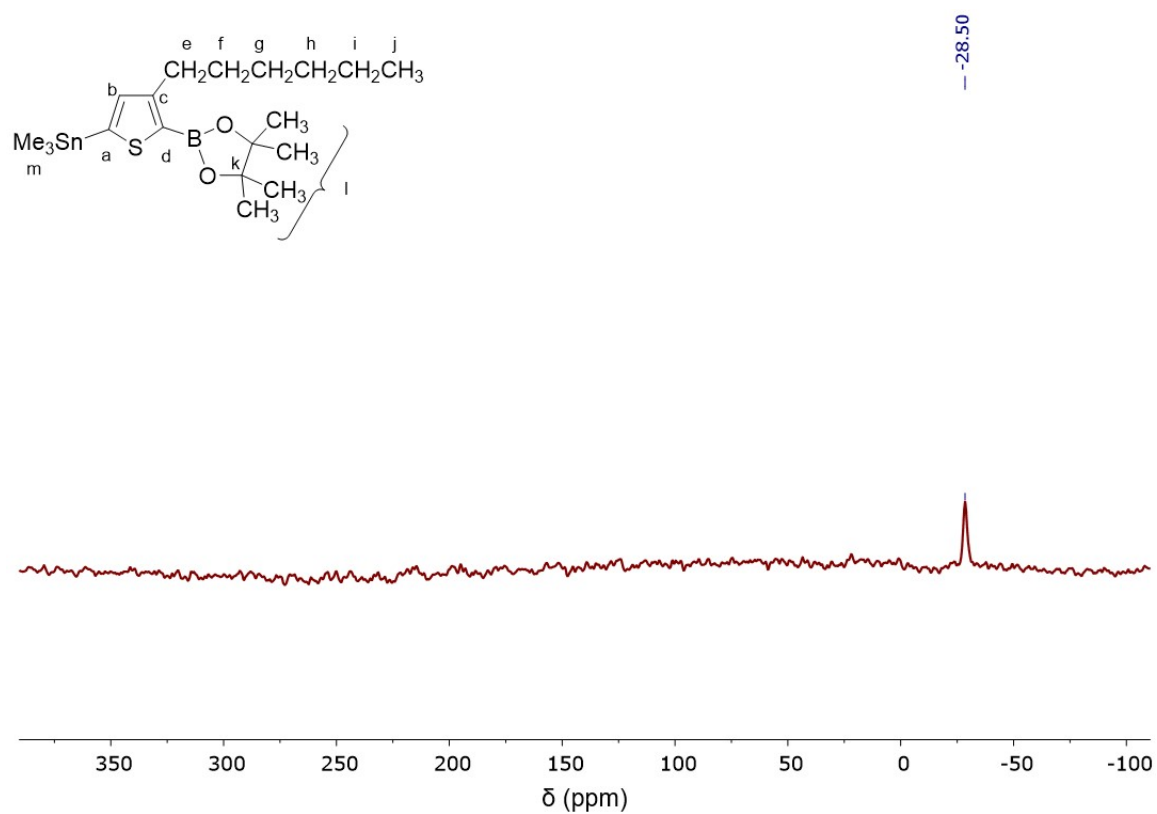
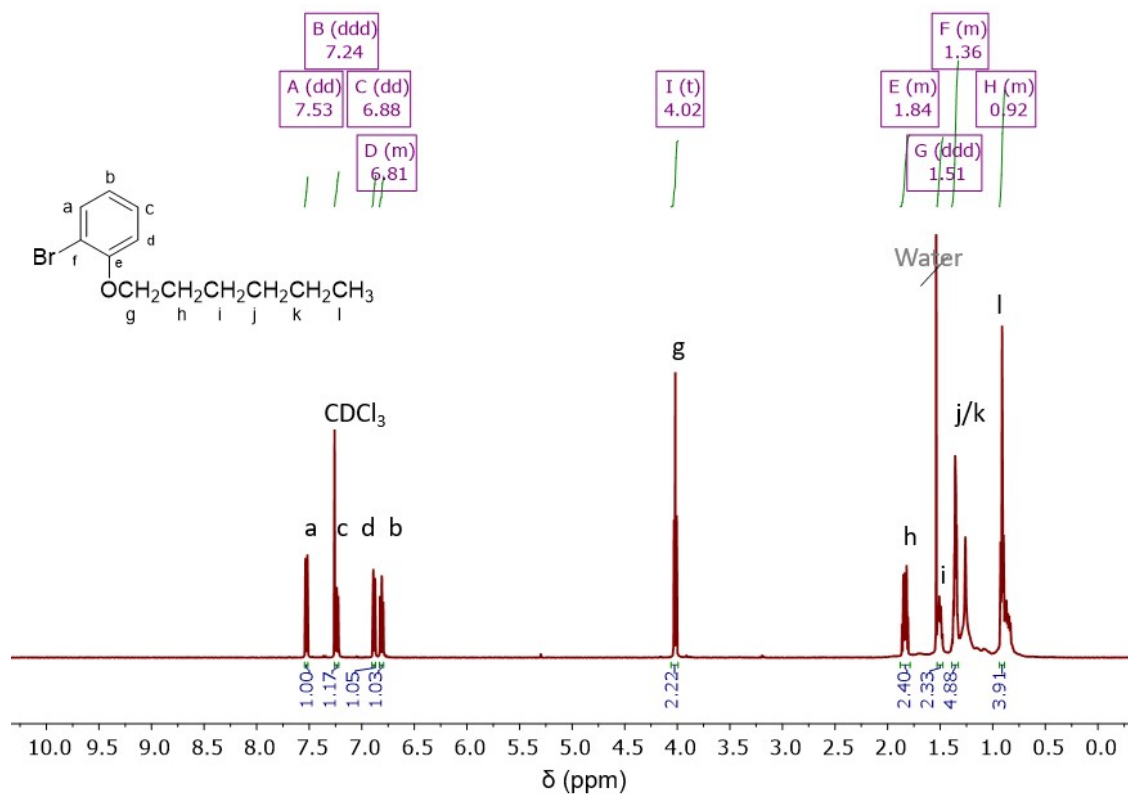
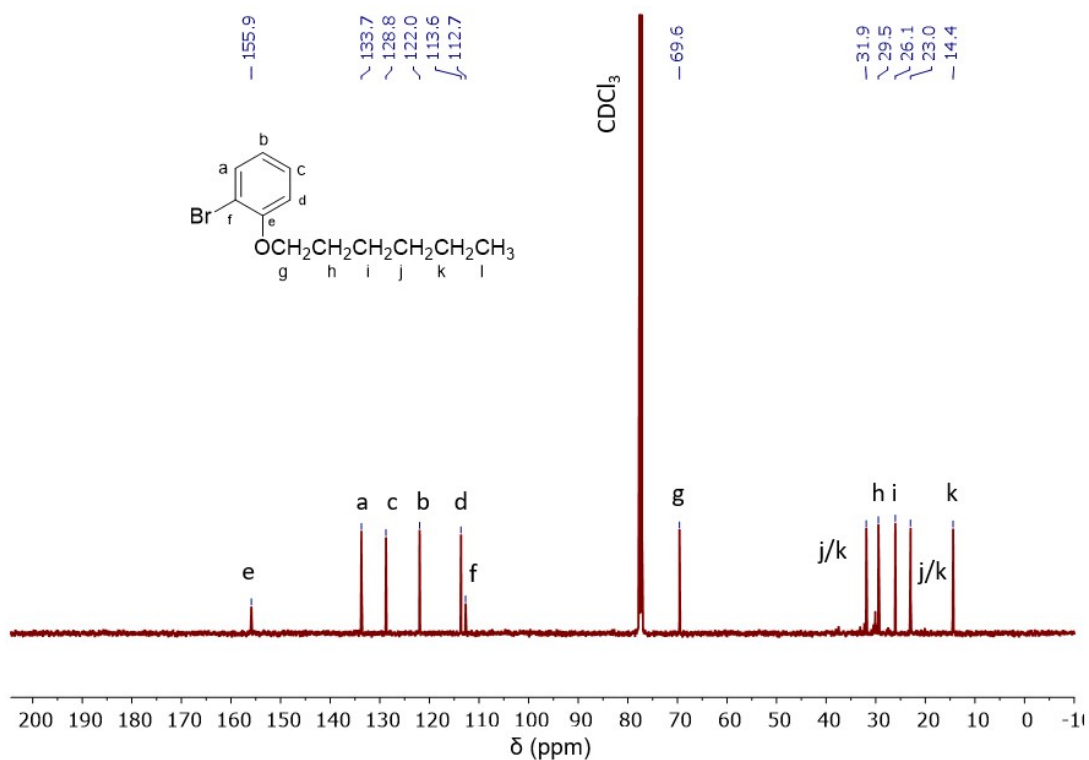
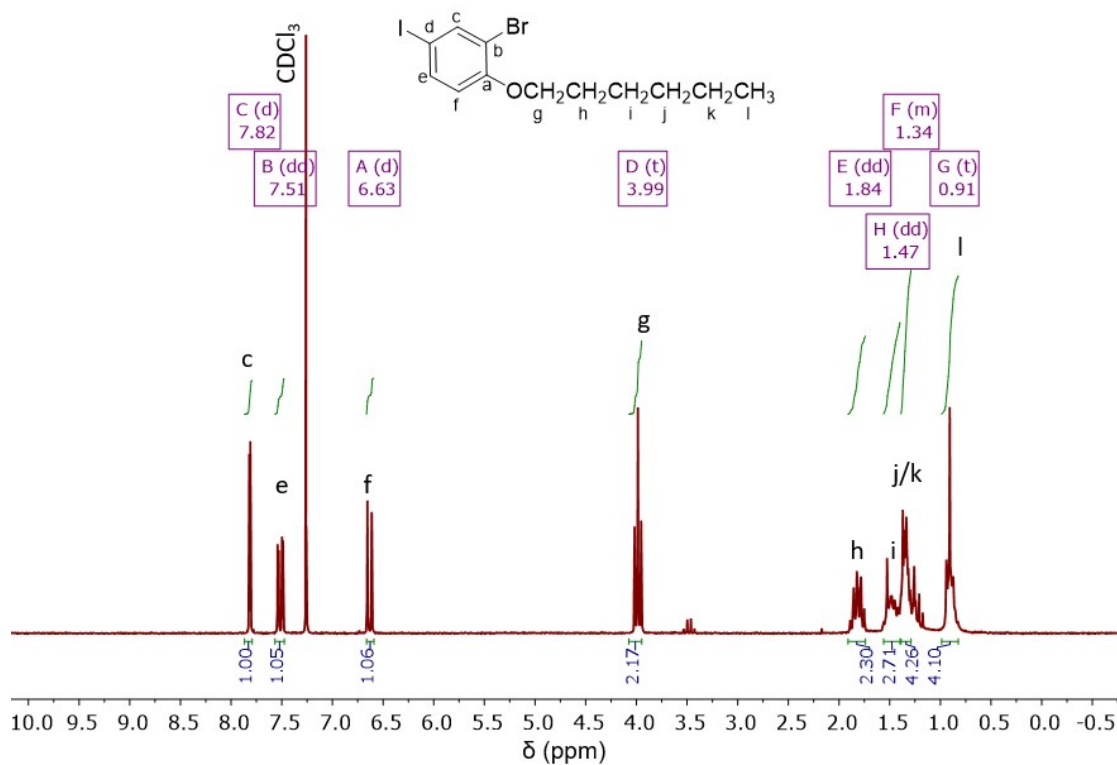
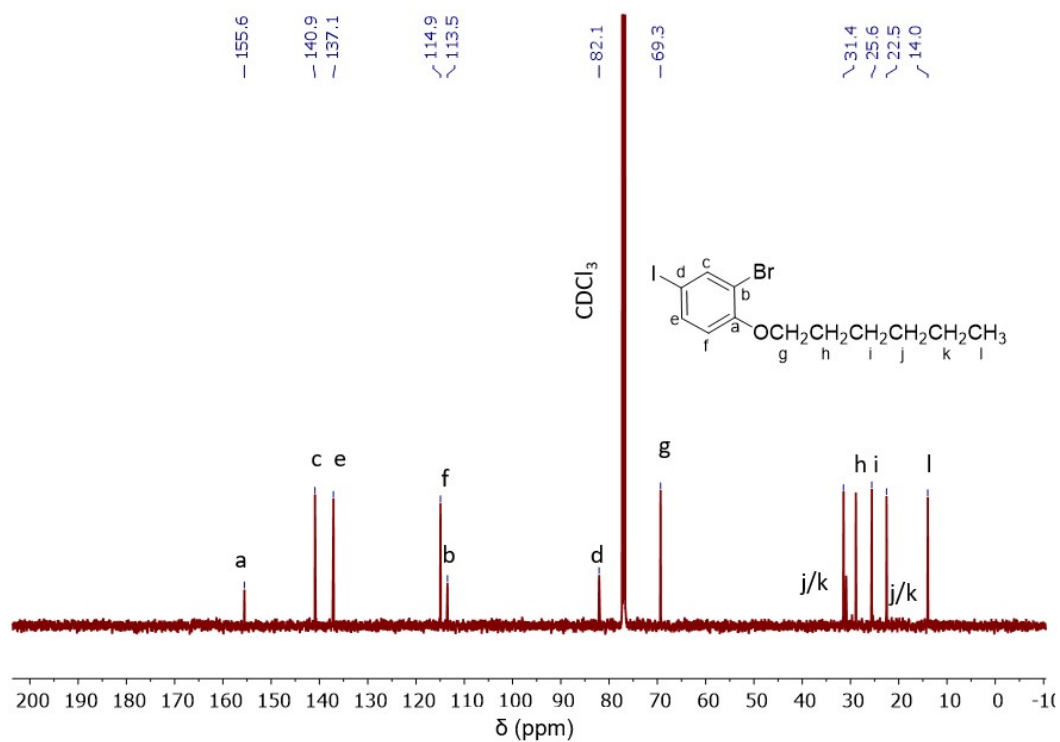
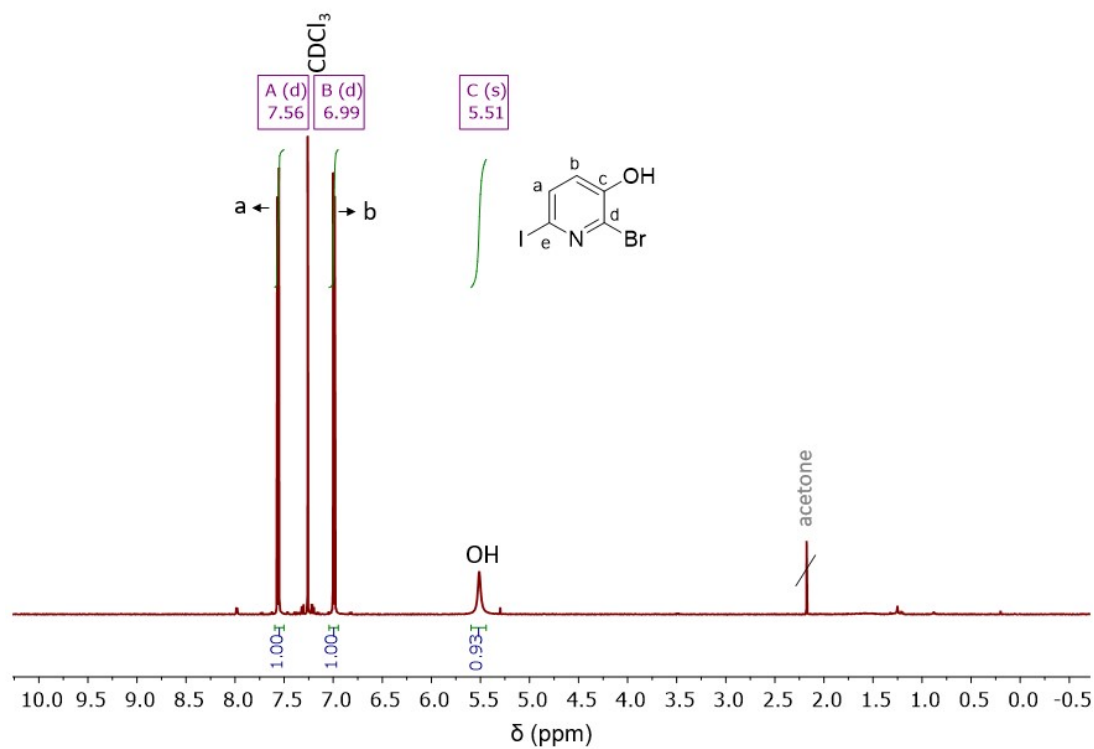
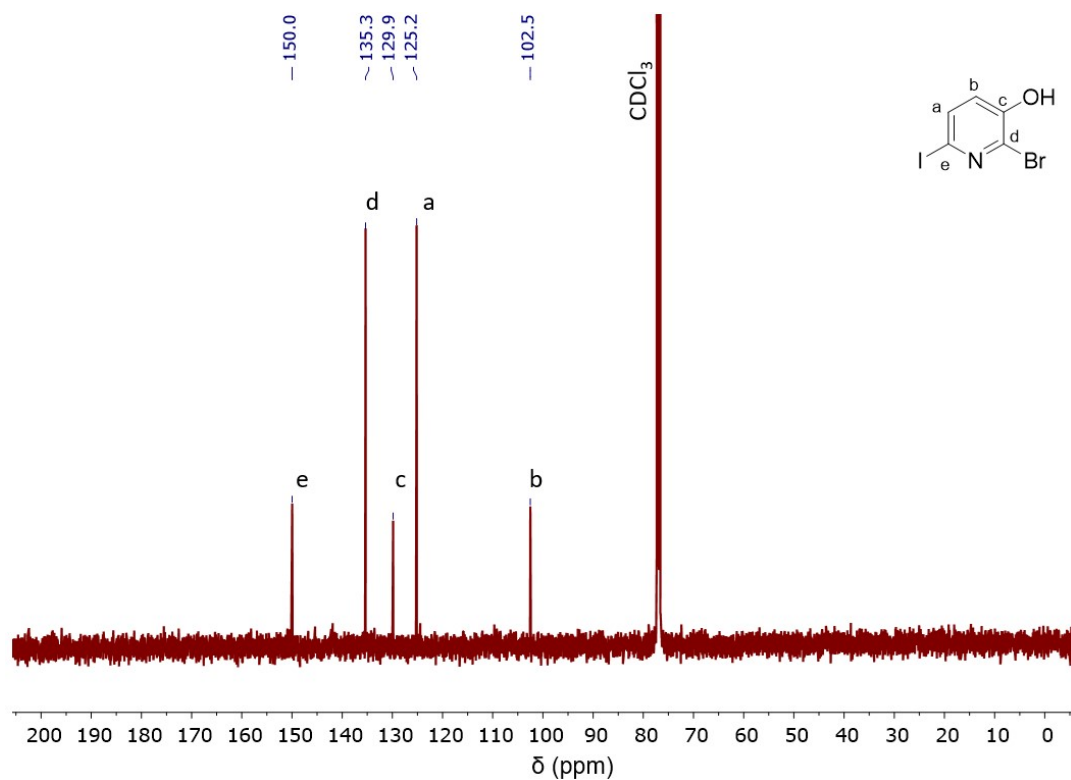


Figure SI- 40. $^{119}\text{Sn}\{^1\text{H}\}$ NMR (160 MHz) spectrum of **13** in CDCl_3 .

1-Bromo-2-(hexyloxy)benzene (15)**Figure SI- 41.** ¹H NMR (500 MHz) spectrum of **15** in CDCl₃.**Figure SI- 42.** ¹³C{¹H} NMR (126 MHz) spectrum of **15** in CDCl₃.

1-Bromo-2-(hexyloxy)-5-iodobenzene (16)

Figure SI- 43. ¹H NMR (500 MHz) spectrum of **16** in CDCl₃.

Figure SI- 44. ¹³C{¹H} NMR (126 MHz) spectrum of **16** in CDCl₃.

2-Bromo-6-iodo-3-pyridinol (18)**Figure SI- 45.** ^1H NMR (500 MHz) spectrum of **18** in CDCl_3 .**Figure SI- 46.** $^{13}\text{C}\{^1\text{H}\}$ NMR (126 MHz) spectrum of **18** in CDCl_3 .

2-Bromo-3-(hexyloxy)-6-iodopyridine (**8**)

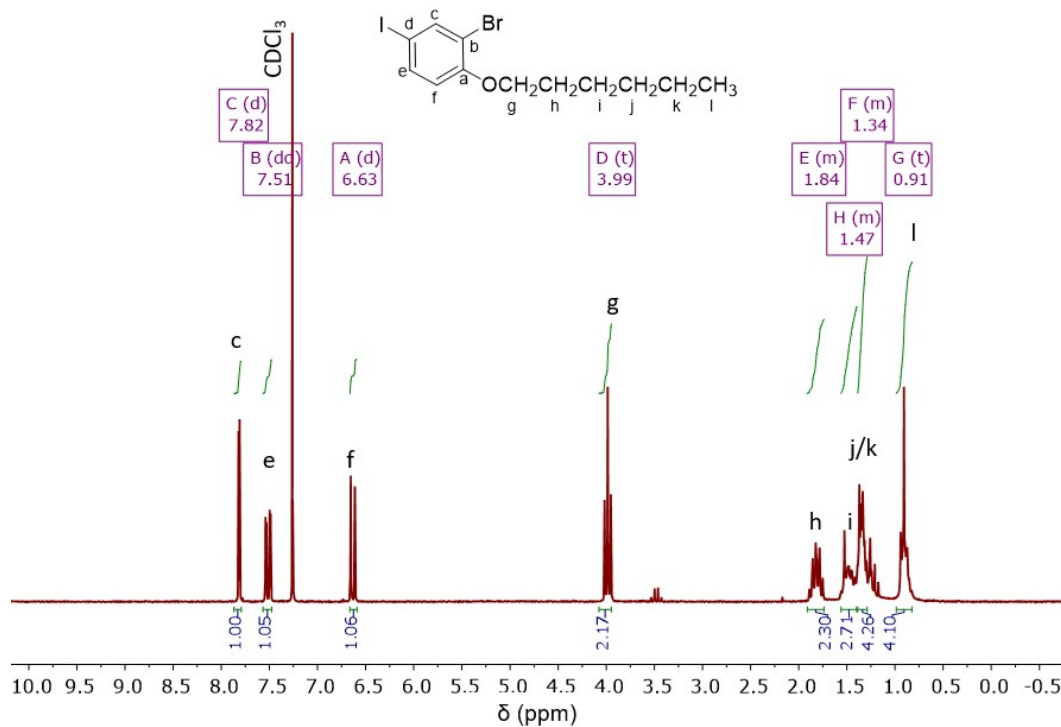


Figure SI- 47. ¹H NMR (500 MHz) spectrum of **8** in CDCl₃.

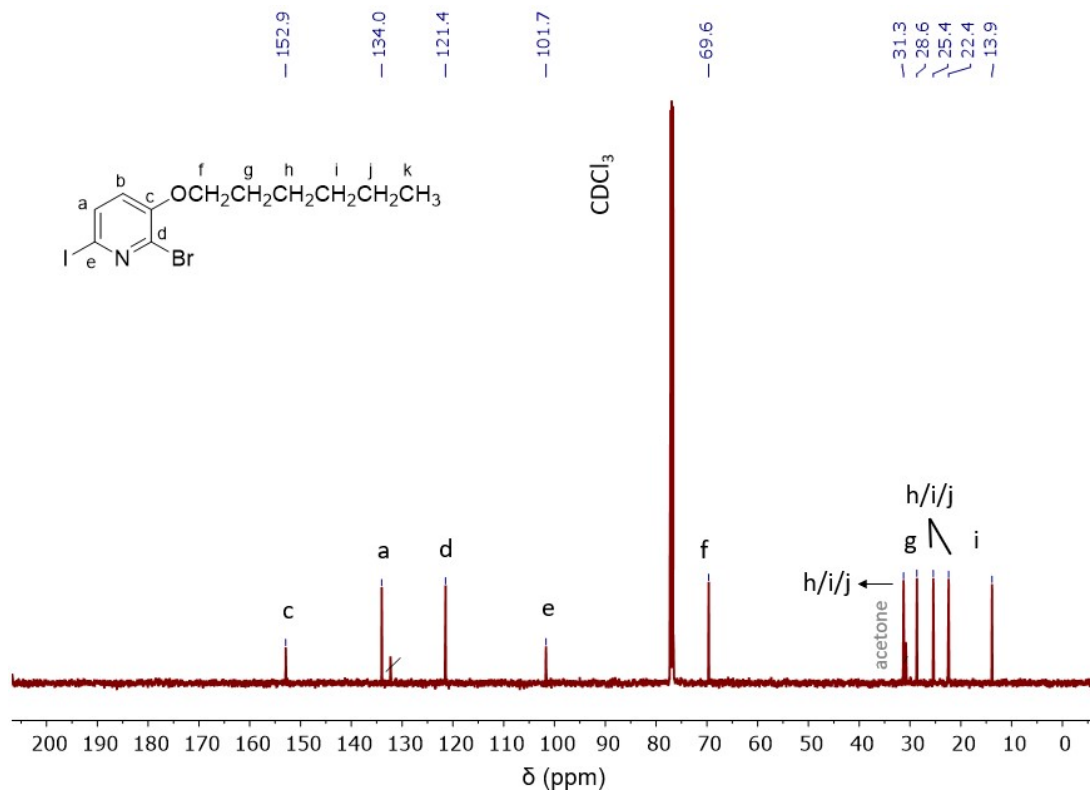


Figure SI- 48. ¹³C{¹H} NMR (126 MHz) spectrum of **8** in CDCl₃.

2-(5-(4-Bromo-3-(hexyloxy)phenyl)-3-hexylthiophen-2-yl)-4,4,5,5-tetramethyl-1,3,2-dioxaborolane (5)

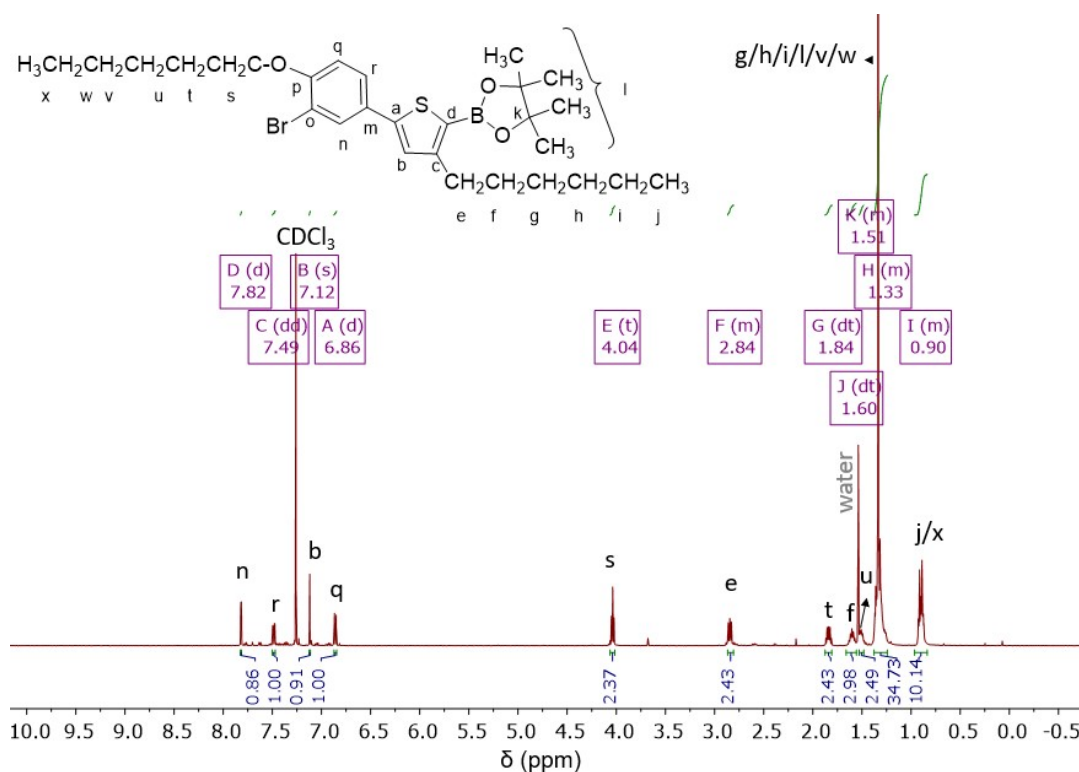


Figure SI- 49. ^1H NMR (500 MHz) spectrum of **5** in CDCl_3 .

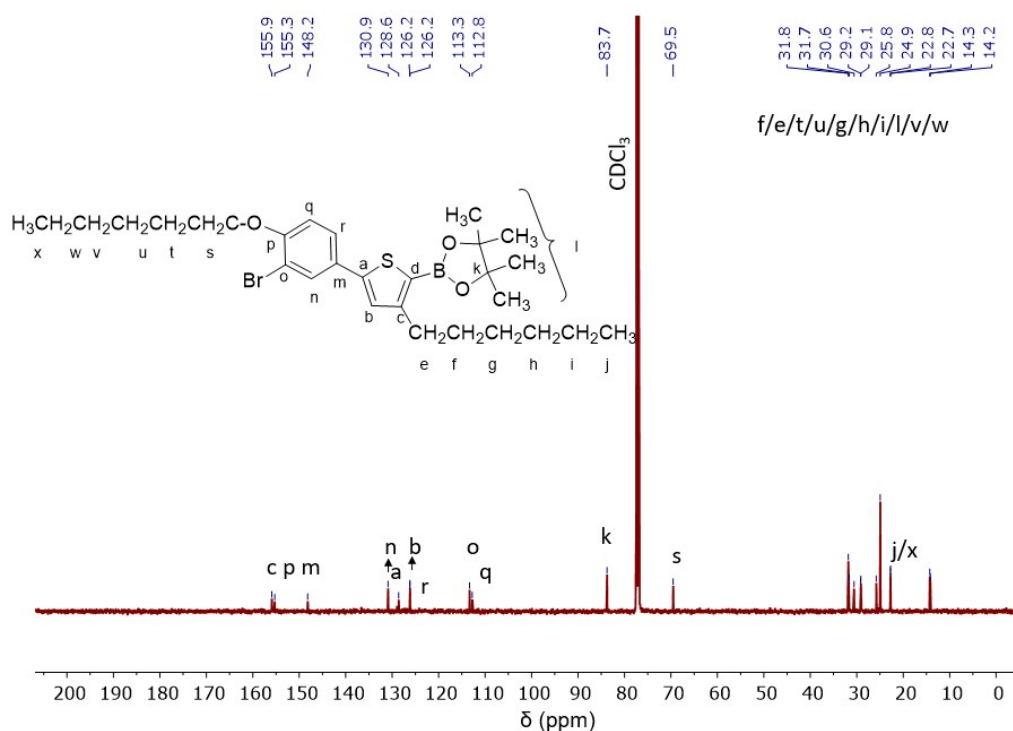
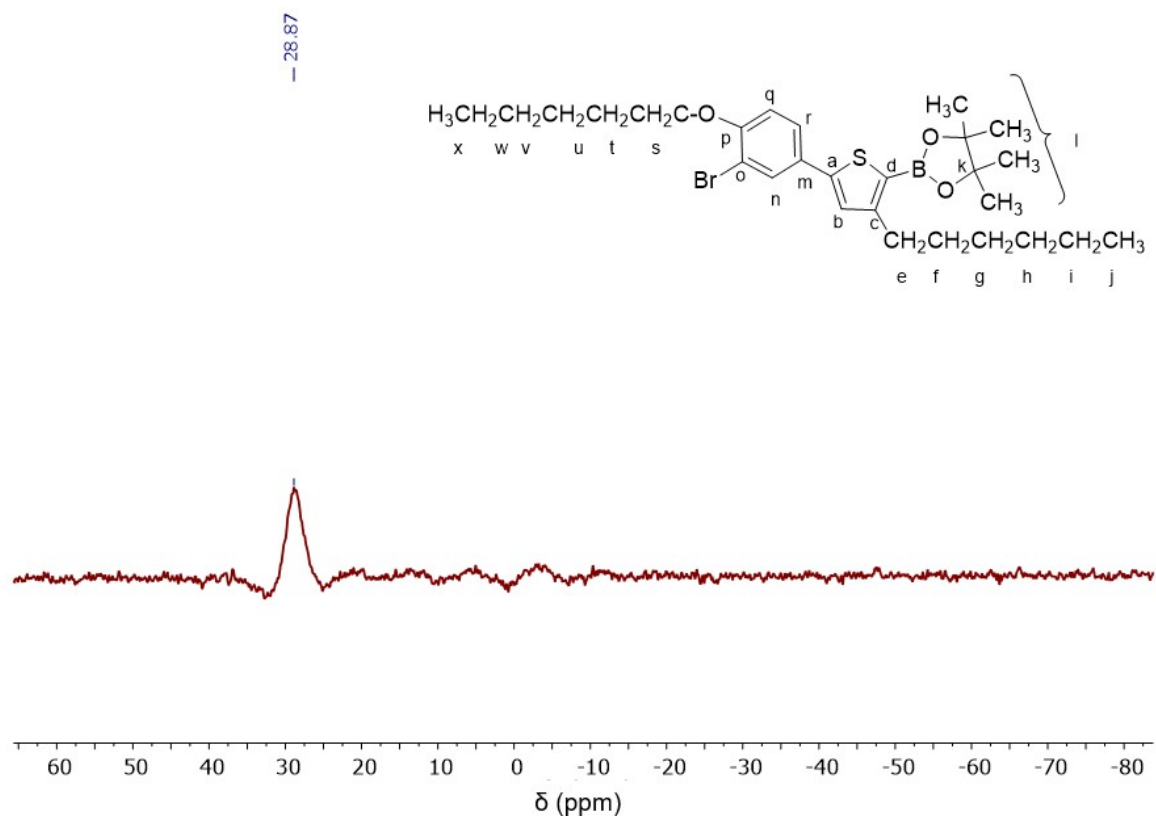


Figure SI- 50. $^{13}\text{C}\{^1\text{H}\}$ NMR (126 MHz) spectrum of **5** in CDCl_3 .



2-Bromo-6-(4-hexyl-5-(4,4,5,5-tetramethyl-1,3,2-dioxaborolan-2-yl)thiophen-2-yl)-3-(hexyloxy)pyridine (6)

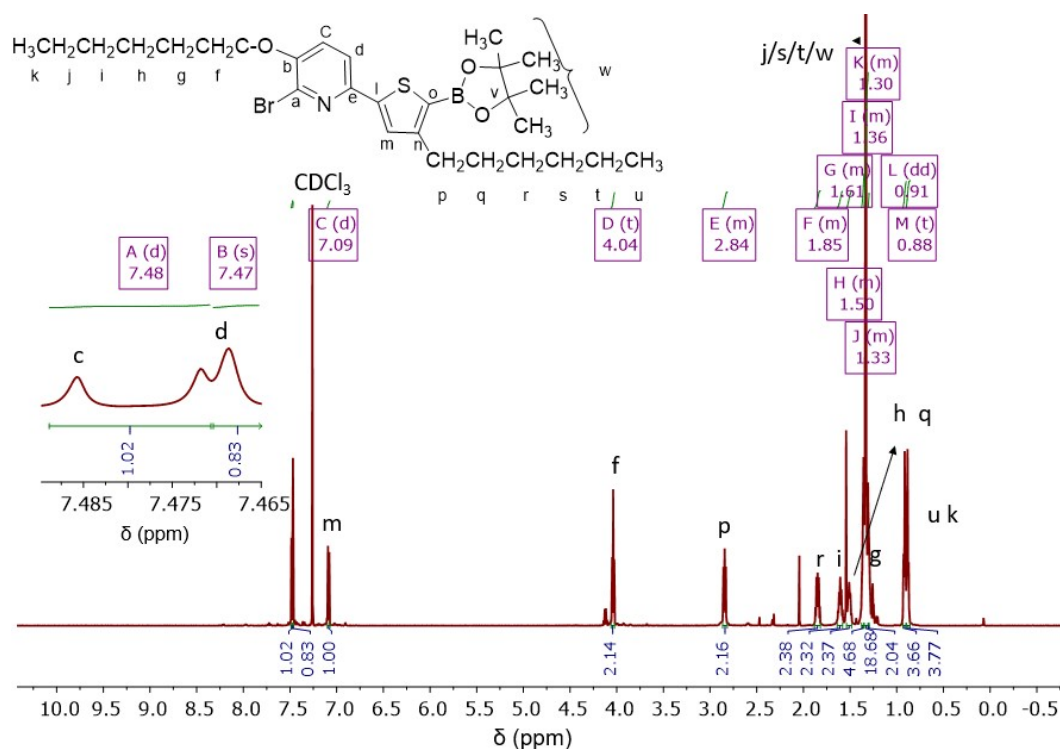


Figure SI- 52. ¹H NMR (500 MHz) spectrum of **6** in CDCl₃.

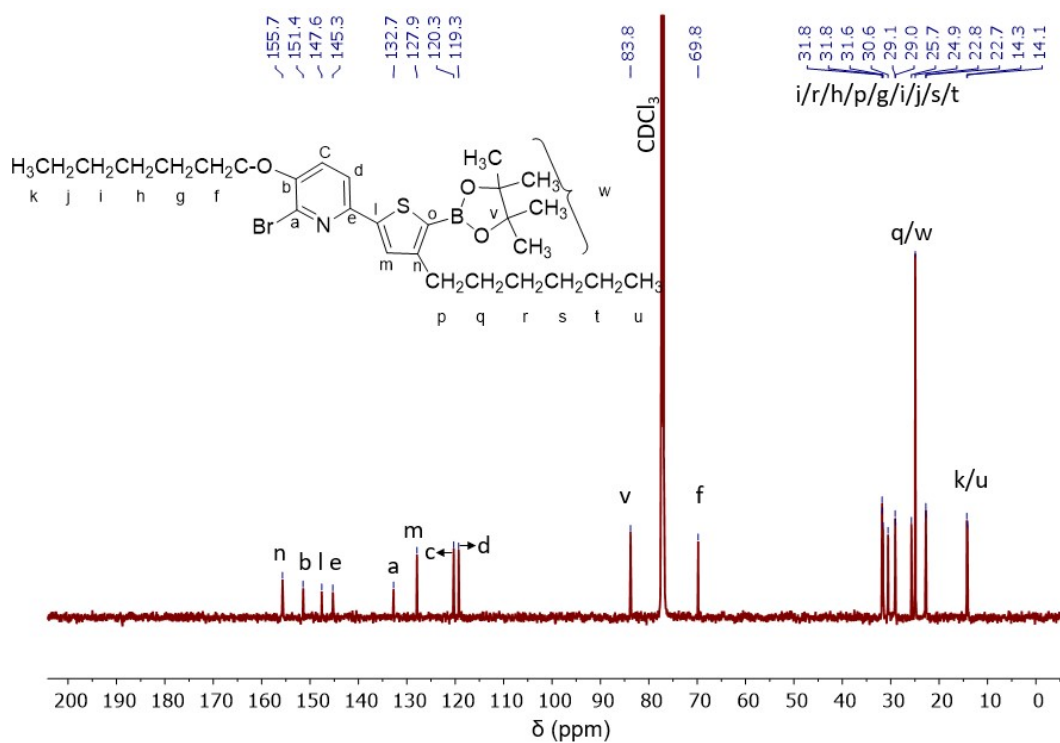
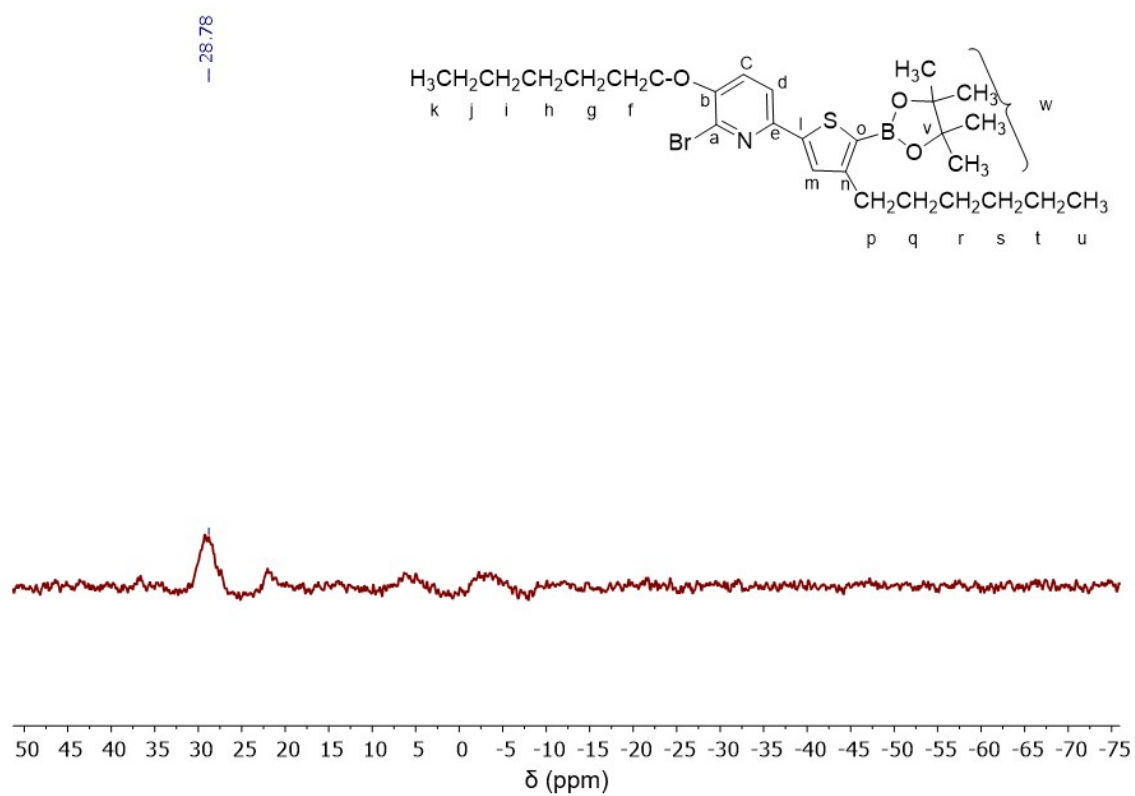
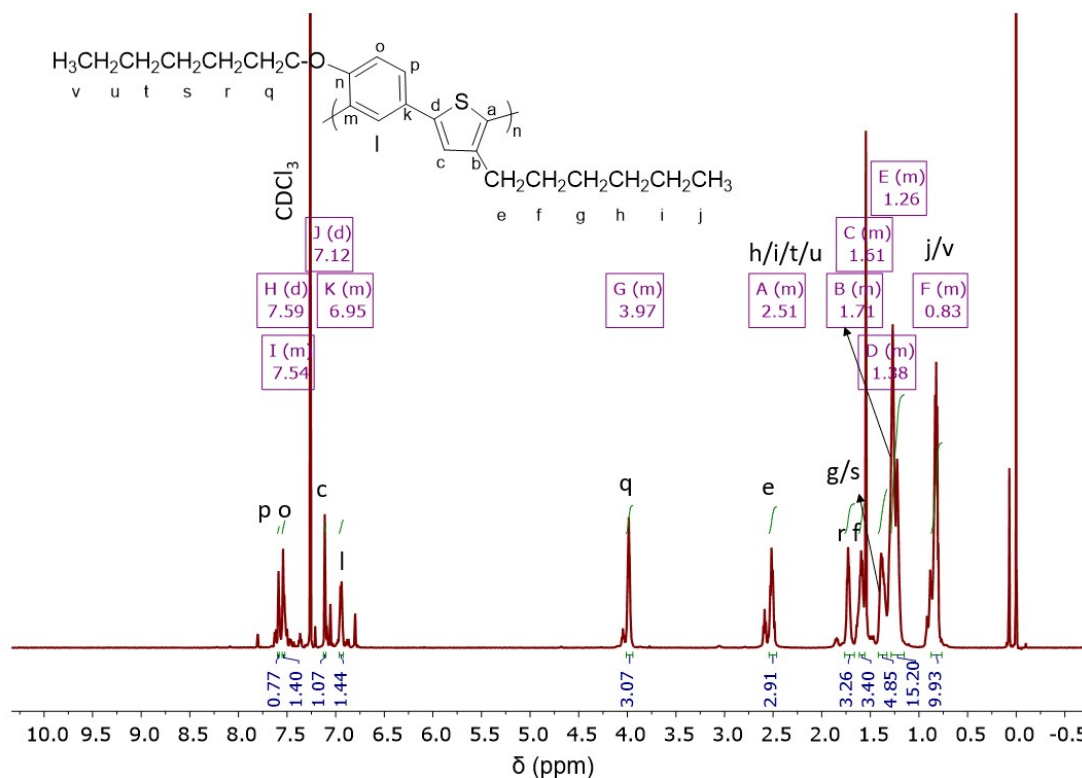
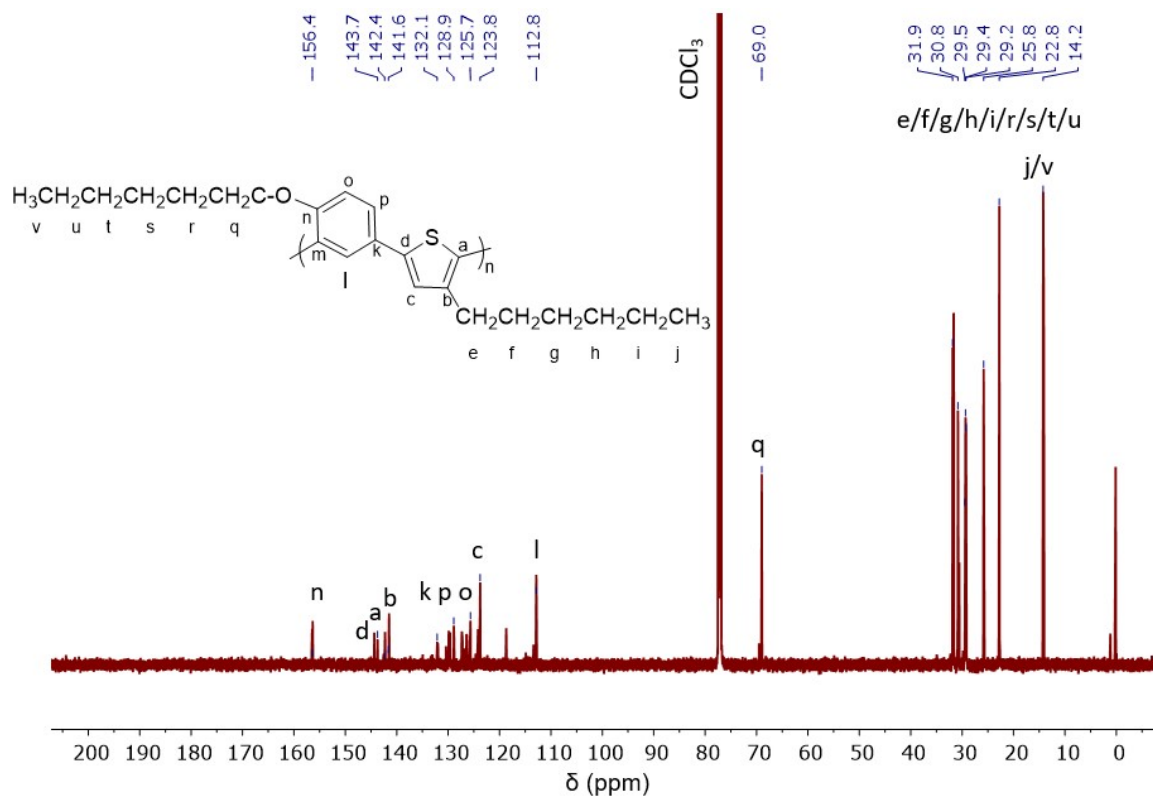


Figure SI- 53. ¹³C{¹H} NMR (126 MHz) spectrum of **6** in CDCl₃.



Poly-(1,4-(3-hexyl)-thiophene-2,6-(3-hexyloxy)-phenylene) O1

Figure SI- 55. ^1H NMR (600 MHz) spectrum of **O1** in CDCl_3 .

Figure SI- 56. $^{13}\text{C}\{^1\text{H}\}$ NMR (126 MHz) spectrum of **O1** in CDCl_3 .

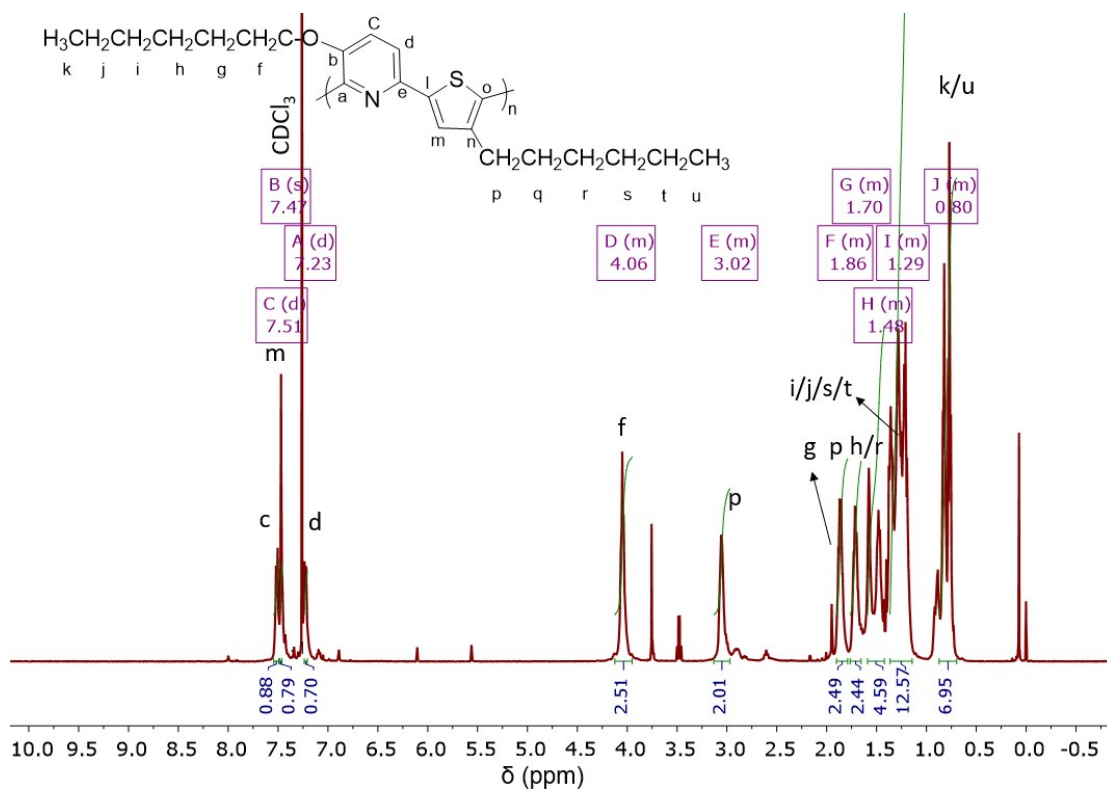
Poly-(2,6-(3-hexyloxy)-pyridine-1,4-(3-hexyl)-thiophene) O2


Figure SI- 57. ^1H NMR (600 MHz) spectrum of **O2** in CDCl_3 .

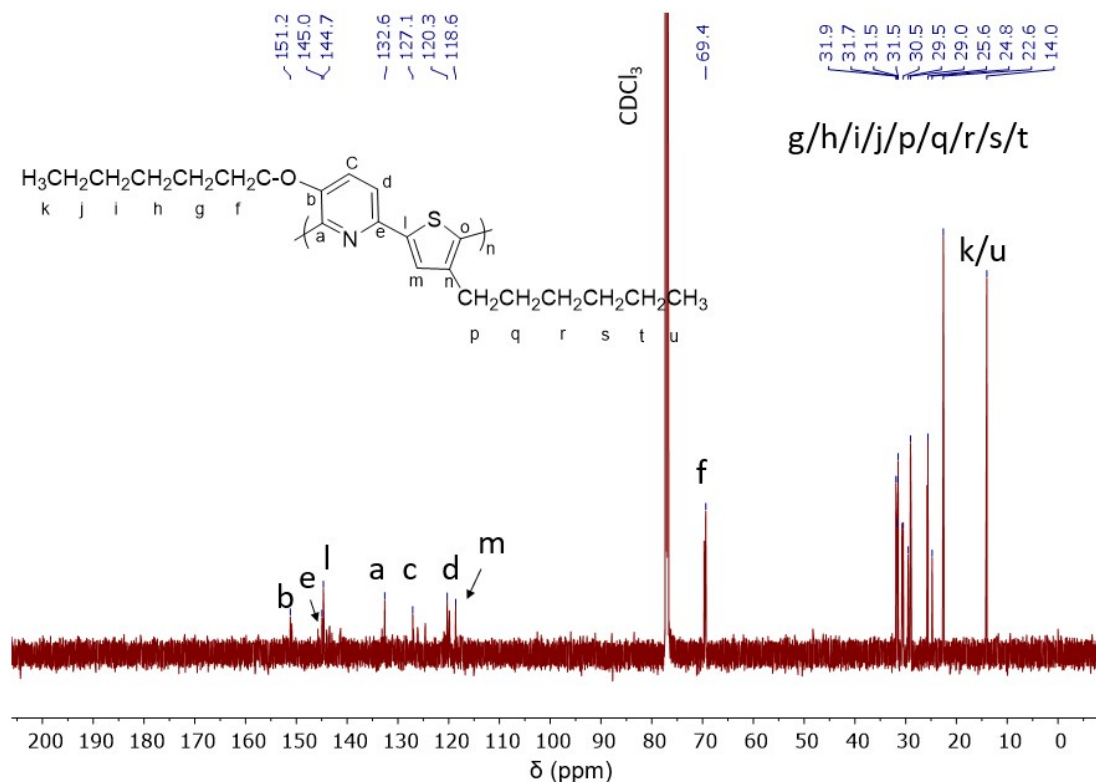


Figure SI- 58. $^{13}\text{C}\{^1\text{H}\}$ NMR (126 MHz) spectrum of **O2** in CDCl_3 .

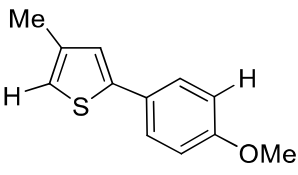
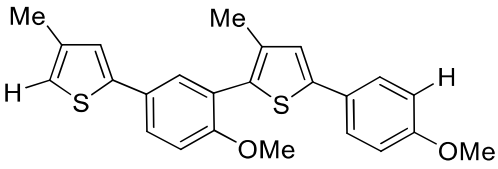
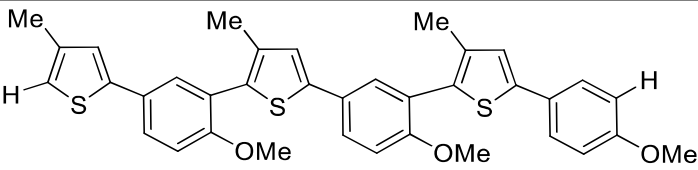
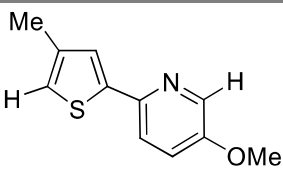
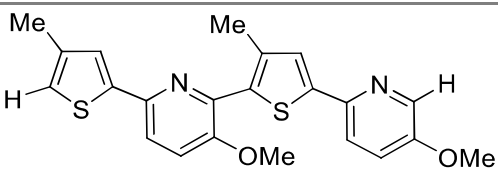
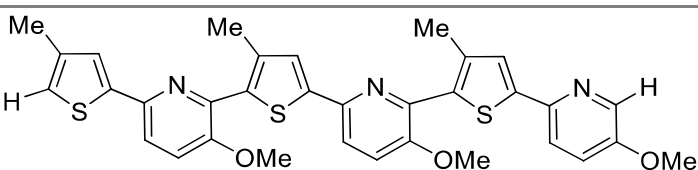
Molecule	E_{homo} (eV)	E_{lumo} (eV)	HOMO-LUMO (eV)	$UV_{\lambda\text{max}}$
 <p style="text-align: center;">S1</p>	-0.66	-5.32	4.66	4.37 eV 284 nm
 <p style="text-align: center;">S1-2</p>	-1.09	-5.17	4.08	3.71 eV 334 nm
 <p style="text-align: center;">S1-3</p>	-1.22	-5.17	3.95	3.60 eV 344 nm
 <p style="text-align: center;">S2</p>	-1.01	-5.43	4.42	4.12 eV 301 nm
 <p style="text-align: center;">S2-2</p>	-1.45	-5.15	3.70	3.39 eV 366 nm
 <p style="text-align: center;">S2-3</p>	-1.57	-5.11	3.54 eV	3.14 eV 395 nm

Table SI- 10. Molecular orbital energies (HOMO, LUMO), HOMO-LUMO gaps and calculated absorption wavelength from the monomers **S1** and **S2**, dimers **S1-2**, **S2-2** and trimers **S1-3** and **S2-3**.

Molecular Orbitals

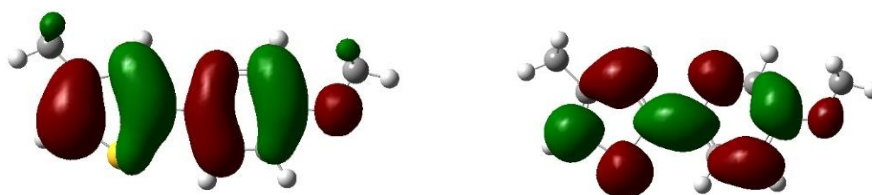


Figure SI- 59. Molecular orbitals of **S1** (displayed with an isovalue of 0.02): HOMO (left) and LUMO (right).

Symmetry = C1

B3LYP/6-31G(d)

E=-937.92384330 Ha

ATOM	SYMBOL	X	Y	Z
1	C	0.919567	-1.27171	0.406397
2	C	0.202495	-0.11965	0.026458
3	C	0.942719	1.019296	-0.3243
4	C	2.305746	-1.28042	0.435678
5	C	3.028695	-0.12825	0.092916
6	C	2.337051	1.028512	-0.28737
7	O	4.386986	-0.23991	0.159257
8	C	5.17097	0.896508	-0.16902
9	H	6.211054	0.589787	-0.04309
10	H	4.958857	1.741717	0.500202
11	H	5.010153	1.212673	-1.20889
12	C	-1.26411	-0.08968	0.000244
13	C	-2.09817	0.981374	0.214313
14	S	-2.21246	-1.52477	-0.35591
15	C	-3.4927	0.677175	0.105882
16	C	-3.70004	-0.64286	-0.19261
17	C	-4.58667	1.689834	0.310417
18	H	-4.64793	-1.14832	-0.32613
19	H	-1.72578	1.966456	0.477531
20	H	2.867164	1.93065	-0.57012

21	H	2.856642	-2.16721	0.732714
22	H	0.379007	-2.16713	0.701041
23	H	-4.50626	2.513021	-0.4107
24	H	-4.53606	2.132805	1.313026
25	H	-5.57636	1.237493	0.193371
26	H	0.419699	1.912838	-0.65257

Table SI- 11. xyz Coordinates from the DFT calculations of molecule **S1-1**.

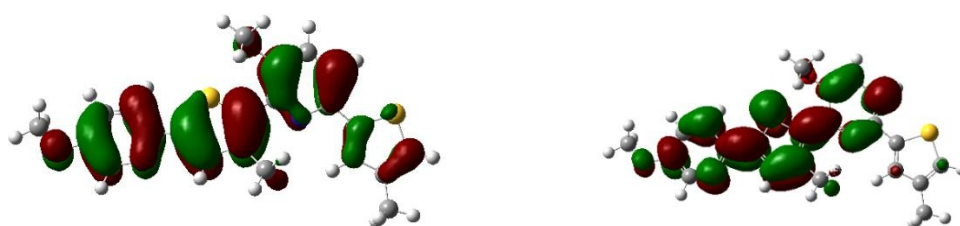


Figure SI- 60. Molecular orbitals of dimer of **S1-2** (displayed with an isovalue of 0.02): HOMO (left) and LUMO (right).

Symmetry = C1

B3LYP/6-31G(d)

E=-1874.65930957 Ha

ATOM	SYMBOL	X	Y	Z
1	C	3.731042	2.085738	-0.2582
2	C	3.613124	0.686968	-0.20421
3	C	2.339871	0.137835	0.014373
4	C	2.611913	2.893348	-0.0812
5	C	1.359116	2.333192	0.164789
6	C	1.201117	0.930374	0.220664
7	O	0.285024	3.184532	0.306807
8	C	-0.17714	3.342686	1.651613
9	H	0.609483	3.779838	2.281548
10	H	-0.49898	2.38655	2.08117
11	H	-1.03006	4.023003	1.603646

12	C	4.769996	-0.20031	-0.37253
13	C	4.965114	-1.44927	0.166722
14	S	6.14669	0.247599	-1.36493
15	C	6.207604	-2.06095	-0.19387
16	C	6.948125	-1.25221	-1.01438
17	C	6.641177	-3.41983	0.285194
18	H	7.923617	-1.45748	-1.43645
19	H	4.247525	-1.91384	0.835787
20	C	-0.10053	0.284968	0.456328
21	H	2.68957	3.975488	-0.11856
22	H	4.703265	2.542901	-0.41938
23	S	-1.54105	0.799555	-0.40522
24	C	-0.37885	-0.79078	1.280292
25	C	-2.51777	-0.43894	0.352016
26	C	-1.74783	-1.18612	1.212042
27	C	0.60748	-1.46963	2.195853
28	H	-2.15814	-1.98273	1.824591
29	C	-3.9472	-0.58294	0.059467
30	H	6.694037	-3.45706	1.380542
31	H	7.627826	-3.68472	-0.10719
32	H	5.934198	-4.19712	-0.03094
33	H	1.462242	-0.82536	2.419751
34	H	0.999293	-2.39549	1.753573
35	H	0.12683	-1.74391	3.14184
36	C	-4.5737	-1.84176	0.168892
37	C	-4.74196	0.505222	-0.33017
38	C	-6.10277	0.360646	-0.60096
39	C	-6.70565	-0.89659	-0.476
40	C	-5.92691	-1.9973	-0.08638
41	H	-4.29717	1.493601	-0.40844
42	H	-6.67741	1.230888	-0.89597
43	O	-8.02416	-1.1575	-0.70918

44	H	-6.407	-2.96756	-0.00659
45	C	-8.85728	-0.08562	-1.12366
46	H	-9.85205	-0.51427	-1.25904
47	H	-8.51627	0.347283	-2.07404
48	H	-8.90464	0.706865	-0.36421
49	H	-3.98039	-2.71067	0.437897
50	H	2.21837	-0.93936	-0.01817

Table SI- 12. xyz Coordinates from the DFT calculations of molecule **S1-2**.

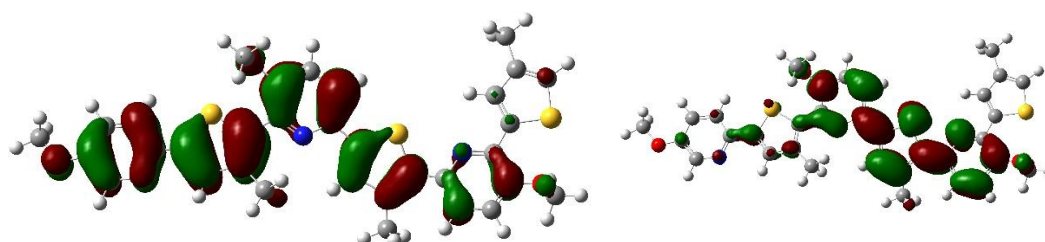


Figure SI- 61. Molecular orbitals of trimer of **S1-3** (displayed with an isovalue of 0.02): HOMO (left) and LUMO (right).

Symmetry = C1

B3LYP/6-31G(d)

E=-2811.39411966 Ha

ATOM	SYMBOL	X	Y	Z
1	C	-0.14973	2.12917	0.231239
2	C	-0.27217	0.731206	0.156165
3	C	-1.55522	0.172038	0.269528
4	C	-1.2745	2.924965	0.423375
5	C	-2.54159	2.354251	0.536371
6	C	-2.70406	0.953057	0.459961
7	O	-3.62146	3.196516	0.686578
8	C	-4.16198	3.244615	2.010709
9	H	-3.40881	3.608455	2.722758
10	H	-4.52353	2.260952	2.333247
11	H	-5.00005	3.943794	1.973248

12	C	0.889824	-0.13935	-0.0526
13	C	0.936594	-1.36959	-0.66401
14	S	2.486067	0.303268	0.513662
15	C	2.230837	-1.96955	-0.70452
16	C	3.193538	-1.1777	-0.10839
17	C	2.484256	-3.29201	-1.38097
18	C	4.634246	-1.42512	0.052607
19	H	0.065815	-1.82713	-1.1231
20	C	-4.01895	0.300647	0.576645
21	H	-1.19404	4.006159	0.4782
22	H	0.824974	2.595361	0.118626
23	S	-5.39965	0.87603	-0.34206
24	C	-4.3538	-0.81559	1.3211
25	C	-6.42932	-0.39325	0.28332
26	C	-5.7185	-1.19359	1.146234
27	C	-3.43154	-1.55177	2.258694
28	H	-6.1705	-2.01816	1.688395
29	C	-7.83906	-0.50751	-0.10294
30	H	1.839536	-3.40303	-2.2599
31	H	2.269401	-4.13737	-0.71368
32	H	3.524264	-3.38617	-1.70623
33	H	-2.58359	-0.93293	2.564558
34	H	-3.02498	-2.46082	1.795802
35	H	-3.97134	-1.86416	3.159915
36	C	-8.47855	-1.76454	-0.09977
37	C	-8.60269	0.607491	-0.4787
38	C	-9.94618	0.490541	-0.83595
39	C	-10.5633	-0.76577	-0.81435
40	C	-9.81542	-1.89329	-0.44132
41	H	-8.14807	1.594513	-0.47652
42	H	-10.497	1.380793	-1.11628
43	O	-11.8678	-1.00125	-1.13656

44	H	-10.3055	-2.86185	-0.44244
45	C	-12.6699	0.099799	-1.53547
46	H	-13.6587	-0.31112	-1.74783
47	H	-12.2749	0.580813	-2.44075
48	H	-12.7532	0.849829	-0.737
49	C	5.108984	-2.69105	0.441156
50	C	5.567232	-0.39667	-0.1447
51	C	6.950393	-0.58984	0.007004
52	C	7.386758	-1.87443	0.393183
53	C	6.473389	-2.90644	0.603501
54	H	4.405274	-3.48975	0.650327
55	H	6.855297	-3.8724	0.920008
56	O	8.727168	-2.12079	0.607422
57	C	7.871322	0.526357	-0.25051
58	C	9.429025	-2.57071	-0.556
59	H	9.020124	-3.52603	-0.91152
60	H	10.4703	-2.70366	-0.2556
61	H	9.374273	-1.82859	-1.36234
62	C	7.636978	1.611326	-1.06583
63	S	9.433851	0.697678	0.535829
64	C	9.70548	2.224959	-0.23819
65	C	8.678447	2.589344	-1.06833
66	H	6.741208	1.705663	-1.67124
67	H	10.62465	2.767866	-0.05576
68	C	8.64191	3.848866	-1.8909
69	H	9.544002	4.449577	-1.73893
70	H	7.776684	4.47075	-1.62907
71	H	8.564873	3.623532	-2.96205
72	H	5.206439	0.589332	-0.41901
73	H	-1.66984	-0.90455	0.205958
74	H	-7.90763	-2.6523	0.155709

Table SI- 13. xyz values from the DFT of Molecule **S1-3**.

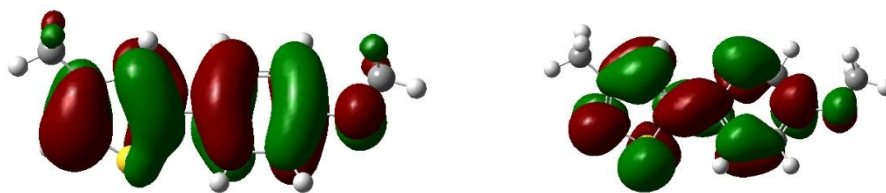


Figure SI- 62. Molecular orbitals of **S2** (displayed with an isovalue of 0.02): HOMO (left) and LUMO (right).

Symmetry = C1

B3LYP/6-31G(d)

E= -953.96099057 Ha

ATOM	SYMBOL	X	Y	Z
1	C	0.947856	-1.40437	-0.00064
2	C	0.232807	-0.18984	-6.9e-05
3	N	0.872	0.992888	0.000307
4	C	2.332228	-1.38134	-0.00064
5	C	2.993317	-0.1468	-0.00017
6	C	2.206566	1.014343	0.000228
7	O	4.35428	-0.18103	-0.00018
8	C	5.053967	1.056726	0.000464
9	H	6.11473	0.799992	0.000539
10	H	4.823161	1.649479	0.895786
11	H	4.823468	1.650221	-0.89445
12	C	-1.23392	-0.12938	-3.2e-05
13	C	-2.01257	1.002383	-0.00027
14	S	-2.24648	-1.56324	0.000529
15	C	-3.41877	0.746435	-8.9e-05
16	C	-3.68882	-0.59695	0.000347
17	C	-4.46534	1.827525	-0.00042
18	H	-4.65952	-1.07615	0.000487
19	H	-1.57185	1.992456	-0.00057
20	H	2.6608	2.001487	0.000548

21	H	2.919373	-2.29446	-0.00105
22	H	0.425336	-2.35644	-0.00113
23	H	-4.36888	2.472663	0.881699
24	H	-5.47567	1.406608	0.000075
25	H	-4.36939	2.471662	-0.88333

Table SI- 14. xyz Coordinates from the DFT calculations of molecule **S2-1**.

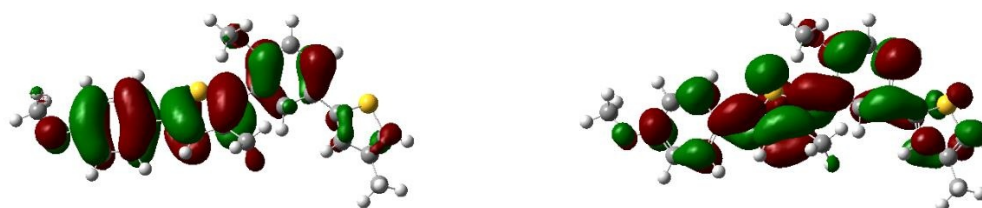


Figure SI- 63. Molecular orbitals of dimer of **S2-2** (displayed with an isovalue of 0.02): HOMO (left) and LUMO (right).

Symmetry = C1

B3LYP/6-31G(d)

E=-1906.73623146 Ha

ATOM	SYMBOL	X	Y	Z
1	C	3.733679	2.148625	-0.27105
2	C	3.562851	0.757823	-0.17116
3	N	2.348121	0.201341	-0.0349
4	C	2.605586	2.956381	-0.19884
5	C	1.352041	2.377464	-0.03628
6	C	1.245343	0.966827	0.037441
7	O	0.236105	3.183077	0.015992
8	C	-0.09177	3.638404	1.334768
9	H	0.724803	4.243038	1.750821
10	H	-0.29842	2.793074	2.002507
11	H	-0.99022	4.250453	1.234244
12	C	4.69036	-0.18295	-0.21593
13	C	4.627585	-1.55226	-0.12432
14	S	6.357365	0.337907	-0.39264

15	C	5.897624	-2.20359	-0.19296
16	C	6.92019	-1.30274	-0.33793
17	C	6.076329	-3.69555	-0.11551
18	H	7.979281	-1.51256	-0.41708
19	H	3.684001	-2.07163	-0.01028
20	C	-0.0339	0.262664	0.191374
21	H	2.675008	4.037858	-0.27028
22	H	4.717293	2.588521	-0.40295
23	S	-1.56871	1.022485	-0.22361
24	C	-0.23478	-1.05049	0.605387
25	C	-2.45829	-0.43076	0.147165
26	C	-1.60626	-1.4196	0.579998
27	C	0.825149	-2.02676	1.043478
28	H	-1.97007	-2.39622	0.876416
29	C	-3.91541	-0.52809	0.019376
30	H	5.684082	-4.09292	0.828831
31	H	7.131688	-3.97691	-0.18575
32	H	5.538325	-4.20131	-0.92683
33	H	1.584524	-1.55371	1.670474
34	H	1.35238	-2.44397	0.178381
35	H	0.366819	-2.85348	1.597038
36	N	-4.46708	-1.69911	0.414389
37	C	-4.70953	0.512364	-0.48407
38	C	-6.09078	0.352637	-0.57989
39	C	-6.65001	-0.85878	-0.16745
40	C	-5.77954	-1.85073	0.32111
41	H	-4.25819	1.44594	-0.80675
42	H	-6.70195	1.158435	-0.97045
43	O	-7.97174	-1.18052	-0.19254
44	H	-6.20172	-2.80088	0.643973
45	C	-8.88436	-0.2066	-0.67957
46	H	-9.87367	-0.66228	-0.61226

47	H	-8.67483	0.053912	-1.72605
48	H	-8.86243	0.706498	-0.06902

Table SI- 15. xyz Coordinates from the DFT calculations of molecule **S2-2**.

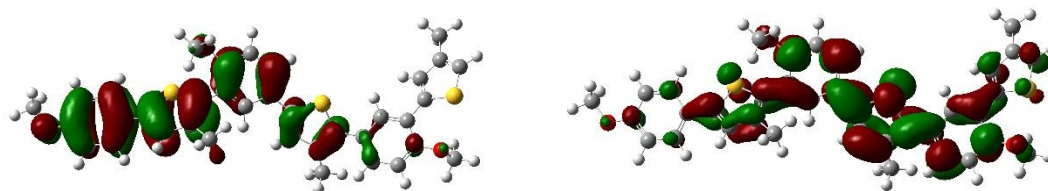


Figure SI- 64. Molecular orbitals of trimer of **S2-3** (displayed with an isovalue of 0.02): HOMO (left) and LUMO (right).

Symmetry = C1

B3LYP/6-31G(d)

E=-2859.51240006 Ha

ATOM	SYMBOL	X	Y	Z
1	C	0.062352	2.069507	0.315208
2	C	-0.13611	0.679128	0.265718
3	N	-1.36619	0.138839	0.254192
4	C	-1.056	2.891031	0.37693
5	C	-2.32674	2.326481	0.38538
6	C	-2.45993	0.917567	0.316337
7	O	-3.43243	3.146423	0.423383
8	C	-3.84162	3.515201	1.746444
9	H	-3.04609	4.072381	2.2584
10	H	-4.10669	2.629707	2.337061
11	H	-4.72127	4.1512	1.629723
12	C	0.979023	-0.27379	0.213735
13	C	0.881536	-1.64278	0.115261
14	S	2.653072	0.21938	0.263455
15	C	2.129966	-2.32199	0.084207
16	C	3.202009	-1.44371	0.165622

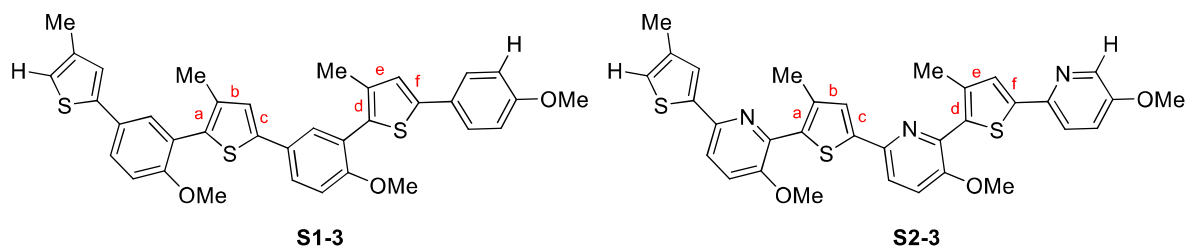
17	C	2.203381	-3.82133	-0.05372
18	C	4.650734	-1.66142	0.167702
19	H	-0.07509	-2.14726	0.056349
20	C	-3.75764	0.230568	0.309231
21	H	-0.9657	3.972738	0.412969
22	H	1.059987	2.496776	0.300157
23	S	-5.24946	1.064916	-0.11927
24	C	-4.00709	-1.11377	0.568855
25	C	-6.18584	-0.39736	0.041388
26	C	-5.38007	-1.44582	0.418842
27	C	-2.99526	-2.15569	0.967849
28	H	-5.77865	-2.43923	0.587237
29	C	-7.63358	-0.44577	-0.18333
30	H	1.224542	-4.22311	-0.3324
31	H	2.498432	-4.30724	0.885536
32	H	2.921108	-4.12612	-0.82342
33	H	-2.27367	-1.77087	1.692094
34	H	-2.4158	-2.48934	0.099862
35	H	-3.50387	-3.02652	1.39554
36	N	-8.22738	-1.64175	0.037277
37	C	-8.37877	0.665116	-0.60439
38	C	-9.75413	0.550275	-0.79832
39	C	-10.3572	-0.68781	-0.56594
40	C	-9.53425	-1.75039	-0.14892
41	H	-7.89369	1.619722	-0.7856
42	H	-10.3271	1.411035	-1.12425
43	O	-11.6803	-0.97309	-0.70512
44	H	-9.99065	-2.72171	0.034143
45	C	-12.5452	0.072487	-1.12602
46	H	-13.5442	-0.36437	-1.17137
47	H	-12.2677	0.448924	-2.12007
48	H	-12.5455	0.906907	-0.41138

49	C	5.254477	-2.92053	0.355912
50	N	5.391941	-0.5524	0.004185
51	C	6.732461	-0.6089	-0.01745
52	C	7.39785	-1.8454	0.127828
53	C	6.641475	-2.99703	0.326294
54	H	4.667449	-3.80747	0.547711
55	H	7.155196	-3.94246	0.475243
56	O	8.772562	-1.9029	0.126832
57	C	7.42149	0.673526	-0.20253
58	C	9.345937	-2.39217	-1.09142
59	H	9.001181	-3.41165	-1.30796
60	H	10.42721	-2.395	-0.94122
61	H	9.094215	-1.73479	-1.93287
62	C	6.797739	1.87296	-0.464
63	S	9.160498	0.901592	-0.10361
64	C	8.992302	2.596175	-0.42397
65	C	7.686499	2.980497	-0.59432
66	H	5.720314	1.941446	-0.55843
67	H	9.871733	3.226934	-0.46884
68	C	7.235023	4.386577	-0.88348
69	H	8.084393	5.074146	-0.94549
70	H	6.560175	4.75536	-0.10105
71	H	6.688136	4.440798	-1.83303

Table SI- 16. xyz Coordinates from the DFT calculations of molecule **S2-3**.

Bond length alternation (BLA) values

The BLA values for **S1-3** and **S2-3** were accessible by subtraction of the longer C-C bond with the shorter C=C bond in both inner thiophene rings.



S1-3									
r_a (Å)	r_b (Å)	r_c (Å)	Δr_{ba} (Å)	Δr_{bc} (Å)	r_d (Å)	r_e (Å)	r_f (Å)	Δr_{ed} (Å)	Δr_{ref} (Å)
1.38173	1.42712	1.37458	0.04539	0.05254	1.38287	1.42683	1.37493	0.04396	0.0519
S2-3									
r_a (Å)	r_b (Å)	r_c (Å)	Δr_{ba} (Å)	Δr_{bc} (Å)	r_d (Å)	r_e (Å)	r_f (Å)	Δr_{ed} (Å)	Δr_{ref} (Å)
1.38826	1.42157	1.37598	0.03331	0.04559	1.39171	1.42050	1.37514	0.02879	0.04536

Table SI-17. Bond lengths for C-C/C=C units and BLA values for **S1-3** and **S2-3**.

Trimer	δr_{ba} (Å)	δr_{bc} (Å)	δr_{ed} (Å)	δr_{ref} (Å)
S1-3	0.04539	0.05254	0.04396	0.0519
S2-3	0.03331	0.04559	0.02879	0.04536

Table SI-18. BLA values for **S1-3** and **S2-3** in direct comparison.

Comparing the BLA values of **S1-3** and **S2-3** lead to the conclusion that the thiophene rings in **S2-3** represent a more quinoidal structure than in **S1-3** since the bond length of the central C-C unit is shorter than expected as has a tendency to form a C=C unit.

Literature

- [1] A. C. J. Heinrich, University of Kiel (Kiel), **2014**.
- [2] X. Liu, J. Long, G. Wang, Y. Pei, B. Zhao, S. Tan, *Dyes Pigment* **2015**, *121*, 118-127.
- [3] A. C. J. Heinrich, B. Thiedemann, P. J. Gates, A. Staubitz, *Org. Lett.* **2013**, *15*, 4666-4669.
- [4] J. Y. Hwang, L. A. Arnold, F. Zhu, A. Kosinski, T. J. Mangano, V. Setola, B. L. Roth, R. K. Guy, *Journal of Medicinal Chemistry* **2009**, *52*, 3892-3901.
- [5] M. S. Yusubov, E. N. Tveryakova, E. A. Krasnokutskaya, I. A. Perederyna, V. V. Zhdankin, *Synthetic Communications* **2007**, *37*, 1259-1265.
- [6] M. Gao, M. Wang, Q.-H. Zheng, *Bioorg Med Chem Lett* **2016**, *26*, 3694-3699.
- [7] A. K. Parhi, A. Xiang, J. D. Bauman, D. Patel, R. S. Vijayan, K. Das, E. Arnold, E. J. Lavoie, *Bioorg Med Chem* **2013**, *21*, 6435-6446.

-
- [8] J. Tauc, R. Grigorovici, A. Vancu, *physica status solidi (b)* **1966**, *15*, 627-637.
- [9] a) J. H. Nobbs, *Review of Progress in Coloration and Related Topics* **1985**, *15*, 66-75; b) E. A. Davis, N. F. Mott, *The Philosophical Magazine: A Journal of Theoretical Experimental and Applied Physics* **1970**, *22*, 0903-0922.
- [10] M. J. Frisch, G. W. Trucks, H. B. Schlegel, G. E. Scuseria, M. A. Robb, J. R. Cheeseman, G. Scalmani, V. Barone, G. A. Petersson, H. Nakatsuji, X. Li, M. Caricato, A. V. Marenich, J. Bloino, B. G. Janesko, R. Gomperts, B. Mennucci, H. P. Hratchian, J. V. Ortiz, A. F. Izmaylov, J. L. Sonnenberg, Williams, F. Ding, F. Lipparini, F. Egidi, J. Goings, B. Peng, A. Petrone, T. Henderson, D. Ranasinghe, V. G. Zakrzewski, J. Gao, N. Rega, G. Zheng, W. Liang, M. Hada, M. Ehara, K. Toyota, R. Fukuda, J. Hasegawa, M. Ishida, T. Nakajima, Y. Honda, O. Kitao, H. Nakai, T. Vreven, K. Throssell, J. A. Montgomery Jr., J. E. Peralta, F. Ogliaro, M. J. Bearpark, J. J. Heyd, E. N. Brothers, K. N. Kudin, V. N. Staroverov, T. A. Keith, R. Kobayashi, J. Normand, K. Raghavachari, A. P. Rendell, J. C. Burant, S. S. Iyengar, J. Tomasi, M. Cossi, J. M. Millam, M. Klene, C. Adamo, R. Cammi, J. W. Ochterski, R. L. Martin, K. Morokuma, O. Farkas, J. B. Foresman, D. J. Fox, Wallingford, CT, **2016**.

5.2. Experimental Section. Supporting Information Chapter 3.1.3.

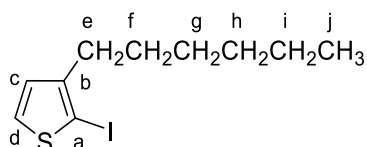
For general methods and materials see beginning of chapter 5.1.

Table of Content

Synthesis	189
Kinetic Studies for P3HT	194
NMR Spectra	197

Synthesis

2-Iodo-3-*n*-hexylthiophene (43)



This procedure was adapted from the literature.^[77]

NIS (3.41 g, 15.1 mmol) was added in one portion to a solution of 3-*n*-hexylthiophene (2.50 g, 14.8 mmol) in glacial acetic acid (25 mL) and chloroform (25 mL) at 17 °C. The solution was stirred for 16 h at 20 °C in absence of light. The reaction was quenched with a saturated solution of Na₂S₂O₃ (40 mL). The mixture was extracted with DCM (2 x 50 mL) and brine (2 x 50 mL). The combined organic layers were dried over MgSO₄, filtered and the solvent was removed *in vacuo*. The product was purified by Kugelrohr distillation (80 °C, 1.3 x 10⁻¹ mbar) to afford an orange oil in a yield of 3.27 g (74 %, 11.2 mmol).

¹H NMR (500 MHz, CDCl₃): δ = 7.38(d, ³J = 5.6Hz, 1H, d), 6.75 (1H, d, ³J = 5.6Hz, c), 2.60 – 2.4 (m, 2H, e), 1.65 – 1.48 (m, 2H, f), 1.41 – 1.29 (m, 6H, h/i/j), 0.90 (d, ³J = 6.9 Hz, 3H, j) ppm.

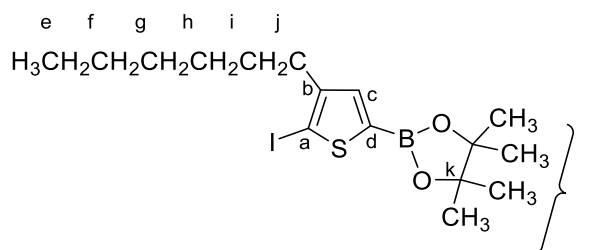
¹³C{¹H} NMR (126 MHz, CDCl₃): δ = 147.9 (b), 130.7 (d), 128.36 (c), 74.3 (a), 32.0 (e), 29.3 (f), 32.52, 30.4, 23.0 (g/h/i), 14.5 (j) ppm.

IR (ATR): $\tilde{\nu}$ = 2953 (m), 2923 (s), 2854 (s), 1456 (m), 1397 (m), 963 (m), 828 (s), 713 (s), 684 (s), 634 (s) cm⁻¹.

HR-MS (ESI, C₁₀H₁₅NaIS): calcd. 293.99337, found 293.92289.

MS (EI, 70 eV, direct inlet, 200 °C): *m/z* (% relative intensity) = 294 (19) [M]⁺, 222.9 (43) [M-C₅H₁₁], 97.0 (100) [M-C₅H₁₁I]⁺.

2-(4-Hexyl-5-iodothiophen-2-yl)-4,4,5,5-tetramethyl-1,3,2-dioxaborolane (**44**)



This procedure was adapted from the literature.^[59]

In a Schlenk flask, a solution of DIPA (1.06 g, 10.4 mmol) in THF (20 mL) was cooled to -78 °C and *n*-BuLi (4.1 mL, 2.5 M in hexanes, 10.2 mmol) was added dropwise over 20 min. The mixture was warmed to 0 °C over the course of 30 min, cooled to -78°C and stirred for 5 min. A solution of 2-Iodo-3-hexylthiophene (**42**) (2.99 g, 10.2 mmol) in THF (20 mL) was added with a syringe pump over the course of 20 min (rate = 0.5 mL / min) and the mixture was stirred for 1 h at this temperature. A solution of *t*PrOBPin (1.91 g, 10.3 mmol) in THF (5 mL) was added with a syringe pump (rate = 1 mL / min) to the orange-green suspension. The reaction mixture was allowed to reach 20 °C and was stirred for further 16 h. Afterwards the reaction was quenched with methanol (100 mL) and all volatiles were removed *in vacuo*. The residue was diluted with DCM (50 mL) and washed with water (2 x 100 mL), brine (2 x 100 mL) and dried over MgSO₄. After filtration, the volatiles were removed *in vacuo* and the mixture was purified by flash chromatography (*n*-hexane: EtOAc, 6:4 R_f = 0.20) to afford an orange oil in a yield of 2.76 g (65%, 6.57 mmol).

¹H NMR (500 MHz, CDCl₃): δ = 7.24(s, 1H, c), 2.53 (dd, ³J = 12.5, 4.6 Hz, 2H, e), 1.67 – 1.48 (m, 2H, f), 1.38 – 1.27 (m, 18H, g/h/i/l), 0.90 (m, 3H, j) ppm.

¹³C{¹H} NMR (126 MHz, CDCl₃): δ = 148.73 (b), 137.61 (c), 84.36 (d), 82.95 (a), 31.78 (e), 30.15 (f), 32.06, 29.07, 22.72 (g/h/i), 24.87 (l), 14.23 (j) ppm.³

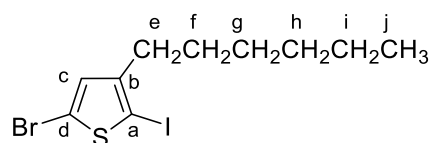
¹¹B{¹H} NMR (160 MHz, CDCl₃): δ = 28.4 ppm.

IR (ATR): $\tilde{\nu}$ = 2976.9 (w), 2925.3 (w), 1540.3 (m), 1428.0 (s), 1370.5 (m), 1326.8 (s), 1294.0 (s), 1267.2 (m), 1138.7 (s), 1024.9 (m), 956.1 (w), 851.1 (s), 662.3 (s) cm⁻¹.

HR-MS (EI, C₁₆H₂₆¹¹BO₂S): calcd. 419.08221, found 419.08159 (R=10000).

MS (EI, 70 eV, direct inlet, 200 °C): *m/z* (% relative intensity) = 420.1 (23) [M]⁺, 349.0 (19) [M-C₅H₁₁], 223.0 (100) [M-C₅H₁₁I]⁺.

³ Carbon d was not possible to identify because the quadrupole moment from the adjacent boron atom.

4- Bromo-5-iodo-3-*n*-hexylthiophene (45)

This procedure was based on the synthesis of 2-Bromo-5-iodo-3-*n*-hexylthiophene.^[92]

2-bromo-4-hexylthiophene (**M1-10**) (1.25 g, 5.07 mmol) was dissolved in a mixture of chloroform (16 ml) and acetic acid (16 mL). NIS (1.20 g, 5.32 mmol) was added to the solution at 0 °C over a period of 3 min.

The solution was stirred for 16 h at 20 °C in absence of light. The reaction was quenched with a saturated solution of Na₂S₂O₃ (50 mL). The mixture was extracted with DCM (2 x 50 mL) and brine (2 x 50 mL) and the combined organic layers were dried over MgSO₄. After filtration, the solvent was removed *in vacuo*. The product was purified by Kugelrohr distillation (110 °C, 9.0 x 10⁻² mbar) to afford a yellow-pink oil in a yield of 1.81 g (96%, 4.87 mmol).

¹H NMR (600 MHz, CDCl₃): δ = 6.72 (s, 1H, c), 2.49 (m, 2H, e), 1.53 (m, 2H, f), 1.32 (6H,m,g/h/i), 0.89 (m, 3H, j) ppm.

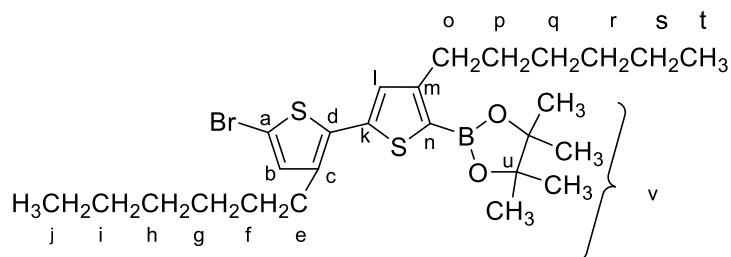
¹³C{¹H} NMR (126 MHz, CDCl₃): δ = 148.2(b), 130.8 (c), 111.7 (d), 72.95 (a), 32.3 (e), 31.6, 28.8, 22.5 (g/h/i), 29.8 (f), 14.0 (j) ppm.

IR (ATR): $\tilde{\nu}$ = 2953(m), 2923 (s), 2854 (s), 1531 (m), 1456 (m), 1407 (m), 1377 (w), 1188 (w), 987 (m) 962 (m), 918 (w),824 (s), 723 (m), 699 (w), 650 (w), 575 (w) cm⁻¹.

HR-MS (ESI, C₁₀H₁₄BrIS): calcd. 371.9044, found 371.9051.

MS (EI, 70 eV, direct inlet, 200 °C): *m/z* (% relative intensity) = 374 (36) [M+2H]⁺, 177.9 (100) [M-Br]⁺.

2-(5'-Bromo-3',4-dihexyl-[2,2'-bithiophen]-5-yl)-4,4,5-trimethyl-1,3,2-dioxaborolane (46)



A solution of **44** (245 mg, 657 μmol), **P1-13** (310 mg, 677 μmol), $[\text{Pd}(\text{PPh}_3)_4]$ (55 mg, 58.6 μmol , 9 mol%) in DMF (4 mL) was heated to 120°C in a microwave apparatus for 15 h. After allowing the mixture to cool to ambient temperature (aprox. 20 °C), water (5 mL) was added and the mixture was extracted with DCM (3 x 10 mL). The organic phase was washed with brine (3 x 5 mL) before drying the organic phase over MgSO_4 . After filtration, the volatiles were removed in vacuo. The mixture was purified by flash chromatography (n-hexane: EtOAc; 70:30; Rf: 0.20) to afford an orange oil in a yield of 270 mg (76%, 503 μmol).

^1H NMR (500.1 MHz, CDCl_3): δ = 6.96 (s, 1H, l), 6.87 (s, 1H, b), 2.86 – 2.82 (m, 2H, e), 2.73 – 2.69 (m, 2H, o), 1.64 – 1.56 (m, 4H, f/p), 1.35 – 1.24 (m, 24H, g/h/i/q/r/s/v), 0.93 – 0.85 (m, 6H, j/t) ppm.

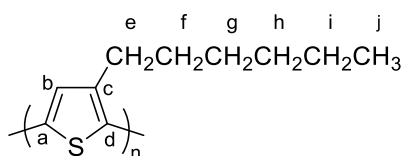
$^{13}\text{C}\{^1\text{H}\}$ NMR (126 MHz, CDCl_3): δ = 154.97 (m), 140.41 (k), 140.30 (c), 132.62 (b), 132.53 (d), 129.41 (l), 127.38 (n), 110.47 (a), 83.65 (u), 31.43 (e), 29.03 (o), 31.58, 30.22 (f/p), 31.63, 31.43, 30.33, 29.13, 28.92, 24.76, 22.64, 22.59 (g/h/i/q/r/s/v), 22.64, 13.93 (j/t) ppm.

$^{11}\text{B}\{^1\text{H}\}$ NMR (160 MHz, CDCl_3): δ = 28.64 ppm.

IR (ATR): $\tilde{\nu}$ = 2955(m), 2925(m), 2856(m), 1526(w), 1459(s), 1426(m), 1371 (m), 1337(s), 1305 (m), 1270(m), 1141 (s), 1045 (m), 959 (w), 854 (s), 830(m), 668(w), 647(m), 578 (w), 517 (w) cm^{-1} .

HR-MS (ESI, $\text{C}_{26}\text{H}_{40}\text{NaBBrO}_2\text{S}_2$): calcd. 561.1643, found 563.1640.

MS (EI, 70 eV, direct inlet, 200 °C): m/z (% relative intensity) = 540.4 (6) $[\text{M}+2\text{H}]^+$, 414.2 (100) $[\text{M} + 2\text{H} - \text{C}_6\text{H}_{12}\text{BO}_2]^+$.

Poly[4-hexyl-2,2'-bithiophene] (47)

In a Schlenk flask, **45** (54 mg, 100 μmol) was dissolved in THF (2 mL). A suspension of $[\text{Pd}(t\text{-Bu}_3\text{P})_2]$ (1 mg, 2 μmol , 2 mmol%), CsF (20 mg, 130 μmol) in degassed water (0.5 mL) and THF (1.5 mL) were added. The mixture was heated at 40 $^\circ\text{C}$ for 24 h under a nitrogen atmosphere. The crude mixture was quenched with a solution of HCl in methanol (1 M, 1 mL) to afford a sticky yellow oil. Water was added (5 mL) and the mixture was extracted with DCM (3 x 10 mL). The organic phase was washed with brine (3 x 5 mL) before being dried over MgSO_4 . After filtration, the volatiles were removed *in vacuo*. The crude product was purified by Soxhlet extraction. First, MeOH (200 mL) was used as solvent and the system was heated at 100 $^\circ\text{C}$ for 8 h. After oligomers and small molecules were removed, the solvent was changed to chloroform and the system was heated at 80 $^\circ\text{C}$ for 4 h. The volatiles were removed *in vacuo* to afford a sticky strong-orange oil in a yield of 15 mg (45%).

$^1\text{H NMR}$ (600 MHz, CDCl_3): δ = 6.97 (d, 3J = 10.1 Hz, 1H, b), 2.87-2.72 (m, 2H, e), 1.94 – 1.75 – 1.67 (m, 2H, f), 1.45 – 1.20 (m, 6H, g/h/i), 0.95 – 0.80 (m, 3H, j) ppm.

$^{13}\text{C}\{^1\text{H}\}$ NMR (126 MHz, CDCl_3): δ = 140.5 (c), 133.7, 130.6 (a/d), 128.8 (b), 31.8, 29.4, 22.8 (g/h/i), 30.7 (f), 29.6 (e), 14.3 (j) ppm.

IR (ATR): $\tilde{\nu}$ = 2920 (s), 2848 (s), 1456 (m), 1269 (w), 1089 (m), 831 (m), 715 (w), 687 (w) cm^{-1} .

λ_{max} (DCM) = 427 nm.

MALDI (Terthiophene) = m/z : 5039.2.

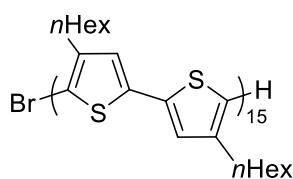
M_n (GPC, conventional method) = 4.56 kDa.

\bar{D} = 2.49

DP (based on GPC measurements) = 13

DP (based on MALDI measurements) = 15

Proposed structure with end groups based on MALDI analysis =



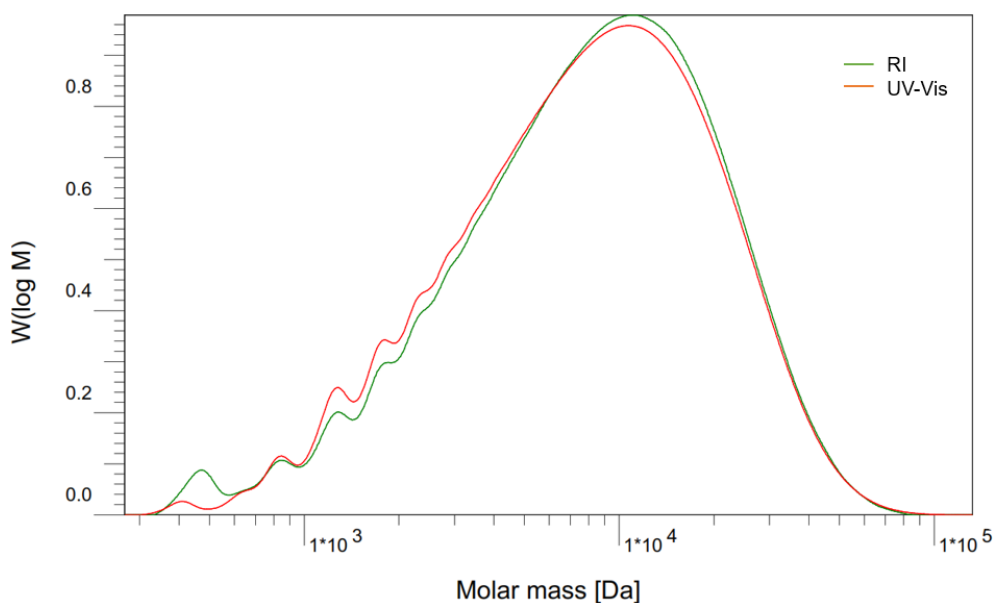


Figure 42. GPC measurement result of **46** using THF as eluent in a concentration of 1 mg/mL, at a flow rate of 1 mL/min. Calibrated against polystyrene standards using a conventional calibration method. Signals from the refractive index (RI) and UV-Vis detectors are shown.

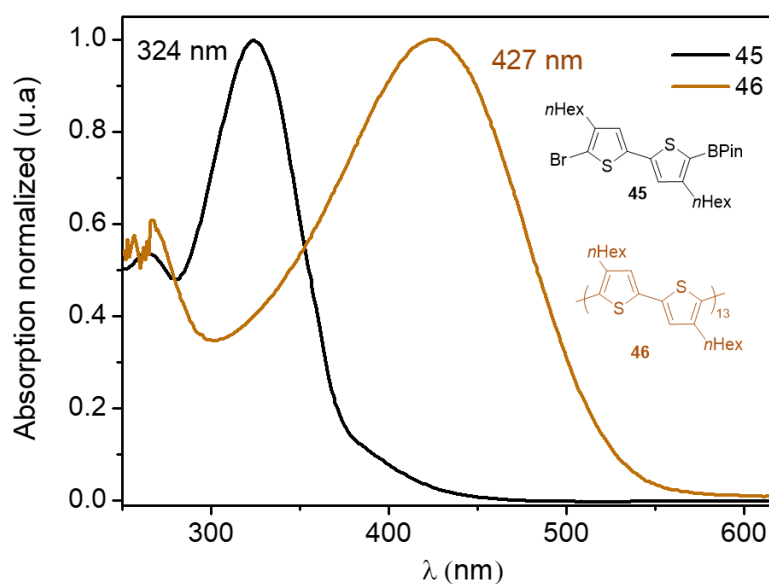
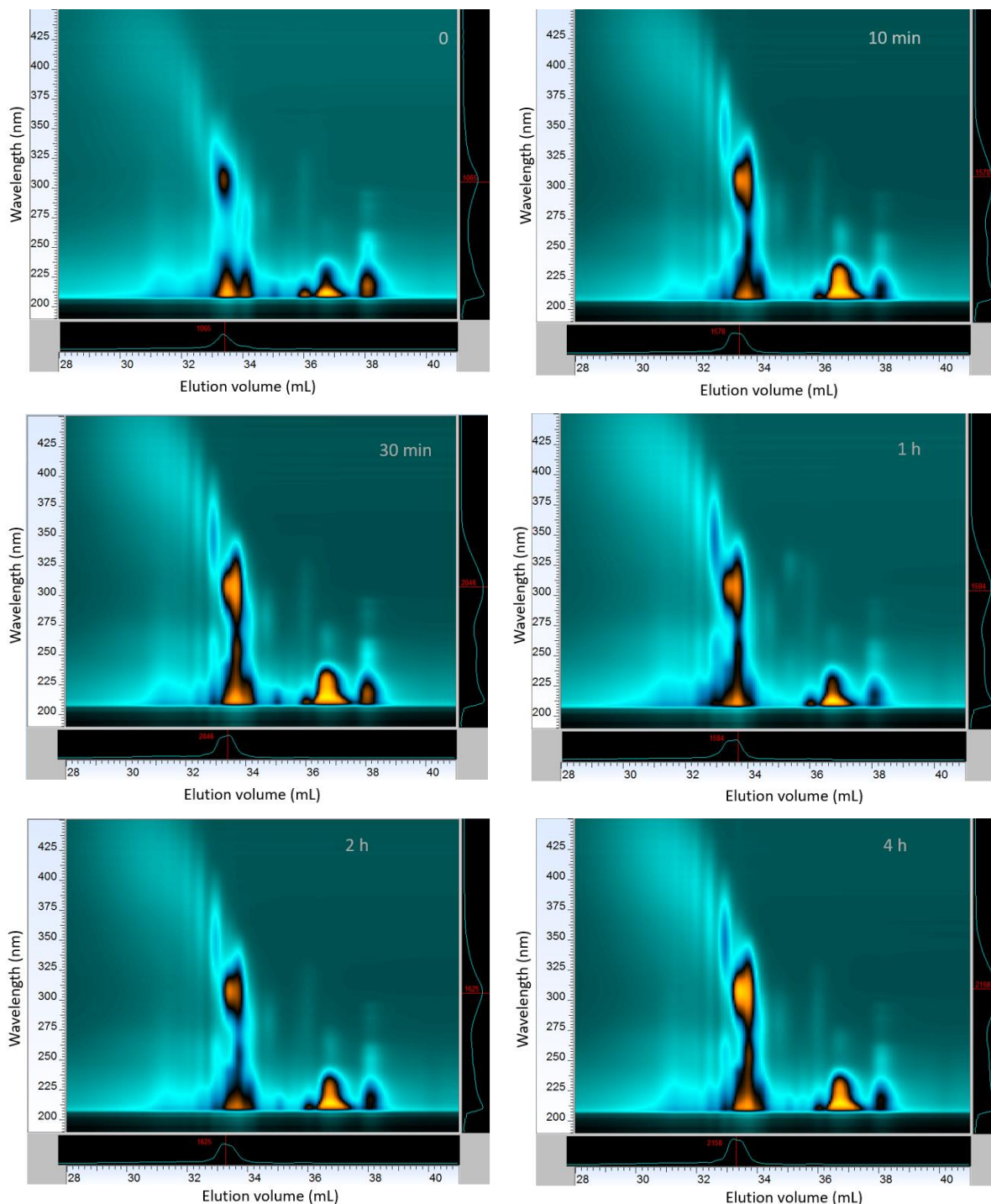


Figure 43. Absorption spectrum from a solution in chloroform of the monomer **45** (3.2 mM) and P3HT **46** (4.8 mM).

Kinetic Studies for P3HT **47**

In a Schlenk tube, a solution of **46** (134 mg, 248 μmol) and 1,3,5-trimethoxy benzene (42 mg, 250 μmol , used as internal standard) in THF (1 mL) was prepared and heated for 2 min at 40 $^{\circ}\text{C}$. Immediately, after a suspension of $[\text{Pd}(\text{t-Bu}_3\text{P})_2]$ (6 mg, 12 μmol , 5% mol), CsF (50 mg, 329 μmol), water (0.6 mL) and THF (stabilizer free, 3.4 mL) was added, a first sample (0.18 mL) was taken out of from the reaction mixture (t_0). After 10 min, 30 min, 1 h, 2 h, 4 h, 6 h, 24 h and 96 h reaction time, a sample was taken out of the reaction mixture.

Every sample was quenched with a solution of HCl in MeOH (2,0 mL, 2 mmol, 1 M), then water (1 mL) was added and the mixture was extracted with DCM (2 x 3 mL). The organic phase was dried over MgSO₄ and filtered over a "mini column". The solution was split in two flasks and the solvents were removed in vacuo. Half of the sample was dissolved in THF for GPC analysis and the second one in CDCl₃ for ¹H NMR analysis.



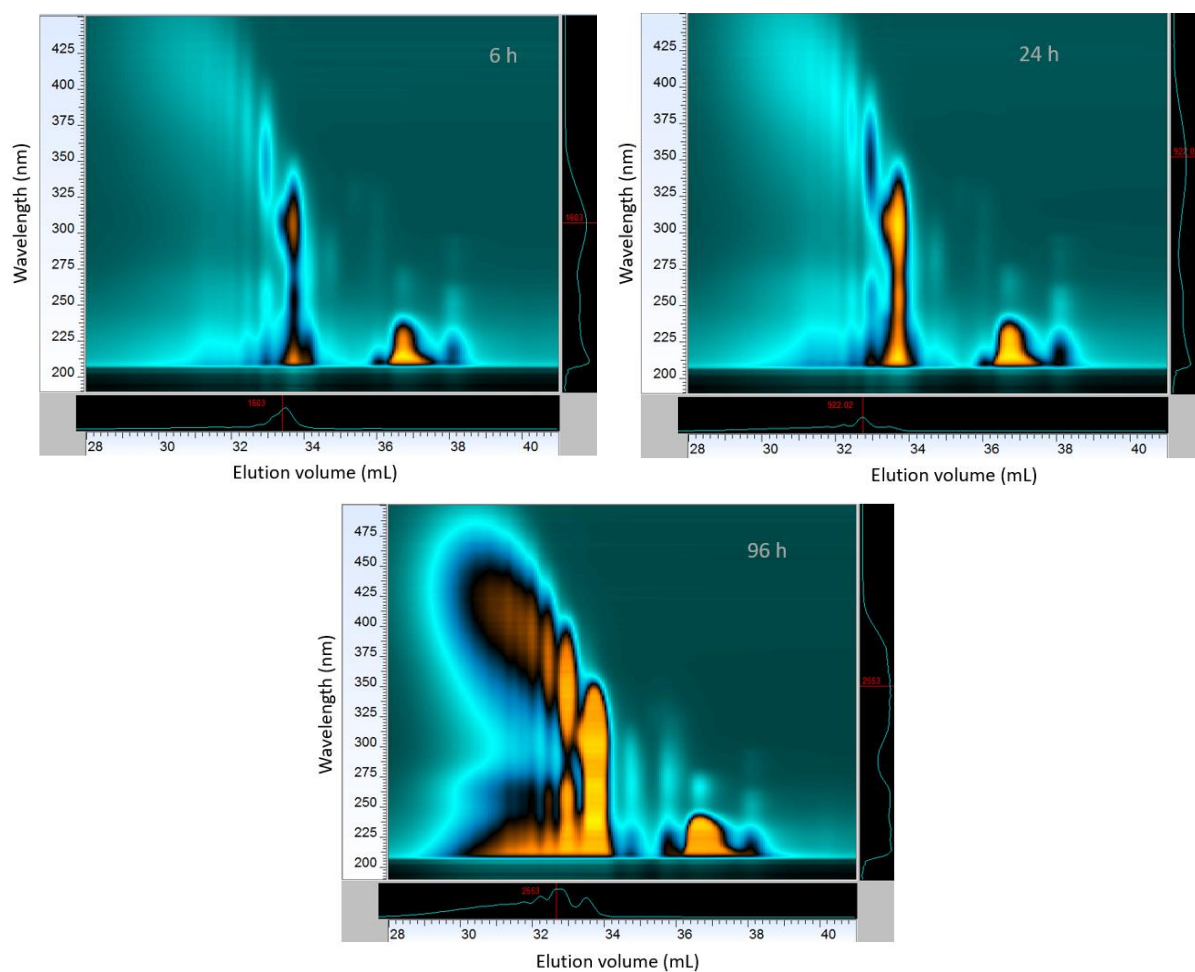


Figure 44. UV-Vis spectrum/ elugram 2D plots from the GPC measurements of the kinetic study of polymerization of **46**. The intensity (Z) of the yellow color is related to the concentration of internal standard, monomer and polymer in each sample.

NMR Spectra

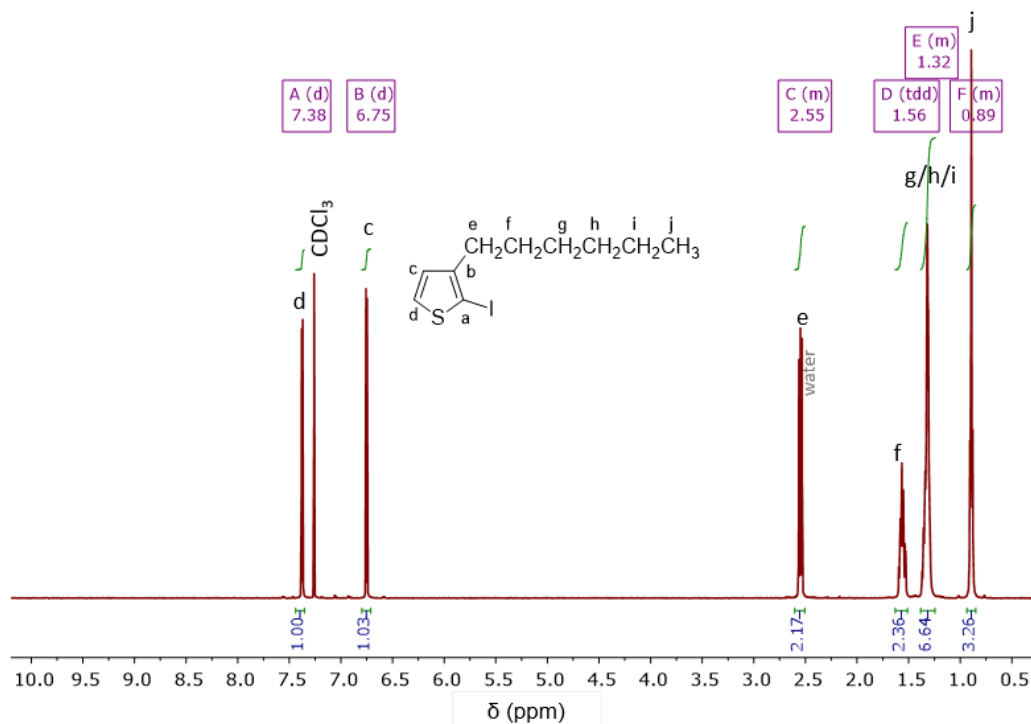
2-Iodo-3-hexylthiophene (**43**)

Figure 45. ^1H NMR (600 MHz) spectrum of **43** in CDCl_3 .

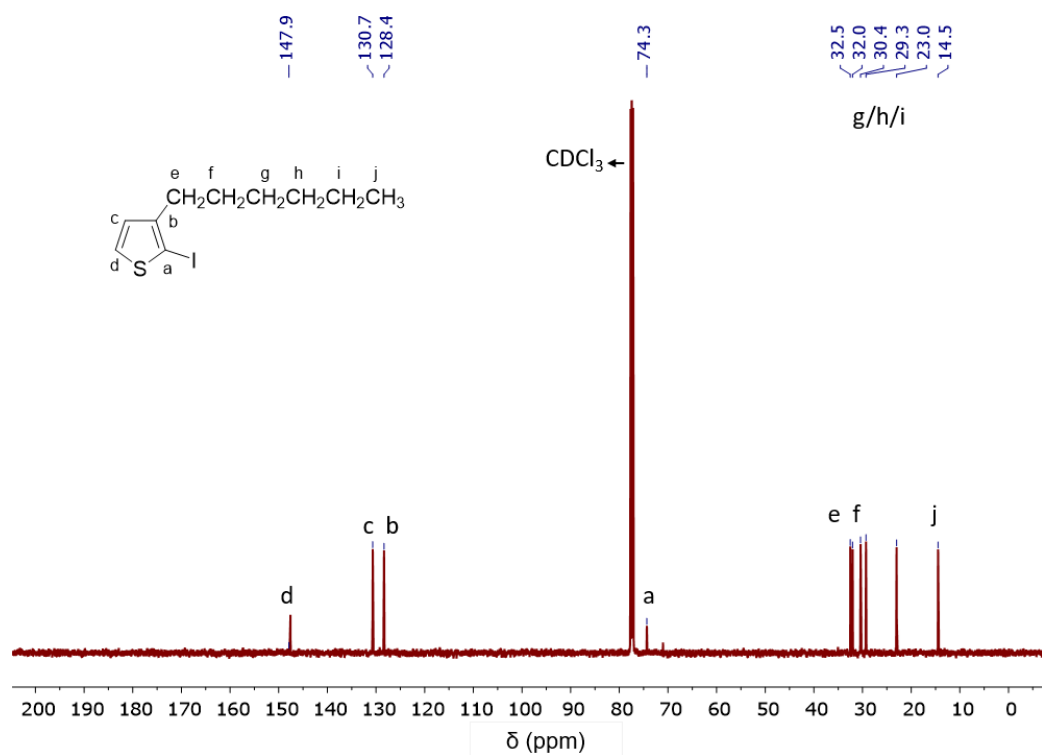
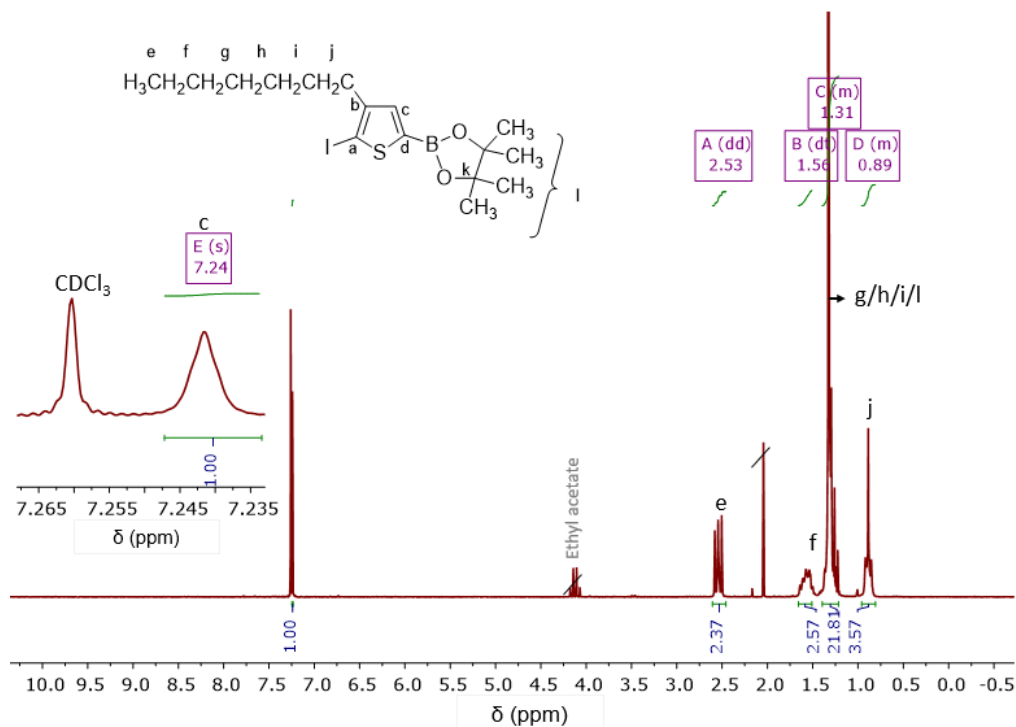
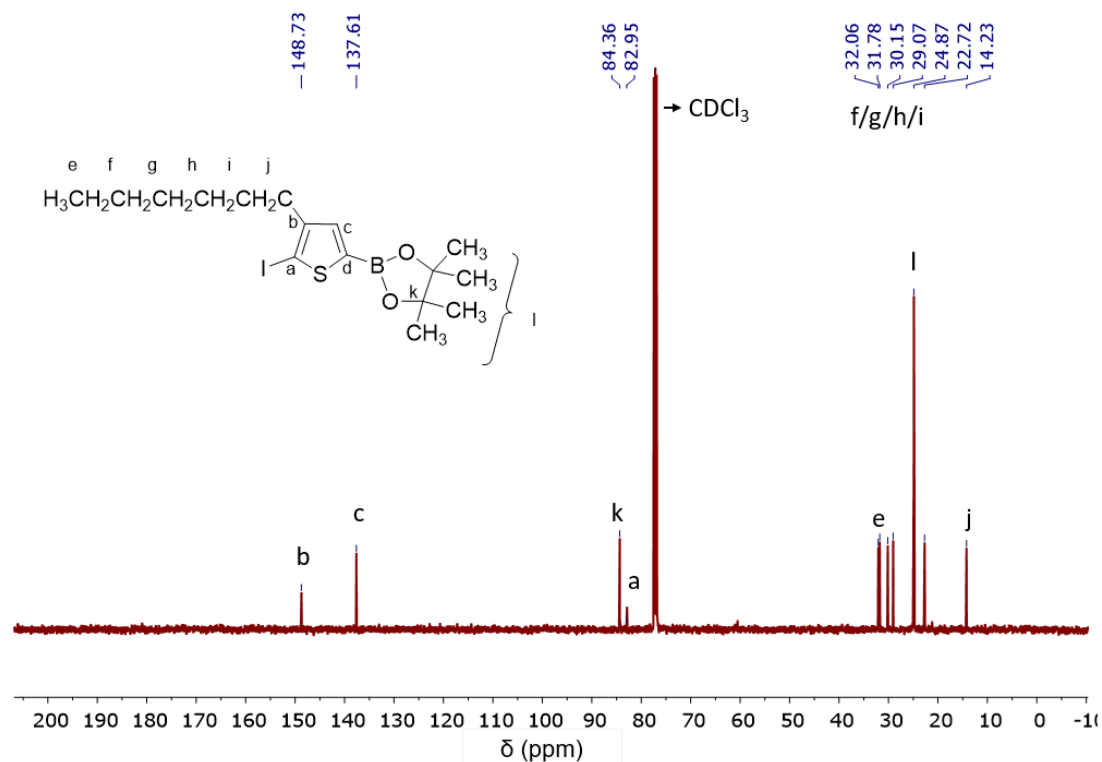


Figure 46. $^{13}\text{C}\{^1\text{H}\}$ NMR (126 MHz) spectrum of **43** in CDCl_3 .

2-(4-Hexyl-5-iodothiophen-2-yl)-4,4,5,5-tetramethyl-1,3,2-dioxaborolane (44)

Figure 47. ¹H NMR (600 MHz) spectrum of **44** in CDCl₃.

Figure 48. ¹³C{¹H} NMR (126 MHz) spectrum of **44** in CDCl₃.

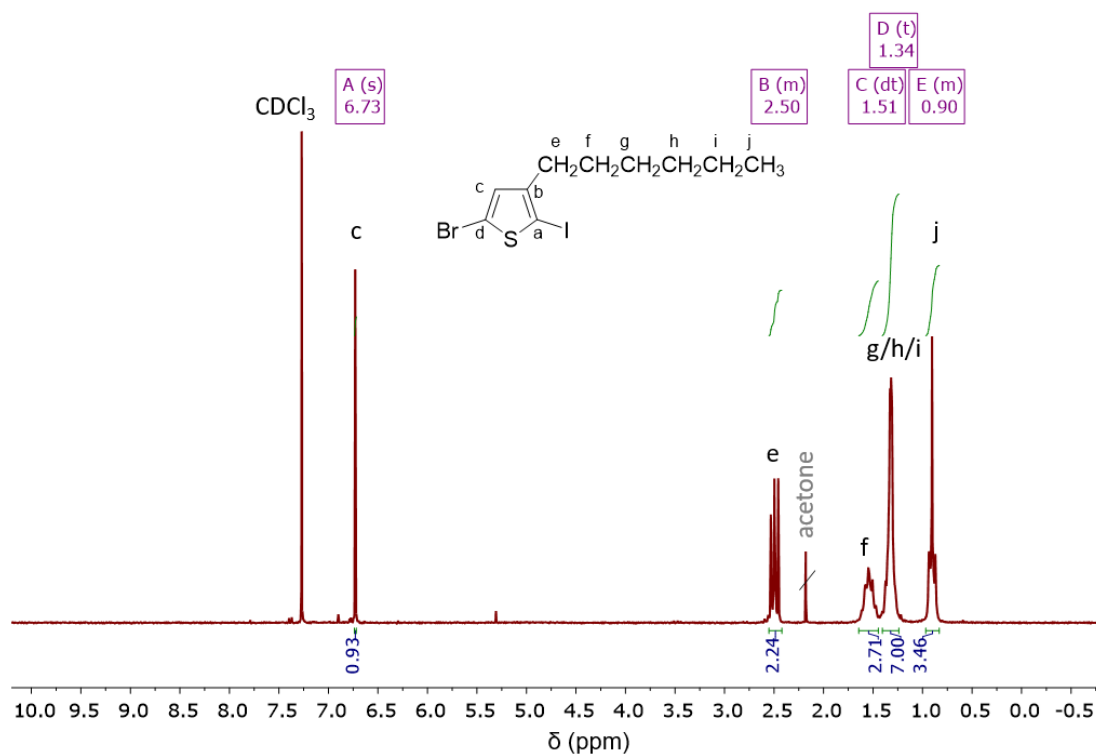
4- Bromo-5-iodo-3-hexylthiophene (**45**)

Figure 49. ¹H NMR (600 MHz) spectrum of **45** in CDCl₃.

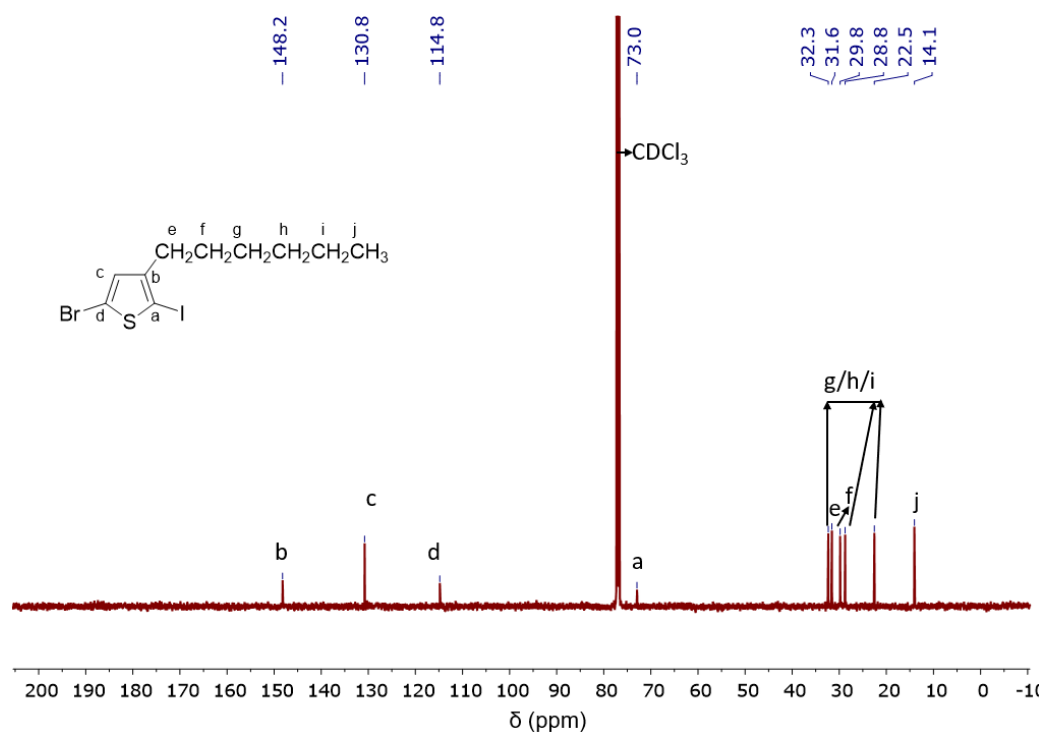


Figure 50. ¹³C{¹H} NMR (126 MHz) spectrum of **45** in CDCl₃.

2-(5'-Bromo-3',4-dihexyl-[2,2'-bithiophen]-5-yl)-4,4,5-trimethyl-1,3,2-dioxaborolane (46)

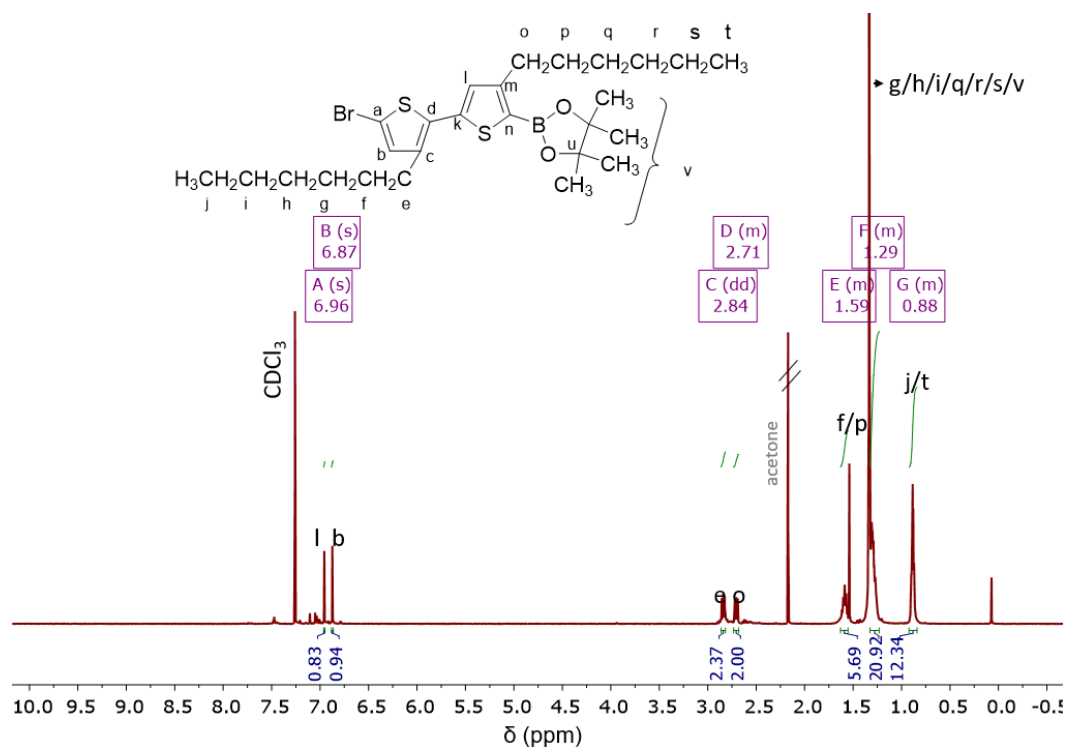


Figure 51. ^1H NMR (600 MHz) spectrum of **46** in CDCl_3 .

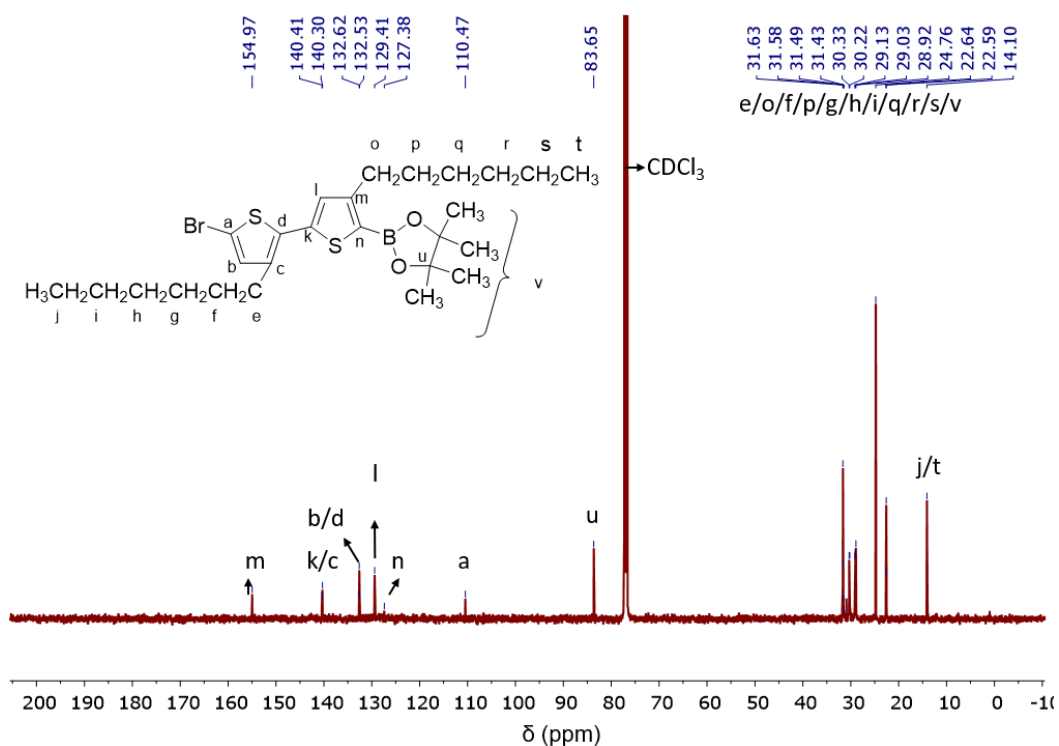


Figure 52. $^{13}\text{C}\{^1\text{H}\}$ NMR (126 MHz) spectrum of **46** in CDCl_3 .

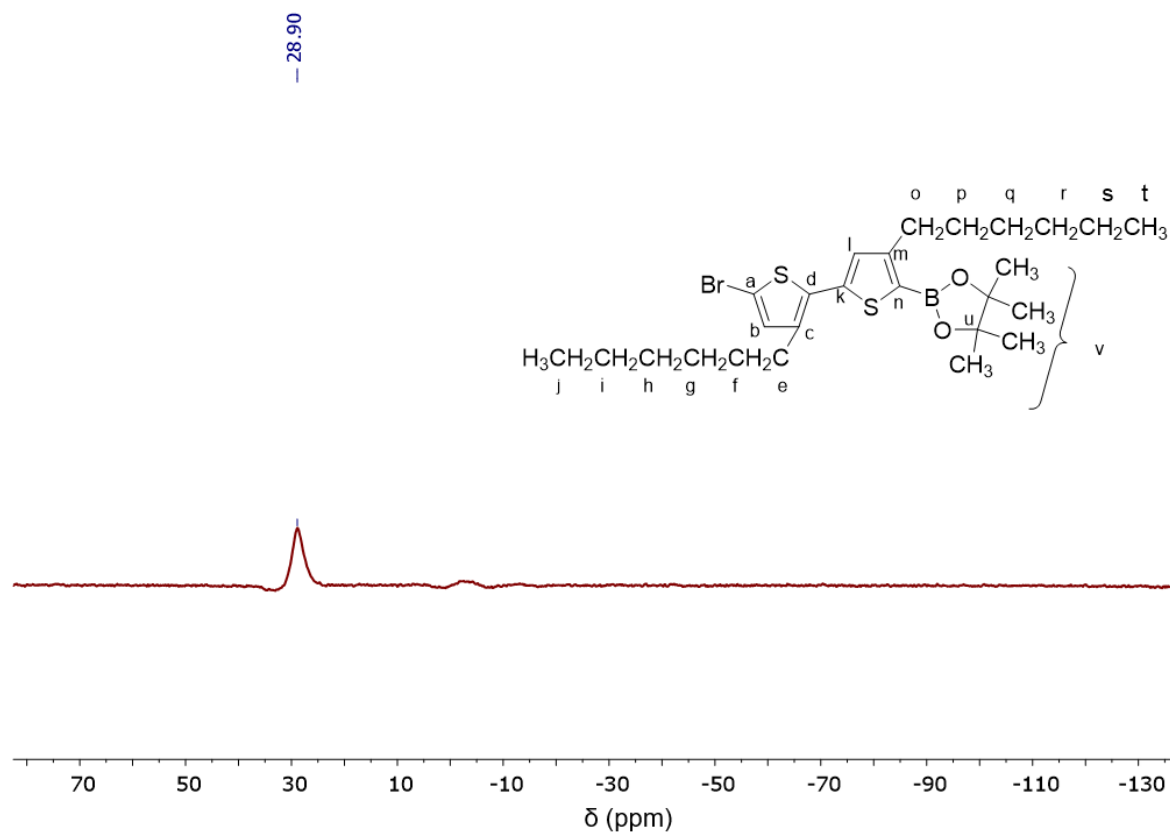


Figure 53. $^{11}\text{B}\{^1\text{H}\}$ NMR (160 MHz) spectrum of **46** in CDCl_3 .

Poly(4-Hexyl-2,2'-bithiophene) (**47**)

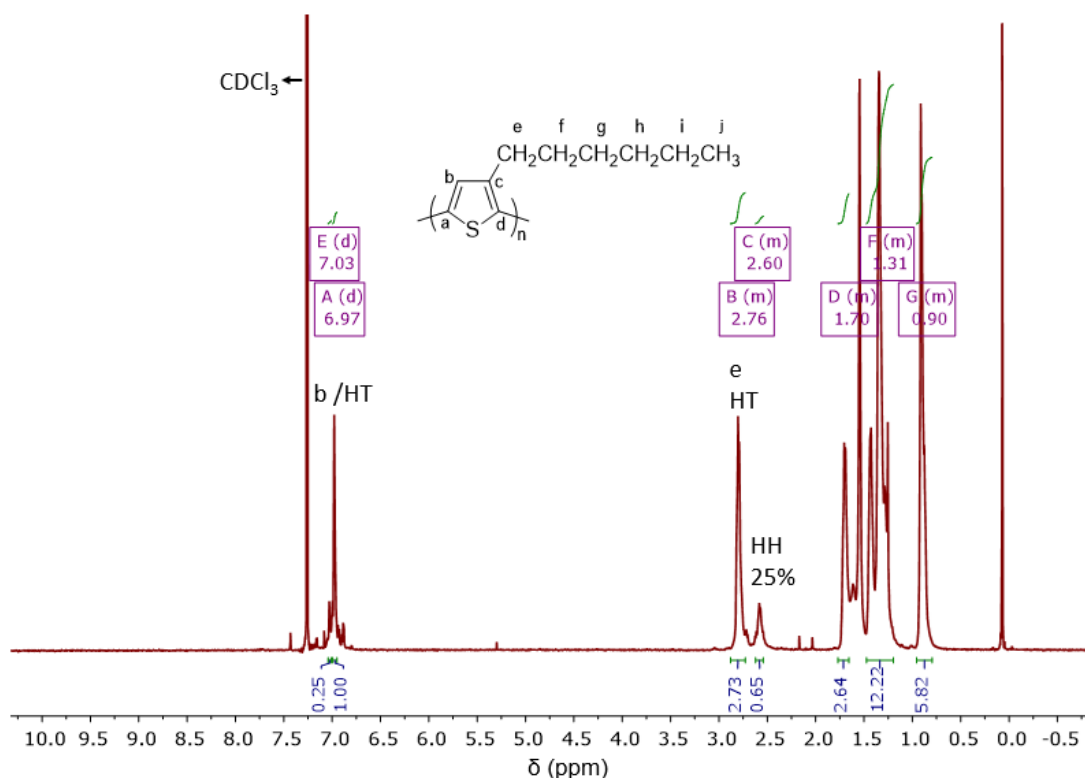


Figure 54. ¹H NMR (600 MHz) spectrum of **47** in CDCl₃.

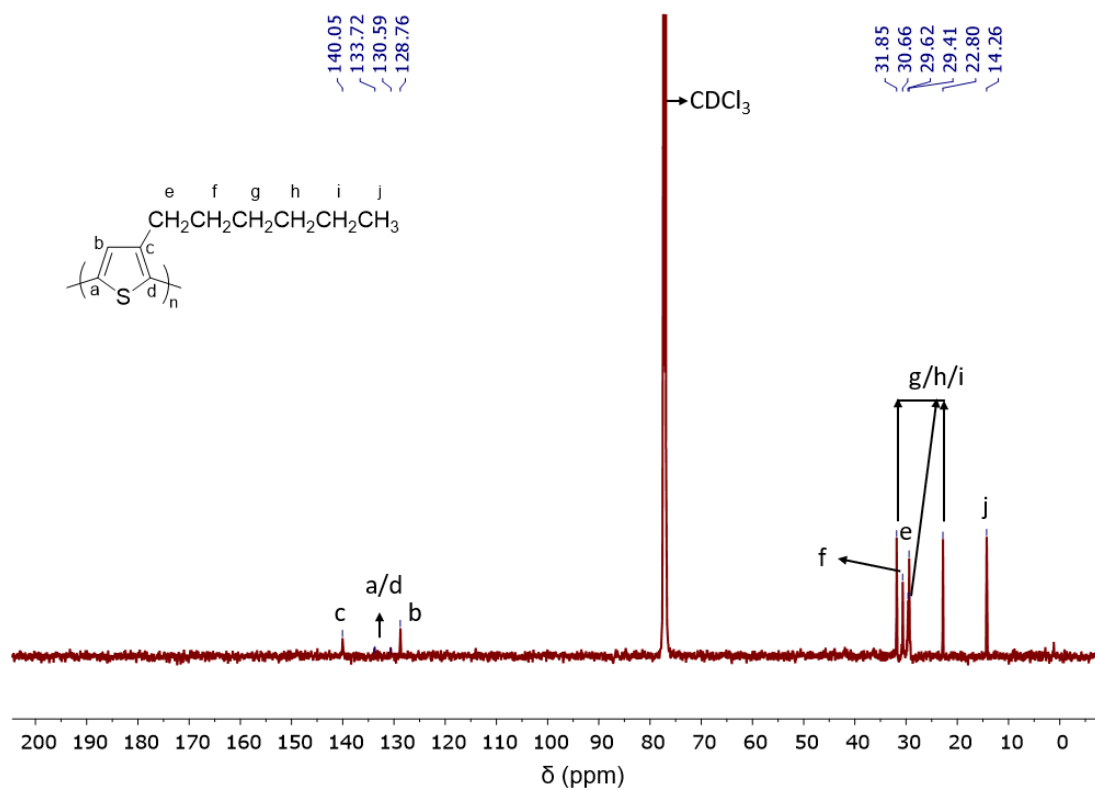


Figure 55. ¹³C{¹H} NMR (126 MHz) spectrum of **47** in CDCl₃.

5.3. Experimental Section. Supporting Information Chapter 3.1.4.

Supporting Information

for

Synthesis of Poly(thiophene-*alt*-pyrrole) from a Difunctionalized Thienylpyrrole by Kumada Polycondensation

Lu-Ying He^a, Sara Urrego-Riveros^a, Paul J. Gates^b, Christian Näther^c, Maren Brinkmann^d, Volker Abetz^{d,c} and Anne Staubitz^{a,*}

^a Otto Diels-Institute for Organic Chemistry, University of Kiel, Otto-Hahn-Platz 4, Kiel 24098 Germany

^b School of Chemistry, University of Bristol, Cantock's Close, Bristol BS8 1TS, UK

^c Institute for Inorganic Chemistry, University of Kiel, Otto-Hahn-Platz 6, Kiel, 24118 Germany

^d Helmholtz-Zentrum Geesthacht, Institute of Polymer Research, Max-Planck-Str. 1, Geesthacht 21502, Germany

* Institute of Physical Chemistry, University of Hamburg, Grindelallee 117, Hamburg 20146, Germany.

Table of Contents

Abbreviations	1
Materials.....	2
GC Calibration.....	3
Lithiation of compound 3 with LDA.....	5
Lithiation of compound 3 with LTMP	6
NMR spectra of crude products obtained via the lithiation of precursor monomer 4	7
MALDI-TOF MS spectra of the poly(thiophene- <i>alt</i> -pyrrole).....	10
NMR spectra for the kinetic study of the polymerization of 7	12
¹ H NMR spectra for PTP (with LiCl and without LiCl).	13
DFT calculations.....	14
DSC heating and cooling curves for PTP at 3 °C /min under N ₂	17
Synthesis.....	18
NMR Spectra.....	21
References.....	33

Abbreviations

A	area
anhyd.	anhydrous
Ar	aryl
ATR	attenuated total reflectance
calcd.	calculated
CI	chemical ionization
COSY	correlated spectroscopy
d	doublet (NMR)
DEPT	distortionless enhancement by polarization transfer
DMF	<i>N,N</i> -dimethylformamide
dppe	1,2- <i>bis</i> (diphenylphosphino)ethane
dppf	1,1'- <i>bis</i> (diphenylphosphino)ferrocene
EI	electron ionization
GC	gas chromatography
GC-MS	gas chromatography-mass spectrometry
HMBC	heteronuclear multiple bond coherence
HPLC	high-performance liquid chromatography
HSQC	heteronuclear single quantum coherence
IR	infrared
m	medium (concerning the intensity) (IR)
m	multiplet (NMR)
MALDI-TOF-MS	matrix-assisted laser desorption/ionization time-of-flight mass spectrometry
M_n	number average molecular weight
M_w	weight average molecular weight
M.p.	melting point
MS	mass spectrometry
MTBE	Methyl <i>tert</i> -butyl ether
MW	microwave
n	amount of substance
RF	response factor
R_f	retention factor
s	strong (concerning the intensity) (IR)
s	singlet (NMR)
SPhos	2-dicyclohexylphosphino-2',6'-dimethoxybiphenyl
t	triplet (NMR)
THF	tetrahydrofuran
TMEDA	<i>N,N,N',N'</i> -tetramethylethylenediamine
TMS	tetramethylsilane
w	weak (concerning the intensity) (IR)

Materials

Chemicals

All reagents were used without further purification unless noted otherwise.

Compound	Supplier	Purity	Comment
Thiophene	Alfa Aesar Inc.	99 %	
Br ₂	Acros Inc.	99+ %	
HBr(48%)	Fisher Scientific	48%	
Natriumthiosulfat	Grüssing Inc.	97 %	
Zinc	J.T.Baker B.V.- Deventer-Holland	-	
Acetic acid	Grüssing Inc.	99.5 %	
Magnesium	Merck Inc.	>99%	
1-Bromohexane	Sigma-Aldrich Inc.	98%	
Ni(dppp)Cl ₂	ABCR Inc.	99%	
<i>N</i> -Bromosuccinimide	Sigma-Aldrich Inc.	98%	
<i>N</i> -iodosuccinimide	molekula	95%	
Pyrrole	Sigma-Aldrich Inc.	98%	
NaH	Acros Inc.	60% disperse in oil	
<i>n</i> -Butyllithium	Acros Inc.	2.5 M in hexane	
Tributyltin chloride	Acros Inc.	95 %	
Tetramethylethyldiamine	Acros Inc.	99.5 %	
Magnesium sulfate	Grüssing Inc.	99 %	
[Pd(PPh ₃) ₄]	ABCR Inc.	99 %	
[Pd(<i>P</i> tBu ₃) ₂]	Strem Chemicals Inc.	>98 %	
Sodium	Merck Inc.	≥ 99 %	
Sodium chloride	Grüssing Inc.	99.5 %	
15-Crown-5	VWR Inc.	98%	
Isopropylmagnesium chloride solution	Sigma-Aldrich Inc.	2 M in THF	
LiCl	Sigma-Aldrich Inc.	99%	

Solvent	Supplier or grade before distillation, drying procedure if applicable
CHCl ₃	VWR Inc., HPLC grade
Diethyl ether	BCD, technical grade
DMF	ABCR, anhydrous, amine free; 99.9%; contains amine and molecular sieves
Hexane	WALTER CMP, technical grade, sodium with benzophenone as an indicator; stored over 3 Å molecular sieves
THF	Sigma Aldrich; Dried over LiAlH ₄ with benzophenone as an indicator, degassed by three freeze-pump-thaw cycles stored over 3 Å molecular sieves
MTBE	Sigma Aldrich; HPLC grade, sodium with benzophenone as an indicator; degassed by three freeze-pump-thaw cycles, stored over 3 Å molecular sieves in the glovebox
Dioxane	Grüssing; Dried over sodium with benzophenone as an indicator; degassed by three freeze-pump-thaw cycles, stored over 3 Å molecular sieves in the glovebox

GC Calibration

The conversion for the polymerization was determined by GC by a multiple point internal standard method, using naphthalene as a standard. The following equation was used for the calculation of the conversion of substances **3**, and **4**.

$$n(\text{analyte}) = \frac{A(\text{analyte})}{A(\text{standard})} \times \frac{n(\text{standard})}{RF}$$

where n is the amount of substance, A is the integrated area and RF is a system specific response factor. For the calibration curve, known amounts of the analytical naphthalene were used. The response factor RF was obtained from the slope of the resulting calibration curve (Figures SI 1 and SI 2).

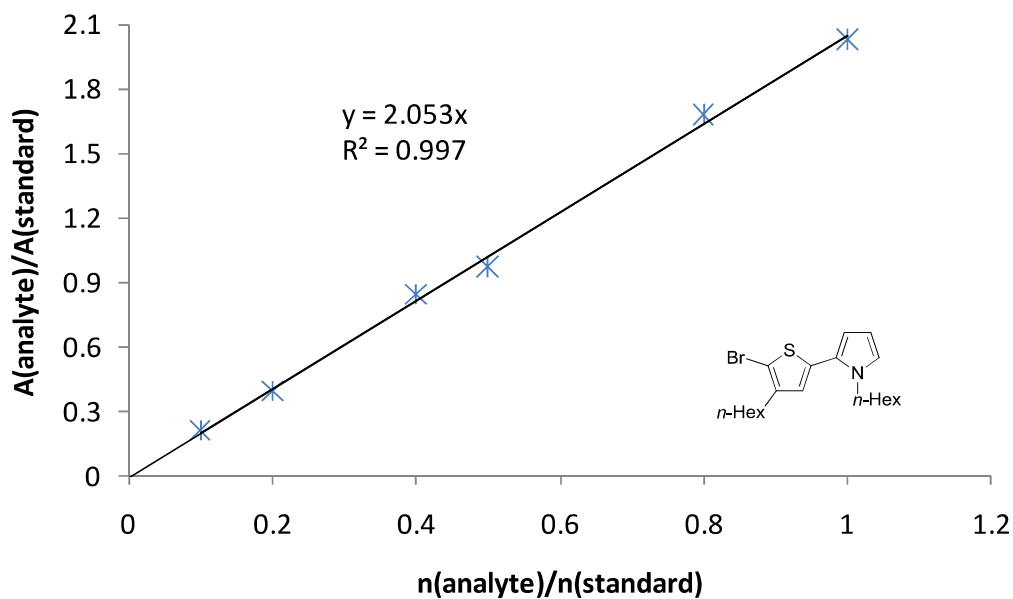


Figure SI 1. Calibration curve for 2-(5-bromo-4-hexylthiophen-2-yl)-1-hexyl-1H-pyrrole **3** using naphthalene as an internal standard.

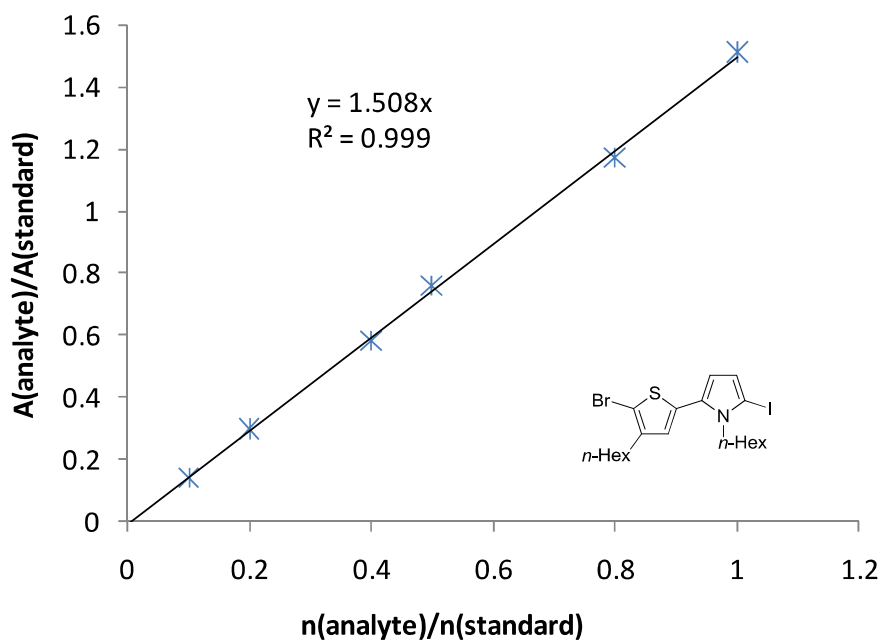
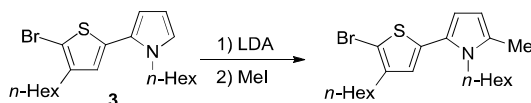


Figure SI 2. Calibration curve for 2-(5-bromo-4-hexylthiophen-2-yl)-1-hexyl-5-iodo-1H-pyrrole **4** using naphthalene as an internal standard.

Lithiation of compound 3 with LDA

Diisopropylamine (111 mg, 155 μ L, 1.10 mmol) was added to THF (10 mL) in one portion. The solution was cooled to 0 $^{\circ}$ C and *n*-BuLi (0.40 mL, 1.00 mmol, 2.5 M in hexanes) was added dropwise in 2 min. After stirring for 20 min at 0 $^{\circ}$ C, the solution was cooled to -78 $^{\circ}$ C and stirring was continued for another 5 min. To this reaction mixture a solution of **3** (397 mg, 1.00 mmol) in anhydrous THF (3 mL) was added via a syringe over the course of 5 min. The reaction mixture was stirred for 6 h at -78 $^{\circ}$ C,* and warmed up 20 $^{\circ}$ C without moving the cooling bath and stirred another 12 h at 20 $^{\circ}$ C. MeI (426 mg, 0.200 mL, 3.00 mmol) was added in one portion. The reaction was quenched with water (5 mL) and the aqueous phase was extracted with ether (2 x 15 mL). The combined organic phase was dried over MgSO₄. The solvent was removed *in vacuo* and the crude product was checked by GC-MS. The GC-MS spectra showed that there was no product detected and still a substantial amount of starting material left; some products from side reactions were also found, such as the quenched products from lithiation of both bromo and iodo groups and halogen dance reaction, which gave 1-hexyl-2-(4-hexylthiophen-2-yl)-1H-pyrrole and 2-bromo-5-(5-bromo-4-hexylthiophen-2-yl)-1-hexyl-1H-pyrrole respectively.

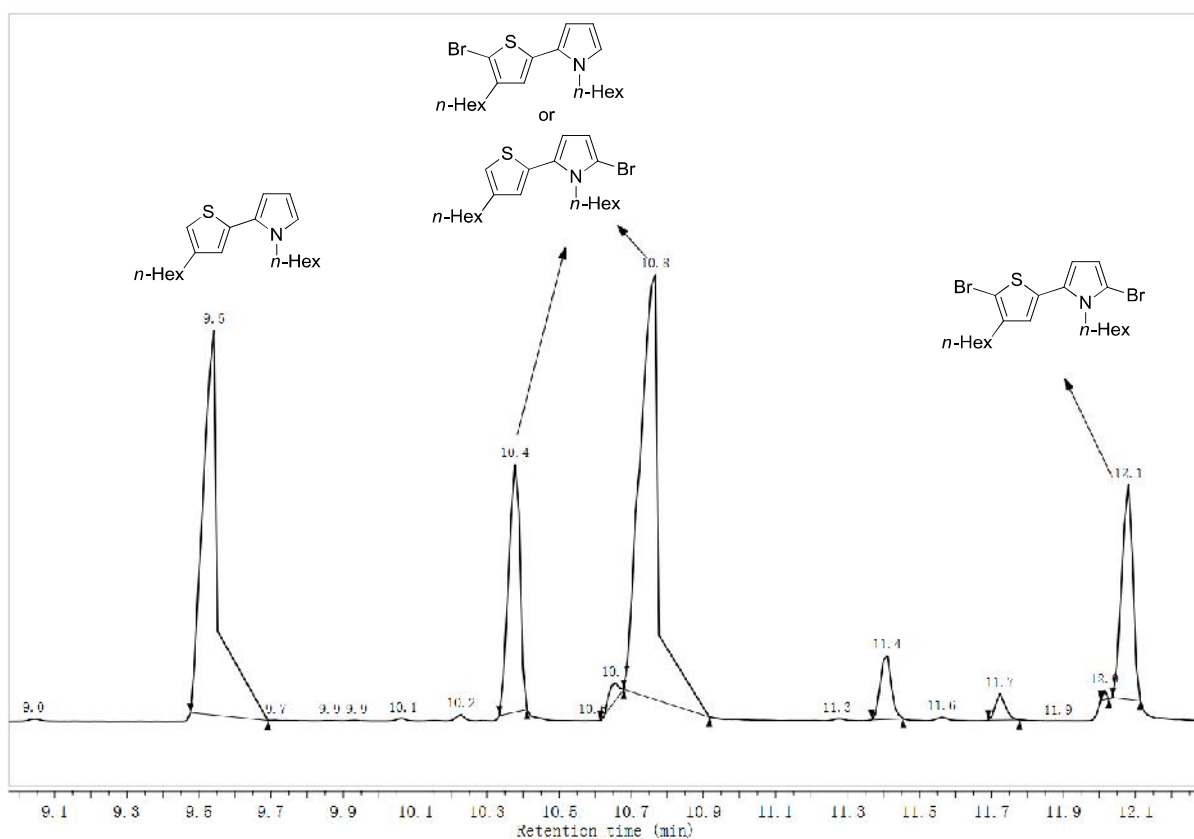
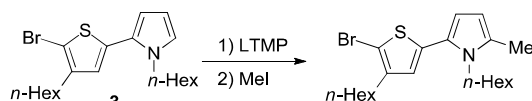


Figure SI 3. GC-MS trace of the lithiation of compound **3** with LDA.

* No product found by GC-MS analysis.

Lithiation of compound **3** with LTMP



2,2,6,6-Tetramethylpiperidine (141 mg, 187 μ L, 1.10 mmol) was added to THF (10 mL) in one portion. The solution was cooled to 0 $^{\circ}$ C and *n*-BuLi (0.40 mL, 1.00 mmol, 2.5 M in hexanes) was added dropwise in 2 min. After stirring for 20 min at 0 $^{\circ}$ C, the solution was cooled to -78 $^{\circ}$ C and stirring was continued for another 5 min. To this reaction mixture a solution of **3** (397 mg, 1.00 mmol) in anhydrous THF (3 mL) was added via a syringe over the course of 5 min. The reaction mixture was stirred for 4 h at -78 $^{\circ}$ C,[†] and warmed up 0 $^{\circ}$ C and stirred another 2 h at 0 $^{\circ}$ C. MeI (426 mg, 0.200 mL, 3.0 mmol) was added in one portion. The reaction was quenched with water (5 mL) and the aqueous phase was extracted with ether (2 x 15 mL). The combined organic phase was dried over MgSO₄. The solvent was removed *in vacuo* and the crude product was analyzed GC-MS and ¹H NMR spectroscopy. This showed that the crude product contained a some product, but also substantial amounts of starting material; and products of side reactions. These were lithiation of both bromo and iodo groups and halogen dance reaction, which gave 1-hexyl-2-(4-hexylthiophen-2-yl)-1*H*-pyrrole and 2-bromo-5-(5-bromo-4-hexylthiophen-2-yl)-1-hexyl-1*H*-pyrrole respectively.

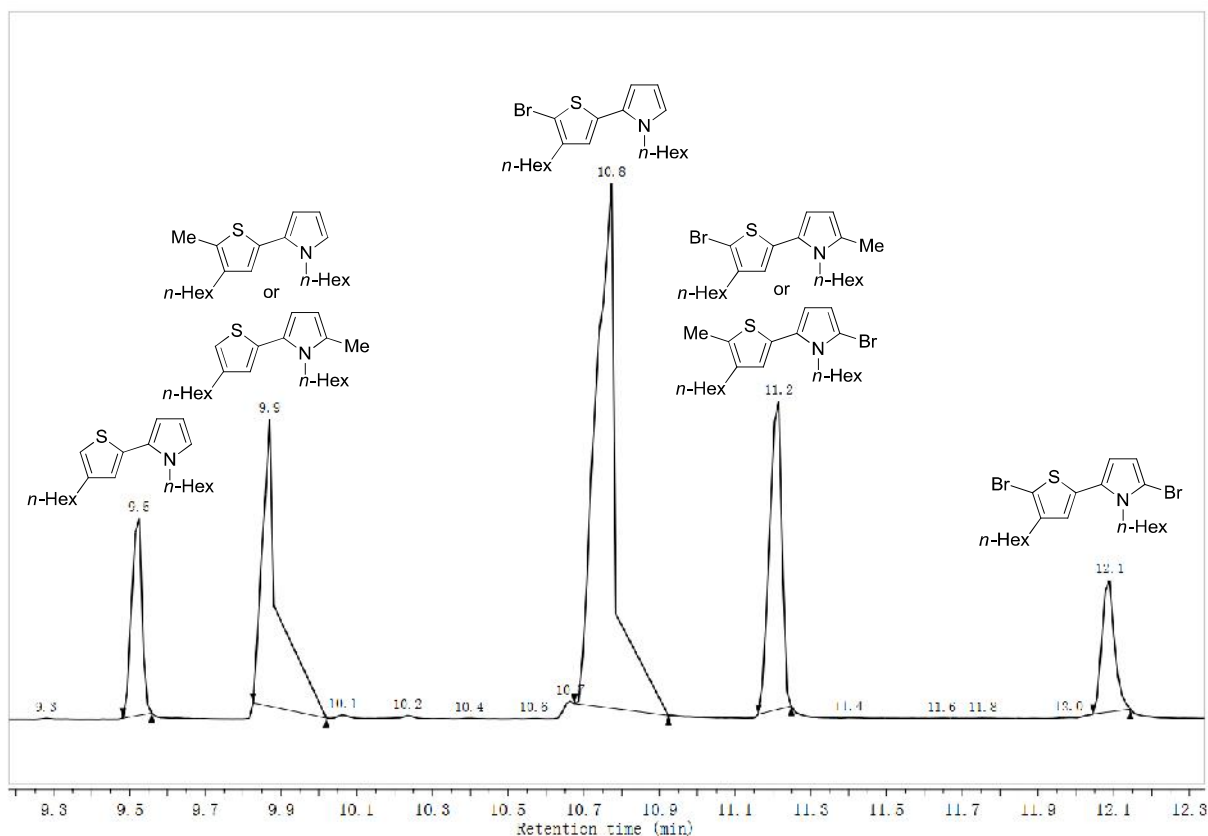
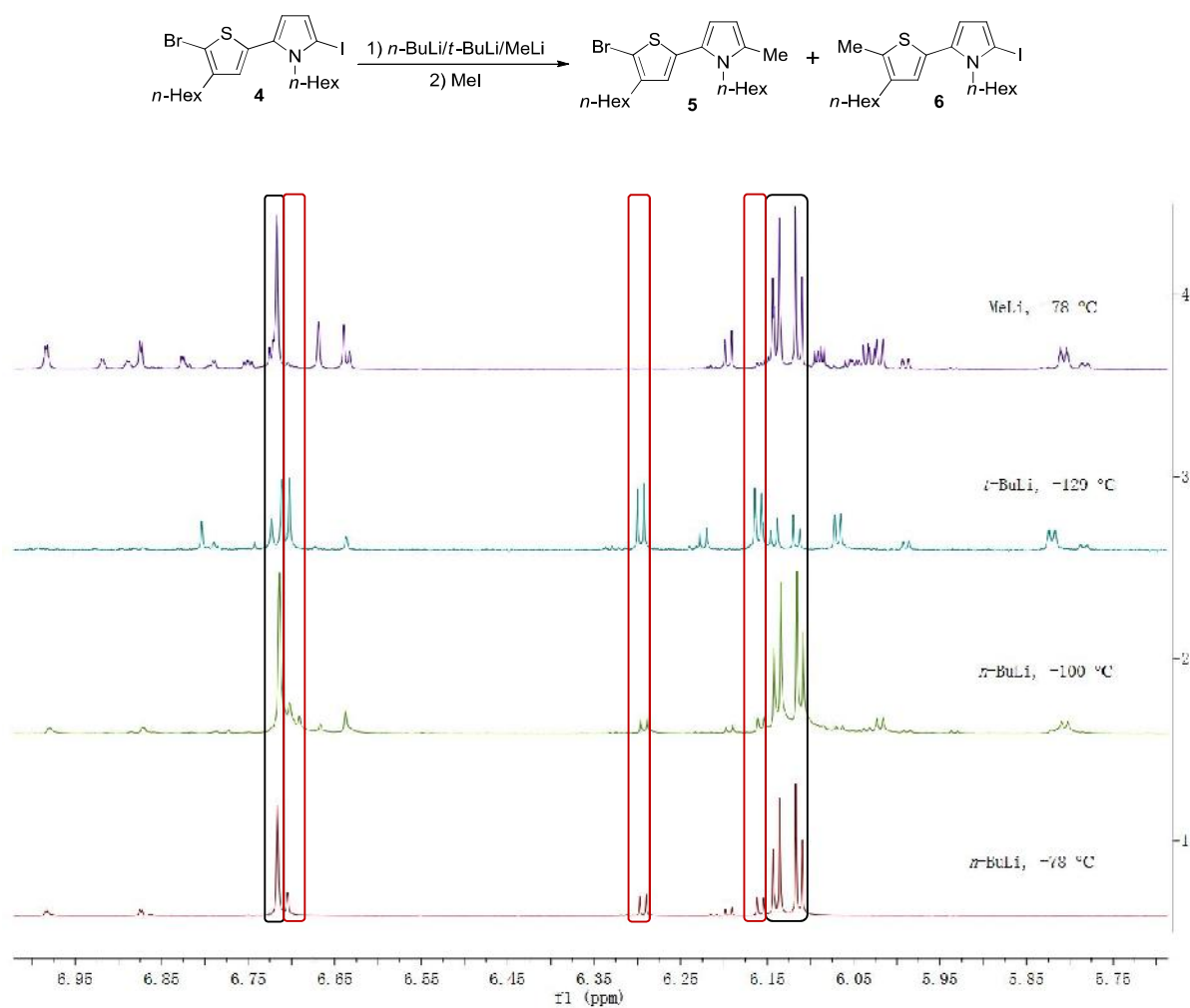
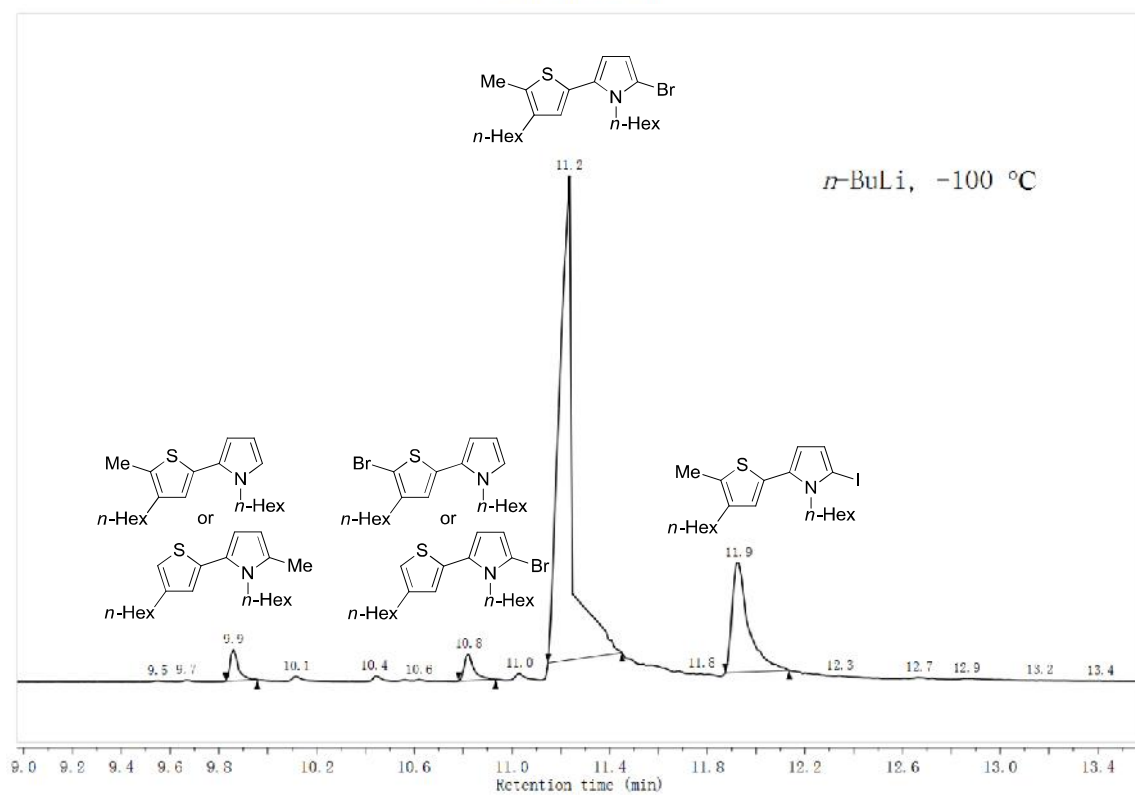
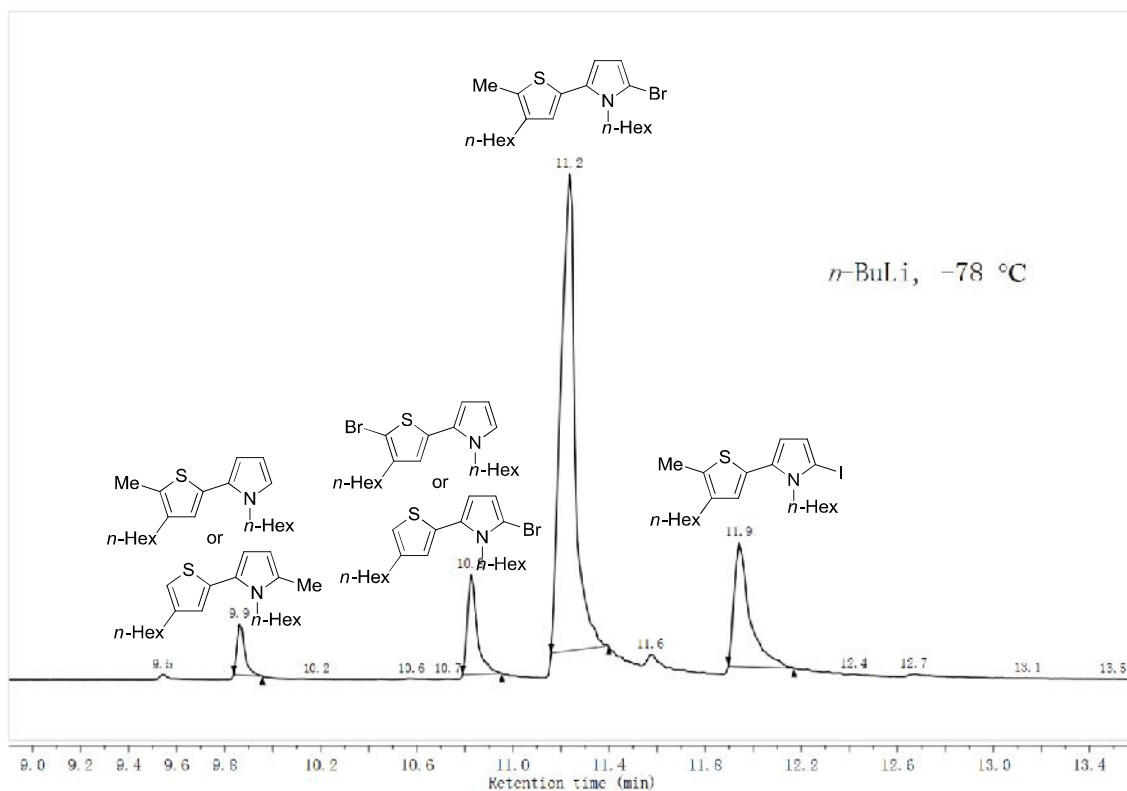


Figure SI 4. GC-MS trace of the lithiation of compound **3** with LTMP.

[†] The GC-MS showed there was a little product, but still a lot of starting mater left and side reactions happened, like lithiation of bromo group and halogen dance reaction.

NMR spectra of crude products obtained via the lithiation of precursor monomer 4.**Figure SI 5.** Signals from compound 5 are marked by the black box, signals from compound 6 are marked by a red box.

GC-MS spectra of crude products obtained via the lithiation of precursor monomer 4.



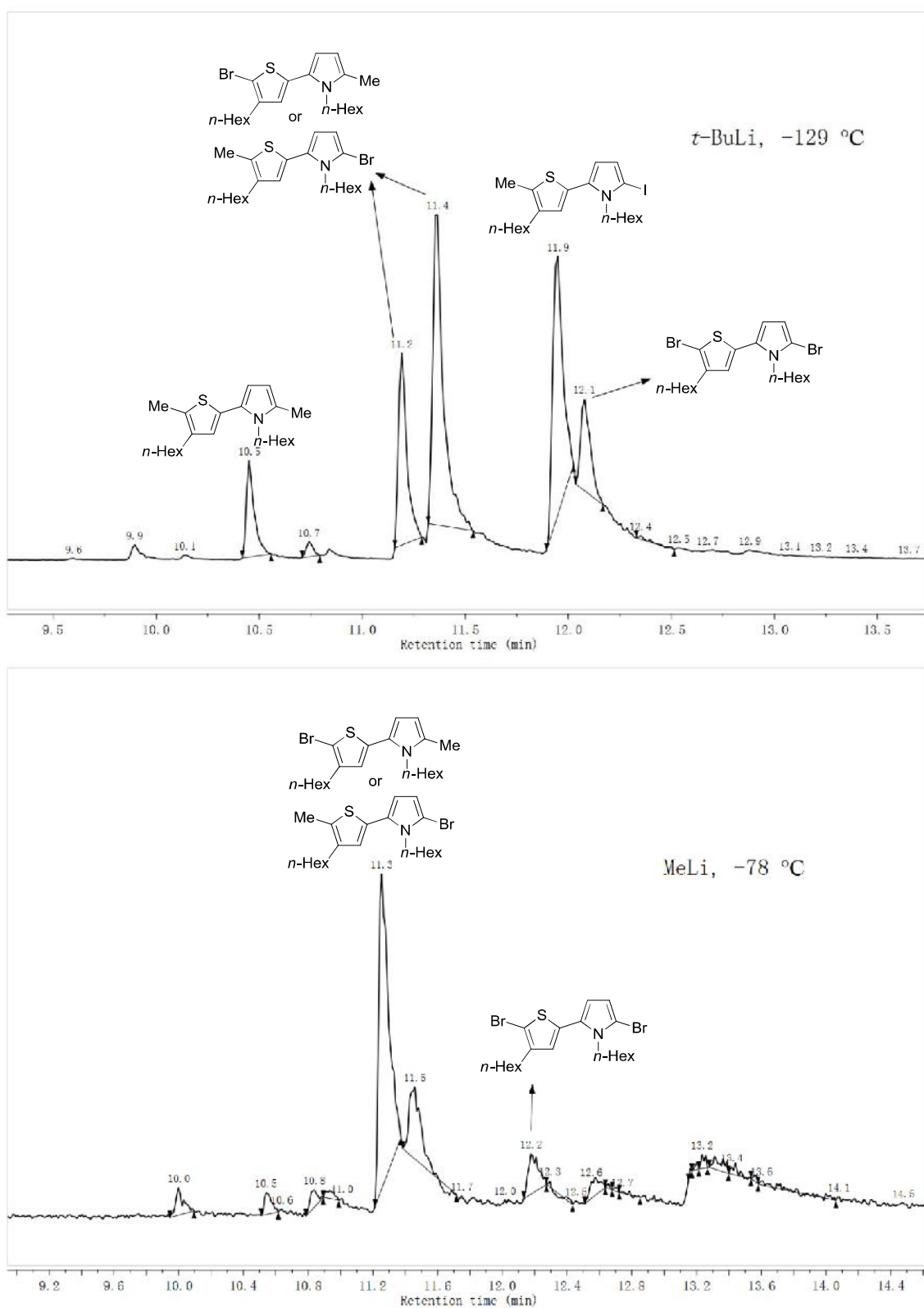
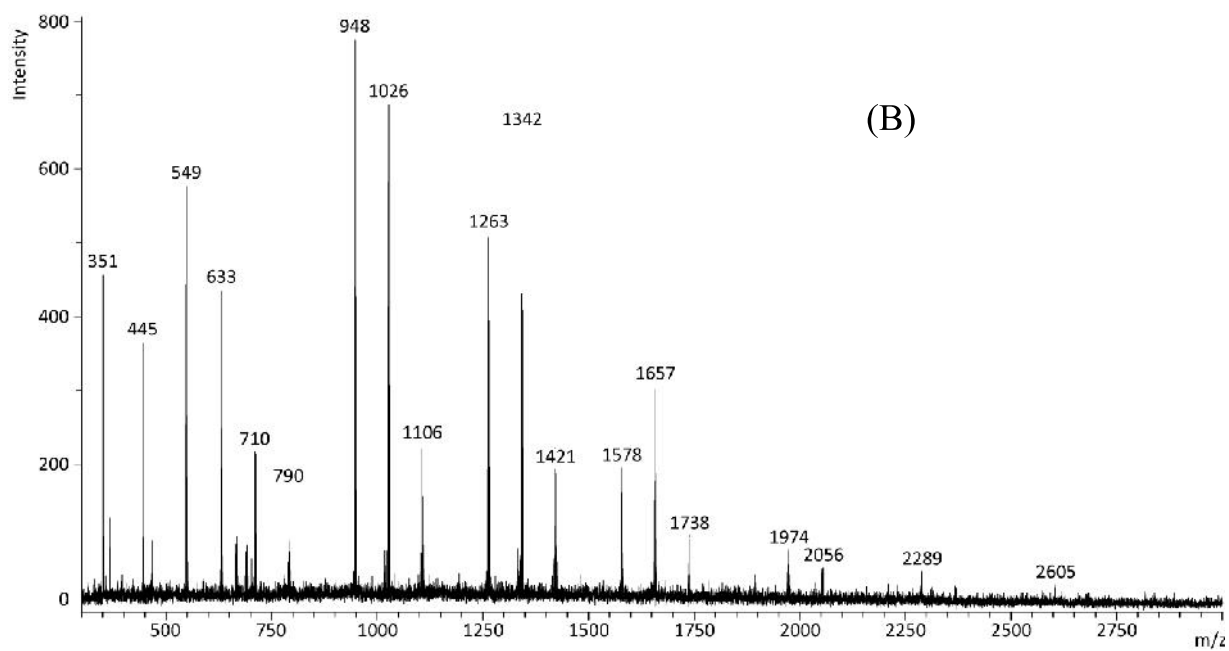
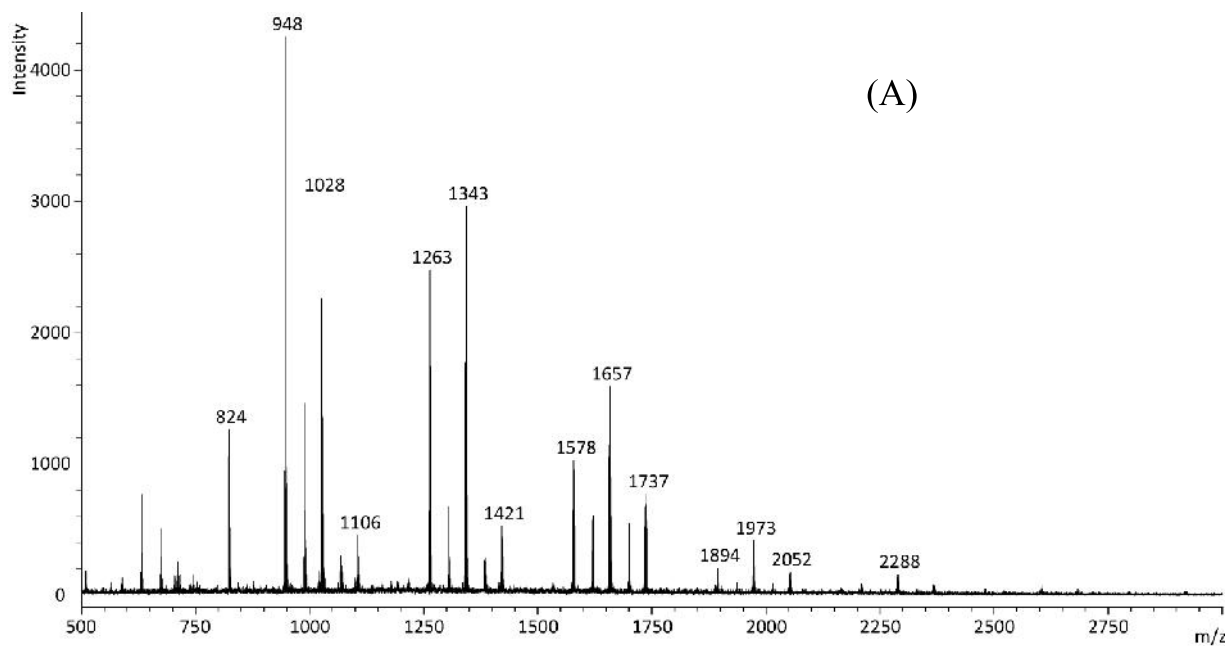


Figure SI 6. Lithiation of precursor monomer 4.

MALDI-TOF MS spectra of the poly(thiophene-*alt*-pyrrole)

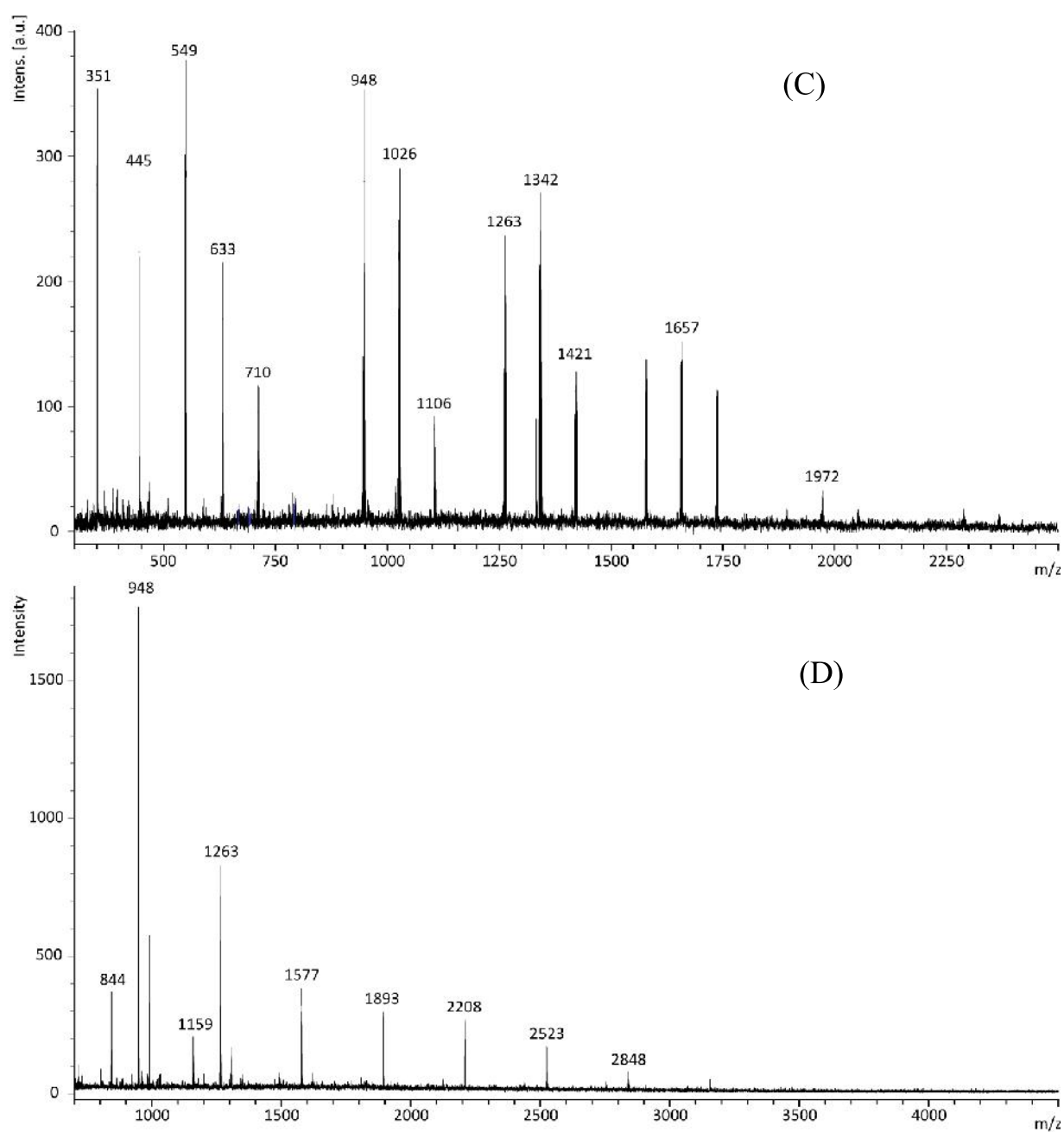


Figure SI 7. (A) polymer synthesized with *i*PrMgCl and [Ni(dppp)Cl₂]; (B) polymer synthesized with *t*BuMgCl·LiCl, 15-crown-5 and [Ni(dppp)Cl₂]; (C) polymer synthesized with *i*PrMgCl and [Pd(*t*Bu₃P)₂] (Table1, entry 6); (D) polymer synthesized with [*i*PrMgCl·LiCl] and [Pd(*t*Bu₃P)₂] (Table1, entry 10).

NMR spectra for the kinetic study of the polymerization of 7.

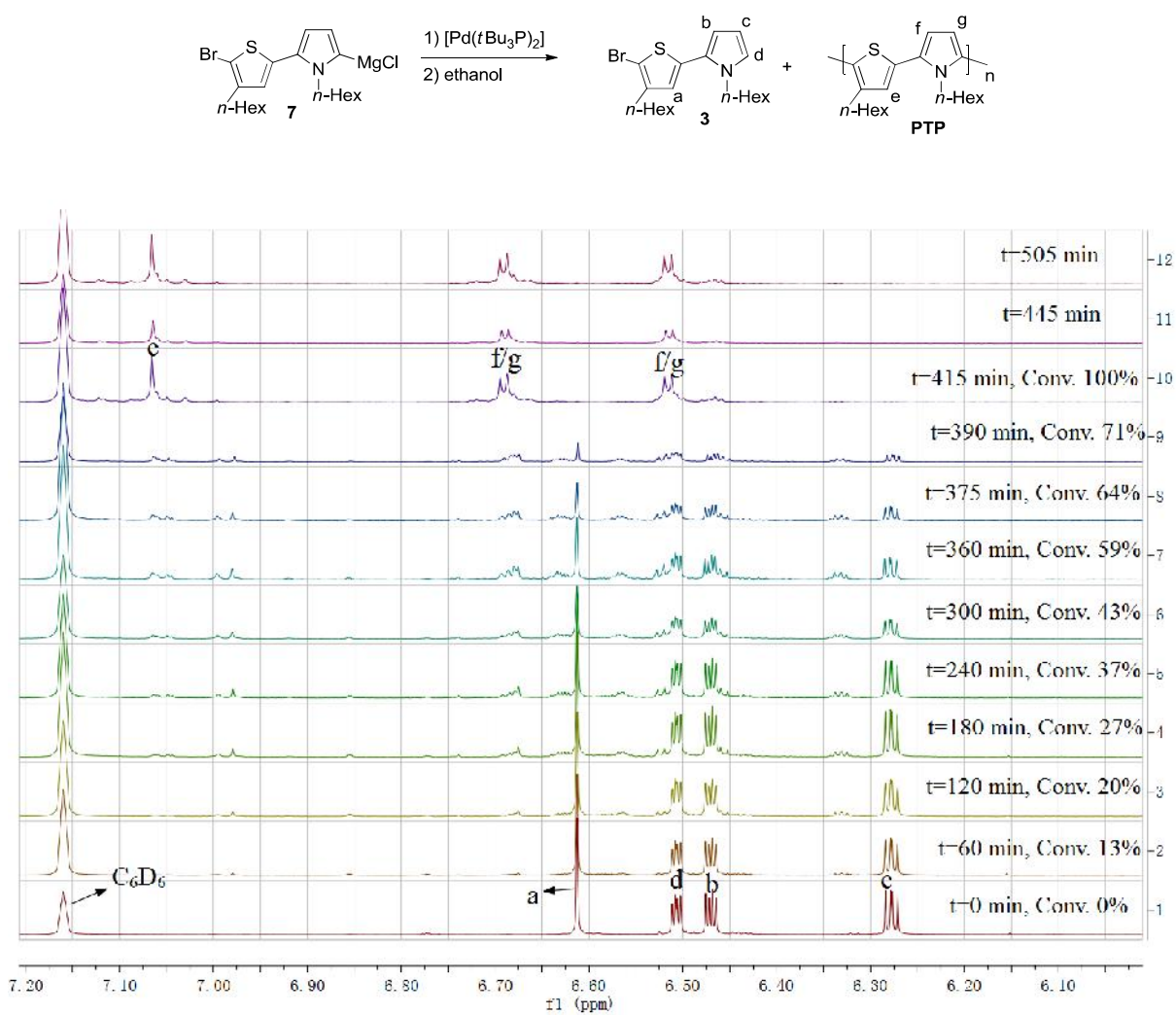


Figure SI 8. ^1H NMR spectra from the polymerization reaction

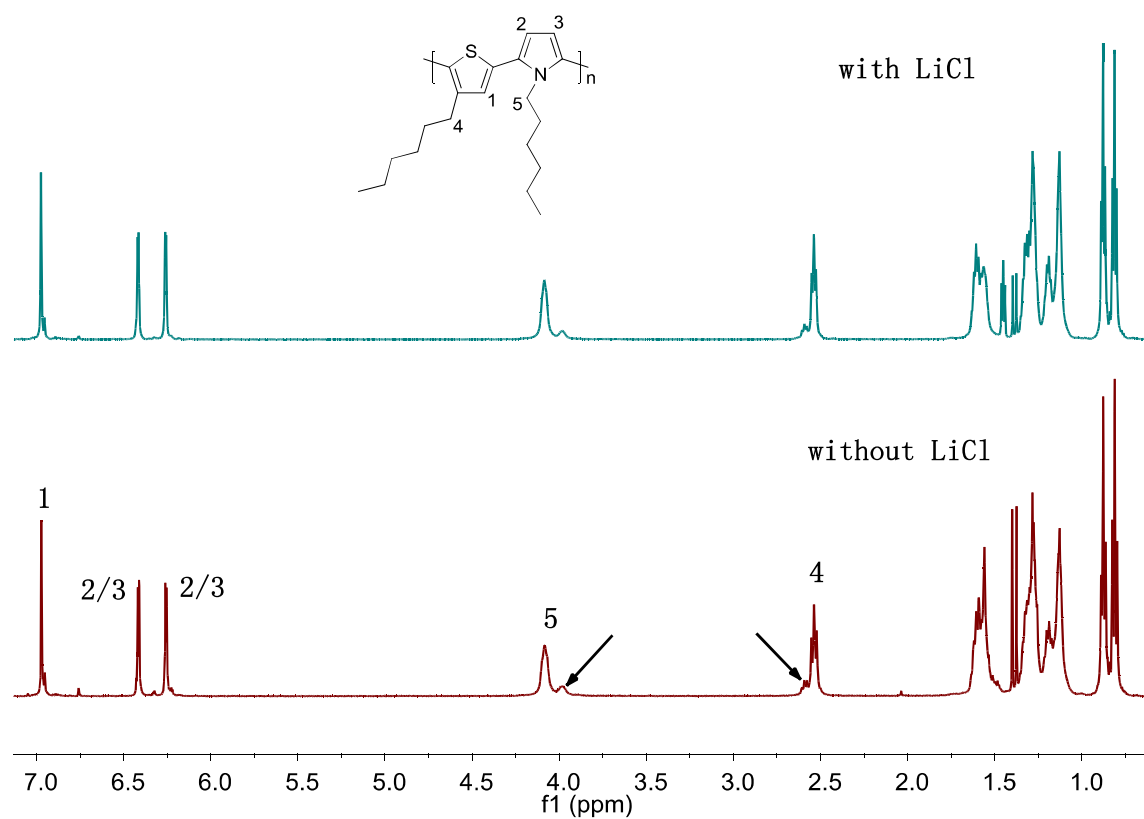
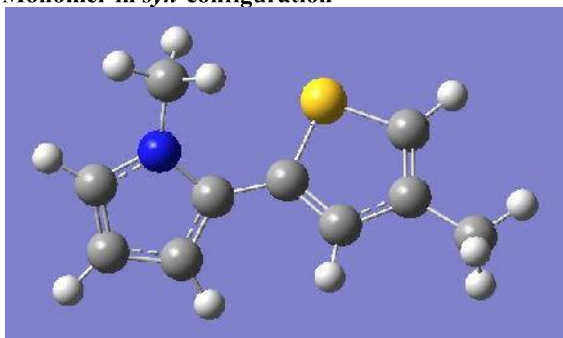
¹H NMR spectra for PTP (with LiCl and without LiCl).

Figure SI 9. ¹H NMR spectra of PTP (without the addition of LiCl [the conditions of Table 2, entry 6] and with the addition of LiCl [the condition of Table 2, entry 10])

DFT calculations

The geometry of the compounds was optimized at the B3LYP level,^{1,2} using the Programme Gaussian 9.0, revision D01.³ The results were visualized with the program GaussView 5.0.⁴ The 6-31+G(d,p) basis set was used for Li, C, N and H.⁵⁻⁷ To estimate the key thermochemical properties, full geometry optimization was followed by vibrational frequency calculations. These confirmed that true minima (only positive frequencies) or transition states (one negative frequency) were obtained. They also allowed to obtain corrections for zero-point energy, internal energy, and free energy (at 298.15K) in the rigid-rotor harmonic oscillator limit. For comparison, the electronic energies, E , the zero-point energy corrected energies E_{ZPE} (at 0 K), enthalpies ΔH (at 298.15 K), and free energies ΔG (at 298.15 K) are given in atomic units. To appreciate the torsions, the dihedral angles between the planes of the heterocycles are also given. They were always measured from the hetero atom in one cycle across the connecting carbon atoms to the hetero atom in the adjacent cycle. The coordinates are presented in Å.

Monomer in *syn*-configuration



Atom nr.	Atom	x	y	z
1	C	-3.598011	-1.246702	0.012960
2	C	-2.258699	-1.204840	-0.313036
3	C	-1.913209	0.158935	-0.467949
4	C	-3.051563	0.920677	-0.230352
5	N	-4.082897	0.038196	0.065238
6	H	-4.250180	-2.084216	0.213849
7	H	-1.608559	-2.059755	-0.432671
8	H	-0.951142	0.563373	-0.748607
9	C	-3.170226	2.371058	-0.245436
10	C	-2.235189	3.271107	0.209321
11	S	-4.502387	3.235767	-1.006723
12	C	-2.564639	4.643856	-0.026557
13	H	-1.334425	2.951682	0.722156
14	C	-3.768943	4.772169	-0.665021
15	H	-4.280034	5.684721	-0.940609
16	C	-5.449810	0.378405	0.425345
17	H	-5.462057	1.227292	1.112130

18	H	-6.053174	0.631808	-0.452678
19	H	-5.902971	-0.480739	0.923414
20	C	-1.697239	5.797404	0.400344
21	H	-1.532374	5.792614	1.484005
22	H	-0.710965	5.750282	-0.075605
23	H	-2.150607	6.756074	0.135029

$$E = -840.643588092$$

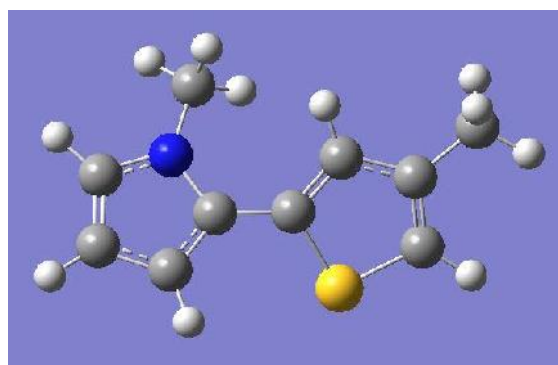
$$E_{ZPE} = -840.458298$$

$$\Delta H = -840.445818$$

$$\Delta G = -840.496644$$

$$\text{Dihedral angle: } -45.5^\circ$$

Monomer in *anti*-configuration



Atom nr.	Atom	x	y	z
1	C	-3.605147	-1.291963	0.094243
2	C	-2.256375	-1.191437	0.363850
3	C	-1.929047	0.184999	0.336123
4	C	-3.089271	0.896898	0.053031
5	N	-4.114292	-0.029976	-0.098288
6	H	-4.248410	-2.156843	0.020982
7	H	-1.586735	-2.016029	0.562381
8	H	-0.962269	0.630086	0.524716
9	C	-3.268247	2.332067	-0.092675
10	C	-4.308638	3.152079	0.282426
11	S	-1.994621	3.286961	-0.835666
12	C	-4.100221	4.540213	-0.003661
13	H	-5.191178	2.785787	0.794802
14	C	-2.885147	4.757695	-0.595831
15	H	-2.459849	5.702955	-0.904792
16	C	-5.496824	0.244773	-0.448259
17	H	-6.104891	0.475075	0.434262
18	H	-5.546309	1.090913	-1.135711
19	H	-5.917813	-0.634293	-0.940628
20	C	-5.094478	5.619736	0.330222
21	H	-6.047630	5.459137	-0.187219
22	H	-5.311473	5.644268	1.404469
23	H	-4.721261	6.606067	0.042611

$$E = -840.627807000$$

$$E_{ZPE} = -840.441907$$

$$\Delta H = -840.429540$$

$$\Delta G = -840.479843$$

Dihedral angle: -143.0°

Dimer in *anti-syn-anti* configuration



Atom nr.	Atom	x	y	z
1	C	-3.651073	-1.161035	0.403877
2	C	-3.205025	-1.031856	1.702670
3	C	-3.019031	0.349781	1.941613
4	C	-3.360278	1.036893	0.781412
5	N	-3.744597	0.088456	-0.160178
6	H	-3.909465	-2.039178	-0.169979
7	H	-3.037668	-1.841370	2.398617
8	H	-2.696246	0.815003	2.862336
9	C	-3.327620	2.467105	0.528524
10	C	-4.152505	3.267606	-0.229244
11	S	-2.088087	3.444493	1.291111
12	C	-3.812732	4.656633	-0.217012
13	H	-5.016837	2.886890	-0.761431
14	C	-2.710831	4.926228	0.566415
15	C	-4.140699	0.330218	-1.536454
16	H	-5.207685	0.566900	-1.619982
17	H	-3.566209	1.160762	-1.950354
18	H	-3.936788	-0.566749	-2.124799
19	C	-4.594345	5.693707	-0.977746
20	H	-4.596368	5.476860	-2.052588
21	H	-5.641196	5.715837	-0.653146
22	H	-4.175251	6.690579	-0.828745
23	C	-2.121195	6.228333	0.885813
24	C	-2.633235	7.241372	1.684421
25	C	-1.701738	8.299075	1.693630
26	H	-3.577941	7.194811	2.207019
27	C	-0.625476	7.924839	0.896224
28	H	-1.793958	9.247946	2.202662
29	C	0.581035	8.682433	0.600753
30	C	1.309073	8.808675	-0.560871
31	S	1.292298	9.678487	1.861176
32	C	2.425468	9.700780	-0.464891
33	H	1.035085	8.311698	-1.484498
34	C	2.527374	10.250502	0.785022
35	H	3.262289	10.962219	1.136119
36	N	-0.884717	6.651389	0.411586
37	C	-0.026065	5.887905	-0.480625

38	H	-0.216394	4.824221	-0.342139
39	H	-0.211192	6.139920	-1.531267
40	H	1.018860	6.097425	-0.248301
41	C	3.354540	10.001887	-1.610134
42	H	3.872531	9.098330	-1.952549
43	H	2.809342	10.406473	-2.470730
44	H	4.114659	10.732993	-1.322841

$$E = -1680.06131435$$

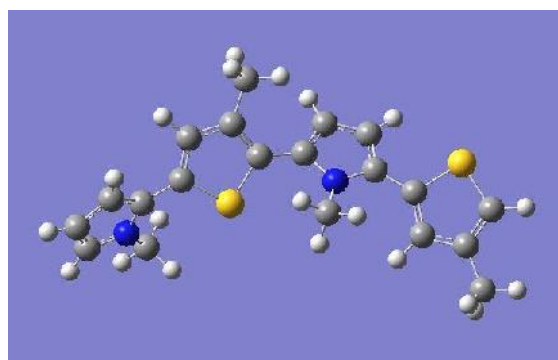
$$E_{\text{ZPE}} = -1679.709231$$

$$\Delta H = -1679.684762$$

$$\Delta G = -1679.765134$$

Dihedral angle: -145.6° , 73.4° , -142.6°

Dimer in *syn-syn-anti* conformation



Atom Nr.	Atom	x	y	z
1	C	-3.565279	-1.293821	0.097448
2	C	-2.762197	-1.139530	-1.013423
3	C	-2.623066	0.251230	-1.232854
4	C	-3.345189	0.916819	-0.247905
5	N	-3.920592	-0.051866	0.565219
6	H	-3.914304	-2.185457	0.597710
7	H	-2.333214	-1.938468	-1.601238
8	H	-2.082825	0.737150	-2.032802
9	C	-3.469255	2.352782	-0.055341
10	C	-2.489437	3.291424	-0.279857
11	S	-4.976680	3.161192	0.347485
12	C	-2.909311	4.648701	-0.145894
13	H	-1.474383	3.009153	-0.537713
14	C	-4.244125	4.759276	0.194966
15	C	-4.727125	0.168755	1.755013
16	H	-4.300406	0.970412	2.361342
17	H	-5.760252	0.432465	1.505588
18	H	-4.734928	-0.749306	2.345375
19	C	-1.974874	5.810533	-0.353767
20	H	-1.259200	5.899821	0.472683
21	H	-1.390134	5.679315	-1.270819
22	H	-2.521233	6.753339	-0.421257
23	C	-4.993964	5.964188	0.526768
24	C	-4.672014	6.968652	1.432386

25	C	-5.714025	7.915942	1.418214
26	H	-3.794452	6.972583	2.062661
27	C	-6.670675	7.482825	0.506234
28	H	-5.800621	8.801157	2.032158
29	C	-7.925626	8.118452	0.145075
30	C	-9.153849	7.575297	-0.160530
31	S	-8.018781	9.871842	0.097103
32	C	-10.177969	8.541646	-0.421276
33	H	-9.340858	6.507295	-0.157766
34	C	-9.706469	9.822098	-0.305314
35	H	-10.257654	10.743761	-0.433970
36	N	-6.221629	6.287909	-0.039719
37	C	-6.821147	5.595780	-1.173117
38	H	-6.031442	5.146258	-1.776362
39	H	-7.505809	4.802765	-0.854199
40	H	-7.374436	6.313437	-1.779630
41	C	-11.599193	8.181467	-0.761512
42	H	-11.652303	7.596646	-1.687267
43	H	-12.057411	7.575934	0.028986
44	H	-12.213863	9.075259	-0.896053

E = -1680.06245192
 E_{ZPE} = -1679.710327
 ΔH = -1679.685933
 ΔG = -1679.765589

Dihedral angles: -43.8°, -55.3°, -145.0°

Dimer in *syn-syn-syn* conformation

Atom nr.	Atom	x	y	z
1	C	-3.545984	-1.283615	0.014435
2	C	-2.685902	-1.101936	-1.048593
3	C	-2.542473	0.293789	-1.230152
4	C	-3.319054	0.934829	-0.270625
5	N	-3.931842	-0.053640	0.489557
6	H	-3.916896	-2.187260	0.475865
7	H	-2.222691	-1.886204	-1.630149
8	H	-1.963302	0.799185	-1.989804
9	C	-3.459336	2.365832	-0.053902
10	C	-2.473947	3.312254	-0.213012
11	S	-4.987126	3.160361	0.295103
12	C	-2.905575	4.664837	-0.070462
13	H	-1.446787	3.038729	-0.429027
14	C	-4.255313	4.763489	0.210154
15	C	-4.802066	0.137679	1.638946
16	H	-4.411210	0.925721	2.285934
17	H	-5.821009	0.404949	1.340059
18	H	-4.838769	-0.793843	2.206699
19	C	-1.967779	5.834092	-0.210867
20	H	-1.278896	5.897260	0.640365
21	H	-1.353674	5.733695	-1.112647
22	H	-2.514067	6.777725	-0.265371
23	C	-5.024779	5.958731	0.533063

24	C	-4.750411	6.940122	1.478737
25	C	-5.795050	7.884699	1.438255
26	H	-3.904929	6.928669	2.151484
27	C	-6.701289	7.474877	0.466873
28	H	-5.920931	8.751414	2.071088
29	C	-7.928381	8.146385	0.067614
30	C	-8.115043	9.504160	-0.050926
31	S	-9.459664	7.312745	-0.179336
32	C	-9.458741	9.896367	-0.348256
33	H	-7.296172	10.207417	0.055652
34	C	-10.288744	8.812474	-0.456092
35	H	-11.342356	8.806270	-0.700741
36	N	-6.223849	6.295047	-0.084733
37	C	-6.770172	5.630154	-1.261997
38	H	-5.959686	5.137533	-1.799828
39	H	-7.520288	4.878273	-0.997370
40	H	-7.233438	6.371437	-1.914293
41	C	-9.890822	11.325324	-0.539580
42	H	-9.708612	11.920055	0.362937
43	H	-9.338435	11.802916	-1.357034
44	H	-10.956689	11.390944	-0.773118

E = -1680.06154718
 E_{ZPE} = -1679.709623
 ΔH = -1679.685105
 ΔG = -1679.765260

Dihedral angles: -43.5°, -55.6°, 45.7°

Dimer in *anti-anti-anti* configuration

This hypothetical structure could not be optimized as it was either too high in energy or did not exist as a stable structure.

DSC heating and cooling curves for PTP at 3 °C /min under N₂.

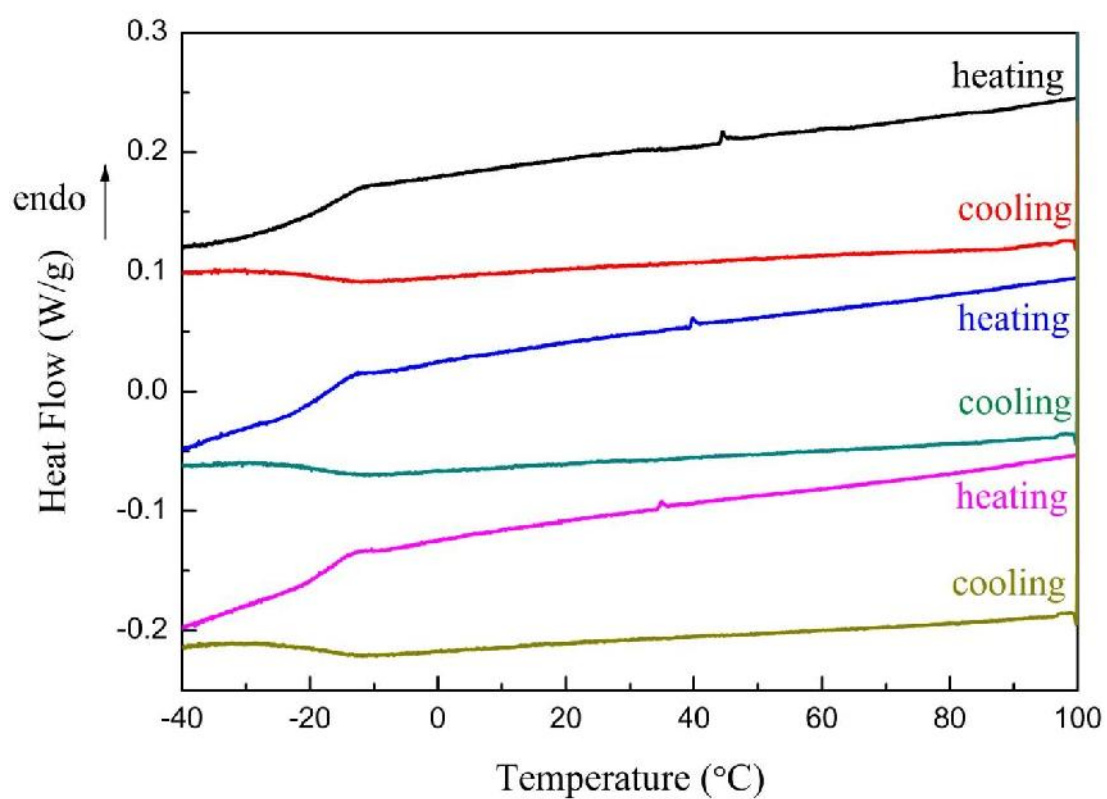
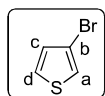


Figure SI 10. A sample of the polymer was subjected to DSC using three heating and cooling samples. All three measurements suggest a T_g of ca. -14 °C.

Synthesis**3-Bromothiophene (9)**

3-Bromothiophene was prepared similar to a method described by Bjørnholm et al.⁸ and was modified as follows: To a solution of thiophene (16.0 mL, 200 mmol), 48% aqueous HBr (100 mL) and diethyl ether (25 mL), a solution of bromine (33.4 mL, 650 mmol) in 48% aqueous HBr (80 mL) was added under vigorous stirring in a dropwise fashion within 3.5 h by using an addition funnel at 22 °C. The reaction mixture was stirred for another 19 h at 22 °C. Then the mixture was quenched by an aqueous saturated solution of Na₂S₂O₃ (150 mL). The aqueous layer was extracted with dichloromethane (3 x 100 mL). The combined organic phases were washed with brine (150 mL) and dried over MgSO₄. The solvent was removed *in vacuo* to receive a red brown oil, which was used in the subsequent step without further purification.

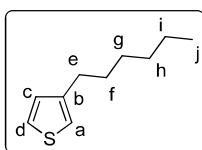
Zinc (52.5 g, 800 mmol) was dispersed in a mixture of water (240 mL) and acetic acid (50 mL) and heated to reflux for 30 min. Then the oil bath was removed and the red brown oil from the reaction described above was dissolved in acetic acid (50 mL) and added dropwise over the course of 3 h. After completion of the addition, the reaction mixture was heated up for another 4 h to reflux. The solution was filtered and the filter cake washed with *n*-hexane (50 mL). Then the aqueous phase was extracted with *n*-hexane (3 x 150 mL). The combined organic phase was dried over MgSO₄. The solvent was removed *in vacuo* and the crude product was purified by vigreux distillation (50 °C, 6 mbar) to receive 15.6 g (48%, lit.⁸ 21%) of slightly yellow oil.

¹H NMR (500 MHz, CDCl₃): δ = 7.28 (dd, ³*J* = 5.1 Hz, ⁴*J* = 3.2 Hz, 1 H, H-d), 7.24 (dd, ⁴*J* = 3.2 Hz, ⁴*J* = 1.3 Hz, 1 H, H-a), 7.03 (dd, ³*J* = 5.1 Hz, ⁴*J* = 1.3 Hz, 1 H, H-c) ppm.

¹³C NMR (126 MHz, CDCl₃): δ = 130.0 (C-c), 126.6 (C-d), 122.7 (C-a), 110.0 (C-b) ppm.

HRMS (EI-sector) *m/z*: [M]⁺ Calcd for [C₄H₃BrS]⁺ 161.9139; Found 161.9143.

IR (ATR): $\tilde{\nu}$ = 3110 (m), 1493 (s), 1442 (w), 1399 (w), 1353 (m), 1195 (m), 1085 (m), 973 (w), 880 (s), 845 (s), 797 (w), 758 (vs), 677 (m), 621 (w), 584 (s) cm⁻¹.

3-Hexylthiophene (10)

3-Hexylthiophene was prepared similarly to a method described by Ng et al.⁹ and was modified as follows: magnesium (2.55 g, 105 mmol) was stirred without solvent under nitrogen for 1 h in order to activate the surface. A solution of 1-bromohexane (14.9 g, 90.0 mmol) in dry diethyl ether (75 mL) was added dropwise to a suspension of the activated magnesium in diethyl ether (45 mL) within 1 h at 20 °C. The reaction mixture was heated to reflux for another 1 h. The resulting Grignard reagent was added to 3-bromothiophene (12.23 g, 75.00 mmol) and [Ni(dppp)Cl₂] (81 mg, 15 mmol, 0.2 mol%) in diethyl ether (45 mL) at 0 °C via syringe over the course of 30 min and the mixture was stirred for 4 h at 20 °C. The reaction mixture was quenched with aqueous hydrochloric acid (1 M, 60 mL) at 0 °C. Then the aqueous layer was extracted with diethyl ether (4 x 50 mL). The combined organic layers were dried over MgSO₄ and the volatiles were removed *in vacuo*. The residue was purified by vigreux distillation (110 °C, 6 mbar) to yield 10.2 g (81%, lit.⁹ 71%) of colorless oil.

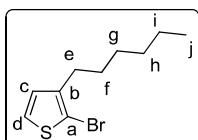
¹H NMR (500 MHz, CDCl₃): δ = 7.24 (dd, ³*J* = 4.9 Hz, ⁴*J* = 2.9 Hz, 1 H, H-d), 6.95 (dd, ³*J* = 4.9 Hz, ⁴*J* = 1.2 Hz, 1 H, H-c), 6.93 (dd, ⁴*J* = 2.9 Hz, ⁴*J* = 1.2 Hz, 1 H, H-a), 2.64 (t, ³*J* = 7.6 Hz, 2 H, H-e), 1.66-1.60 (m, 2 H, H-f), 1.38-1.30 (m, 6 H, H-g, h, i), 0.91 (t, ³*J* = 7.0 Hz, 3 H, H-j) ppm.

^{13}C NMR (126 MHz, CDCl_3): δ = 143.3 (C-b), 128.3 (C-c), 125.0 (C-d), 119.8 (C-a), 31.7, 30.5, 30.3, 29.0 (C-e, f, g, h), 22.6 (C-i), 14.1 (C-j) ppm.

HRMS (EI-sector) m/z : $[\text{M}]^+$ Calcd for $[\text{C}_{10}\text{H}_{16}\text{S}]^+$ 168.0973; Found 168.0972.

IR (ATR): $\tilde{\nu}$ = 2995 (m), 2925 (s), 2855 (m), 1537 (w), 1478 (m), 1409 (w), 1377 (w), 1234 (w), 1153 (w), 1079 (w), 936 (w), 855 (m), 834 (m), 769 (s), 680 (m), 660 (w), 632 (m), 577 (w) cm^{-1} .

2-Bromo-3-hexylthiophene (11)



2-Bromo-3-hexylthiophene was prepared similarly to a method described by Carlsen et al.¹⁰ and was modified as follows: 3-hexylthiophene (12.0 g, 71.3 mmol) was dissolved in glacial acetic acid (100 mL) under an air atmosphere. Then NBS (12.7 g, 71.5 mmol) was added in one portion. The reaction mixture was stirred for 2.5 h at 22 °C. Then the solution was poured into water (200 mL) and diethyl ether (250 mL). After extraction, the organic phase was separated and washed with aqueous NaOH (2 M, 5 x 150 mL), followed by water (3 x 150 mL). The organic layer was dried over MgSO_4 and then the solvent was removed *in vacuo*. The crude product was purified by vigreux distillation (130 °C, 4×10^{-2} mbar) to receive 13.5 g (77%, lit.¹⁰ 92%) of light yellow oil.

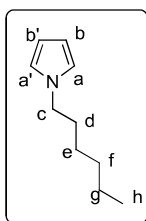
^1H NMR (500 MHz, CDCl_3): δ = 7.18 (d, 3J = 5.6 Hz, 1 H, H-d), 6.79 (d, 3J = 5.6 Hz, 1 H, H-c), 2.56 (t, 3J = 7.6 Hz, 2 H, H-e), 1.60-1.54 (m, 2 H, H-f), 1.36-1.27 (m, 6 H, H-g, h, i), 0.88 (t, 3J = 7.0 Hz, 3 H, H-j) ppm.

^{13}C NMR (126 MHz, CDCl_3): δ = 142.0 (C-b), 128.2 (C-c), 125.1 (C-d), 108.8 (C-a), 31.6, 29.7, 29.4, 28.9 (C-e, f, g, h), 22.6 (C-i), 14.1 (C-j) ppm.

HRMS (EI-sector) m/z : $[\text{M}]^+$ Calcd for $[\text{C}_{10}\text{H}_{15}\text{BrS}]^+$ 246.0078; Found 246.0086.

IR (ATR): $\tilde{\nu}$ = 2995 (m), 2924(s), 2855(m), 1539(w), 1457 (m), 1409(m), 1377 (w), 1275(w), 1261(w), 1228(w), 1087(w), 991(s), 874(w), 829(m), 764(s), 750(s), 711(s), 683(s), 634(s), 580(m), 466(w) cm^{-1} .

1-Hexyl-1H-pyrrole (12)



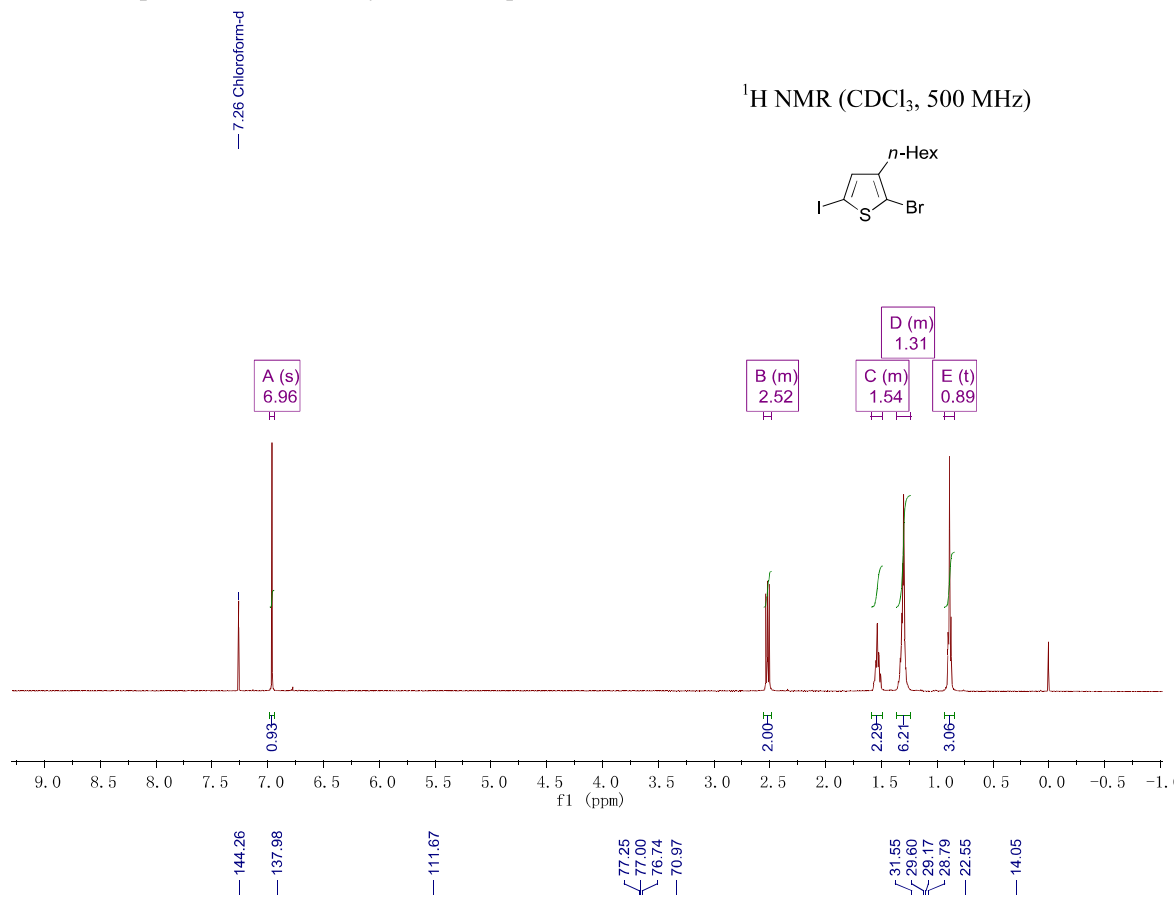
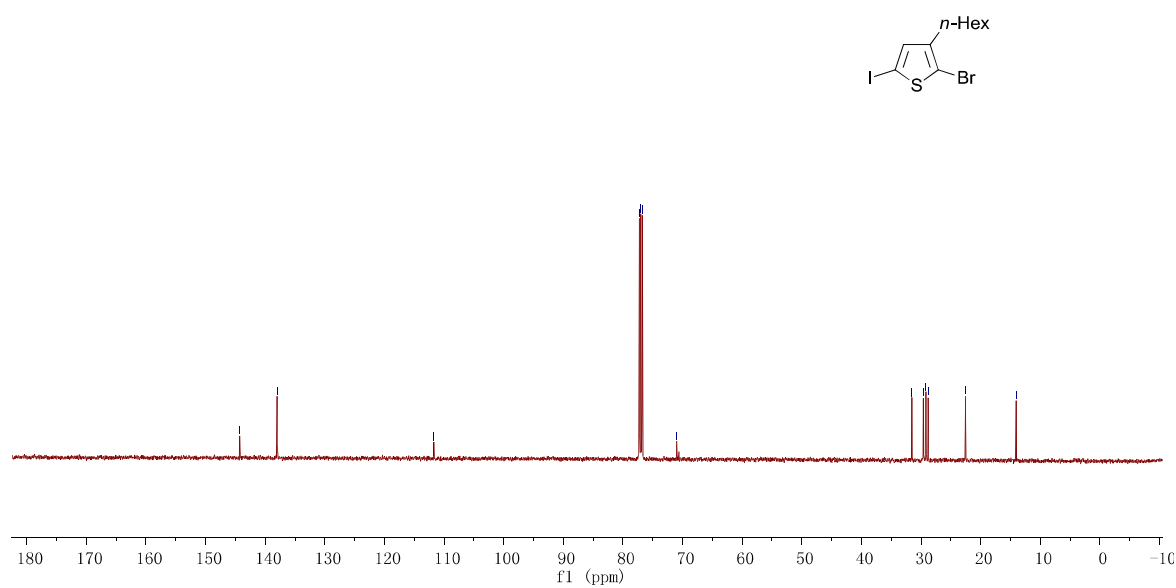
1-Hexyl-1H-pyrrole was prepared similarly to a method described by Piomelli et al.¹¹ and was modified as follows: pyrrole (10.0 mL, 144 mmol) was added dropwise over the course of 30 min at 0 °C to a stirred solution of sodium hydride (10.7g of 60% mineral oil dispersion, 267 mmol) in DMF (320 mL). After hydrogen evolution had ceased, 1-bromohexane (29.6 mL, 210 mmol) was added in one portion. The reaction mixture was allowed to warm up to 20 °C within 15 min by removing the cooling bath and it was stirred at 20 °C for 9 h. The reaction was quenched by adding water (80 mL). DCM (100 mL) was added and the organic layer was washed with water (6 x 300 mL) and dried over MgSO_4 . After the solvent was removed *in vacuo*, the product (17.54 g, 81%) was obtained by vigreux distillation (115 °C, 6 mbar) as colorless oil.

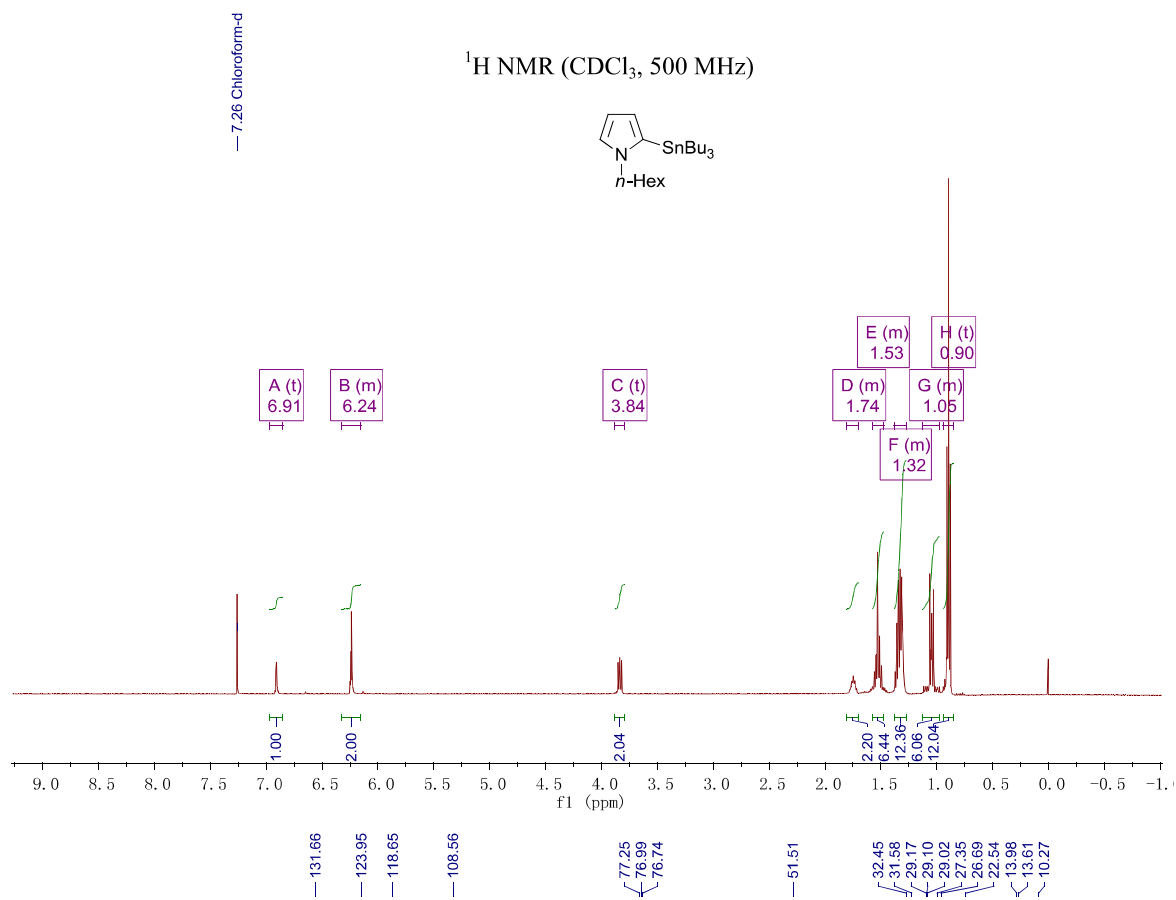
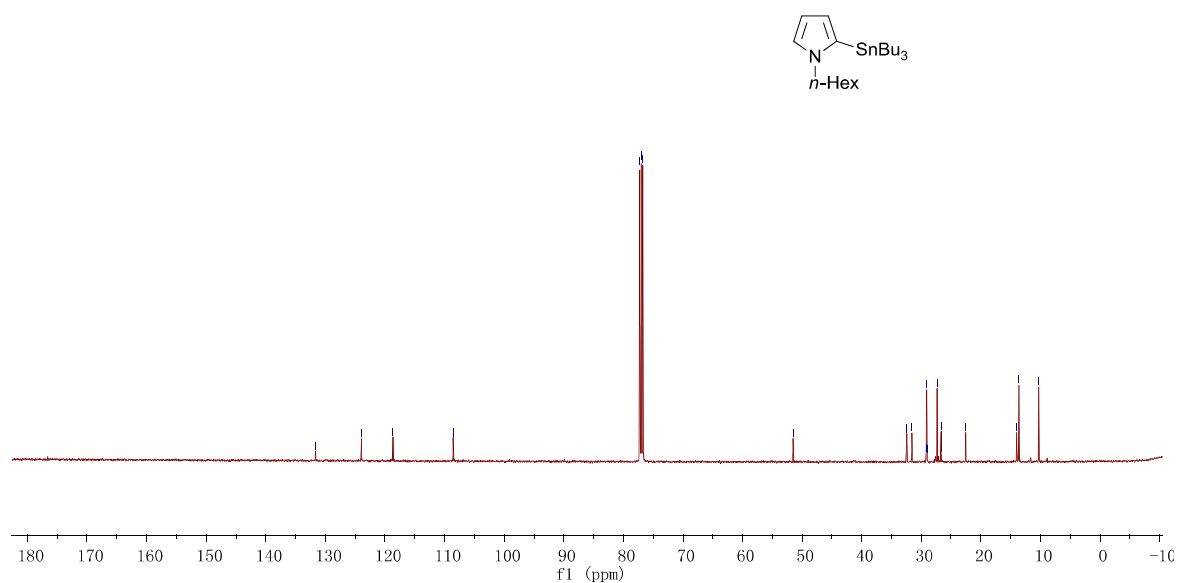
^1H NMR (500 MHz, CDCl_3): δ = 6.68 (a t, $^{12,3}J$ = 2.1 Hz, 2 H, H-a, a'), 6.16 (a t, $^{12,3}J$ = 2.1 Hz, 2 H, H-b, b'), 3.89 (t, 3J = 7.2 Hz, 2 H, H-c), 1.81-1.76 (m, 2 H, H-d), 1.36-1.32 (m, 6 H, H-e, f, g), 0.92 (t, 3 H, 3J = 6.8 Hz, H-h) ppm.

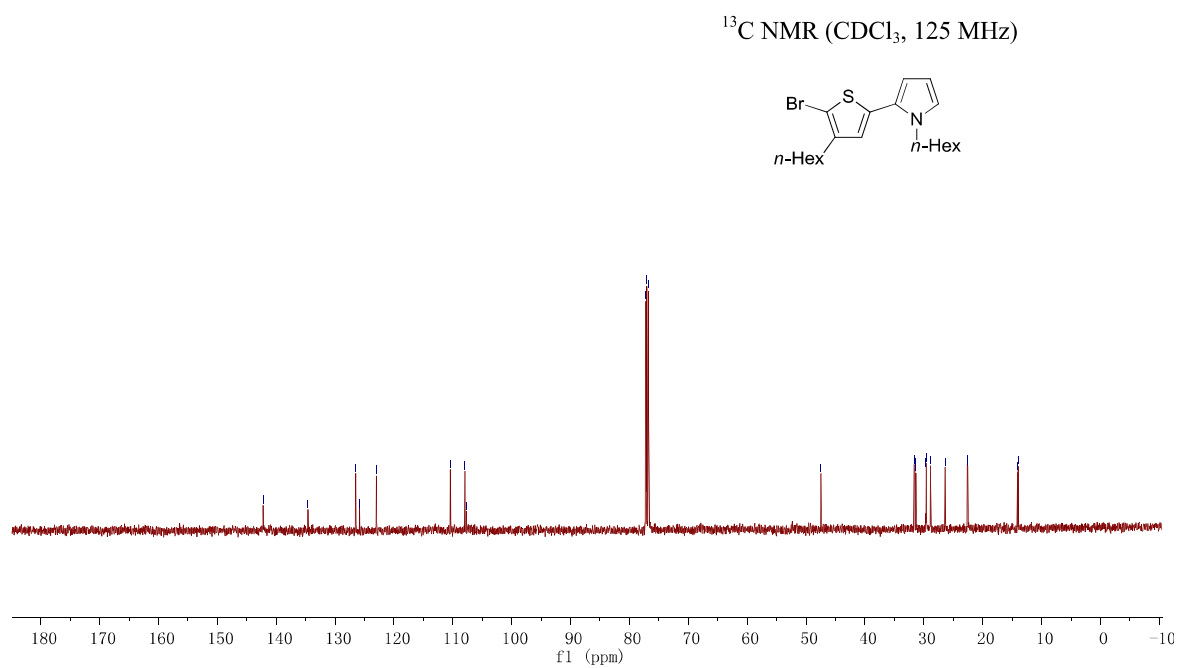
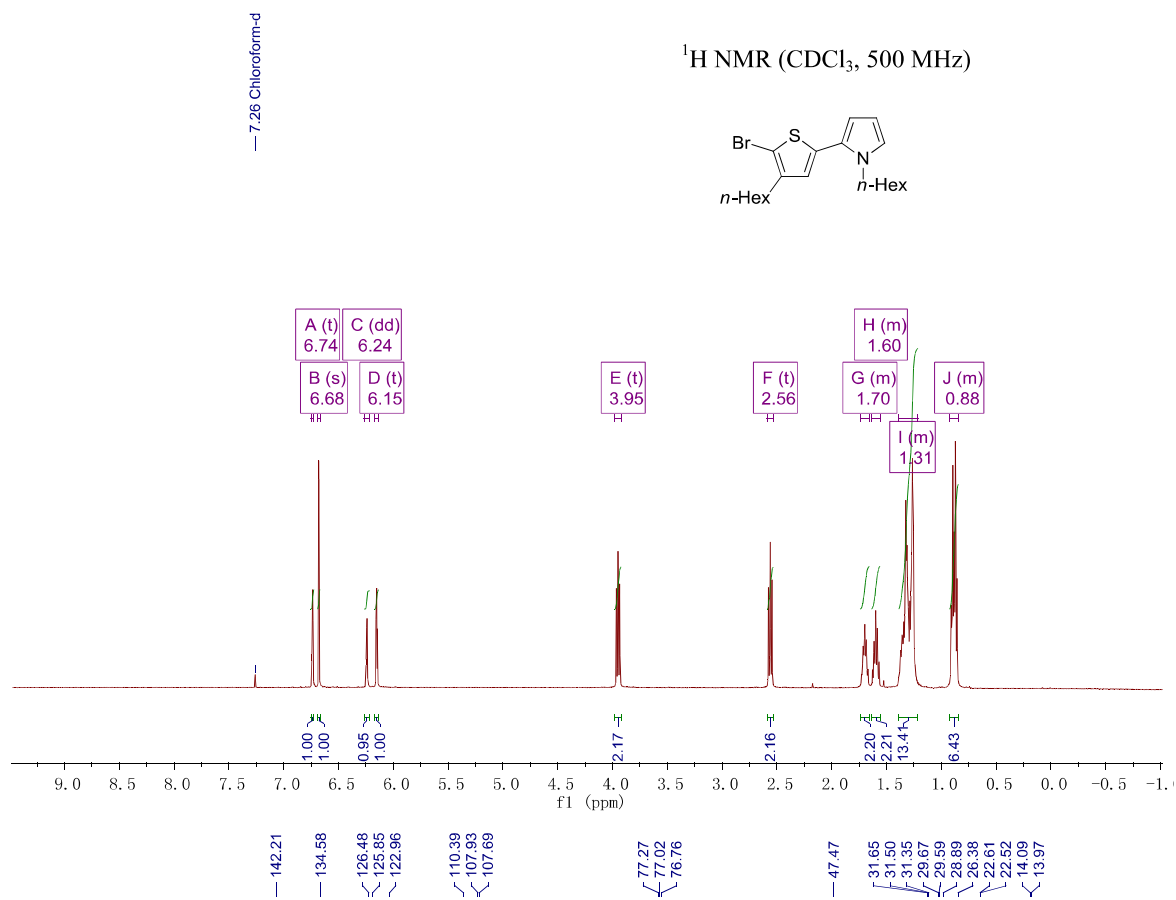
^{13}C NMR (126 MHz, CDCl_3): δ = 120.5 (C-a, a'), 107.8 (C-b, b'), 49.7 (C-c), 31.6 (C-d), 31.4 (C-e), 26.5 (C-f), 22.5 (C-g), 14.0 (C-h) ppm.

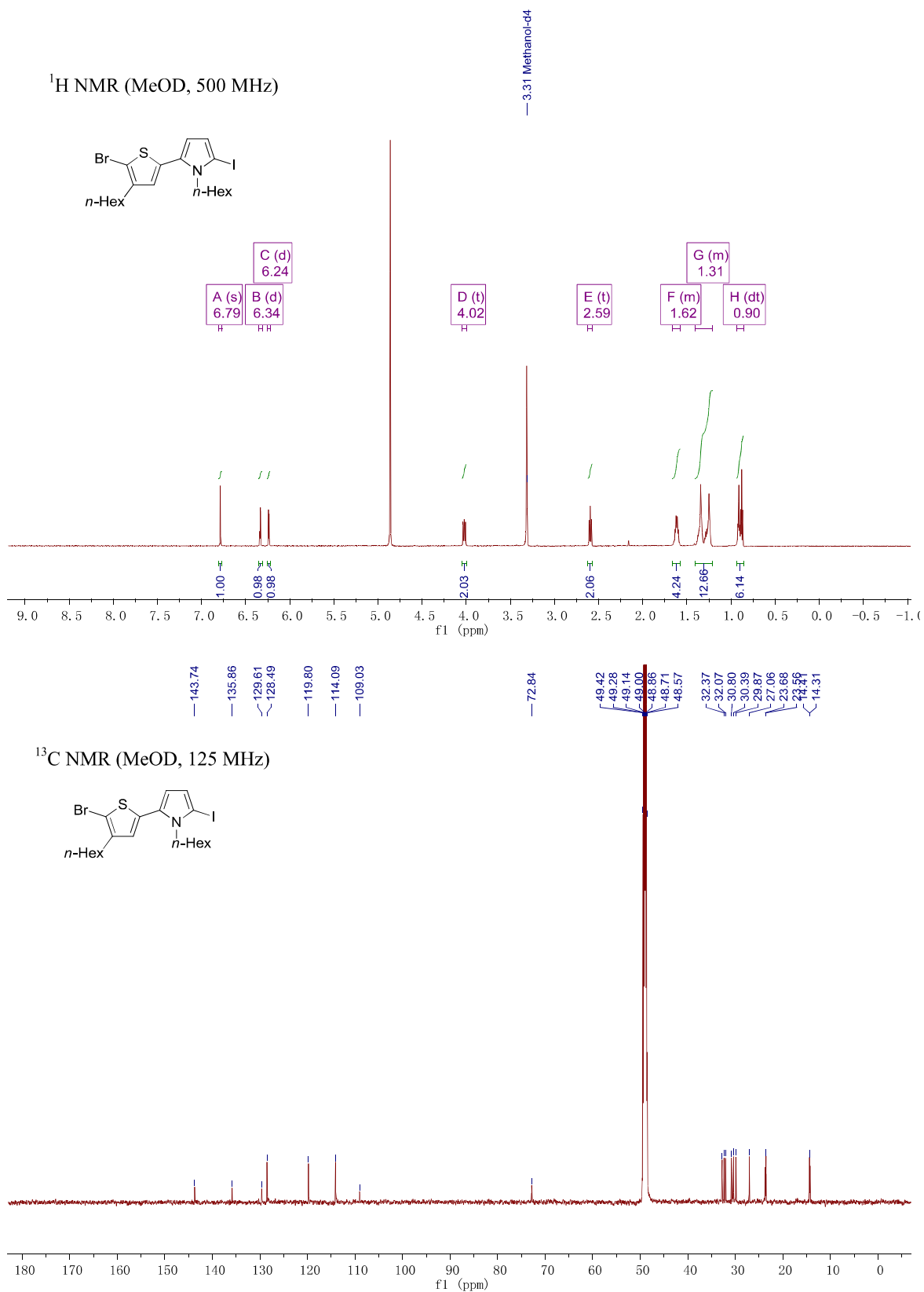
HRMS (EI-sector) m/z : $[\text{M}]^+$ Calcd for $[\text{C}_{10}\text{H}_{17}\text{N}]^+$ 151.1361; Found 151.1363.

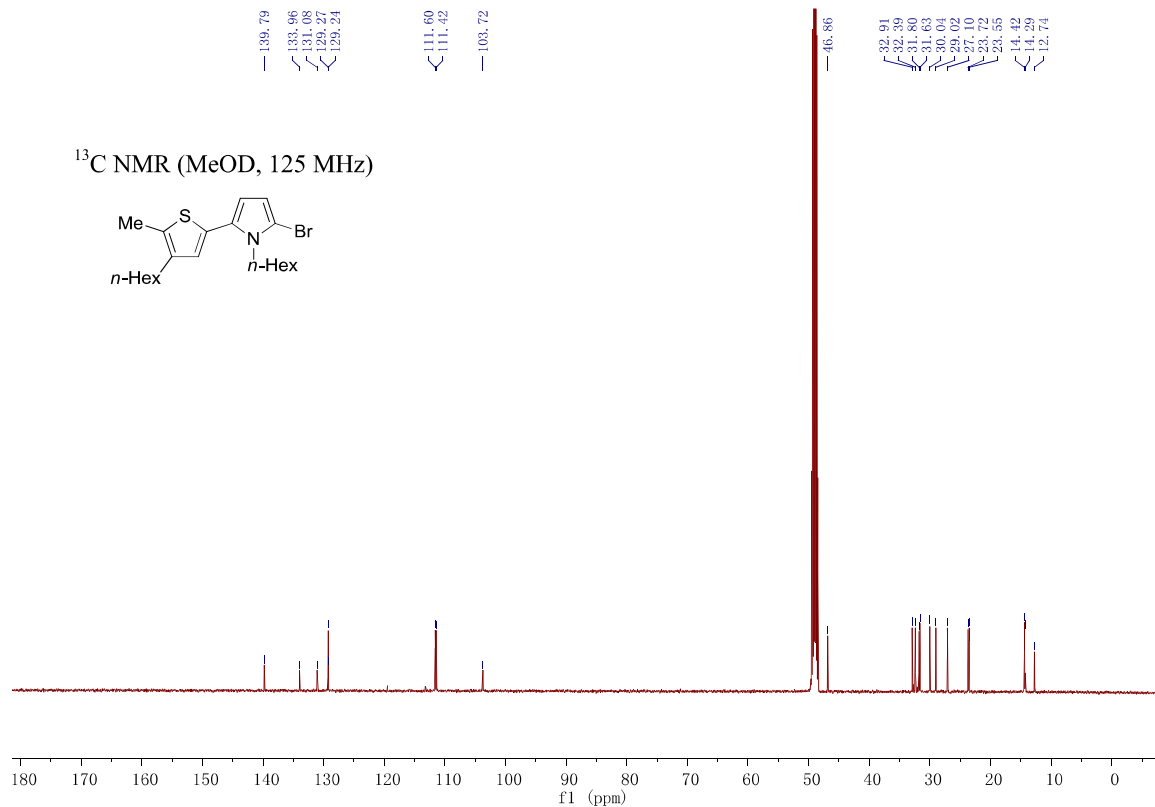
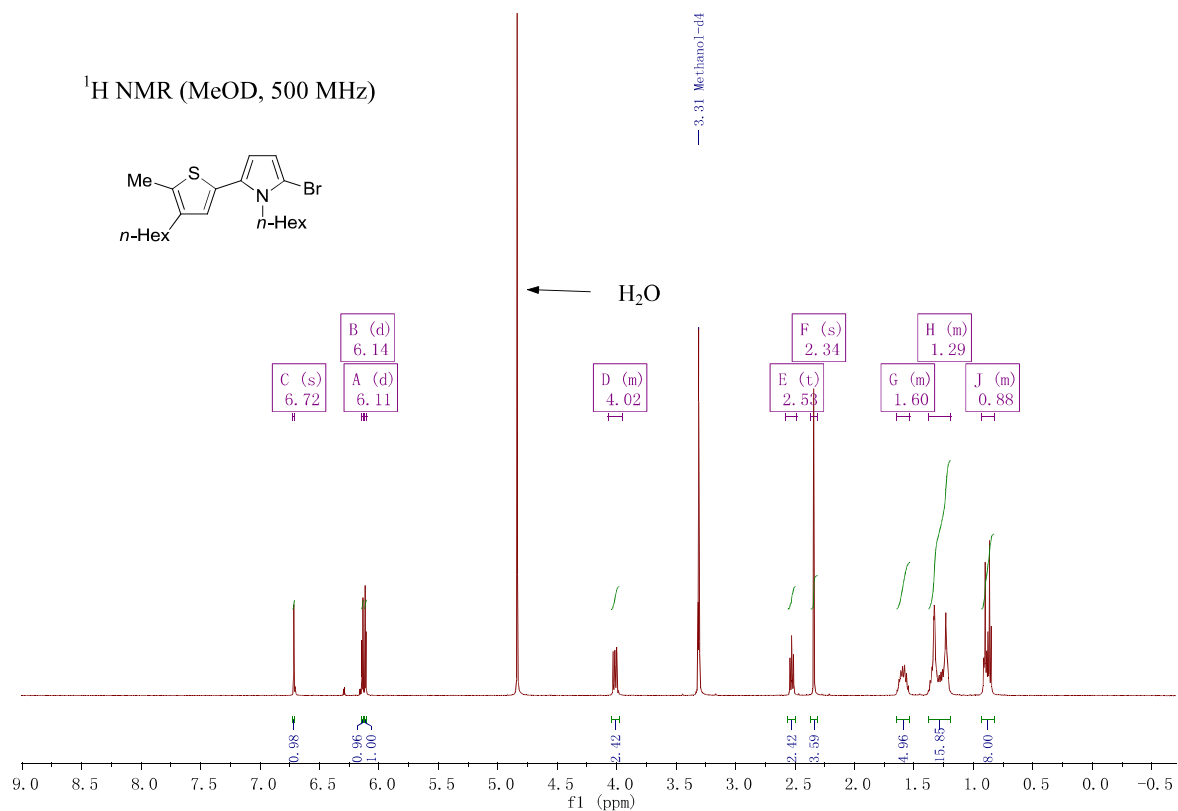
IR (ATR): $\tilde{\nu}$ = 2957 (m), 2928 (s), 2858 (m), 1537 (w), 1500 (s), 1465 (w), 1377 (w), 1281 (s), 1088 (s), 1063 (m), 968 (w), 716 (vs), 650 (w), 616 (s) cm^{-1} .

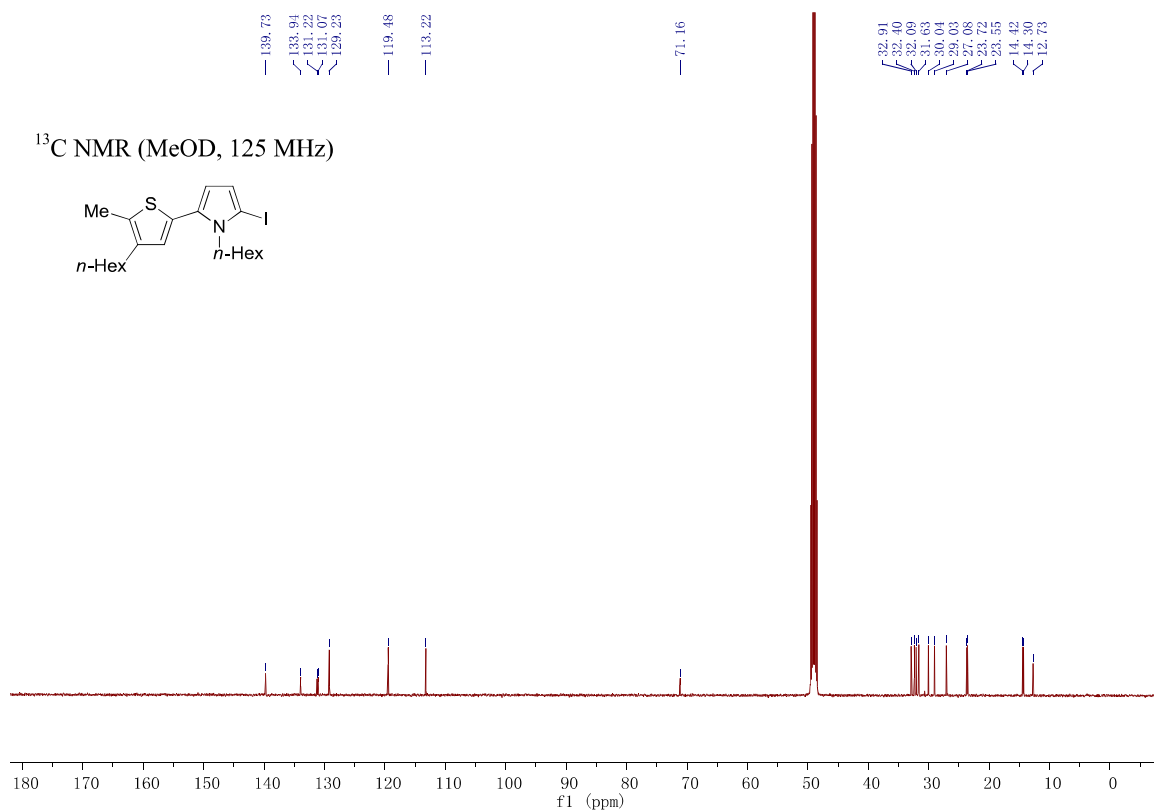
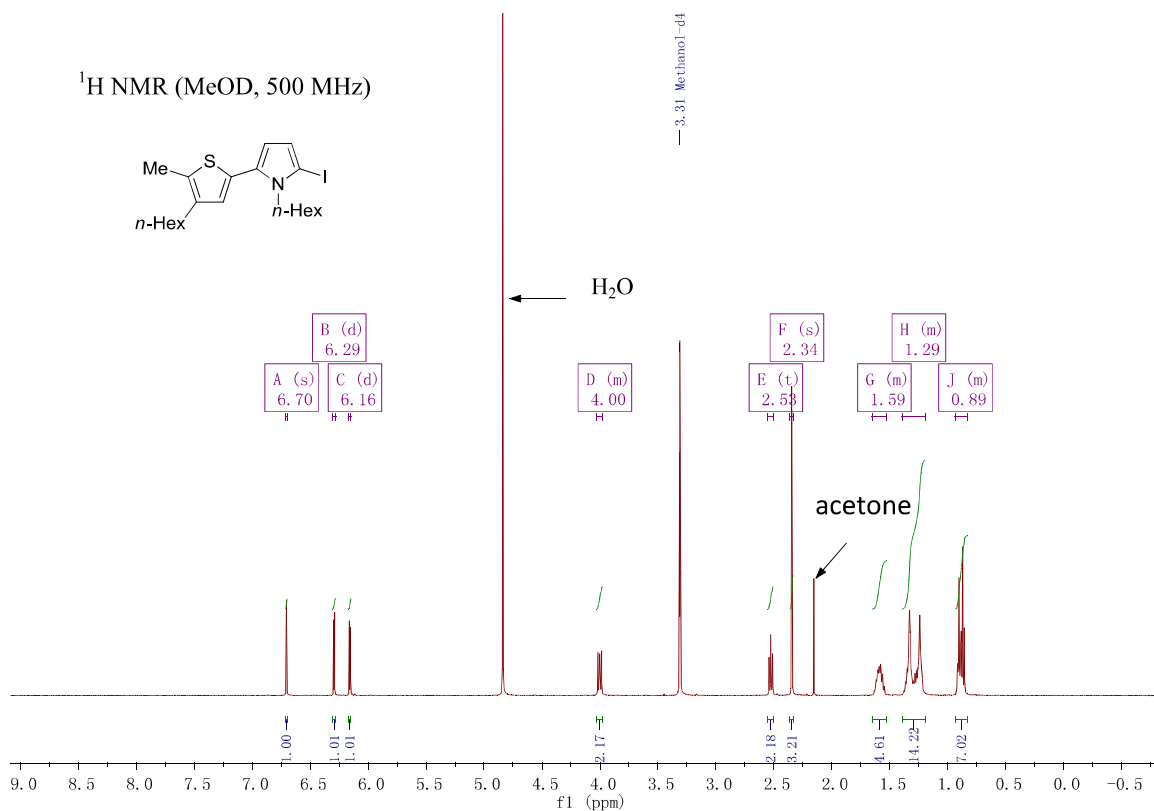
NMR Spectra
3-Bromothiophene2-Bromo-3-hexyl-5-iodothiophene (1)¹³C NMR (CDCl₃, 125 MHz)

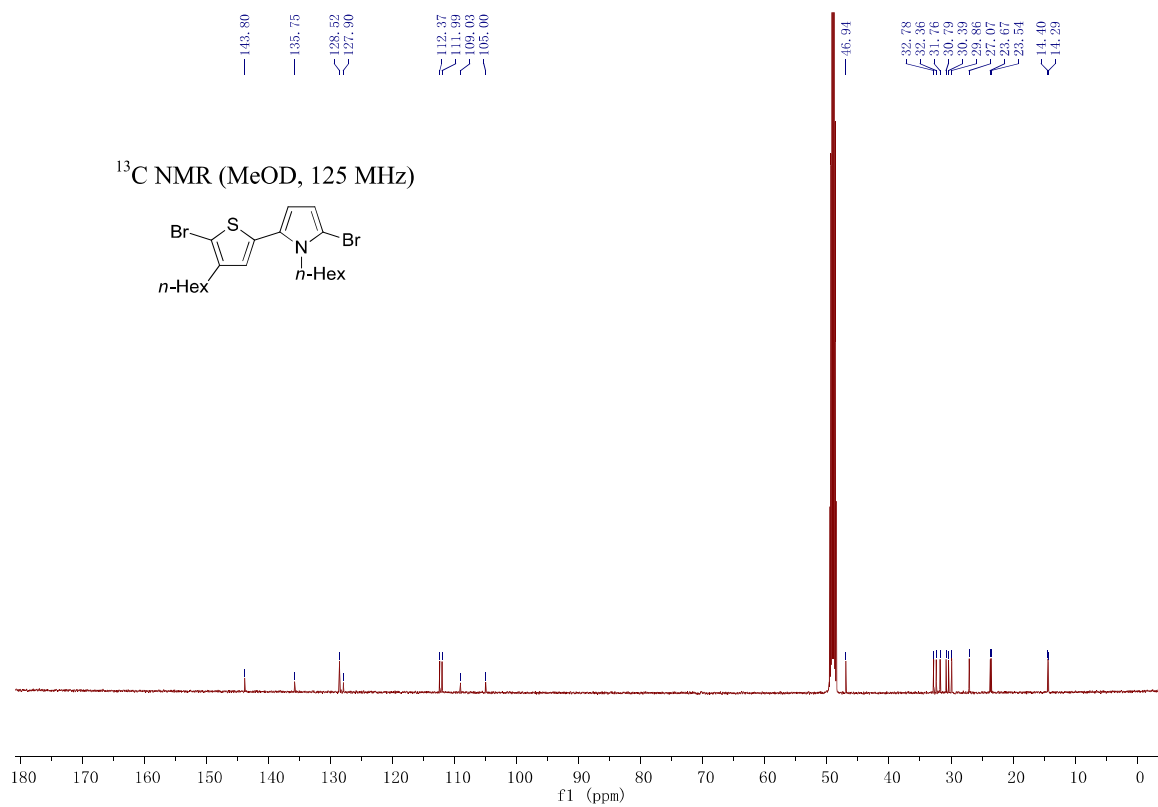
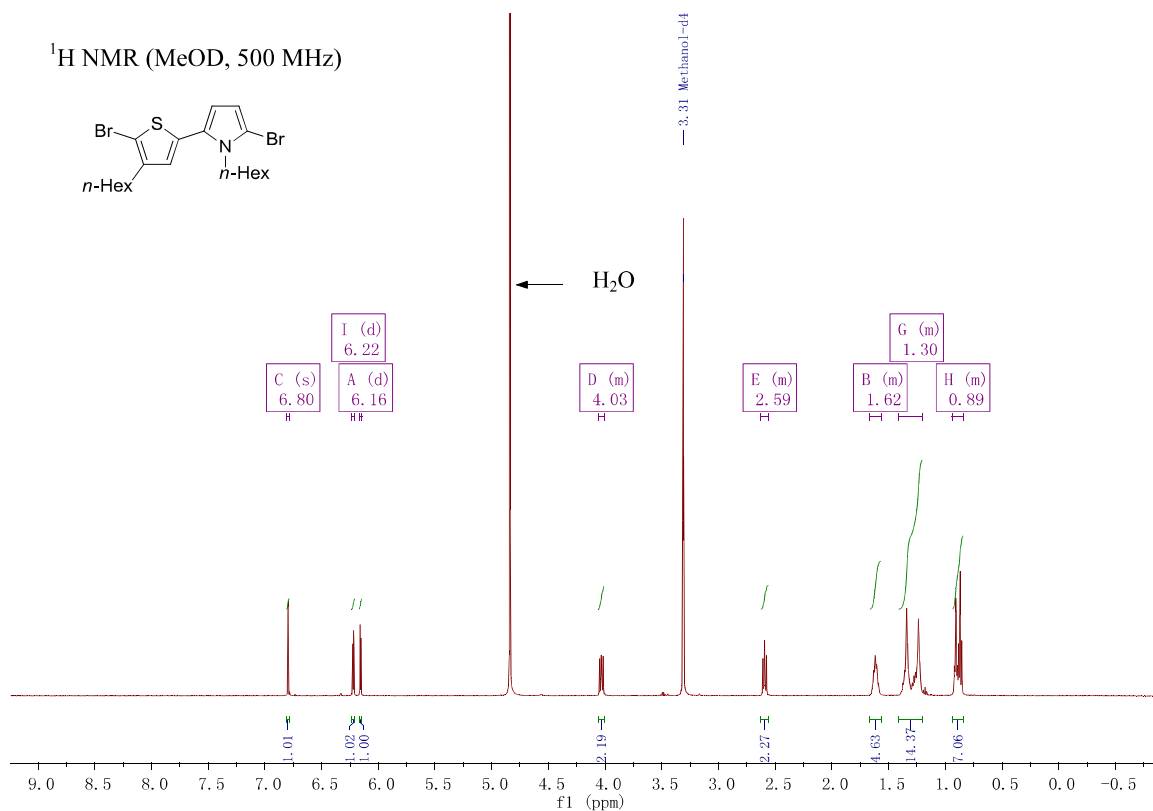
1-Hexyl-2-(tributylstannyl)-1*H*-pyrrole (2)¹³C NMR (CDCl₃, 125 MHz)

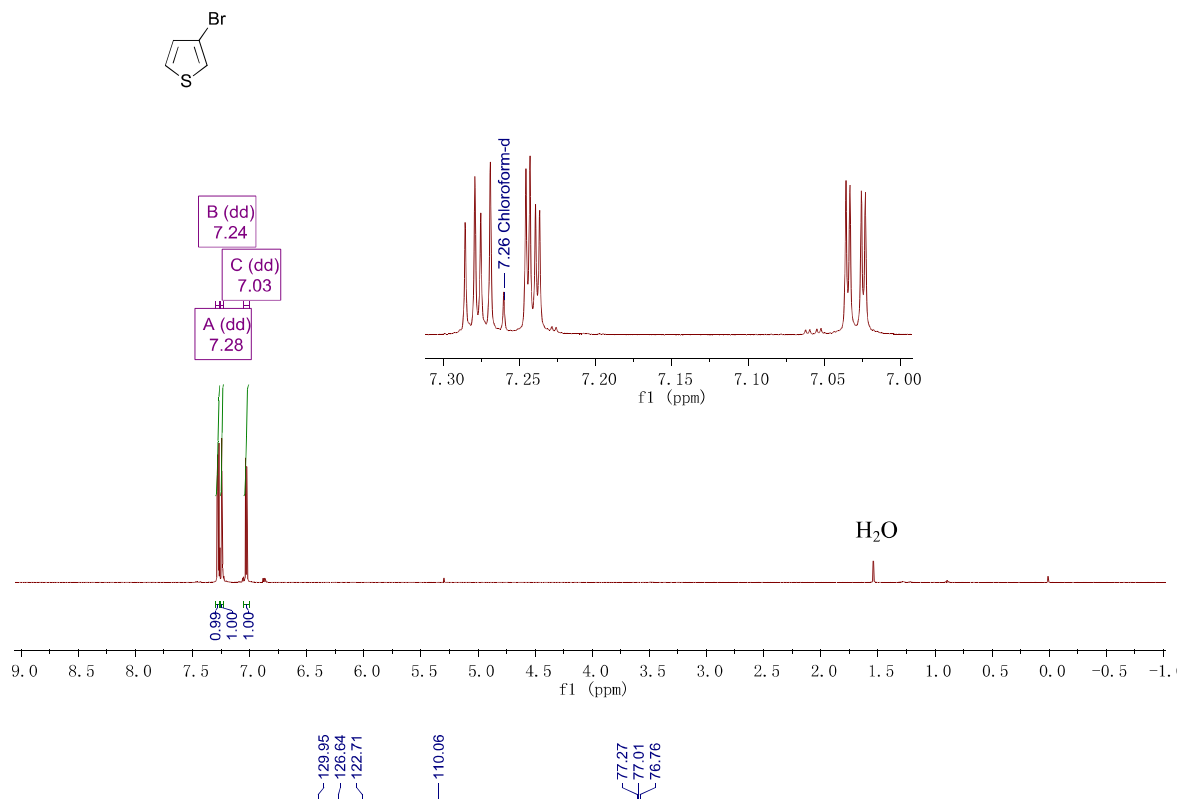
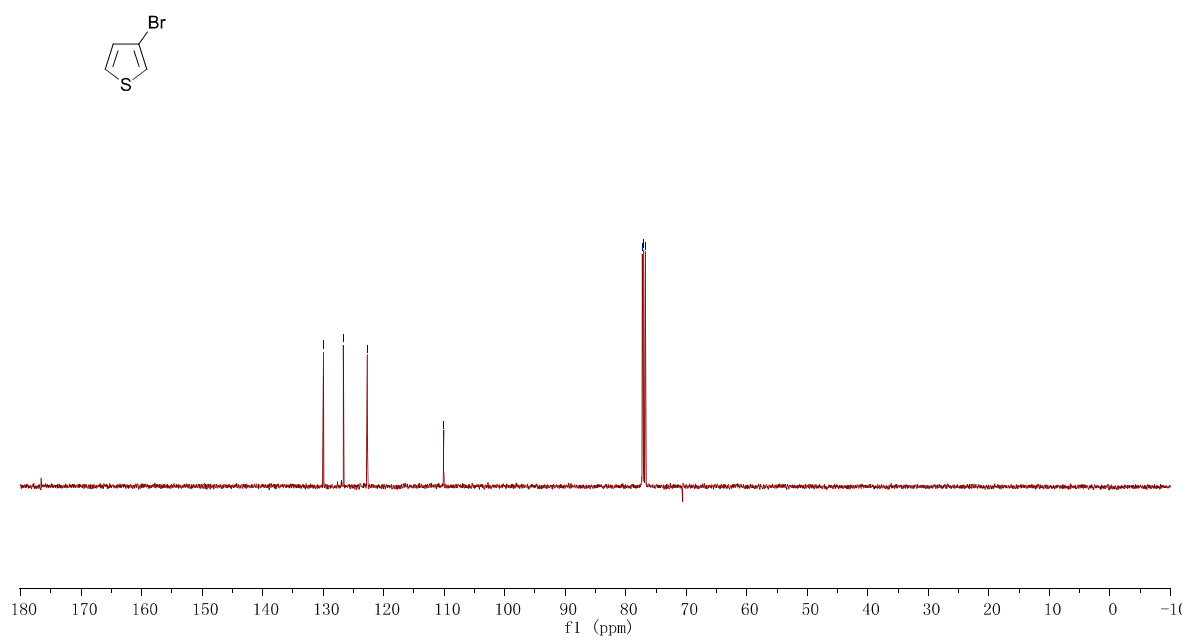
2-(5-Bromo-4-hexylthiophen-2-yl)-1-hexyl-1H-pyrrole (3)

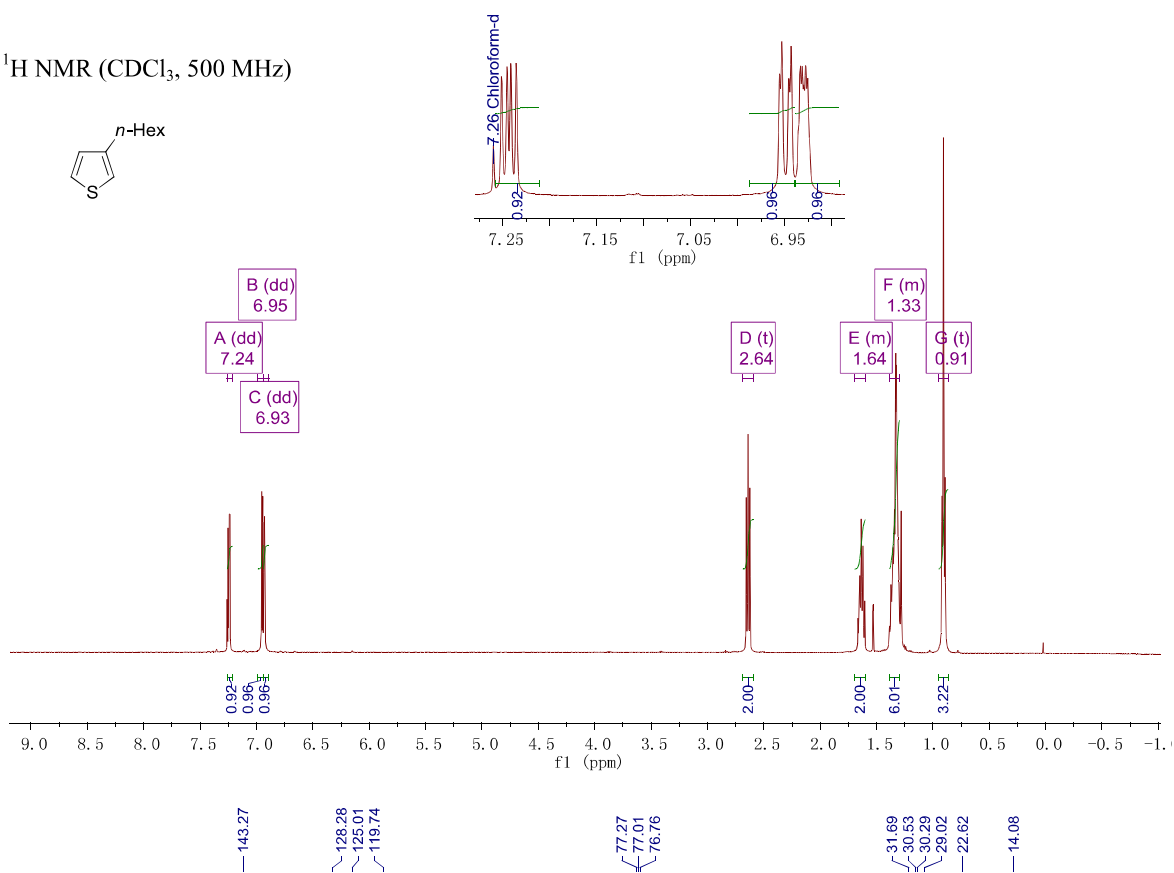
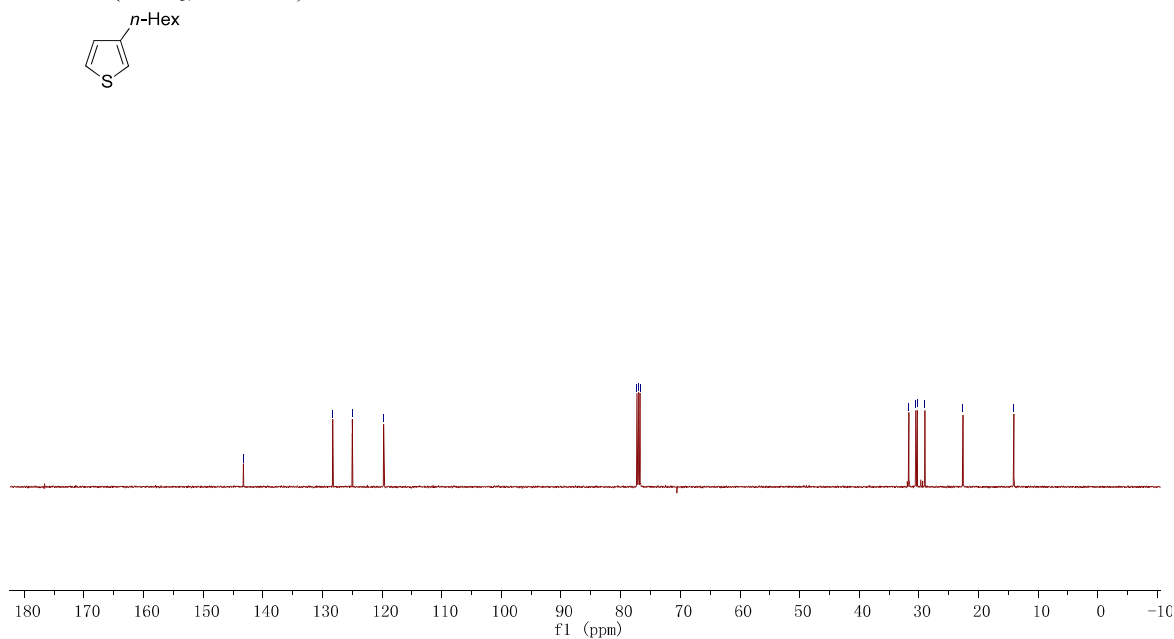
2-(5-Bromo-4-hexylthiophen-2-yl)-1-hexyl-5-iodo-1*H*-pyrrole (4)


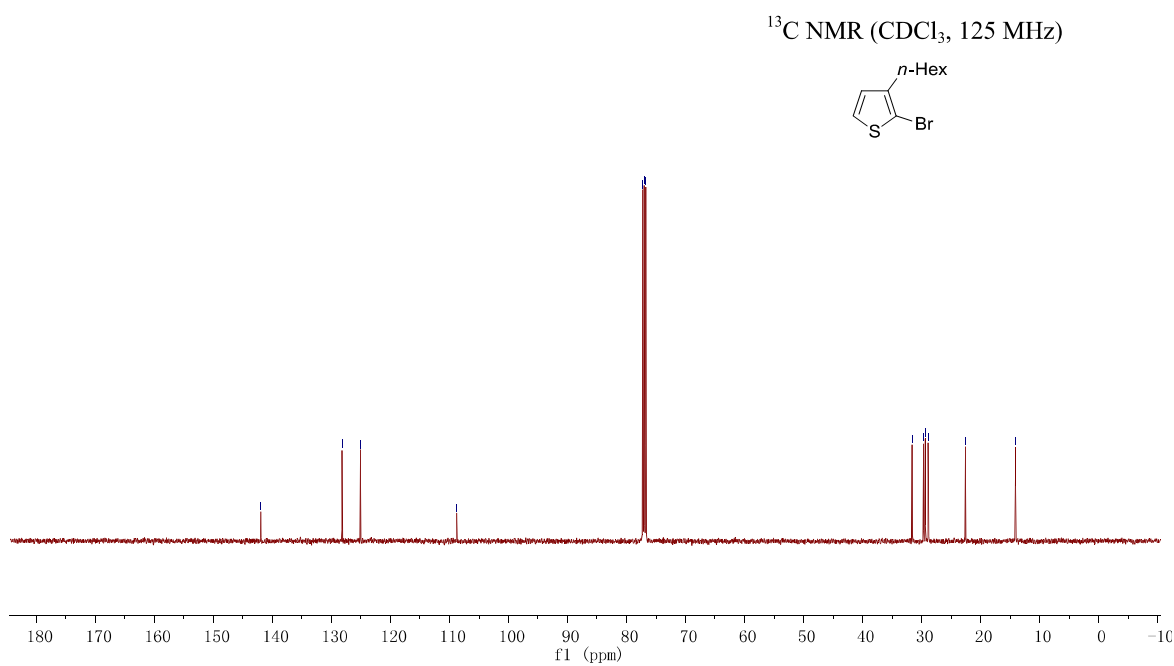
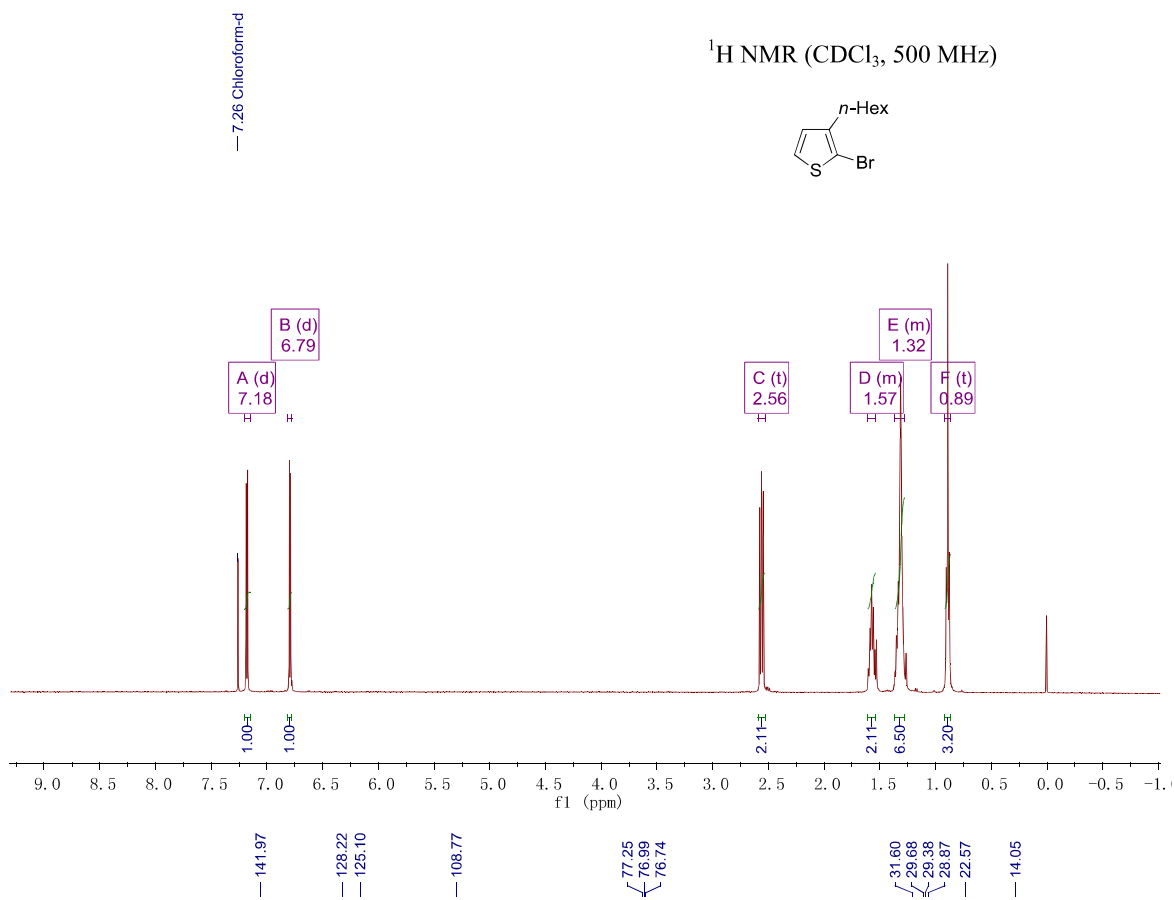
2-Bromo-1-hexyl-5-(4-hexyl-5-methylthiophen-2-yl)-1H-pyrrole (5)

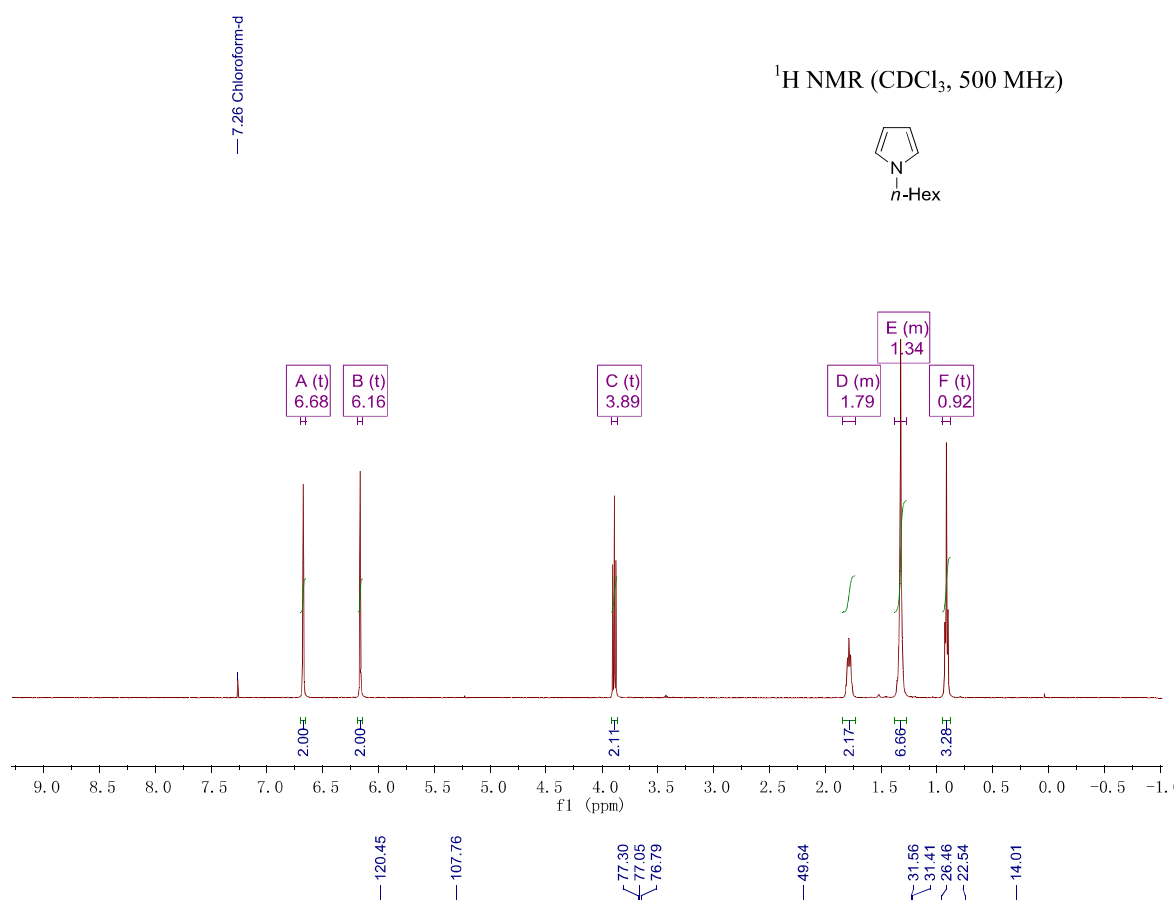
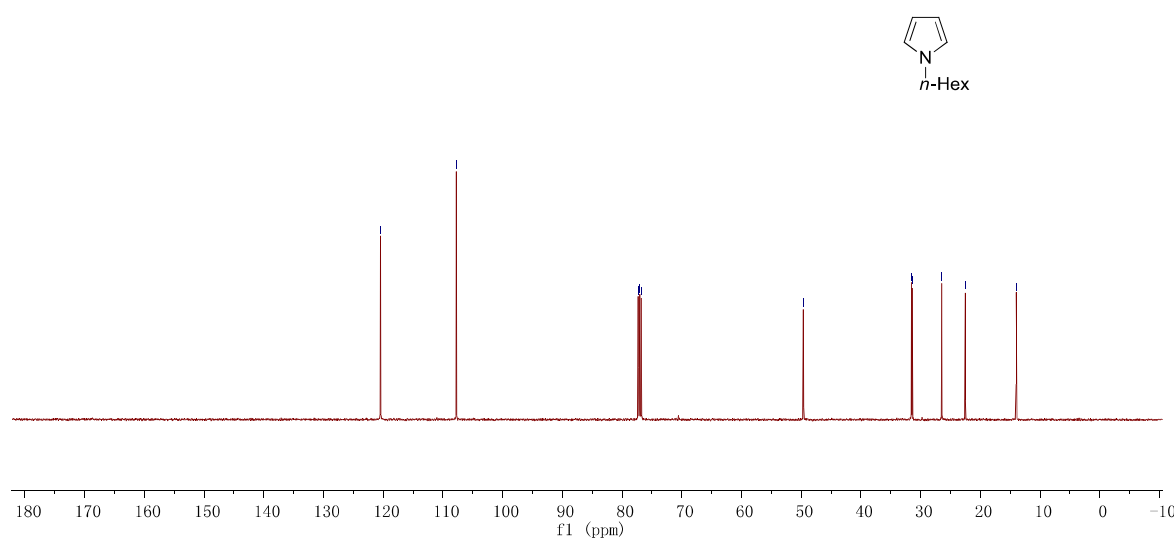
1-Hexyl-2-(4-hexyl-5-methylthiophen-2-yl)-5-iodo-1*H*-pyrrole (6)

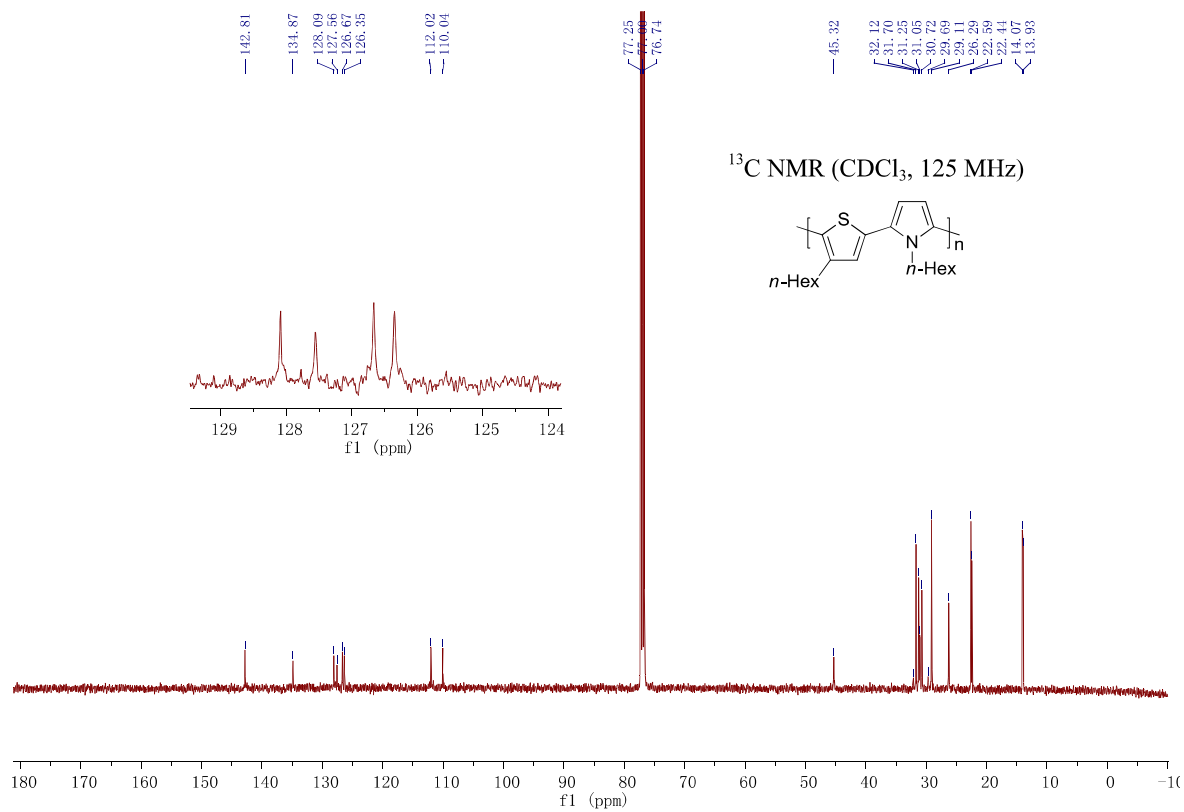
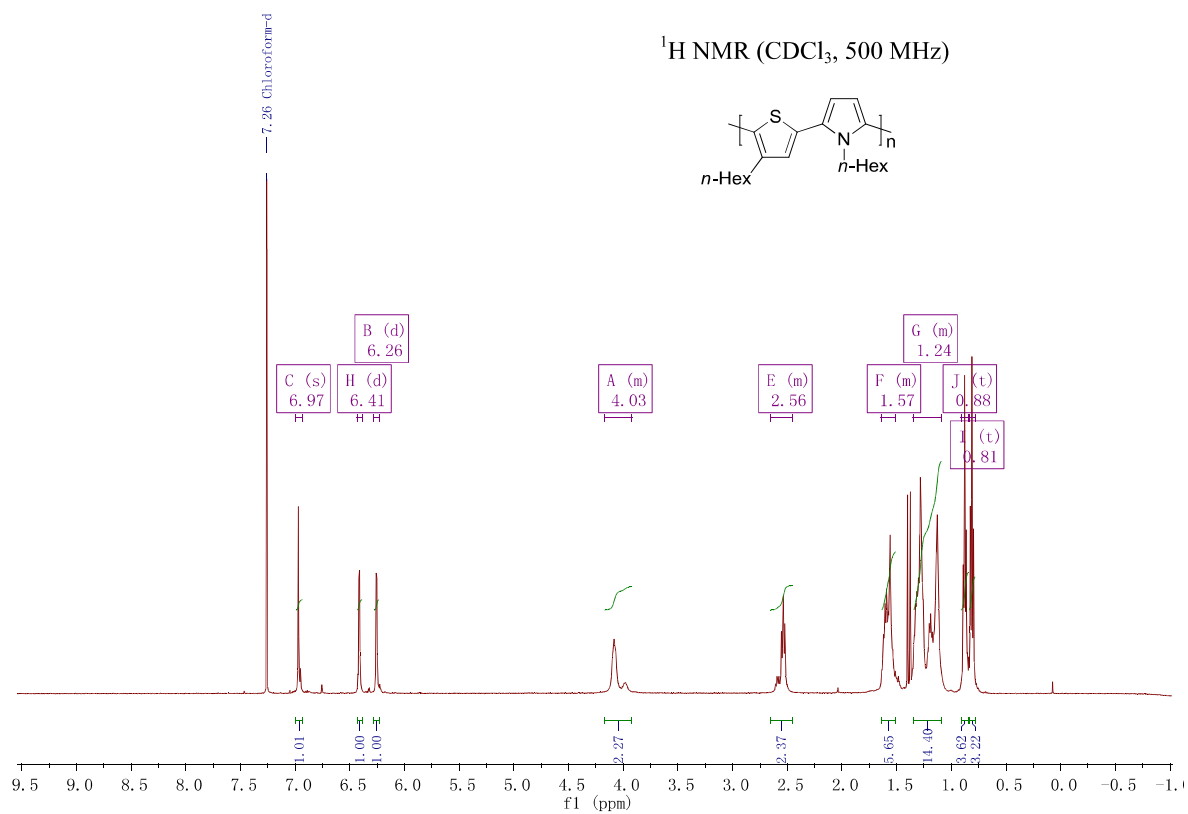
2-Bromo-5-(5-bromo-4-hexylthiophen-2-yl)-1-hexyl-1H-pyrrole (8)

3-Bromothiophene (9) $^1\text{H NMR}$ (CDCl_3 , 500 MHz) $^{13}\text{C NMR}$ (CDCl_3 , 125 MHz)

3-Hexylthiophene (10) ^1H NMR (CDCl_3 , 500 MHz) ^{13}C NMR (CDCl_3 , 125 MHz)

2-Bromo-3-hexylthiophene (11)

1-Hexyl-1*H*-pyrrole (12)**¹³C NMR (CDCl₃, 125 MHz)**

Poly(thiophene-*alt*-pyrrole) (PTP) (of Table 2, entry 9)

References

1. Lee, C. T.; Yang, W. T.; Parr, R. G. *Phys. Rev. B* **1988**, *37*, 785-789.
2. Becke, A. D. *J. Chem. Phys.* **1993**, *98*, 5648-5652.
3. Gaussian 09, Revision D.01, M. J. Frisch, G. W. Trucks, H. B. Schlegel, G. E. Scuseria, M. A. Robb, J. R. Cheeseman, G. Scalmani, V. Barone, B. Mennucci, G. A. Petersson, H. Nakatsuji, M. Caricato, X. Li, H. P. Hratchian, A. F. Izmaylov, J. Bloino, G. Zheng, J. L. Sonnenberg, M. Hada, M. Ehara, K. Toyota, R. Fukuda, J. Hasegawa, M. Ishida, T. Nakajima, Y. Honda, O. Kitao, H. Nakai, T. Vreven, J. A. Montgomery, Jr., J. E. Peralta, F. Ogliaro, M. Bearpark, J. J. Heyd, E. Brothers, K. N. Kudin, V. N. Staroverov, T. Keith, R. Kobayashi, J. Normand, K. Raghavachari, A. Rendell, J. C. Burant, S. S. Iyengar, J. Tomasi, M. Cossi, N. Rega, J. M. Millam, M. Klene, J. E. Knox, J. B. Cross, V. Bakken, C. Adamo, J. Jaramillo, R. Gomperts, R. E. Stratmann, O. Yazyev, A. J. Austin, R. Cammi, C. Pomelli, J. W. Ochterski, R. L. Martin, K. Morokuma, V. G. Zakrzewski, G. A. Voth, P. Salvador, J. J. Dannenberg, S. Dapprich, A. D. Daniels, O. Farkas, J. B. Foresman, J. V. Ortiz, J. Cioslowski, and D. J. Fox, Gaussian, Inc., Wallingford CT, 2013.
4. Gaussian, Inc. 340 Quinnipiac St Bldg 40, Wallingford, CT 06492 USA, Copyright 2000-2008 Semichem. Inc. Authors: R. D. Dennington II, T. A. Keith, J. M. Millan.
5. Ditchfie.R; Hehre, W. J.; Pople, J. A. *J. Chem. Phys.* **1971**, *54*, 724-728.
6. Harihara.Pc; Pople, J. A. *Theoret. Chim. Acta* **1973**, *28*, 213-222.
7. Hehre, W. J.; Ditchfie.R; Pople, J. A. *J. Chem. Phys.* **1972**, *56*, 2257-2261.
8. Nielsen, C. B.; Bjørnholm, T. *Org. Lett.* **2004**, *6*, 3381-3384.
9. Zhang, Y.; Zhao, C. C.; Yang, J. H.; Kapiamba, M.; Haze, O.; Rothberg, L. J.; Ng, M. K. *J. Org. Chem.* **2006**, *71*, 9475-9483.
10. Hoffmann, K. J.; Carlsen, P. H. J. *Synth. Commun.* **1999**, *29*, 1607-1610.
11. Tarzia, G.; Duranti, A.; Tontini, A.; Spadoni, G.; Mor, M.; Rivara, S.; Plazzi, P. V.; Kathuria, S.; Piomelli, D. *Bioorganic & Medicinal Chemistry* **2003**, *11*, 3965-3973.
12. Katritzky, A. R.; Akhmedov, N. G.; Doskocz, J.; Hall, C. D.; Akhmedova, R. G.; Majumder, S. *Magn. Reson. Chem.* **2007**, *45*, 532-543.

**5.4. Experimental Section. Supporting Information Chapter
3.2.2**

CHEMISTRY

A **European** Journal

Supporting Information

Negishi's Reagent Versus Rosenthal's Reagent in the Formation of Zirconacyclopentadienes

Sara Urrego-Riveros^{+, [a]} Isabel-Maria Ramirez y Medina^{+, [a]} Daniel Duvinage,^[b] Enno Lork,^[b] Frank D. Sönnichsen,^[c] and Anne Staubitz^{*[a]}

chem_201902255_sm_miscellaneous_information.pdf

Table of contents

1	General Considerations	2
2	Syntheses	10
3	Reaction Monitoring Using Rosenthal's Zirconocene vs. Negishi's Reagent for the Synthesis of Zirconacyclopentadienes.....	18
4	Air Stability Tests	32
5	Literature	36
6	Spectra	37
7	Crystal Structures	100

1 General Considerations

1.1 Abbreviations

br	broad
BTMSA	bis(trimethylsilyl)acetylene
calcd.	calculated
Cp	cyclopentadienyl
d	doublet (NMR)
EI	electron impact
GB	glove box
IR	infrared spectroscopy
m	multiplet (NMR)
m	medium (IR)
NMR	nuclear magnetic resonance
Pin	pinacol
[PdCl ₂ (dppf)]	[1,1'-bis(diphenylphosphino)ferrocene]dichloropalladium(II)
[Pd(PPh ₃) ₄]	tetrakis(triphenylphosphine)palladium(0)
ppm	parts per million
R	resolution (mass spectrometry)
s	singlet (NMR)
s	strong (IR)
SPS	solvent purification system
t	triplet (NMR)
TLC	thin layer chromatography
THF	tetrahydrofuran
TMS	tetramethylsilane
w	weak (IR)

1.2 Chemicals and Solvents

All reactions were carried out using standard Schlenk techniques under a dry, inert nitrogen or argon atmosphere unless noted otherwise. Some reactions were performed inside a nitrogen filled glovebox from Inert, Innovative Technology, Inc. Company (< 0.1 ppm O_2 and < 0.1 ppm H_2O). All dry solvents were taken from the solvent purification system (SPS), degassed by freeze-pump-thaw cycles and stored under a nitrogen atmosphere unless noted otherwise. All chemicals were commercially available and were used without further purification unless noted otherwise.

Table S 1. List of supplier and purity of used chemicals.

Reagent	Supplier	Purity	Comments
Ammonium chloride	Carl Roth	$\geq 99.5\%$	
Bis(trimethylsilyl)acetylene	Sigma Aldrich	99%	stored in a freezer in a GB
1-Bromo-4-iodobenzene	Alfa Aesar	98%	
1-Bromo-2-(2-trimethylsilylethynyl)benzene	Sigma Aldrich	98%	
2-Bromothiophene	Sigma Aldrich	98%	
Copper (II) chloride	Alfa Aesar	99.995%	
Copper (I) iodide	Alfa Aesar	99.998%	stored in a GB
<i>N</i> -Bromosuccinimide	Merck	99%	
<i>n</i> -Butyllithium	Acros Organics	n. a.	Titrated with Lin& Paquette-Method ^[1]
Diphenylacetylene	Sigma Aldrich	98%	
1,6-Heptadiyne			
Iodine	ABCR	99%	
Iodobenzene	Alfa Aesar	98%	
<i>n</i> -Iodosuccinimide	MOLEKULA	95%	
2-Iodothiophene	TCI	$\geq 98\%$	
LiCl	Sigma Aldrich	$\geq 99\%$	anhydrous
Magnesium sulfate	Grüssing	99%	
2-Methoxythiophene	Alfa Aesar	99%	
1-(1-Naphthyl)-2-(trimethylsilyl)acetylene	Sigma Aldrich	97%	
1,8-Nonadiyne	Sigma Aldrich	98%	
1,7-Octadiyne	VWR Chemicals	98%	

[PdCl ₂ (dppf)]		Sigma Aldrich	n.a.	
[Pd(PPh ₃) ₄]		TCI	> 97%	stored in a freezer in a GB
Sodium carbonate		VWR Chemicals	n.a.	ACS, Reag. Ph. Eur.
Sodium hydrogen carbonate		VWR Chemicals	n.a.	ACS, Reag. Ph. Eur.
Sodium sulfate		Grüssing	99%	
Sodium thiosulfate		Grüssing	97%	
<i>p</i> -Toluenesulfonic acid·H ₂ O		Acros Organics	97.5 %	
Trimethylstannyl chloride		Sigma Aldrich	99 %	Stored in a GB
Zirconocene dichloride		abcr	99%	stored in a freezer inside a GB

Table S2. List of suppliers and purity of used solvents.

Solvent	Comments
Acetic acid	Alfa Aesar, 99+%
Chloroform	VWR Chemicals; ACS, Reag. Ph. Eur.
Dichloromethane	VWR Chemicals; for HPLC; dry from the SPS
Diethyl ether	VWR Chemicals; for HPLC; dry, distilled from sodium / benzophenone
<i>N,N</i> -Dimethylformamide	Extra dry from Acros Organics; 99.8%
Ethyl acetate	VWR Chemicals; ACS, Reag. Ph. Eur.
Ethanol	VWR Chemicals, ACS, Reag. Ph. Eur.
<i>n</i> -Hexane	VWR Chemicals; ACS, Reag. Ph. Eur.
<i>n</i> -Pentane	VWR Chemicals; for HPLC; dry from the SPS and degassed
Pyridine	Acros Organics 99.8%; dried over KOH, degassed, stored over 4 Å molecule sieves
Triethylamine	Grüssing; 99%; dry, distilled over CaH ₂ ; degassed
<i>t</i> -Butanol	VWR Chemicals, ACS, Reag. Ph. Eur.
Tetrahydrofuran	VWR Chemicals; for HPLC; dry from the SPS and degassed
Toluene	VWR Chemicals; for HPLC; dry, from the SPS and degassed

1.3 Analytical Instruments

^1H , $^{13}\text{C}\{^1\text{H}\}$, ^{19}F , $^{29}\text{Si}\{^1\text{H}\}$, $^{11}\text{B}\{^1\text{H}\}$ and $^{119}\text{Sn}\{^1\text{H}\}$ NMR spectra were recorded on a Bruker Avance Neo 500, Bruker Avance Neo 600 or Bruker DPX-200 spectrometer at 300 K. All ^1H NMR and $^{13}\text{C}\{^1\text{H}\}$ NMR spectra were referenced against the solvent residual proton signals (^1H), or the solvent itself (^{13}C). The reference for the $^{119}\text{Sn}\{^1\text{H}\}$ NMR spectra was calculated based on the ^1H NMR spectrum of TMS. ^{19}F and $^{11}\text{B}\{^1\text{H}\}$ NMR spectra were referenced against $\text{BF}_3 \cdot \text{Et}_2\text{O}$ in CDCl_3 . $^{29}\text{Si}\{^1\text{H}\}$ NMR spectra were referenced against TMS in CDCl_3 . All chemical δ shifts are given in parts per million (ppm) and all coupling constants J in Hz. The exact assignment of the peaks was proved by two-dimensional NMR spectroscopy such as ^1H COSY, ^{13}C HSQC or $^1\text{H}/^{13}\text{C}$ HMBC when possible.

Electron Impact (EI) ionization mass spectra were obtained on the double focusing mass spectrometer MAT 95XL or MAT 8200 from FINNIGAN mat. Samples were measured by direct inlet or indirect inlet method with a source temperature of 200°C . The ionization energy of the electron impact ionization was 70 eV. All signals were reported with the quotient from mass to charge m/z . High resolution (HR) mass spectra were recorded on the double focusing mass spectrometer MAT 95XL from FINNIGAN MAT. Precision weights were determined via the peak-matching method. The reference substance was perfluorokerosene (PFK). The resolution (R) of the peak-matching performance was 10000. The calculated isotopic distribution for each ion was in agreement with experimental values.

IR spectra were recorded on a NICOLET Thermo IS10 SCIENTIFIC IR spectrometer with a diamond-ATR-unit. The resolution was 4 cm^{-1} . Relative intensities of the IR bands were described by s = strong, m = medium or w = weak.

All melting points were measured with a BÜCHI Melting Point M-560 apparatus and are uncorrected.

Thin layer chromatography (TLC) was carried out on aluminum plates coated with silica gel 60 F_{254} with a layer thickness of 0.2 mm from Fluka or Macherey-Nagel. All bands were detected by using a fluorescent lamp (254 nm and 366 nm). Column chromatography was carried out by using the column machine PuriFlash 4250 from Interchim. Silica gel columns of the type PF-15SiHP-F0012, PF-15SiHP-F0025, PF-50SiHP-JP-F0080, PF-50SiHP-JP-F0120, and PF-50SiHP-JP-F0220 were used. The injection of the sample was made via dry load. The column material of the dry load was Celite 503 from Macherey-Nagel.

1.4 Crystallography

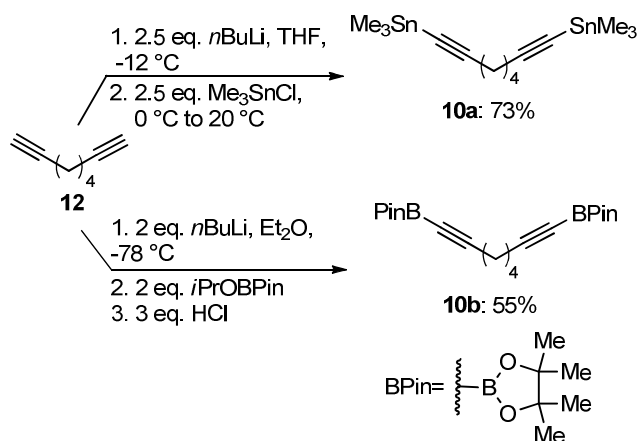
Crystallography. Intensity data of **11d**, **11f**, **11h**, **11i**, **11j**, **11k** and **11l** were collected on a Bruker Venture D8 diffractometers at 100 K with Mo-K α (0.7107 Å) radiation. All structures were solved by intrinsic phasing and refined based on F² by use of the SHELX^[2] program package as implemented in OLex2 1.2.^[3] All non-hydrogen atoms were refined using anisotropic displacement parameters. Hydrogen atoms attached to carbon atoms were included in geometrically calculated positions using a riding model. Crystal and refinement data are collected in Tables S3-5.

A rotational disorder was resolved for the thiophene groups of compound **11f**. The refinement led to a split atom model for each group with refined occupancies of 76:24 and 53:47, respectively. Compound **11h** comprised two crystallographically independent conformers. The fluorine atoms of the two CF₃-groups of compound **11i** were disordered and were refined with split occupancies of 71:29 and 57:43, respectively. The C-F-distances were restrained to be equal. Compound **11k** crystallized with one molecule of toluene per asymmetric unit. The toluene was disordered over two positions with split occupancies of 65:35. Compound **11l** crystallized with a half molecule in the asymmetric unit. The Zr-atom was located on the Wyckoff-Position 4e of space group C2/c.

Crystallographic data for the structural analyses have been deposited with in Cambridge Crystallographic Data Centre. Copies of this information may be obtained free of charge from The Director, CCDC, 12 Union Road, Cambridge CB2 1EZ, UK (Fax: +44-1223-336033; e-mail: deposit@ccdc.cam.ac.uk or <http://www.ccdc.cam.ac.uk>).

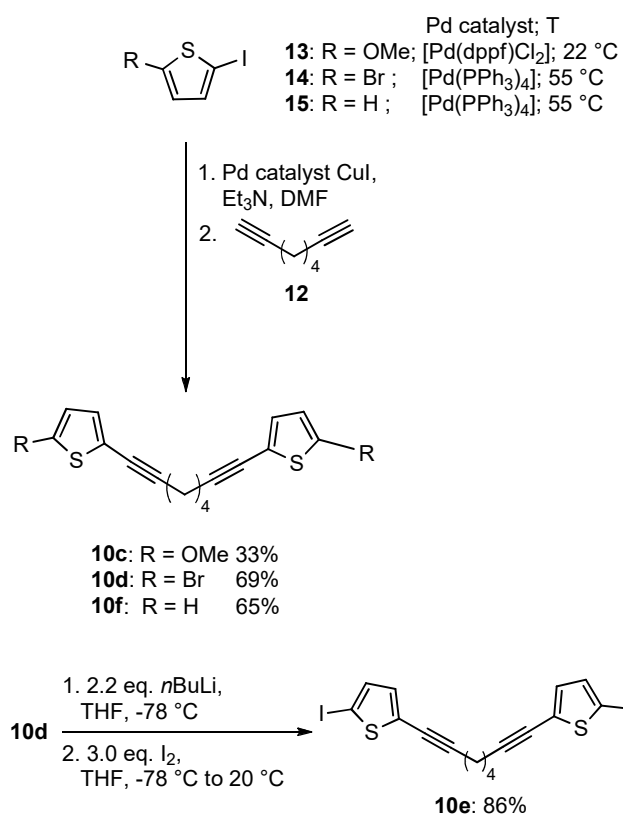
1.5 Results and Discussion of the Precursor Synthesis

The dialkynes **11a-11f** required for the synthesis of the zirconacyclopentadienes were prepared by two methods starting with 1,7-octadiyne (**12**): the first method was based on the deprotonation of **12**, followed by a nucleophilic substitution either with trimethyltin chloride or *isopropyl* pinacol boronic ester to give **10a** and **10b** in yields of 73% and 55%, respectively (Scheme 6).^[4]



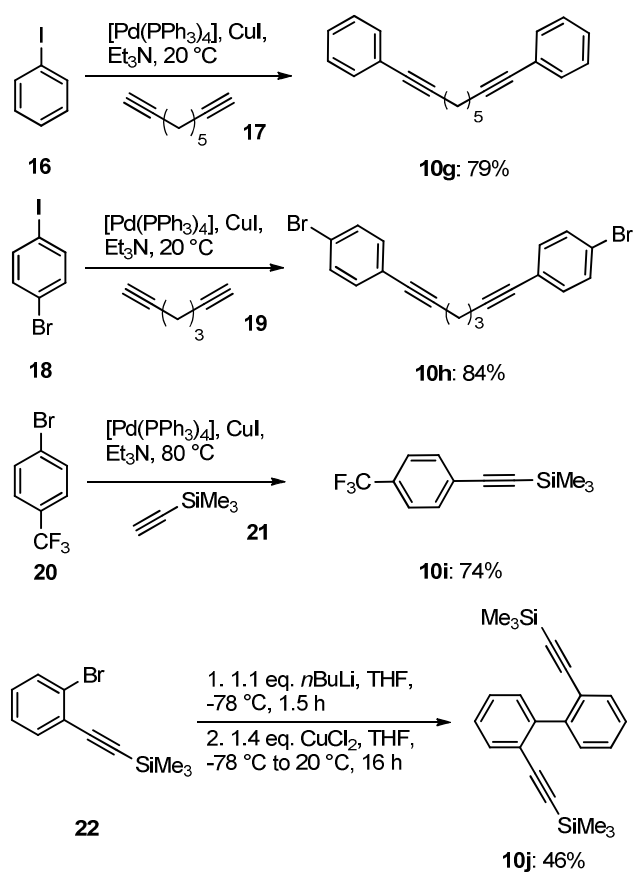
Scheme S1. Synthetic route to form the dialkynes **10a** and **11b** by nucleophilic substitution.

The second route was based on Sonogashira cross coupling reactions of two equivalents of functionalized thiophenes **13**, **14** or **15** with 1,7-octadiyne (**12**) using different Pd sources and temperatures (Scheme 7). The yields ranged from 33% for the electron rich compound **13** up to 69% and 65% for 2-bromo-5-iodothiophene (**14**) and 5-iodothiophene (**15**) respectively. The product of the Sonogashira reaction between the 2-iodo-5-bromothiophene (**14**) and 1,7-octadiyne (**12**) gave the dialkyne **10d**, which contained two bromide groups.^[5] The substituents were transformed into iodide groups via bromo-lithium exchange followed by iodination in order to prepare compound **10e**.^[6] The diynes **10d** and **10e** are of high interest for this study, because with these compounds it is possible to synthesize functionalized heterocycles, which are useful for further polymerizations (materials science) and other reactions. With these functionalities it can be analyzed a potential difference in the stability aryl iodides vs. aryl bromides under the experimentally more extreme Negishi conditions, which are both prone to halogen metal exchange reactions, but to a different extent.



Scheme S2. Synthetic path to form the dialkynes **10c-10f**.

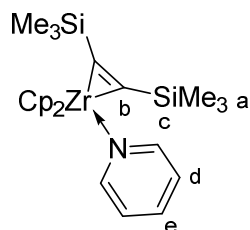
The dialkynes **10g** and **10h** and the monoalkyne **10i** were prepared by a Sonogashira reaction between the benzene derivatives **16**, **18** and **20** and 1,8-nonadiyne (**17**), 1,4-heptadiyne (**19**)^[7] and trimethylsilylacetylene (**21**)^[8] respectively (Scheme 8). The dialkyne **10j** was prepared by the Ullman reaction between the aryllithium species, formed *in situ* from the bromide-lithium exchange of the starting material **19** with *n*BuLi, and an equivalent of **19**.^[9] The monoalkynes **10k** and **10l** were obtained from commercial sources.



Scheme S3. Synthetic path to form the alkynes **10g-10j**.

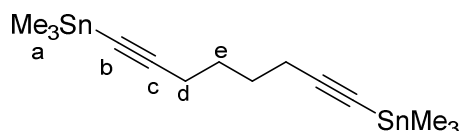
2 Syntheses

Rosenthal's Zirconocene (9)^[6, 10]



In a GB, zirconocene dichloride (5.00 g, 17.1 mmol) and bis(trimethylsilyl)acetylene (2.91 g, 17.1 mmol) were dissolved in tetrahydrofuran (100 mL). At the Schlenk line, *n*-butyllithium (2.5 M in hexanes, 13.7 mL, 34.2 mmol) was added dropwise over the course of 40 min at -78 °C to the colorless solution. The yellow mixture was stirred for 10 min and the reaction was allowed to warm to 22 °C over 2 h by removing the cooling bath. During that, the color changed from yellow to dark red. The flask was transferred into a GB and pyridine (1.38 mL, 17.1 mmol) was added leading to a color change from dark red to purple. The solvent was removed *in vacuo* under inert conditions until only ca. 1 mL remained. *n*-Pentane (250 mL) was added and the solution was stirred for further 48 h. Then, the crude compound was filtered with PTFE syringe filters (0.45 μm pore size) and placed in a -30 °C freezer in the GB for 72 h. The supernatant was removed by decantation and dried *in vacuo* to afford long black-purple crystals in a yield of 5.06 g (63%). **¹H NMR** (500 MHz, C₆D₆): δ 8.89-8.82 (m, 2H, c), 6.86-6.71 (m, 1H, e), 6.46-6.34 (m, 2H, d), 5.47 (s, 10H, Cp), 0.32 (s, 18H, a) ppm; **¹³C{¹H} NMR** (126 MHz, C₆D₆): δ 153.9 (d), 136.5 (f), 123.1 (e), 111.1 (b), 106.4 (Cp), 2.5 (c) ppm. The data are consistent with the literature.^[6, 10]

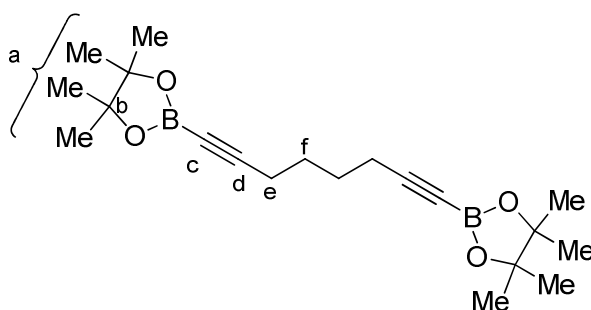
1,8-bis(Trimethylstannyl)octa-1,7-diyne (10a)^[4a]



n-Butyllithium (19.6 mL, 2.4 M in hexanes) was added dropwise over the course of 8 min to a solution of 1,7-octadiyne (2.00 g, 18.8 mmol) in THF (47 mL) at -12 °C under nitrogen atmosphere. The slightly yellow slurry was stirred for 80 min at 0 °C and trimethylstannyl chloride (9.38 g, 47.1 mmol) in THF (10 mL) was added. After removal of the cooling bath, the slightly yellow solution was stirred for 2 h at 22 °C and was quenched with a saturated solution of ammonium chloride (1 x 5 mL). The crude product was extracted with diethyl ether (3 x 10 mL) and dried over magnesium sulfate, filtered, and the volatiles were removed *in vacuo*. The yellow oil was purified by sublimation (75 °C, 4.5 · 10⁻² mbar) to afford a slightly yellow solid

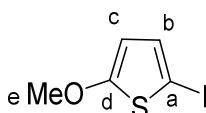
in a yield of 6.00 g (73%). **M.p.**: 70 °C; **¹H NMR** (500 MHz, C₆D₆): δ 2.16-2.09 (m, 4 H, d), 1.63-1.53 (m, 4 H, e), 0.16 (s, 18H, a) ppm; **¹³C{¹H} NMR** (126 MHz, CDCl₃): δ 110.4 (c), 82.2 (b), 28.3 (e), 19.8 (d), -8.3 (a) ppm; **¹¹⁹Sn{¹H} NMR** (187 MHz, C₆D₆): δ -73.2 ppm.; **IR** (ATR): ν 3619 (w), 2984 (w), 2942 (m), 2866 (w), 2147 (m), 1548 (m), 1459 (m), 1373 (m), 1326 (m), 1307 (m), 1191 (m), 1028 (m), 925 (m), 771 (s), 721 (s), 538 (s), 516 (s) cm⁻¹; **HR-MS** (EI, [M-H]⁺, C₁₃H₂₃¹²⁰Sn₂): *m/z* calcd. 418.9843, found 418.9844 (R = 10000); **MS** (EI, 70 eV, direct inlet, 200 °C): *m/z* (% relative intensity) = 419 (20) [M]⁺, 329 (100) [M-OC₄H₉]⁺. The data are consistent with the literature.^[4a]

1,8-bis(4,4,5,5-Tetramethyl-1,3,2-dioxaborolan-2-yl)octa-1,7-diyne^[4b]



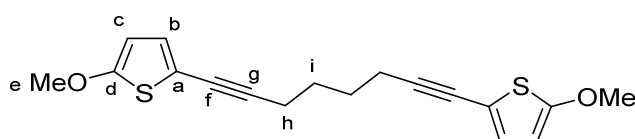
n-Butyllithium (14.5 mL, 2.4 M in hexanes) was added dropwise over the course of 30 min to a solution of 1,7-octadiyne (2.34 mL, 17.6 mmol) in diethyl ether (350 mL) at -78 °C under nitrogen atmosphere. The resulting slurry was mechanically stirred for 15 min and isopropylpinacol borate (6.56 g, 34.9 mmol) was added at once and the slurry was stirred at 22 °C for 3 h. HCl (28 mL, 2 M in diethyl ether) was added at -40 °C and the mixture was stirred until it reached 22 °C. It was stirred for a further 1 h at this temperature. Afterwards the mixture was filtered and concentrated to dryness. The residue was dried via oil pump vacuum (2.0·10⁻¹ mBar) at 50 °C for 3h. The crude product was then recrystallized in *n*-hexane (1 x 20 mL) and hot filtered to afford a white solid in a yield of 3.64 g (58%). **M.p.**: 129 °C; **¹H NMR** (500 MHz, C₆D₆): 1.82-1.78 (m, 4H, f), 1.29-1.24 (m, 4H, e), 1.00 (s, 24H, a) ppm; **¹³C{¹H} NMR** (126 MHz, C₆D₆): 83.83 (b), 69.2 (d), 27.5 (f), 24.9 (a), 19.2 (e) ppm; **¹¹B NMR** (160 MHz, C₆D₆): δ 24.6 ppm; **IR** (ATR): ν 2975 (w), 2923 (w), 1577 (w), 1430 (m), 1369 (m), 1316 (s), 1265 (m), 1165 (s), 1074 (w), 966 (w), 847 (s), 727 (s), 696 (s), 672 (m) cm⁻¹; **HR-MS** (EI, C₂₀H₃₂O₄¹⁰B₂): *m/z* calcd. 356.25538, found 356.25674 (R = 10000); **MS** (EI, 70 eV, direct inlet, 200 °C): *m/z* (% relative intensity) = 358 (9) [M]⁺, 285 (100) [M-OC₄H₉]⁺. The data are consistent with the literature.^[4b]

5-Methoxy-2-iodothiophene (13)^[11]

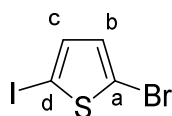


This reaction was not carried out under inert conditions. 2-Methoxythiophene (1.00 g, 8.76 mmol.) was dissolved in ethanol (17.5 mL). *N*-Iodosuccinimide (1.97 g, 8.76 mmol) and *p*-toluenesulfonic acid (170 mg, 870 mmol, 10 mol%) were added and reaction was stirred for 10 min at 22 °C. A saturated solution of sodium thiosulfate (17.5 mL) was added. The mixture was extracted with ethyl acetate (1 x 26 mL) and the organic phase was washed with a solution of sodium carbonate (1 M, 1 x 18 mL), dried over magnesium sulfate and filtered. The volatiles were removed *in vacuo*. The crude product was purified by column chromatography (silica gel, *n*-hexane, $R_f = 0.33$) to afford a yellow oil (1.36 g, 65%). **¹H NMR** (500 MHz, CDCl₃): δ 6.91 (d, ³*J* = 4.0 Hz, 1H, b), 5.93 (d, ³*J* = 4.0 Hz, 1H, c), 3.87 (s, 3H, e) ppm; **¹³C{¹H} NMR** (126 MHz, CDCl₃): δ 170.1 (d), 134.6 (b), 106.0 (c), 60.6 (e), 57.4 (a) ppm; **IR** (ATR): ν 2932 (w), 2821 (w), 1541 (m), 1464 (m), 1419 (m), 1367 (w), 1320 (w), 1277 (w), 1232 (w), 1219 (w), 1195 (m), 1179 (m), 1147 (w), 1098 (w), 1074 (w), 1057 (m), 1044 (m), 992 (m), 968 (w), 931 (m), 848 (w), 808 (w), 758 (m), 736 (w), 718 (w) cm⁻¹; **HR-MS** (EI, C₅H₅OSI): *m/z* calcd. 239.91004, found 239.90994 (R = 10000); **MS** (EI, 70 eV, indirect inlet, 200 °C): *m/z* (% relative intensity) = 240 (100) [M]⁺, 98 (77) [M-CH₃-I]⁺. The data are consistent with the literature.^[11]

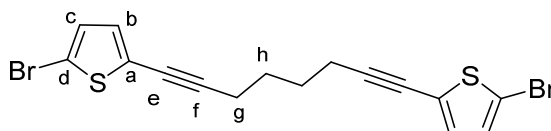
1,8-bis(5-Methoxy-thiophen-2-yl)octa-1,7-diyne^[5]



In a GB, a mixture of 5-methoxy-2-iodothiophene (**15**) (2.00 g, 8.33 mmol), [PdCl₂(dppf)] (607 mg, 830 μmol) and copper (I) iodide (158 mg, 830 μmol) in triethylamine (4.5 mL) and *N,N*-dimethylformamide (14 mL) was stirred at 20 °C. After addition of 1,7-octadiyne (441 mg, 4.16 mmol), the red-brown suspension was stirred under for further 20 h. The reaction was quenched with a saturated solution of ammonium chloride (1 x 50 mL) and the aqueous layer was extracted with diethyl ether (3 x 50 mL). The combined organic layers were washed with water (1 x 100 mL), separated and the organic phase was dried over magnesium sulfate. After filtration, the solvents were removed *in vacuo*. The product was purified by column chromatography (silica gel, 1:5 dichloromethane/*n*-hexane, $R_f = 0.14$) to give an orange yellow solid (455 mg, 33%). **M.p.**: 36 °C; **¹H NMR** (500 MHz, CDCl₃): δ 6.77 (d, ³*J* = 4.0 Hz, 2H, b), 6.02 (d, ³*J* = 4.0 Hz, 2H, c), 3.87 (s 6H, e), 2.47-2.41 (m, 4H, g), 1.75-1.65 (m, 4H, h) ppm; **¹³C{¹H} NMR** (126 MHz, CDCl₃): δ 165.9 (d), 129.6 (b), 110.6 (c), 103.8 (a), 91.6 (g), 74.7 (f), 60.3 (e), 27.9 (h), 19.4 (i) ppm; **IR** (ATR): ν 2945 (w), 1542 (m), 1488 (s), 1458 (m), 1449 (m), 1424 (s), 1344 (w), 1329 (w), 1251 (m), 1197 (m), 1154 (w), 1045 (s), 1008 (w), 987 (m), 903 (w), 859 (w), 773 (s), 739 (m), 728 (m), 712 (m) cm⁻¹; **HR-MS** (EI, C₁₈H₁₈O₂S₂): *m/z* calcd. 330.07427, found 330.07389 (R = 10000); **MS** (EI, 70 eV, direct inlet, 200 °C): *m/z* (% relative intensity) = 330 (16) [M]⁺, 315 (100) [M-CH₃]⁺. The data are consistent with the literature.^[5]

2-Bromo-5-iodothiophene (14)^[11]

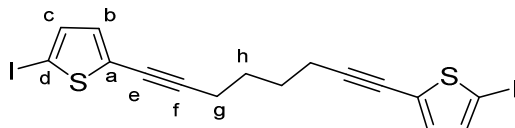
This reaction was not carried out under Schlenk conditions. To a solution of 2-bromothiophene (10.0 g, 61.3 mmol) in ethanol (123 mL), *n*-iodosuccinimide (15.2 g, 67.4 mmol, 1.1 eq) and *p*-toluenesulfonic acid (1.17 g, 6.13 mmol, 10 mol%) were added at 22 °C. The reaction mixture was stirred for 10 min at 50 °C. It was taken out of the heating bath and a saturated solution of sodium thiosulfate (1 x 123 mL) was added. The mixture was extracted with ethyl acetate (3 x 100 mL) and the organic phase was washed with a 1 M solution of sodium carbonate (1 x 200 mL). The organic phase was dried over magnesium sulfate, filtered, and dried *in vacuo*. Purification by Kugelrohrdistillation ($9 \cdot 10^{-2}$ mbar, 48-50 °C) gave 2-bromo-5-iodo-thiophene as colorless oil (13.6 g, 77%). **¹H NMR** (500 MHz, CDCl₃): δ 7.04 (d, ³J = 3.8 Hz, 1H, c), 6.75 (d, ³J = 3.8 Hz, 1H, b) ppm; **¹³C{¹H} NMR** (126 MHz, CDCl₃): δ 137.6 (c), 131.8 (b), 115.3 (a), 72.4 (d) ppm; **IR** (ATR): ν 3091 (w), 1731 (w), 1567 (w), 1508 (m), 1397 (m), 1202 (m), 968 (s), 929 (m), 780 (s) cm⁻¹; **HR-MS** (EI, C₄H₂⁷⁹BrIS): *m/z* calcd. 287.80998, found 287.81052 (R = 10000); **MS** (EI, 70 eV, indirect inlet, 200 °C): *m/z* (% relative intensity) = 288 (92) [M]⁺, 82 (100). The data are consistent with the literature.^[11]

1,8-bis(5-Bromo-thiophen-2-yl)octa-1,7-diyne (10d)

In a GB, a mixture of 2-bromo-5-iodothiophene (5.00 g, 17.3 mmol), [Pd(PPh₃)₄] (404 mg, 2 mol%, 350 μmol) and copper iodide (66.7 mg, 2 mol%, 350 μmol) in dry triethylamine (5.00 mL) and dry *N,N*-dimethylformamide (9.00 mL) was stirred at 20 °C. After addition of 1,7-octadiyne (920 mg, 8.65 mmol), the red suspension was stirred under a nitrogen atmosphere at 55 °C for 20 h. Then, the reaction was quenched with a saturated solution of ammonium chloride (1 x 50 mL). The mixture was extracted with diethyl ether (3 x 100 mL) and the combined organic layers were washed with water (1 x 100 mL). They were separated and dried over magnesium sulfate. The volatiles were removed *in vacuo*. The residue was purified by column chromatography (silica gel, *n*-hexane; R_f = 0.24) to obtain a yellow oil, which crystallised at 0-5 °C (2.57 g, 69%). **M.p.**: 53 °C; **¹H NMR** (500 MHz, CDCl₃): δ 6.88 (d, ³J = 3.9 Hz, 2H, b), 6.86 (d, ³J = 3.9 Hz, 2H, c), 2.51-2.43 (m, 4H, g), 1.79-1.69 (m, 4H, h); **¹³C{¹H} NMR** (126 MHz, CDCl₃): δ 131.5 (b), 129.9 (c), 125.9 (a), 111.7 (d), 95.1 (f), 73.6 (e), 27.7 (g), 19.4 (h) ppm; **IR** (ATR): ν 3091 (w), 3079 (w), 2949 (w), 2926 (m), 2898 (w), 2859 (w), 2823

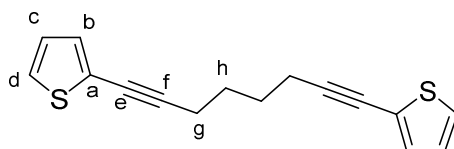
(w), 2226 (w), 1749 (w), 1587 (w), 1526 (w), 1452 (w), 1428 (m), 1418 (m), 1326 (m), 1305 (w), 1222 (w), 1188 (m), 1111 (w), 1054 (w), 991 (m), 964 (m), 893 (w), 876 (w), 793 (s), 757 (m), 727 (w) cm^{-1} ; **HR-MS** (EI, $\text{C}_{16}\text{H}_{12}^{79}\text{Br}_2\text{S}_2$): m/z calcd. 425.87472, found 425.87555 ($R = 10000$); **MS** (EI, 70 eV, direct inlet, 200 °C): m/z (% relative intensity) = 428 (100) $[\text{M}]^+$.

1,8-bis(5-Iodothiophen-2-yl)octa-1,7-diyne (10e)



To a solution of 1,8-bis(5-bromo-thiophen-2-yl)octa-1,7-diyne (**11d**) (800 mg, 1.87 mmol) in THF (13 mL) at -78 °C, *n*-butyllithium (2.50 M in hexanes, 1.6 mL, 4.1 mmol) was added dropwise over the course of 15 min. The red solution was stirred for 60 min and iodine (1.42 g, 5.61 mmol) in THF (2.70 mL) was added within 5 min. The brown suspension was warmed to 20 °C over the course of 2 h by removing the cooling bath. The reaction mixture was quenched with a saturated solution of sodium thiosulfate (1 x 25 mL) and it was extracted with diethyl ether (3 x 30 mL). The combined organic layers were dried over magnesium sulfate. The solvents were removed *in vacuo*. The crude product was purified by column chromatography (silica gel, *n*-hexane; $R_f = 0.14$) to obtain a yellow oil (836 mg, 86%), which crystallized at 0-5 °C. **M.p.**: 73 °C; **$^1\text{H NMR}$** (500 MHz, CDCl_3): δ 7.07 (d, $^3J = 3.8$ Hz, 2H, c), 6.77 (d, $^3J = 3.8$ Hz, 2H, b), 2.53-2.43 (m, 4H, g), 1.79-1.68 (m, 4H, h) ppm; **$^{13}\text{C}\{^1\text{H}\}$ NMR** (126 MHz, CDCl_3): δ 136.9 (c), 132.5 (b), 130.4 (a), 96.0 (f), 73.3 (e), 73.1 (d), 27.7 (g), 19.4 (h) ppm; **IR** (ATR): ν 3072 (w), 2946 (w), 2924 (w), 2896 (w), 2857 (w), 2223 (w), 1752 (w), 1590 (w), 1519 (w), 1451 (w), 1434 (w), 1417 (m), 1325 (w), 1304 (w), 1220 (w), 1185 (m), 1052 (w), 987 (w), 942 (m), 891 (w), 877 (w), 794 (s), 755 (m) cm^{-1} ; **HR-MS** (EI, $\text{C}_{16}\text{H}_{12}\text{I}_2\text{S}_2$): m/z calcd. 521.84700, found 521.84899 ($R = 10000$); **MS** (EI, 70 eV, direct inlet, 200 °C): m/z (% relative intensity) = 522 (100) $[\text{M}]^+$.

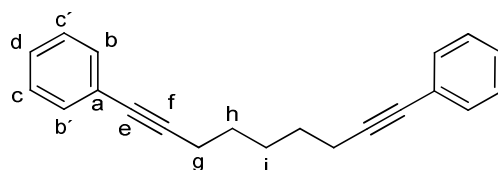
1,8-bis(Thiophen-2-yl)octa-1,7-diyne (10f)^[5]



In a GB, a mixture of 2-iodothiophene (5.00 g, 23.8 mmol), $[\text{Pd}(\text{PPh}_3)_4]$ (555 mg, 480 μmol) and copper (I) iodide (91.4 mg, 480 μmol) in triethylamine (8 mL) and *N,N*-dimethylformamide (14 mL) was stirred at 20 °C. After addition of 1,7-octadiyne (0.59 g, 5.65 mmol), the red-brown suspension was stirred under a nitrogen atmosphere at 55 °C for 20 h. The reaction was quenched with a saturated solution of ammonium chloride (1 x 30 mL). The aqueous layer was

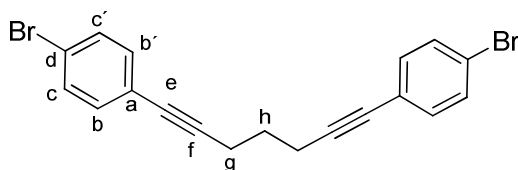
extracted with diethyl ether (3 x 30 mL) and the combined organic layers were washed with water (1 x 100 mL). The phases were separated and dried over magnesium sulfate. The volatiles were removed *in vacuo*. The residue was purified by column chromatography (silica gel, 1/20 dichloromethane/*n*-hexane, $R_f = 0.18$) to give the product as a yellow waxy solid (2.09 g, 65%). **M.p.:** 44 °C; **$^1\text{H NMR}$** (500 MHz, CDCl_3): δ 7.17 (dd, $^3J = 5.2$ Hz, $^4J = 1.0$ Hz, 2H, d), 7.12 (dd, $^3J = 3.6$ Hz, $^4J = 1.0$ Hz, 2H, b), 6.94 (dd, $^3J = 5.2$ Hz, $^3J = 3.6$ Hz, 2H, c), 2.54-2.43 (m, 4H, g), 1.82-1.72 (m, 4H, h) ppm; **$^{13}\text{C}\{^1\text{H}\}$ NMR** (126 MHz, CDCl_3): δ 131.2 (b), 126.9 (d), 126.1 (c), 124.2 (a), 94.0 (f), 74.2 (e), 27.9 (g), 19.4 (h) ppm; **IR** (ATR): ν 3107 (w), 2939 (w), 2860 (w), 1516 (w), 1449 (w), 1427 (m), 1355 (w), 1294 (w), 1275 (w), 1237 (w), 1222 (w), 1185 (m), 1141 (w), 1083 (w), 1043 (w), 1015 (w), 897 (w), 846 (m), 829 (s), 741 (w), 691 (s), 662 (m) cm^{-1} ; **HR-MS** (EI, $\text{C}_{16}\text{H}_{14}\text{S}_2$): m/z calcd. 270.05314, found 270.05306 ($R = 12000$); **MS** (EI, 70 eV, direct inlet, 200 °C): m/z (% relative intensity) = 270 (100) $[\text{M}]^+$, 242 (70) $[\text{M}-\text{C}_2\text{H}_4]^+$. The data are consistent with the literature.^[5]

1,9-Diphenylnona-1,8-diyne (10g)

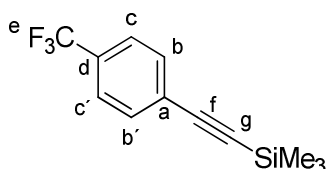


In a GB, a mixture of iodobenzene (2.00 g, 9.80 mmol), $[\text{Pd}(\text{PPh}_3)_4]$ (453 mg, 392 μmol , 4 mol%) and copper iodide (74.7 mg, 392 μmol , 4 mol%) in dry triethylamine (20 mL) was stirred at 20 °C. After addition of 1,8-nonadiyne (294 mg, 4.90 mmol), the suspension was stirred under a nitrogen atmosphere at 20 °C for 48 h. The reaction was quenched with a saturated solution of ammonium chloride (1 x 30 mL) and was extracted with dichloromethane (3 x 30 mL). The combined organic layers were washed with water (1 x 90 mL). They were separated and dried over magnesium sulfate. The volatiles were removed *in vacuo*. The residue was purified by column chromatography (silica gel, *n*-pentane, $R_f = 0.05$) to give a colorless oil (1.06 g, 79%). **$^1\text{H NMR}$** (600 MHz, CDCl_3): δ 7.45-7.35 (m, 4H, b, b'), 7.30-7.23 (m, 6H, c, c', d), 2.49-2.42 (m, 4H, g), 1.71-1.63 (m, 6H, h, i) ppm; **$^{13}\text{C}\{^1\text{H}\}$ NMR** (151 MHz, CDCl_3): δ 131.7 (b, b'), 128.3 (c, c'), 127.6 (d), 124.1 (a), 90.3 (f), 80.9 (e), 28.4 (h), 28.3 (i), 19.5 (g) ppm; **IR** (ATR): ν 3053 (w), 2935 (w), 2858 (w), 2231 (w), 1597 (w), 1570 (w), 1488 (m), 1441 (m), 1330 (w), 1069 (w), 1026 (w), 912 (w), 753 (s), 689 (s) cm^{-1} ; **HR-MS** (EI, $\text{C}_{21}\text{H}_{20}$): m/z calcd. 272.15595, found 272.15599 ($R = 10000$); **MS** (EI, 70 eV, direct inlet, 200 °C): m/z (% relative intensity) = 272 (46) $[\text{M}]^+$, 115 (100).

* This signal was overlapping with the solvent signal.

1,7-bis(4-Bromophenyl)hepta-1,6-diyne (10h)^[7]

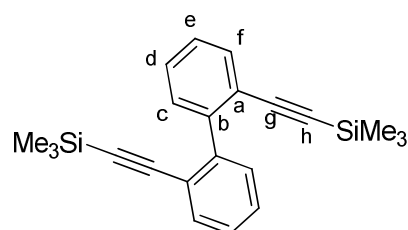
In a GB, a mixture of 1-bromo-4-iodobenzene (2.00 g, 7.07 mmol), [Pd(PPh₃)₄] (327 mg, 283 μmol, 4 mol%) and copper iodide (54 mg, 283 μmol, 4 mol%) in dry triethylamine (20 mL) was stirred at 20 °C. After addition of 1,6-heptadiyne (326 mg, 3.54 mmol), the suspension was stirred under a nitrogen atmosphere at 20 °C for 24 h. The reaction was quenched with a saturated solution of ammonium chloride (1 x 30 mL). The mixture was extracted with dichloromethane (3 x 30 mL) and the combined organic layers were washed with water (1 x 90 mL) and dried over magnesium sulfate. The volatiles were removed *in vacuo* and the residue was purified by column chromatography (silica gel, *n*-pentane, R_f = 0.15) to give a colorless solid (1.20 g, 84%). **M.p.:** 61 °C; **¹H NMR** (600 MHz, CDCl₃): δ 7.47-7.41 (m, 4H, c, c'), 7.30-7.26 (m, 4H, b, b'), 2.59 (t, ³J = 7.0 Hz, 4H, g), 1.92 (p, ³J = 7.0 Hz, 2H, h) ppm; **¹³C{¹H} NMR** (151 MHz, CDCl₃): δ 133.1 (b, b'), 131.5 (c, c'), 122.7 (d), 121.8 (a), 90.4 (f), 80.3 (e), 27.7 (h), 18.7 (g) ppm; **IR** (ATR): ν 3071 (w), 2953 (w), 2903 (w), 2828 (w), 2236 (w), 2146 (w), 1900 (w), 1779 (w), 1651 (w), 1583 (w), 1481 (m), 1454 (w), 1423 (w), 1392 (w), 1351 (w), 1318 (w), 1291 (w), 1253 (w), 1199 (w), 1175 (w), 1096 (w), 1065 (m), 1043 (w), 1009 (m), 907 (w), 857 (w), 821 (s), 761 (m), 736 (w), 703 (w) cm⁻¹; **HR-MS** (EI, C₁₉H₁₄⁷⁹Br₂): *m/z* calcd. 399.94568, found 399.94568 (R = 10000); **MS** (EI, 70 eV, direct inlet, 200 °C): *m/z* (% relative intensity) = 400 (20) [M]⁺, 242 (100) [M-C₆H₄Br]⁺. The data are consistent with the literature.^[7]

4-Trifluoromethyl-phenylethynyltrimethylsilane (10i)^[8]

1-Bromo-4-(trifluoromethyl)benzene (1.53 g, 6.82 mmol) was dissolved in triethylamine (10 mL). Trimethylsilylacetylene (736 mg, 7.50 mmol), [Pd(PPh₃)₄] (46.2 mg, 40.0 μmol) and copper iodide (8 mg, 40.0 μmol) were added and the reaction mixture was heated to 80 °C for 12 h in a microwave apparatus. Then, the mixture was filtered to remove insoluble by-products and was diluted with diethyl ether (1 x 40 mL). It was washed with a saturated solution of ammonium chloride (1 x 40 mL). The aqueous layer was extracted with diethyl ether (3 x 40 mL) and the combined organic layers were washed with water (1 x 40 mL). The organic phase was dried using magnesium sulfate and the volatiles were removed *in vacuo* leaving a

yellow oil. Purification by column chromatography (silica gel, *n*-pentane, $R_f = 0.47$) gave 4-(trifluoromethylphenyl)ethynyltrimethylsilane as a colorless oil (1.23 g, 74%). **$^1\text{H NMR}$** (500 MHz, CDCl_3): δ 7.56 (s, 4H, b, b', c, c'), 0.27 (s, 9H, SiMe_3) ppm; **$^{13}\text{C}\{^1\text{H}\}$ NMR** (126 MHz, CDCl_3): δ 132.3 (s, b, b'), 130.3 (q, $^2J_{\text{C-F}} = 32.7$ Hz, d), 127.1 (q, $^5J_{\text{C-F}} = 1.5$ Hz, a), 125.3 (q, $^3J_{\text{C-F}} = 3.8$ Hz, c, c'), 123.0 (s, e), 103.6 (s, f), 97.3 (s, g), -0.1 (s, SiMe_3) ppm; **$^{19}\text{F NMR}$** (471 MHz, CDCl_3): δ -63.4 ppm; **$^{29}\text{Si}\{^1\text{H}\}$ NMR** (99 MHz, CDCl_3): δ -17.1 ppm; **IR** (ATR): ν 2961 (w), 2162 (w), 1614 (w), 1405 (w), 1320 (s), 1250 (m), 1220 (w), 1166 (m), 1126 (s), 1104 (m), 1066 (s), 1014 (w), 861 (s), 838 (s), 759 (m), 699 (w), 656 (m) cm^{-1} ; **HR-MS** (EI, $\text{C}_{12}\text{H}_{13}\text{F}_3\text{Si}$): m/z calcd. 242.07331, found 242.07332 ($R = 10000$); **MS** (EI, 70 eV, indirect inlet, 200 °C): m/z (% relative intensity) = 242 (12) $[\text{M}]^+$, 227 (100) $[\text{M}-\text{CH}_3]^+$. The data are consistent with the literature.^[8]

2,2'-bis((Trimethylsilyl)ethynyl)biphenyl (10j)^[9]



To a solution of 1-bromo-2-(2-trimethylsilylethynyl)benzene (1.20 g, 4.74 mmol) in tetrahydrofuran (24 mL), *n*-butyllithium (2.5 M in hexanes, 2.10 mL, 5.2 mmol) was added dropwise over the course of 8 min. The reaction mixture was stirred for 1.5 h, then copper(II) chloride (0.88 g, 6.5 mmol) was added. The red-brownish mixture was allowed to warm up by removing the cooling bath and was stirred at 20 °C for further 16 h. The reaction mixture was quenched with a saturated solution of ammonium chloride (1 x 100 mL) and extracted with ethyl acetate (3 x 50 mL). The combined organic layers were washed with water (1 x 100 mL) and dried over magnesium sulfate. Filtration, removing of the solvents *in vacuo* and purification by column chromatography (silica gel, *n*-pentane, $R_f = 0.1$) gave the product as a slightly yellow oil (378 mg, 46%). **$^1\text{H NMR}$** (600 MHz, CDCl_3): δ 7.55 (d, $^3J = 7.2$ Hz, 2H, c), 7.44 (d, $^3J = 7.5$ Hz, 2H, f), 7.37-7.31 (m, 2H, d), 7.29 (t, $^3J = 7.5$ Hz, 2H, e), 0.06 (s, 18H, SiMe_3) ppm; **$^{13}\text{C}\{^1\text{H}\}$ NMR** (151 MHz, CDCl_3): δ 143.6 (b), 132.2 (f), 130.2 (d), 127.8 (e), 127.2 (c), 122.7 (a), 104.7 (g), 97.5 (h), -0.2 (SiMe_3) ppm; **$^{29}\text{Si}\{^1\text{H}\}$ NMR** (99 MHz, C_6D_6): δ -18.3 ppm; **IR** (ATR): ν 3061 (w), 2957 (w), 2897 (w), 2158 (w), 1466 (w), 1437 (w), 1247 (m), 1212 (w), 1095 (w), 1062 (w), 1047 (w), 1002 (w), 946 (w), 858 (s), 836 (s), 752 (s), 697 (m) cm^{-1} ; **HR-MS** (APCI pos, $\text{C}_{22}\text{H}_{27}\text{Si}_2$): m/z calcd. 347.16458, found 347.16410; **MS** (EI, 70 eV, direct inlet, 200 °C): m/z (% relative intensity) = 346 (27) $[\text{M}]^+$, 73 (100) (SiMe_3)⁺. The data are consistent with the literature.^[9]

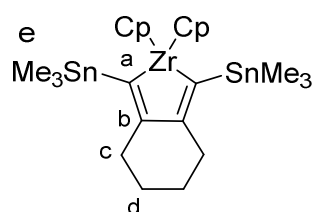
3 Reaction Monitoring Using Rosenthal's Zirconocene vs. Negishi's Reagent for the Synthesis of Zirconacyclopentadienes.

General Procedure for the Synthesis of the Zirconacyclopentadienes and Reaction Monitoring.

A mixture of a "Cp₂Zr" species, either from Negishi's reagent or Rosenthal's reagent, and a diyne (**10a-l**) was stirred at 22 °C in THF or toluene (amounts see below). A defined sample (0.3 mL) of the reaction was taken after 10 min, 30 min, 1 h, 3 h and 22 h and the solvent was removed immediately *in vacuo* at 22 °C. The reaction monitorings were analyzed by ¹H NMR spectroscopic measurements of each sample. Naphthalene in C₆D₆ was added in an equimolar amount to the sample and used as an internal standard.

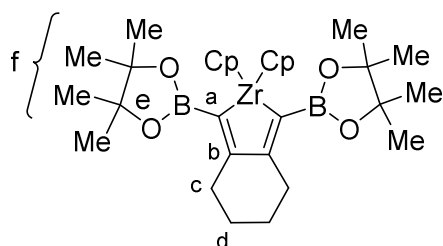
3.1 Reactions with the Negishi's reagent

Reaction Monitoring of the Formation of Zirconacyclopentadiene **11a**^[4a]



To a solution of Cp₂ZrCl₂ (67.7 mg, 231 μmol) in THF (2.0 mL) at -78 °C, *n*-butyllithium (0.18 mL, 463 μmol; 2.59 M in hexanes) was added dropwise over the course of 1 min. The reaction mixture was stirred at -78 °C for 1 h and a solution of diyne **10a** (100 mg, 231 μmol) in THF (1.0 mL) was added. The reaction was allowed to warm to 22 °C and samples (0.3 mL) were taken for the reaction monitoring after the defined times. The partial formation of the zirconacyclopentadiene **11a** was observed after 10 min of reaction. Over time, the mixture turned from yellow to bright orange. After 22 h, the reaction mixture was yellowish again.

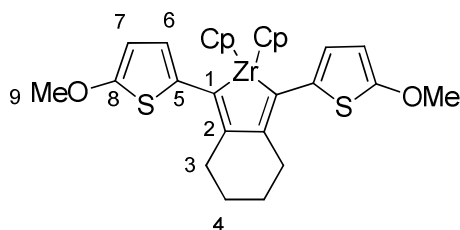
Reaction Monitoring of the Formation of Zirconacyclopentadiene **11b**^[12]



To a solution of Cp₂ZrCl₂ (81.6 mg, 279 μmol) in THF (2 mL) at -78 °C, *n*-butyllithium (0.22 mL, 558 μmol; 2.59 M in hexanes) was added dropwise over the course of 1 min. The reaction mixture was stirred at -78 °C for 1 h and a solution of diyne **10b** (100 mg, 279 μmol) in THF

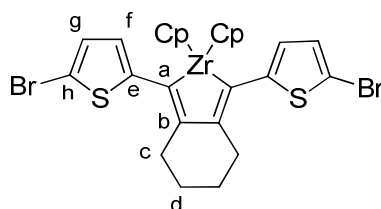
(1.0 mL) was added. The reaction was allowed to warm to 22 °C and samples (0.3 mL) were taken for the reaction monitoring after the defined times. The partial formation of the zirconacyclopentadiene **11b** was observed after 10 min of reaction. Over this time, the mixture turned from yellow to bright orange. After 22 h, the reaction mixture was yellowish again.

Reaction Monitoring of the Formation of Zirconacyclopentadiene **11c**^[5]



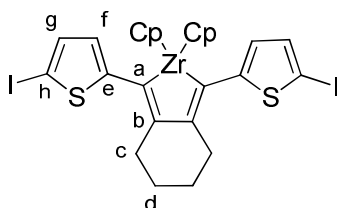
To a solution of Cp_2ZrCl_2 (88.7 mg, 303 μmol) in THF (1.5 mL) at -78 °C, *n*-butyllithium (0.23 mL, 606 μmol ; 2.59 M in hexanes) was added dropwise over the course of 1 min. The reaction mixture was stirred at -78 °C for 1 h and a solution of diyne **10c** (100 mg, 303 μmol) in THF (0.5 mL) was added. The reaction was allowed to warm to 22 °C and samples (0.3 mL) were taken for the reaction monitoring after the defined times. A low amount of formation of the zirconacyclopentadiene **11c** was observed after 10 min of reaction. Over time, the mixture turned from yellow to orange-brown. After 22 h, the reaction mixture was yellowish again.

Reaction Monitoring of the Formation of Zirconacyclopentadiene **11d**



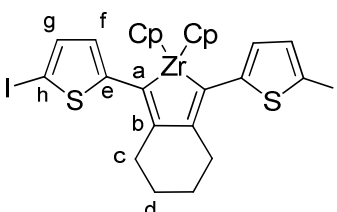
To a solution of zirconocene dichloride (68.7 mg, 235 μmol) in THF (1.5 mL) at -78 °C, *n*-butyllithium (0.18 mL, 470 μmol ; 2.59 M in hexanes) was added dropwise over the course of 1 min. The reaction mixture was stirred at -78 °C for 1 h and a solution of diyne **10d** (100 mg, 235 μmol) in THF (0.5 mL) was added. The reaction was allowed to warm to 22 °C and samples (0.3 mL) were taken for the reaction monitoring after the defined times. A low amount of formation of the zirconacyclopentadiene **11d** was observed after 10 min of reaction. Over time, the mixture turned from yellow to orange. After 22 h, the reaction mixture was yellowish again.

Reaction Monitoring of the Formation of Zirconacyclopentadiene **11e**



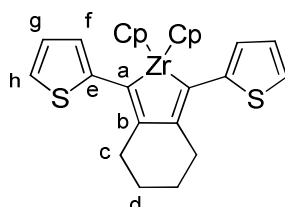
To a solution of zirconocene dichloride (56.1 mg, 192 μmol) in THF (1.5 mL) at $-78\text{ }^\circ\text{C}$, *n*-butyllithium (0.15 mL, 384 μmol ; 2.59 M in hexanes) was added dropwise over the course of 1 min. The reaction mixture was stirred at $-78\text{ }^\circ\text{C}$ for 1 h and a solution of diyne **10e** (100 mg, 192 μmol) in THF (0.5 mL) was added. The reaction was allowed to warm to $22\text{ }^\circ\text{C}$ and samples (0.3 mL) were taken for the reaction monitoring after the defined times. No formation of the zirconacyclopentadiene **11e** was observed after 10 min of reaction. Over time, the mixture did not change the color.

Reaction Monitoring of the Formation of Zirconacyclopentadiene **11e** with BTMSA in the Reaction Mixture



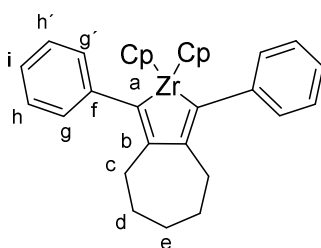
To a solution of zirconocene dichloride (83.9 mg, 287 μmol) in THF (3.0 mL) at $-78\text{ }^\circ\text{C}$, *n*-butyllithium (0.23 mL, 574 μmol ; 2.50 M in hexanes) was added dropwise over the course of 1-2 min. The reaction mixture was stirred at $-78\text{ }^\circ\text{C}$ for 1 h. Then, a solution of bis(trimethylsilyl)acetylene (48.9 mg, 287 μmol) in THF (0.5 mL) was added and one minute later a solution of diyne **10e** (150 mg, 287 μmol) in THF (0.5 mL) was added. The reaction was allowed to warm to $22\text{ }^\circ\text{C}$ and samples (0.3 mL) were taken for the reaction monitoring after the defined times. A low amount of formation of the zirconacyclopentadiene **11e** was observed after 10 min of reaction. Over time, the mixture turned from yellow to orange-red. After 22 h, the reaction mixture was bright yellow again.

Reaction Monitoring of the Formation of Zirconacyclopentadiene **11f**^[5]



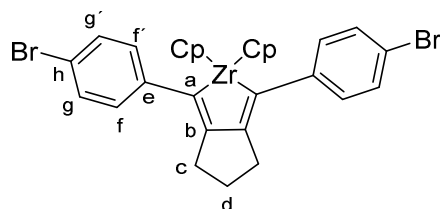
To a solution of zirconocene dichloride (108 mg, 370 μmol) in THF (1.5 mL) at $-78\text{ }^\circ\text{C}$, *n*-butyllithium (0.29 mL, 740 μmol ; 2.59 M in hexanes) was added dropwise over the course of 1 min. The reaction mixture was stirred at $-78\text{ }^\circ\text{C}$ for 1 h and a solution of diyne **10f** (100 mg, 370 μmol) in THF (0.5 mL) was added. The reaction was allowed to warm to $22\text{ }^\circ\text{C}$ and samples (0.3 mL) were taken for the reaction monitoring after the defined times. High formation of the zirconacyclopentadiene **11f** was observed after 10 min of reaction. Over time, the mixture turned from yellow to orange-red. After 22 h, the reaction mixture was yellowish again.

Reaction Monitoring of the Formation of Zirconacyclopentadiene **11g**



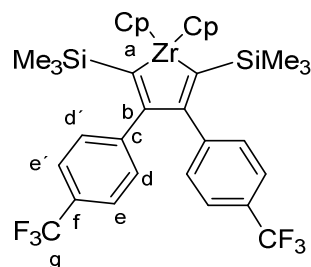
To a solution of Cp_2ZrCl_2 (161 mg, 551 μmol) in THF (5 mL) at $-78\text{ }^\circ\text{C}$, *n*-butyllithium (0.44 mL, 1.10 mmol; 2.50 M in hexanes) was added dropwise over the course of 2 min. The reaction mixture was stirred at $-78\text{ }^\circ\text{C}$ for 1 h and a solution of diyne **10g** (150 mg, 551 μmol) in THF (0.5 mL) was added. The reaction was allowed to warm to $22\text{ }^\circ\text{C}$ and after 3 h of reaction the solvent was removed *in vacuo*. After removing of the solvent, the sample could not be completely redissolved in deuterated solvents so that the conversion could not be determined by ^1H NMR with an internal standard. The reaction was repeated. After filtration of the reaction mixture over celite and removing of the solvent, an orange-pink solid-like film was obtained (239 mg, 88%, purity 90%).

Reaction Monitoring of the Formation of Zirconacyclopentadiene **11h**^[13]



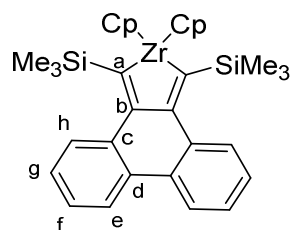
To a solution of Cp_2ZrCl_2 (109 mg, 373 μmol) in THF (3 mL) at $-78\text{ }^\circ\text{C}$, *n*-butyllithium (0.30 mL, 746 μmol ; 2.50 M in hexanes) was added dropwise over the course of 2 min. The reaction mixture was stirred at $-78\text{ }^\circ\text{C}$ for 1 h and a solution of diyne **10h** (150 mg, 373 μmol) in THF (0.5 mL) was added. The reaction was allowed to warm to $22\text{ }^\circ\text{C}$ and samples (0.3 mL) were taken for the reaction monitoring after the defined times. Formation of the zirconacyclopentadiene **11h** was observed after 10 min of reaction. Over this time, the mixture turned from yellow to orange-red.

Reaction Monitoring of the Formation of Zirconacyclopentadiene **11i**



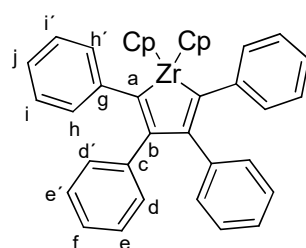
To a solution of Cp_2ZrCl_2 (90 mg, 309 μmol) in THF (3 mL) at -78°C , *n*-butyllithium (250 μL , 618 μmol ; 2.50 M in hexanes) was added dropwise over the course of 1 min. The reaction mixture was stirred at -78°C for 1 h and a solution of acetylene **10i** (150 mg, 618 μmol) in THF (0.5 mL) was added. The reaction was allowed to warm to 22°C and samples (0.3 mL) were taken for the reaction monitoring after the defined times. Formation of the zirconacyclopentadiene **11i** was observed after 10 min of reaction. Over this time, the mixture turned from yellow to orange. After 22 h the reaction mixture turned lighter in color.

Reaction Monitoring of the Formation of Zirconacyclopentadiene **11j**^[9]



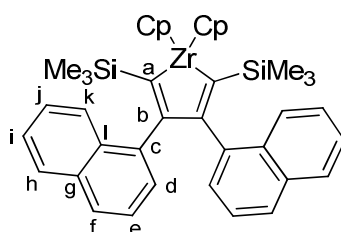
To a solution of Cp_2ZrCl_2 (84 mg, 288 μmol) in THF (5 mL) at -78°C , *n*-butyllithium (230 μL , 576 μmol ; 2.50 M in hexanes) was added dropwise over the course of 1 min. The reaction mixture was stirred at -78°C for 1 h and a solution of diyne **10j** (100 mg, 288 μmol) in THF (0.5 mL) was added. The reaction was allowed to warm to 22°C and samples (0.3 mL) were taken for the reaction monitoring after the defined times. Formation of the zirconacyclopentadiene **11j** was observed after 10 min of reaction. Over this time, the mixture turned from yellow to orange-red. After 22 h the reaction mixture went to bright orange.

Reaction Monitoring of the Formation of Zirconacyclopentadiene **11k**^[13]



To a solution of Cp_2ZrCl_2 (123 mg, 421 μmol) in THF (3 mL) at -78°C , *n*-butyllithium (330 μL , 842 μmol ; 2.50 M in hexanes) was added dropwise over the course of 2 min. The reaction mixture was stirred at -78°C for 1 h and a solution of diphenylacetylene (**10k**) (150 mg, 842 μmol) in THF (2 mL) was added. The reaction was allowed to warm to 22°C and samples (0.3 mL) were taken for the reaction monitoring after the defined times. Formation of the zirconacyclopentadiene **11k** was observed after 10 min of reaction. Over this time, the mixture turned from yellow to orange-red. After 22 h the reaction mixture changed to bright orange.

Reaction Monitoring of the Formation of Zirconacyclopentadiene **11l**

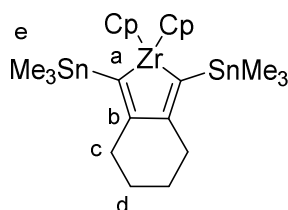


To a solution of Cp_2ZrCl_2 (97 mg, 334 μmol) in THF (3 mL) at -78°C , *n*-butyllithium (270 μL , 668 μmol ; 2.50 M in hexanes) was added dropwise over the course of 1 min. The reaction mixture was stirred at -78°C for 1 h and a solution of 1-(1-naphthyl)-2-(trimethylsilyl)acetylene (**10l**) (150 mg, 668 μmol) in THF (0.5 mL) was added. The reaction was allowed to warm to 22°C and samples (0.3 mL) were taken for the reaction monitoring after the defined times. Formation of the zirconacyclopentadiene **11l** was observed after 10 min of reaction. Over this time, the mixture turned from yellow to orange. After 22 h the reaction mixture changed to bright orange-yellow.

3.2 Reactions with the Rosenthal's Reagent

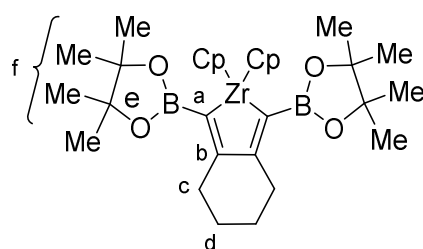
In the case of the reactions with Rosenthal's zirconocene, two reaction pots with the same amount were made: one for the reaction monitoring and one was stirred for 10 min and was used for further analytics and crystallization purposes. An exception was **11g**, where no reaction monitoring by ^1H NMR measurements could be performed.

Reaction Monitoring and Synthesis of Zirconacyclopentadiene **11a**^[4a]



In a GB, a solution of zirconocene **9** (108 mg, 230 μmol) and diyne **10a** (100 mg, 230 μmol) in toluene (5 mL) was stirred at 22 °C. Samples (0.3 mL) were taken for the reaction monitoring after the defined times. The formation of the zirconacyclopentadiene **11a** was observed after 10 min of reaction. Over this time the mixture turned to bright orange. The second reaction mixture was filtered over celite, the solvent was removed *in vacuo* and a bright orange-yellow solid was obtained for further analysis (141 mg, 94%). **^1H NMR** (500 MHz, C_6D_6) δ 6.00 (s, 10H, Cp), 2.22-2.15 (m, 4H, c), 1.57-1.50 (m, 4H, d), 0.20 (d, 18H, e; $^2J_{\text{Sn-H}} = 24$ Hz) ppm; **$^{13}\text{C}\{^1\text{H}\}$ NMR** (126 MHz, C_6D_6): δ 206.1 (a), 150.7 (b), 111.4 (Cp), 38.7 (c), 23.1(d), -6.7 (e; $^1J_{\text{Sn-C}} = 146$ Hz) ppm; **$^{119}\text{Sn}\{^1\text{H}\}$ NMR** (187 MHz, CDCl_3): δ -81.3 ppm; **HR-MS** (EI, $\text{C}_{24}\text{H}_{36}\text{Sn}_2\text{Zr}$): m/z calcd 653.99153, found 653.99188 (R = 10000); **MS** (EI, 70 eV, direct inlet, 200 °C): m/z (% relative intensity) = 654 (5) $[\text{M}]^+$, 155 $[\text{M}-\text{C}_{12}\text{H}_{12}]^+$, (100).

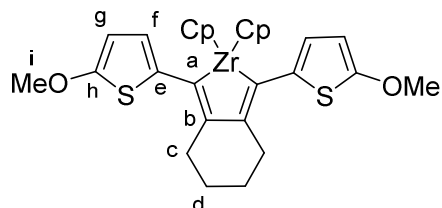
Reaction Monitoring and Synthesis of Zirconacyclopentadiene **11b**^[12]



In a GB, a solution of zirconocene **9** (132 mg, 280 μmol) and diyne **10b** (100 mg, 280 μmol) in toluene (5 mL) was stirred at 22 °C. Samples (0.3 mL) were taken for the reaction monitoring after the defined times. The formation of the zirconacyclopentadiene **11b** was observed after 10 min of reaction. Over this time the mixture turned to bright orange. The second reaction mixture was filtered over celite, the solvent was removed *in vacuo* and a bright orange-yellow solid was obtained for further analysis (151 mg, 93%). **^1H NMR** (500 MHz, C_6D_6): δ 6.37(s, 10, Cp), 2.59-2.54 (m, 4 m, c), 1.65-1.58 (m, 4H, d), 1.10 (s, 24H, f) ppm; **$^{13}\text{C}\{^1\text{H}\}$ NMR** (126 MHz, C_6D_6): δ 147.0 (b), 111.7 (Cp), 81.5(e), 35.4 (c), 24.9 (f), 23.5(d) ppm; **$^{11}\text{B}\{^1\text{H}\}$ NMR** (160 MHz, C_6D_6): δ 30.9 ppm; **HR-MS** (EI, $\text{C}_{30}\text{H}_{42}^{10/11}\text{B}_2\text{O}_4^{90}\text{Zr}$): m/z calcd. 577.23471, found 577.23484 (R = 10000); **MS** (EI, 70 eV, direct inlet, 200 °C): m/z (% relative intensity) = 578 (13) $[\text{M}]^+$, 83 (100).

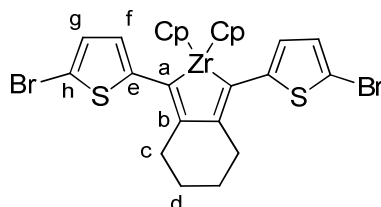
[†] The signal from the carbon atom bond to boron was not visible due to the high quadrupole moment of the boron nucleus

Reaction Monitoring and Synthesis of Zirconacyclopentadiene **11c**^[5]



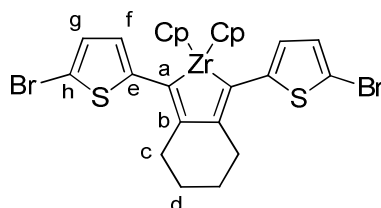
In a GB, a solution of zirconocene **9** (214 mg, 454 μmol) and diyne **10c** (150 mg, 454 μmol) in toluene (6 mL) was stirred at 22 °C. Samples (0.3 mL) were taken for the reaction monitoring after the defined times. The formation of the zirconacyclopentadiene **11c** was observed after 10 min of reaction. Over this time the mixture turned to yellowish brown. The second reaction mixture was filtered over celite, the solvent was removed *in vacuo* and a dark greenish-purple solid was obtained for further analysis (233 mg, 93%). **¹H NMR** (500 MHz, C₆D₆): δ 6.07 (d, $^3J = 3.8$ Hz, 2H, g), 6.05 (s, 10H, Cp), 5.77 (d, $^3J = 3.7$ Hz, 2H, f), 3.43 (s, 6H, i), 2.80-2.75 (m, 4H, c), 1.63-1.56 (m, 2H, d) ppm; **¹³C{¹H} NMR** (126 MHz, C₆D₆): δ 177.9 (a), 165.7 (h), 141.3 (b), 136.8 (e), 119.9 (f), 112.1 (Cp), 104.1 (g), 59.7 (i), 30.7 (c), 24.4 (d) ppm; **HR-MS** (EI, C₂₈H₂₈O₂S₂⁹⁰Zr): *m/z* calcd. 550.05723, found 550.05796 (R = 10000); **MS** (EI, 70 eV, direct inlet, 200 °C): *m/z* (% relative intensity) = 550 (74) [M]⁺, 220 (100) [Cp₂Zr]⁺.

Reaction Monitoring and Synthesis of Zirconacyclopentadiene **11d**



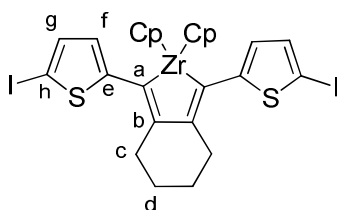
In a GB, a solution of zirconocene **9** (165 mg, 352 μmol) and diyne **10d** (150 mg, 352 μmol) in toluene (6 mL) was stirred at 22 °C. Samples (0.3 mL) were taken for the reaction monitoring after the defined times. The formation of the zirconacyclopentadiene **11d** was observed after 10 min of reaction. Over this time the mixture turned to dark red. The second reaction mixture was filtered over celite, the solvent was removed *in vacuo* and a dark red solid was obtained for further analysis (210 mg, 93%). Crystals could be obtained from a saturated toluene solution. **¹H NMR** (600 MHz, C₆D₆): δ 6.82 (d, $^3J = 3.8$ Hz, 2H, g), 5.84 (s, 10H, Cp), 5.69 (d, $^3J = 3.8$ Hz, 1H, f), 2.49 (m, 4H, c), 1.50-1.46 (m, 4H, d) ppm; **¹³C{¹H} NMR** (126 MHz, C₆D₆): δ 177.0 (a), 151.8 (e), 143.0 (b), 130.2 (g), 121.8 (f), 112.3 (Cp), 109.4 (h), 30.1 (c), 23.8 (d) ppm; **HR-MS** (EI, C₂₆H₂₂⁷⁹Br₂S₂⁹⁰Zr): *m/z* calcd. 645.85712, found 645.85714 (R = 10000); **MS** (EI, 70 eV, direct inlet, 200 °C): *m/z* (% relative intensity) = 646 (38) [M]⁺, 301 (100).

Reaction Monitoring of the Formation of Zirconacyclopentadiene **11d** in THF



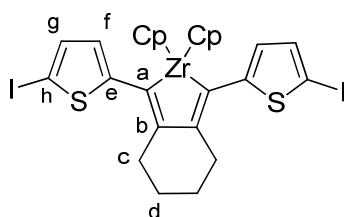
In a GB, a solution of zirconocene **9** (111 mg, 235 μmol) and diyne **10d** (100 mg, 235 μmol) in THF (6 mL) was stirred at 22 °C. Samples (0.3 mL) were taken for the reaction monitoring after the defined times. The formation of the zirconacyclopentadiene **11d** was observed after 10 min of reaction. Over this time the mixture turned to dark red. After 22 h, the zirconacyclopentadiene partly decomposed to starting material.

Reaction Monitoring and Synthesis of Zirconacyclopentadiene **11e**



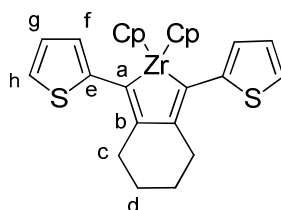
In a GB, a solution of zirconocene **9** (135 mg, 287 μmol) and diyne **10e** (150 mg, 287 μmol) in toluene (6 mL) was stirred at 22 °C. Samples (0.3 mL) were taken for the reaction monitorings after the defined times. The formation of the zirconacyclopentadiene **11e** was observed after 10 min of reaction. Over this time the mixture turned to dark red. The second reaction mixture was filtered over celite, the solvent was removed *in vacuo* and a dark red solid was obtained for further analysis (194 mg, 91%). **¹H NMR** (500 MHz, C_6D_6): δ 7.03 (d, $^3J = 3.7$ Hz, 2H, g), 5.85 (s, 10H, Cp), 5.65 (d, $^3J = 3.7$ Hz, 2H, f), 2.52-2.45 (m, 4H, c), 1.50-1.44 (m, 4H, d) ppm; **¹³C{¹H} NMR** (126 MHz, C_6D_6): δ 176.9 (a), 156.1 (e), 142.8 (b), 137.1 (g), 129. (f), 112.1 (Cp), 70.0 (h), 29.9 (c), 23.6 (d) ppm; **HR-MS** (EI, $\text{C}_{26}\text{H}_{22}\text{I}_2\text{S}_2^{90}\text{Zr}$): m/z calcd. 741.82939, found 741.82934 ($R = 10000$); **MS** (EI, 70 eV, direct inlet, 200 °C): m/z (% relative intensity) = 742 (44) $[\text{M}]^+$, 347 (100).

Stability Test of Zirconacyclopentadiene **11e** in Toluene with LiCl



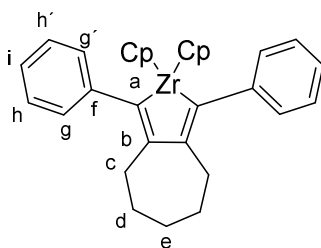
A mixture of zirconacyclopentadiene **11e** (50 mg, 67 μmol) and LiCl (89.5 mg, 134 μmol) in toluene (3 mL) was stirred at 22 °C in a GB. The stability of the zirconacyclopentadiene **11e** was observed by ^1H NMR measurements after 10 min, 30 min, 60 min, 3 h and 22 h. The color of the reaction mixture turned over the time of 22 h from dark red to bright yellow and a precipitate was formed.

Reaction Monitoring and Synthesis of Zirconacyclopentadiene **11f**^[5, 14]



In a GB, a solution of zirconocene **9** (261 mg, 555 μmol) and diyne **10f** (150 mg, 555 μmol) in toluene (6 mL) was stirred at 22 °C. Samples (0.3 mL) were taken for the reaction monitoring after the defined times. The formation of the zirconacyclopentadiene **11f** was observed after 10 min of reaction. Over this time the mixture turned to dark red. The second reaction mixture was filtered over celite, the solvent was removed *in vacuo* and a red solid was obtained for further analysis (259 mg, 95%). Crystals could be obtained from a saturated toluene solution ^1H NMR (500 MHz, C_6D_6): δ 6.96 (dd, $^3J = 5.2$ Hz, $^4J = 1.0$ Hz, 2H, h), 6.90 (dd, $^3J = 5.2$ Hz, 3.5 Hz, 2H, g), 6.21 (dd, $^3J = 3.5$ Hz, $^4J = 1.0$ Hz, 2H, f), 6.00 (s, 10H, Cp), 2.70-2.65 (m, 4H, c), 1.59-1.52 (m, 4H, d) ppm; $^{13}\text{C}\{^1\text{H}\}$ NMR (126 MHz, C_6D_6): δ 177.9 (a), 150.3 (e), 142.4 (b), 127.3 (g), 123.0 (h), 121.4 (f), 112.2 (Cp), 30.1 (c), 24.0 (d) ppm; HR-MS (EI, $\text{C}_{26}\text{H}_{24}\text{S}_2^{90}\text{Zr}$): m/z calcd. 490.03610, found 490.03669 ($R = 10000$); MS (EI, 70 eV, direct inlet, 200 °C): m/z (% relative intensity) = 490 (19) $[\text{M}]^+$, 220 (100) $[\text{Cp}_2\text{Zr}]^+$.

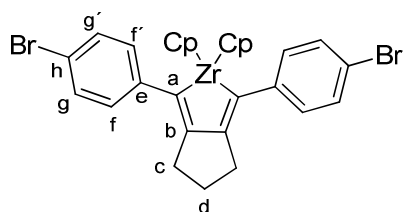
Reaction Monitoring and Synthesis of Zirconacyclopentadiene **11g**



A solution of zirconocene **9** (259 mg, 552 μmol) and diyne **10g** (150 mg, 551 μmol) in toluene (6 mL) was stirred at 22 °C for 3 h. The reaction mixture was filtered over celite. The solvent was removed *in vacuo* and an orange-pink solid-like film was obtained (248 mg, 91%, 92% purity). Crystal data could not be received, the compound was just forming gel-like needles. ^1H NMR (500 MHz, C_6D_6): δ 7.42-7.23 (m, 4H, g, g'), 7.09-6.95 (m, 6H, h, h', i), 5.93 (s, 10H, Cp), 2.38-2.31 (m, 4H, c), 1.61-1.50 (m, 6H, d, e) ppm;

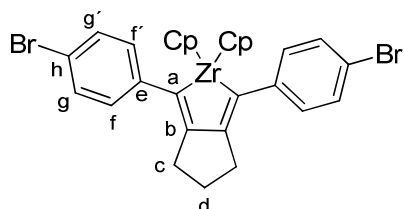
$^{13}\text{C}\{^1\text{H}\}$ NMR (126 MHz, C_6D_6): δ 189.3 (a), 149.6 (b), 137.9 (f), 128.6 (g, g'), 126.3 (h, h'), 123.3 (i), 112.2 (Cp), 31.6 (c), 31.1 (d, e) ppm; **HR-MS** (EI, $\text{C}_{31}\text{H}_{30}^{90}\text{Zr}$): m/z calcd. 492.13891, found 492.13982 ($R = 10000$); **MS** (EI, 70 eV, direct inlet, 200 °C): m/z (% relative intensity) = 492 (8) $[\text{M}]^+$, 220 (100) $[\text{Cp}_2\text{Zr}]^+$.

Reaction Monitoring and Synthesis of Zirconacyclopentadiene **11h**^[13]



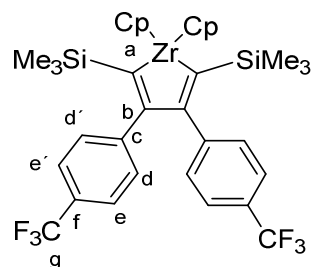
A solution of zirconocene **9** (176 mg, 373 μmol) and diyne **11h** (150 mg, 373 μmol) in toluene (6 mL) was stirred at 22 °C. Samples (0.3 mL) were taken for the reaction monitoring after the defined times. The formation of the zirconacyclopentadiene **11h** was observed after 10 min of reaction. Over this time, the mixture turned to orange-red. The second reaction mixture was filtered over celite, the solvent was removed *in vacuo* and a reddish-orange solid was obtained for further analysis (223 mg, 96%). Crystals could be obtained from a saturated toluene solution. ^1H NMR (600 MHz, C_6D_6): δ 7.49-7.44 (m, 4H, g, g'), 6.80-6.74 (m, 4H, f, f'), 5.70 (s, 10H, Cp), 2.33 (t, $^3J = 7.1$ Hz, 4H, c), 1.26 (p, $^3J = 7.1$ Hz, 2H, d) ppm; $^{13}\text{C}\{^1\text{H}\}$ NMR (151 MHz, C_6D_6): δ 182.2 (a), 149.0 (b), 131.7 (g, g'), 128.0 (f, f'), 126.2 (e), 117.8 (h), 110.4 (Cp), 35.6 (c), 22.5 (d) ppm; **HR-MS** (EI, $\text{C}_{29}\text{H}_{24}^{79/81}\text{Br}_2^{90}\text{Zr}$): m/z calcd. 621.92728, found 621.92652 ($R = 10000$); **MS** (EI, 70 eV, direct inlet, 200 °C): m/z (% relative intensity) = 620 (69) $[\text{M}]^+$, 220 (100) $[\text{Cp}_2\text{Zr}]^+$.

Reaction Monitoring of the Formation of Zirconacyclopentadiene **11h** in THF^[13]



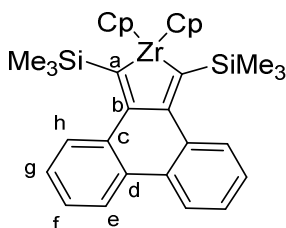
A solution of zirconocene **9** (117 mg, 249 μmol) and diyne **11h** (100 mg, 249 μmol) in THF (6 mL) was stirred at 22 °C. Samples (0.3 mL) were taken for the reaction monitoring after the defined times. The formation of the zirconacyclopentadiene **11h** was observed after 10 min of reaction. Over this time, the mixture turned to orange-red. After 22 h, the zirconacyclopentadiene partly decomposed.

Reaction Monitoring and Synthesis of Zirconacyclopentadiene **11i**



A solution of zirconocene **9** (146 mg, 310 μmol) and acetylene **10i** (150 mg, 619 μmol) in toluene (6 mL) was stirred at 22 °C. Samples (0.3 mL) were taken for the reaction monitoring after the defined times. The formation of the zirconacyclopentadiene **11i** was observed after 10 min of reaction. Over this time, the mixture turned to orange-yellow. The second reaction mixture was filtered over celite, the solvent was removed *in vacuo* and a bright yellow solid was obtained for further analysis (206 mg, 94%). Crystals could be obtained from a saturated toluene solution. $^1\text{H NMR}$ (600 MHz, C_6D_6): δ 7.11 (d, $^3J = 7.8$ Hz, 4H, e, e'), 6.49 (d, $^3J = 7.8$ Hz, 4H, d, d'), 6.09 (s, 10H, Cp), -0.28 (s, 18H, SiMe_3) ppm; $^{13}\text{C}\{^1\text{H}\}$ NMR (151 MHz, C_6D_6): δ 206.3 (a), 149.4 (c) 148.2 (b), 130.2 (d, d'), 127.5 (q, $^2J = 32.2$ Hz, f)†, 125.0 (q, $^1J_{\text{C-F}} = 271.7$ Hz, g), 124.0 (q, $^3J_{\text{C-F}} = 3.8$ Hz, e, e'), 111.7 (Cp), 2.70 (SiMe_3) ppm; $^{19}\text{F NMR}$ (471 MHz, C_6D_6): δ -62.1 ppm; $^{29}\text{Si}\{^1\text{H}\}$ NMR (99 MHz, C_6D_6): δ -15.4 ppm; **MS** (EI, 70 eV, direct inlet, 200 °C): compound shows no molecule ion.

Reaction Monitoring and Synthesis of Zirconacyclopentadiene **11j**^[9]

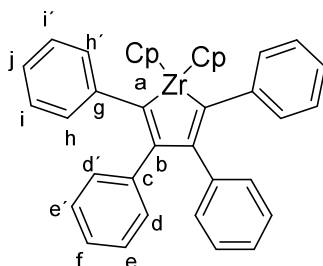


A solution of zirconocene **9** (166 mg, 352 μmol) and diyne **10j** (122 mg, 352 μmol) in toluene (3 mL) was stirred at 25 °C. Samples (0.3 mL) were taken for the reaction monitoring after the defined times. The formation of the zirconacyclopentadiene **11j** was observed after 10 min of reaction. Over this time, the mixture turned to red. The second reaction mixture was filtered over celite, the solvent was removed *in vacuo* and an orange-red solid was obtained for further analysis (192 mg, 96%). Crystals could be obtained from a saturated toluene solution. $^1\text{H NMR}$ (600 MHz, C_6D_6): δ 7.60 (dd, $^3J = 7.6$ Hz, $^4J = 1.3$ Hz, 2H, e), 7.51 (dd, $^3J = 7.6$ Hz, $^4J = 1.3$ Hz, h), 7.14 (td, $^3J = 7.6$ Hz, $^4J = 1.3$ Hz, 2H, f), 7.07 (td, $^3J = 7.6$ Hz, $^4J = 1.3$ Hz, 2H, g), 5.94 (s, 10H, Cp), 0.21 (s, 18H, SiMe_3) ppm;

† This signal is overlapping with the solvent signal.

$^{13}\text{C}\{^1\text{H}\}$ NMR (151 MHz, C_6D_6): δ 208.9 (a), 137.5 (b), 136.2 (c or d), 133.7 (d or c), 129.7 (h), 128.8 (f), 126.9 (g), 123.7 (e), 110.2 (Cp), 3.8 (SiMe₃) ppm; $^{29}\text{Si}\{^1\text{H}\}$ NMR (99 MHz, C_6D_6): δ -12.0 ppm; **HR-MS** (EI, $\text{C}_{32}\text{H}_{36}^{28}\text{Si}_2^{90}\text{Zr}$): m/z calcd. 566.13971, found 566.13966 (R = 10000); **MS** (EI, 70 eV, direct inlet, 200 °C): m/z (% relative intensity) = 566 (5) $[\text{M}]^+$, 220 (100) $[\text{Cp}_2\text{Zr}]^+$.

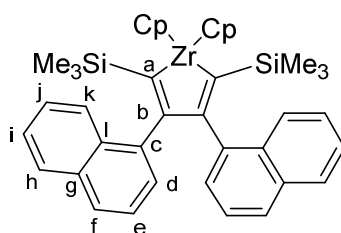
Reaction Monitoring and Synthesis of Zirconacyclopentadiene **11k**^[13]



A solution of zirconocene **9** (198 mg, 421 μmol) and diphenylacetylene (**10k**) (150 mg, 842 μmol) in toluene (6 mL) was stirred at 22 °C. Samples (0.3 mL) were taken for the reaction monitoring after the defined times. The formation of the zirconacyclopentadiene **11k** was observed after 10 min of reaction. Over this time, the mixture turned to orange-pink. The second reaction mixture was filtered over celite, the solvent was removed *in vacuo* and an orange-pink solid was obtained for further analysis (231 mg, 95%). Single crystals could be obtained from a saturated toluene solution. ^1H NMR (500 MHz, C_6D_6): δ 7.06-7.01 (m, 4H, i, i'), 7.00-6.93 (m, 4H, d, d'), 6.86-6.82 (m, 4H, e, e'), 6.82-6.79 (m, 2H, j), 6.76-6.71 (m, 2H, f), 6.71-6.66 (m, 4H, h, h'), 6.00 (s, 10H, Cp) ppm;

$^{13}\text{C}\{^1\text{H}\}$ NMR (126 MHz, C_6D_6): δ 194.8 (a), 148.6 (b), 142.8 (g), 141.7 (c), 131.3 (d, d'), 128.3 (i, i'), 127.2 (h, h'), 127.1 (e, e'), 125.1 (f), 123.4 (j), 112.3 (Cp) ppm; **HR-MS** (EI, $\text{C}_{38}\text{H}_{30}^{90}\text{Zr}$): m/z calcd. 576.13891, found 576.13987 (R = 10000); **MS** (EI, 70 eV, direct inlet, 200 °C): m/z (% relative intensity) = 576 (18) $[\text{M}]^+$, 220 (100) $[\text{Cp}_2\text{Zr}]^+$.

Reaction Monitoring and Synthesis of Zirconacyclopentadiene **11l**

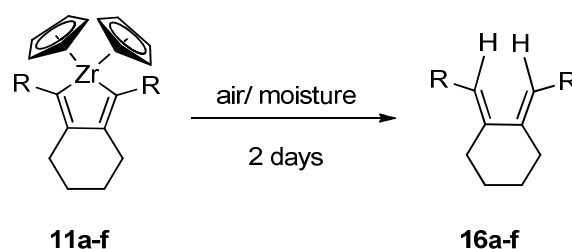


A solution of zirconocene **9** (158 mg, 335 μmol) and 1-(1-naphthyl)-2-(trimethylsilyl)acetylene (**10l**) (150 mg, 669 μmol) in toluene (6 mL) was stirred at 22 °C. Samples (0.3 mL) were taken for the reaction monitoring after the defined times. The formation of the zirconacyclopentadiene **11l** was observed after 10 min of reaction. Over this time, the mixture turned to yellow-orange. The second reaction mixture was filtered over celite, the solvent was removed *in vacuo* and

an orange-yellow solid was obtained for further analysis (202 mg, 90%). Crystals could be obtained from a saturated toluene solution. **¹H NMR** (600 MHz, C₆D₆): δ 8.32 (dq, ³J = 8.4 Hz, ⁴J = 0.9 Hz, 2H, k), 7.46 (ddd, ³J = 8.4 Hz, ³J = 6.8 Hz, ⁴J = 1.3 Hz, 2H, j), 7.38 (ddt, ³J = 8.1 Hz, ⁴J = 1.2 Hz, 0.6 Hz, 2H, h), 7.21 (ddd, ³J = 8.1 Hz, ³J = 6.8 Hz, ⁴J = 1.3 Hz, 2H, i), 7.02 (d, ³J = 8.1 Hz, 2H, f), 6.84 (dd, ³J = 7.0 Hz, ⁴J = 1.3 Hz, 2H, d), 6.59 (dd, ³J = 8.2 Hz, ³J = 7.0 Hz, 2H, e), 6.34 (s, 10H, Cp), -0.39 (m, 18H, SiMe₃) ppm; **¹³C{¹H} NMR** (151 MHz, C₆D₆): δ 207.7 (a), 150.0 (b), 142.6 (c), 133.4 (l), 132.8 (g), 128.0 (h), 126.8 (k), 126.0 (d), 125.8 (f), 124.8 (j), 124.6 (i), 124.0 (e), 111.1 (Cp), 2.1 ppm; **²⁹Si{¹H} NMR** (99 MHz, C₆D₆): δ -14.9 ppm; **MS** (EI, 70 eV, direct inlet, 200 °C): compound shows no molecular ion.

4 Air Stability Tests

The zirconacyclopentadienes **11a-f** were exposed to compressed air and normal atmospheric conditions in order to study their stability under such conditions. The samples were then analyzed by ^1H NMR spectroscopy. After flushing the zirconacyclopentadienes with compressed air for 10 min and 30 min no change was observed in the spectra. This procedure was repeated with the same sample the next day obtaining the same result. A significant change was observed only when the samples were exposed to normal atmospheric conditions for one further day. Under such conditions new signals were observed presumably arising from the ring-opening of the zirconacyclopentadienes **11a-f**. After 2 days the zirconacyclopentadienes were completely decomposed. Because the main difference between compressed air and atmospheric air is the higher moisture content in the latter, we assume that the decomposition is a protonolysis that forms the dienes **16a-f** (Scheme S4). Those types of decomposition products are already known from the literature, when the zirconacyclopentadienes were exposed to acidic conditions, for example in the formation of **3** (Scheme 1, main manuscript).^[9, 15] The structure of the compounds **16a-f** was confirmed by two-dimensional NMR and mass spectrometry.



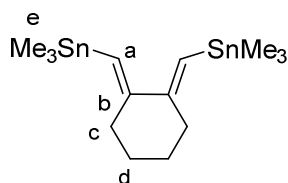
Scheme S4. Decomposition path of the zirconacyclopentadienes **11a-f** to the dienes **16a-f**.

4.1 General procedure for the air stability test

Zirconacyclopentadienes **11a-f** were stirred in toluene under normal atmospheric conditions for 24 h. After normal work up with water and dichloromethane and drying of the organic layer over magnesium sulfate, the solvents were removed *in vacuo*. The main product of decomposition was analyzed by NMR spectroscopy and MS spectrometry.

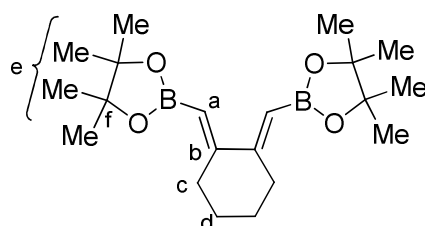
A second by-product was observed in all of the decomposition tests by NMR spectroscopic analysis; however it was not possible to isolate this compound. The chemical shifts were (^1H δ (C_6D_6): 6.30 (ddd, 2H), 6.50 (ddd, 2H), 2.68 (m, 2H) ppm. ^{13}C δ (C_6D_6): 132, 133, 41 ppm.

Decomposition of Zirconacyclopentadiene **11a**



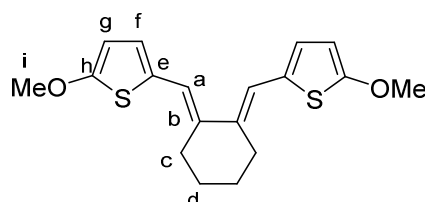
A sample of zirconacyclopentadiene **11a** (50.0 mg, 116 μmol) was exposed to the air under normal atmospheric conditions during 24 h to yield a white-yellowish solid (32 mg, 73 μmol , 63%). $^1\text{H NMR}$ (600 MHz, C_6D_6): δ 6.03 (s, 2H, a), 2.13 (m, 4H, c), 1.57 (m, 4H, d), 0.18 (m, 18H, e) ppm; $^{13}\text{C}\{^1\text{H}\}$ NMR (126 MHz, C_6D_6): δ 111.1 (a), 82.5 (b), 28.5 (c), 20.1(d), -8.04(e) ppm; MS (EI, 70 eV, direct inlet, 200 $^\circ\text{C}$): m/z (% relative intensity) = 419 (40) $[\text{M}-\text{CH}_3]^+$, 241 (100) $[\text{M}-\text{C}_5\text{H}_{13}\text{Sn}]^+$.

Decomposition of Zirconacyclopentadiene **11b**



A sample of zirconacyclopentadiene **11b** (50.0 mg, 140 μmol) was exposed to the air under normal atmospheric conditions during 24 h to yield a pink-yellowish solid (20 mg, 56 μmol , 40%). $^1\text{H NMR}$ (600 MHz, C_6D_6): δ 5.95 (s, 2H, a), 2.99 (m, 4H, c), 1.62 (dt, $^3J = 6.4, 3.0$ Hz, 4H, d), 1.05 (s, 24H, e) ppm; $^{13}\text{C}\{^1\text{H}\}$ NMR (126 MHz, C_6D_6): δ 167.5 (b), 82.7 (f), 34.0 (c), 27.4 (d), 25.0 (e) ppm; ^sMS (EI, 70 eV, direct inlet, 200 $^\circ\text{C}$): m/z (% relative intensity) = 360(12) $[\text{M}]^+$, 44 (100) $[\text{M}-\text{C}_{20}\text{H}_{34}\text{BO}]^+$.

Decomposition of Zirconacyclopentadiene **11c**

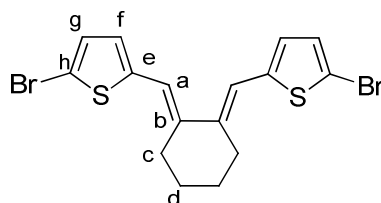


A sample of zirconacyclopentadiene **11c** (50.0 mg, 150 μmol) was exposed to the air under normal atmospheric conditions during 24 h to yield a yellowish solid (41 mg, 123 μmol , 82%).

^s Carbon b was not possible to identify carbon d because the quadrupole moment from the adjacent boron atom.

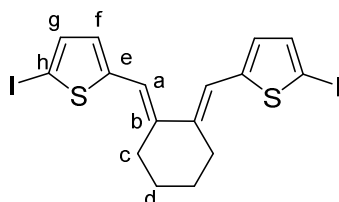
$^1\text{H NMR}$ (600 MHz, C_6D_6): δ 6.7(s, 2H, a), 6.58 (d, $^3J = 3.9$ Hz, 4H, g), 5.96 (d, $^3J = 3.9$ Hz, 4H, f), 3.32 (s, 6H, i), 2.66 (d, $^3J = 1.7$ Hz, 4H, c), 1.44 (m, 4H, d) ppm; **$^{13}\text{C}\{^1\text{H}\}$ NMR** (126 MHz, C_6D_6): δ 166.8 (h), 139.1 (b) 128.4 (e), 125.9 (g), 118.7(a), 104.0 (f), 59.6 (i), 30.3(c), 25.9 (d) ppm; **MS** (EI, 70 eV, direct inlet, 200 °C): m/z (% relative intensity) = 332 (100) $[\text{M}]^+$.

Decomposition of Zirconacyclopentadiene **11d**



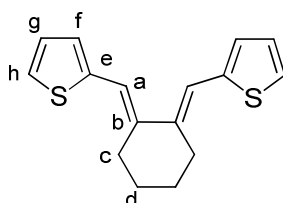
A sample of zirconacyclopentadiene **11d** (50.0 mg, 96.2 μmol) was exposed to air under normal atmospheric conditions during 24 h to yield an orange solid (36.0 mg, 83.7 μmol , 87%). **$^1\text{H NMR}$** (600 MHz, C_6D_6): δ 6.58 (d, $^3J = 3.8$ Hz, 2H, g), 6.27 (d, $^3J = 3.8$ Hz, 2H, f), 6.04 (s, 2H, a), 2.46 (t, $^3J = 5.8$ Hz, 2H, c), 1.40 (dt, $^3J = 10.1, 5.0$ Hz, 2H, d) ppm; **$^{13}\text{C NMR}$** (126 MHz, C_6D_6): δ 142.8 (e), 139.6 (b), 130.2 (f), 128.75 (g), 117.5 (a), 74.0 (h), 31.4 (c), 24.4 (d) ppm; **MS** (EI, 70 eV, direct inlet, 200 °C): m/z (% relative intensity) = 428 (24) $[\text{M}]^+$, 270 (100).

Decomposition of Zirconacyclopentadiene **11e**



A sample of zirconacyclopentadiene **11e** (50 mg, 95.8 μmol) was exposed to air under normal atmospheric conditions during 24 h to yield a yellowish solid (49 mg, 93 μmol , 97%). **$^1\text{H NMR}$** (600 MHz, C_6D_6): δ 6.92 (d, $^3J = 3.83$ Hz, 2H, g), 6.57 (s, 2H, a), 6.33 (d, $^3J = 3.83$ Hz, 4H, f), 2.40 (d, 4H, c), 1.32 (m, 4H, d) ppm; **$^{13}\text{C}\{^1\text{H}\}$ NMR** (126 MHz, C_6D_6): δ 14.7 (e), 142.1 (b), 137.1 (f), 129.5 (g), 118.0 (a), 73.9 (h), 30.3 (c), 24.4 (d) ppm; **MS** (EI, 70 eV, direct inlet, 200 °C): m/z (% relative intensity) = 524 (30) $[\text{M}]^+$, 237 (100) $[\text{M}-\text{C}_6\text{H}_3\text{S}]^+$.

Decomposition of Zirconacyclopentadiene **11f**



A sample of zirconacyclopentadiene **11f** (50 mg, 138 μmol) was exposed to air under normal atmospheric conditions during 24 h to yield a yellowish solid (29.7 mg, 109 μmol , 79%). **^1H NMR** (600 MHz, C_6D_6): δ 6.90 (d, $^3J = 5.1$ Hz, 2H, g), 6.87 (d, $^3J = 3.4$ Hz, 2H, h), 6.84 (s, 2H, a), 6.80 (dd, $^3J = 5.1$ Hz, $^4J = 3.6$ Hz, 2H, f), 2.69-2.63 (m, 4H, c), 1.41 (m, 2H, d) ppm; **$^{13}\text{C}\{^1\text{H}\}$ NMR** (126 MHz, C_6D_6): δ 141.82 (e), 141.79 (b), 128.35 (h), 127.20 (f), 125.27 (g), 118.36 (a), 30.39 (c), 24.78 (d) ppm; **MS** (EI, 70 eV, direct inlet, 200 $^\circ\text{C}$): m/z (% relative intensity) = 272 (62) $[\text{M}]^+$, 111 (100).

5 Literature

- [1] H.-S. Lin, L. A. Paquette, *Synth. Commun.* **1994**, *24*, 2503-2506.
- [2] a) G. Sheldrick, *Acta Cryst. A* **2008**, *64*, 112-122; b) L. Farrugia, *J. Appl. Cryst.* **1999**, *32*, 837-838.
- [3] O. V. Dolomanov, L. J. Bourhis, R. J. Gildea, J. A. K. Howard, H. Puschmann, *J. Appl. Cryst.* **2009**, *42*, 339-341.
- [4] a) K. Oouchi, M. Mitani, M. Hayakawa, T. Yamada, T. Mukaiyama, *J. Organomet. Chem.* **1996**, *516*, 111-114; b) V. Gandon, D. Leca, T. Aechtner, K. P. C. Vollhardt, M. Malacria, C. Aubert, *Org. Lett.* **2004**, *6*, 3405-3407.
- [5] I.-M. Ramirez y Medina, M. Rohdenburg, F. Mostaghimi, S. Grabowsky, P. Swiderek, J. Beckmann, J. Hoffmann, V. Dorcet, M. Hissler, A. Staubitz, *Inorg. Chem.* **2018**, *57*, 12562-12575.
- [6] J. Linshoeft, E. J. Baum, A. Hussain, P. J. Gates, C. Näther, A. Staubitz, *Angew. Chem. Int. Ed.* **2014**, *53*, 12916-12920.
- [7] G. Wang, C. Chen, J. Peng, *Chem. Commun.* **2016**, *52*, 10277-10280.
- [8] T. Shimada, K. Mukaide, A. Shinohara, J. W. Han, T. Hayashi, *J. Am. Chem. Soc.* **2002**, *124*, 1584-1585.
- [9] G. R. Kiel, M. S. Ziegler, T. Tilley, *Angew. Chem. Int. Ed.* **2017**, *122*, 4839-4844.
- [10] a) J. Linshoeft, E. J. Baum, A. Hussain, P. J. Gates, C. Näther, A. Staubitz, *Angew. Chem.* **2014**, *126*, 13130-13134; b) U. Rosenthal, A. Ohff, W. Baumann, A. Tillack, H. Görls, V. V. Burlakov, V. B. Shur, *Zeitschrift für anorganische und allgemeine Chemie* **1995**, *621*, 77-83.
- [11] J. Grolleau, P. Frère, F. Gohier, *Synthesis* **2015**, *47*, 3901-3906.
- [12] G. He, L. Kang, W. Torres Delgado, O. Shynkaruk, M. J. Ferguson, R. McDonald, E. Rivard, *J. Am. Chem. Soc.* **2013**, *135*, 5360-5363.
- [13] a) B. Jiang, T. D. Tilley, *J. Am. Chem. Soc.* **1999**, *121*, 9744-9745; b) I. t. l. p. t. z. w. n. isolated.
- [14] C. Hay, M. Hissler, C. Fischmeister, J. Rault-Berthelot, L. Toupet, L. Nyulászi, R. Réau, *Chem. Eur. J.* **2001**, *7*, 4222-4236.
- [15] E. Negishi, S. J. Holmes, J. M. Tour, J. A. Miller, F. E. Cederbaum, D. R. Swanson, T. Takahashi, *J. Am. Chem. Soc.* **1989**, *111*, 3336-3346.

6 Spectra

6.1 Isolated Compounds

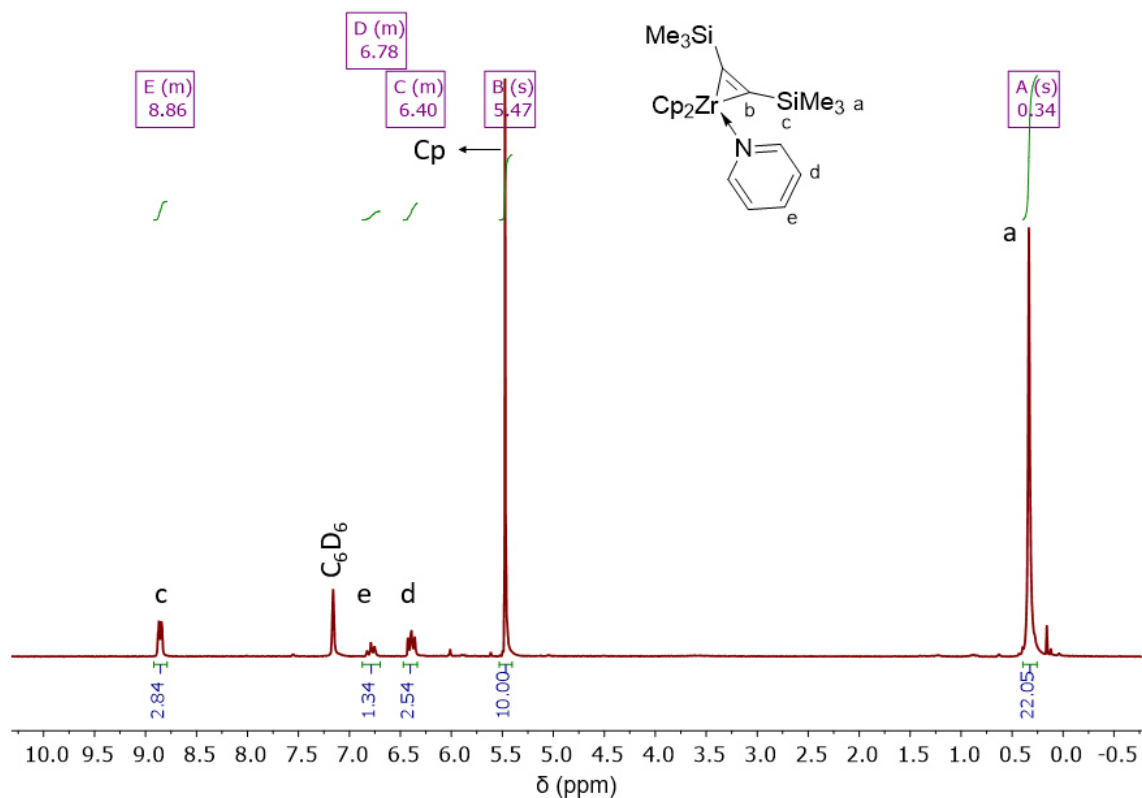


Figure S1. ^1H NMR (500 MHz) spectrum of Rosenthal's zirconocene in C_6D_6 .

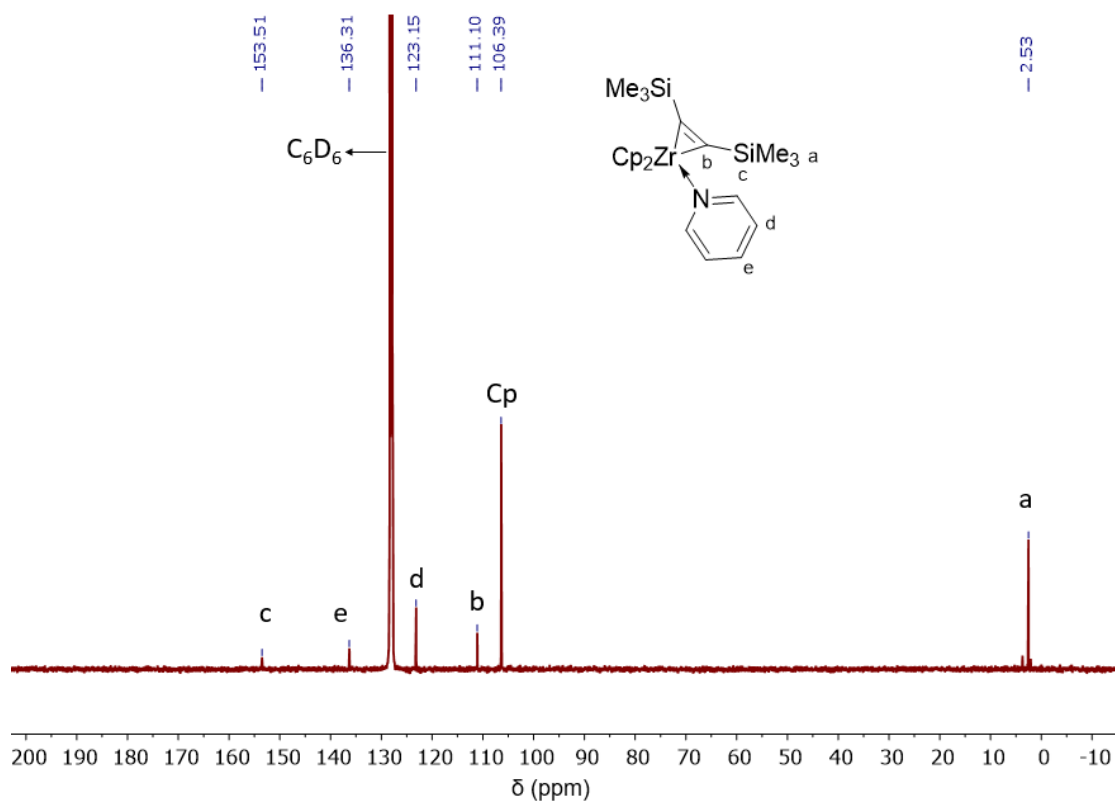


Figure S2. $^{13}\text{C}\{^1\text{H}\}$ NMR (126 MHz) spectrum of Rosenthal's zirconocene in C_6D_6 .

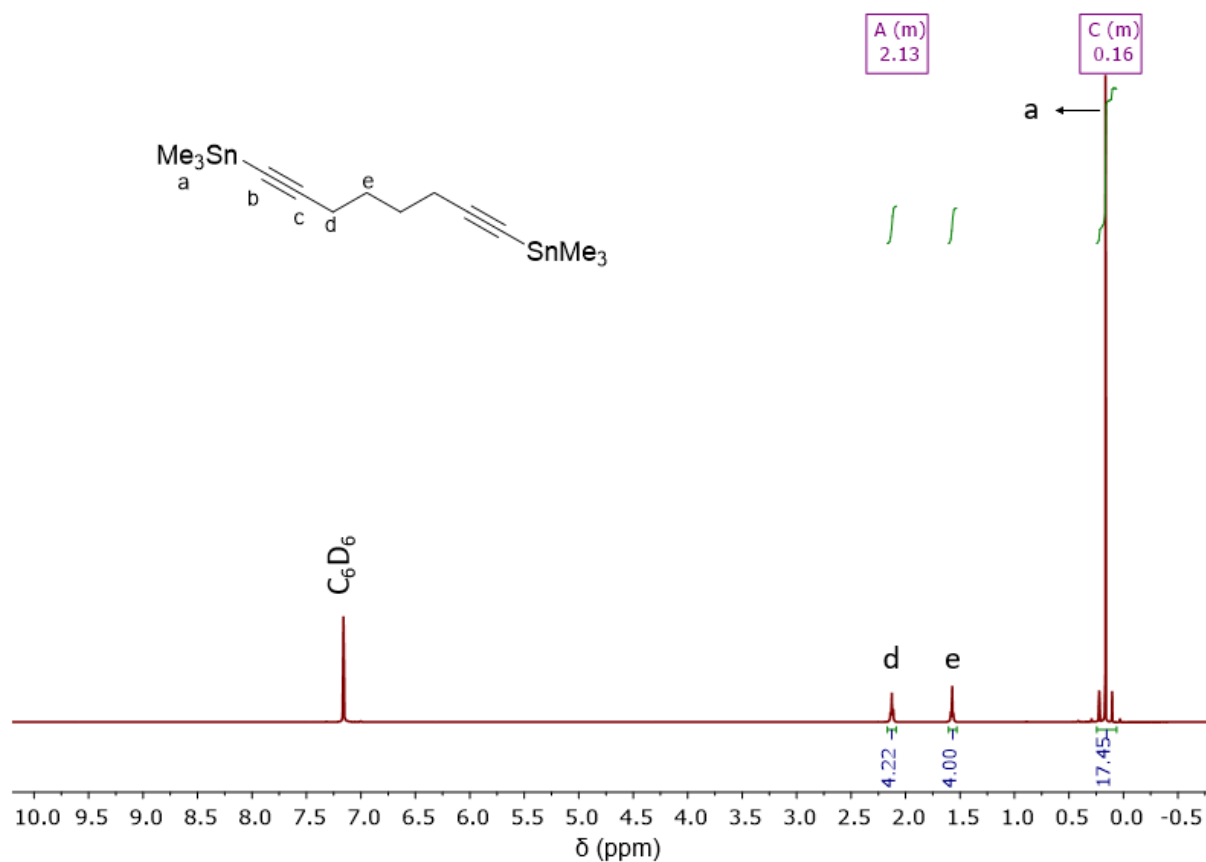


Figure S3. ¹H NMR (500 MHz) spectrum of 1,8-bis(trimethylstannyl)octa-1,7-diyne in CDCl₃.

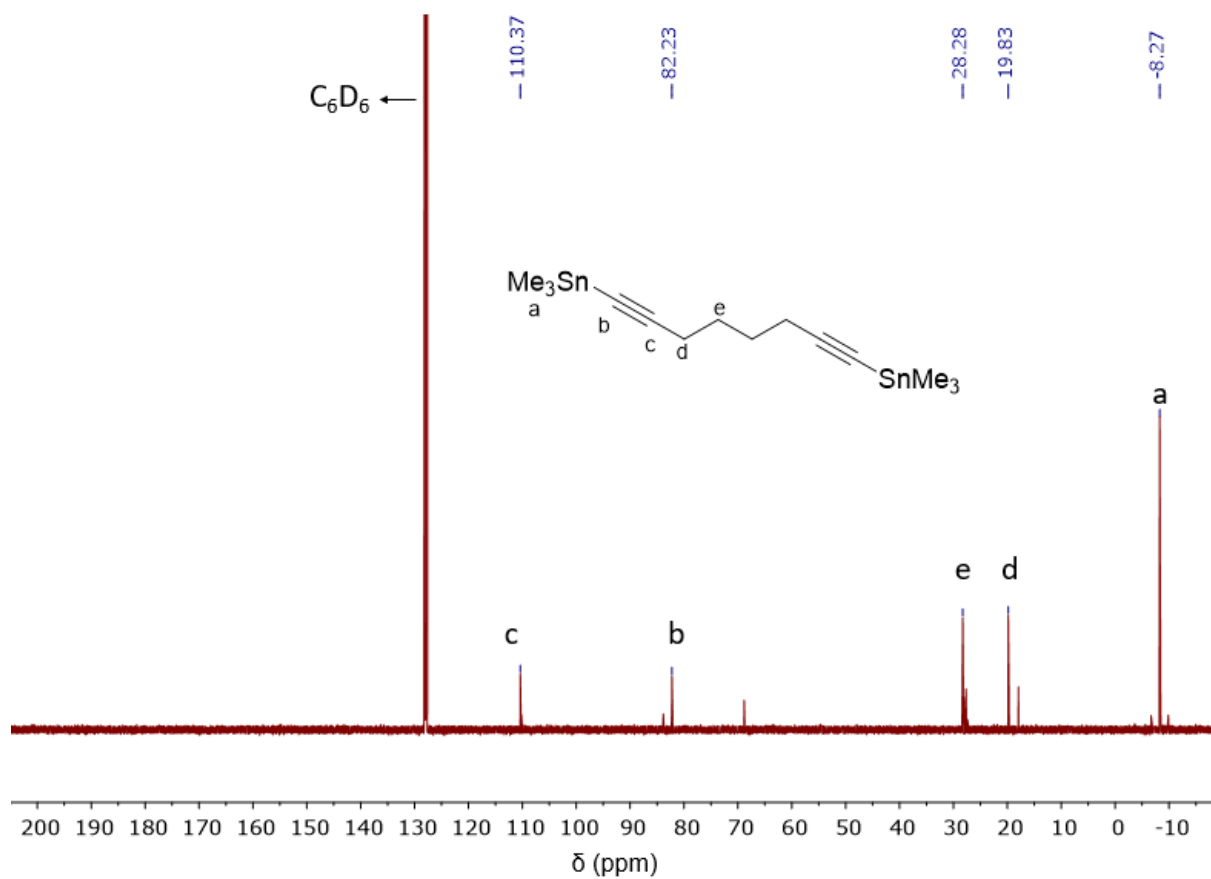


Figure S4. ¹³C{¹H} NMR (126 MHz) spectrum of 1,8-bis(trimethylstannyl)octa-1,7-diyne in CDCl₃.

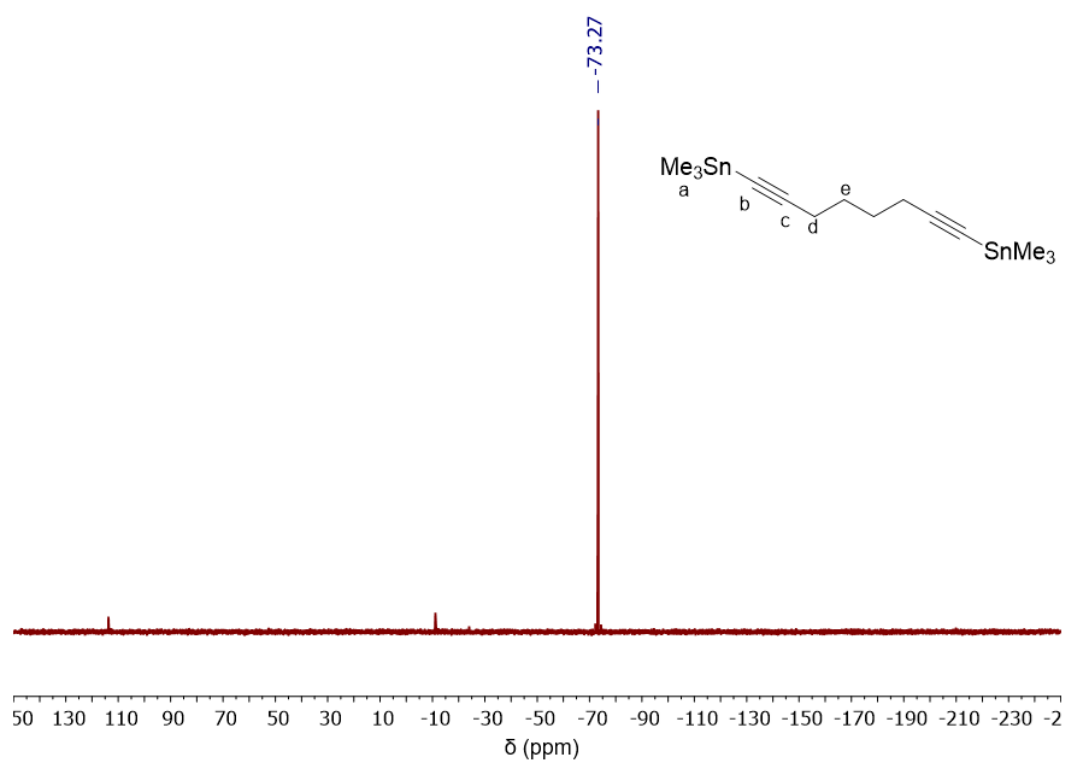


Figure S5. $^{119}\text{Sn}\{^1\text{H}\}$ NMR (187 MHz) spectrum of 1,8-bis(trimethylstannyl)octa-1,7-diyne in CDCl_3 .

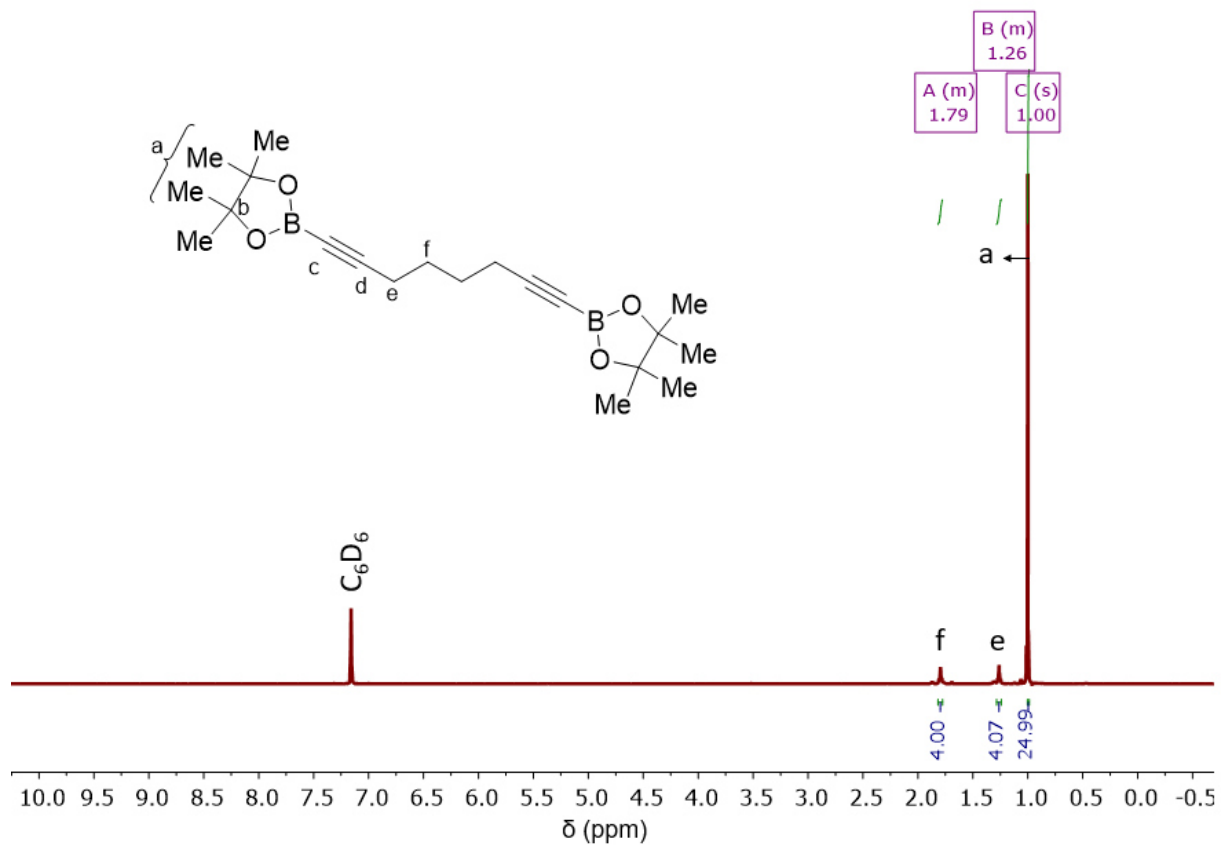


Figure S6. ^1H NMR (500 MHz) spectrum of 1,8-bis(4,4,5,5-tetramethyl-1,3,2-dioxaborolan-2-yl)octa-1,7-diyne in C_6D_6 .

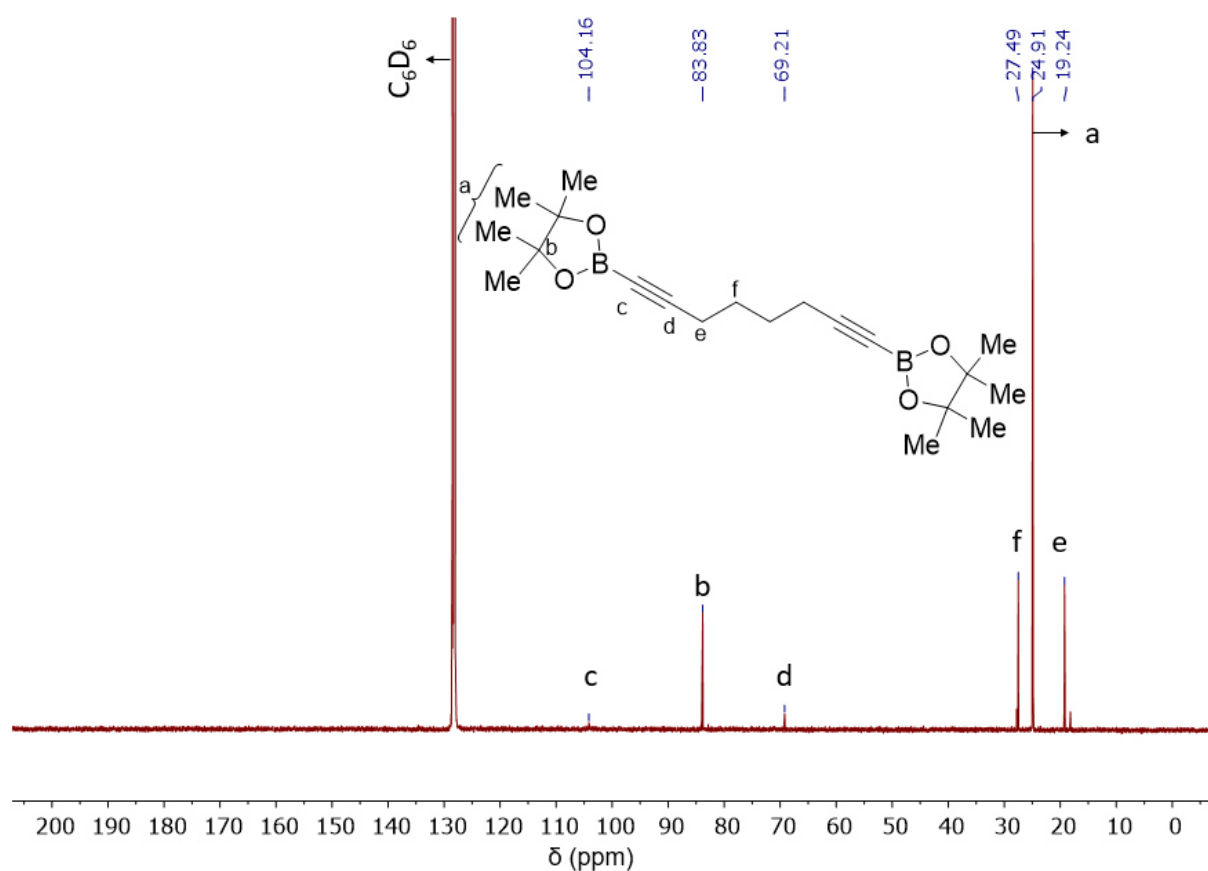


Figure S7. $^{13}\text{C}\{^1\text{H}\}$ NMR (126 MHz) spectrum of 1,8-bis(4,4,5,5-tetramethyl-1,3,2-dioxaborolan-2-yl)octa-1,7-diyne in C_6D_6 .

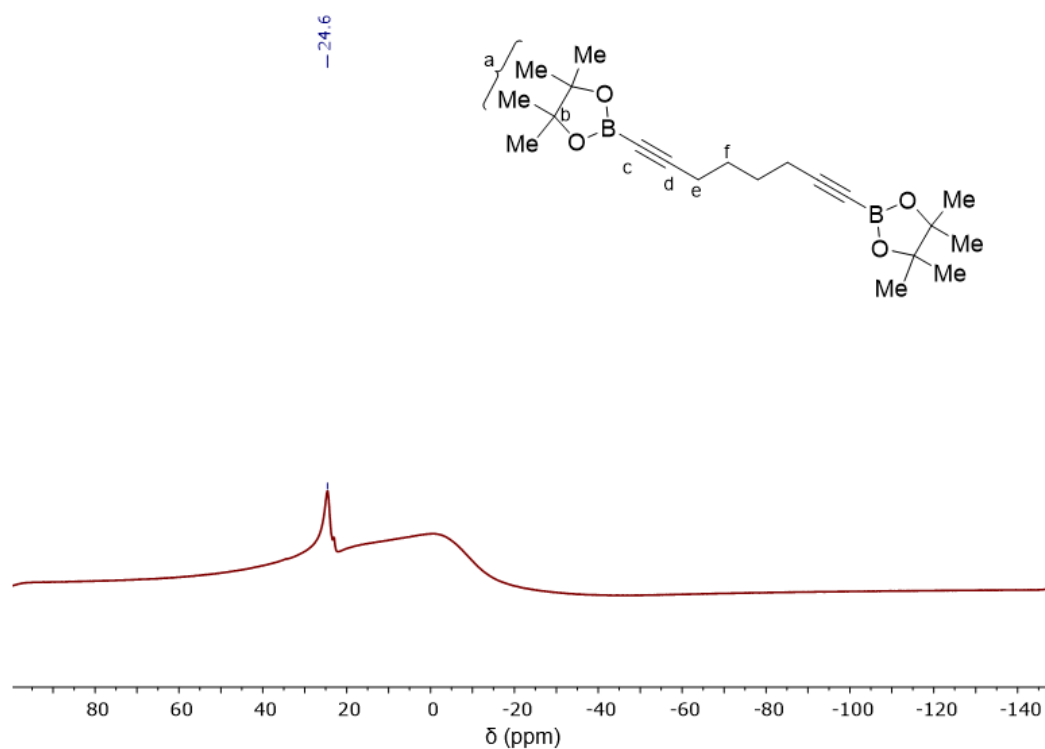


Figure S8. $^{11}\text{B}\{^1\text{H}\}$ NMR (160 MHz, C_6D_6): spectrum of 1,8-bis(4,4,5,5-tetramethyl-1,3,2-dioxaborolan-2-yl)octa-1,7-diyne in C_6D_6 .

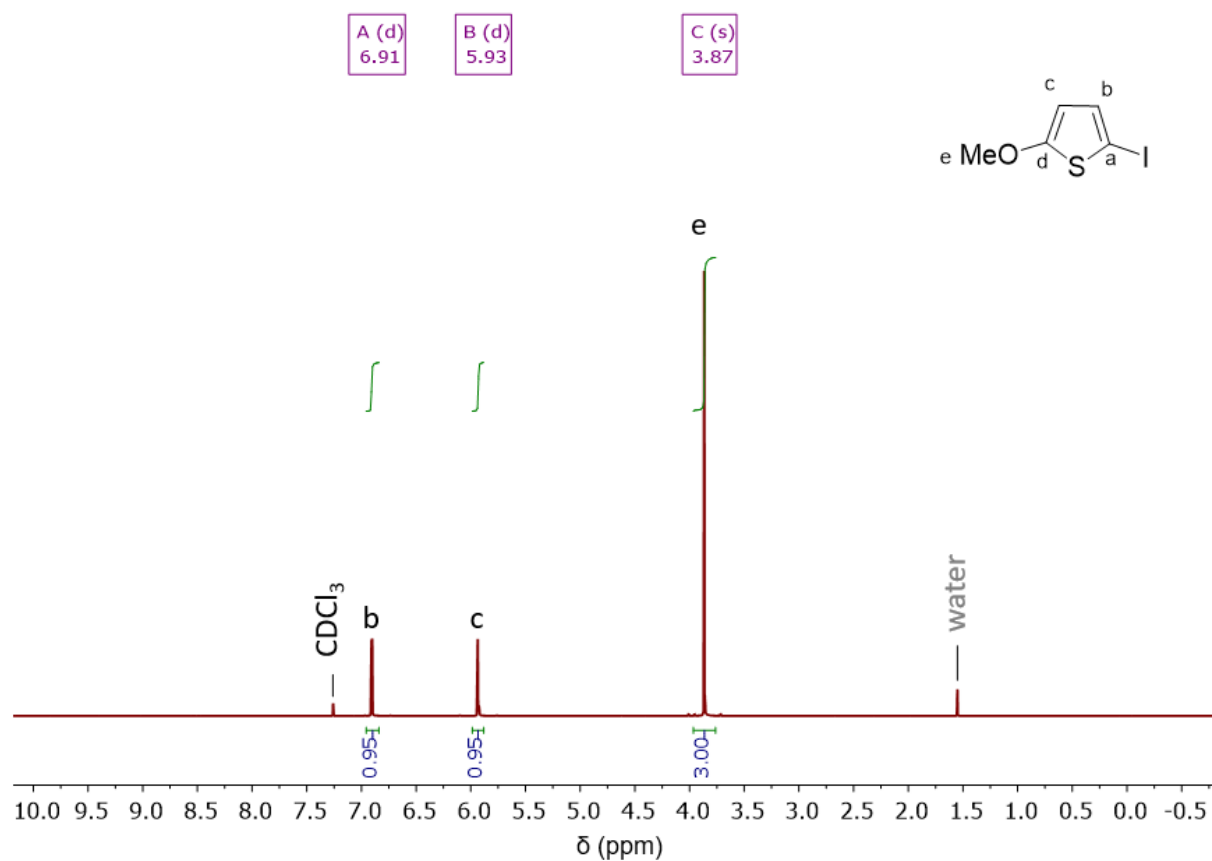


Figure S9. ^1H NMR (500 MHz) spectrum of 5-methoxy-2-iodothiophene in CDCl_3 .

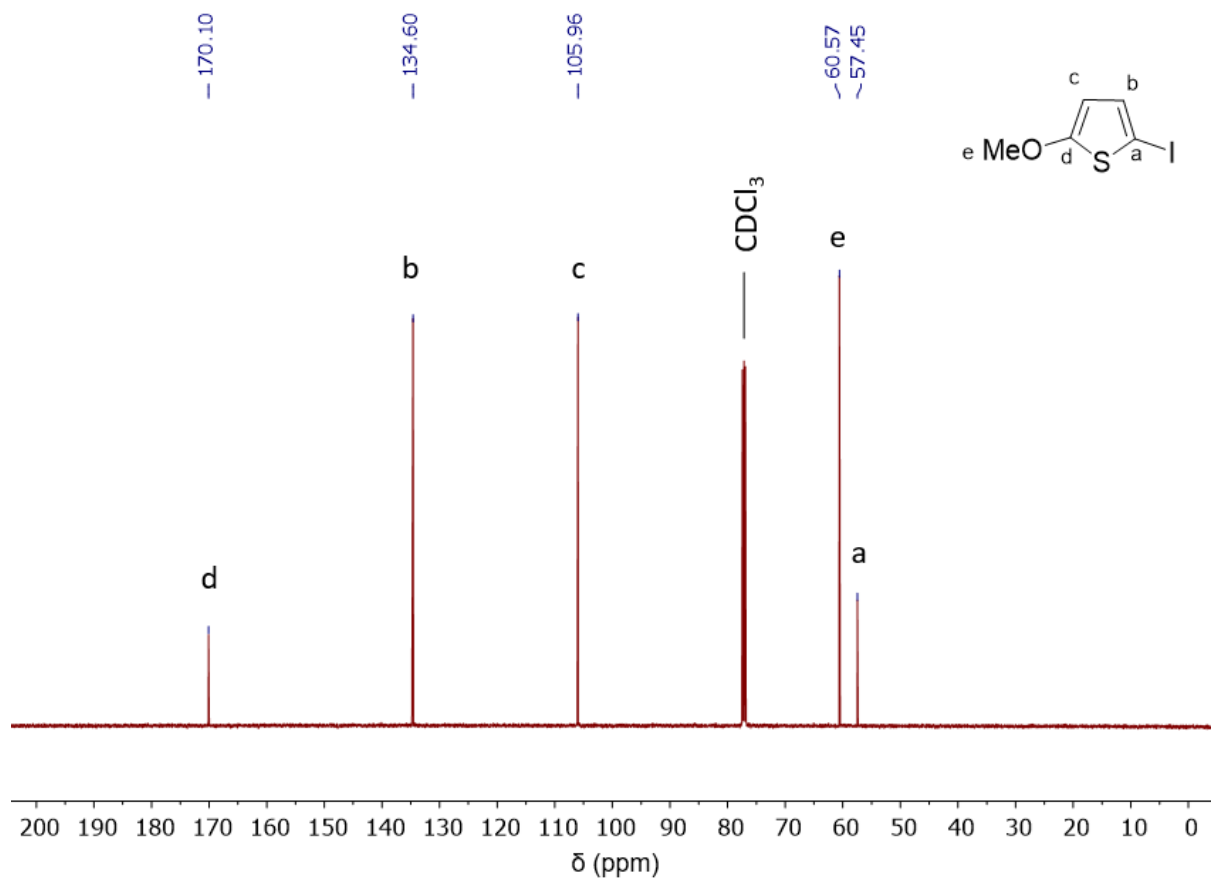


Figure S10. $^{13}\text{C}\{^1\text{H}\}$ NMR (126 MHz) spectrum of 5-methoxy-2-iodothiophene in CDCl_3 .

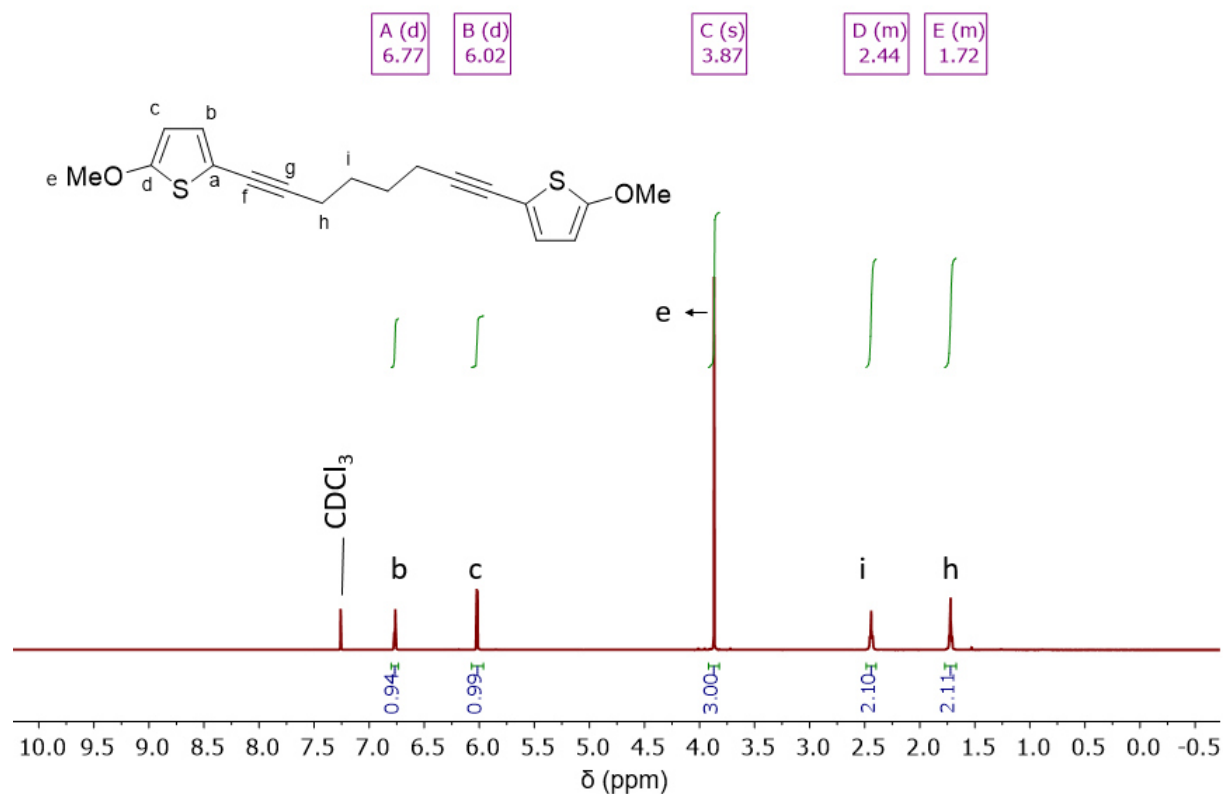


Figure S11. ^1H NMR (500 MHz) spectrum of 1,8-bis(5-methoxy-thiophen-2-yl)octa-1,7-diyne in CDCl_3 .

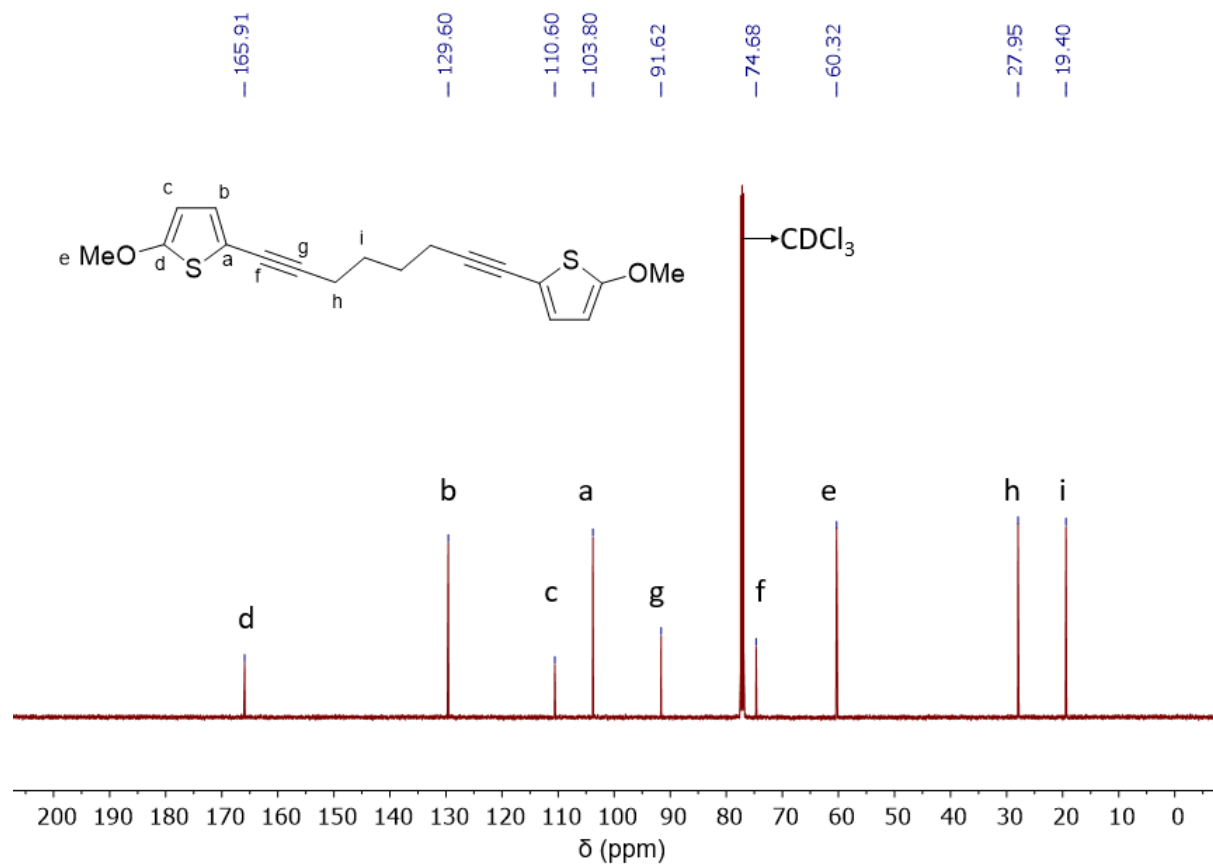


Figure S12. $^{13}\text{C}\{^1\text{H}\}$ NMR (126 MHz) spectrum of 1,8-bis(5-methoxy-thiophen-2-yl)octa-1,7-diyne in CDCl_3 .

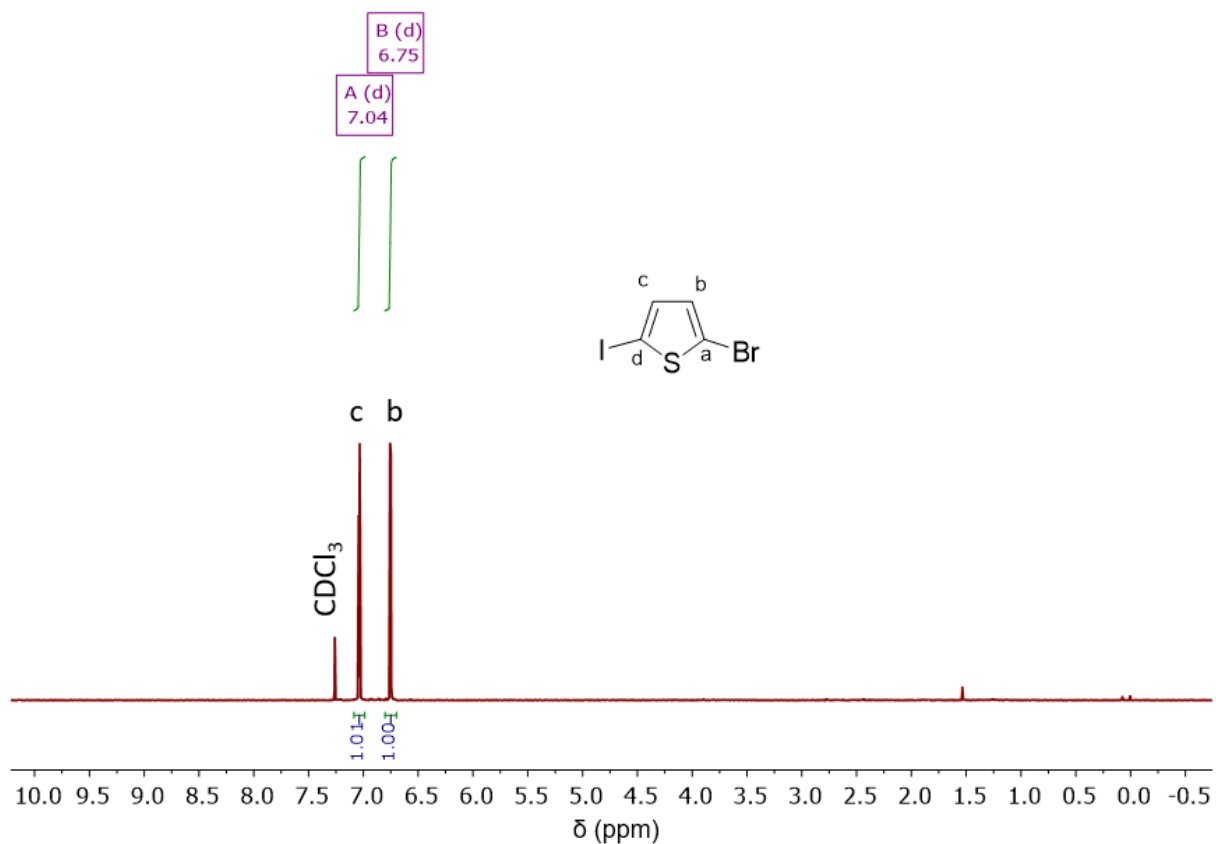


Figure S13. ^1H NMR (500 MHz) spectrum of 2-bromo-5-iodothiophene in CDCl_3 .

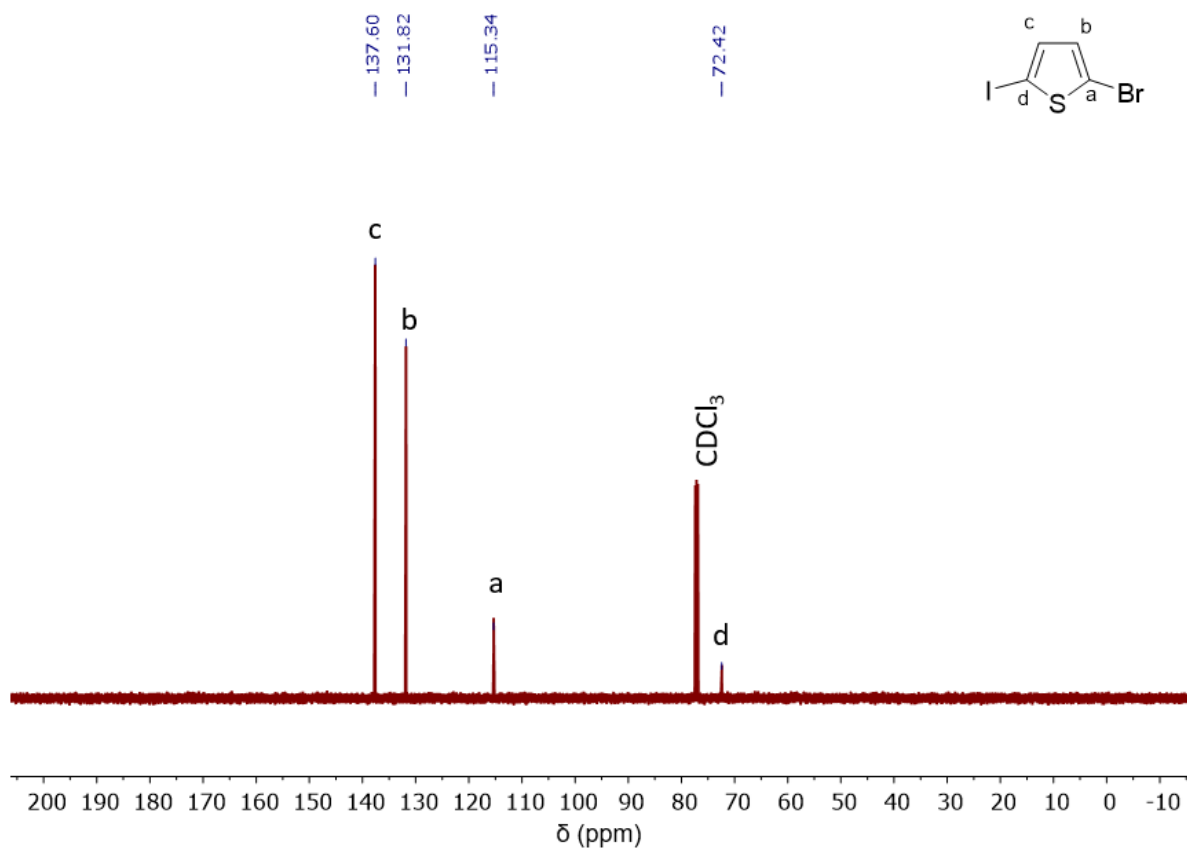


Figure S14. $^{13}\text{C}\{^1\text{H}\}$ NMR (126 MHz) spectrum of 2-bromo-5-iodothiophene in CDCl_3 .

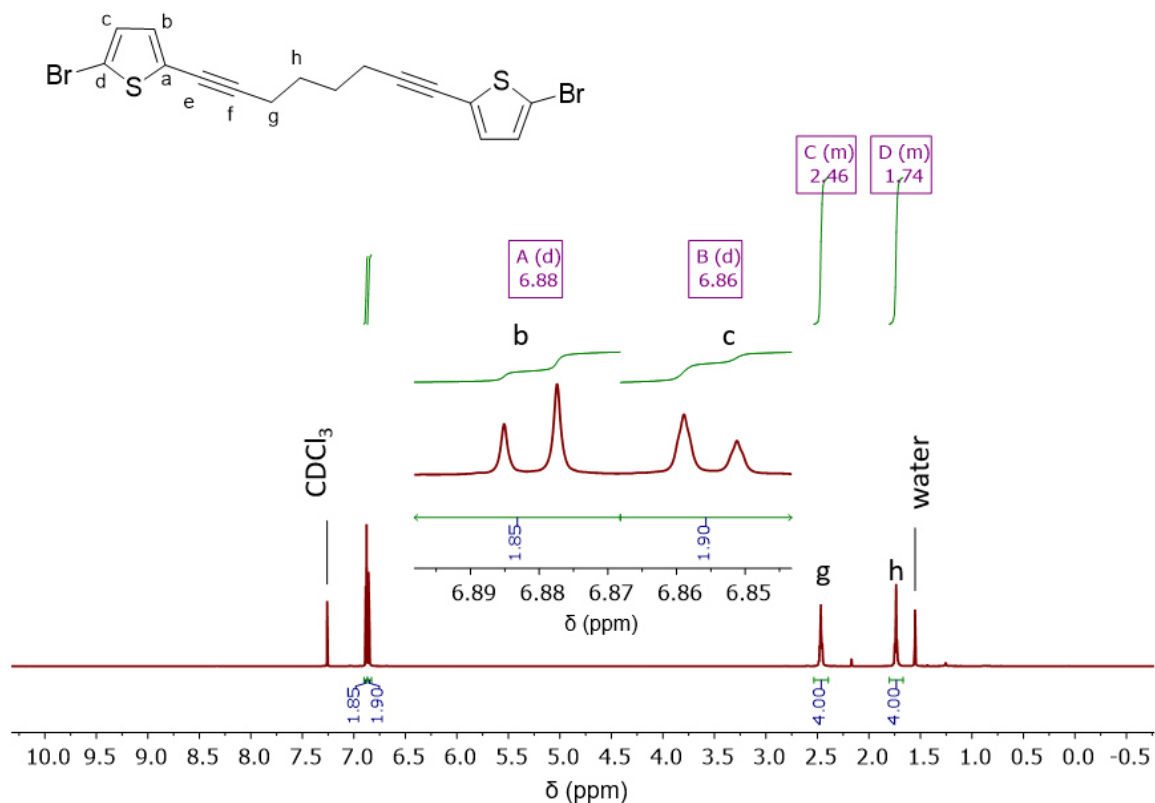


Figure S15. ¹H NMR (500 MHz) spectrum of 1,8-bis(5-bromo-thiophen-2-yl)octa-1,7-diyne in CDCl₃.

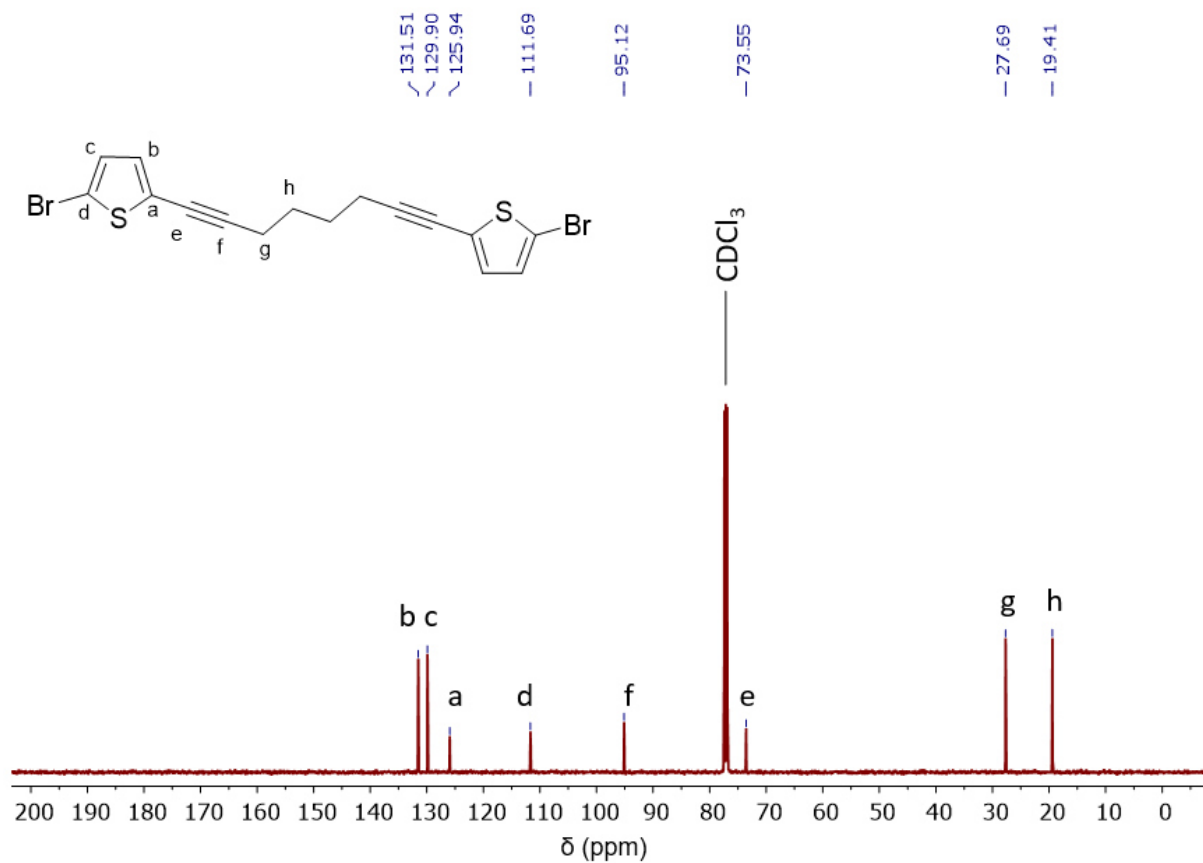


Figure S16. ¹³C{¹H} NMR (126 MHz) spectrum of 1,8-bis(5-bromo-thiophen-2-yl)octa-1,7-diyne in CDCl₃.

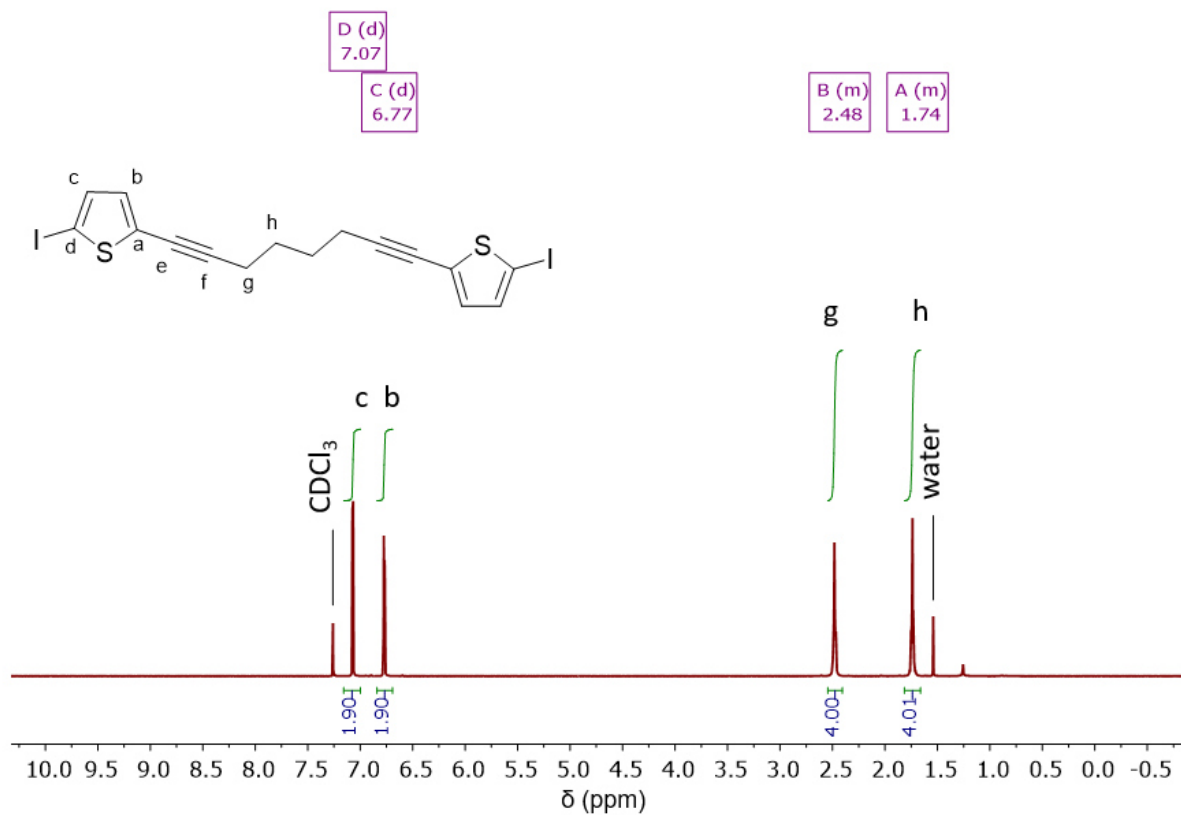


Figure S17. ^1H NMR (500 MHz) spectrum of 1,8-bis(5-iodo-thiophen-2-yl)octa-1,7-diyne in CDCl_3 .

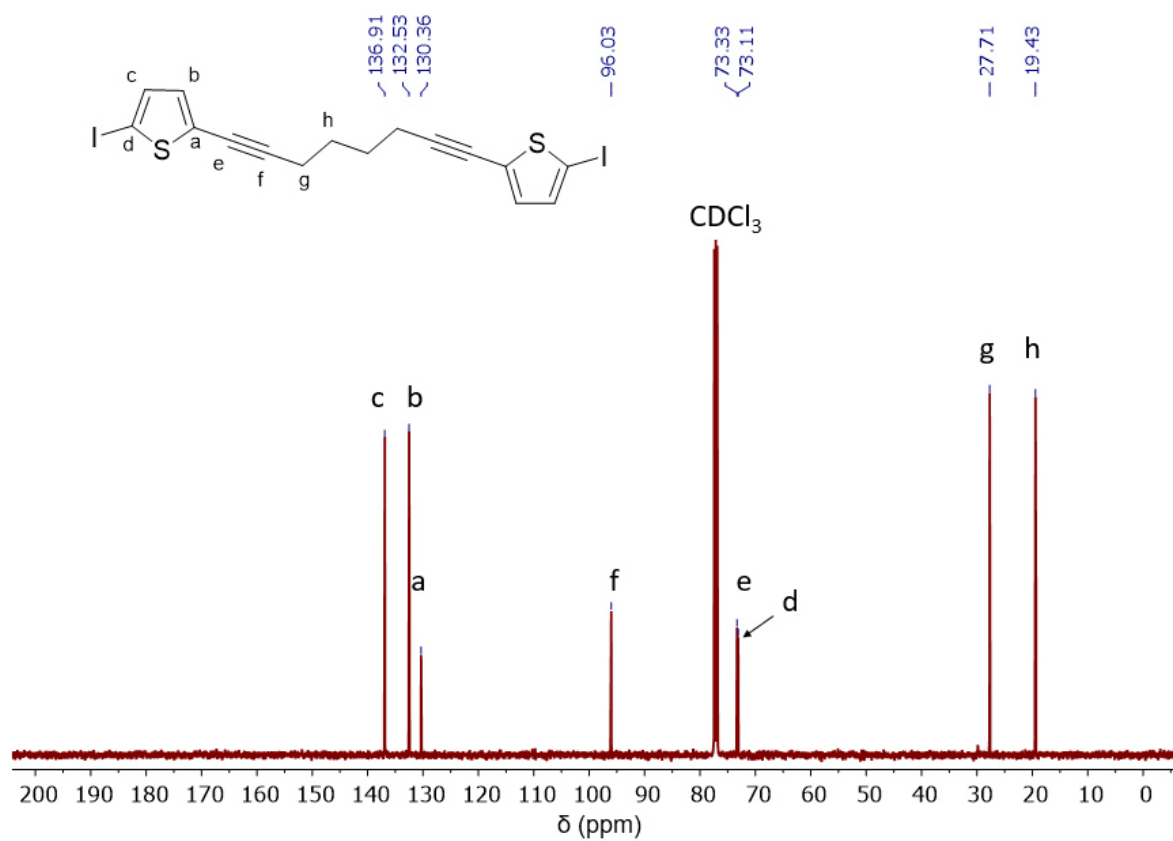


Figure S18. $^{13}\text{C}\{^1\text{H}\}$ NMR (126 MHz) spectrum of 1,8-bis(5-iodo-thiophen-2-yl)octa-1,7-diyne in CDCl_3 .

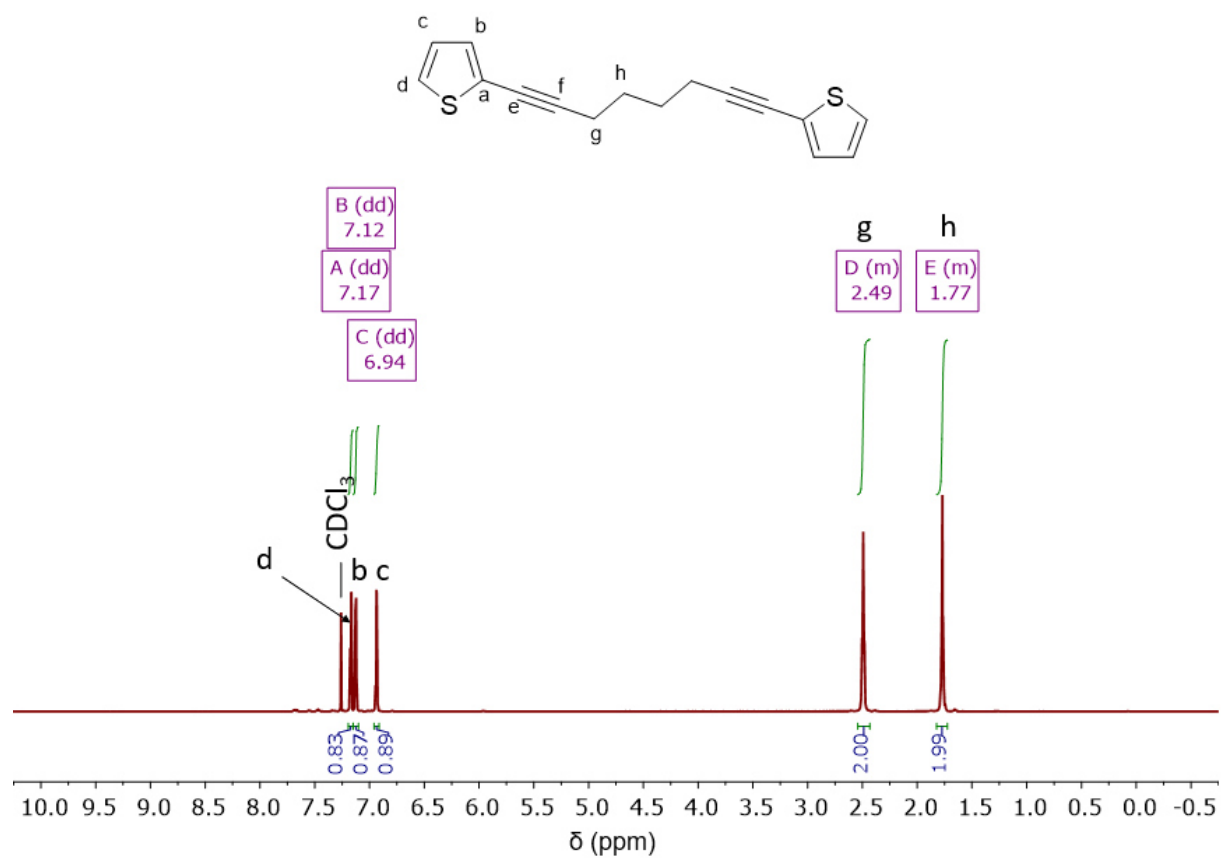


Figure S19. ^1H NMR (500 MHz) spectrum of 1,8-bis(thiophen-2-yl)octa-1,7-diyne in CDCl_3 .

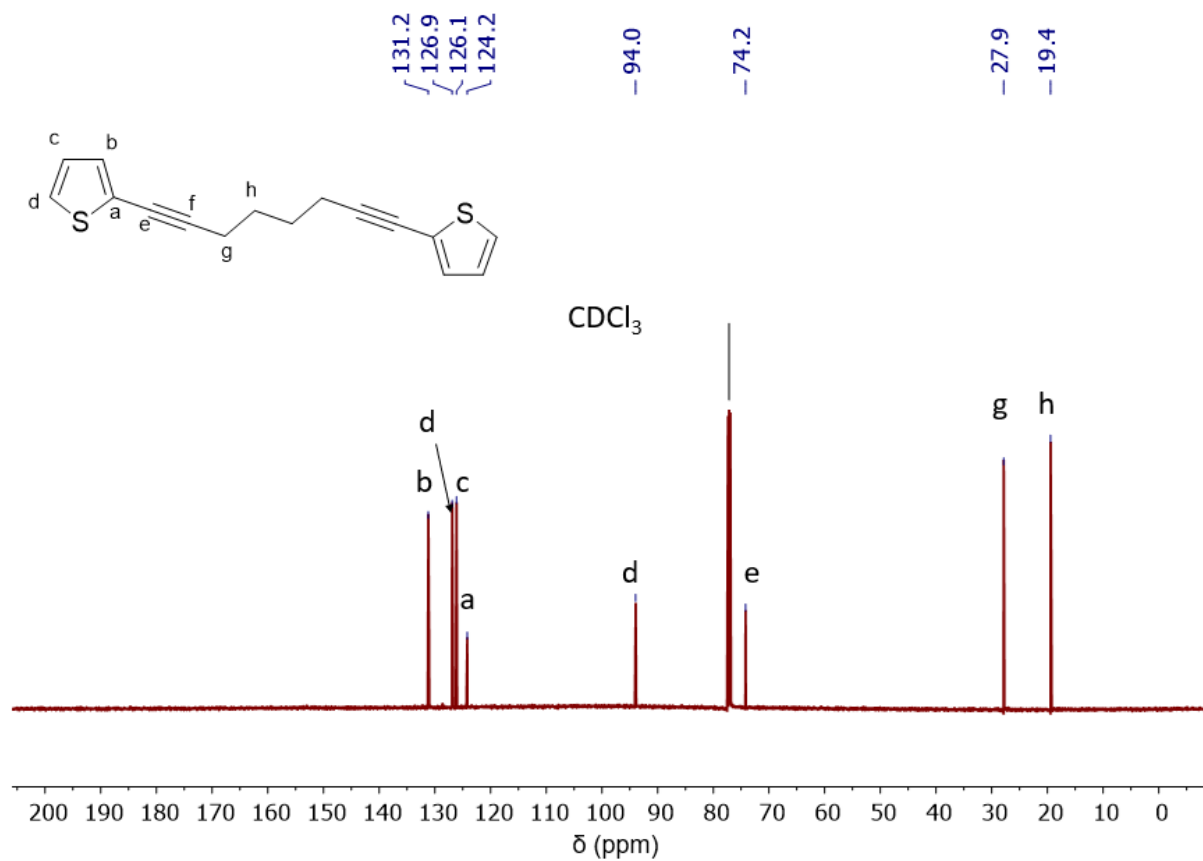


Figure S20. $^{13}\text{C}\{^1\text{H}\}$ NMR (126 MHz) spectrum of 1,8-bis(thiophen-2-yl)octa-1,7-diyne in CDCl_3 .

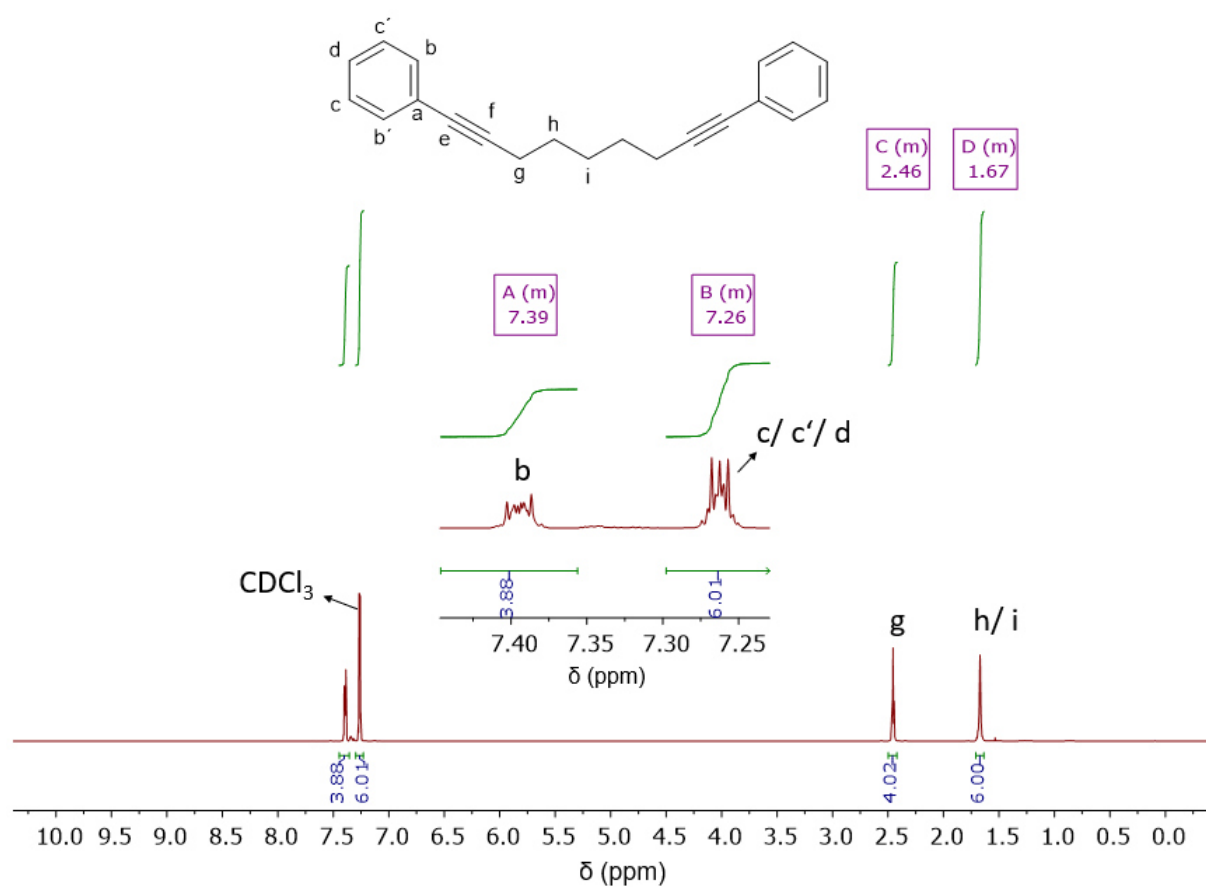


Figure S21. ^1H NMR (600 MHz) spectrum of 1,9-diphenylnona-1,8-diyne in CDCl_3 .

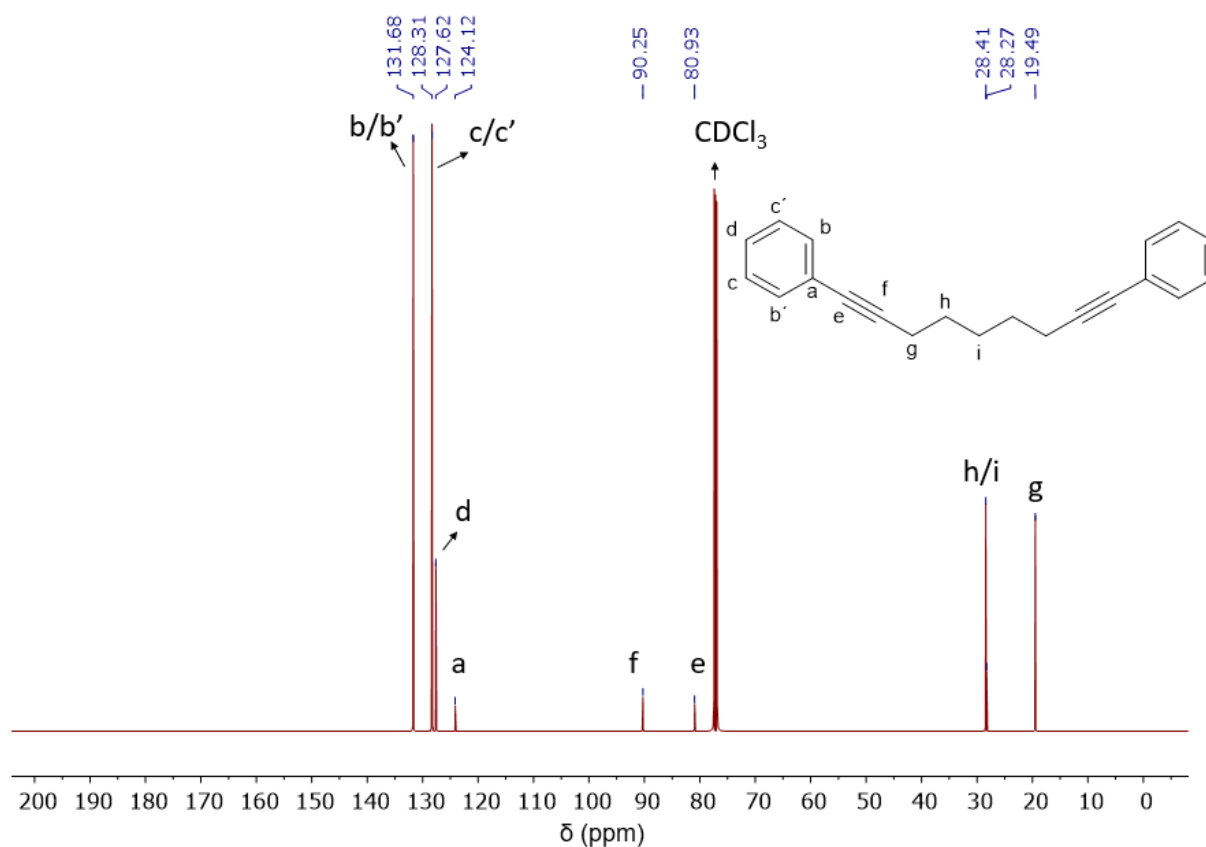


Figure S22. $^{13}\text{C}\{^1\text{H}\}$ NMR (151 MHz) spectrum of 1,9-diphenylnona-1,8-diyne in CDCl_3 .

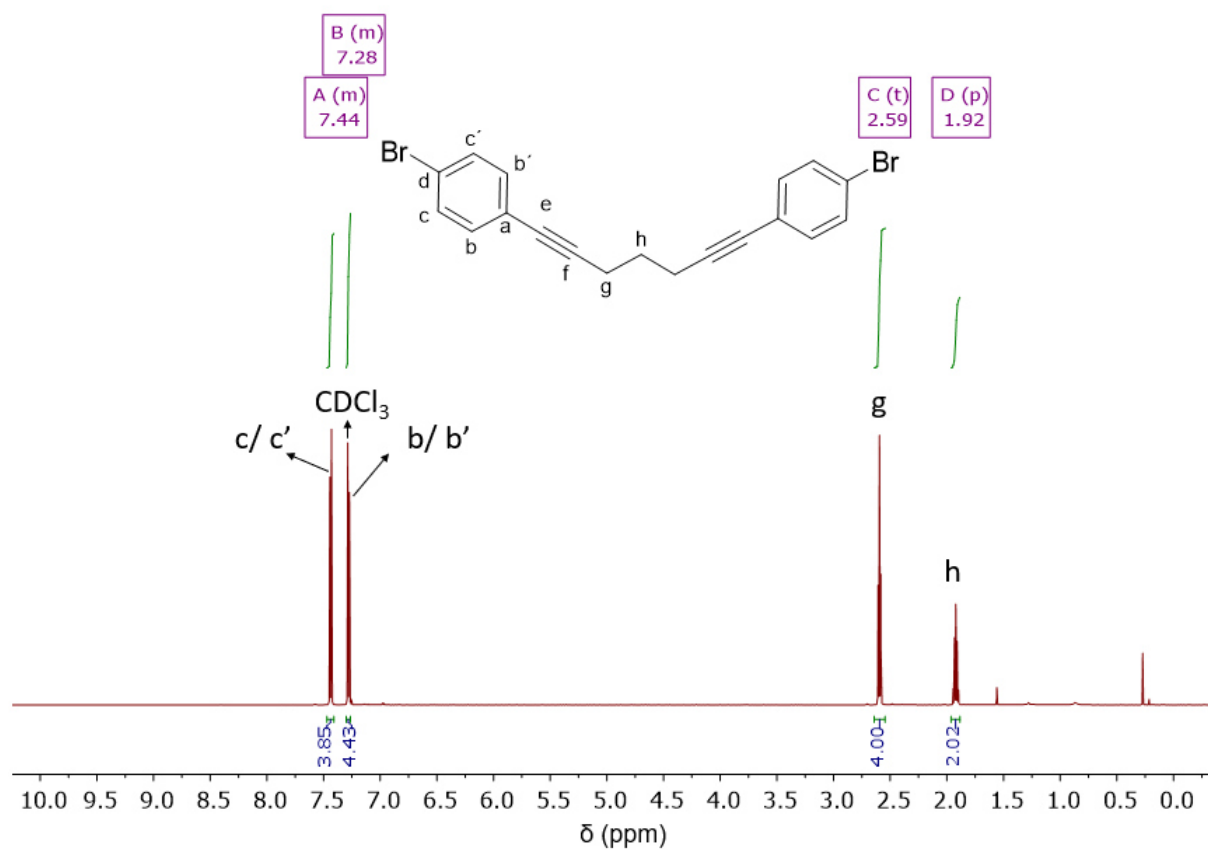


Figure S23. ^1H NMR (600 MHz) spectrum of 1,7-bis(4-bromophenyl)hepta-1,6-diyne in CDCl_3 .

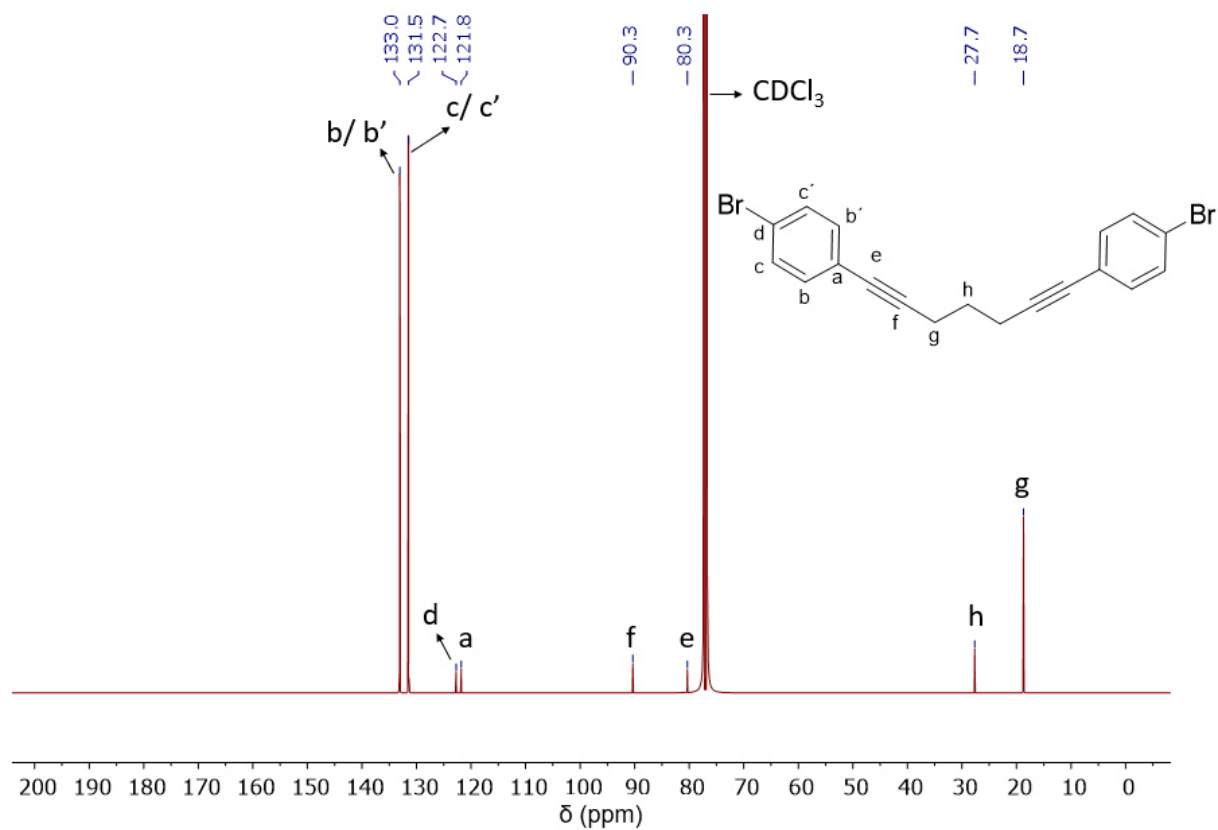
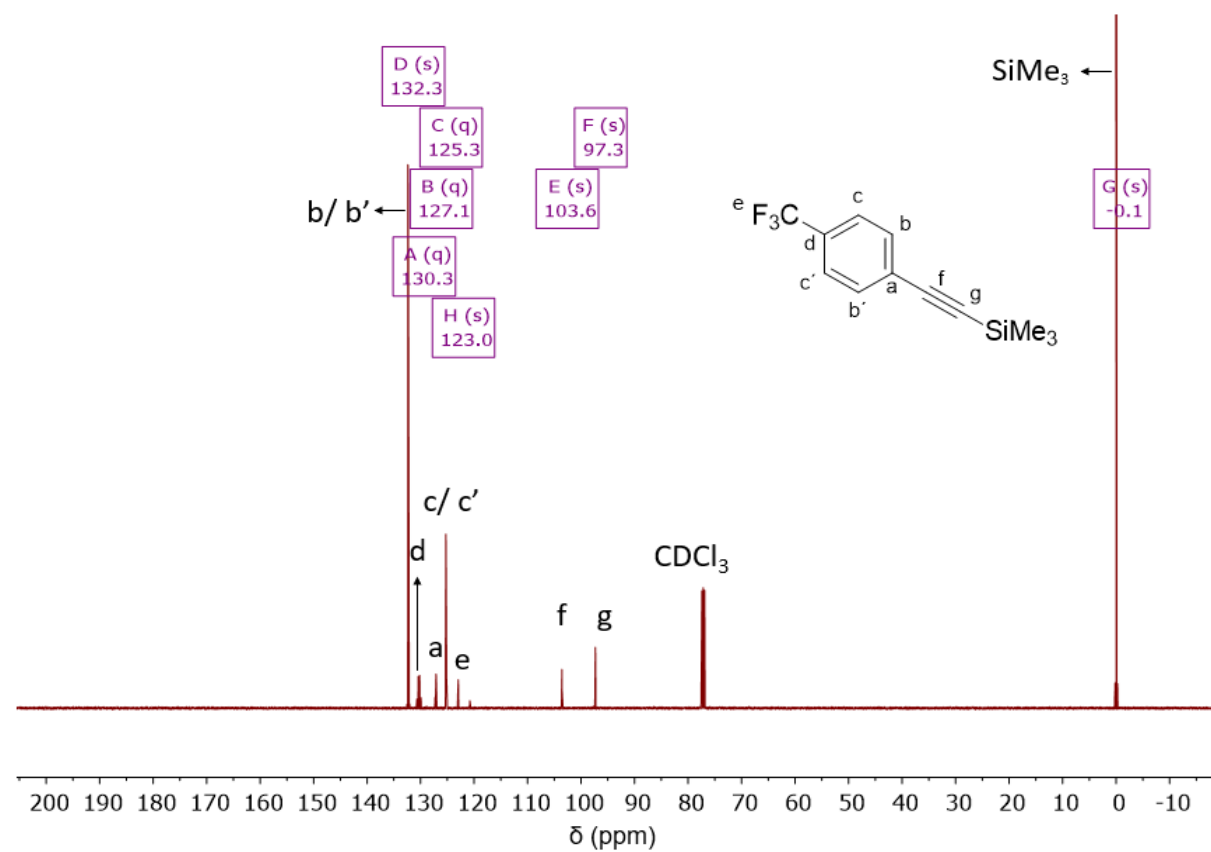
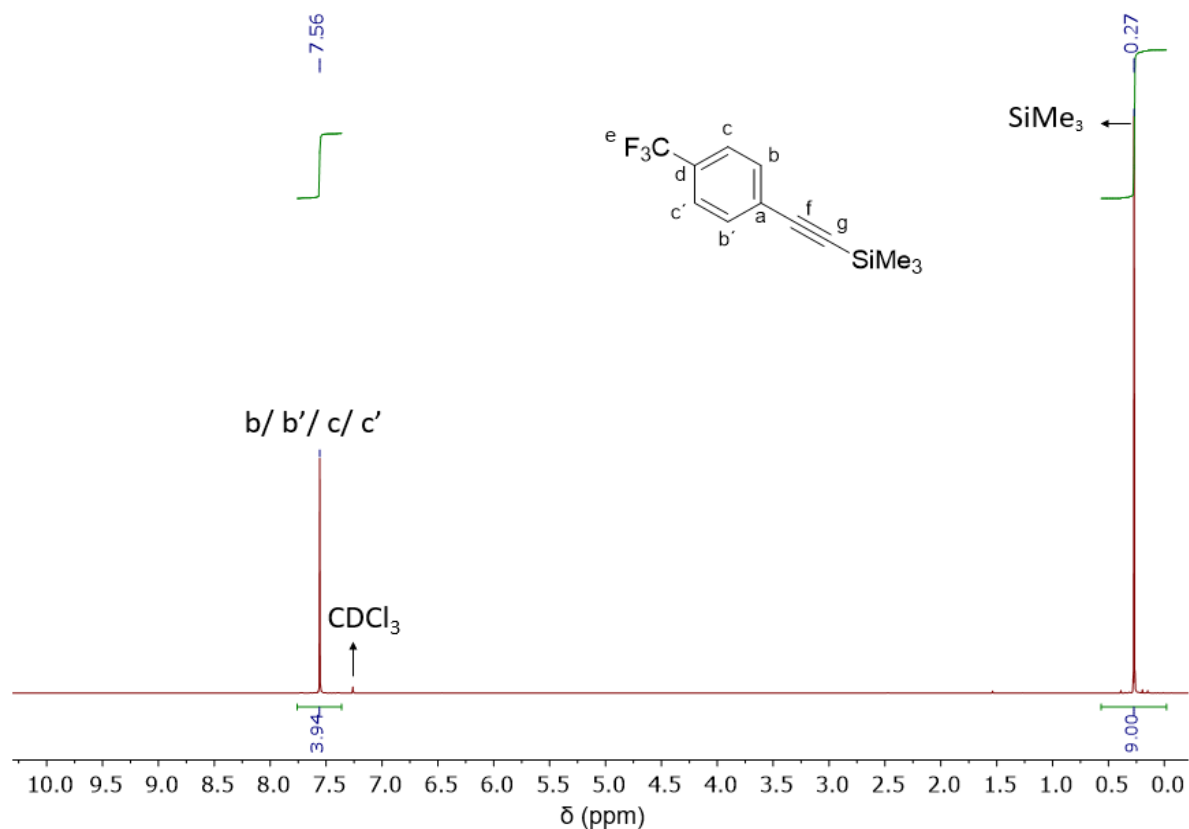


Figure S24. $^{13}\text{C}\{^1\text{H}\}$ NMR (151 MHz) spectrum of 1,7-bis(4-bromophenyl)hepta-1,6-diyne in CDCl_3 .



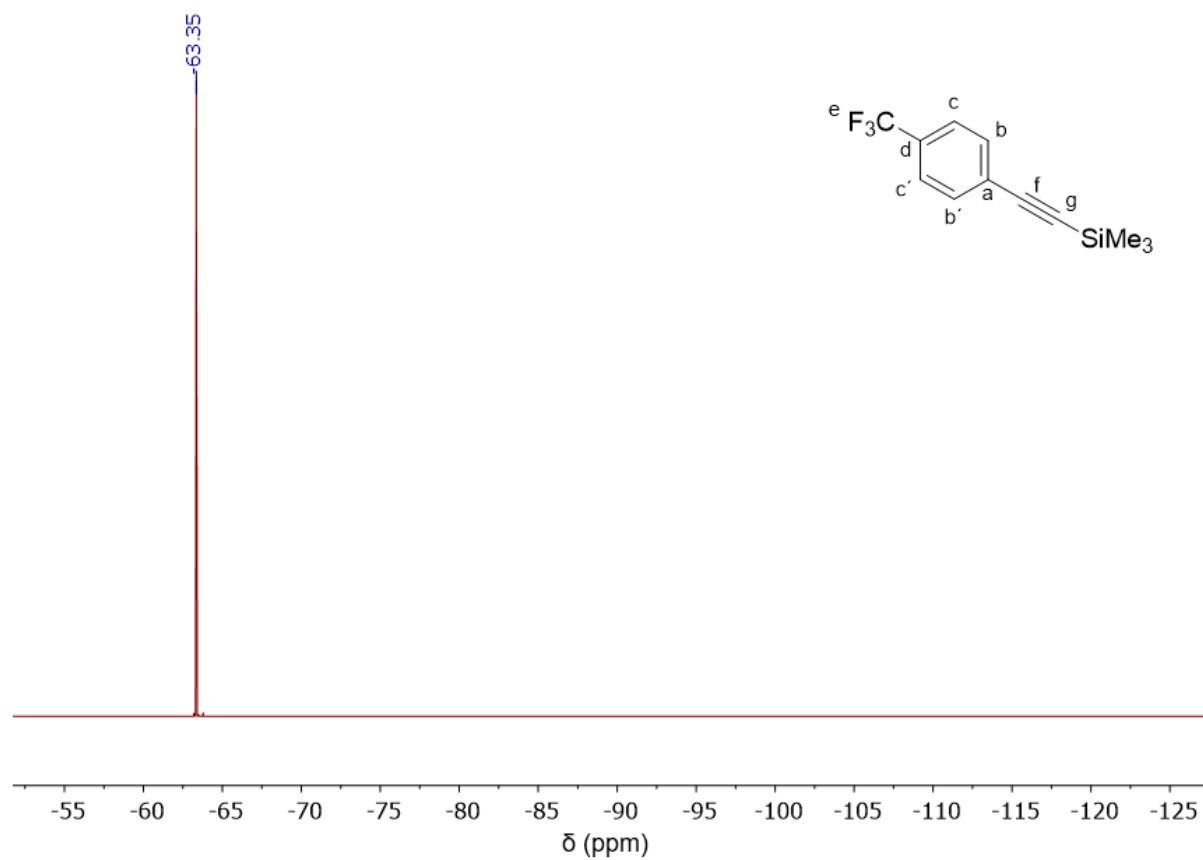


Figure S27. ^{19}F NMR (471 MHz) spectrum of 4-trifluoromethyl-phenylethyne-trimethylsilane in CDCl_3 .

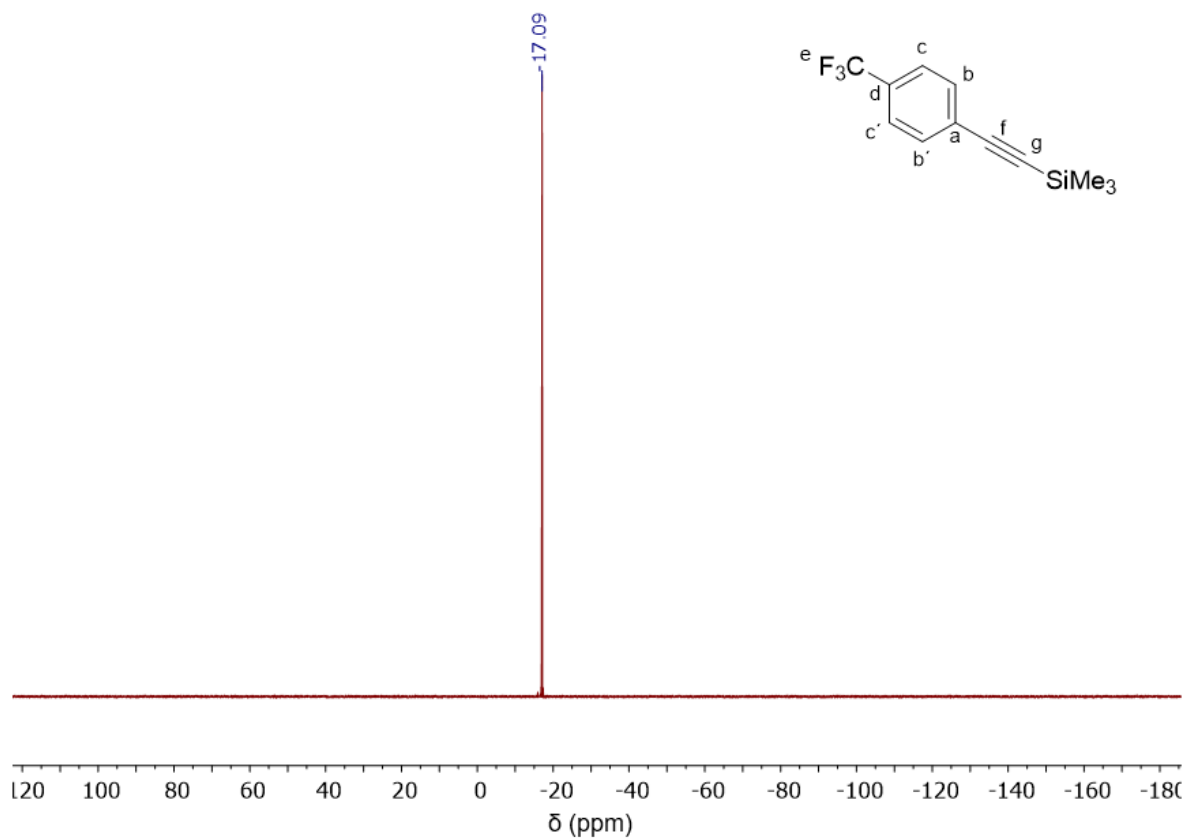


Figure S28. $^{29}\text{Si}\{^1\text{H}\}$ NMR (99 MHz) spectrum of 4-trifluoromethyl-phenylethyne-trimethylsilane in CDCl_3 .

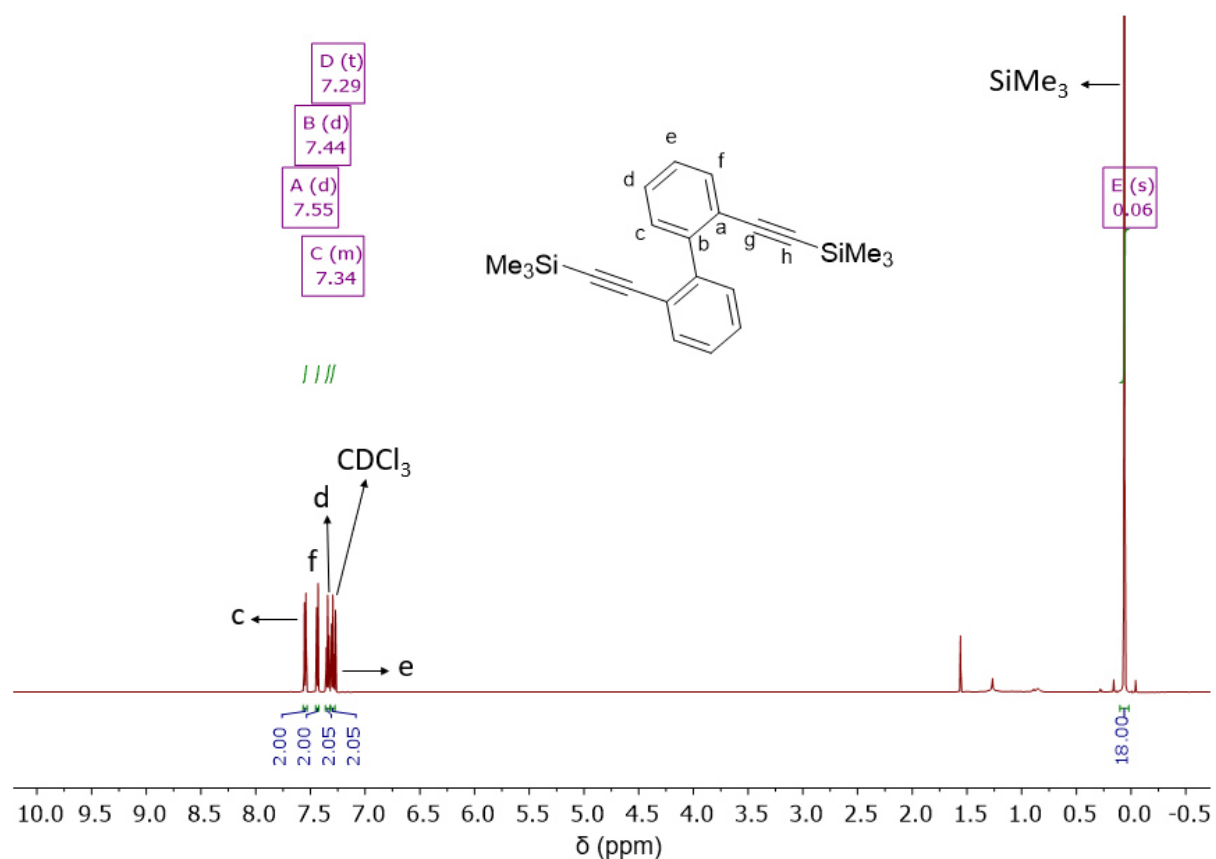


Figure S29. ^1H NMR (600 MHz) spectrum of 2,2'-bis((trimethylsilyl)ethynyl)biphenyl in CDCl_3 .

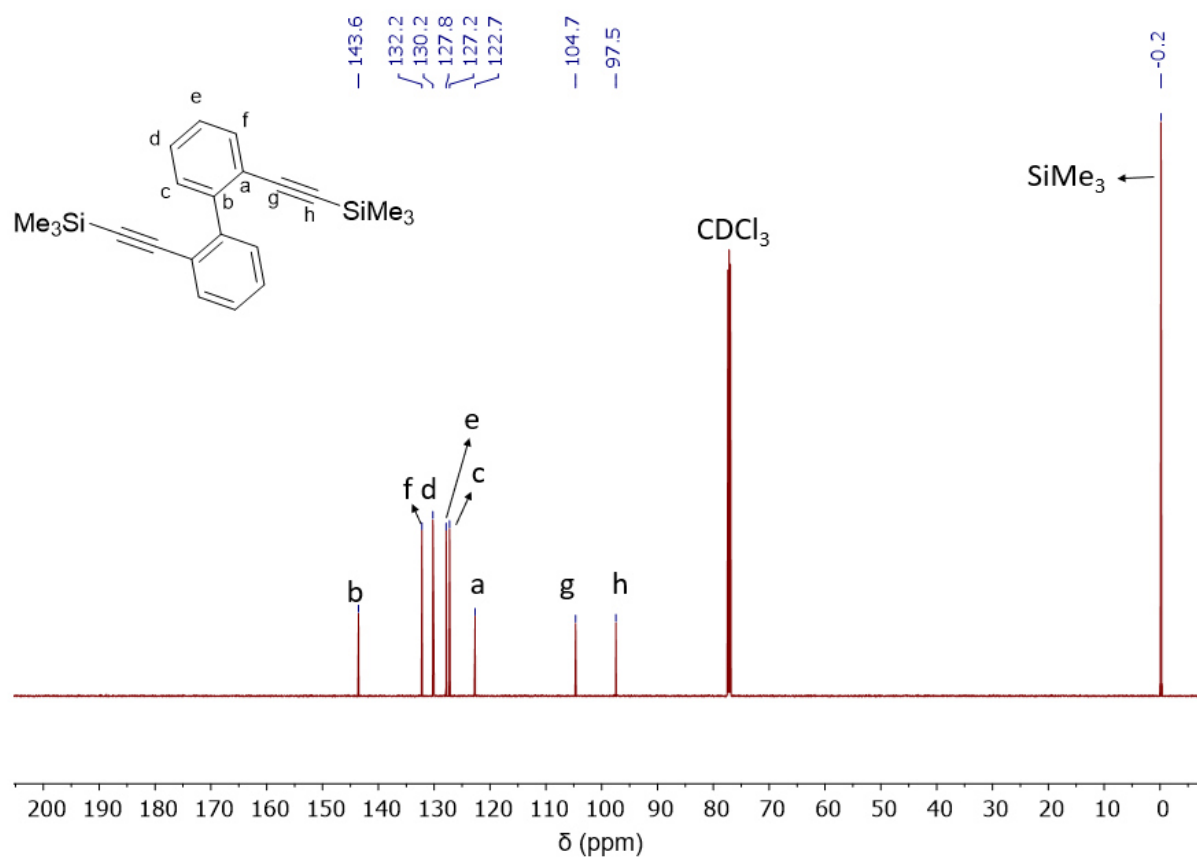


Figure S30. $^{13}\text{C}\{^1\text{H}\}$ NMR (151 MHz) spectrum of 2,2'-bis((trimethylsilyl)ethynyl)biphenyl in CDCl_3 .

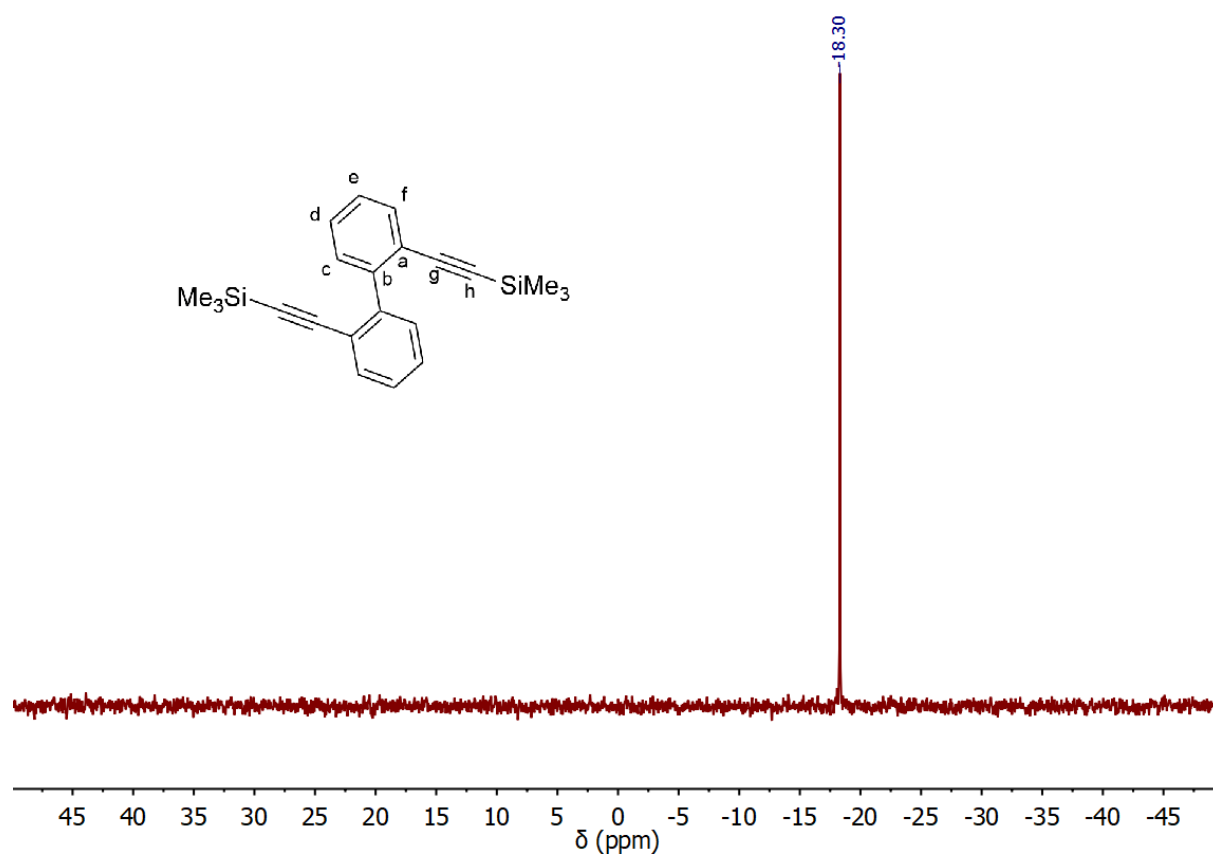


Figure S31. $^{29}\text{Si}\{^1\text{H}\}$ NMR (99 MHz) spectrum of 2,2'-bis((trimethylsilyl)ethynyl)biphenyl in C_6D_6 .

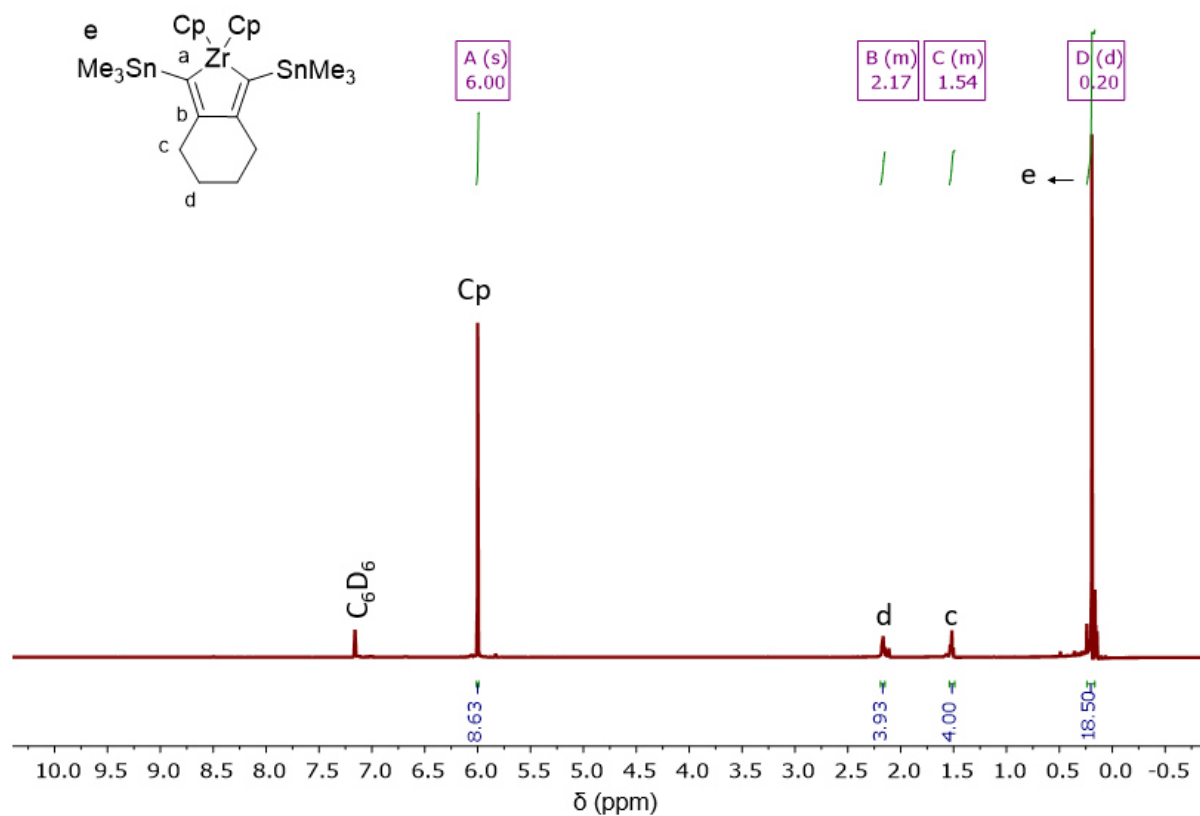


Figure S32. ^1H NMR (500 MHz) spectrum of zirconacyclopentadiene **11a** in C_6D_6 .

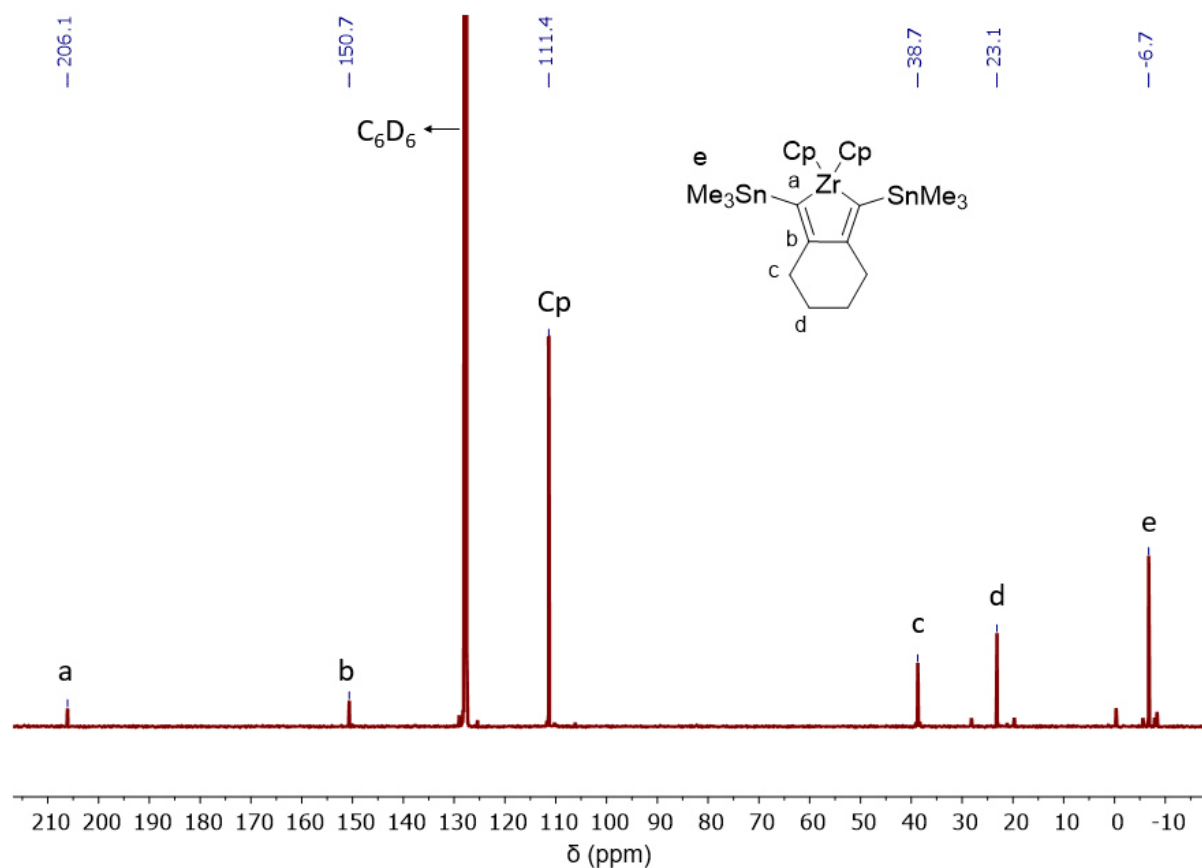


Figure S33. $^{13}\text{C}\{^1\text{H}\}$ NMR (126 MHz) spectrum of zirconacyclopentadiene **11a** in C_6D_6 .

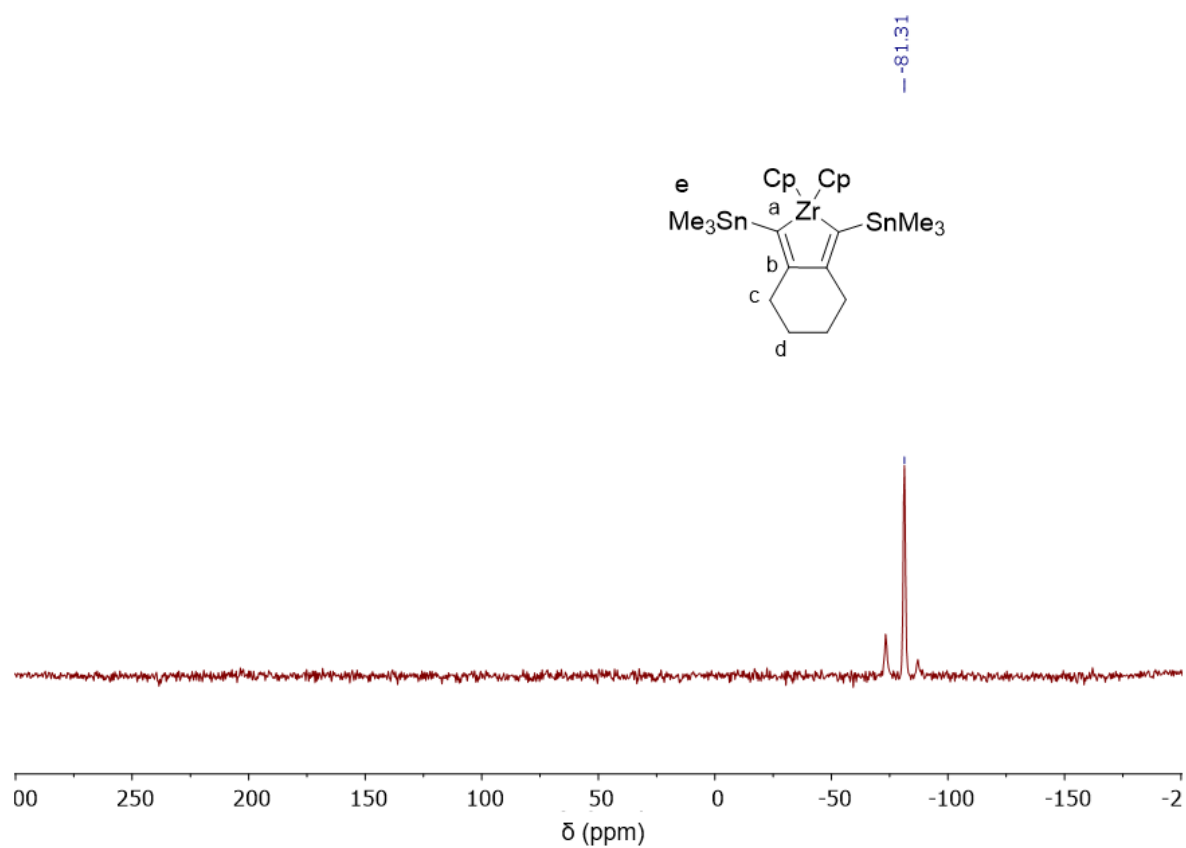


Figure S34. $^{119}\text{Sn}\{^1\text{H}\}$ NMR (187 MHz) spectrum of zirconacyclopentadiene **11a** in C_6D_6 .

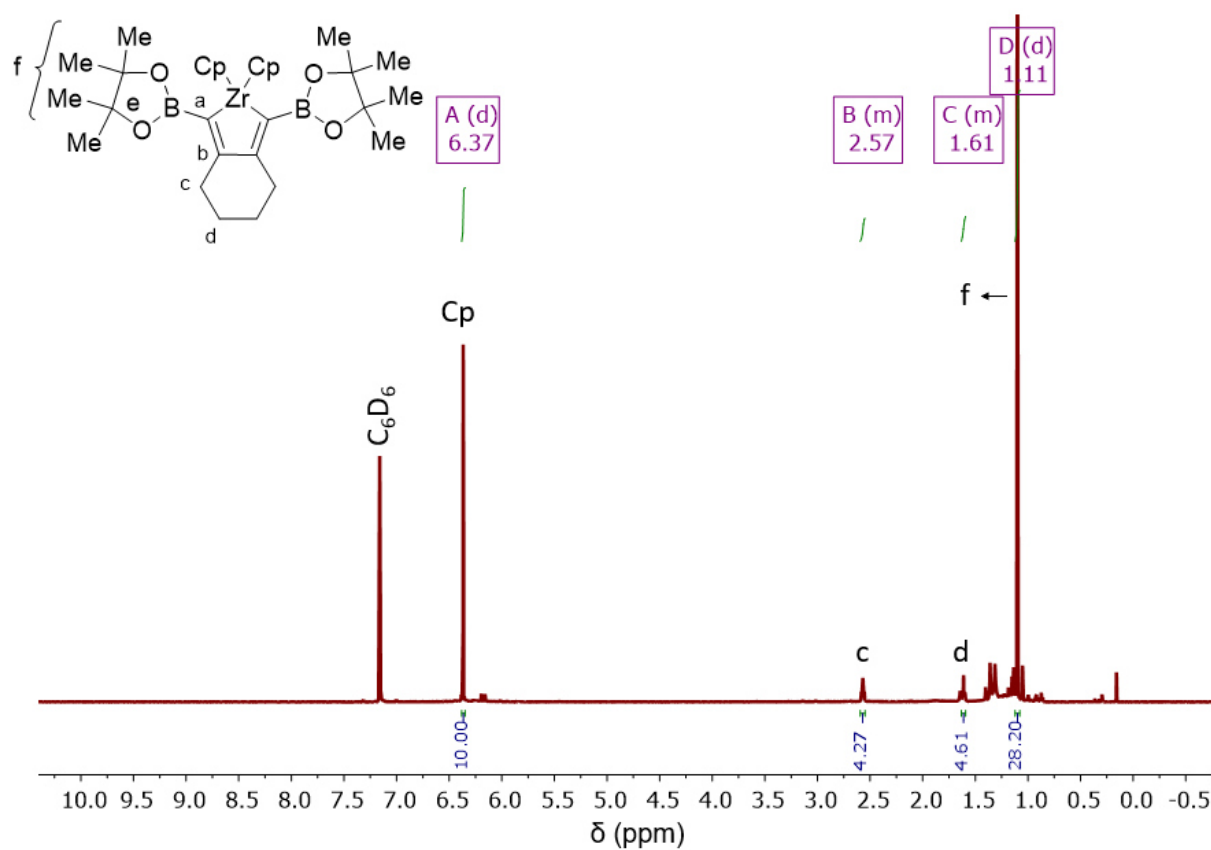


Figure S35. ^1H NMR (500 MHz) spectrum of zirconacyclopentadiene **11b** in C_6D_6 .

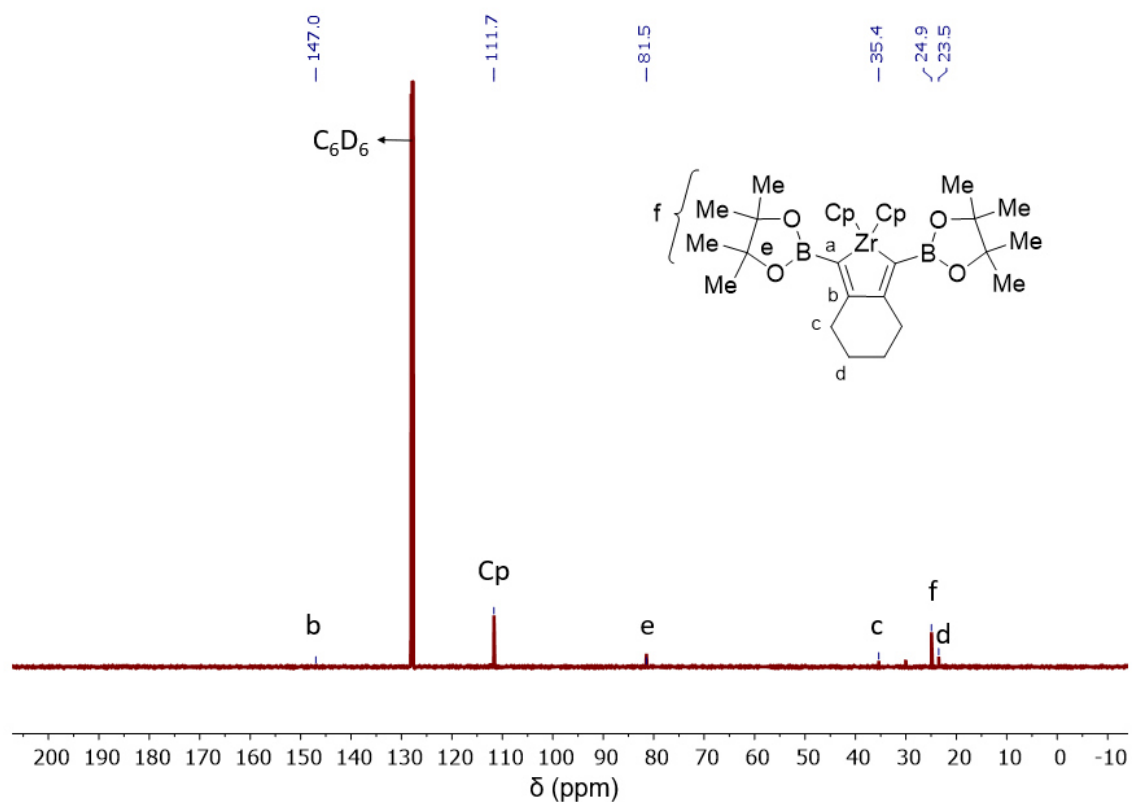


Figure S36. $^{13}\text{C}\{^1\text{H}\}$ NMR (126 MHz) spectrum of zirconacyclopentadiene **11b** in C_6D_6 .

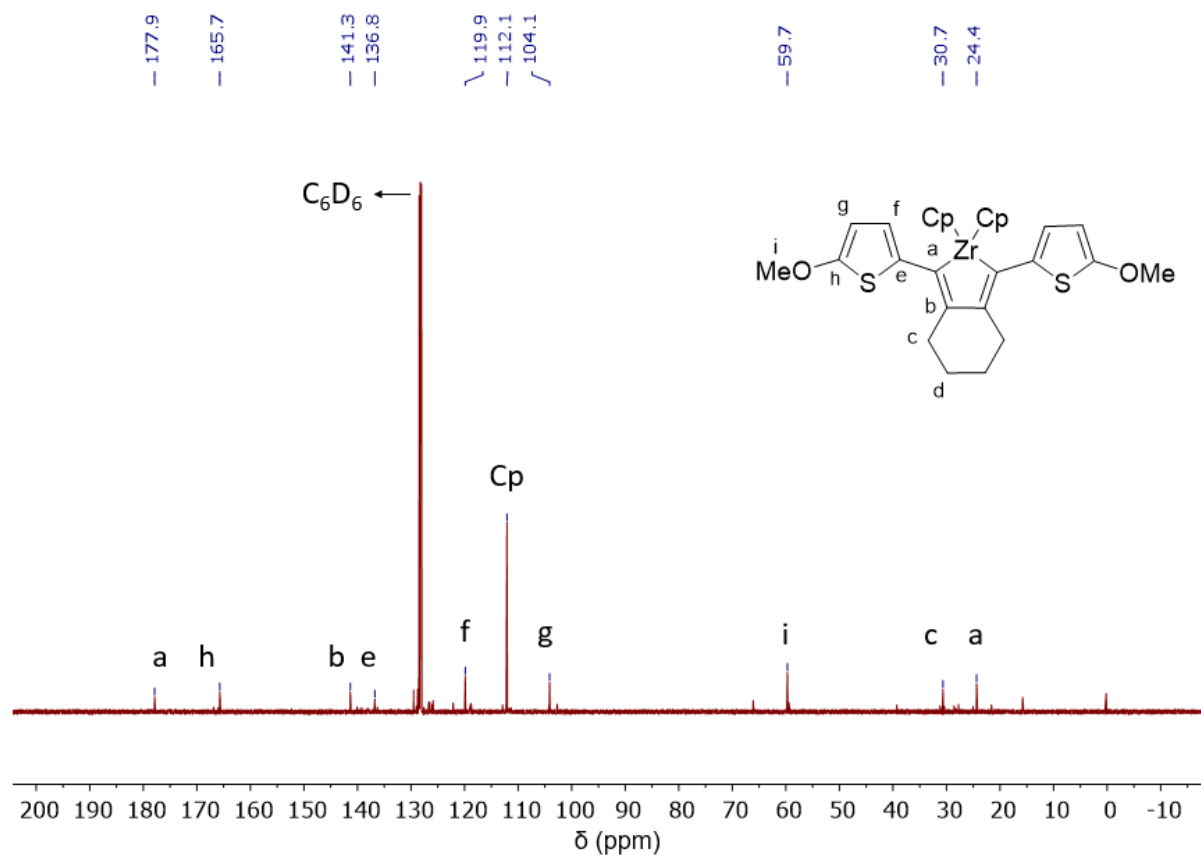


Figure S39. $^{13}\text{C}\{^1\text{H}\}$ NMR (126 MHz) spectrum of zirconacyclopentadiene **11c** in C_6D_6 .

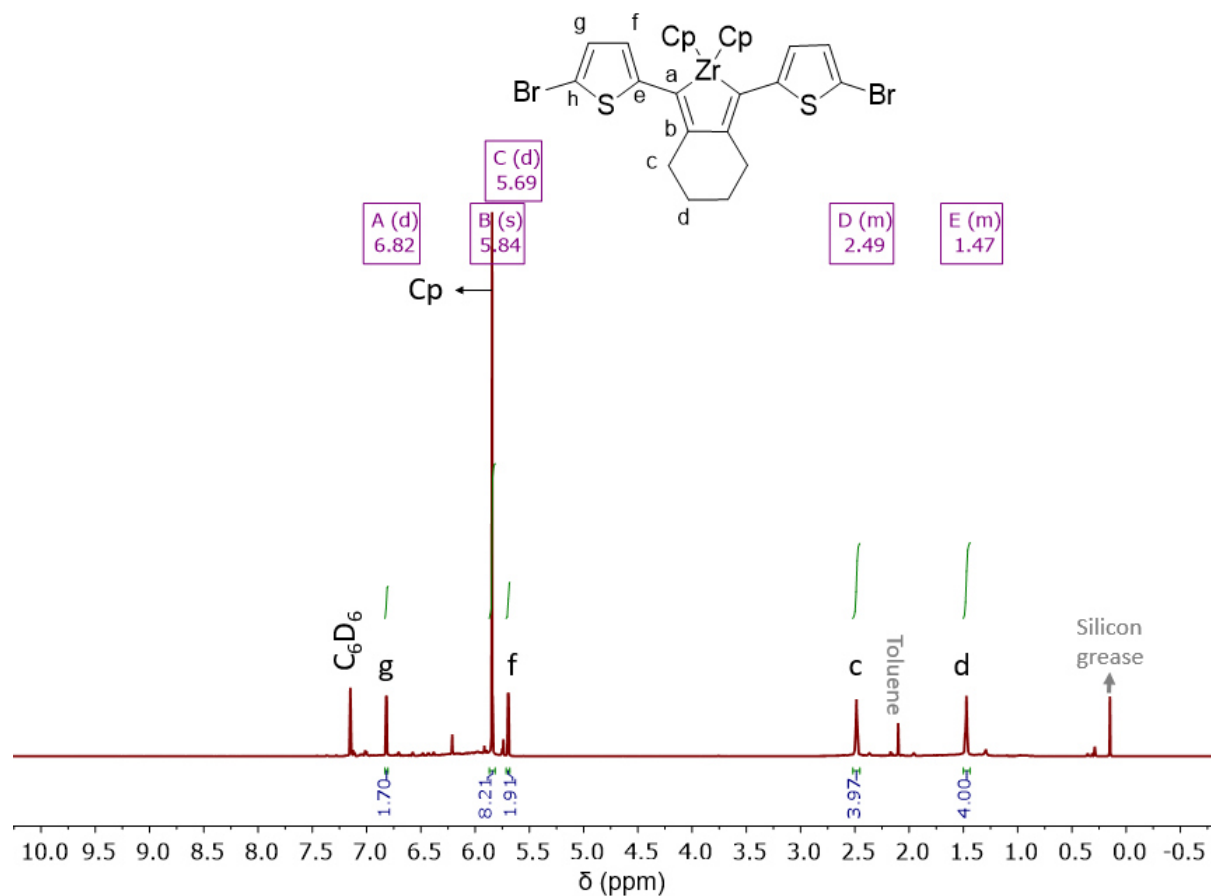


Figure S40. ^1H NMR (500 MHz) spectrum of zirconacyclopentadiene **11d** in C_6D_6 .

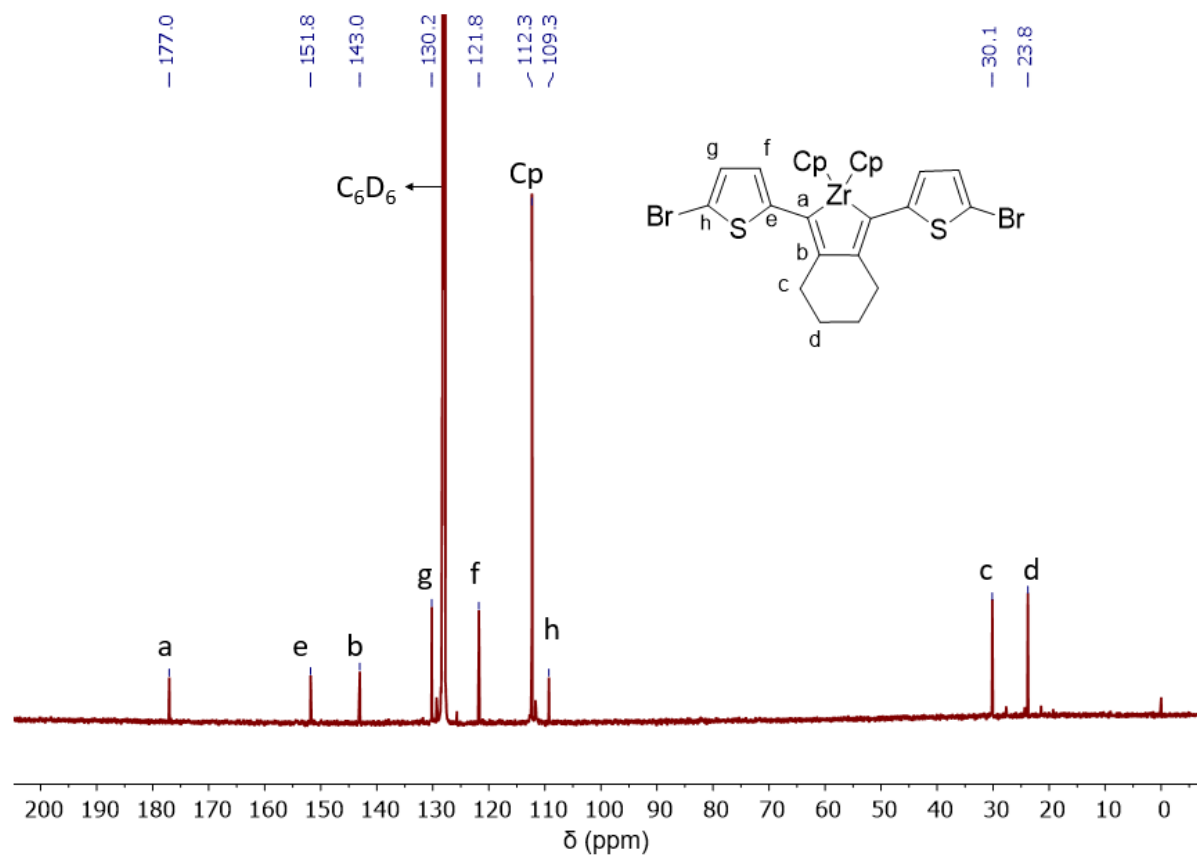


Figure S41. $^{13}\text{C}\{^1\text{H}\}$ NMR (126 MHz) spectrum of zirconacyclopentadiene **11d** in C_6D_6 .

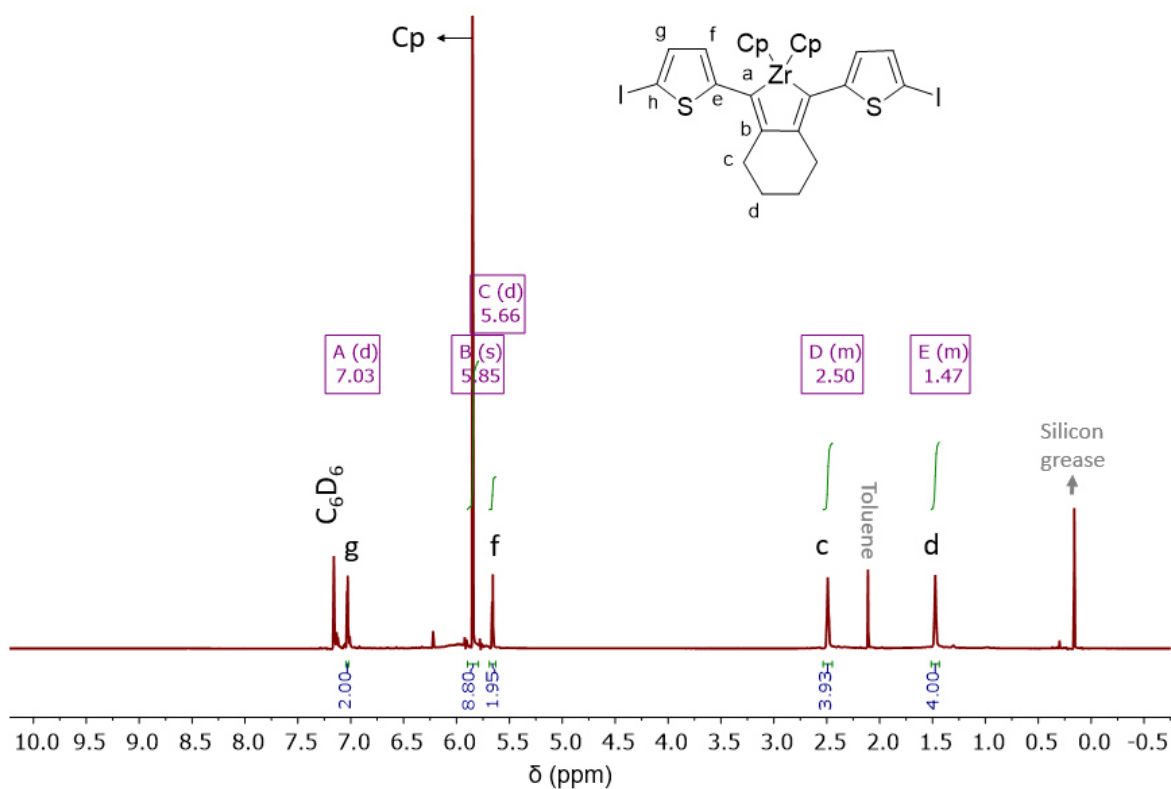


Figure S42. ^1H NMR (500 MHz) spectrum of zirconacyclopentadiene **11e** in C_6D_6 .

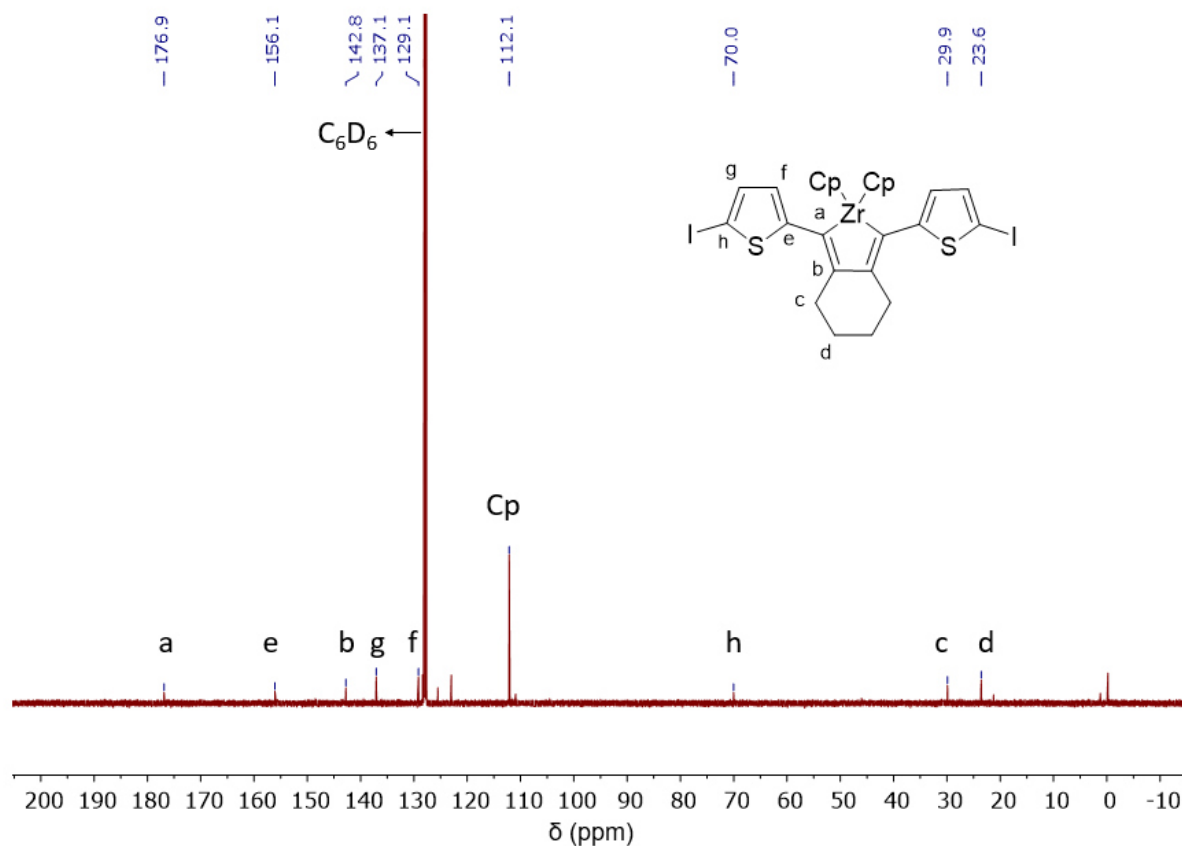


Figure S43. $^{13}\text{C}\{^1\text{H}\}$ NMR (126 MHz) spectrum of zirconacyclopentadiene **11e** in C_6D_6 .

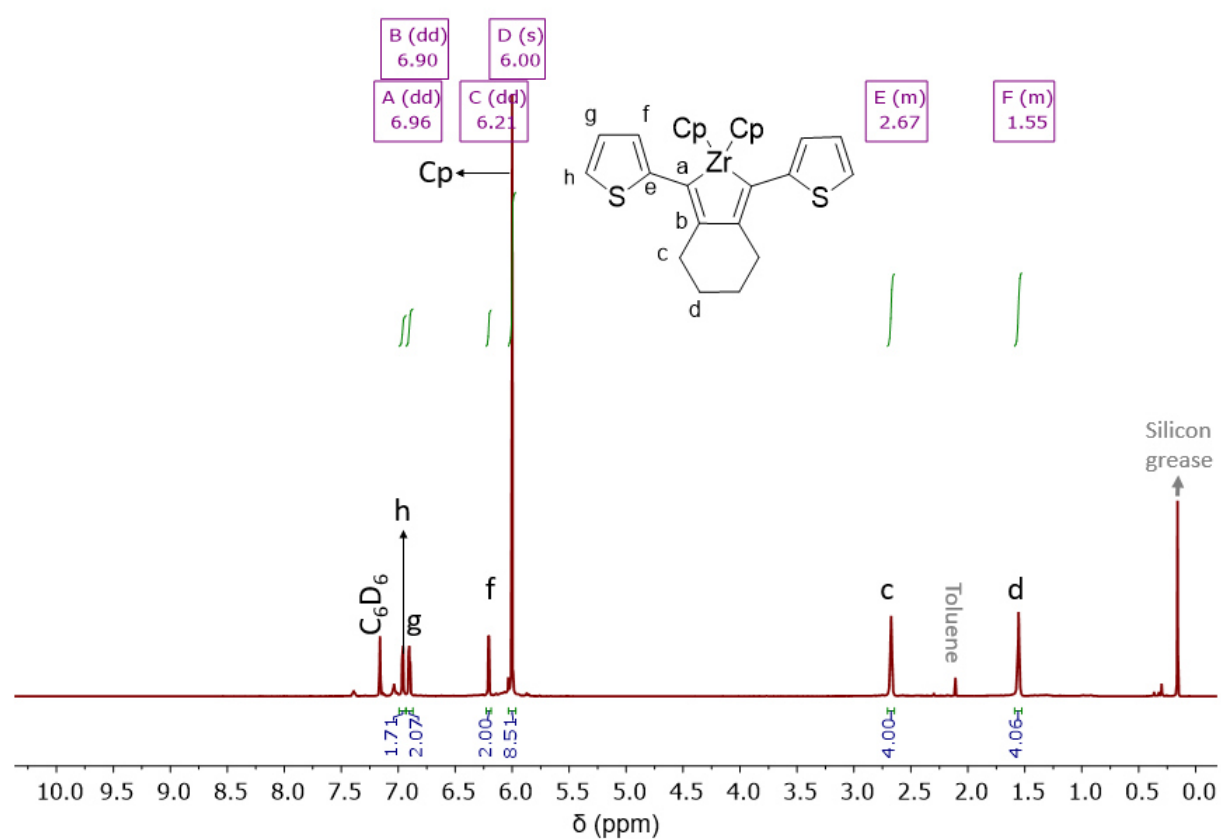


Figure S44. ^1H NMR (500 MHz) spectrum of zirconacyclopentadiene **11f** in C_6D_6 .

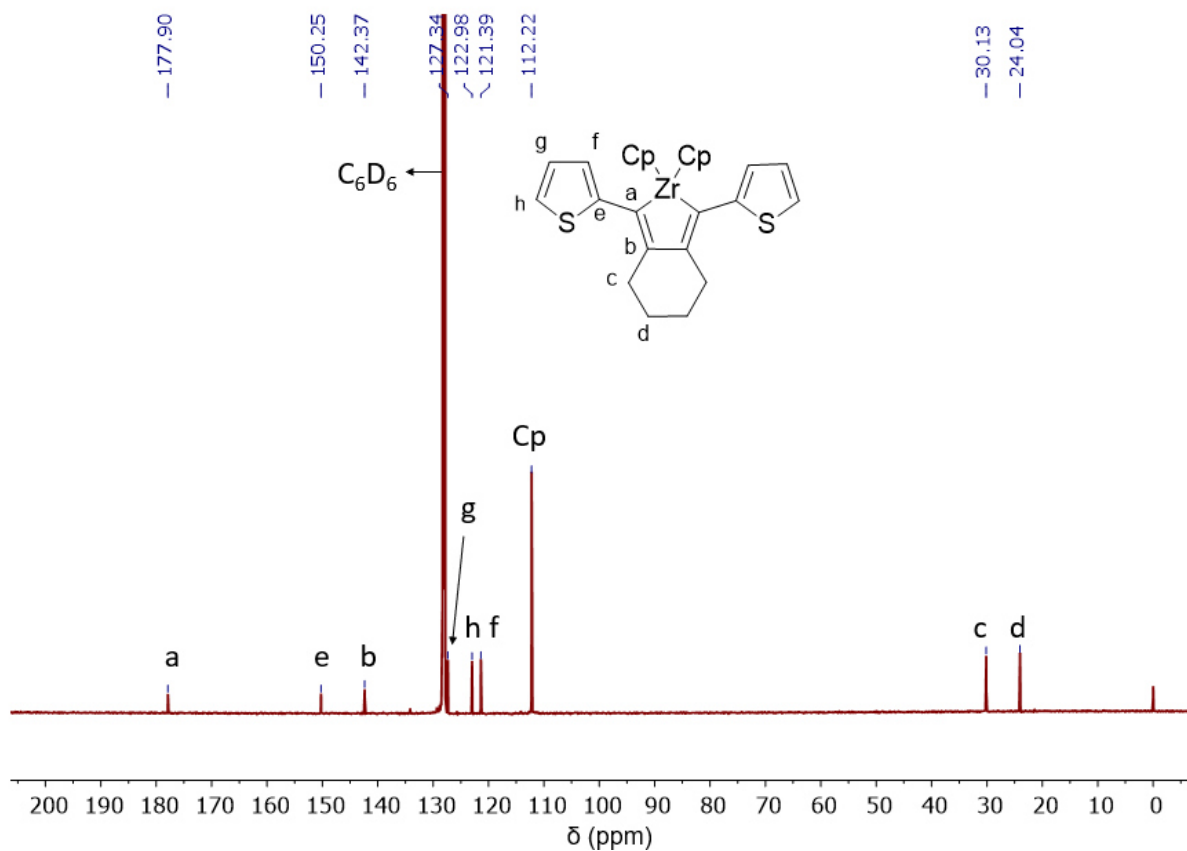


Figure S45. $^{13}\text{C}\{^1\text{H}\}$ NMR (126 MHz) spectrum of zirconacyclopentadiene **11f** in C_6D_6 .

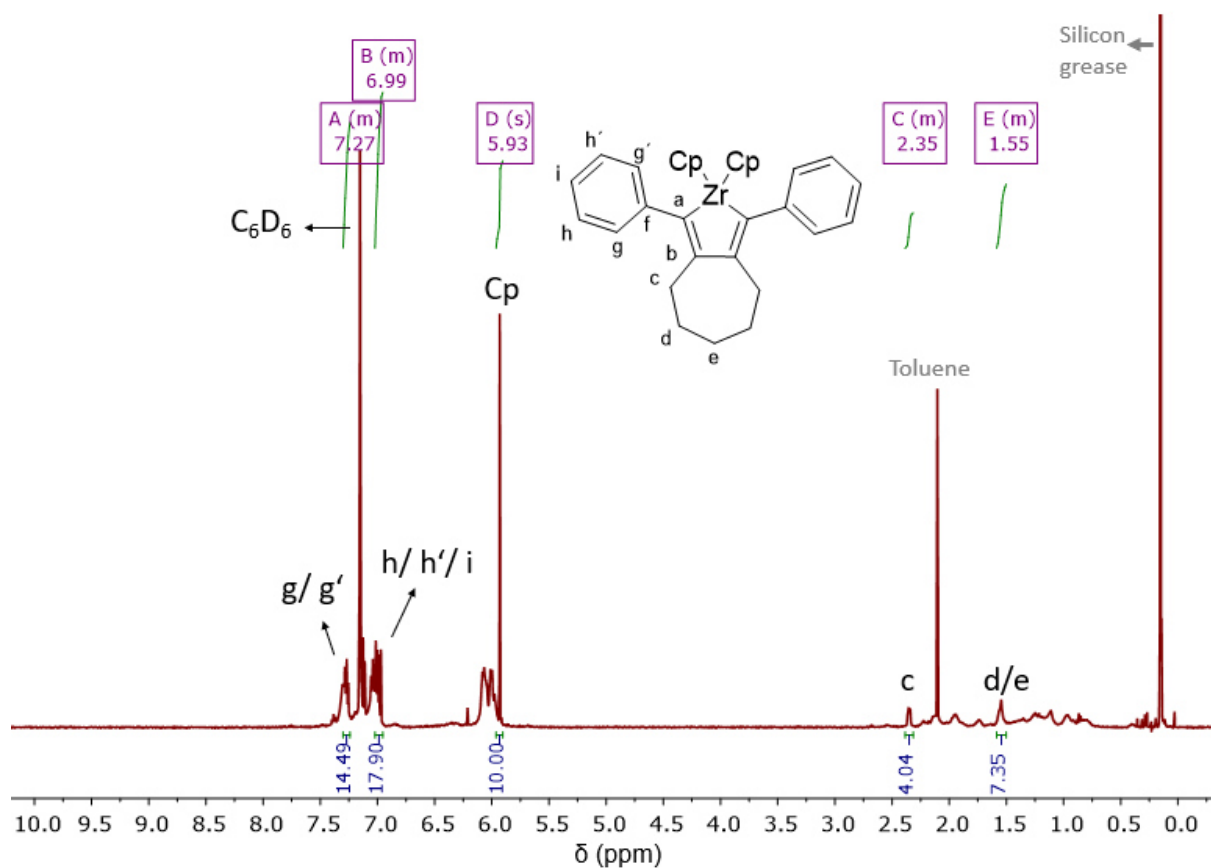


Figure S46. ^1H NMR (500 MHz) spectrum of zirconacyclopentadiene **11g** in C_6D_6 .

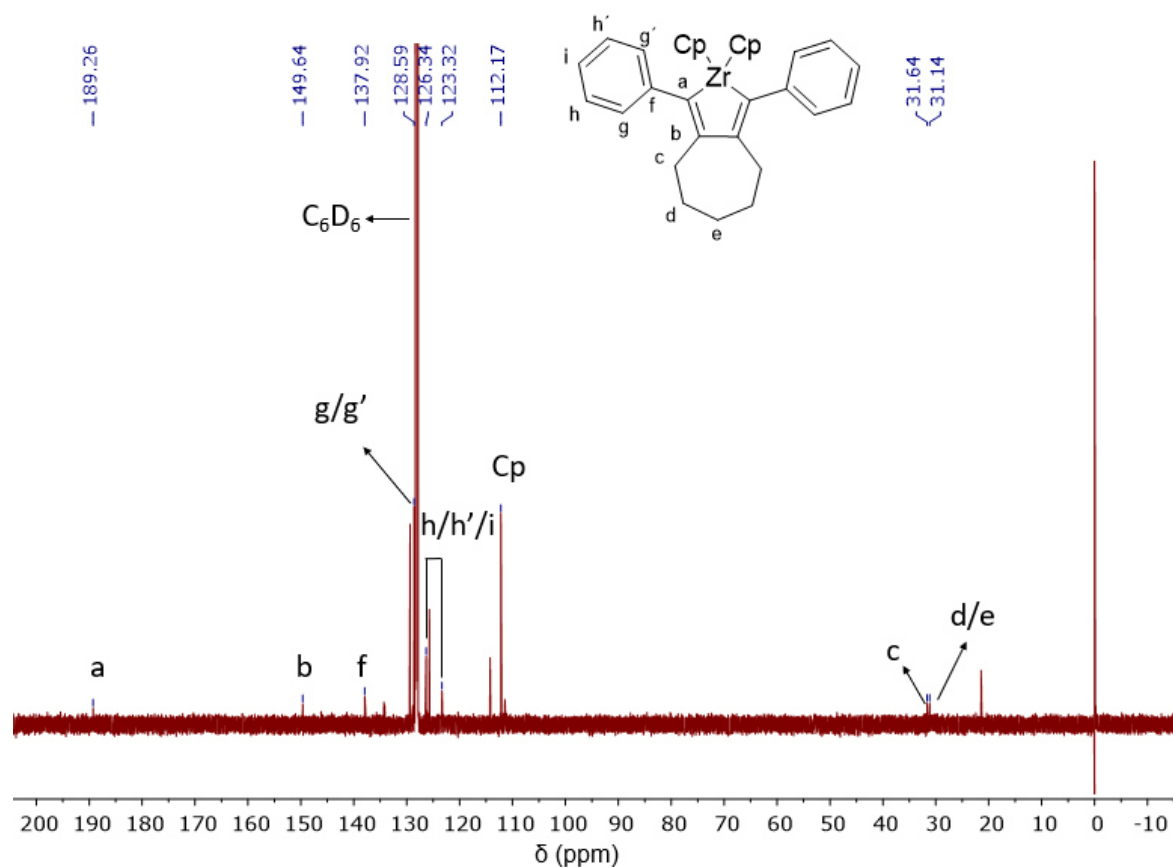


Figure S47. $^{13}\text{C}\{^1\text{H}\}$ NMR (126 MHz) spectrum of zirconacyclopentadiene **11g** in C_6D_6 .

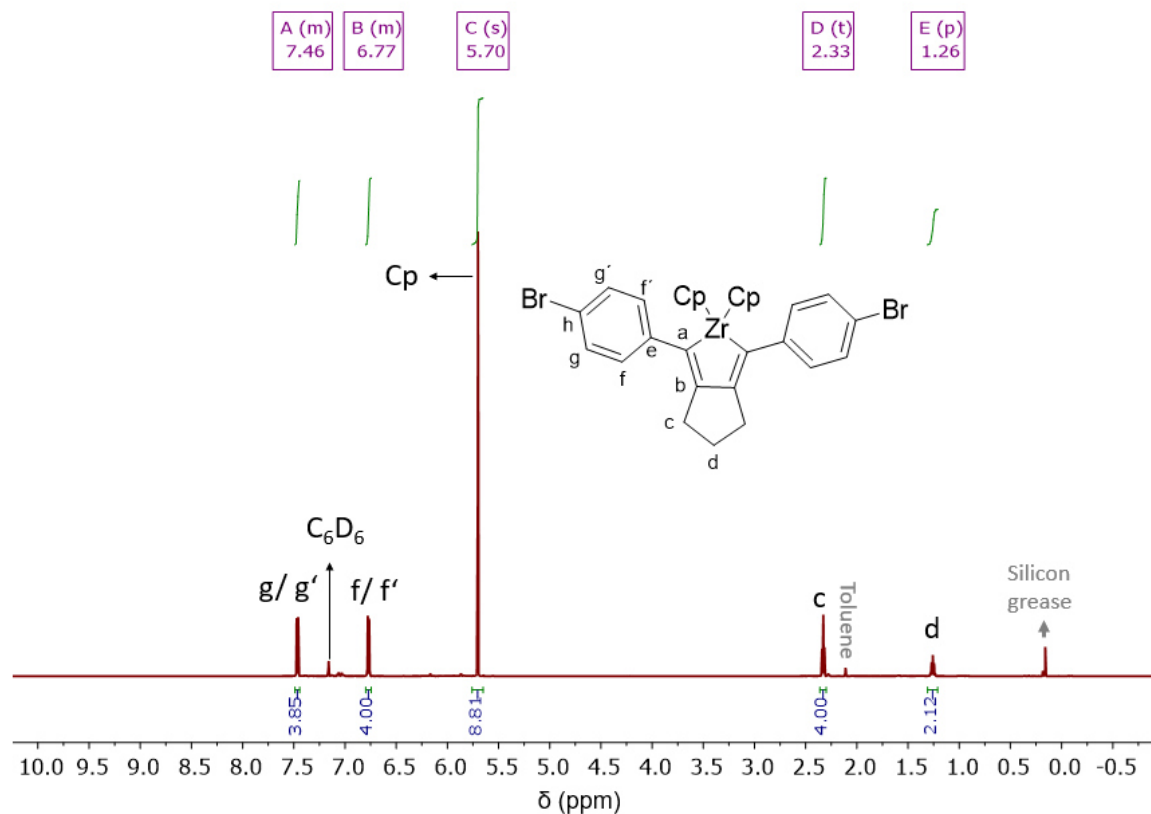


Figure S48. ^1H NMR (600 MHz) spectrum of zirconacyclopentadiene **11h** in C_6D_6 .

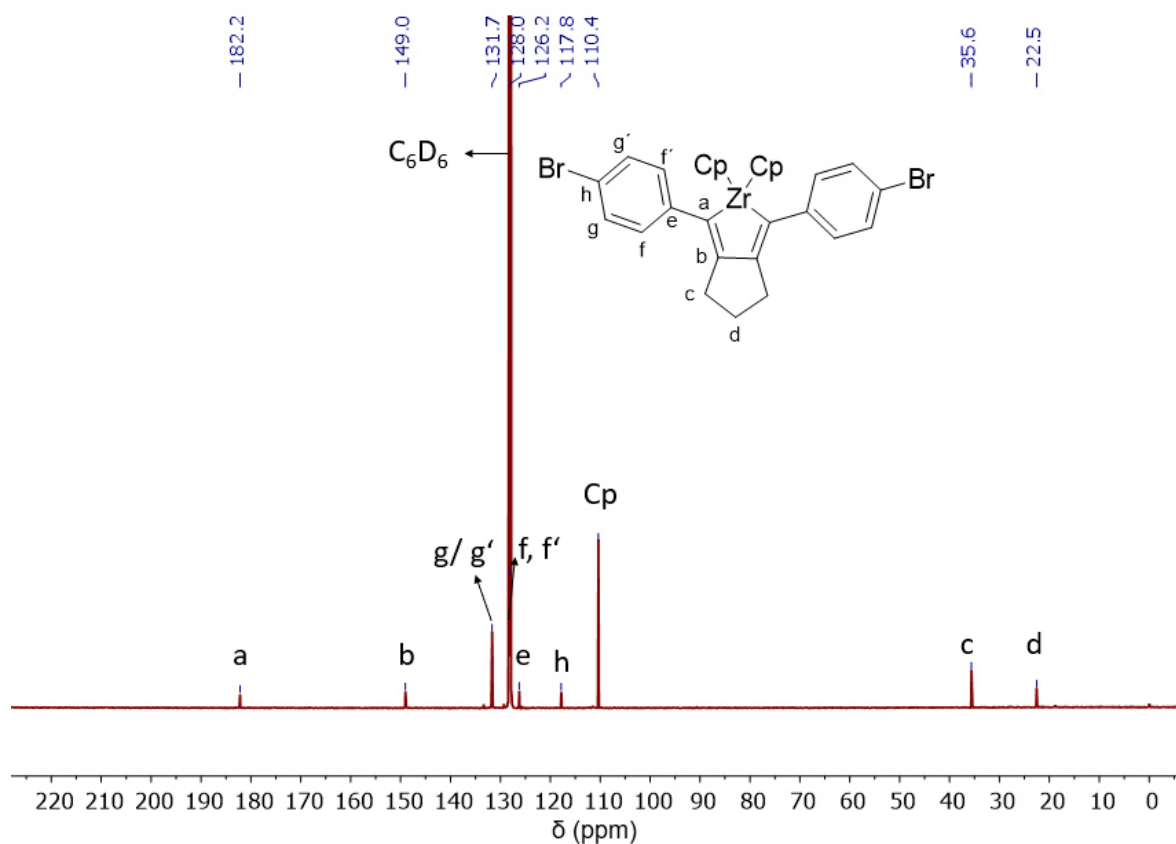


Figure S49. $^{13}\text{C}\{^1\text{H}\}$ NMR (151 MHz) spectrum of zirconacyclopentadiene **11h** in C_6D_6 .

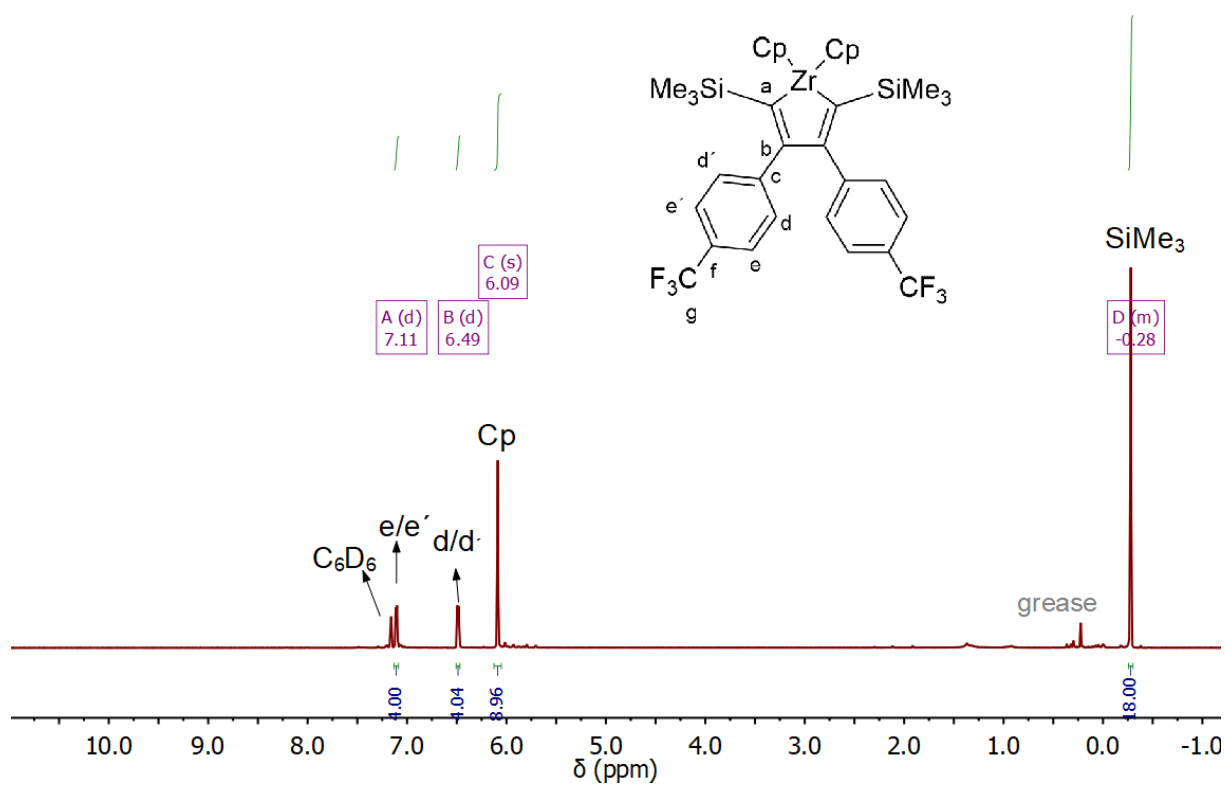


Figure S50. ^1H NMR (600 MHz) spectrum of zirconacyclopentadiene **11i** in C_6D_6 .

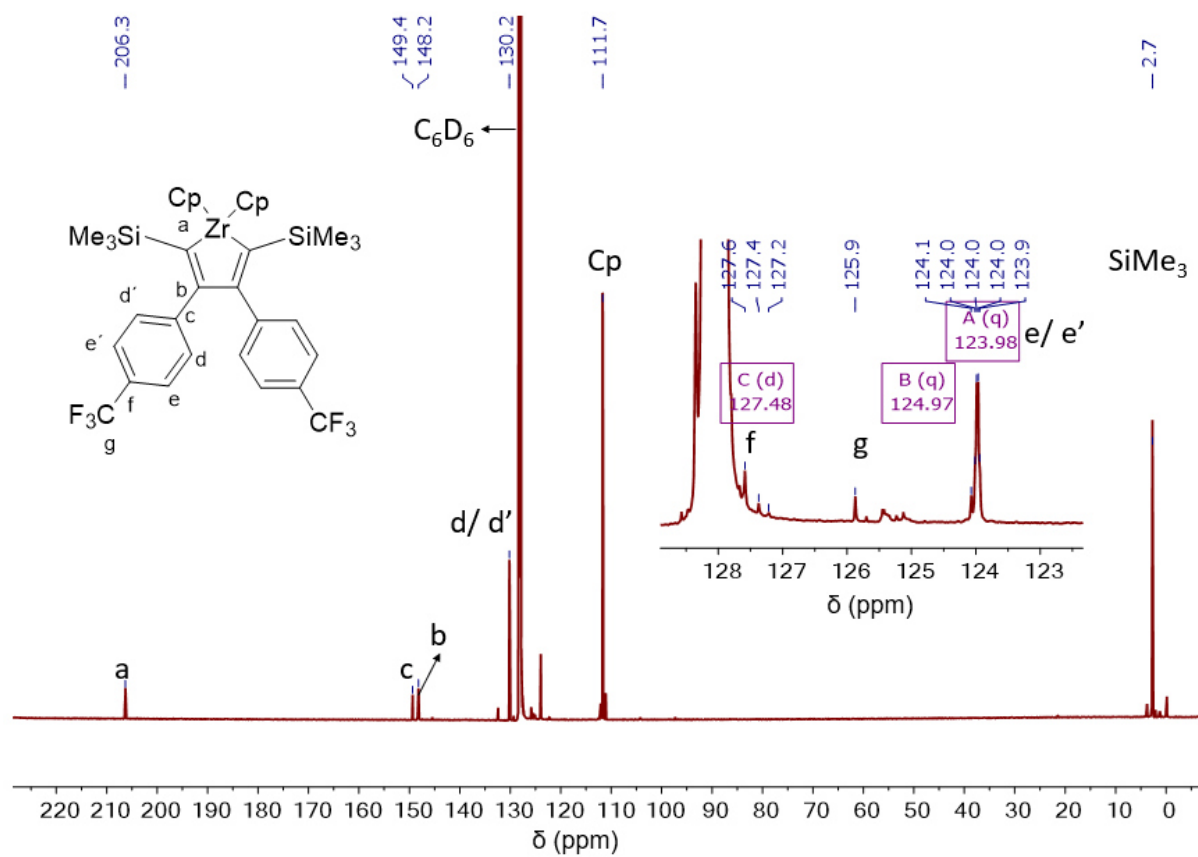


Figure S51. $^{13}\text{C}\{^1\text{H}\}$ NMR (151 MHz) spectrum of zirconacyclopentadiene **11i** in C_6D_6 .

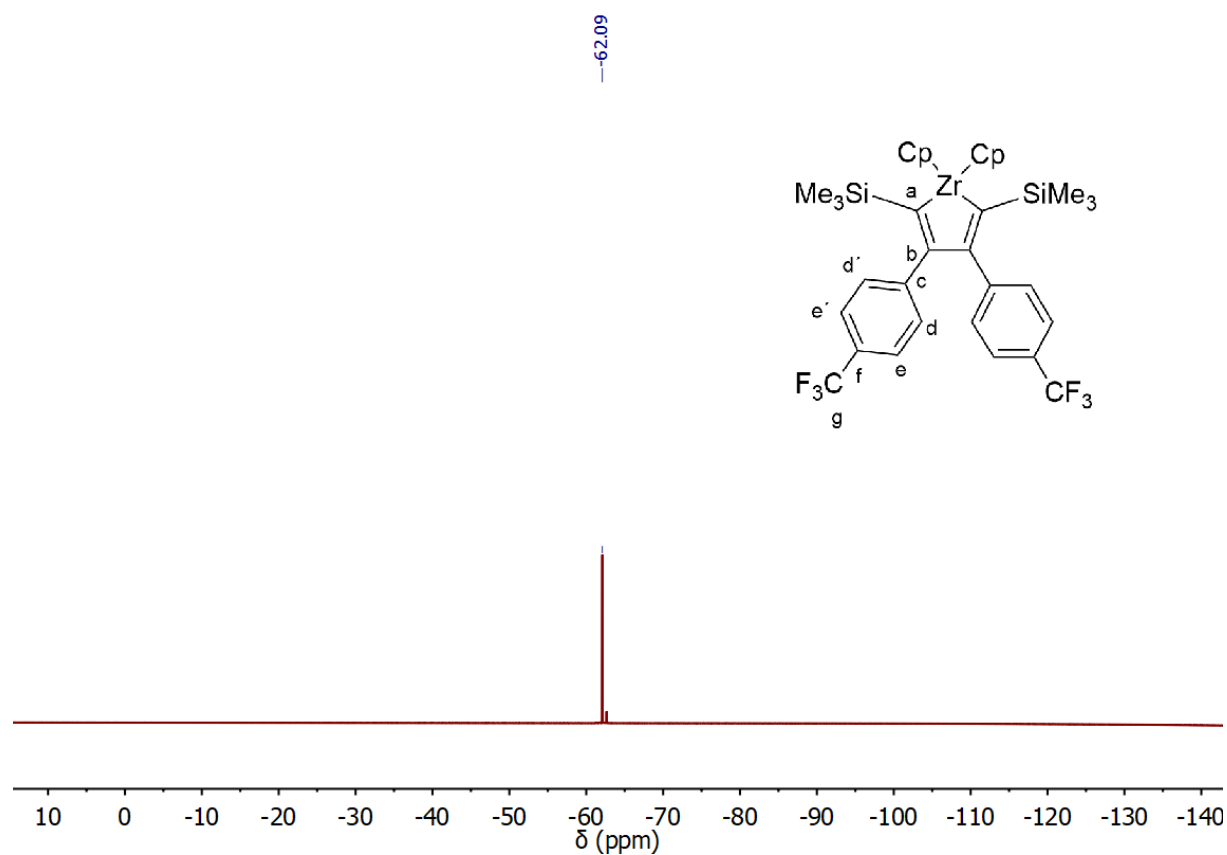


Figure S52. ^{19}F NMR (471 MHz) spectrum of zirconacyclopentadiene **11i** in C_6D_6 .

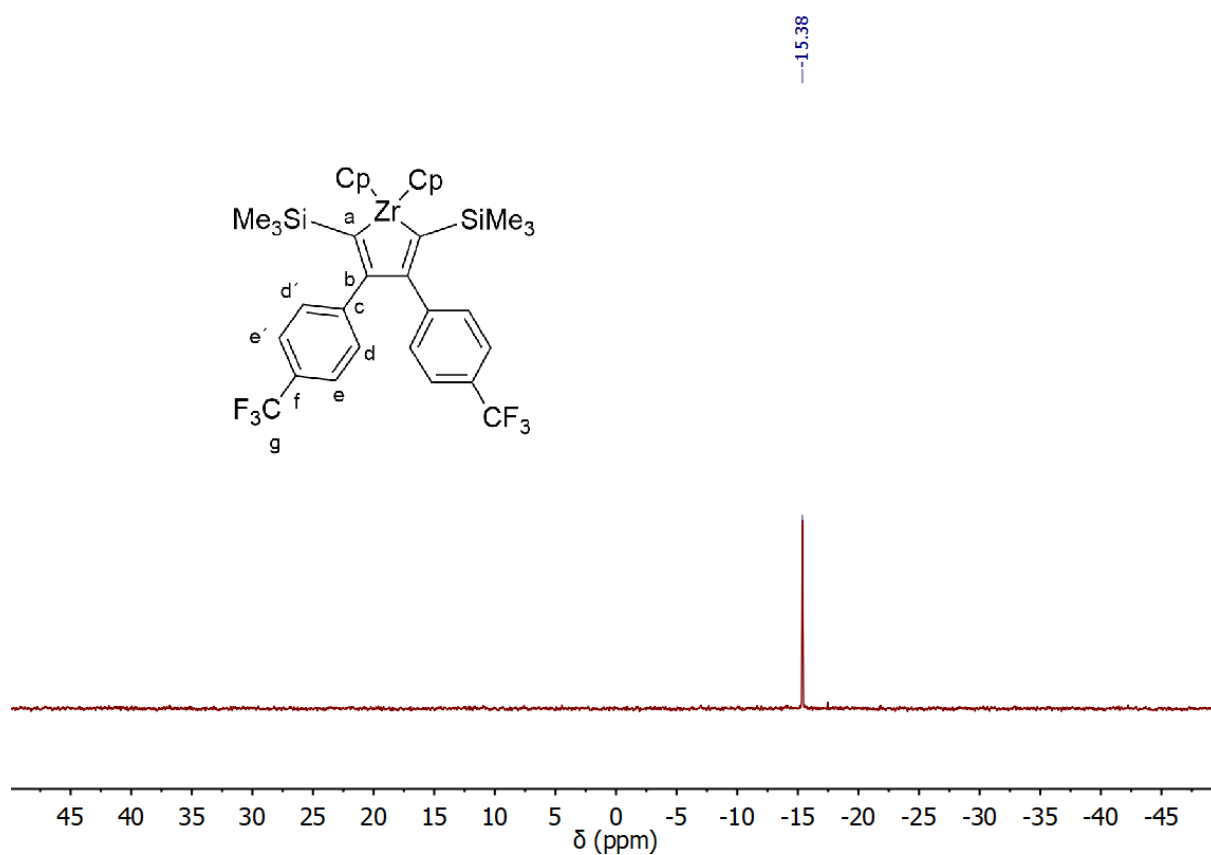


Figure S53. ²⁹Si{¹H} NMR (99 MHz) spectrum of zirconacyclopentadiene **11i** in C₆D₆.

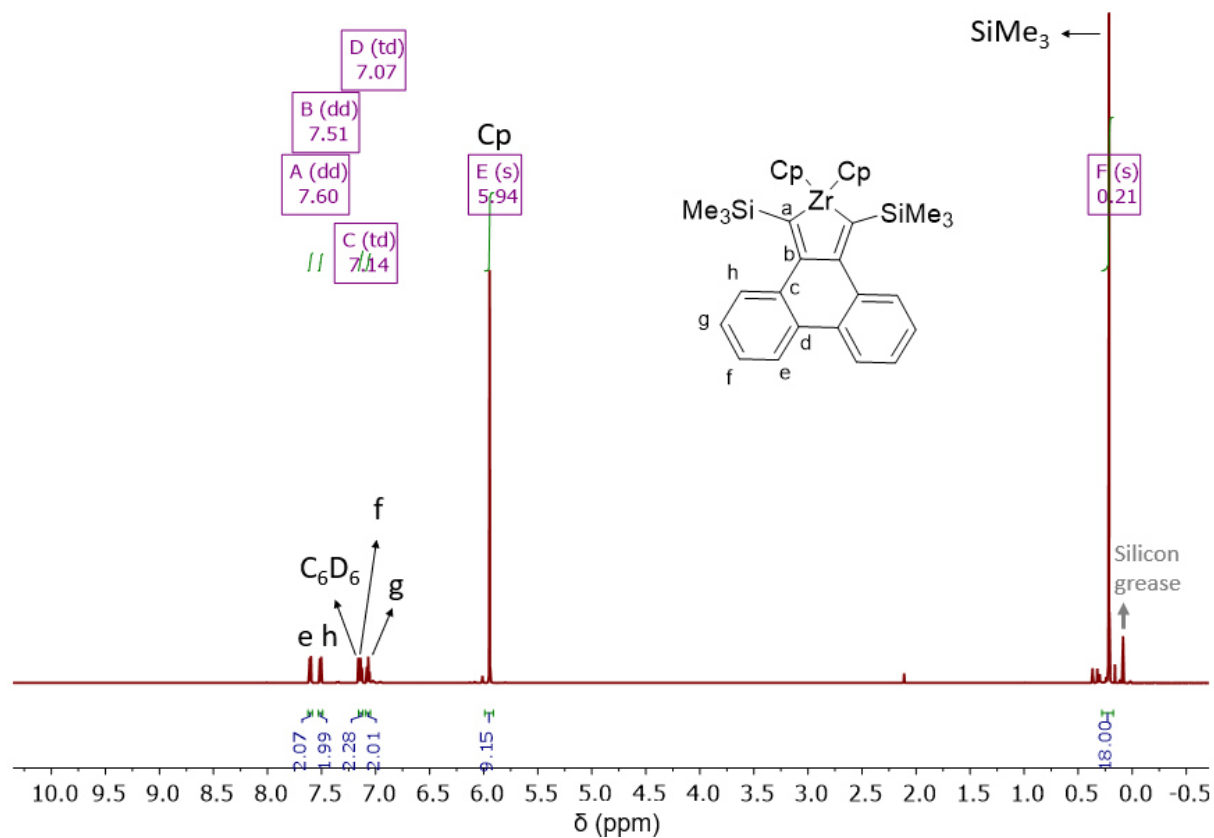


Figure S54. ¹H NMR (600 MHz) spectrum of zirconacyclopentadiene **11j** in C₆D₆.

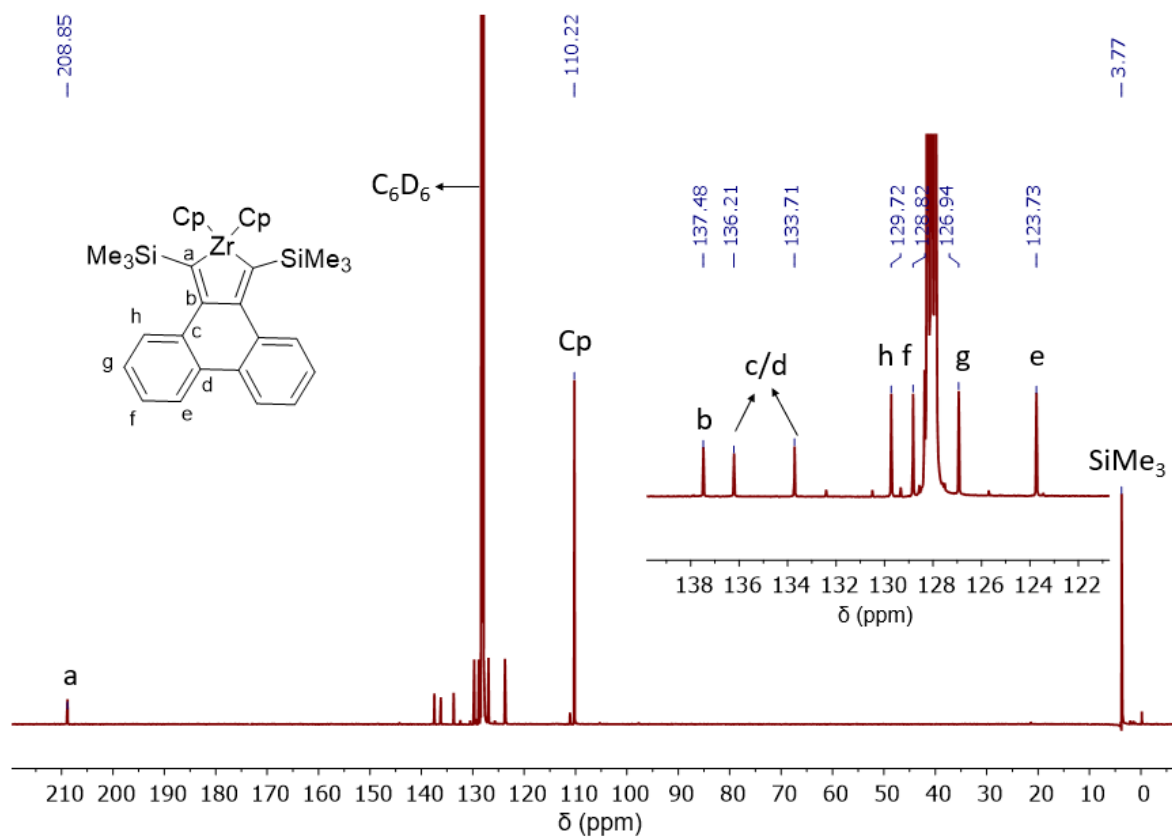


Figure S55. ^{13}C NMR (151 MHz) spectrum of zirconacyclopentadiene **11j** in C_6D_6 .

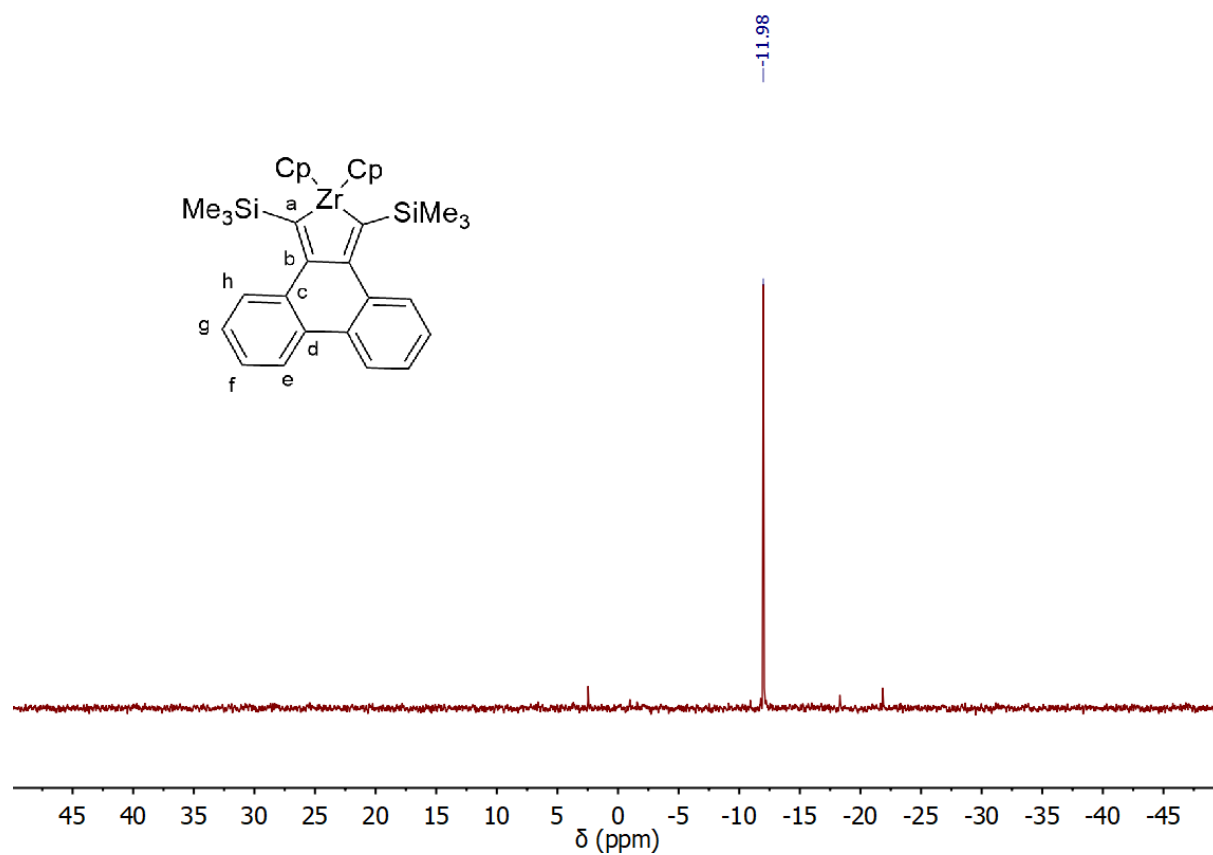


Figure S56. $^{29}\text{Si}\{^1\text{H}\}$ NMR (99 MHz) spectrum of zirconacyclopentadiene **11j** in C_6D_6 .

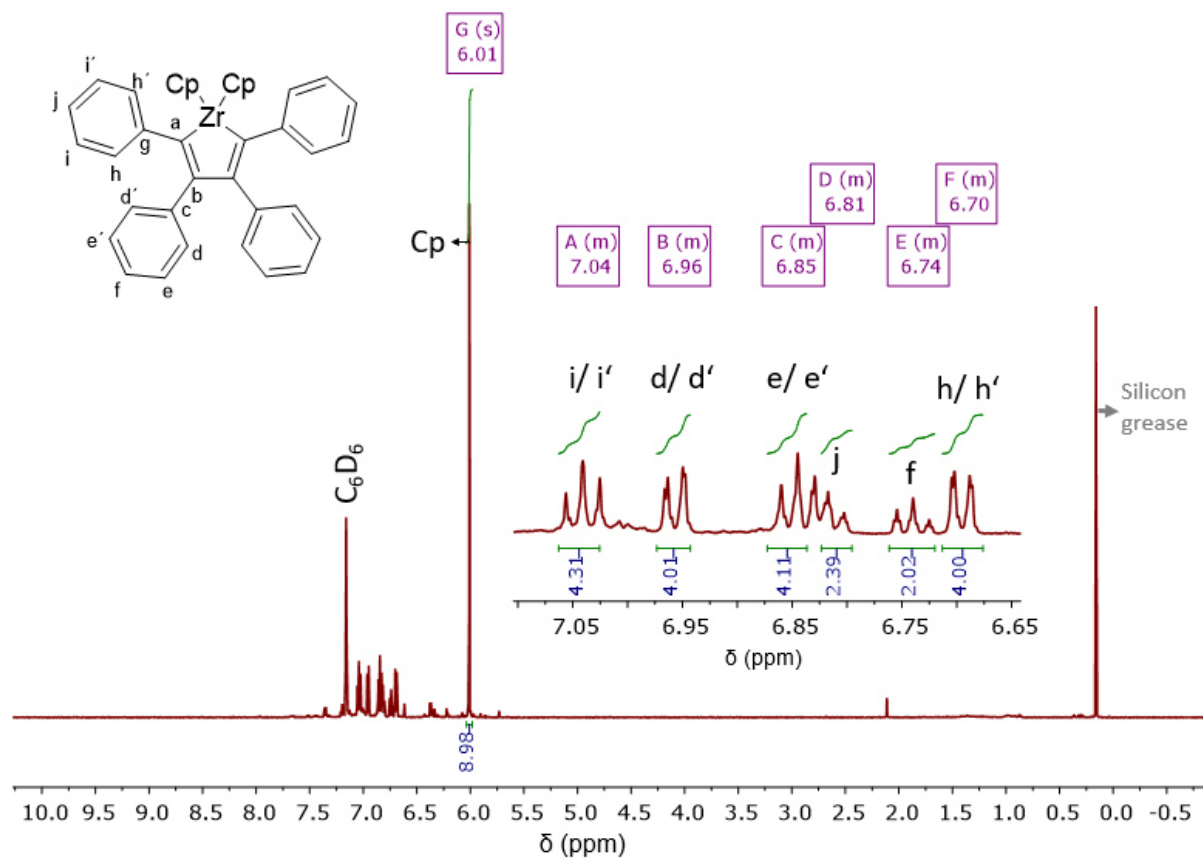


Figure S57. ^1H NMR (500 MHz) spectrum of zirconacyclopentadiene **11k** in C_6D_6 .

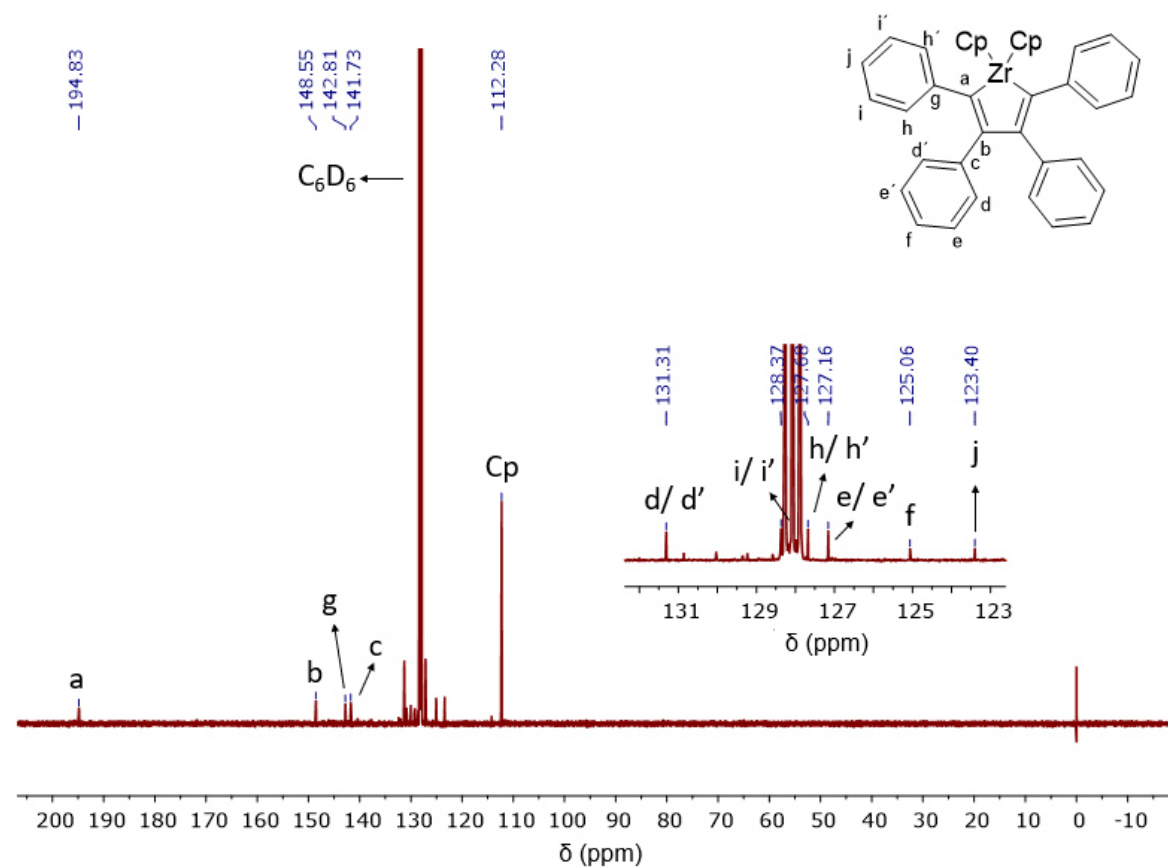


Figure S58. $^{13}\text{C}\{^1\text{H}\}$ NMR (126 MHz) spectrum of zirconacyclopentadiene **11k** in C_6D_6 .

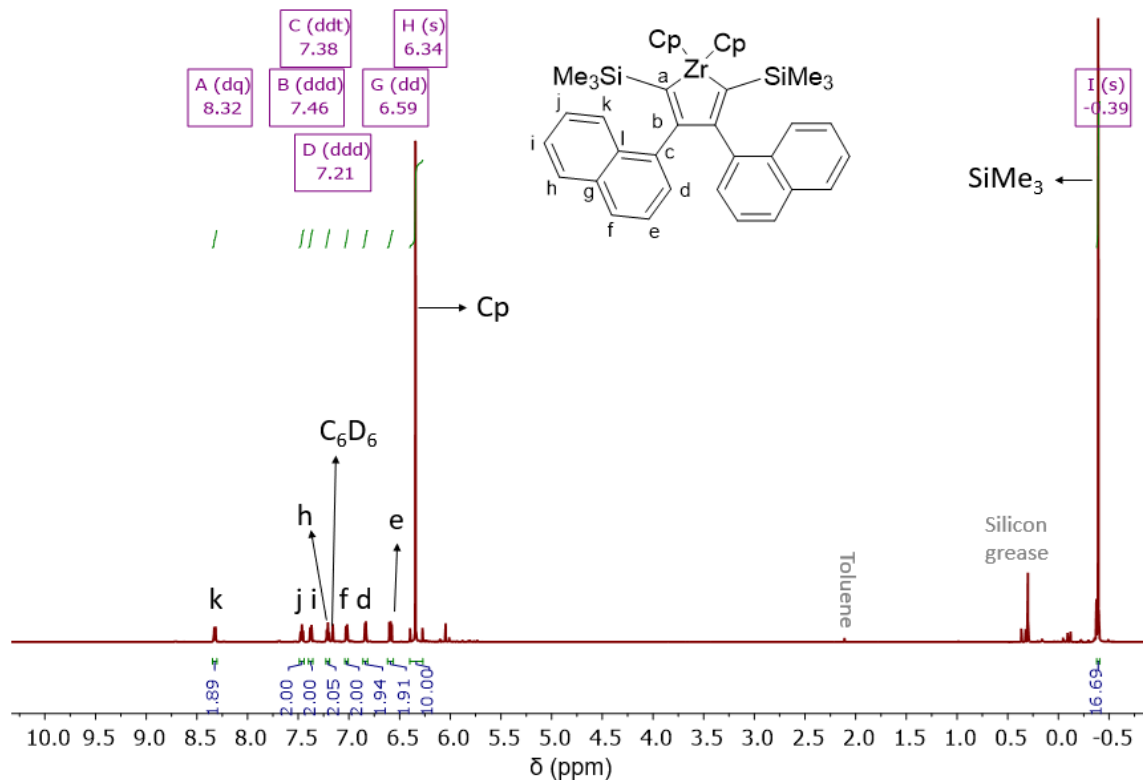


Figure S59. ^1H NMR (500 MHz) spectrum of zirconacyclopentadiene **11I** in C_6D_6 .

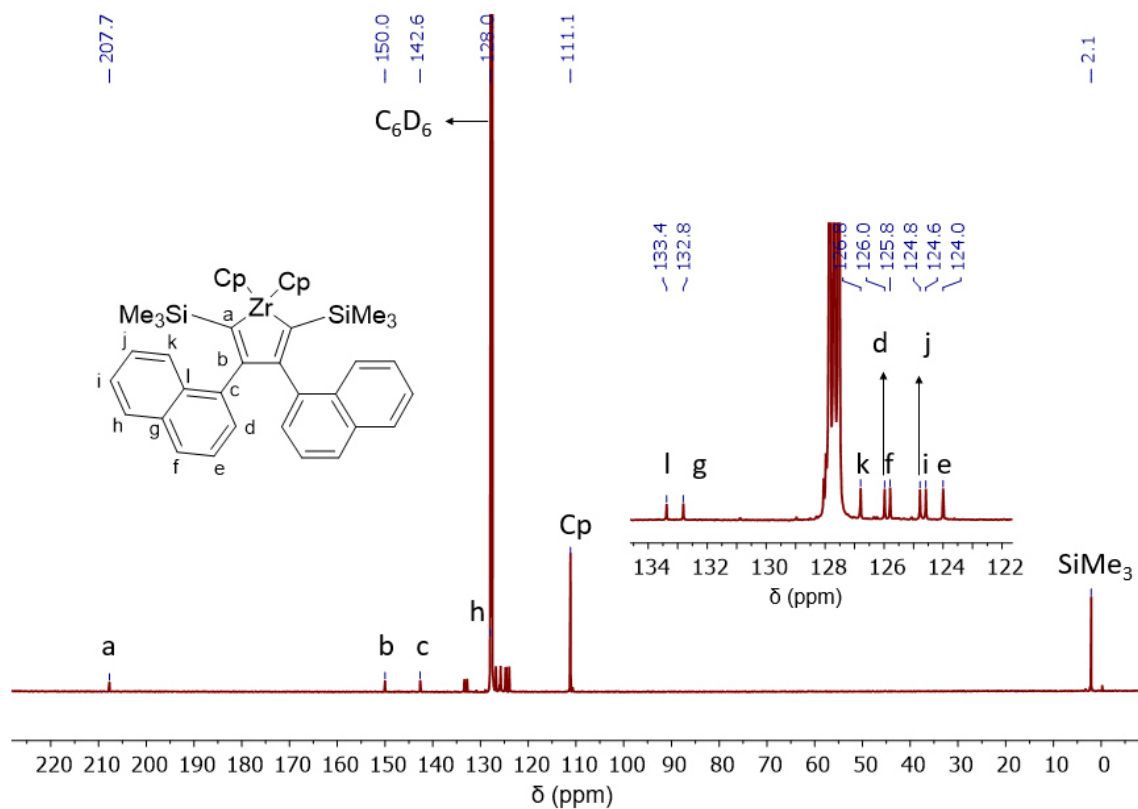


Figure S60. $^{13}\text{C}\{^1\text{H}\}$ NMR (126 MHz) spectrum of zirconacyclopentadiene **11I** in C_6D_6 .

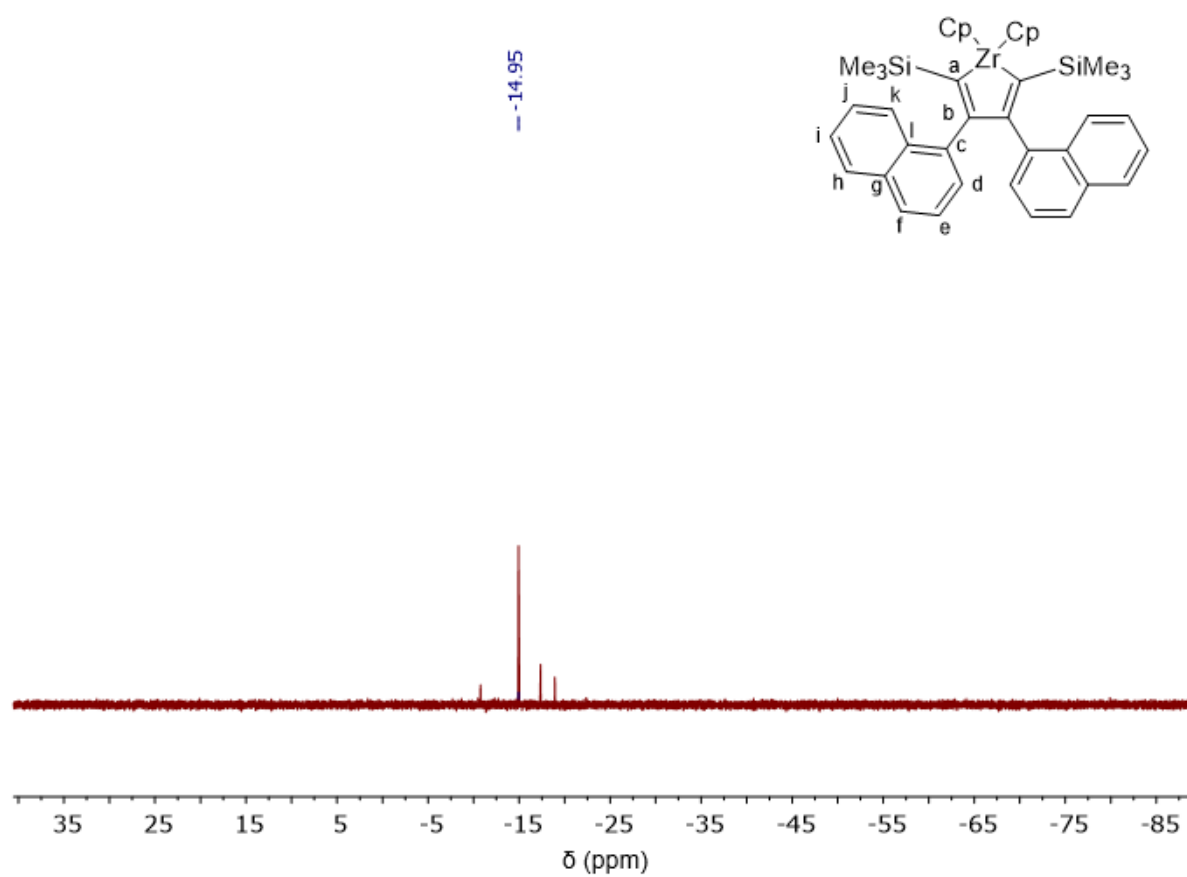


Figure S61. $^{29}\text{Si}\{^1\text{H}\}$ NMR (99 MHz) spectrum of zirconacyclopentadiene **11I** in C_6D_6 .

6.2 Reaction Monitoring Experiments

Negishi conditions

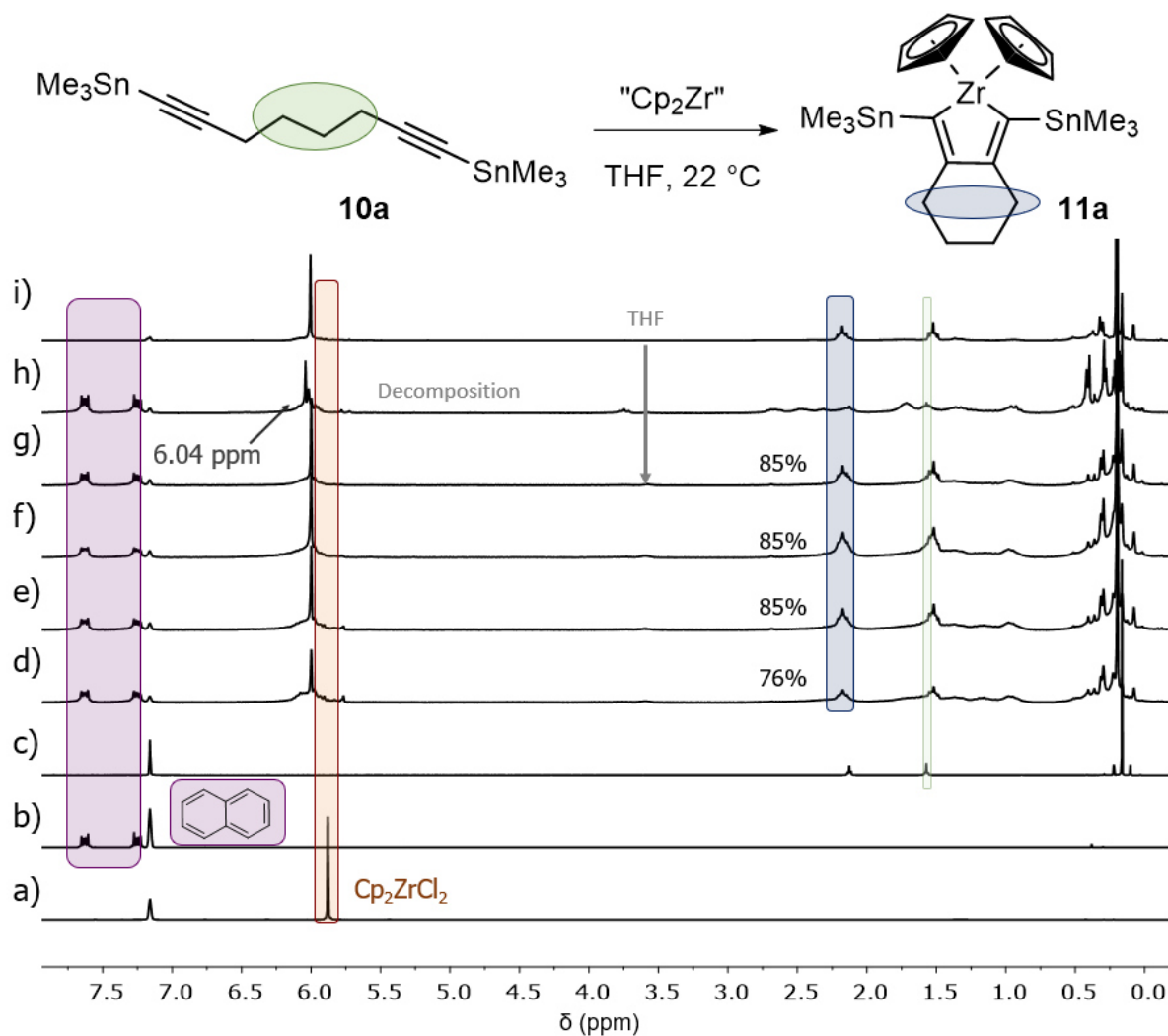


Figure S62. ¹H NMR spectra (recorded at 300 K, 200 MHz in C₆D₆) of the reaction monitoring for the synthesis of zirconacyclopentadiene **11a** using Negishi's reagent with naphthalene as standard (1 eq.). a) Starting material Cp₂ZrCl₂. b) Naphthalene. c) Starting material **10a**. Reaction monitoring after d) 10 min. e) 30 min. f) 1 h. g) 3 h and h) 22 h. i) zirconacyclopentadiene **11a** that had been previously isolated.

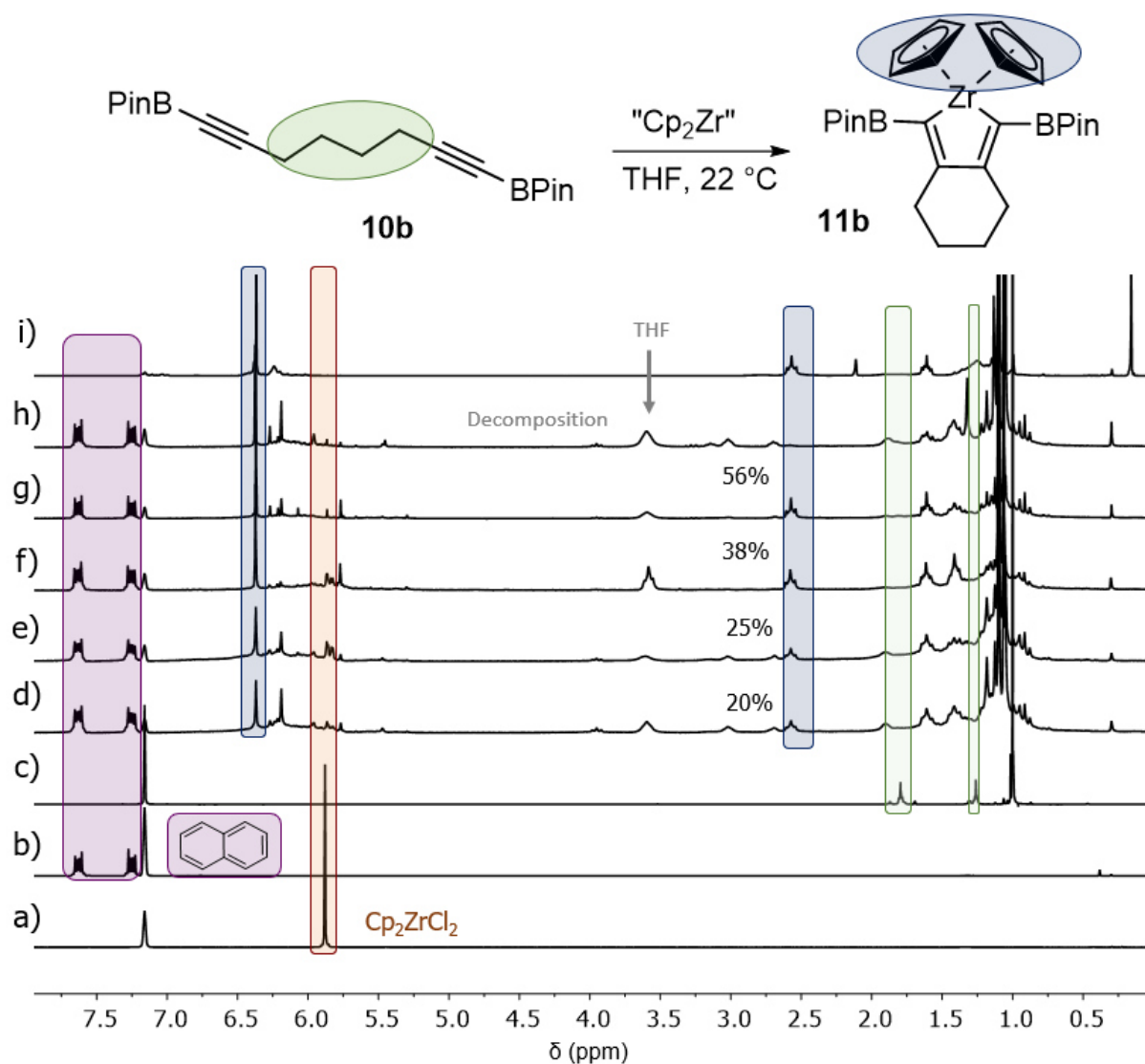


Figure S63. ¹H NMR spectra (recorded at 300 K, 200 MHz in C₆D₆) of the reaction monitoring for the synthesis of zirconacyclopentadiene **11b** using Negishi's reagent with naphthalene as standard (1 eq.). a) Starting material Cp₂ZrCl₂. b) Naphthalene. c) Starting material **10b**. Reaction monitoring after d) 10 min. e) 30 min. f) 1 h. g) 3 h and h) 22 h. i) zirconacyclopentadiene **11b** that had been previously isolated.

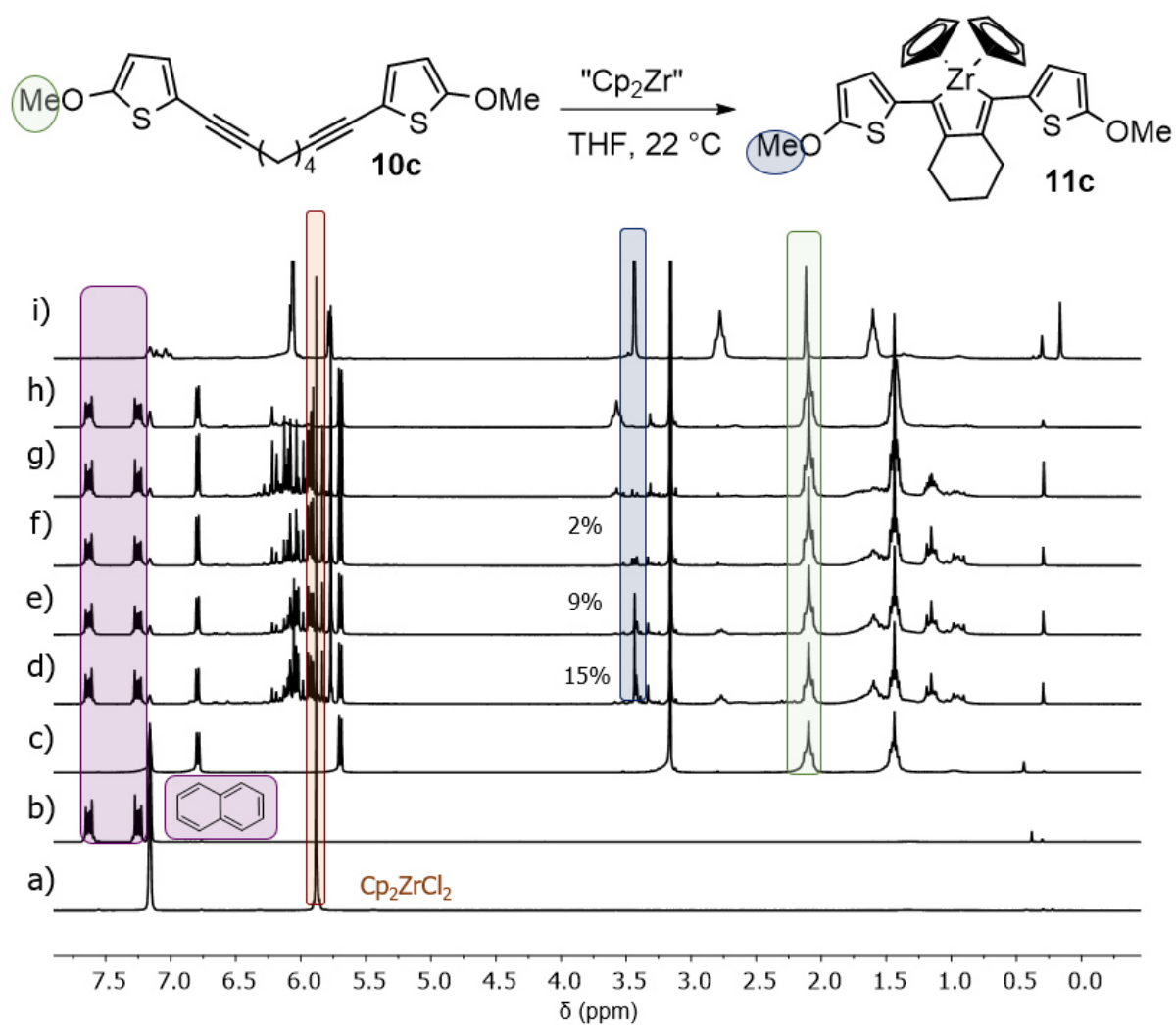


Figure S64. ¹H NMR spectra (recorded at 300 K, 200 MHz in C₆D₆) of the reaction monitoring for the synthesis of zirconacyclopentadiene **11c** using Negishi's reagent with naphthalene as standard (1 eq.). a) Starting material Cp₂ZrCl₂. b) Naphthalene. c) Starting material **10c**. Reaction monitoring after d) 10 min. e) 30 min. f) 1 h. g) 3 h and h) 22 h. i) zirconacyclopentadiene **11c** that had been previously isolated.

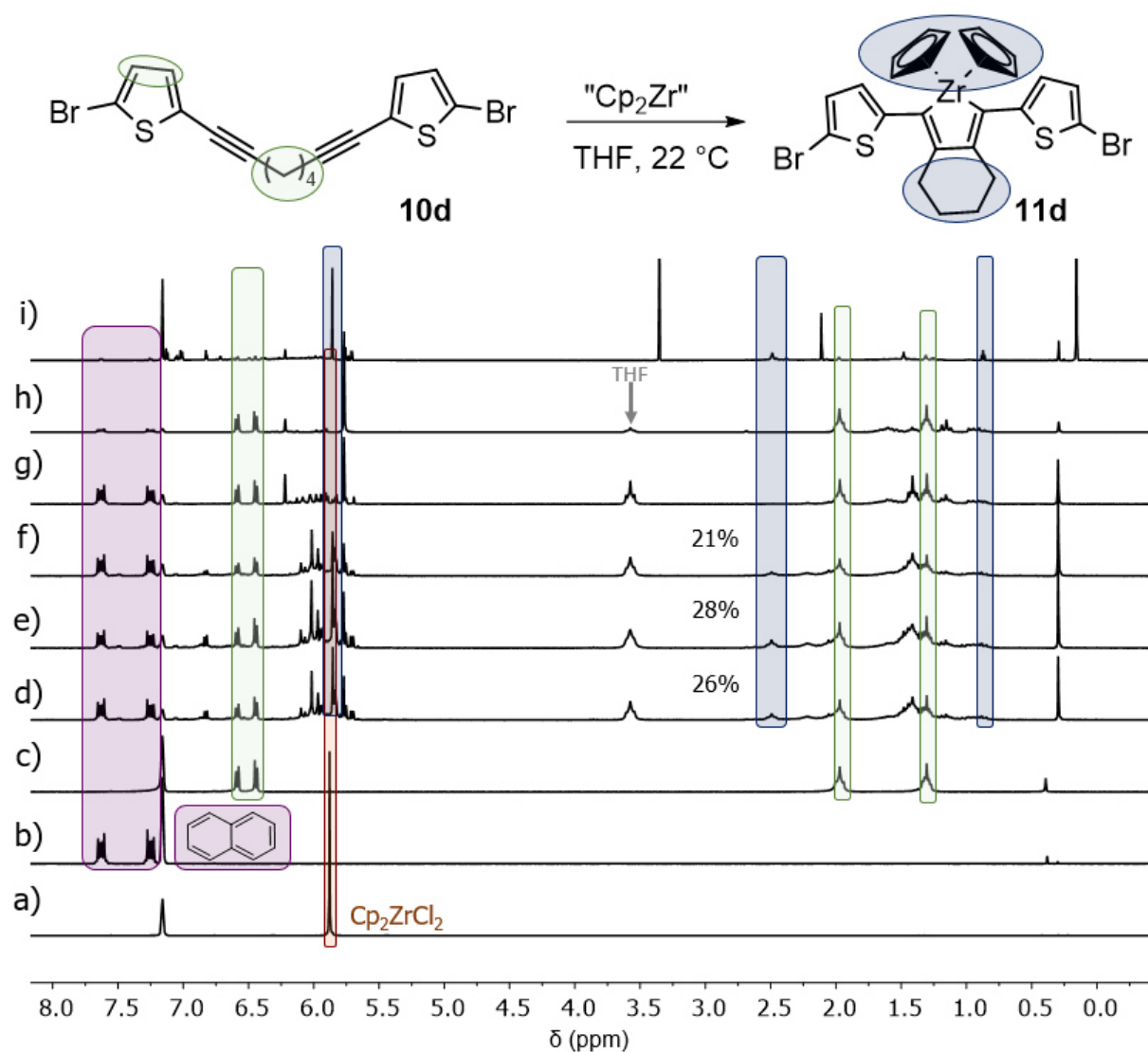


Figure S65. ¹H NMR spectra (recorded at 300 K, 200 MHz in C₆D₆) of the reaction monitoring for the synthesis of zirconacyclopentadiene **11d** using Negishi's reagent with naphthalene as standard (1 eq.). a) Starting material Cp₂ZrCl₂. b) Naphthalene. c) Starting material **10d**. Reaction monitoring after d) 10 min. e) 30 min. f) 1 h. g) 3 h and h) 22 h. i) zirconacyclopentadiene **11d** that had been previously isolated.

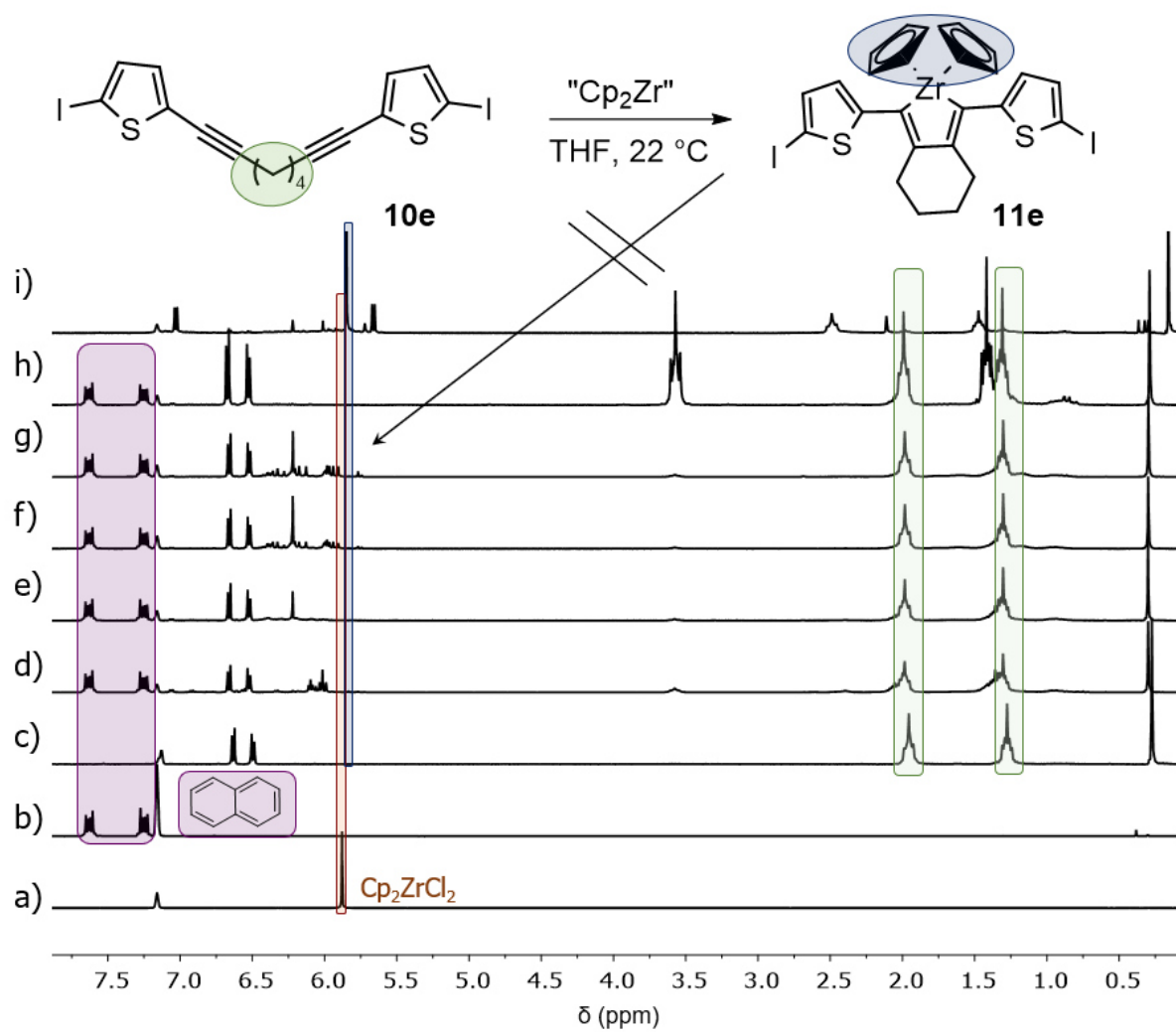


Figure S66. ^1H NMR spectra (recorded at 300 K, 200 MHz in C_6D_6) of the reaction monitoring for the synthesis of zirconacyclopentadiene **11e** using Negishi's reagent with naphthalene as standard (1 eq.). a) Starting material Cp_2ZrCl_2 . b) Naphthalene. c) Starting material **10e**. Reaction monitoring after d) 10 min. e) 30 min. f) 1 h. g) 3 h and h) 22 h. i) zirconacyclopentadiene **11e** that had been previously isolated.

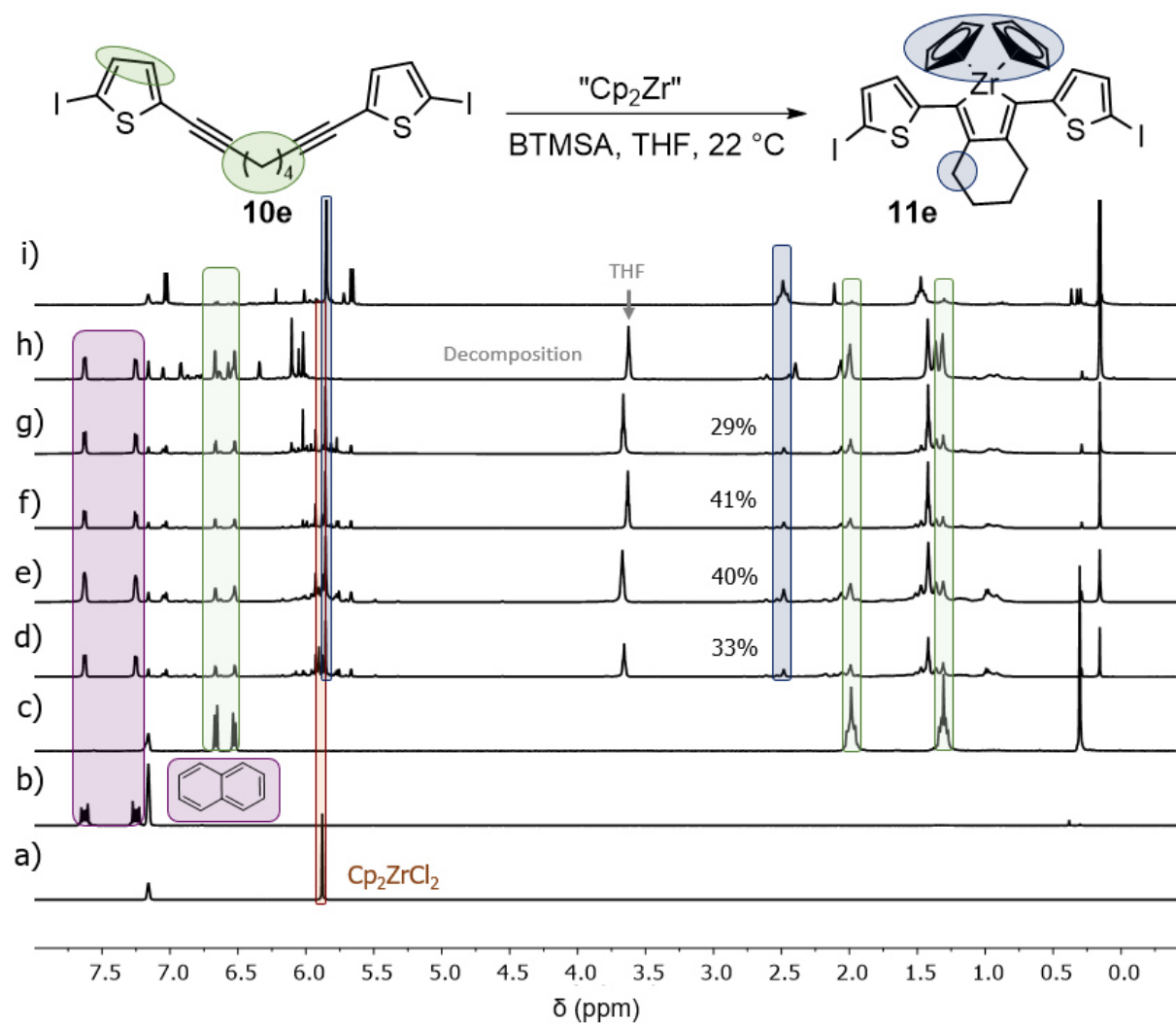


Figure S67. ¹H NMR spectra (recorded at 300 K, 600 MHz in C₆D₆) of the reaction monitoring for the synthesis of zirconacyclopentadiene **11e** using Negishi's reagent and BTMSA as ligand with naphthalene as standard (1 eq.). a) Starting material Cp₂ZrCl₂. b) Naphthalene. c) Starting material **10e**. Reaction monitoring after d) 10 min. e) 30 min. f) 1 h. g) 3 h and h) 22 h. i) zirconacyclopentadiene **11e** that had been previously isolated.

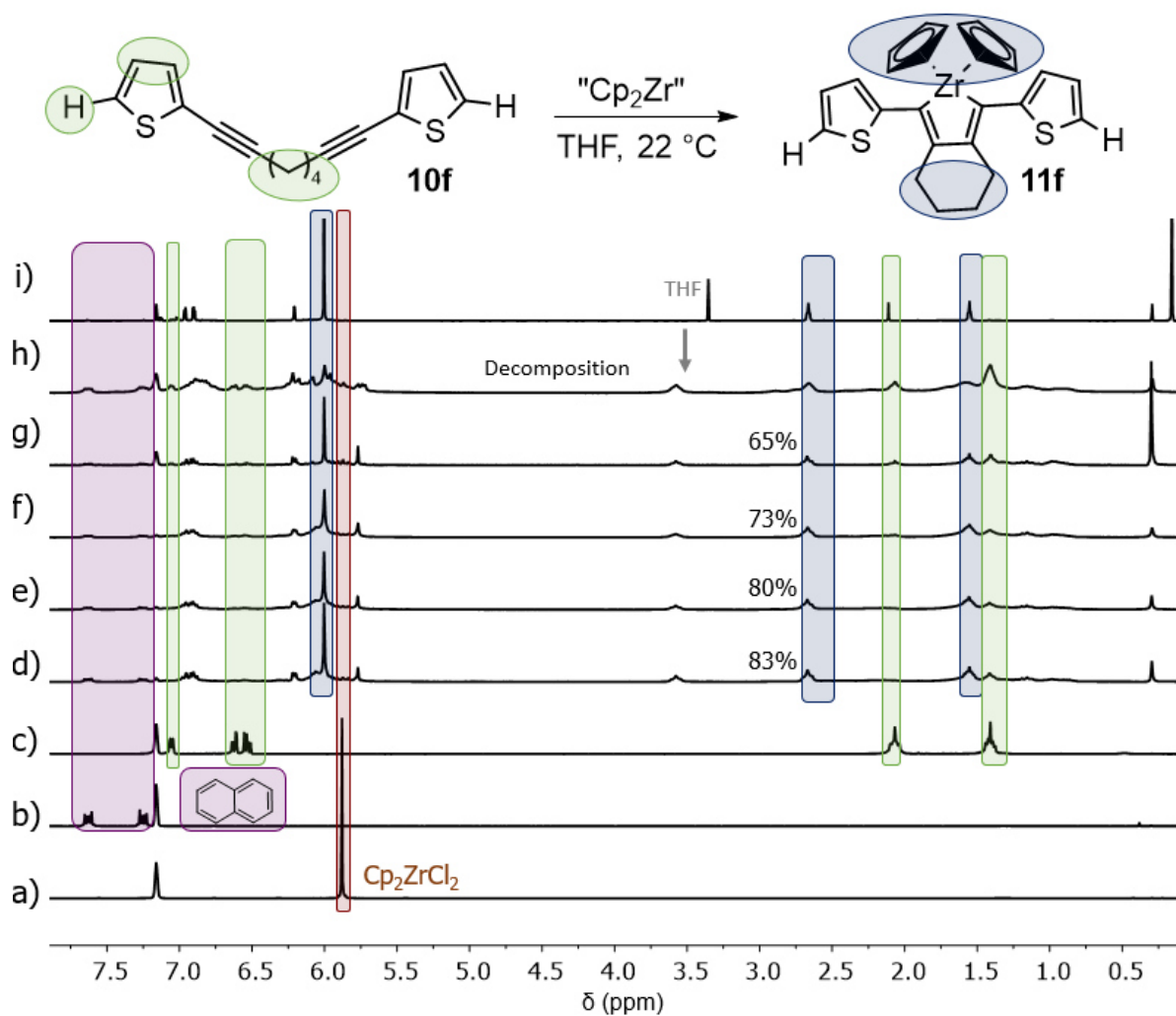


Figure S68. ¹H NMR spectra (recorded at 300 K, 200 MHz in C₆D₆) of the reaction monitoring for the synthesis of zirconacyclopentadiene **11f** using Negishi's reagent with naphthalene as standard (1 eq.). a) Starting material Cp₂ZrCl₂. b) Naphthalene. c) Starting material **10f**. Reaction monitoring after d) 10 min. e) 30 min. f) 1 h. g) 3 h and h) 22 h. i) zirconacyclopentadiene **11f** that had been previously isolated.

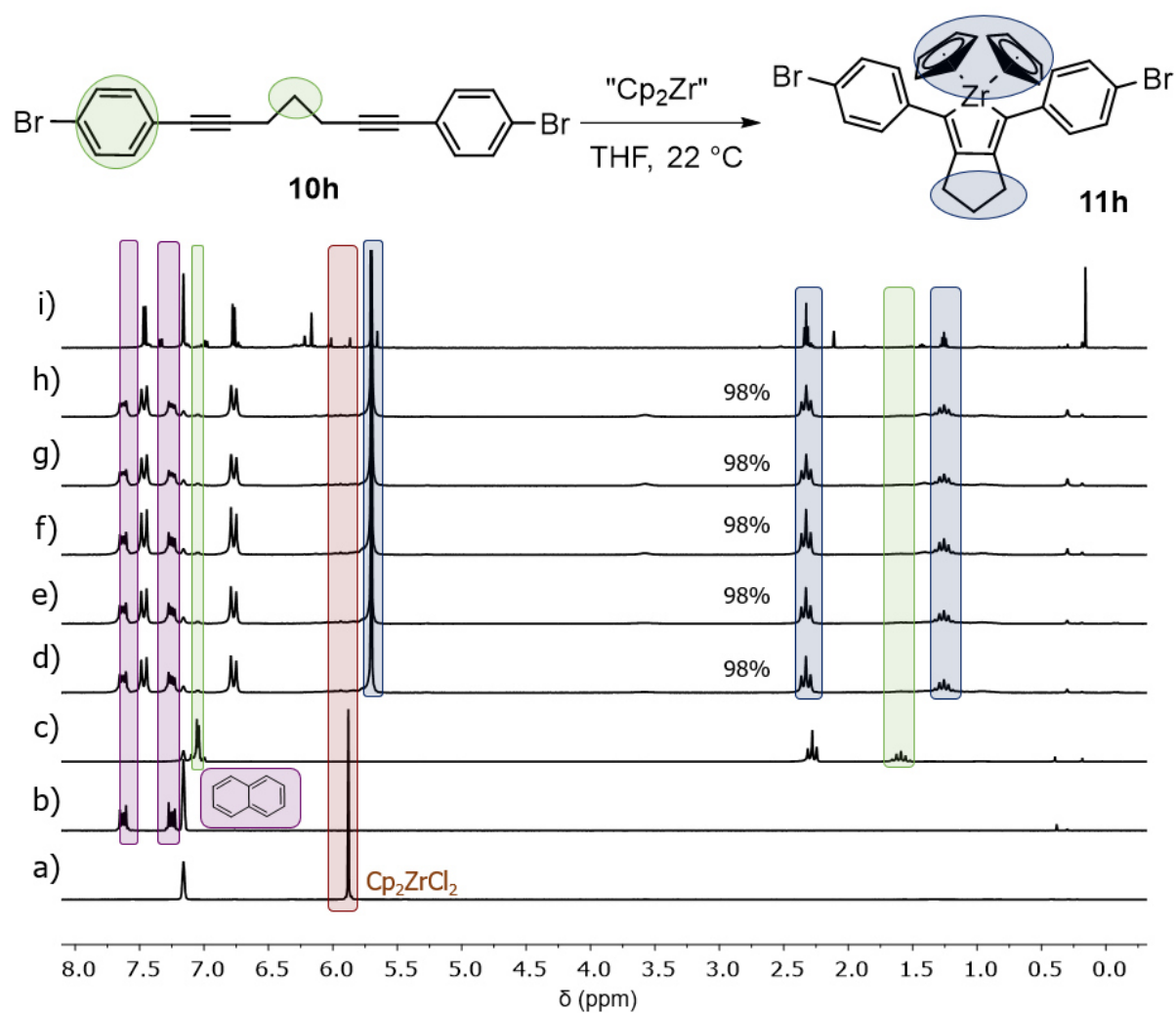


Figure S69. ¹H NMR spectra (recorded at 300 K, 200 MHz in C₆D₆) of the reaction monitoring for the synthesis of zirconacyclopentadiene **11h** using Negishi's reagent with naphthalene as standard (1 eq.). a) Starting material Cp₂ZrCl₂. b) Naphthalene. c) Starting material **10h**. Reaction monitoring after d) 10 min. e) 30 min. f) 1 h. g) 3 h and h) 22 h. i) zirconacyclopentadiene **11h** that had been previously isolated.

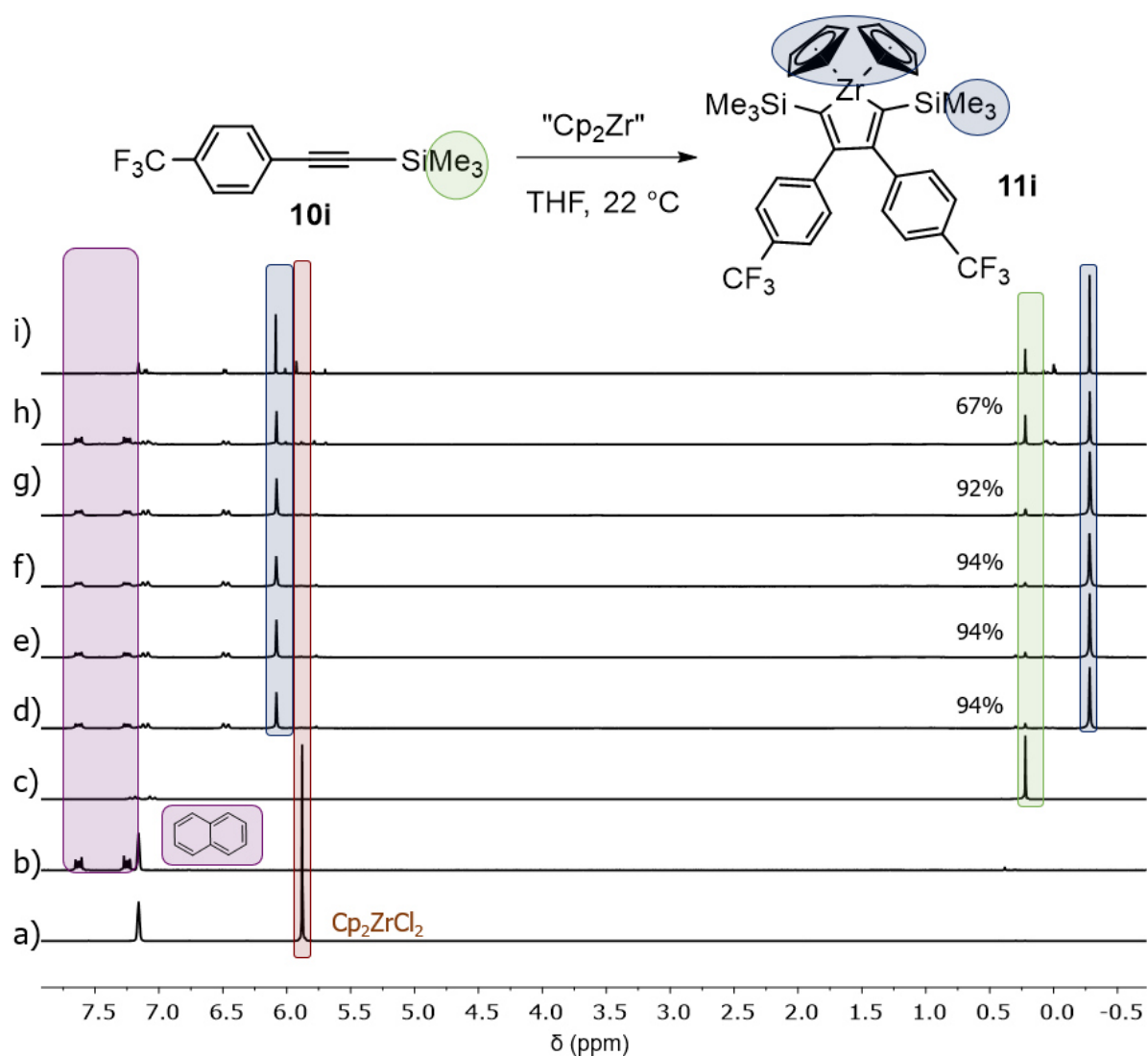


Figure S70. ¹H NMR spectra (recorded at 300 K, 200 MHz in C₆D₆) of the reaction monitoring for the synthesis of zirconacyclopentadiene **11i** using Negishi's reagent with naphthalene as standard (1 eq.). a) Starting material Cp₂ZrCl₂. b) Naphthalene. c) Starting material **10i**. Reaction monitoring after d) 10 min. e) 30 min. f) 1 h. g) 3 h and h) 22 h. i) zirconacyclopentadiene **11i** that had been previously isolated.

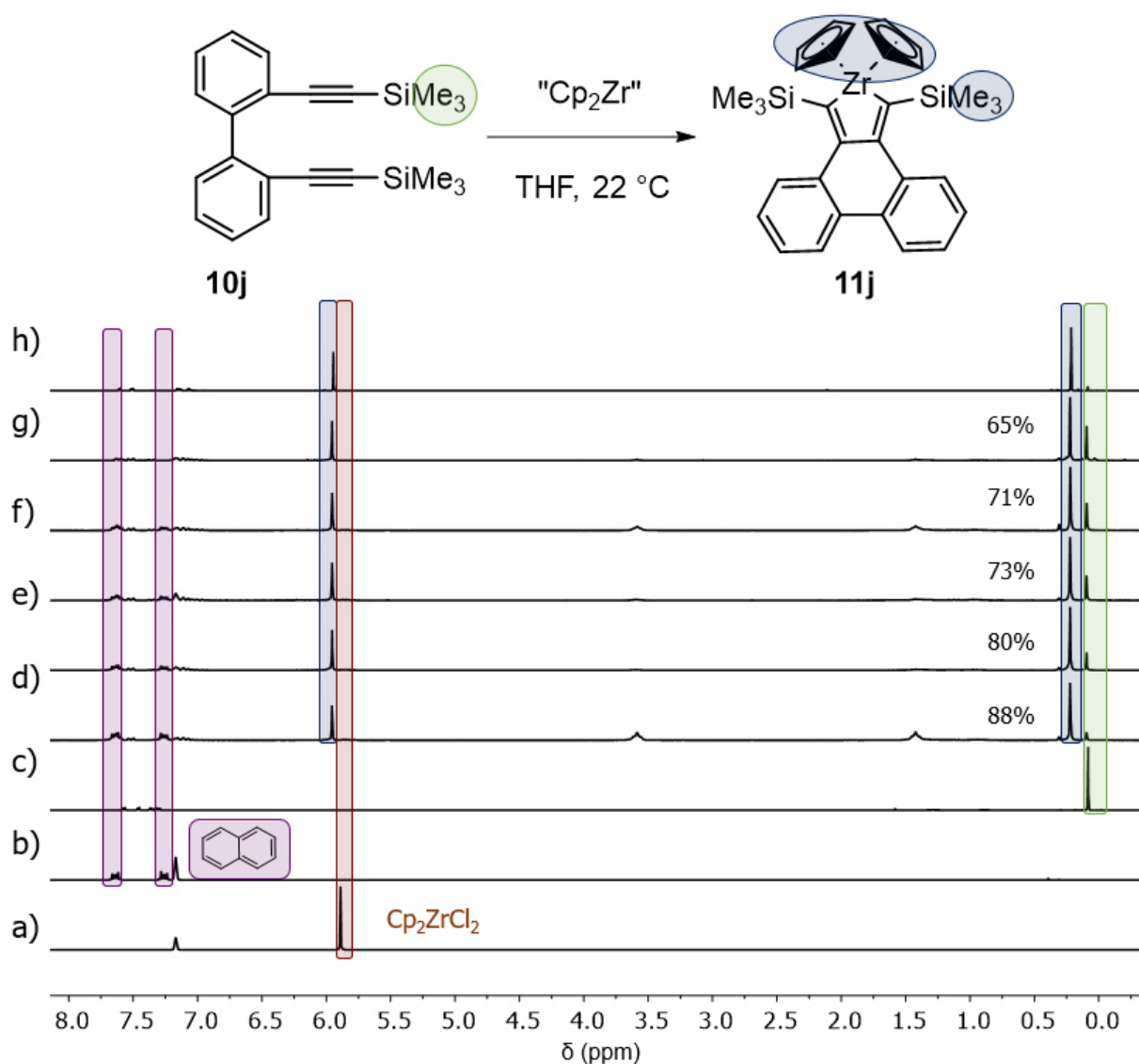


Figure S71. ¹H NMR spectra (recorded at 300 K, 200 MHz in C₆D₆) of the reaction monitoring for the synthesis of zirconacyclopentadiene **11j** using Negishi's reagent with naphthalene as standard (1 eq.). a) Starting material Cp₂ZrCl₂. b) Naphthalene. c) Starting material **10j**. Reaction monitoring after d) 10 min. e) 30 min. f) 1 h. g) 3 h and h) 22 h. i) zirconacyclopentadiene **11j** that had been previously isolated.

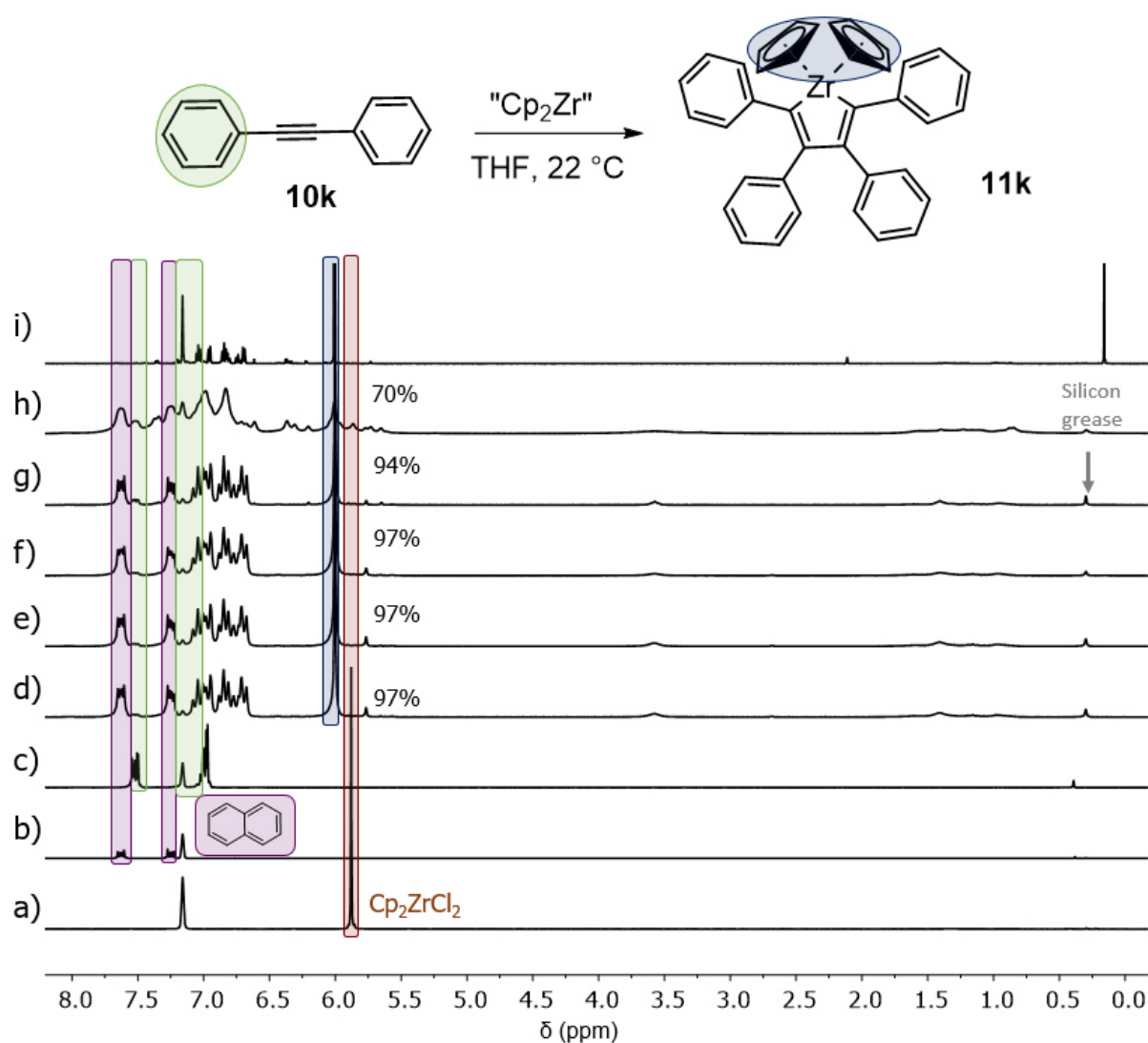


Figure S72. ¹H NMR spectra (recorded at 300 K, 200 MHz in C₆D₆) of the reaction monitoring for the synthesis of zirconacyclopentadiene **11k** using Negishi's reagent with naphthalene as standard (1 eq.). a) Starting material Cp₂ZrCl₂. b) Naphthalene. c) Starting material **10k**. Reaction monitoring after d) 10 min. e) 30 min. f) 1 h. g) 3 h and h) 22 h. i) zirconacyclopentadiene **11k** that had been previously isolated.

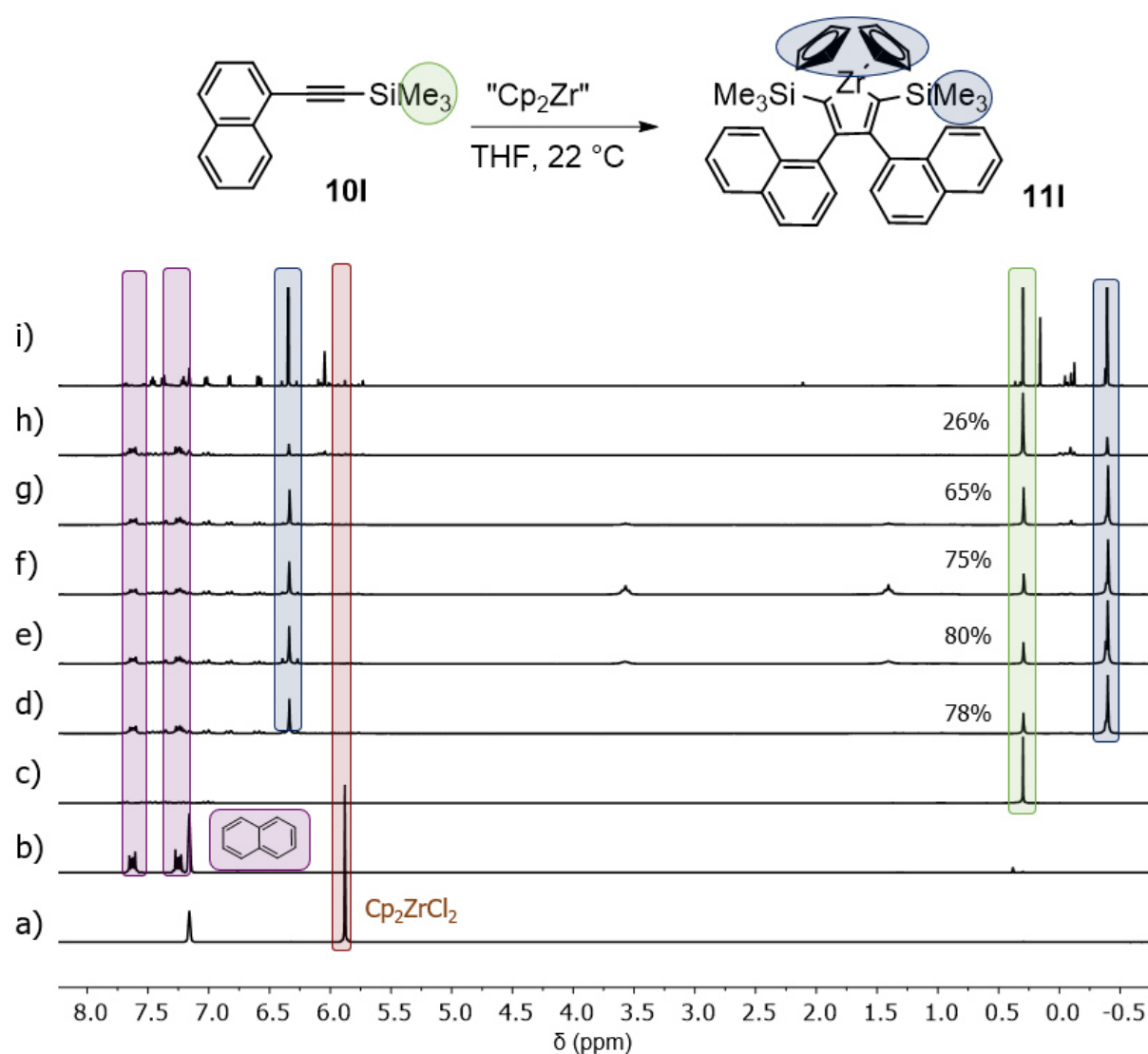


Figure S73. ¹H NMR spectra (recorded at 300 K, 200 MHz in C₆D₆) of the reaction monitoring for the synthesis of zirconacyclopentadiene **11I** using Negishi's reagent with naphthalene as standard (1 eq.). a) Starting material Cp₂ZrCl₂. b) Naphthalene. c) Starting material **10I**. Reaction monitoring after d) 10 min. e) 30 min. f) 1 h. g) 3 h and h) 22 h. i) zirconacyclopentadiene **11I** that had been previously isolated.

Rosenthal conditions

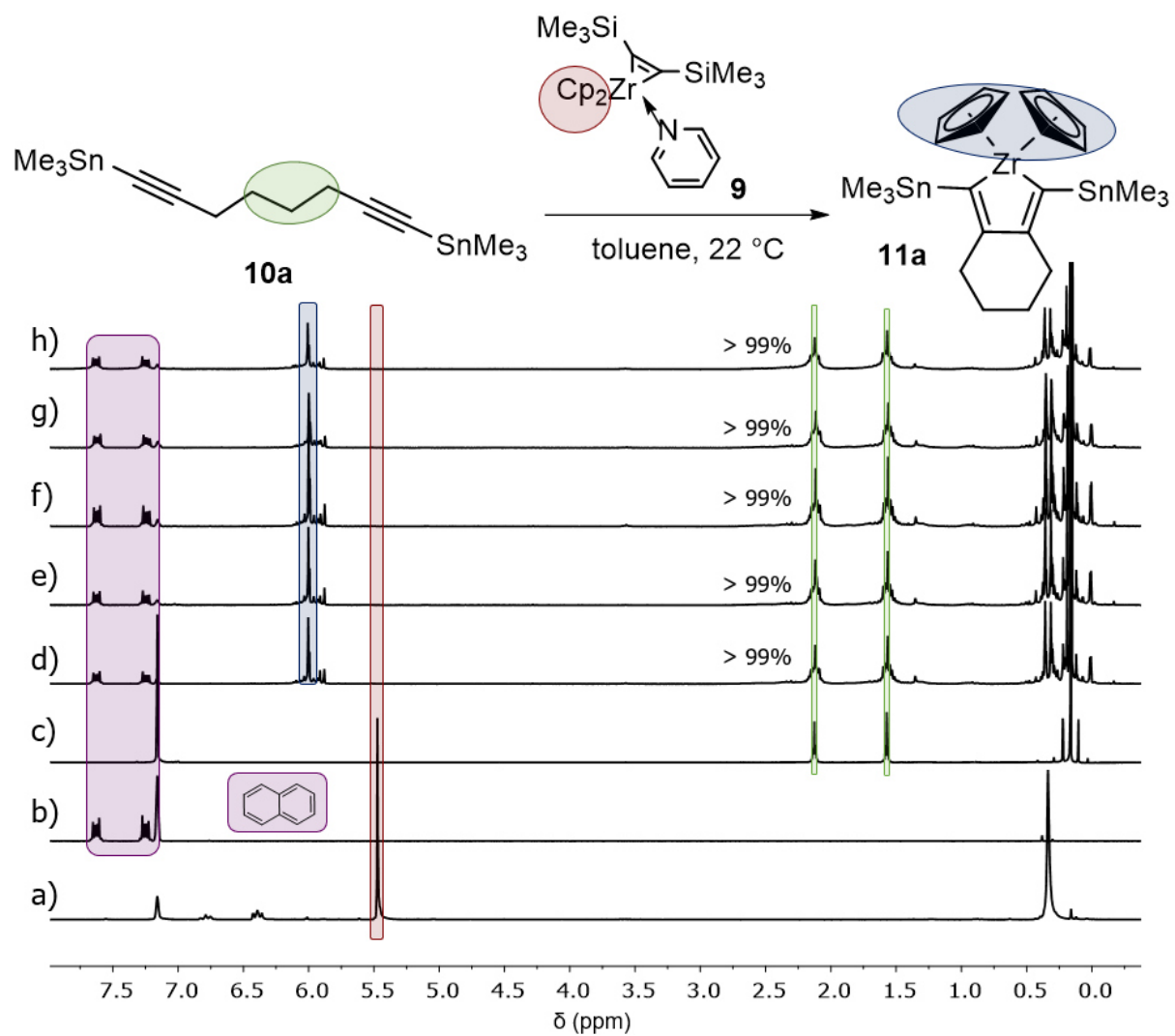


Figure S74. ¹H NMR spectra (recorded at 300 K, 200 MHz in C₆D₆) of the reaction monitoring for the synthesis of zirconacyclopentadiene **11a** using Rosenthal's reagent with naphthalene as standard (1 eq.). a) Rosenthal's reagent (**9**). b) Naphthalene. c) Starting material **10a**. Reaction monitoring after d) 10 min. e) 30 min. f) 1 h. g) 3 h and h) 22 h.

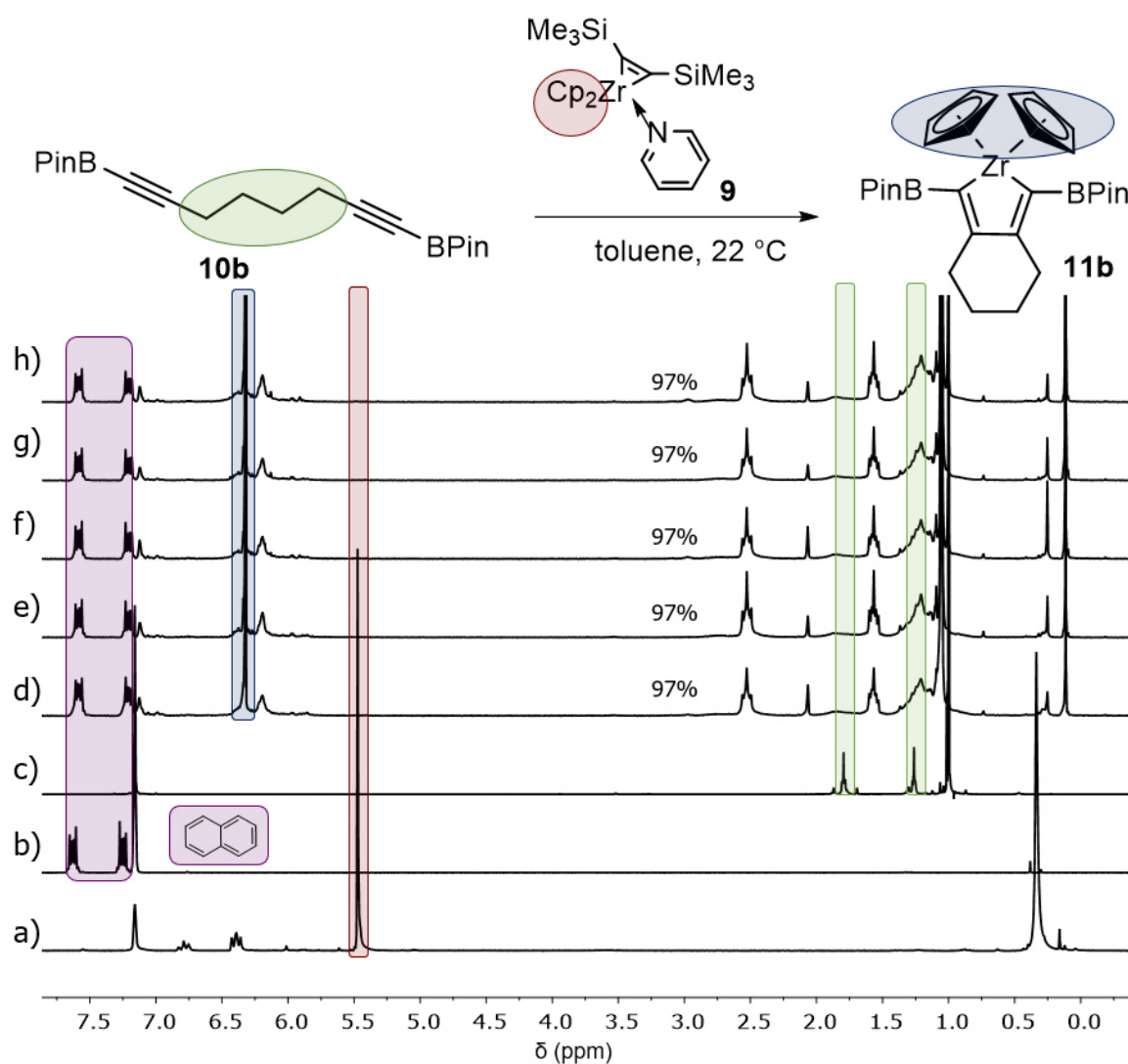


Figure S75. ¹H NMR spectra (recorded at 300 K, 200 MHz in C₆D₆) of the reaction monitoring for the synthesis of zirconacyclopentadiene **11b** using Rosenthal's reagent with naphthalene as standard (1 eq.). a) Rosenthal's reagent (**9**). b) Naphthalene. c) Starting material **10b**. Reaction monitoring after d) 10 min. e) 30 min. f) 1 h. g) 3 h and h) 22 h.

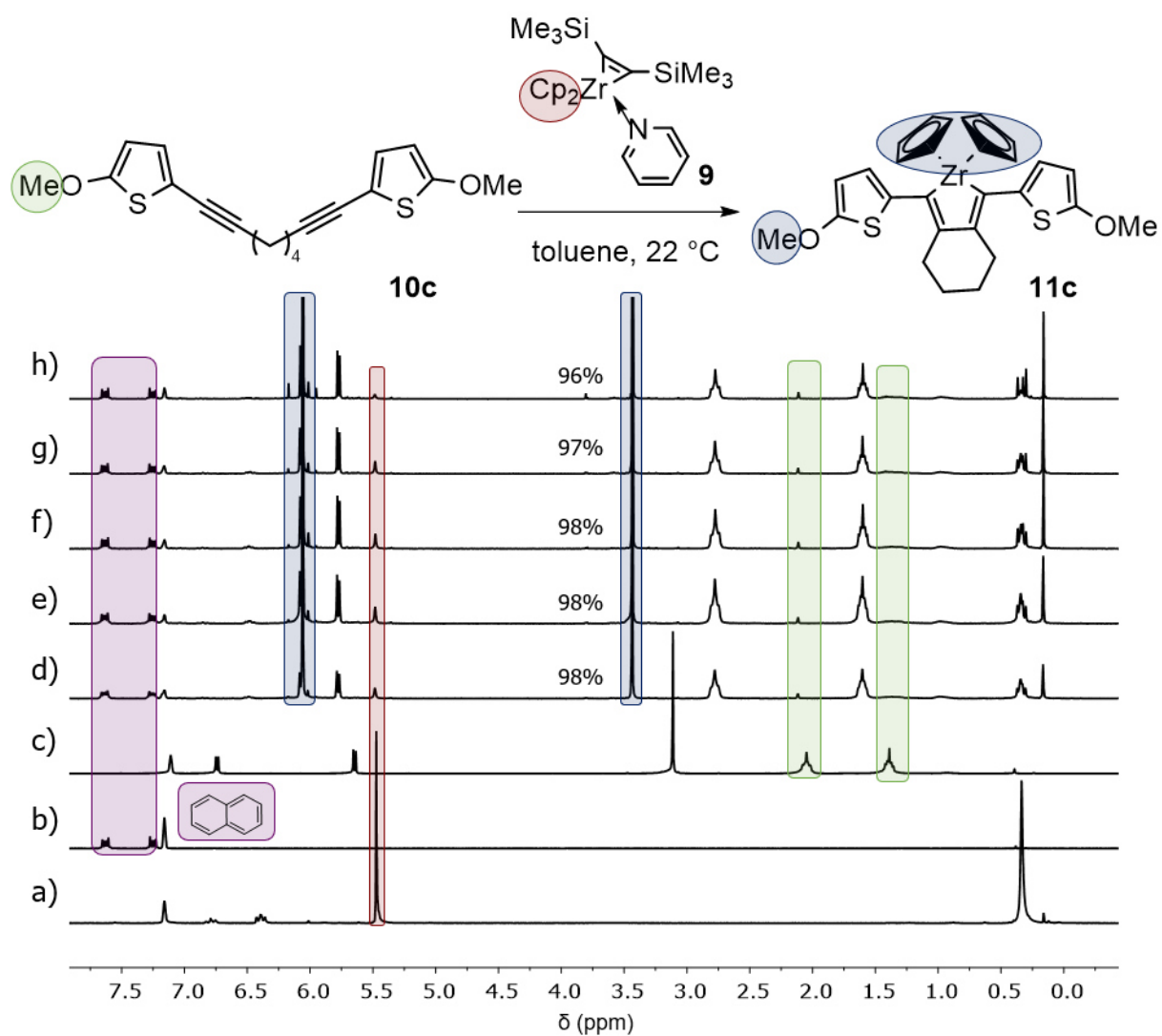


Figure S76. ¹H NMR spectra (recorded at 300 K, 200 MHz in C₆D₆) of the reaction monitoring for the synthesis of zirconacyclopentadiene **11c** using Rosenthal's reagent with naphthalene as standard (1 eq.). a) Rosenthal's reagent (**9**). b) Naphthalene. c) Starting material **10c**. Reaction monitoring after d) 10 min. e) 30 min. f) 1 h. g) 3 h and h) 22 h.

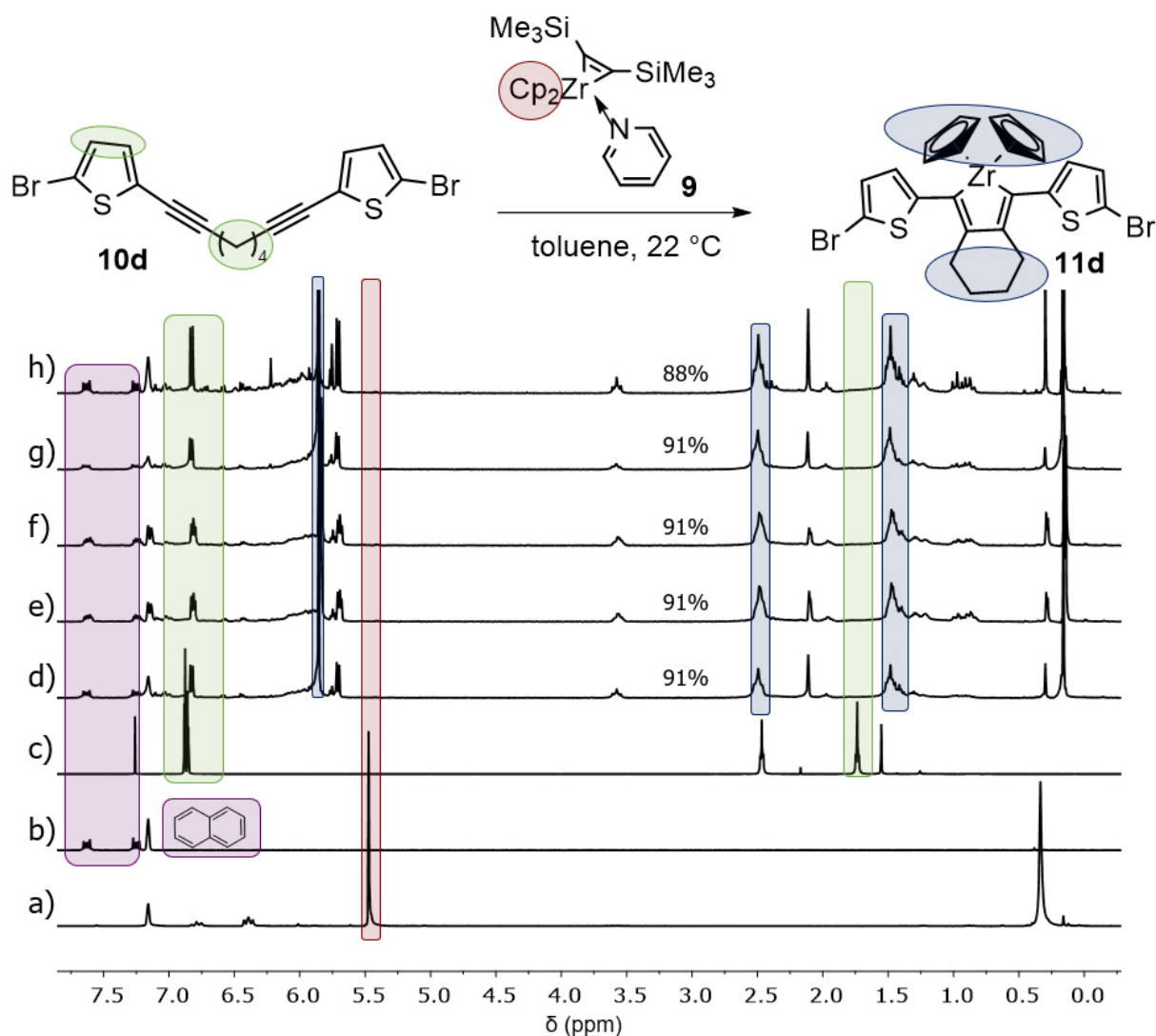


Figure S77. ¹H NMR spectra (recorded at 300 K, 200 MHz in C₆D₆) of the reaction monitoring for the synthesis of zirconacyclopentadiene **11d** using Rosenthal's reagent with naphthalene as standard (1 eq.). a) Rosenthal's reagent (**9**). b) Naphthalene. c) Starting material **10d**. Reaction monitoring after d) 10 min. e) 30 min. f) 1 h. g) 3 h and h) 22 h.

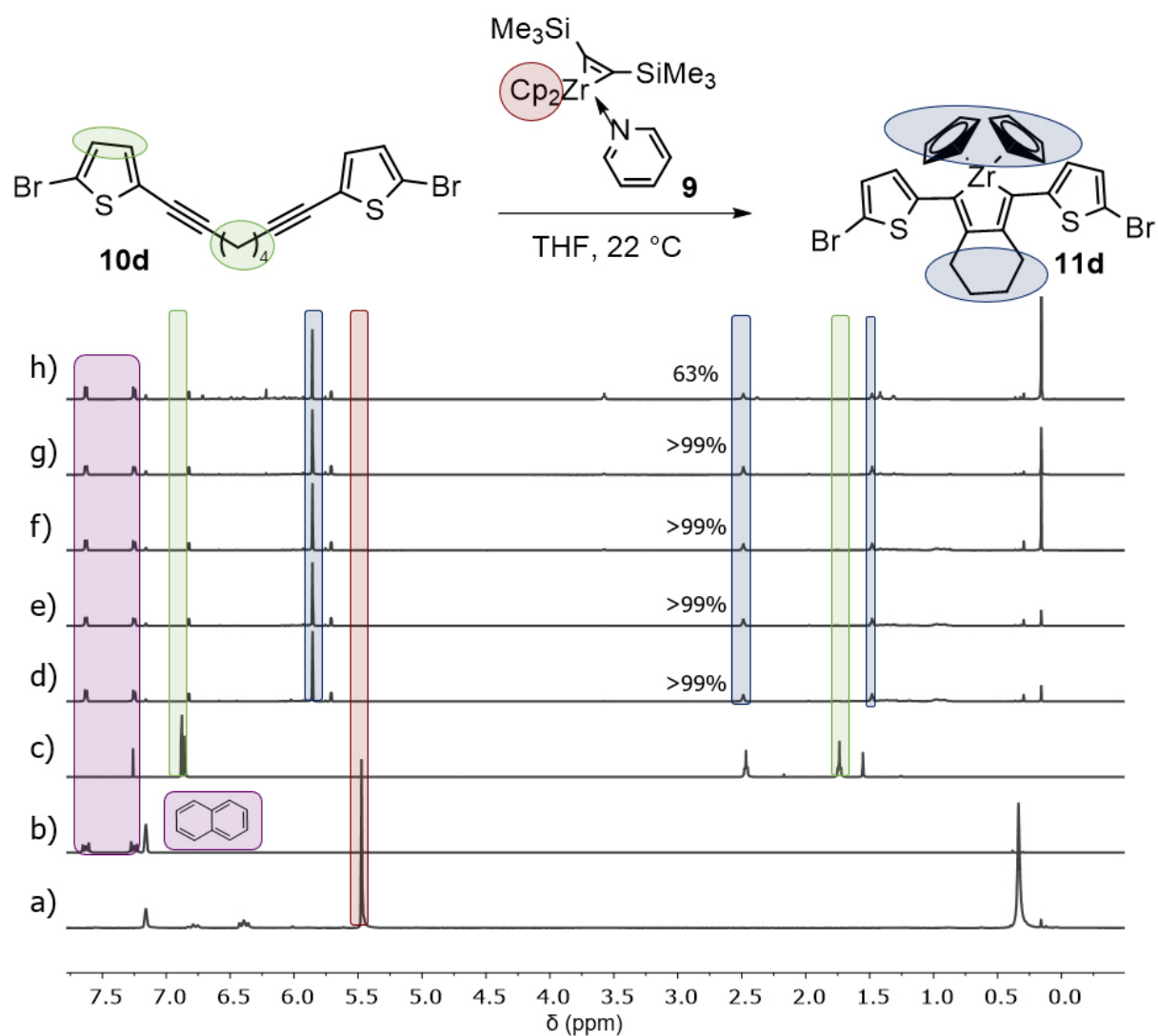


Figure S78. ¹H NMR spectra (recorded at 300 K, 600 MHz in C₆D₆) of the reaction monitoring for the synthesis of zirconacyclopentadiene **11d** using Rosenthal's reagent with naphthalene as standard (1 eq.). a) Rosenthal's reagent (**9**). b) Naphthalene. c) Starting material **10d**. Reaction monitoring after d) 10 min. e) 30 min. f) 1 h. g) 3 h and h) 22 h.

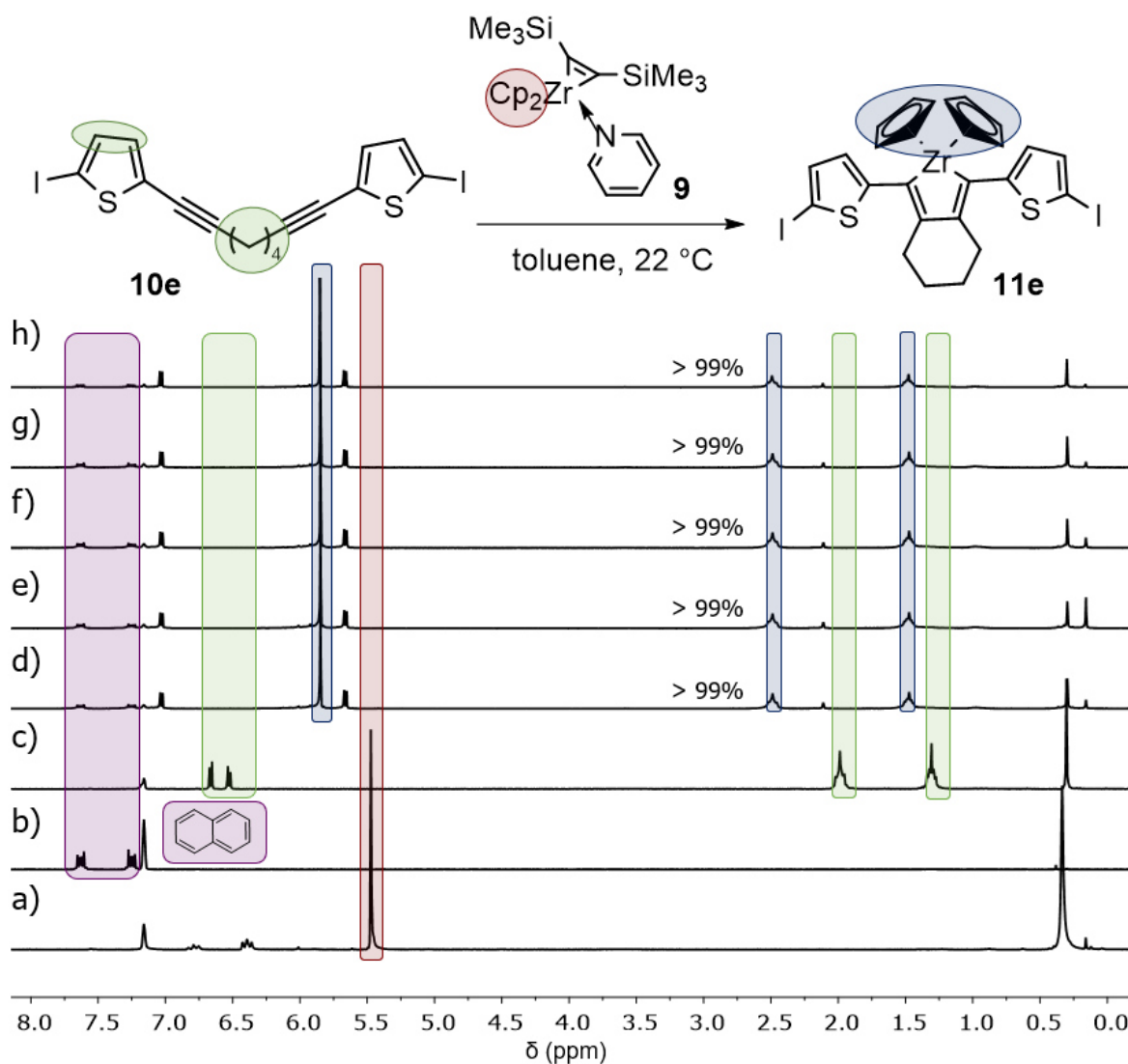


Figure S79. ¹H NMR spectra (recorded at 300 K, 200 MHz in C₆D₆) of the reaction monitoring for the synthesis of zirconacyclopentadiene **11e** using Rosenthal's reagent with naphthalene as standard (1 eq.). a) Rosenthal's reagent (**9**). b) Naphthalene. c) Starting material **10e**. Reaction monitoring after. d) 10 min. e) 30 min. f) 1 h. g) 3 h and h) 22 h.

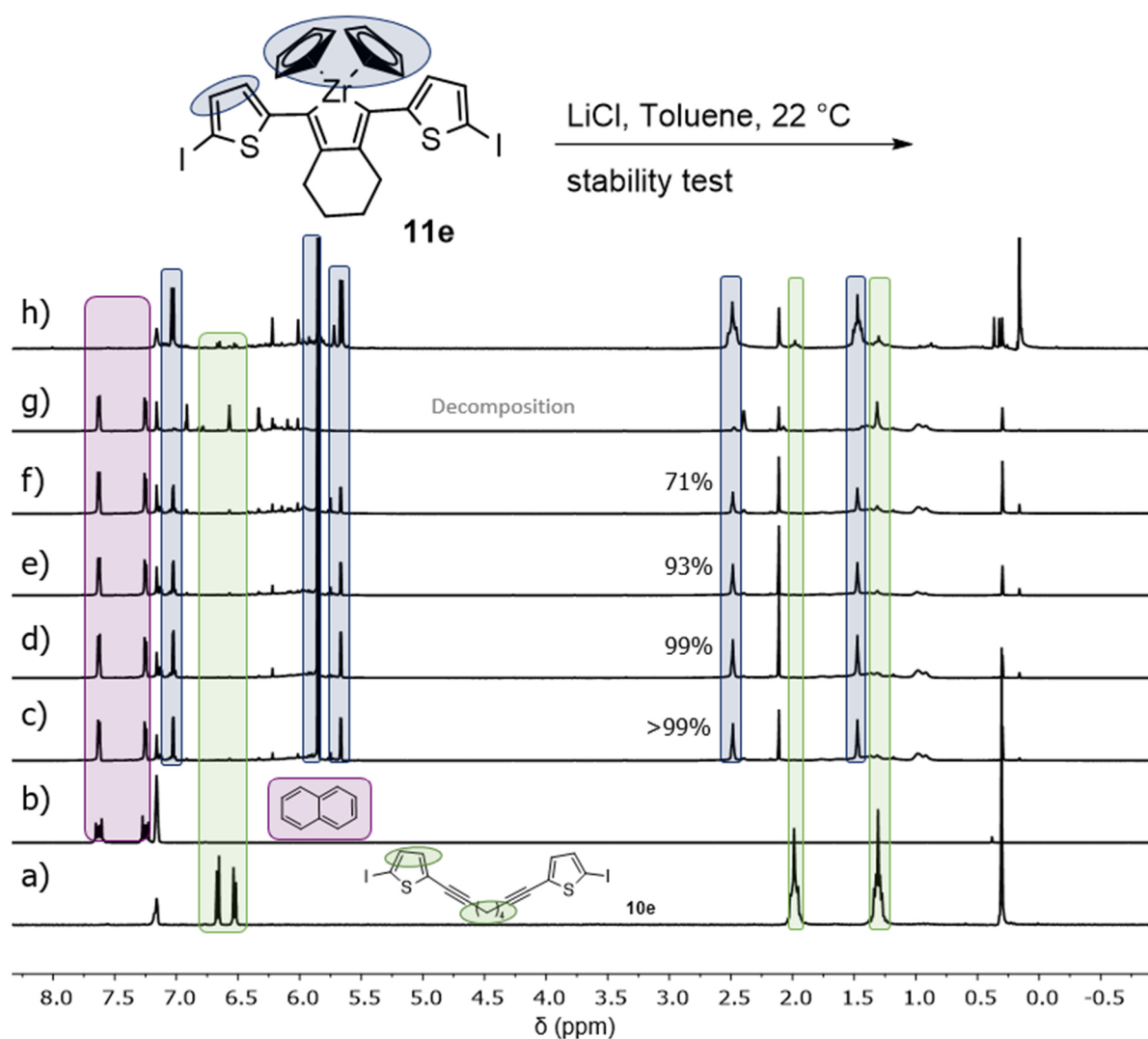


Figure S80. ¹H NMR spectra (recorded at 300 K, 600 MHz in C₆D₆) of the reaction monitoring for the stability test of zirconacyclopentadiene **11e** with naphthalene as standard (1 eq.). a) Naphthalene. b) Starting material **10e**. Reaction monitoring after. c) 10 min. d) 30 min. e) 1 h. f) 3 h. g) 22 h. and h) isolated zirconacyclopentadiene **11e**.

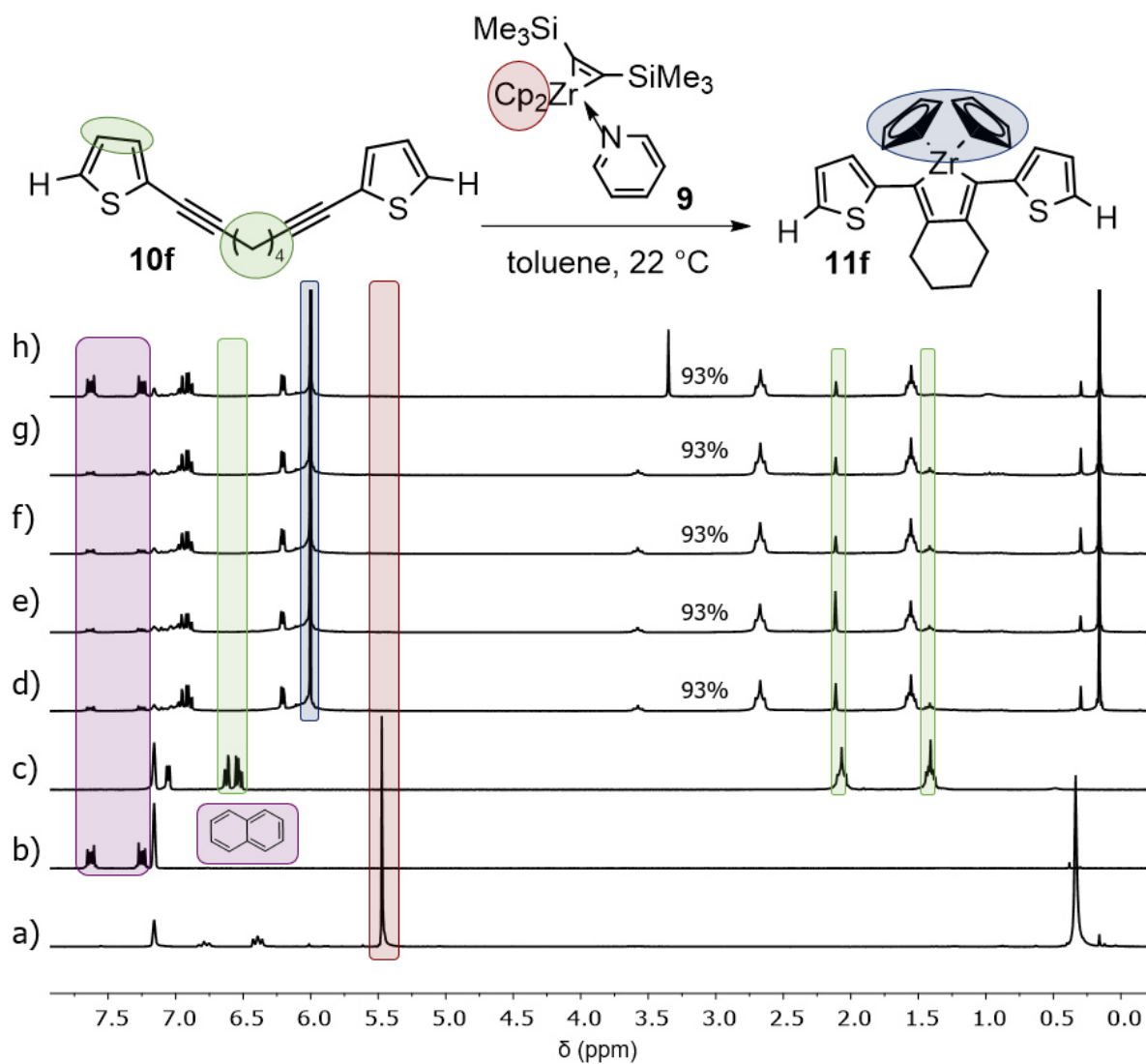


Figure S81. ¹H NMR spectra (recorded at 300 K, 200 MHz in C₆D₆) of the reaction monitoring for the synthesis of zirconacyclopentadiene **11f** using Rosenthal's reagent with naphthalene as standard (1 eq.). a) Rosenthal's reagent (**9**). b) Naphthalene. c) Starting material **10f**. Reaction monitoring after. d) 10 min. e) 30 min. f) 1 h. g) 3 h and h) 22 h.

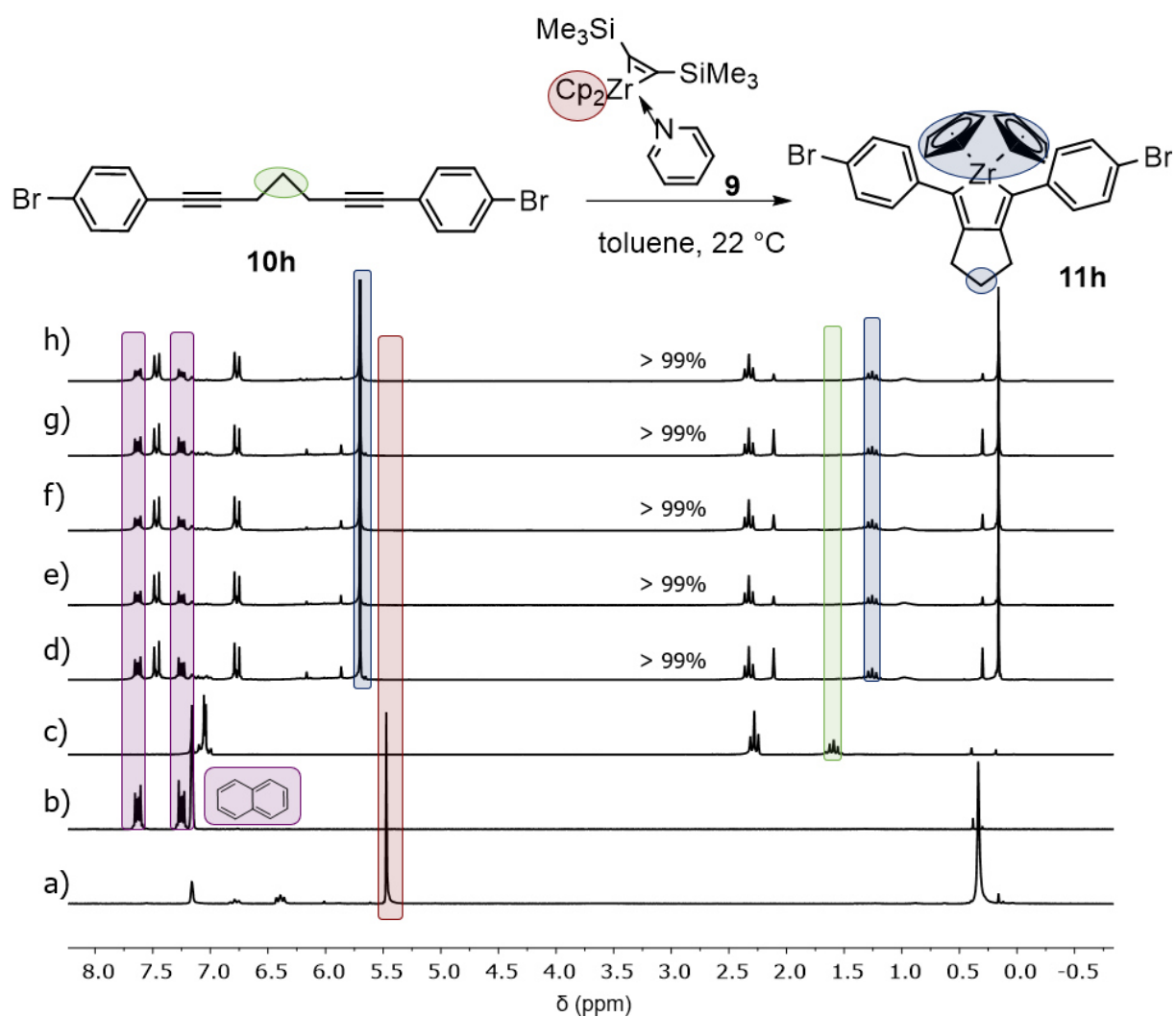


Figure S82. ¹H NMR spectra (recorded at 300 K, 200 MHz in C₆D₆) of the reaction monitoring for the synthesis of zirconacyclopentadiene **11h** using Rosenthal's reagent with naphthalene as standard (1 eq.). a) Rosenthal's reagent (**9**). b) Naphthalene. c) Starting material **10h**. Reaction monitoring after. d) 10 min. e) 30 min. f) 1 h. g) 3 h and h) 22 h.

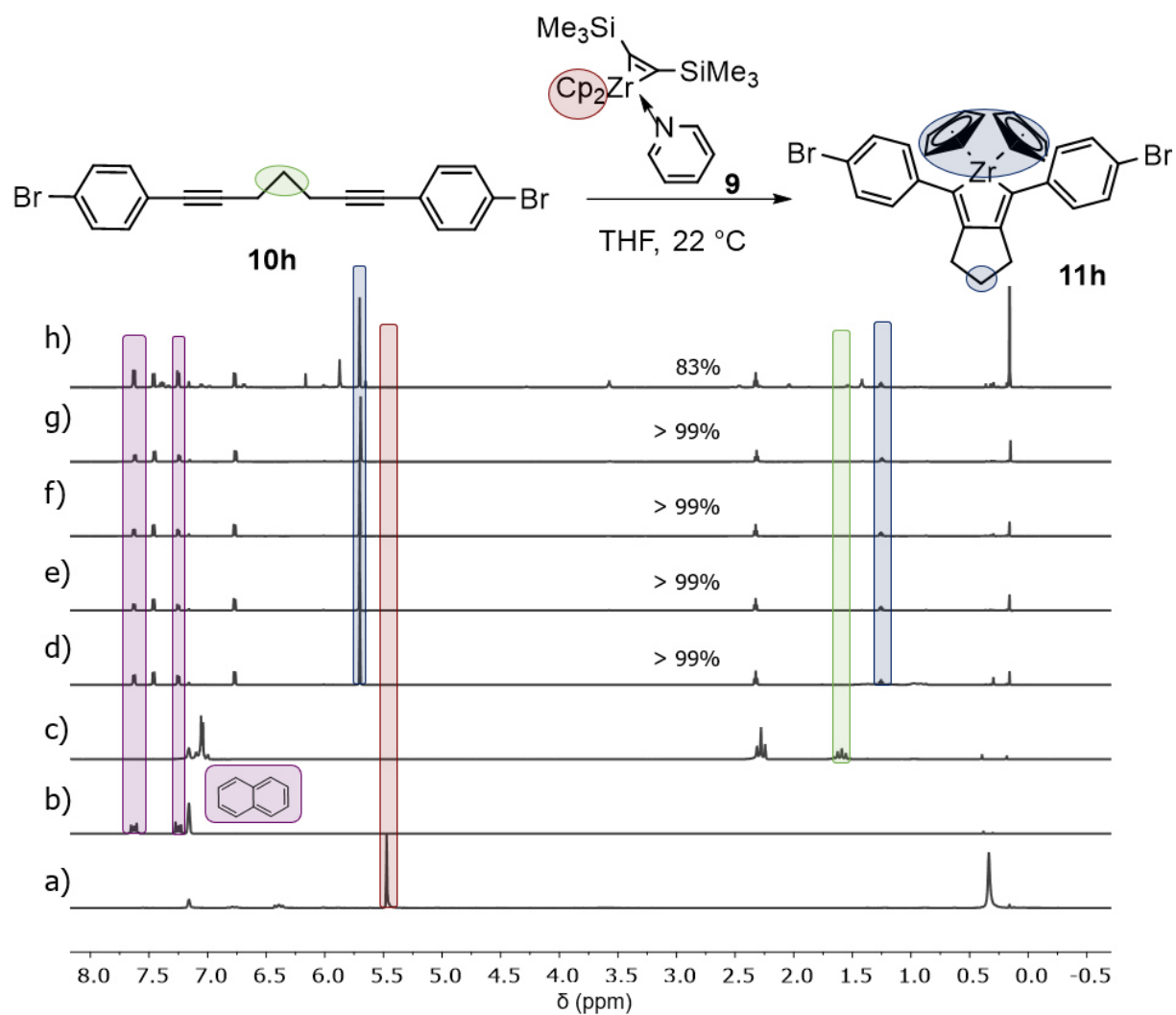


Figure 83. ¹H NMR spectra (recorded at 300 K, 600 MHz in C₆D₆) of the reaction monitoring for the synthesis of zirconacyclopentadiene **11h** using Rosenthal's reagent with naphthalene as standard (1 eq.). a) Rosenthal's reagent (**9**). b) Naphthalene. c) Starting material **10h**. Reaction monitoring after. d) 10 min. e) 30 min. f) 1 h. g) 3 h and h) 22 h.

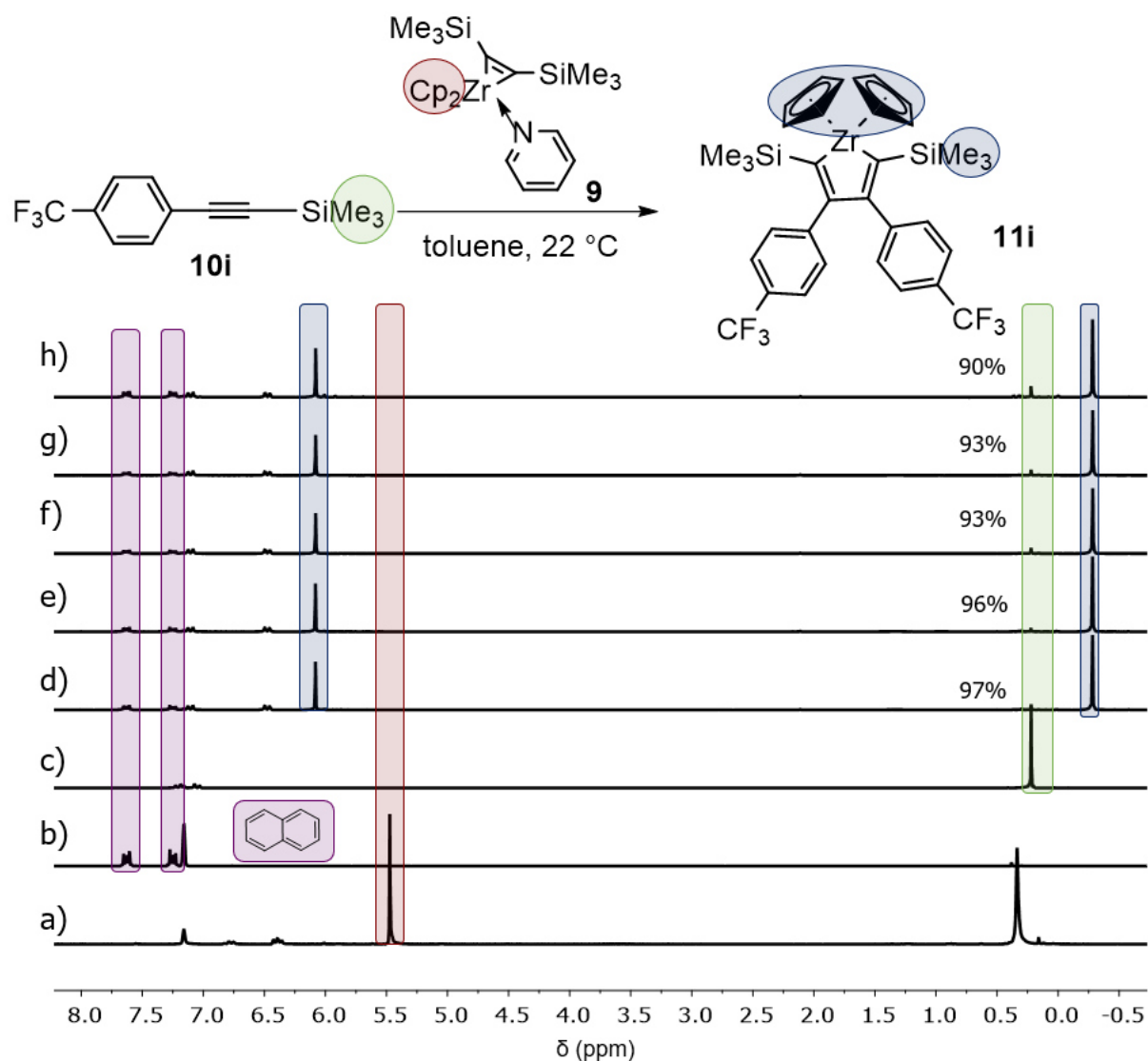


Figure S84. ¹H NMR spectra (recorded at 300 K, 200 MHz in C₆D₆) of the reaction monitoring for the synthesis of zirconacyclopentadiene **11i** using Rosenthal's reagent with naphthalene as standard (1 eq.). a) Rosenthal's reagent (**9**). b) Naphthalene. c) Starting material **10i**. Reaction monitoring after d) 10 min. e) 30 min. f) 1 h. g) 3 h and h) 22 h.

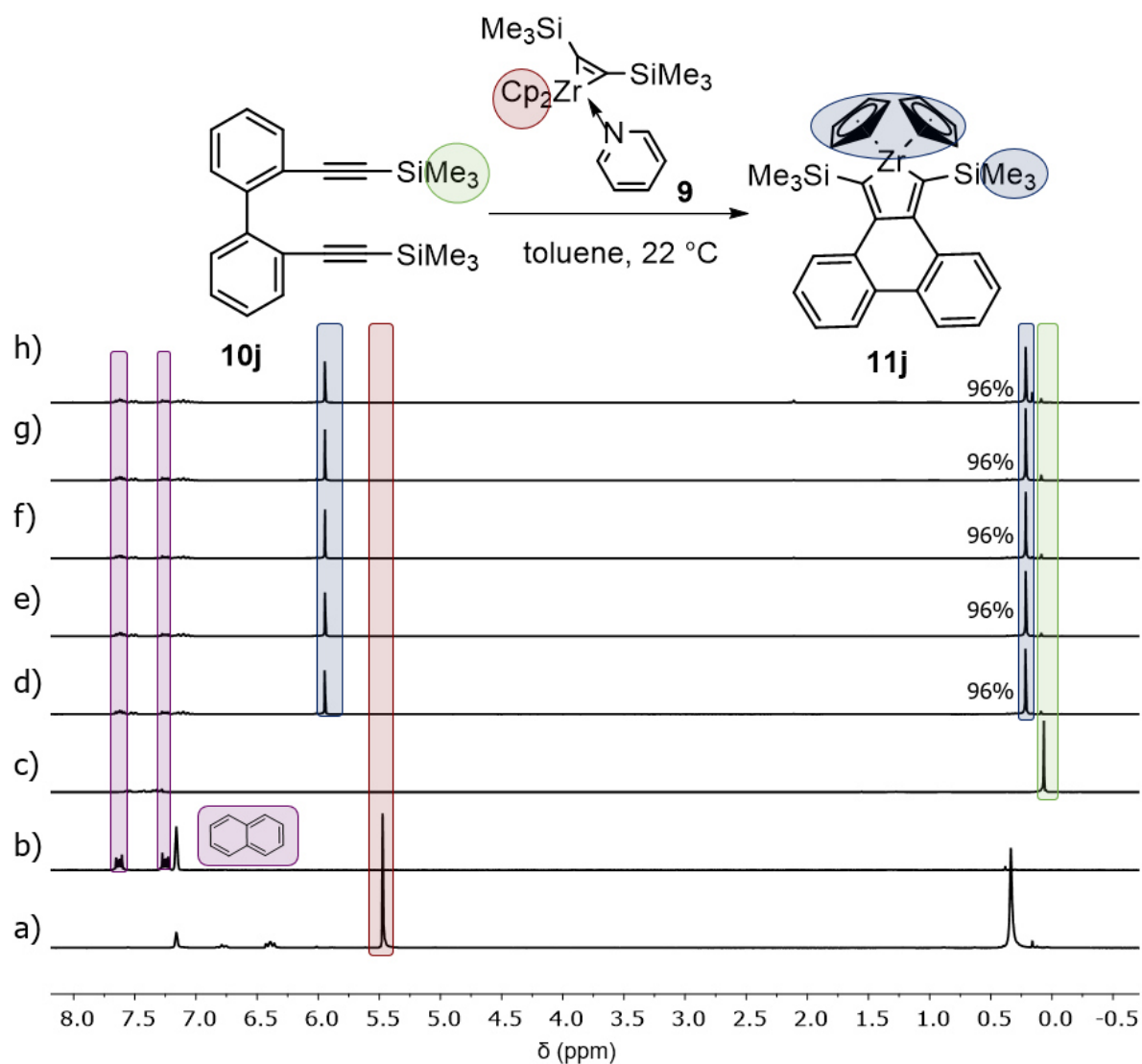


Figure S85. ¹H NMR spectra (recorded at 300 K, 200 MHz in C₆D₆) of the reaction monitoring for the synthesis of zirconacyclopentadiene **11j** using Rosenthal's reagent with naphthalene as standard (1 eq.). a) Rosenthal's reagent (**9**). b) Naphthalene. c) Starting material **10j**. Reaction monitoring after. d) 10 min. e) 30 min. f) 1 h. g) 3 h and h) 22 h.

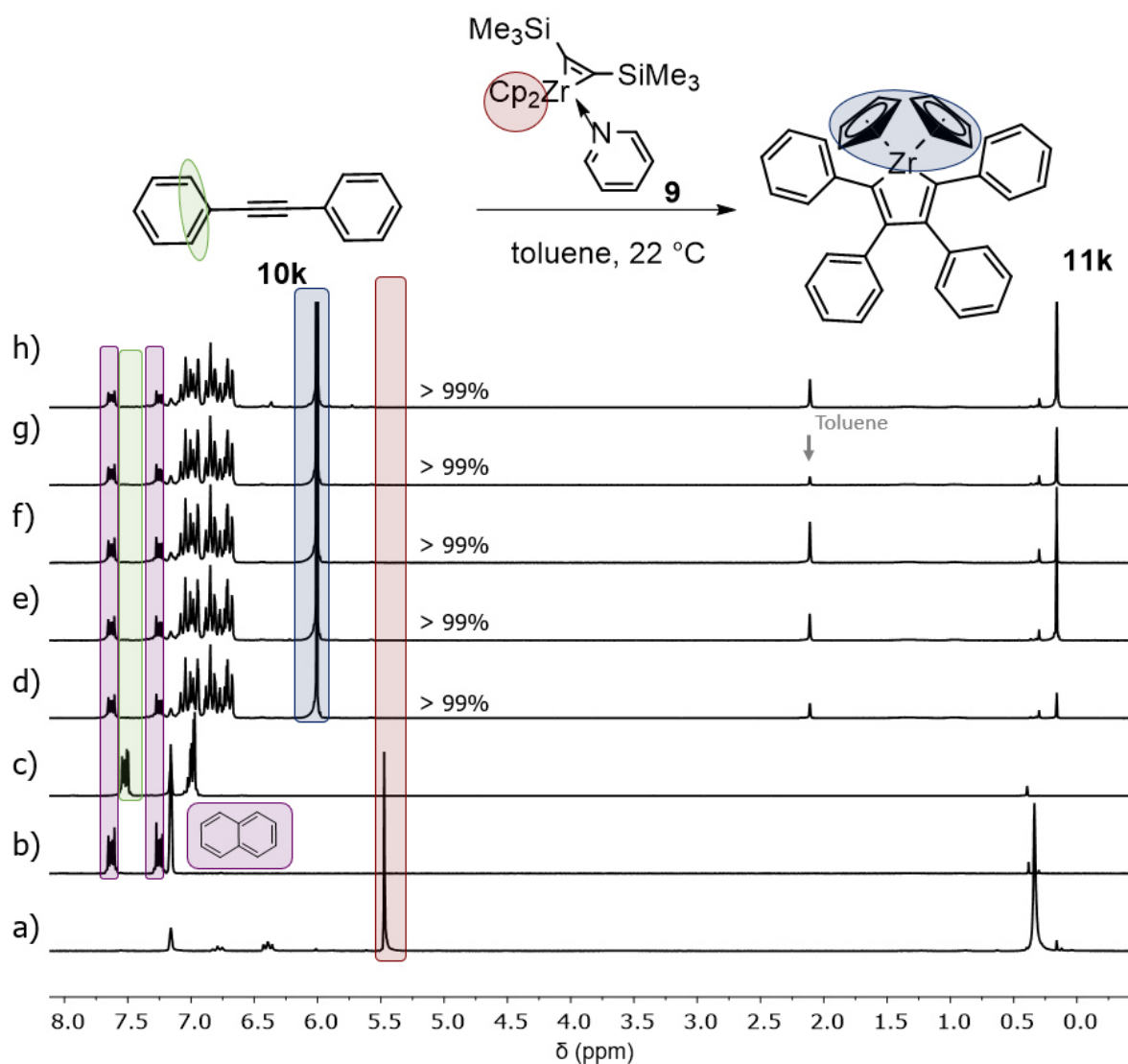


Figure S86. ¹H NMR spectra (recorded at 300 K, 200 MHz in C₆D₆) of the reaction monitoring for the synthesis of zirconacyclopentadiene **11k** using Rosenthal's reagent with naphthalene as standard (1 eq.). a) Rosenthal's reagent (**9**). b) Naphthalene. c) Starting material **10k**. Reaction monitoring after d) 10 min. e) 30 min. f) 1 h. g) 3 h and h) 22 h.

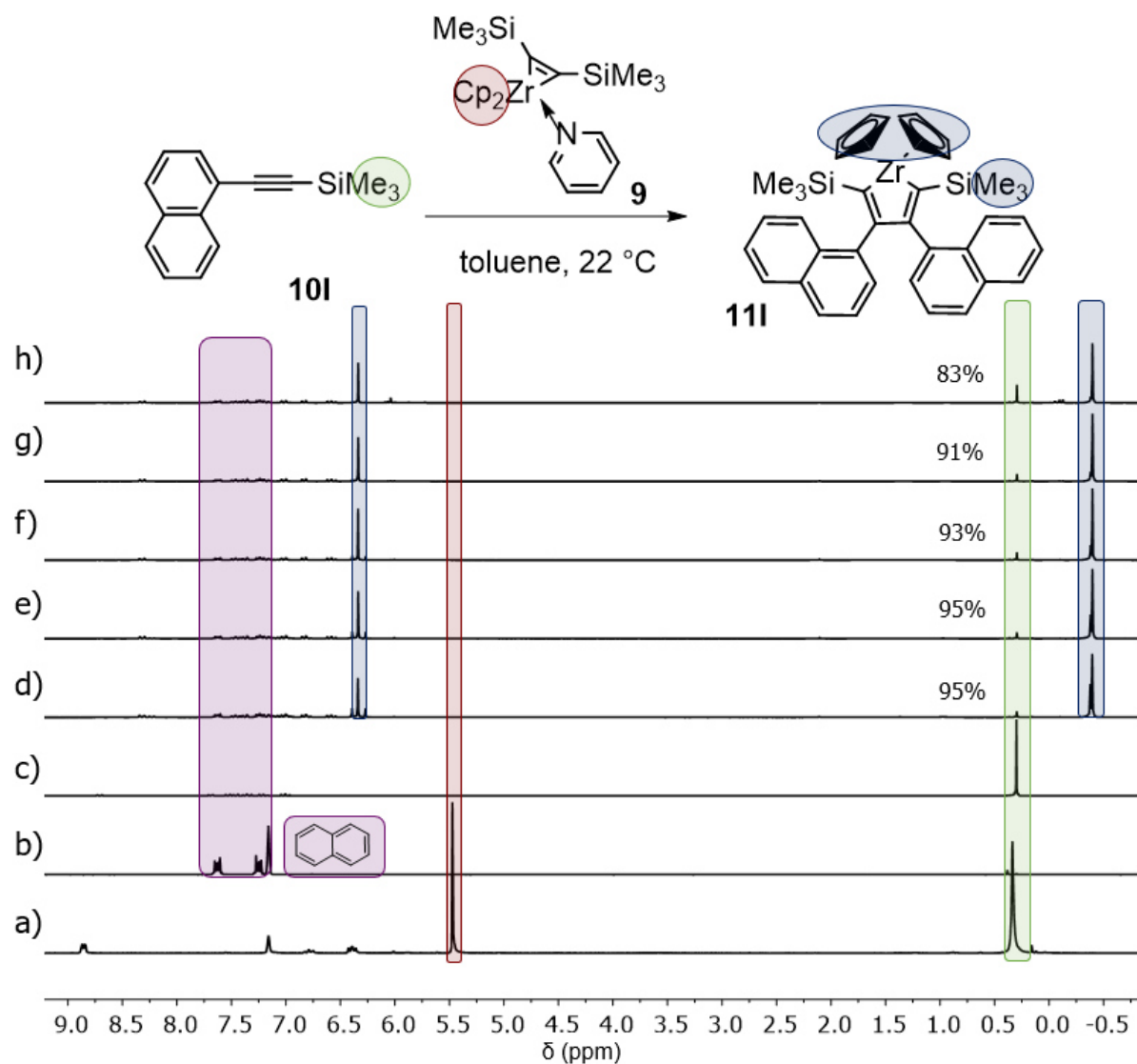


Figure S87. ¹H NMR spectra (recorded at 300 K, 200 MHz in C₆D₆) of the reaction monitoring for the synthesis of zirconacyclopentadiene **11I** using Rosenthal's reagent with naphthalene as standard (1 eq.). a) Rosenthal's reagent (**9**). b) Naphthalene. c) Starting material **10I**. Reaction monitoring after d) 10 min. e) 30 min. f) 1 h. g) 3 h and h) 22 h.

6.3 Air Stability Tests

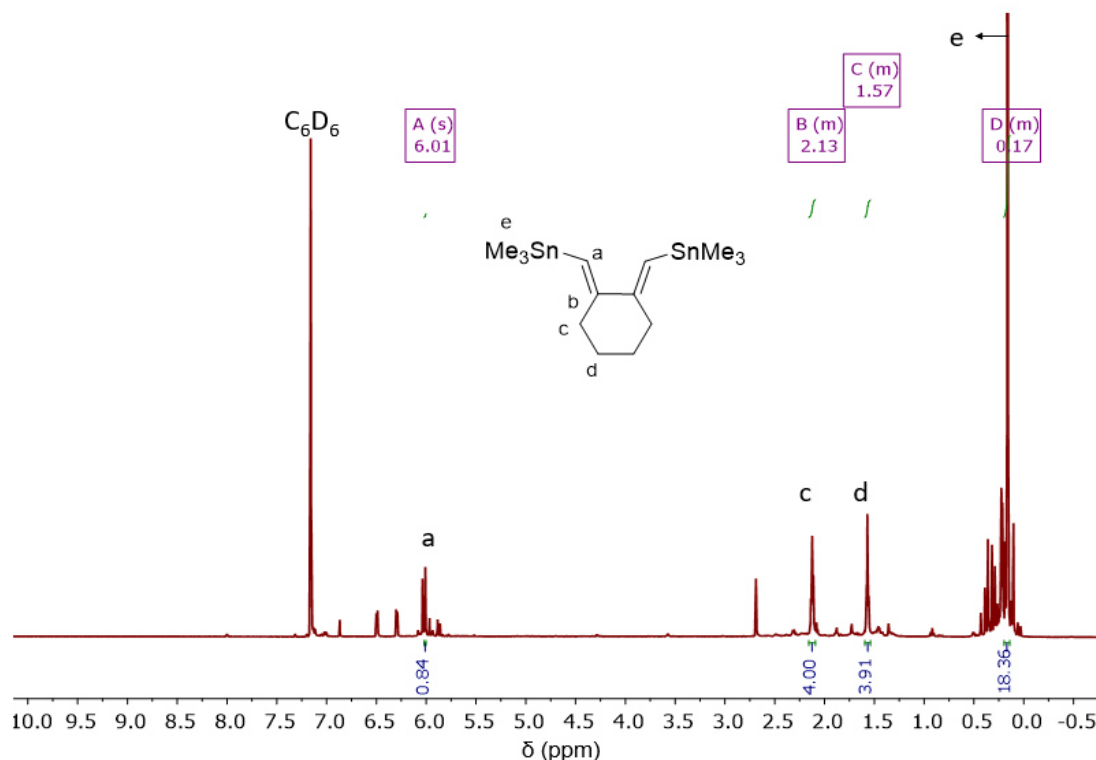


Figure S88. ^1H NMR (500 MHz) spectrum of (1*E*,2*E*)-1,2-bis(trimethylstannyl)methylene)cyclohexane main product in the decomposition of zirconacyclopentadiene **11a** under air, in C_6D_6 .

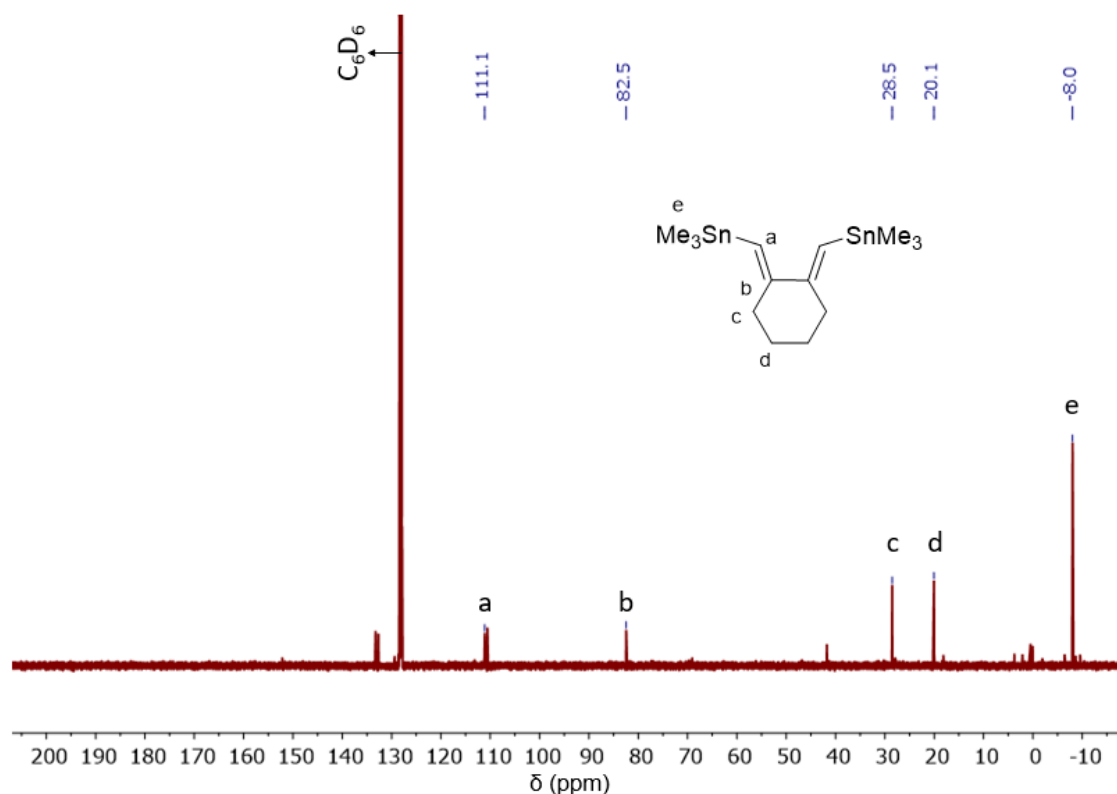


Figure S89. $^{13}\text{C}\{^1\text{H}\}$ NMR (126 MHz) spectrum of (1*E*,2*E*)-1,2-bis(trimethylstannyl)methylene)cyclohexane main product of the decomposition of zirconacyclopentadiene **11a** under air, in C_6D_6 .

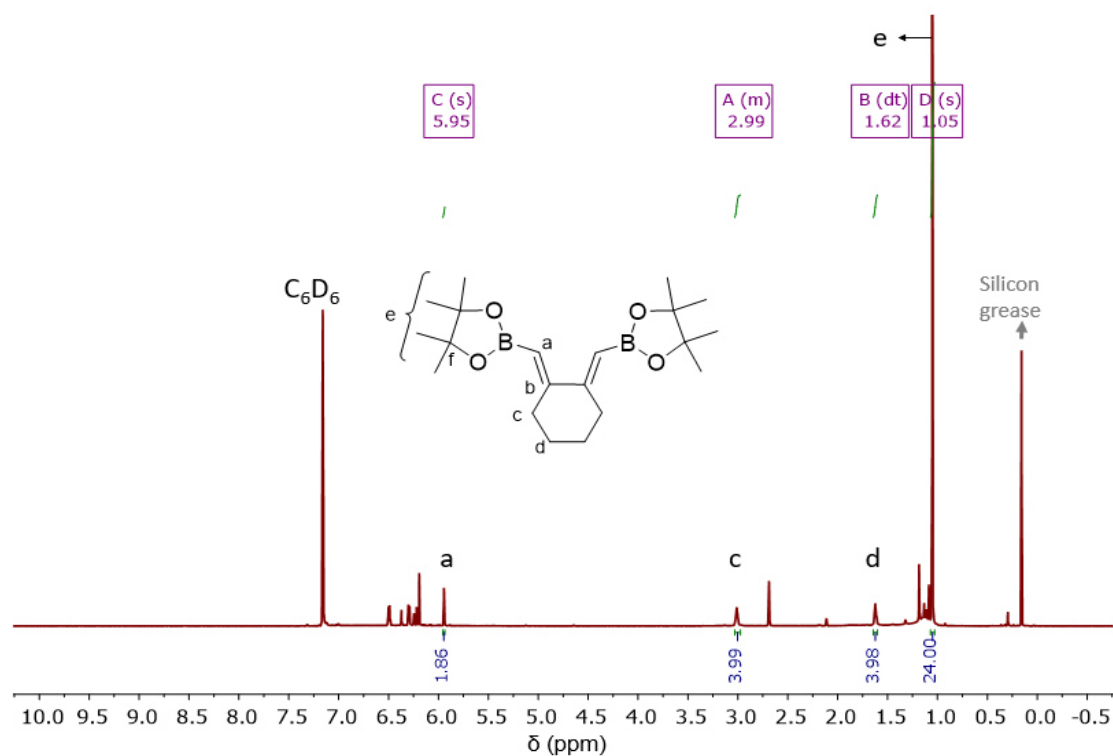


Figure S90. ^1H NMR (500 MHz) spectrum of (1*E*,2*E*)-1,2-bis((4,4,5,5-tetramethyl-1,3,2-dioxaborolan-2-yl)methylene)cyclohexane main product of the decomposition of zirconacyclopentadiene **11b** under air, in C_6D_6 .

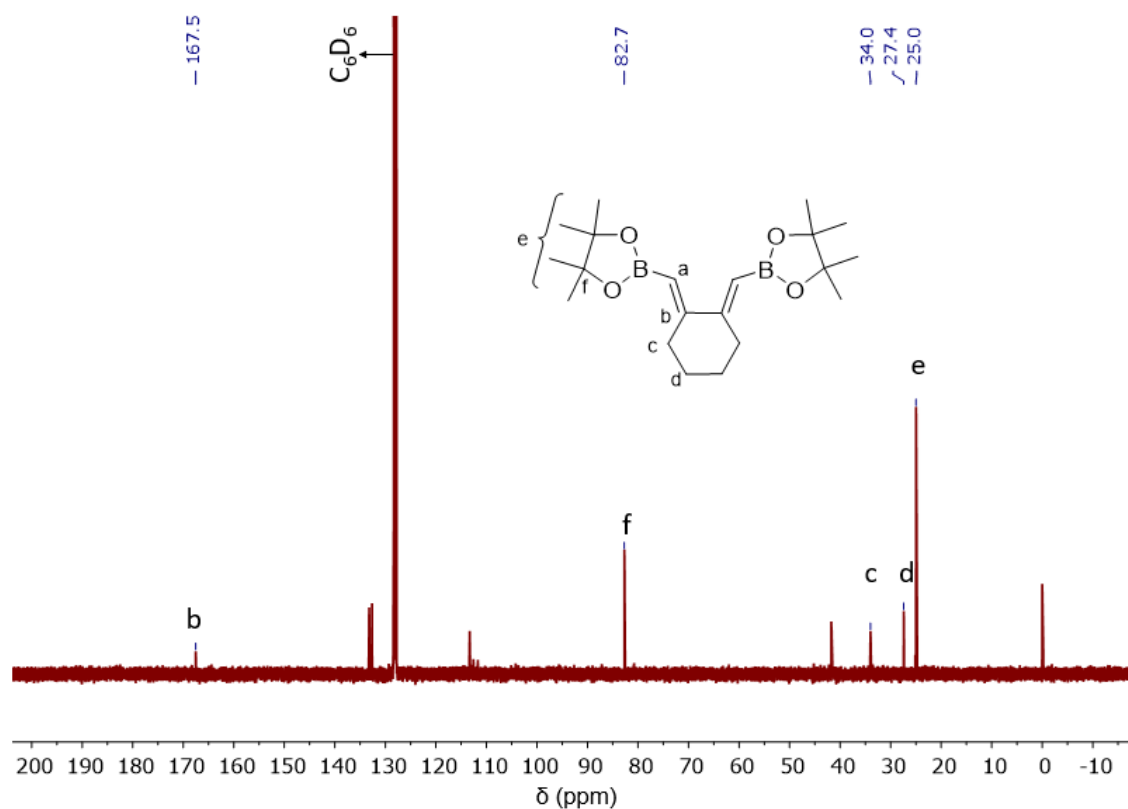


Figure S91. $^{13}\text{C}\{^1\text{H}\}$ NMR (126 MHz) spectrum of (1*E*,2*E*)-1,2-bis((4,4,5,5-tetramethyl-1,3,2-dioxaborolan-2-yl)methylene)cyclohexane main product of the decomposition of zirconacyclopentadiene **11b** under air, in C_6D_6 .

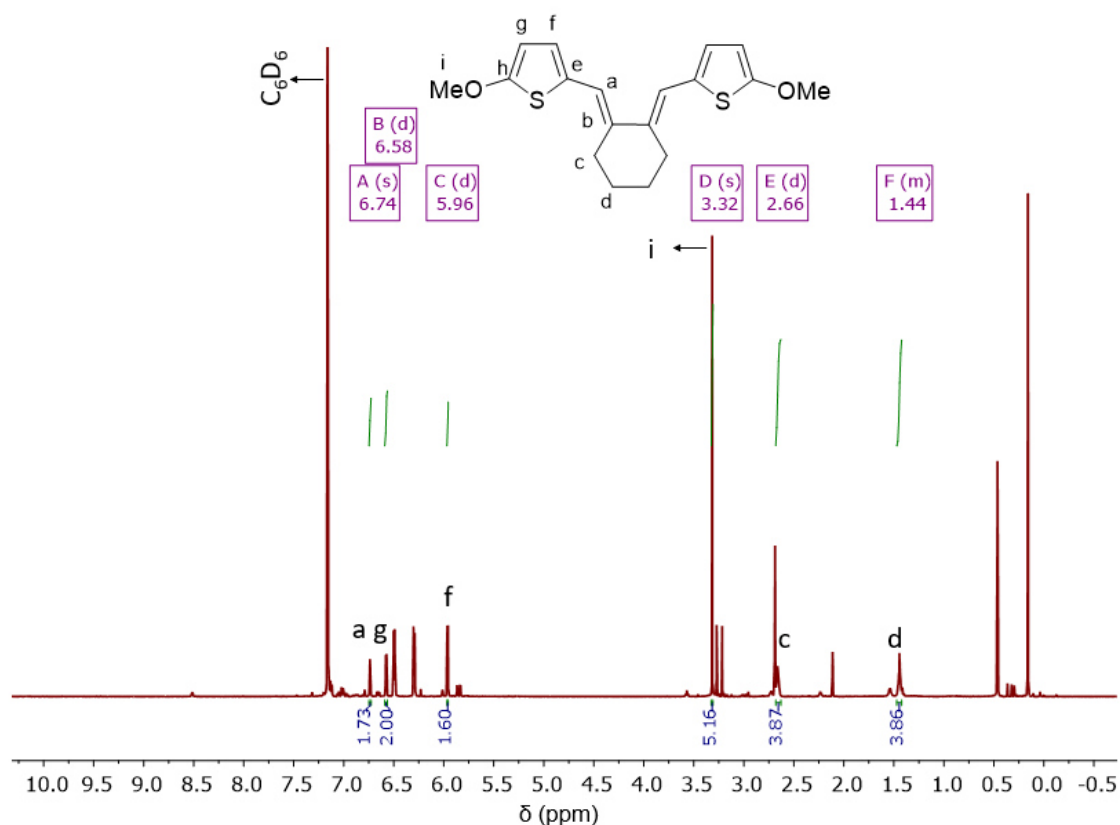


Figure S92. ¹H NMR (500 MHz) spectrum of (1*E*, 2*E*)-1, 2-bis((5-methoxythiophen-2-yl)methylene)cyclohexane main product of the decomposition of zirconacyclopentadiene **11c** under air, in C₆D₆.

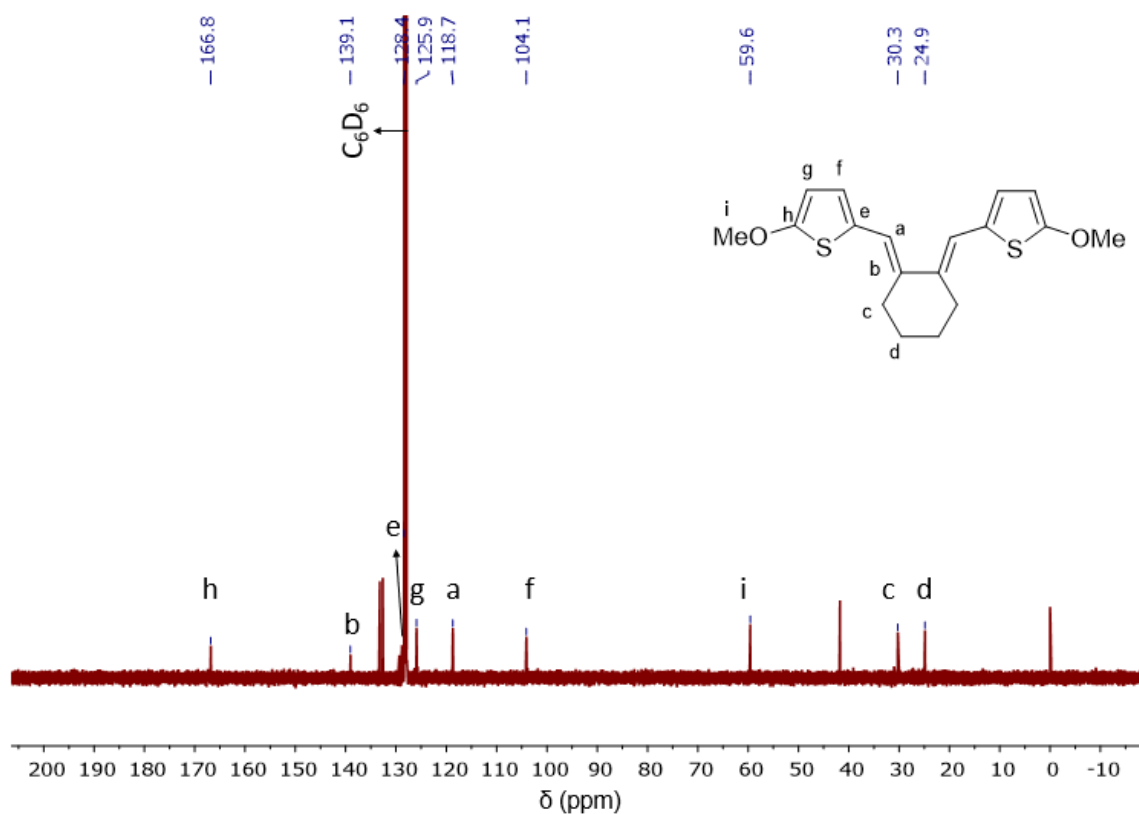


Figure S93. ¹³C{¹H} NMR (126 MHz) spectrum of (1*E*, 2*E*)-1, 2-bis((5-methoxythiophen-2-yl)methylene)cyclohexane main product of the decomposition of zirconacyclopentadiene **11c** under air, in C₆D₆.

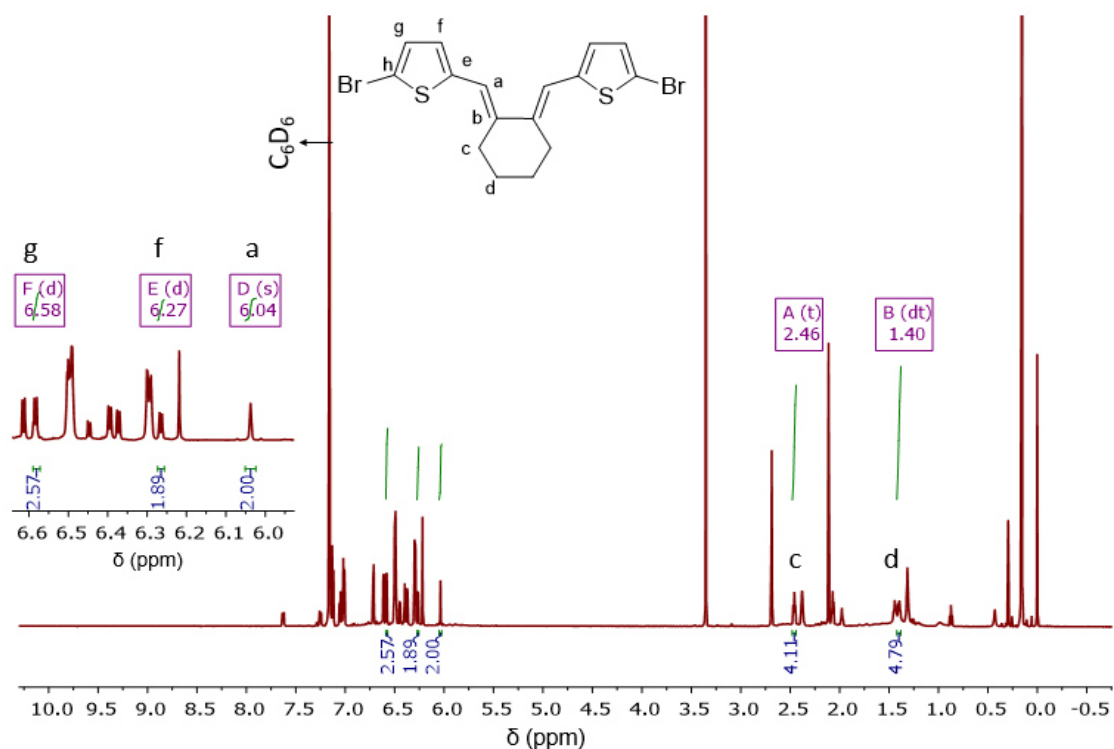


Figure S94. ^1H NMR (500 MHz) spectrum of $(1E,2E)$ -1,2-bis((5-bromothiophen-2-yl)methylene)cyclohexane main product of the decomposition of zirconacyclopentadiene **11d** under air, in C_6D_6 .

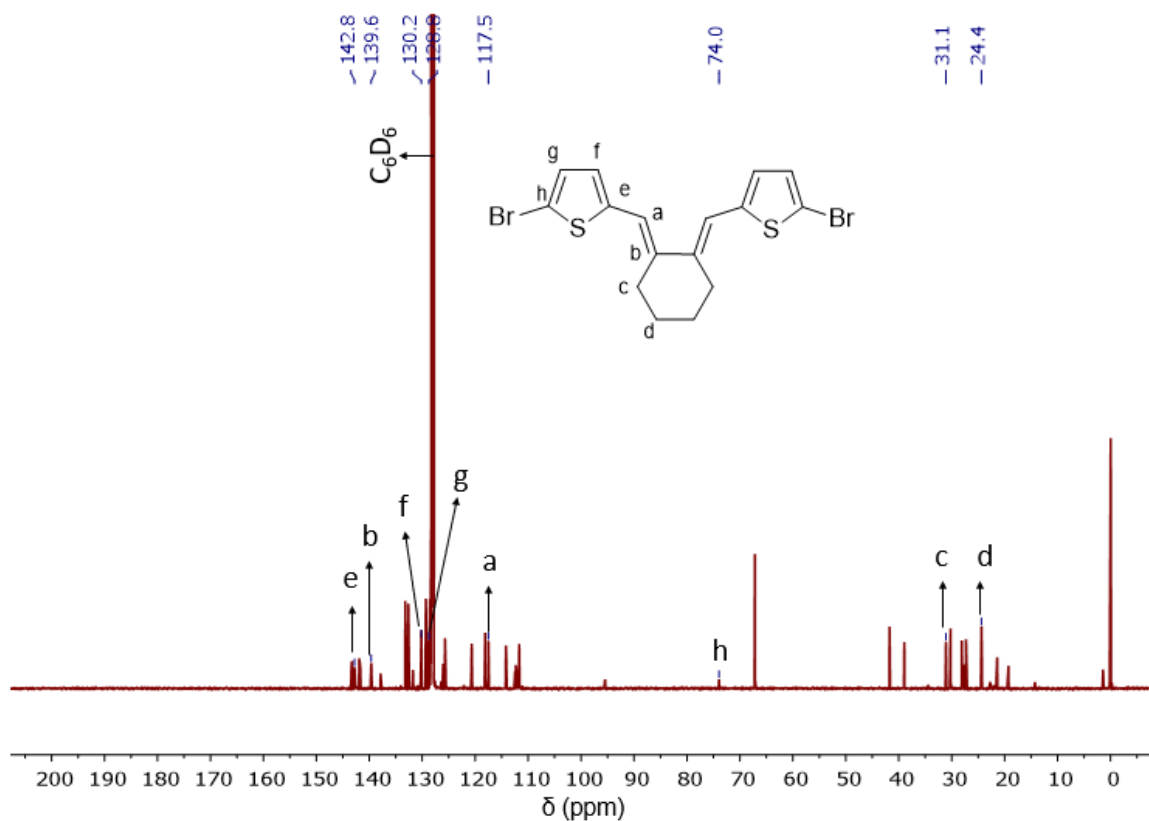


Figure S95. $^{13}\text{C}\{^1\text{H}\}$ NMR (126 MHz) spectrum of $(1E,2E)$ -1,2-bis((5-bromothiophen-2-yl)methylene)cyclohexane main product of the decomposition of zirconacyclopentadiene **11d** under air, in C_6D_6 .

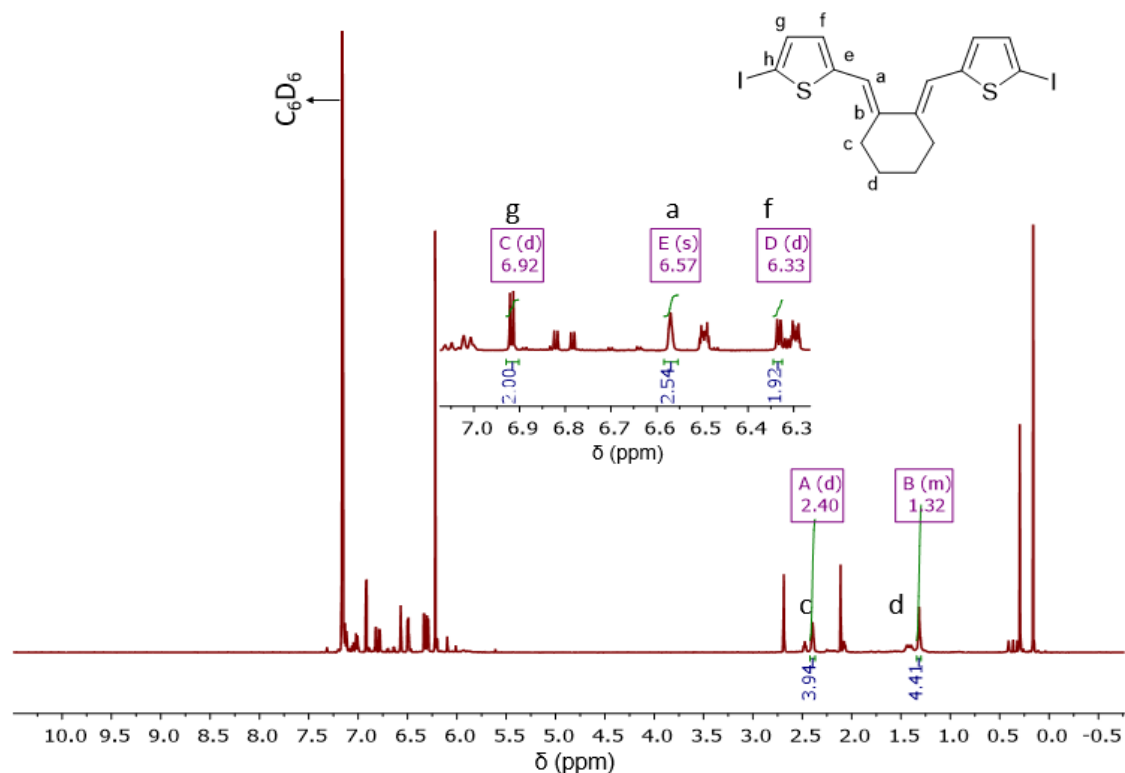


Figure S96. ^1H NMR (500 MHz) spectrum of (1*E*,2*E*)-1,2-bis((5-iodothiophen-2-yl)methylene)cyclohexane main product of the decomposition of zirconacyclopentadiene **11e** under air, in C_6D_6 .

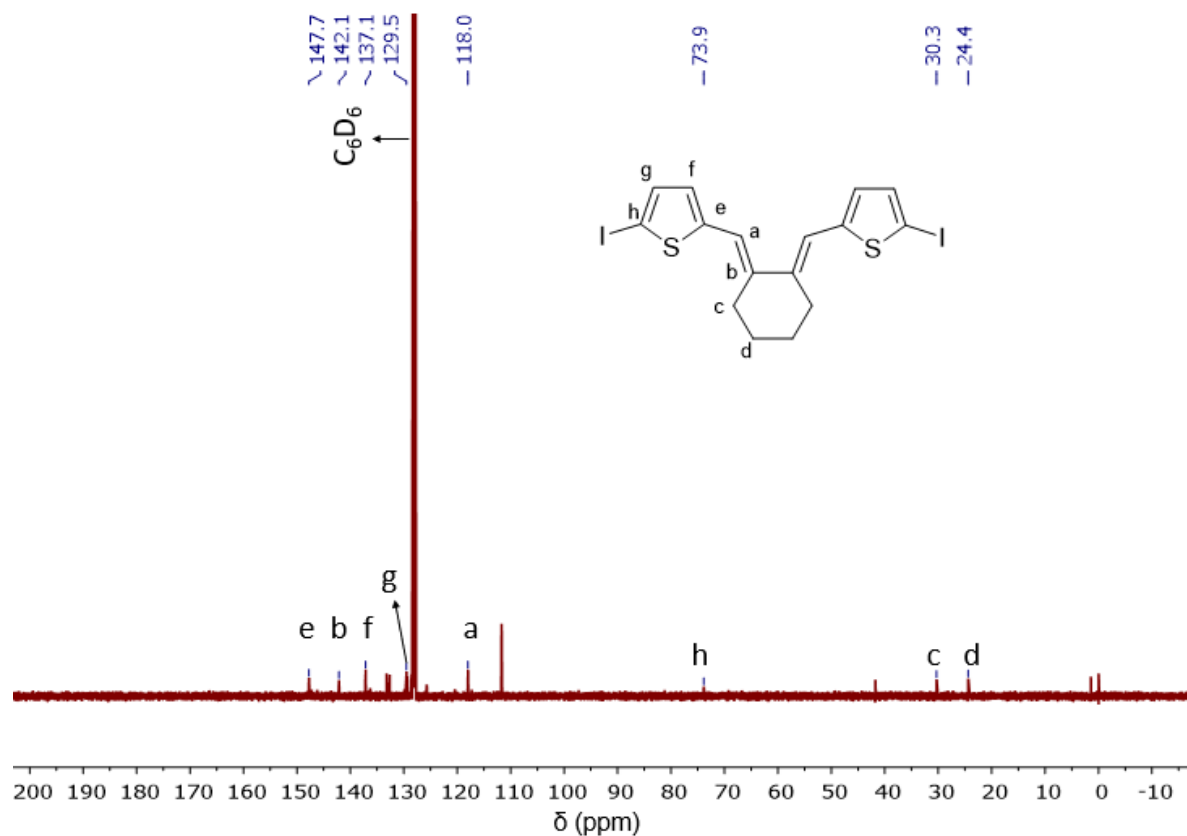


Figure S97. $^{13}\text{C}\{^1\text{H}\}$ NMR (126 MHz) spectrum of (1*E*,2*E*)-1,2-bis((5-iodothiophen-2-yl)methylene)cyclohexane main product of the decomposition of zirconacyclopentadiene **11e** under air, in C_6D_6 .

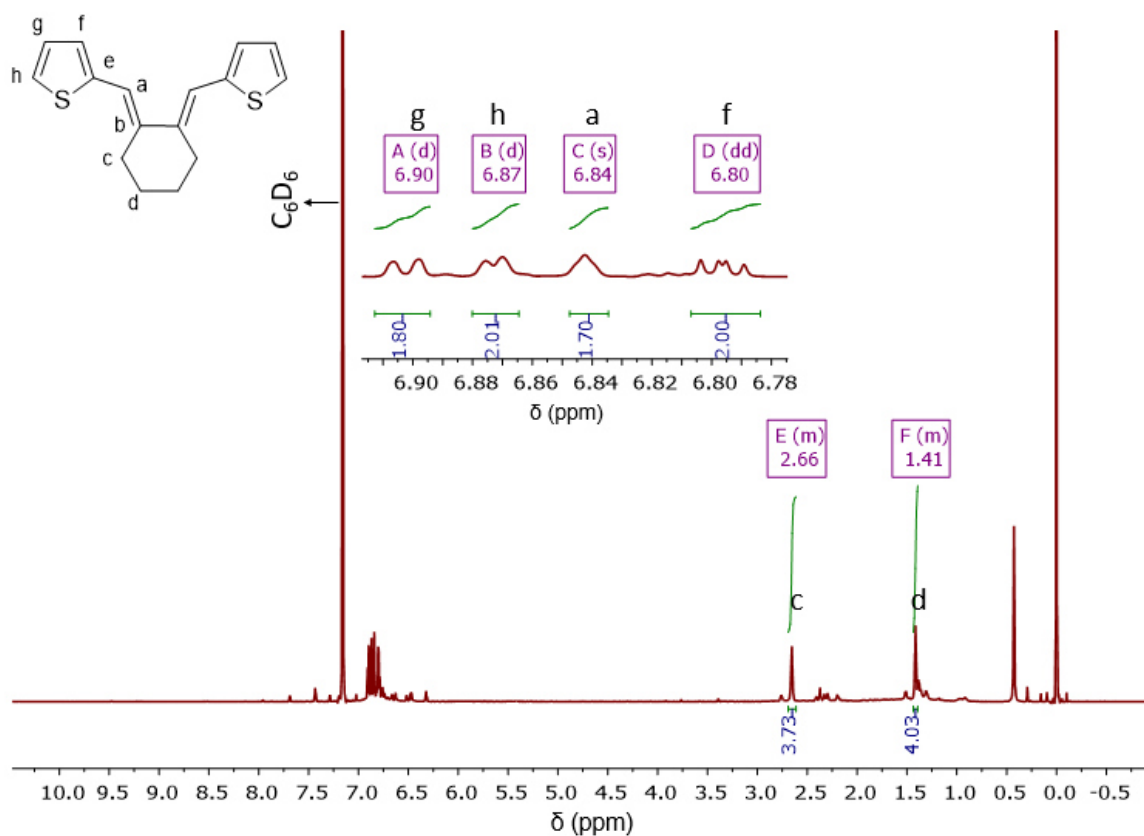


Figure S98. ^1H NMR (500 MHz) spectrum of (1*E*,2*E*)-1,2-bis(thiophen-2-ylmethylene)cyclohexane main product of the decomposition of zirconacyclopentadiene **11f** under air, in C_6D_6 .

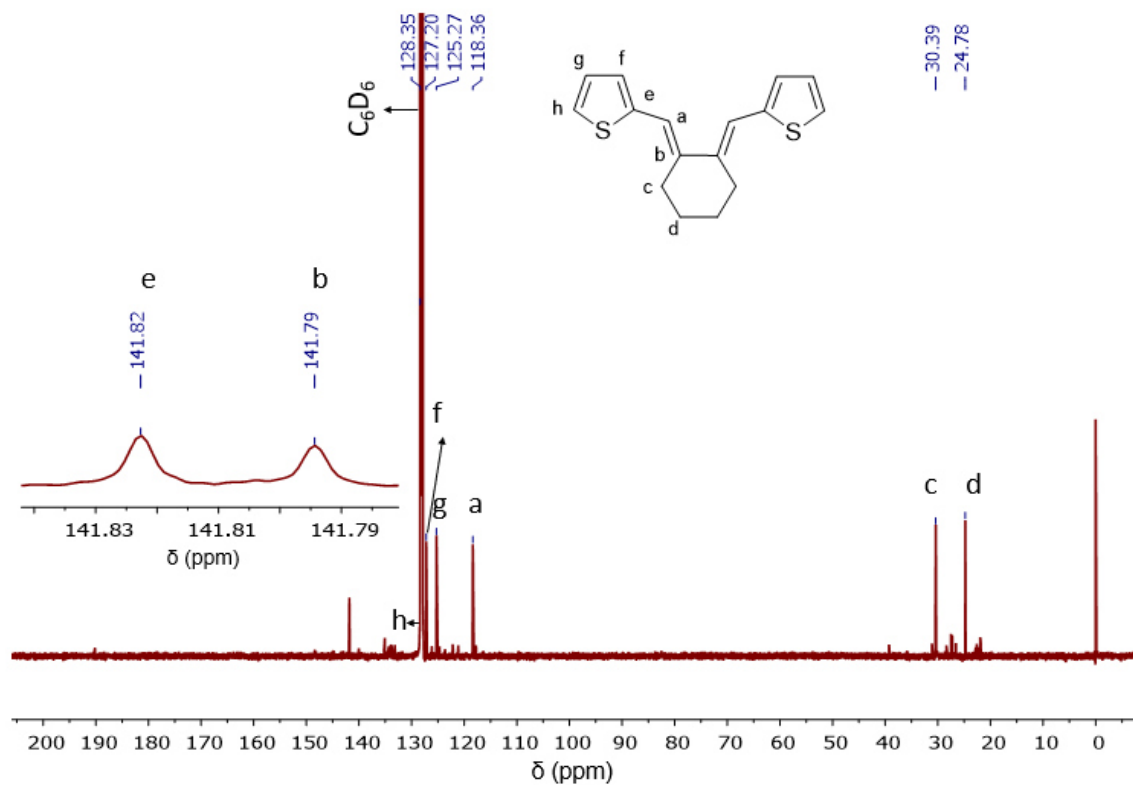


Figure S99. $^{13}\text{C}\{^1\text{H}\}$ NMR (126 MHz) spectrum of (1*E*,2*E*)-1,2-bis(thiophen-2-ylmethylene)cyclohexane main product of the decomposition of zirconacyclopentadiene **11f** under air, in C_6D_6 .

7 Crystal Structures

Table S3. Crystal data and structure refinement of **11d** and **11f**.

	11d	11f
Empirical formula	C ₂₆ H ₂₂ S ₂ Br ₂ Zr	C ₂₆ H ₂₄ S ₂ Zr
Formula weight	649.59	491.79
Temperature/K	100.0	100.0
Crystal system	monoclinic	monoclinic
Space group	P2 ₁ /c	P2 ₁ /c
a/Å	15.0327(11)	9.6714(3)
b/Å	8.6378(6)	12.0118(4)
c/Å	18.2944(17)	18.6458(7)
α/°	90	90
β/°	100.400(4)	99.1990(10)
γ/°	90	90
Volume/Å ³	2336.5(3)	2138.24(13)
Z	4	4
ρ _{calc} /cm ³	1.847	1.528
μ/mm ⁻¹	4.082	0.720
F(000)	1280.0	1008.0
Crystal size/mm ³	0.22 × 0.2 × 0.15	0.3 × 0.25 × 0.25
Radiation	MoKα (λ = 0.71073)	MoKα (λ = 0.71073)
2θ range for data collection/°	4.528 to 59.998	5.576 to 57
Index ranges	-21 ≤ h ≤ 21, -12 ≤ k ≤ 11, -25 ≤ l ≤ 25	-12 ≤ h ≤ 12, -16 ≤ k ≤ 16, -25 ≤ l ≤ 25
Reflections collected	55126	49315
Independent reflections	6820 [R _{int} = 0.0475, R _{sigma} = 0.0291]	5401 [R _{int} = 0.0225, R _{sigma} = 0.0120]
Data/restraints/parameters	6820/0/281	5401/18/300
Goodness-of-fit on F ²	1.041	1.078
Final R indexes [I >= 2σ (I)]	R ₁ = 0.0271, wR ₂ = 0.0534	R ₁ = 0.0230, wR ₂ = 0.0528
Final R indexes [all data]	R ₁ = 0.0378, wR ₂ = 0.0573	R ₁ = 0.0253, wR ₂ = 0.0542
Largest diff. peak/hole / e Å ⁻³	0.58/-0.64	0.48/-0.35
CCDC Number	1900225	Our experimental data is in agreement with the literature. ^[14]

Table S4. Crystal data and structure refinement of **11h** and **11i**.

	11h	11i
Empirical formula	C ₂₉ H ₂₄ Br ₂ Zr	C ₃₄ H ₃₆ F ₆ Si ₂ Zr
Formula weight	623.52	706.03
Temperature/K	100.0	100.0
Crystal system	triclinic	monoclinic
Space group	P-1	P2 ₁ /n
a/Å	9.0975(3)	9.2700(4)
b/Å	13.0160(4)	13.8588(6)
c/Å	22.4469(8)	26.4170(12)
α/°	74.3840(10)	90
β/°	83.3870(10)	93.081(2)
γ/°	70.9900(10)	90
Volume/Å ³	2419.18(14)	3388.9(3)
Z	4	4
ρ _{calc} /g/cm ³	1.712	1.384
μ/mm ⁻¹	3.773	0.450
F(000)	1232.0	1448.0
Crystal size/mm ³	0.35 × 0.2 × 0.15	0.2 × 0.2 × 0.15
Radiation	MoKα (λ = 0.71073)	MoKα (λ = 0.71073)
2θ range for data collection/°	4.738 to 59	4.584 to 66.472
Index ranges	-12 ≤ h ≤ 12, -18 ≤ k ≤ 18, -31 ≤ l ≤ 31	-14 ≤ h ≤ 14, -21 ≤ k ≤ 21, -40 ≤ l ≤ 40
Reflections collected	81502	81669
Independent reflections	13464 [R _{int} = 0.0704, R _{sigma} = 0.0347]	13006 [R _{int} = 0.0350, R _{sigma} = 0.0259]
Data/restraints/parameters	13464/0/578	13006/78/450
Goodness-of-fit on F ²	1.025	1.089
Final R indexes [I ≥ 2σ (I)]	R ₁ = 0.0244, wR ₂ = 0.0570	R ₁ = 0.0365, wR ₂ = 0.0854
Final R indexes [all data]	R ₁ = 0.0297, wR ₂ = 0.0585	R ₁ = 0.0485, wR ₂ = 0.0906
Largest diff. peak/hole / e Å ⁻³	0.75/-0.64	0.92/-0.87
CCDC Number	1900228	1900226

Table S5. Crystal data and structure refinement of **11j**, **11k** and **11l**.

	11j	11k	11l
Empirical formula	C ₃₂ H ₃₆ Si ₂ Zr	C ₄₅ H ₃₈ Zr	C ₄₀ H ₄₂ Si ₂ Zr
Formula weight	568.01	669.97	670.13
Temperature/K	100.0	100.0	100.0
Crystal system	monoclinic	triclinic	monoclinic
Space group	C2	P-1	C2/c
a/Å	12.1783(5)	11.0860(4)	21.8814(9)
b/Å	28.7591(12)	11.3088(4)	10.8845(4)
c/Å	24.7926(10)	14.1880(5)	14.3210(6)
α/°	90	90.1010(10)	90
β/°	95.4680(10)	108.9690(10)	98.3850(10)
γ/°	90	90.0260(10)	90
Volume/Å ³	8643.8(6)	1682.14(10)	3374.3(2)
Z	12	2	4
ρ _{calc} /cm ³	1.309	1.323	1.319
μ/mm ⁻¹	0.483	0.358	0.424
F(000)	3552.0	696.0	1400.0
Crystal size/mm ³	0.18 × 0.16 × 0.16	0.2 × 0.15 × 0.15	0.37 × 0.19 × 0.16
Radiation	MoKα (λ = 0.71073)	MoKα (λ = 0.71073)	MoKα (λ = 0.71073)
2θ range for data collection/°	4.952 to 54.966	4.706 to 55.994	4.922 to 61.14
Index ranges	-13 ≤ h ≤ 15, -37 ≤ k ≤ 37, -32 ≤ l ≤ 32	-14 ≤ h ≤ 14, -14 ≤ k ≤ 14, -18 ≤ l ≤ 17	-31 ≤ h ≤ 31, -15 ≤ k ≤ 15, -20 ≤ l ≤ 20
Reflections collected	80826	35430	36277
Independent reflections	19556 [R _{int} = 0.0316, R _{sigma} = 0.0316]	8114 [R _{int} = 0.0244, R _{sigma} = 0.0219]	5186 [R _{int} = 0.0359, R _{sigma} = 0.0243]
Data/restraints/parameters	19556/1/966	8114/0/480	5186/0/198
Goodness-of-fit on F ²	1.145	1.060	1.064
Final R indexes [I ≥ 2σ (I)]	R ₁ = 0.0373, wR ₂ = 0.0810	R ₁ = 0.0344, wR ₂ = 0.0910	R ₁ = 0.0282, wR ₂ = 0.0656
Final R indexes [all data]	R ₁ = 0.0399, wR ₂ = 0.0818	R ₁ = 0.0384, wR ₂ = 0.0939	R ₁ = 0.0369, wR ₂ = 0.0697
Largest diff. peak/hole / e Å ⁻³	1.04/-0.57	2.02/-0.60	0.45/-0.34
CCDC Number	1915992	1900380	1900227

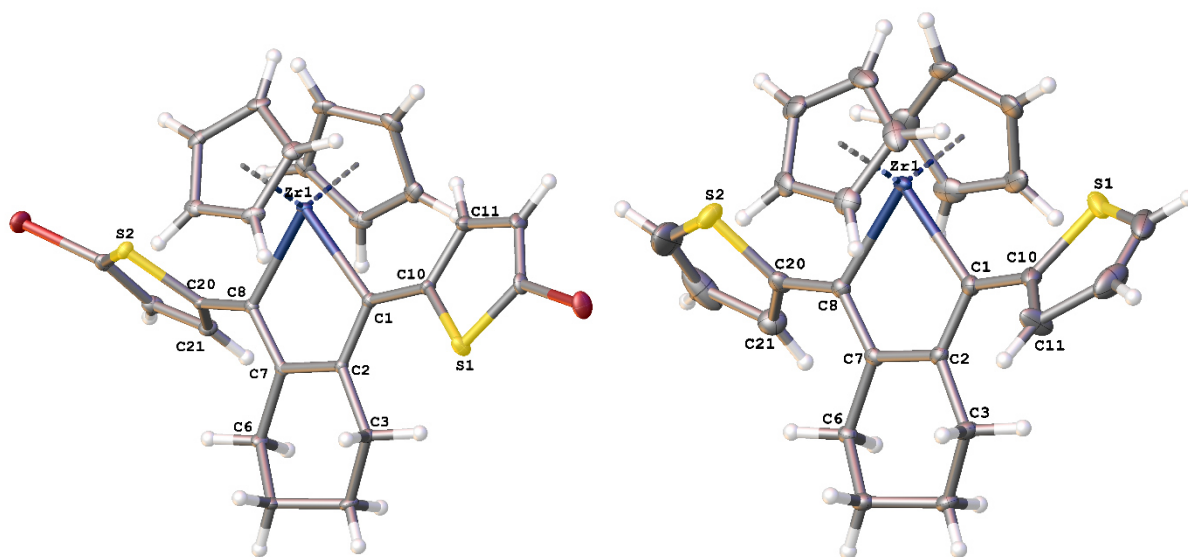


Figure S100. Molecular structures of **11d** and **11f** showing 50% probability ellipsoids and the crystallographic numbering scheme. Only the major parts of the disordered molecule of **11f** is shown for clarity.

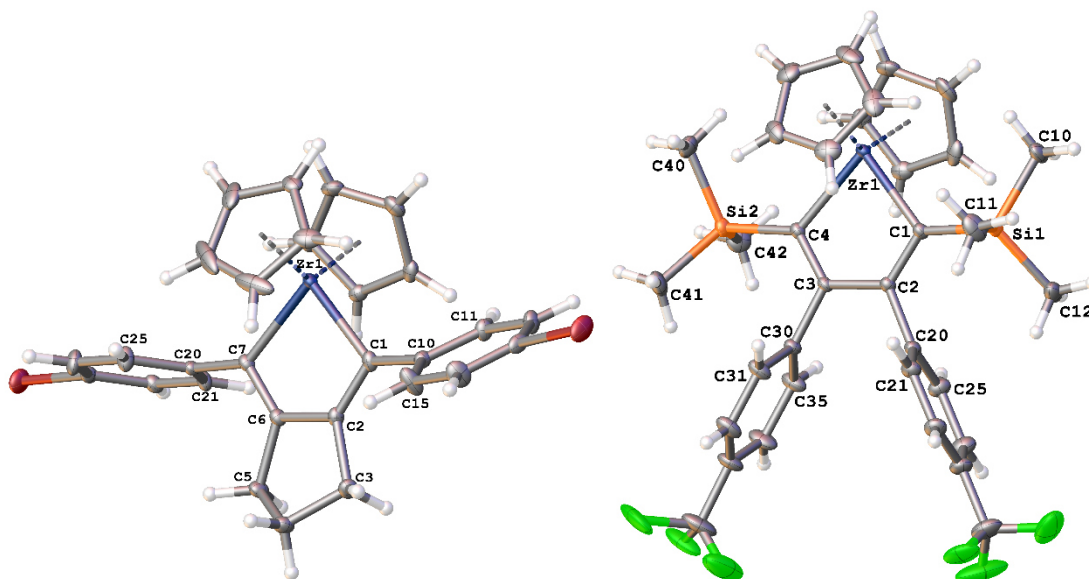


Figure S101. Molecular structures of **11h** (only one independent molecule is shown) and **11i** showing 50% probability ellipsoids and the crystallographic numbering scheme. Only the major parts of the disordered molecule of **11i** is shown for clarity.

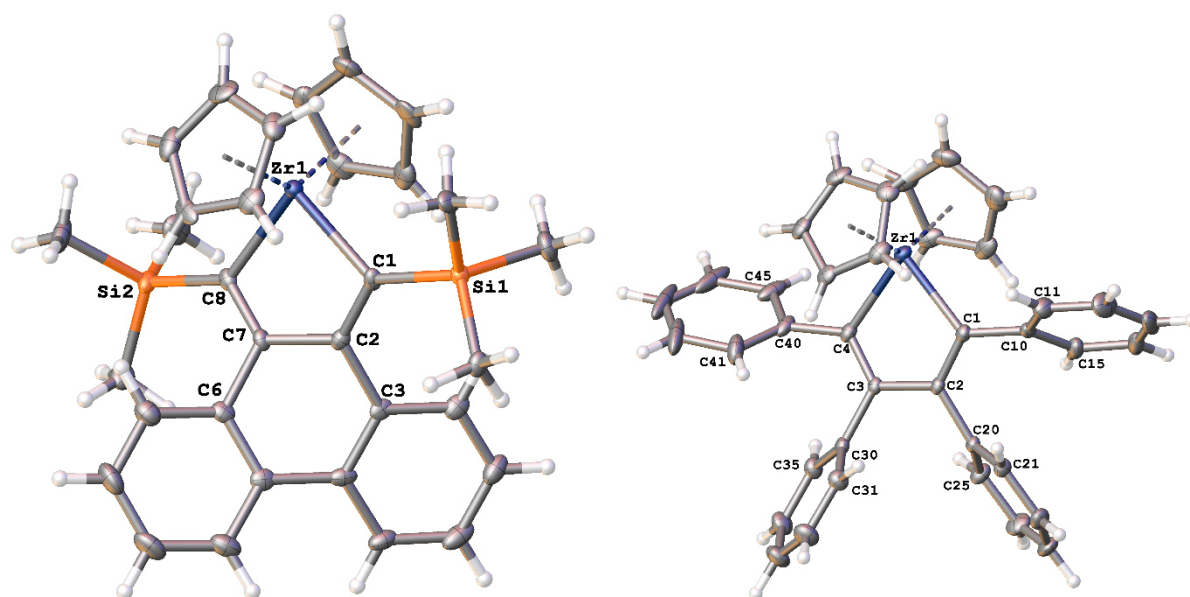


Figure S102. Molecular structures of **11j** and **11k** showing 50% probability ellipsoids and the crystallographic numbering scheme.

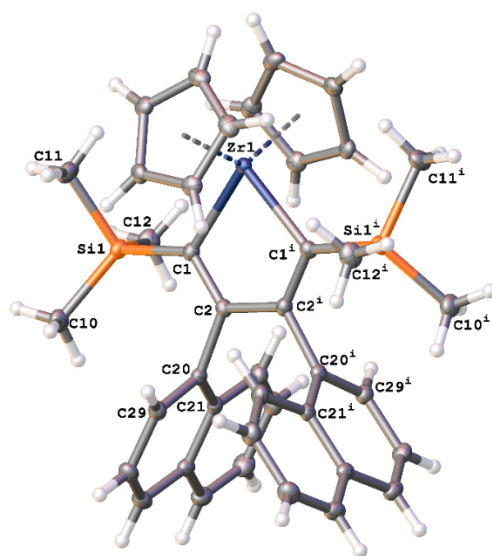


Figure S103. Molecular structure of **11l** showing 50% probability ellipsoids and the crystallographic numbering scheme.

Table S6. Selected Bond Parameters of Molecular Structures **11d**, **11f** and **11h**.

	11d	11f	11h
Bond lengths [Å] and angles [°]			
Zr(1)-C(1)	2.2878(2)	2.2619(2)	2.2468(2)
C(1)-C(2)	1.369(3)	1.3665(2)	1.361(2)
C(1)-C(10)	1.451(3)	1.460(2)	1.470(2)
C(2)-C(7)	1.481(3)	1.4866(2)	-
C(2)-C(6)	-	-	1.502(2)
C(2)-C(3)	1.525(3)	1.5199(2)	1.529(2)
C(2)-C(1)-Zr(1)	112.23(2)	112.84(2)	101.94(2)
C(8)-Zr(1)-C(1)	76.40(7)	76.52(5)	-
C(7)-Zr(1)-C(1)	-	-	86.12(6)
Zr(1)-C(1)-C(2)-C(7)	8.3(2)	7.58(2)	-
Zr(1)-C(1)-C(2)-C(6)	-	-	5.28(2)
Zr(1)-C(1)-C(10)- C(11)	-23.0(3)	125.5(6)	-65.3(2)

Table S7. Selected Bond Parameters of Molecular Structures **11i** and **11j**.

	11i	11j
Bond lengths [Å] and angles [°]		
Zr(1)-C(1)	2.2633(2)	2.250(5)
C(1)-C(2)	1.3660(2)	1.365(7)
C(1)-Si(1)	1.8723(2)	1.875(5)
C(2)-C(3)	1.5056(2)	1.505(7)
C(2)-C(20)	1.5005(2)	-
C(2)-C(1)-Zr(1)	105.71(9)	100.1(3)
C(1)-Zr(1)-C(4)	82.69(5)	-
C(1)-Zr(1)-C(8)	-	87.00(2)
Zr(1)-C(1)-C(2)-C(3)	-2.16(2)	155.5(4)
C(8)-Zr(1)-C(1)-C(2)	-	1.8(3)
C(1)-C(2)-C(20)-C(21)	75.78(2)	-

Table S8. Selected Bond Parameters of Molecular Structures **11k** and **11l**.

	11k	11l
Bond lengths [Å] and angles [°]		
Zr(1)-C(1)	2.2588(2)	2.2684(2)
C(1)-C(2)	1.359(2)	1.3667(2)
C(1)-Si(1)	-	1.8752(2)
C(1)-C(10)	1.483(2)	-
C(2)-C(3)	1.498(2)	-
C(2)-C(20)	1.499(2)	1.5079(2)
C(2)-C(1)-Zr(1)	109.09(2)	106.00(9)
C(1)-Zr(1)-C(4)	79.37(6)	-
Zr(1)-C(1)-C(2)-C(3)	-7.40(2)	-
C(1)-C(2)-C(20)-C(21)	54.6(2)	83.36(2)
Zr(1)-C(1)-C(10)-C(11)	71.8(2)	-

5.5. Experimental Section. Supporting Information Chapter 3.2.3.

General Considerations	344
Synthesis.....	350
NMR Spectra	361
Single Crystal Data.....	377

General Considerations

Abbreviations

ATR	attenuated total reflectance
br	broad
calcd.	calculated
δ	chemical shift in parts per million
COSY	correlated spectroscopy
Cp	cyclopentadienyl
DCM	dichloromethane
DSC	differential scanning calorimetry
DIPA	<i>N,N</i> -diisopropylamine
DMF	<i>N,N</i> -dimethylformamide
DEPT	distortionless enhancement by polarization transfer
d	doublet (NMR)
EI	electron impact
EtOAc	ethyl acetate
GPC	gel permeation chromatography
GB	glovebox
HMBC	heteronuclear multiple bond coherence
HSQC	heteronuclear single quantum coherence
HOMO	highest occupied molecular orbital
HR-MS	high resolution mass spectrometry
IR	infrared spectroscopy
LUMO	lowest unoccupied molecular orbital
λ_{\max}	maximum absorption wavelength
m	medium (IR)
m	multiplet (NMR)

NBS	<i>N</i> -bromosuccinimide
NIS	<i>N</i> -iodosuccinimide
NMR	nuclear magnetic resonance
ppm	parts per million
Ph	phenyl group
PL	photoluminescence
λ_{PL}	photoluminescence emission wavelength
\bar{D}	polydispersity index
R	resolution (mass spectrometry)
R_f	retention factor
s	singlet (NMR)
SPS	solvent purification system
s	strong (IR)
$\text{Cp}_2\text{Zr}(\text{pyr})(\text{Me}_3\text{SiC}\equiv\text{CSiMe}_3)$	Rosenthal's reagent
THF	tetrahydrofuran
TMS	tetramethylsilane
TGA	thermogravimetric analysis
TLC	thin layer chromatography
TEA	triethylamine
t	triplet (NMR)
UV-Vis	ultraviolet visible spectroscopy
w	weak (IR)

Chemicals and Solvents

All reactions were carried out using standard Schlenk techniques under a dry, inert nitrogen or argon atmosphere unless noted otherwise. Some reactions were performed inside a nitrogen filled glovebox from Inert Innovative Technology, Inc. Company (with < 0.1 ppm O₂ and < 0.1 ppm H₂O). Separations using centrifugation were carried out with a centrifuge EBA 20 from the company Hettich Zentrifugen. All dry solvents were obtained from the solvent purification system (SPS), degassed by freeze-pump-thaw cycles and stored under a nitrogen atmosphere unless noted otherwise. All chemicals were commercially available and were used without further purification unless noted otherwise.

The preparation of the 1,8-bis(trimethylstannyl)octa-1,7-diyne (**M2-10b**), 1,8-bis(4,4,5,5-Tetramethyl-1,3,2-dioxaborolan-2-yl)octa-1,7-diyne (**M2-10b**) and the Rosenthal reagent (**M2-9**) were already described in the supporting information of chapter 3.2.2. (See chapter 5.4.). The synthesis of 2-Bromo-4-hexyl-5-iodothiophene (**44**) and 2-Bromo-3-n-

hexylthiophene (**42**) was described in the supporting information of the chapter 3.1.3. (see chapter 5.2.). The synthesis of 2-bromo-3-hexyl-5-iodothiophene (**P1-1**) was described in the experimental part from *Tetrahedron*, **2015**, *71* (33), 5399-5406 (see Chapter 5.3.).

Reagent	Supplier	Purity	Comments
Ammonium chloride	Carl Roth	≥ 99.5%	
2-Bromothiophene	Sigma Aldrich	98%	
Copper (I) chloride	Alfa Aesar	99.999%	stored in a glove box (GB)
Copper (I) iodide	Alfa Aesar	99.998%	stored in a GB
<i>n</i> -Butyllithium	Acros Organics	n. a.	2.5 M in hexanes
Diphenyltin dichloride	VWR Chemicals	96%	distilled
Iodine	AppliChem	Pure Ph. Eur.	
2-Iodothiophene	TCI	≥ 98%	
Magnesium sulfate	Grüssing	99%	
<i>N</i> -Iodosuccinimide	MOLEKULA	95%	
1,7-Octadiyne	VWR Chemicals	98%	
[PdCl ₂ (dppf)]	Sigma Aldrich	n.a.	
[Pd(PPh ₃) ₄]	TCI	> 97%	stored in a freezer in a GB
[Pd(<i>t</i> Bu ₃ P) ₂]	TCI	> 98%	Stored in a freezer in a GB
Sodium carbonate	VWR Chemicals	n.a.	ACS, Reag. Ph. Eur.
Sodium hydrogen carbonate	VWR Chemicals	n.a.	ACS, Reag. Ph. Eur.
Sodium sulfate	Grüssing	99%	
Sodium thiosulfate	Grüssing	97%	
<i>p</i> -Toluenesulfonic acid·H ₂ O	Acros Organics	97.5 %	
Trimethylstannyl chloride	Sigma Aldrich	99 %	Stored in a GB
Zirconocene dichloride	abcr	99%	stored in a freezer inside a GB
Bis(trimethylsilyl)acetylene	Sigma Aldrich	99%	stored in a freezer in a GB

Table 5: List of supplier and purity of used chemicals.

Solvent	Comments
Acetic acid	Alfa Aesar, 99+%
Chloroform	VWR Chemicals; ACS, Reag. Ph. Eur.
Dichloromethane	VWR Chemicals; for HPLC; dry from the SPS
Diethyl ether	VWR Chemicals; for HPLC; dry, distilled from sodium / benzophenone
Dioxane	ABC R GmbH, distilled and degassed by SPT
<i>N,N</i> -Dimethylformamide	Extra dry from Acros Organics; 99.8%
Ethyl acetate	VWR Chemicals; ACS, Reag. Ph. Eur.
Ethanol	VWR Chemicals, ACS, Reag. Ph. Eur.
<i>n</i> -Hexane	VWR Chemicals; ACS, Reag. Ph. Eur.
<i>n</i> -Pentane	VWR Chemicals; for HPLC; dry from the SPS and degassed
Pyridine	Acros Organics 99.8%; dried over KOH, degassed, stored over 4 Å molecule sieves
Triethylamine	Grüssing; 99%; dry, distilled over CaH ₂ ; degassed
<i>t</i> -Butanol	VWR Chemicals, ACS, Reag. Ph. Eur.
Tetrahydrofuran	VWR Chemicals; for HPLC; dry from the SPS and degassed
Toluene	VWR Chemicals; for HPLC; dry, from the SPS and degassed

Table 6: List of suppliers and purity of used solvents.

Analytical Instruments

¹H NMR, ¹³C{¹H} NMR, ¹¹B{¹H} NMR and ¹¹⁹Sn{¹H} NMR spectrum were recorded on a Bruker Avance Neo 500 (for isolated compounds and kinetic experiments). All ¹H NMR and ¹³C{¹H} NMR were referenced against the solvent residual proton signals (¹H), or the solvent itself (¹³C). ¹¹⁹Sn{¹H} NMR spectrum were calculated based on the ¹H NMR spectrum of TMS. ¹¹B{¹H} NMR spectrum were referenced against BF₃·Et₂O in CDCl₃. All chemical shifts δ are given in parts per million (ppm) and all coupling constants *J* in Hz. The exact elucidation of the compounds was proved by ¹H, ¹³C DEPT and two-dimensional NMR spectroscopy such as ¹H COSY, ¹³C{¹H} HSQC or ¹H/¹³C{¹H} HMBC when possible.

Electron impact (EI) ionization mass spectra were recorded on a double focusing mass spectrometer MAT 95+ or MAT 8200 from FINNIGAN mat. Samples were measured by direct

inlet or indirect inlet method with a source temperature of 200° C. The ionization energy of the electron impact ionization was 70 eV. All signals were reported with the quotient from mass to charge m/z . Accurate masses were determined via the peak-matching method. The resolution (R) of the peak-matching performance was 10 000. The calculated isotopic distribution for each ion agreed with experimental values.

High-resolution accurate-mass electrospray ionization (ESI) spectra were recorded on a Bruker Daltonics microTOF II mass spectrometer. High resolution accurate-mass MALDI mass spectrum and MALDI MS analysis of the polymers **47**, **56** and **61** were recorded on a Bruker Daltonics ultrafleXtreme TOF/TOF mass spectrometer using graphite as the matrix. IR spectra were recorded on a NICOLET Thermo IS10 SCIENTIFIC IR spectrometer with a diamond-ATR-unit. The resolution was 4 cm^{-1} . Relative intensities of the IR bands were described by s = strong, m = medium or w = weak.

UV-Vis measurements were recorded on a Jasco spectrometer model V-630, with dichloromethane as a solvent.

Fluorescence measurements were recorded on a Photon Technology International spectrometer with a lamp power supply LPS-220B, Motor Driver MD-5020 and 1Photomultiplier 814. Dichloromethane was used as a solvent.

All melting points were measured with a BÜCHI Melting Point M-560 using a heating ramp of 5 K / min.

Thin layer chromatography (TLC) was carried out on aluminium plates coated with silica gel 60 F₂₅₄ with a layer thickness of 0.2 mm from Fluka or Macherey-Nagel. All bands were detected by using a fluorescent lamp (254 nm and 366 nm). Column chromatography was carried out by using the column machine PuriFlash 4250 from Interchim. Silica gel columns of the type PF-15SiHP-F0012, PF-15SiHP-F0025, PF-50SiHP-JP-F0080, PF-50SiHP-JP-F0120, and PF-50SiHP-JP-F0220 were used. The injection of the sample was made via dry load. The column material of the dry load was Celite 503 from Macherey-Nagel.

The molecular weight and molecular weight distribution of all synthesized polymers were determined using a PSS GPC/SEC system 1260/1290. The system was equipped with three PSS-SDV high combination columns (styrene-divinylbenzene copolymer network) with a molecular range from 100-3000 kDa, a refractive index detector (SECurity RID Article Nr. 404-0106), a diode array detector (SECurity DAD Article Nr. 404-0110), a viscometer detector (DVD 1260 Article Nr. 404-0025) and a Light Scattering Detector with 3D spectrum option (SECcurity Multichrom SLD 1000 Article Nr. 404-0196). The columns were heated at 35 °C using a column thermostat (SECcurity TCC6000). THF (HPLC grade without stabilizer) was used as an eluent. The measurements were recorded at 35° C under an eluent flow of 1 mL/min. The apparatus was calibrated using polystyrene standards (PSS) with a conventional calibration.

The electrochemical studies were carried out under argon using an Eco Chemie Autolab PGSTAT 30 potentiostat for cyclic voltammetry with the three-electrode configuration: the working electrode was a platinum disk; the reference electrode was a saturated calomel electrode and the counter-electrode was a platinum wire. All potentials were internally referenced to the ferrocene/ ferrocenium couple. For the measurements, concentrations of 10^{-3} M of the electroactive species were used in freshly distilled and degassed dichloromethane and 0.2 M tetrabutylammonium hexafluorophosphate as the electrolyte.

TGA measurements were performed on a Mettler Toledo DSC 3/TGA + STAR system using aluminium crucibles and under a flow of nitrogen of 20 mL/min.

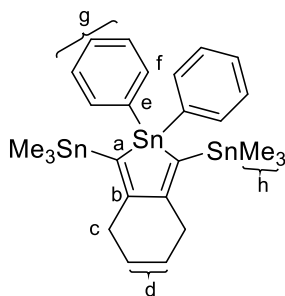
DSC measurements were performed on a Mettler Toledo DSC 3+ STAR system using aluminium pans, under nitrogen atmosphere and a heat flow of 10 K/min.

Crystallography

Single crystals of size ~ 0.3 mm were chosen using a polarizing microscope and mounted on a goniometer head using perfluorinated oil. X-ray diffraction data were collected on a four-circle diffractometer with a Complementary Metal–Oxide–Semiconductor (CMOS) area detector and a microfocus source using Mo K α radiation ($\lambda = 0.71073$ Å) at 100K. The crystal to detector distance was fixed at 40 mm, and the scan width ($\Delta\omega$) was 0.5° per frame during the data collection. The data collection strategy was chosen in such a way as to yield a dataset with $d = 0.7$ Å resolution yet having both high and low angle frames. Cell refinement, data integration, and reduction with face indexing for accurate numerical absorption correction were carried out using the Apex2 software. Data merging and space group determination were performed by XPREP. The crystal structure was solved by direct methods using SHELXS97 and refined according to the spherical-atom approximation (based on F^2) using SHELXL97^[93] included in the WinGX suite.^[94] The hydrogen atoms were fixed stereochemically and the position and isotropic thermal parameters were allowed to refine in the spherical atom model.

Synthesis

2,2-Diphenyl-1,3-bis(trimethylstannyl)-4,5,6,7-tetrahydro-2H-benzo[*c*]stannole (48)



In a glovebox, a solution of 1,8-bis(trimethylstannyl)octa-1,7-diyne (**M2-10a**) (447 mg, 1.03 mmol) and $\text{Cp}_2\text{Zr}(\text{pyr})(\text{Me}_3\text{SiC}\equiv\text{CSiMe}_3)$ (**M2-9**) (488 mg, 1.03 mmol) in toluene (10 mL) was stirred for 2 h at 20 °C. Over this time the mixture turned to bright orange. Ph_2SnCl_2 (354 mg, 1.03 mmol), CuCl (10.2 mg, 103 μmol , 10 mol%) and toluene (2 mL) were added. The reaction was stirred at 20 °C for 3 h, until the mixture turned to dark green.

Outside the glovebox, the reaction was quenched with water (50 mL) and the aqueous layer was extracted with DCM (3 x 100 mL). The combined organic layers were dried over MgSO_4 . After filtration, the volatiles were removed *in vacuo* and the residue was filtered over a short plug of silica using diethyl ether as eluent. After the volatiles were removed in the second filtration, the orange pink oil was filtered by third and last time using deactivated silica (hexane : TEA 10 %) and pentane as eluent to afford a white-pink solid in a yield of 329 mg (45 %, 465 μmol). Single crystals were obtained from a saturated *n*-pentane solution.

M.p.: 77 °C.

$^1\text{H NMR}$ (500.1 MHz, C_6D_6): δ = 7.78 - 7.66 (m, 4H, f), 7.20 – 7.17 (m, 6H, g), 2.70 (t, 3J = 6.7 Hz, 4H, c), 1.72 – 1.47 (m, 4H, d), 0.42 – 0.13 (m, 18H, h; $^2J(^{119}\text{Sn}-^1\text{H})$ = 27 Hz) ppm.

$^{13}\text{C}\{^1\text{H}\}$ NMR (126 MHz, C_6D_6): δ = 166.5 (b), 141.5 (a), 140.2 (e), 137.8 (f), 129.3 (g), 38.0 (c), 24.7 (d), -7.6 (h) ppm.

$^{119}\text{Sn}\{^1\text{H}\}$ NMR (187 MHz, C_6D_6): δ = -35.28, -43.72 ppm.

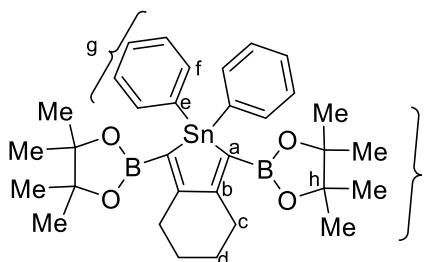
IR (ATR): $\tilde{\nu}$ = 2956(m), 1432 (m), 1262 (s), 1079 (m), 1026 (m), 712 (s), 516 (s) cm^{-1} .

HR-MS (EI, $\text{C}_{26}\text{H}_{36}^{120}\text{Sn}_3$) m/z : calcd. 707.9883, found 707.9883 (R = 10000).

MS (EI, 70 eV, direct inlet, 200 °C): m/z (% relative intensity) = 707 (31) $[\text{M}]^+$, 688.8 (100).

λ_{max} (DCM) = 267 and 316 nm.

2,2-Diphenyl-1,3-bis(4,4,5,5-tetramethyl-1,3,2-dioxaborolan-2-yl)-4,5,6,7-tetrahydro-2H-benzo[c]stannole (49)



In a glovebox, a solution of 1,8-bis(4,4,5,5-tetramethyl-1,3,2-dioxaborolan-2-yl)octa-1,7-diyne (**M2-10b**) (363 mg 1.01 mmol) and $\text{Cp}_2\text{Zr}(\text{pyr})(\text{Me}_3\text{SiC}\equiv\text{CSiMe}_3)$ (**M2-9**) (488 mg, 1.03 mmol) in toluene (10 mL) was stirred for 2h at 20 °C. After a color change to dark red, Ph_2SnCl_2 (348 mg, 1.01 mmol), CuCl (10.0 mg, 101 μmol , 10 mol%) and THF (5 mL) were added to the solution. The mixture was stirred for 6 h at 20 °C until the mixture turned to red-brown color.

Outside the glovebox, the reaction was quenched with water (50 mL) and the aqueous layer was extracted with chloroform (3 x 50 mL). The combined organic layers were dried over MgSO_4 . After filtration, the solvent was removed *in vacuo* and the residue filtered over a short plug of deactivated silica (*n*-hexane/ TEA 10%) using *n*-pentane as eluent. The solvent was removed *in vacuo*, diethyl ether (10 mL) was added and the mixture was centrifuged. The soluble organic phase was concentrated, and the crude solid was crystallized in cyclohexane to afford a colorless solid in a yield of 264 mg (41%, 418 μmol). Single crystals were obtained from a saturated of cyclohexane solution.

M.p.: 165 °C.

^1H NMR (500.1 MHz, C_6D_6): δ = 8.11 - 8.08 (m, 4H, f), 7.31 - 7.23 (m, 6H, g), 3.19 - 3.14 (m, 4H, c), 1.60 - 1.56 (m, 4H, d), 1.07 (s, 24H, i) ppm.

$^{13}\text{C}\{^1\text{H}\}$ NMR (126 MHz, C_6D_6):⁴ δ = 171.0 (b), 141.2 (e), 137.9 (f), 128.7 (g), 82.9 (h), 33.6 (c), 25.0 (d), 23.2 (i) ppm.

$^{119}\text{Sn}\{^1\text{H}\}$ NMR (187 MHz, CDCl_3): δ -34,67 ppm.

$^{11}\text{B}\{^1\text{H}\}$ NMR (160 MHz, C_6D_6): δ = 22.4 ppm.

IR (ATR): $\tilde{\nu}$ = 2975 (w), 2923 (w), 1577 (w), 1430 (m), 1369 (m), 1316 (s), 1265 (m), 1138 (s), 1074 (w), 966 (w), 847 (s), 727 (s), 696 (s), 672 (m) cm^{-1} .

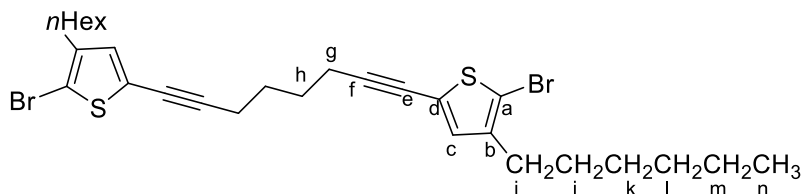
HR-MS (ESI, positive, MeOH, $[\text{M}+\text{H}]^+$, $\text{C}_{32}\text{H}_{42}^{11}\text{B}_2\text{O}_4^{120}\text{Sn}$) m/z : calcd for 633.23639 Found 633.23770.

⁴ The carbon a was not possible to identify, because the quadrupole moment of the adjacent boron atom.

MS (EI, 70 eV, direct inlet, 200 °C): m/z (% relative intensity) = 632 (12) $[M]^+$, 355(100) $[M-C_{18}H_{18}BO_2]^+$.

λ_{\max} (DCM) = 270 nm.

1,8-bis(5-Bromo-4-hexylthiophen-2-yl)octa-1,7-diyne (73)^[78]



In a glovebox, in a Schlenk flask, a solution of **P1-1** (5.40 g, 14.5 mmol), $[Pd(Ph_3)_4]$ (347 mg, 300 μ mol, 4 mol%) CuI (57 mg, 299 μ mol, 4 mol%) and TEA (6 mL) in DMF (12 mL) was stirred at 20 °C. After the addition of 1,7-octadiyne (769 mg, 7.25 mmol), the yellow-brown suspension was stirred under a nitrogen atmosphere at 55 °C for 21 h. Outside the glovebox, the reaction mixture was quenched with a saturated solution of NH_4Cl (100 mL) and extracted with diethyl ether (4 x 60 mL). The organic layers were dried over $MgSO_4$, filtered and concentrated *in vacuo*. The crude product was purified via flash chromatography (silica gel, *n*-hexane; R_f = 0.37) to afford a yellow oil on a yield of 3.81 g (88%, 6.41 mmol).

1H NMR (500 MHz, $CDCl_3$) 6.81 (s, 2H, c), 2.52 - 2.47 (m, 4H, i), 2.47 - 2.44 (m, 4H, g), 1.76 - 1.70 (m, 4H, h), 1.63 - 1.47 (m, 4H, j)*, 1.36 - 1.24 (m, 12H, k/l/m), 0.88 (dd, $^3J = 9.2, 4.6$ Hz, 6H, n) ppm.

* overlapping with the water signal.

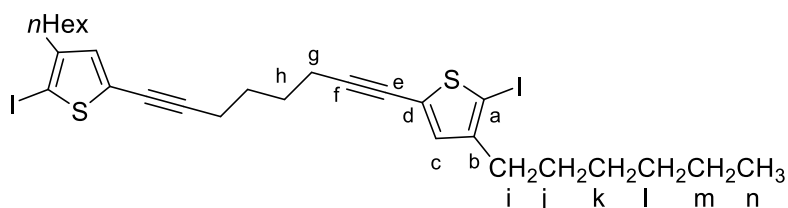
$^{13}C\{^1H\}$ NMR (126 MHz, $CDCl_3$) 142.1 (b), 132.2 (c), 123.9 (d), 108.5 (a), 94.8 (f), 73.9 (e), 31.7, 29.7, 22.7 (k/l/m), 29.5 (i), 29.0 (j), 27.7 (h), 19.4 (g), 14.2 (n) ppm.

IR (ATR): $\tilde{\nu}$ = 2925 (s), 2856 (s), 1547 (w), 1441 (m), 1324 (m), 1196 (m), 1006 (w), 834 (s), 733 (w), 661 (w), 581 (w), 534 (m) cm^{-1} .

HR-MS (ESI, $[M-H]^+$, $C_{28}H_{36}^{79}Br_2S_2$) m/z : calcd. 594.0625, found 594.0620 ($R = 10000$).

MS (EI, 70 eV, direct inlet, 200 °C): m/z (% relative intensity) = 594 (26) $[M]^+$, 84 (100).

The NMR data agree with the data found in the literature.^[78]

1,8-bis(4-Hexyl-5-iodothiophen-2-yl)octa-1,7-diyne (74)^[78]

n-Butyllithium (10.4 mL, 24.9 mmol; 2.5 M in hexanes) was added dropwise within 2 min to a solution of **73** (6.75 mg, 11.3 mmol) in THF (100 mL) at -78 °C. The orange suspension was stirred for 15 min and iodine (6.90 g, 27.2 mmol) in THF (20 mL) was added within 5 min. The red solution was allowed to warm to 20 °C after removal of the cooling bath. The reaction mixture was then quenched with a saturated solution of Na₂S₂O₃ (13 mL). The aqueous layer was extracted with diethyl ether (3 x 50 mL) and the combined organic layers were dried with MgSO₄. After filtration, the volatiles were removed *in vacuo*. The crude product was purified by column chromatography (silica gel, *n*-hexane; R_f = 0.21) to afford a pale-yellow oil in a yield of 7.20 g (92 %, 10.4 mmol).

¹H NMR (500 MHz, CDCl₃) 6.75 (s, 2H, c), 2.50 - 2.44 (m, 8 H, g/i), 1.76 - 1.69 (m, 4H, h), 1.57 - 1.47 (m, 4H, j)*, 1.37 - 1.28 (m, 12H, k/l/m), 0.91 - 0.85 (m, 6H, n) ppm.

* overlapping with the water signal.

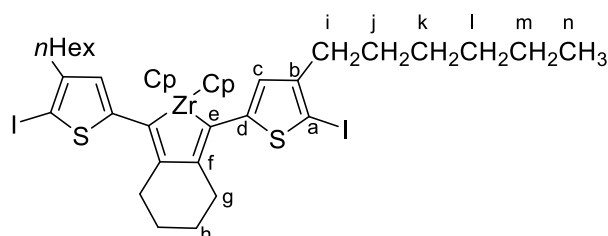
¹³C{¹H} NMR (126 MHz, CDCl₃) 147.3 (b), 131.8 (c), 128.9 (d), 95.7 (f), 74.2, 74.0 (a/e), 32.4, 29.0, 22.7 (k/l/m), 31.8, 19.4 (g/i), 30.0 (j), 27.7 (h). 14.1 (l) ppm.

IR (ATR): $\tilde{\nu}$ = 2924 (s), 2854 (s), 1704 (w), 1538 (w), 1457 (m), 1362 (m), 1324 (m), 1263(w), 1194(m), 835 (s), 738 (s), 658 (w), 560 (w), 533 (m) cm⁻¹.

HR-MS (ESI, C₂₈H₃₆I₂S₂) *m/z*: calcd. 690.03480, found 691.03711 (R= 10000).

MS (EI, 70 eV, direct inlet, 200 °C): *m/z* (% relative intensity) = 690 (100) [M]⁺, 662 (6) [M-C₂H₄]⁺.

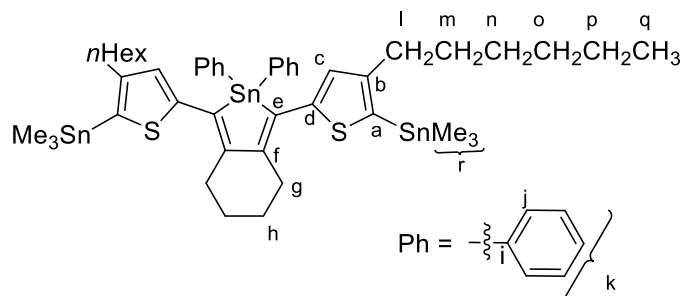
The NMR data agree with the data found in the literature.^[78]

Zirconacyclopentadiene (75)

In a glovebox, **74** (100 mg, 145 μmol) and Cp₂Zr(pyr)(Me₃SiC≡CSiMe₃) (68 mg, 0.14 mmol) were dissolved in toluene (5 mL) and the solution was stirred for 2 h at 20 °C. Over this time the mixture turned to bright orange. The volatiles were removed *in vacuo* to afford a yellow oil in a yield of 124 mg (90 %, 136 μmol).

λ_{\max} (DCM) = 440 nm.

1,3-bis(4-Hexyl-5-(trimethylstannyl)thiophen-2-yl)-2,2-diphenyl-4,5,6,7-tetrahydro-2H-benzo[c]stannole (76)



In a glovebox, a mixture of **70** (504 mg, 523 μmol), $[\text{Pd}(\text{Ph}_3)_4]$ (60 mg, 52 μmol , 10 mol%) and $(\text{SnMe}_3)_2$ (343 mg, 1.04 mol) in toluene (4 mL) was prepared in a microwave vial. The mixture was heated to 120 $^\circ\text{C}$ in a microwave apparatus for 30 min. The volatiles were removed *in vacuo* and the crude product was filtrated using deactivated silica (*n*-hexane : TEA 5%) and *n*-hexane as eluent (R_f = 0.48). The crude product was crystallized using a mixture cyclohexane/DCM to afford a bright yellow solid in a yield of 359 mg (66%, 345 μmol).

M.p.: 131 $^\circ\text{C}$.

^1H NMR (500.1 MHz, C_6D_6): δ = 7.67 – 7.62 (m, 4H, j), 7.35 (dd, $^3J = 6.3, 3.5$ Hz, 6H, k), 6.93 (s, 2H, c), 2.91 - 2.85 (m, 4H, g), 2.49 - 2.41 (m, 4H, l), 1.82 - 1.76 (m, 4H, h), 1.48 – 1.39 (m, 4H, m), 1.28 – 1.18 (m, 12H, n/o/p), 0.91 - 0.79 (m, 6H, q), 0.43 - 0.26 (m, 18H, r, $^2J(^{119}\text{Sn}-^1\text{H}) = 28$ Hz) ppm.

$^{13}\text{C}\{^1\text{H}\}$ NMR (126 MHz, C_6D_6): δ = 150.9 (d), 150.3 (b), 149.2 (f), 137.2 (i), 137.2 (j), 133.7 (a), 132.3 (c), 129.0 (e), 128.6 (k), 31.7 (g), 32.4 (l), 31.6, 29.0, 31.7 (n/o/p) 22.4 (h), 14.0 (q), -7.9 (r) ppm.

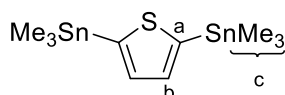
$^{119}\text{Sn}\{^1\text{H}\}$ NMR: δ = -37.72, -83.5 ppm.

IR (ATR): $\tilde{\nu}$ = 2924(s), 2853 (m), 2365 (w), 1429 (m), 1329 (m), 1141 (m), 1023 (m), 852 (w), 812 (m), 724 (s), 695 (s) cm^{-1} .

HR-MS (ESI, $\text{C}_{46}\text{H}_{64}\text{S}_2^{119}\text{Sn}_3$) m/z : calc. 1036.15184, found 1036.15130.

MS (EI, 70 eV, direct inlet, 200 $^\circ\text{C}$): m/z (% relative intensity) = 1040 (100) M^+ .

λ_{\max} (DCM) = 437 nm.

2,5-bis(trimethylstannyl)thiophene (71)^[95]

n-Butyllithium (8 mL, 20 mmol, 2.5 M in hexanes) was added dropwise within 10 min to a solution of thiophene (841 mg, 10.0 mmol) and TMEDA (2.22 g, 19.0 mmol) in *n*-hexane (13 mL) at 0 °C under a nitrogen atmosphere. The reaction mixture was heated to reflux for 45 min. The suspension was cooled to 0 °C and a solution of Me₃SnCl (3.98 g, 20.0 mmol) in THF (7.5 mL) was added. After removal of the cooling bath, the reaction mixture was stirred at 24 °C for 15 h and then quenched with a saturated solution of NH₄Cl (40 mL). The aqueous layer was extracted with diethyl ether (3 x 40 mL) and the combined organic layers were washed with brine (2 x 20 mL). The organic layers were dried over MgSO₄, filtered and the volatiles were removed *in vacuo*. The side products were removed partly by sublimation (40 °C, 2 x 10⁻¹ mbar) and the residue was sublimed (80 °C, 9 x 10⁻² mbar) to afford a white solid in a yield of 1.97 g (48%, 4.78 mmol, *Lit.* yield 51%).

m.p.: 95.5 °C.

¹H NMR (500.1 MHz, CDCl₃): δ = 7.40-7.33 (m, 2H, b), 0.43-0.30 (m, 18 H, c; ²J(¹¹⁹Sn-¹H) = 29 Hz) ppm.

¹³C{¹H} NMR (126 MHz, CDCl₃): δ = 143.18 (a), 135.96 (b), -8.04 (c; ¹J(¹¹⁹Sn-¹³C) = 185 Hz) ppm.

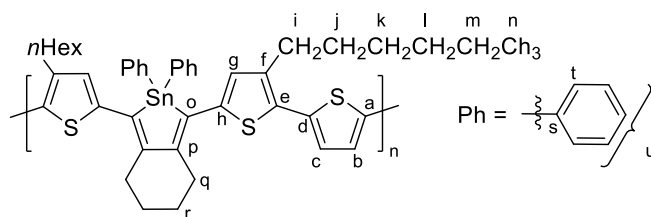
¹¹⁹Sn{¹H} NMR (187 MHz, CDCl₃): δ = -28.14 ppm.

IR (ATR): $\tilde{\nu}$ = 3057 (w), 2982 (w), 2913 (w), 1564 (w), 1477 (w), 1390 (w), 1199 (w), 1255 (w), 1187 (w), 953 (m), 921 (w), 797 (s), 761 (s), 734 (s), 531 (s), 515 (s) cm⁻¹.

HR-MS (EI, C₁₀H₂₀SSn₂) *m/z*: calcd. 407.93204, 409.93216, 411.93280, found 407.93146, 409.93214, 411.93241 (R = 10000).

MS (EI, 70 eV, direct inlet, 200 °C): *m/z* (%) = 411 (8) [M]⁺, 395 (100) [M-CH₃]⁺, 365 (6) [M-C₃H₉]⁺.

Polymer Containing Thiophene and Thionyl Moieties with a Ratio of 3 : 1 (72)



An orange-red solution of **70** (144 mg, 150 μmol), $[\text{Pd}(\text{PPh}_3)_4]$ (8.7 mg, 7.5 μmol , 5 mol%) and 2,5-bis(trimethylstannyl)thiophene (**71**) (61.4 mg, 150 μmol) in toluene (5 mL) was prepared in a glovebox in a microwave vial. The mixture was heated in a microwave apparatus for 2 h at 120 $^\circ\text{C}$. Then, the volatiles were removed *in vacuo* and the crude product was purified by Soxhlet extraction, first with methanol (200 mL) heating the system at 100 $^\circ\text{C}$ for 10 h. After oligomers and small molecules were removed, the solvent was changed to DCM and the system has heated at 80 $^\circ\text{C}$ for 6 h. The volatiles were removed *in vacuo* to afford a purple solid in a yield of 21.3 mg (18%).

^1H NMR (500.1 MHz, C_6D_6): δ = 7.75 – 7.61 (m, 4H, t), 7.44 – 7.33 (m, 6H, u), 7.07 (d, J = 18.3 Hz, 2H, c/b), 6.82 (broad, 2H, g), 2.90 (s, 2H, q), 2.77 – 2.62 (m, 2H, i), 1.83 (broad, 2H, r), 1.66 – 1.47 (m, 2H, j), 1.40 – 1.07 (m, 6H, k/l/m), 0.87 (broad, 3H, n) ppm.

$^{13}\text{C}\{^1\text{H}\}$ NMR (126 MHz, C_6D_6): δ = 146.0 (p), 143.6 (h), 139.5 (o), 138.7 (f), 137.6 (t), 136.5 (a), 135.1 (s), 133.7 (g), 130.7 (e), 129.8 (d), 129.3 (u), 125.8 (c/b), 32.2 (q), 30.6 (j), 29.7 (i), 23.6 (r), 32.1, 29.5, 22.93 (k/l/m), 14.52 (n) ppm.

IR (ATR): $\tilde{\nu}$ = 2919 (m), 2848 (m), 1426 (m), 1071 (w), 992 (w), 787 (m), 715 (s), 685 cm^{-1} .

λ_{max} (CHCl_3) = 530 nm.

M_n (GPC, conventional method, CHCl_3) = 3.94 kDa.

Đ = 1.72.

Variation of the Ratio between the Monomers **70** and **68** and the Type of Catalyst for the Formation of the Polymer **72**.

General procedure for mixtures of **70:71** in molar ratios of 1.00: 1.00, 1.05:1.00, 1.10 : 1.00 and 1.15: 1.00.

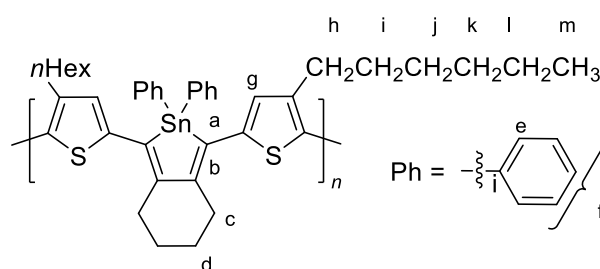
A solution of **70** and 2,5-bis(trimethylstannyl)thiophene (**71**) in a defined molar ratio was prepared with 5 mol% of catalyst, either [Pd(PPh₃)₄] or [Pd(*t*Bu₃P)₂] in toluene in a screw-septum vial. The mixture was heated in screw-septum vial for 15 h at 120 °C in the glovebox. Then, the volatiles were removed *in vacuo*. The crude product was washed several times with methanol, then dissolved in DCM and filtrated over a small plug of celite. The results were summarized in the Table 4 and Figure 35 in the section 3.2.3.

Solutions of **70** (0.05 M), **71** (0.04 M), [Pd(PPh₃)₄] (2.2 x 10⁻³ M) and [Pd(*t*Bu₃P)₂] (2.1 x 10⁻³ M) were prepared in toluene. The volume of each component used for each mixture were taken with a 1 mL syringe. The quantities used of each component for the mixture with different ratio and type of catalyst are summarized in the Table 7.

Entrance	Ratio 70:71	V 70 (mL) / μmol	V 71 (mL) / μmol	V [Pd(PPh ₃) ₄] (mL)	V [Pd(<i>t</i> Bu ₃ P) ₂] (mL)
1	1.00:1.00	0.8 / 42	1.1/ 42	1.0	1.1
2	1.05:1.00	0.8 / 42	1.0 / 40	0.9	1.1
3	1.10:1.00	0.8 / 42	1.0 / 38	1.0	1.0
4	1.15:1.00	0.8 / 42	1.0 / 36	1.0	1.0

Table 7. Quantities used in mL of solutions of each component of the mixture of **51** and **52** in different ratio using as catalyst either [Pd(Ph₃)₄] or [Pd(*t*Bu₃P)₂].

Polymer Containing Thiophene and Thionyl Moieties with a Ratio of 2 : 1 (77)



An orange-red solution of **70** (48.2 mg, 50 μmol), $[\text{Pd}(\text{P}(t\text{-Bu})_3)_2]$ (0.5 mg, 1 μmol , 2 mol%) and **76** (43.3 mg, 50 μmol) in toluene (3 mL) was prepared in the glovebox and heated at 100 $^\circ\text{C}$ for 6 h. The reaction mixture was quenched with water (10 mL) and the aqueous layer was extracted with chloroform (3 x 5 mL). The combined organic phases were dried over MgSO_4 and after filtration the volatiles were removed *in vacuo*. The crude product was purified by Soxhlet extraction, first with methanol (200 mL), heating the system at 100 $^\circ\text{C}$ for 10 h. After oligomers and small molecules were removed, the solvent was changed to chloroform and the system has heated at 80 $^\circ\text{C}$ for 6 h. The volatiles were removed *in vacuo* to afford a brown dark solid in a yield of 34 mg (95%, 47.7 μmol).

$^1\text{H NMR}$ (500 MHz, CDCl_3) 7.65 (s, 4H, e), 7.36 (s, 6H, f), 6.83 (s, 2H, g), 2.85 (s, 4H, h), 2.45 (s, 4H, i), 1.78 (s, 4H, j), 1.30 – 1.05 (m, 8H, k/l), 0.99 – 0.69 (m, 6H, m) ppm.

IR (ATR): $\tilde{\nu}$ = 2358 (m), 1275 (m), 1261 (m), 1099 (br), 799 (w), 764 (s), 750 (s) cm^{-1} .

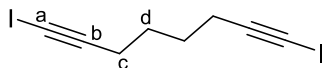
MALDI (CICCA): m/z = 777.5.

GPC (conventional calibration, CHCl_3) = 1.303 kDa.

\bar{D} = 1.43.

λ_{max} (DCM) = 436 nm.

1,8-Diiodoocta-1,7-diyne (77)



This synthetic route was adapted from a similar procedure in literature. [89]

A solution of AgNO_3 (4.05 g, 23.8 mmol), NIS (4.96 g, 22.0 mmol) and 1,7-octadiyne (1.06 g, 10.0 mmol) in DCM (88 mL) was prepared. [96] The mixture was stirred at 20 $^\circ\text{C}$ for 4 h, afterwards the mixture was filtered through a pad of celite, and the solvent was removed *in vacuo*. The impurities of the product were removed by column chromatography (silica gel, 9:1 *n*-pentane/ Et_2OAc ; R_f = 0.20). The crude product was crystallized with *n*-pentane to afford light yellow crystals in a yield of 2.04 g (57%, 5.69 mmol).

M.p.: 79.6 °C.

¹H NMR (500.1 MHz, CDCl₃): δ = 2.45 – 2.36 (m, 4H, c), 1.69 1.58 (m, 4H, d) ppm.

¹³C{¹H} NMR (126 MHz, CDCl₃): δ= 94.21 (b), 27.32 (d), 20.18 (c) ppm.⁵

IR (ATR): $\tilde{\nu}$ = 2935.1 (s), 2857.3 (w), 1459.4 (s), 1422.9 (m), 1342.7 (s), 1220.6 (m), 104.5 (w), 952.9 (m), 733.0 (s) cm⁻¹.

HR-MS (EI, C₈H₈I₂) *m/z*: calcd. 357.8716, found. 357.8700.

⁵ The carbon a was not possible to identify

NMR Spectra

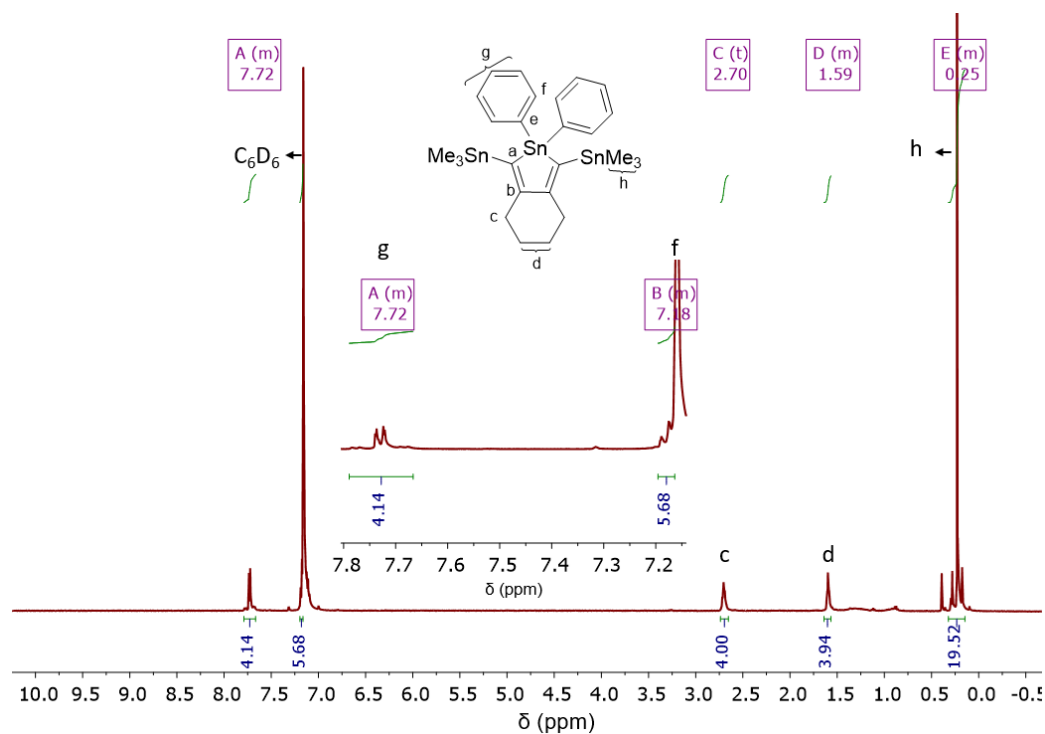
2,2-Diphenyl-1,3-bis(trimethylstannyl)-4,5,6,7-tetrahydro-2H-benzo[*c*]stannole (**48**) in C_6D_6 

Figure 56. 1H NMR (600 MHz) spectrum of **48** in C_6D_6 .

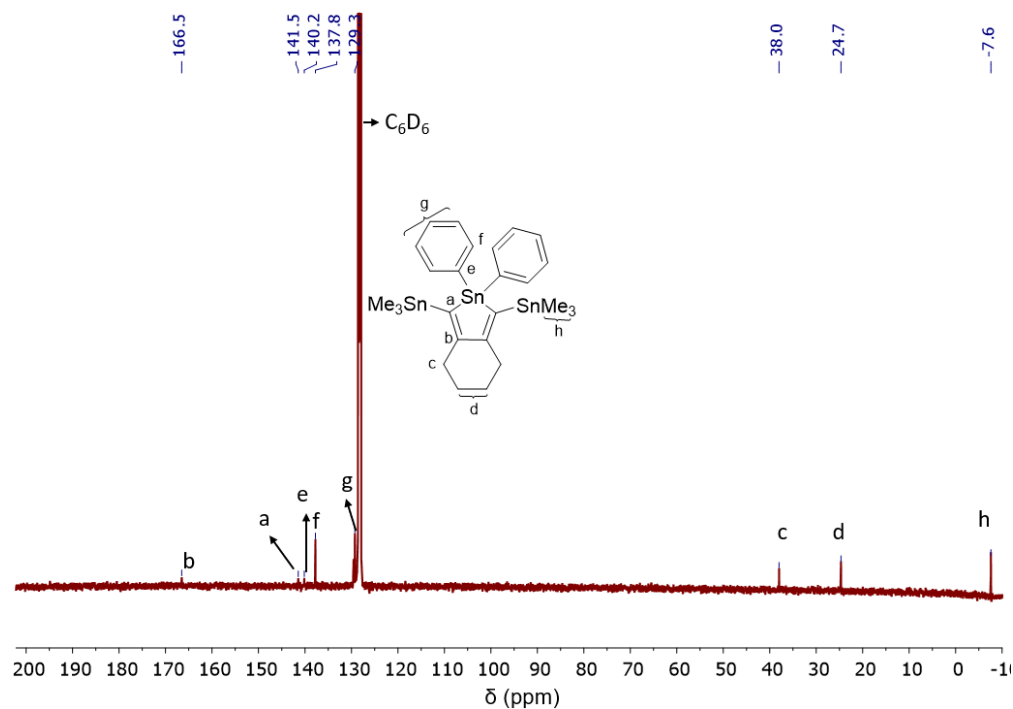


Figure 57. $^{13}C\{^1H\}$ NMR (126 MHz) spectrum of **48** in C_6D_6 .

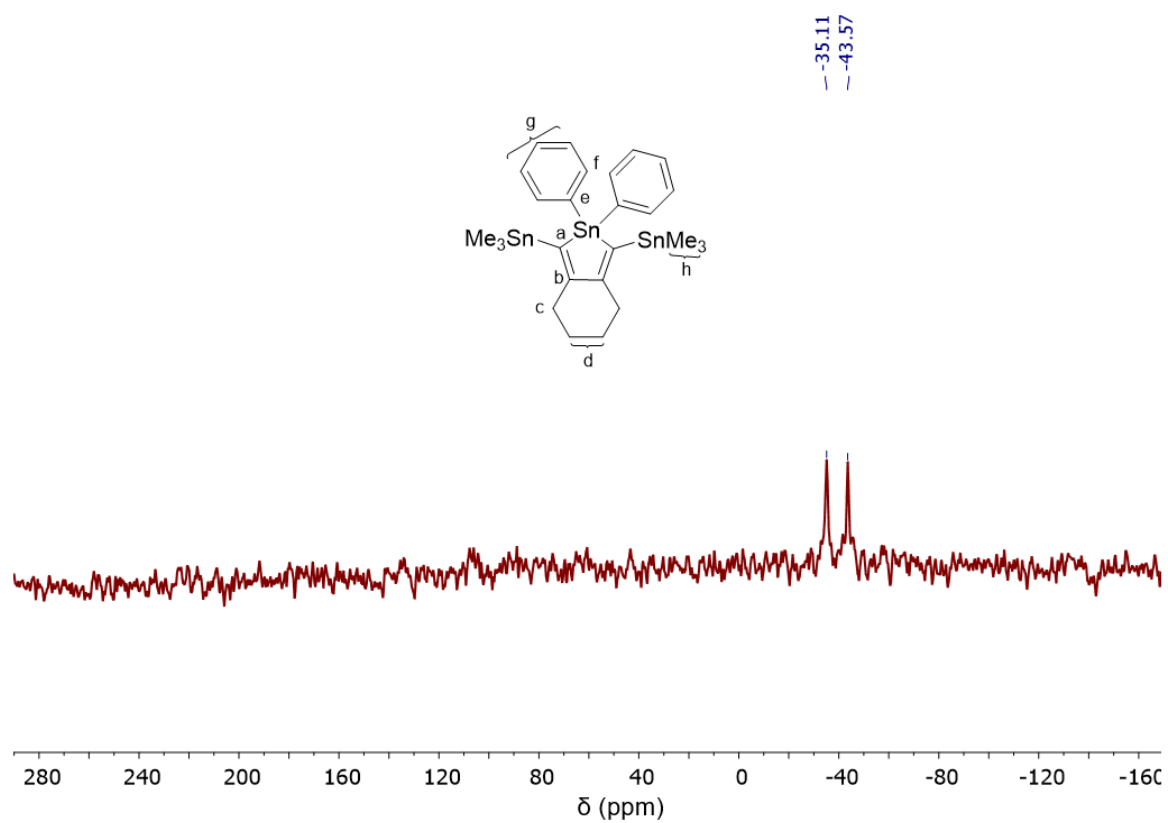


Figure 58. $^{119}\text{Sn}\{^1\text{H}\}$ NMR (160 MHz) spectrum of **48** in C_6D_6 .

2,2-Diphenyl-1,3-bis(4,4,5,5-tetramethyl-1,3,2-dioxaborolan-2-yl)-4,5,6,7-tetrahydro-2H-benzo[c]stannole (49) in C₆D₆

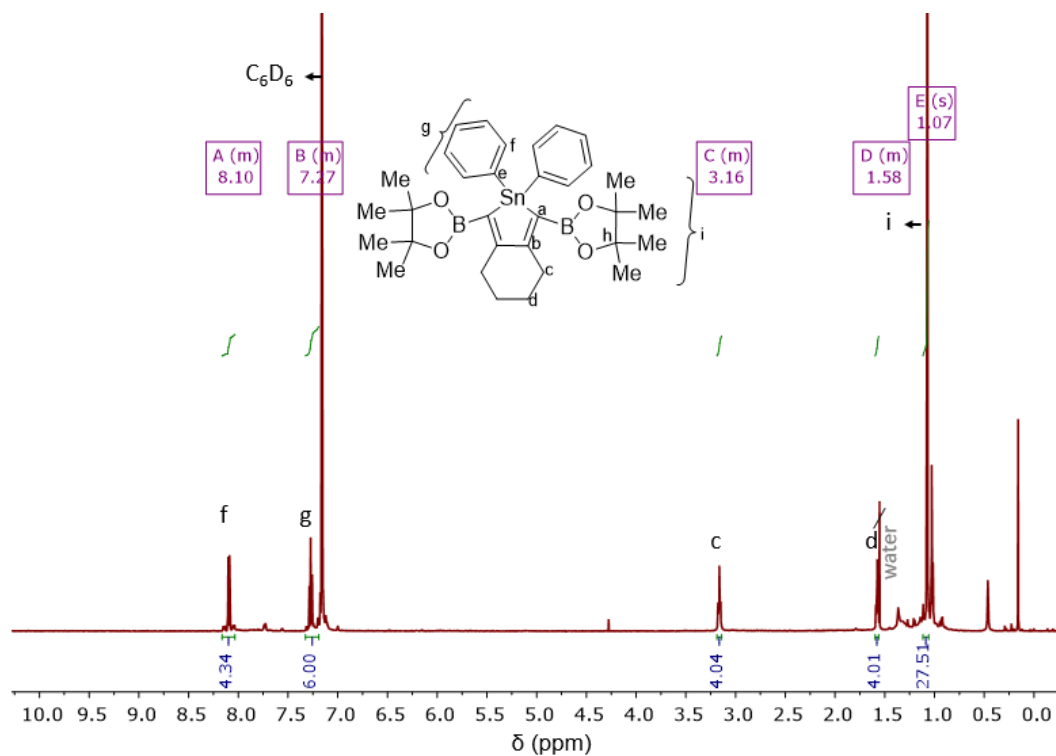


Figure 59. ¹H NMR (600 MHz) spectrum of **49** in C₆D₆.

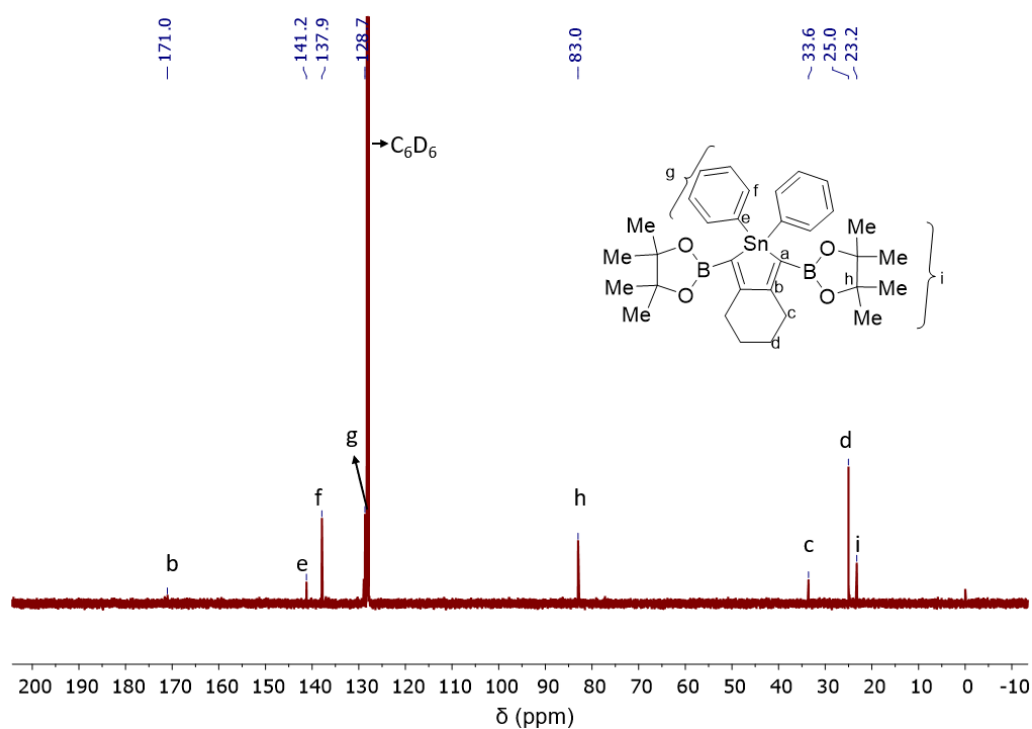
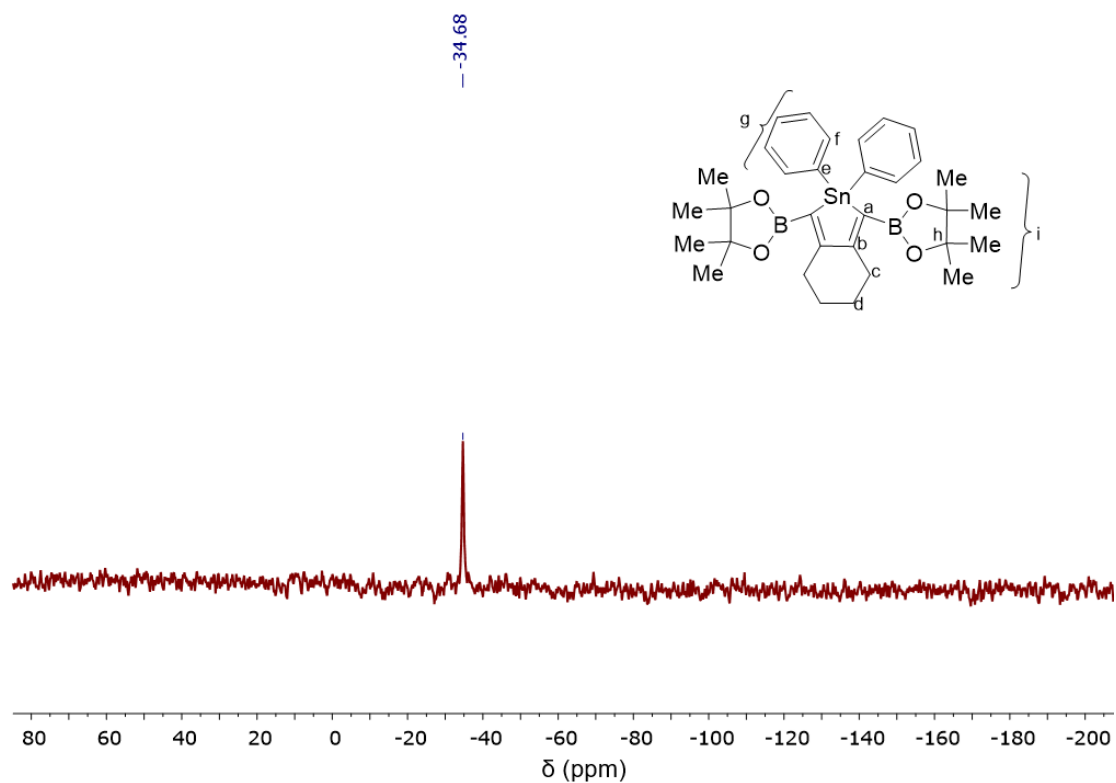
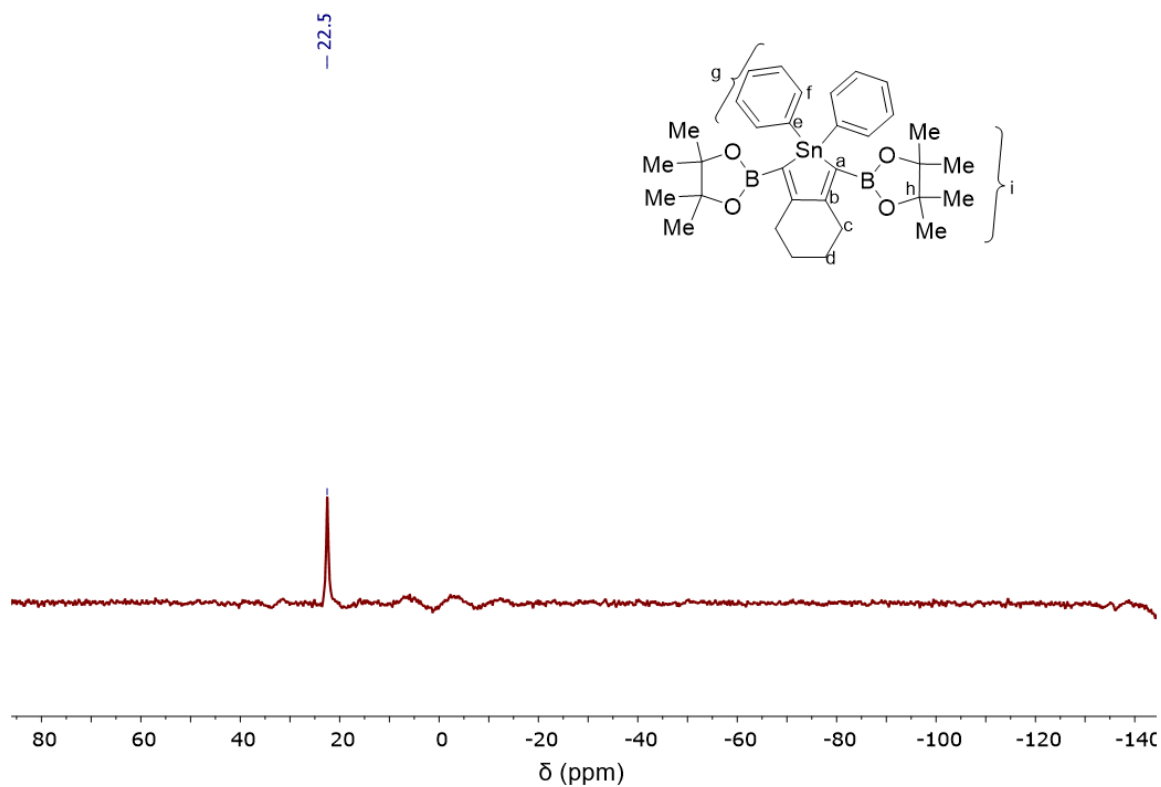
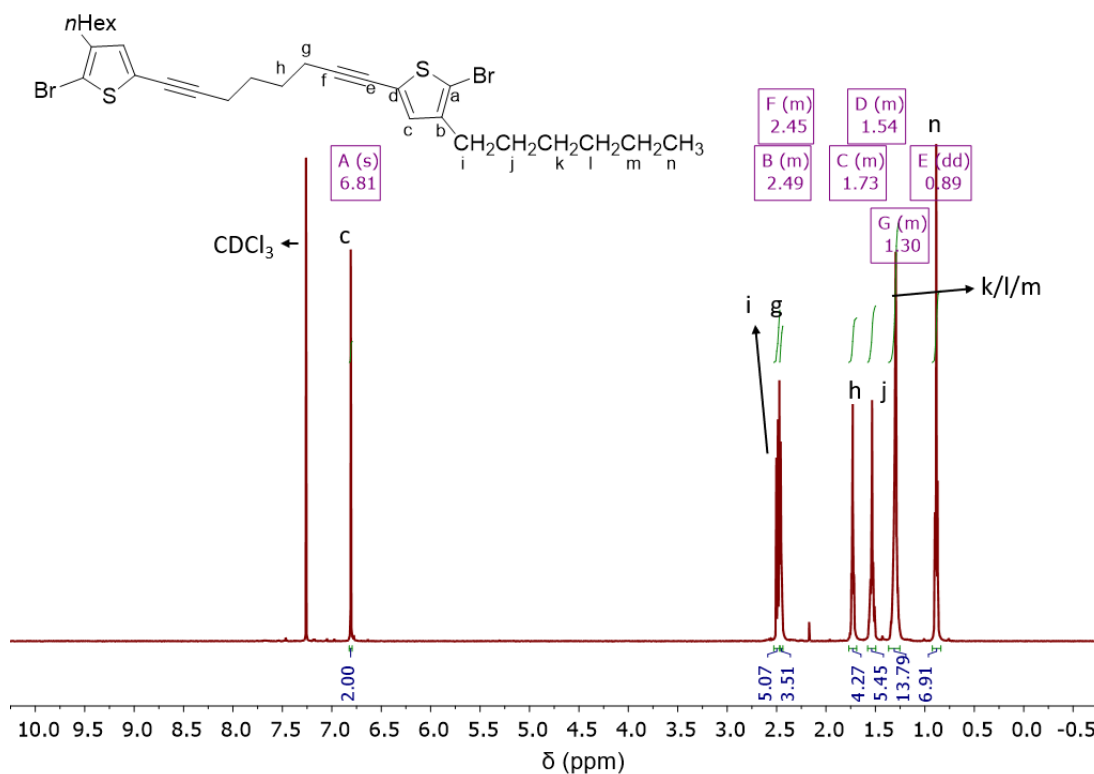
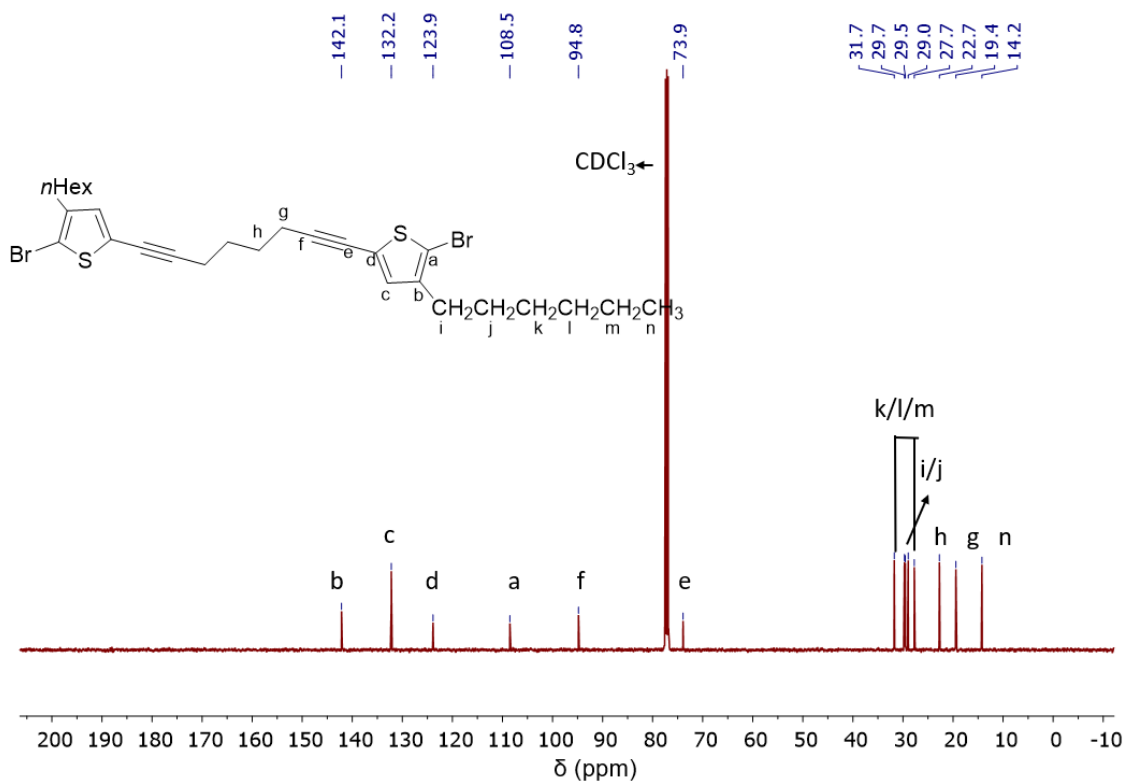
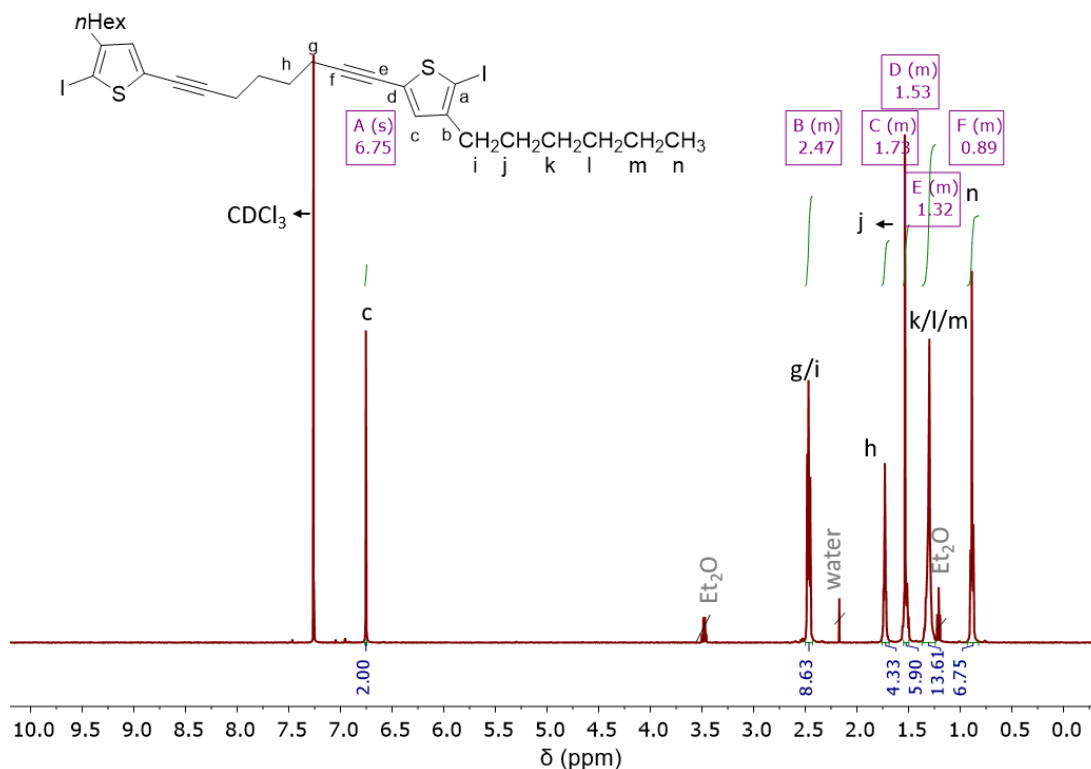
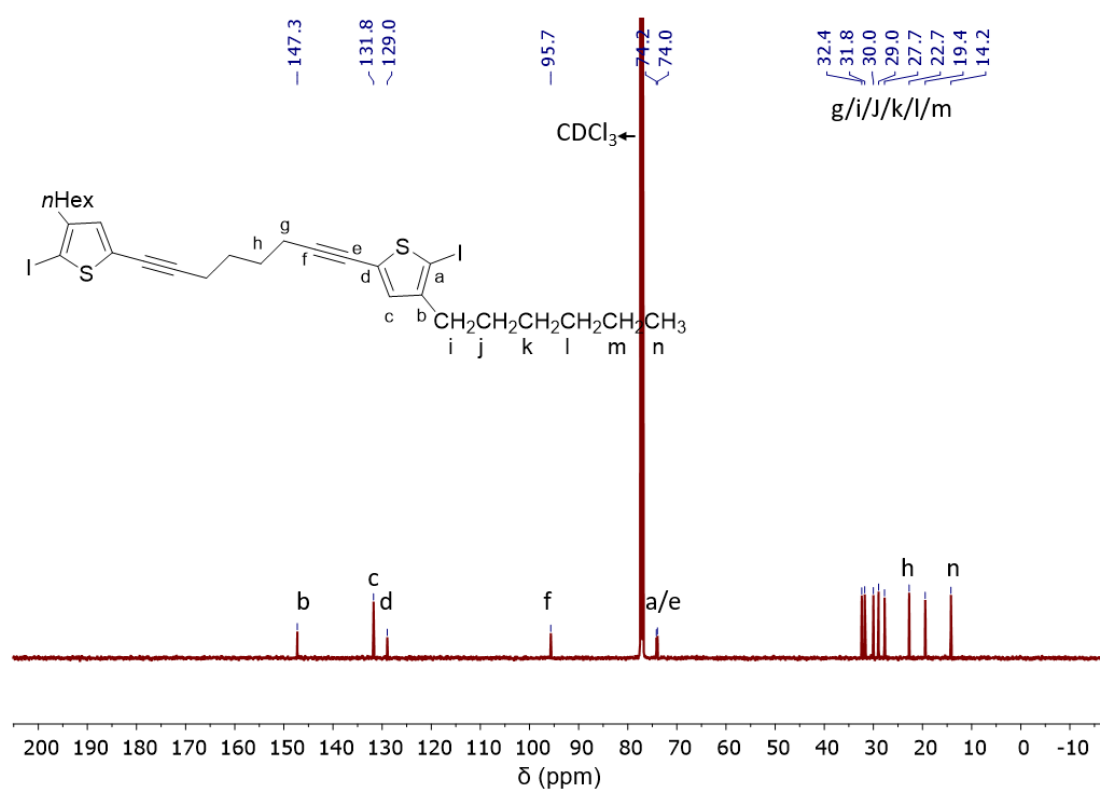


Figure 60. ¹³C{¹H} NMR (126 MHz) spectrum of **49** in C₆D₆.



1,8-bis(5-Bromo-4-hexylthiophen-2-yl)octa-1,7-diyne (73) in CDCl₃^[78]**Figure 63.** ¹H NMR (600 MHz) spectrum of **73** in CDCl₃.**Figure 64.** ¹³C{¹H} NMR (126 MHz) spectrum of **73** in CDCl₃.

1,8-bis(4-Hexyl-5-iodothiophen-2-yl)octa-1,7-diyne (74) in CDCl₃^[78]

Figure 65. ¹H NMR (600 MHz) spectrum of **74** in CDCl₃.

Figure 66. ¹³C{¹H} NMR (126 MHz) spectrum of **74** in CDCl₃.

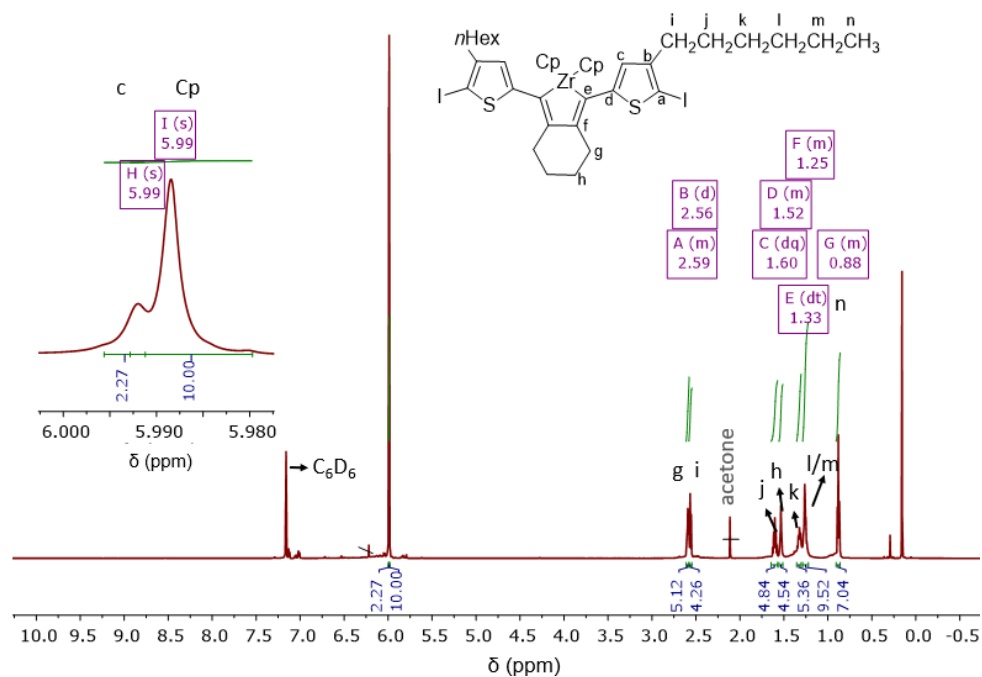
Zirconacyclopentadiene (**75**) in C_6D_6 

Figure 67. 1H NMR (600 MHz) spectrum of **75** in C_6D_6 .

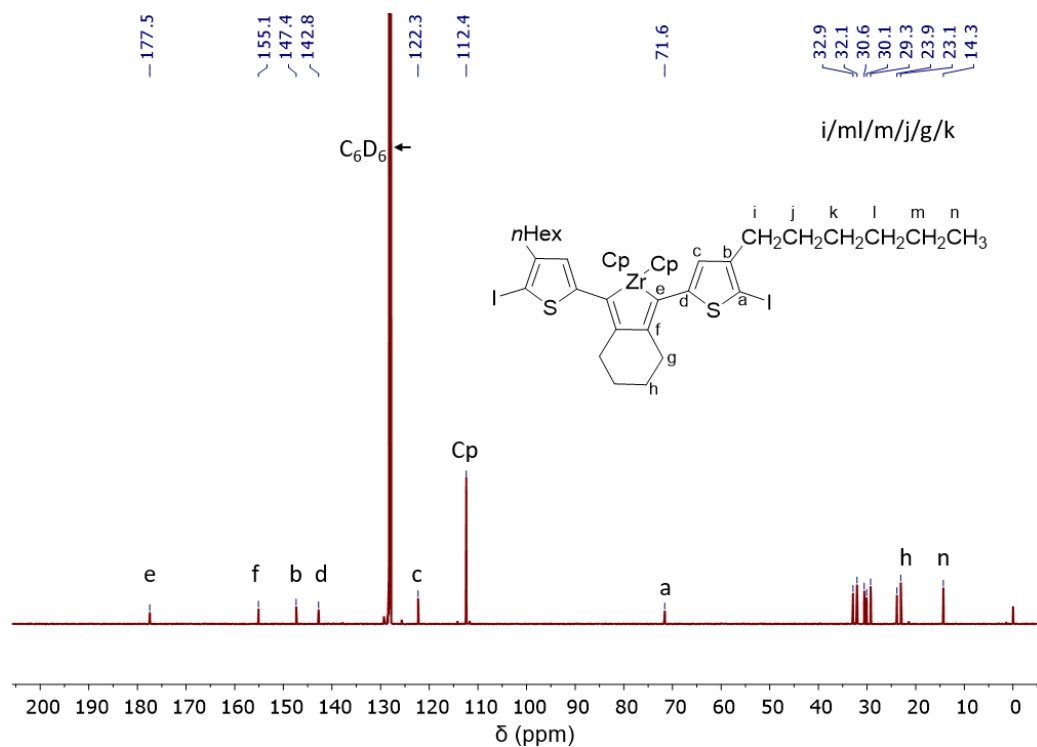


Figure 68. $^{13}C\{^1H\}$ NMR (126 MHz) spectrum of **75** in C_6D_6 .

1,3-bis(4-Hexyl-5-iodothiophen-2-yl)-2,2-diphenyl-4,5,6,7-tetrahydro-2H-benzo[c]stannole (70) in CDCl₃

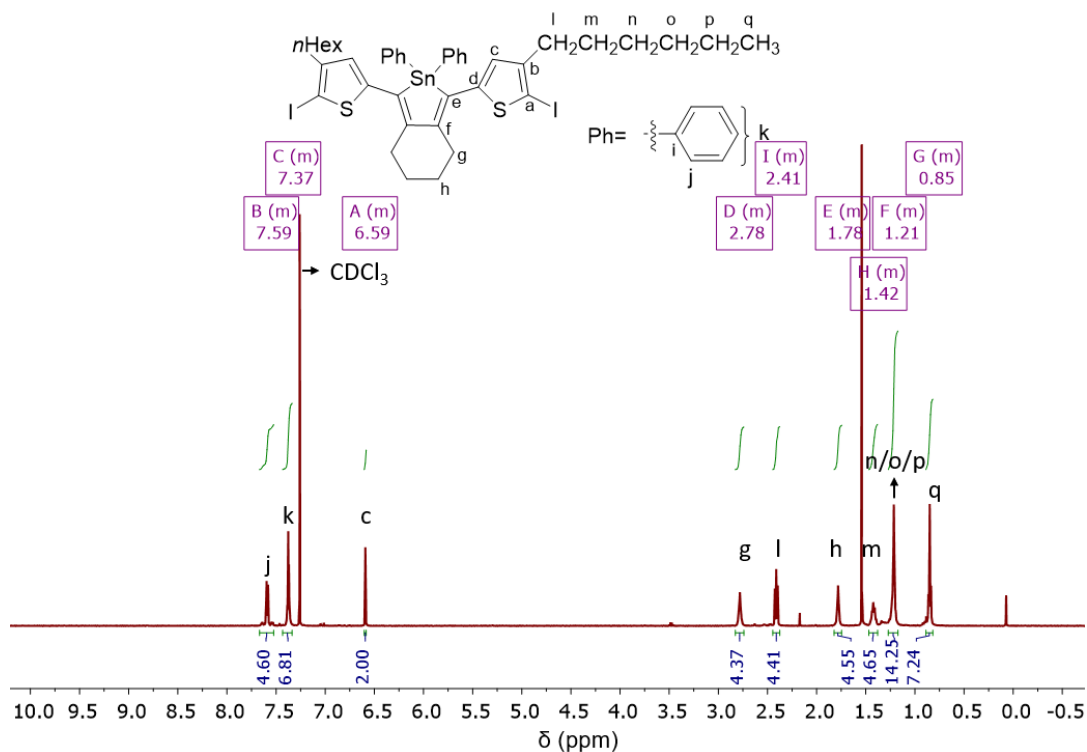


Figure 69. ¹H NMR (600 MHz) spectrum of **70** in CDCl₃.

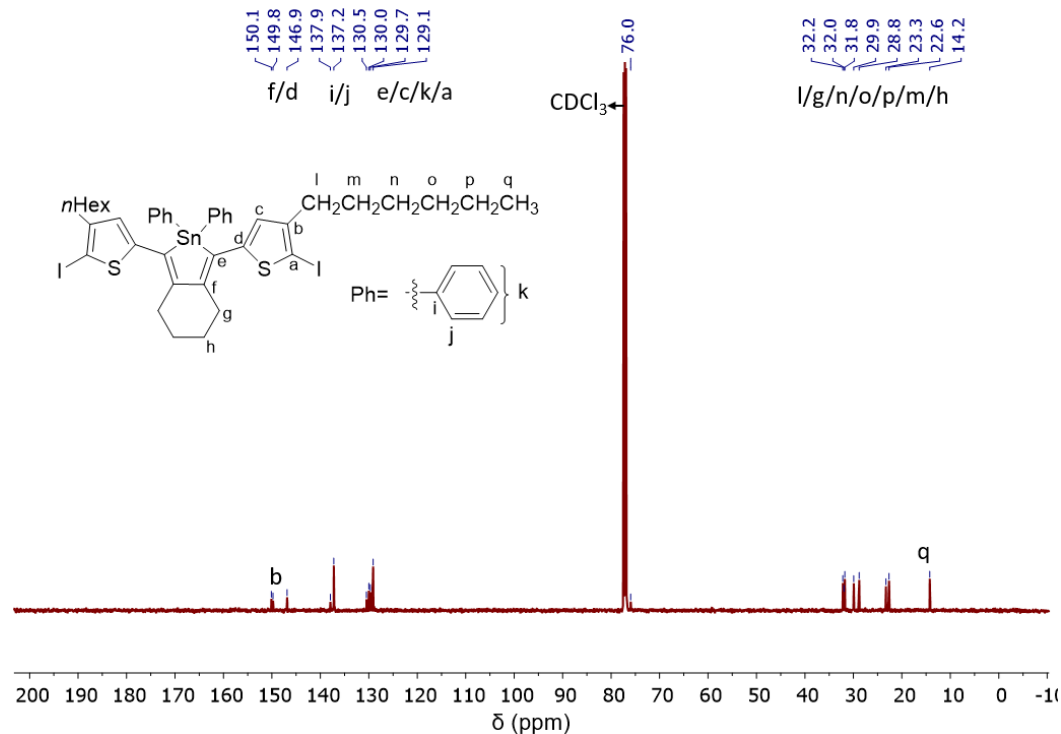


Figure 70. ¹³C{¹H} NMR (126 MHz) spectrum of **70** in CDCl₃.

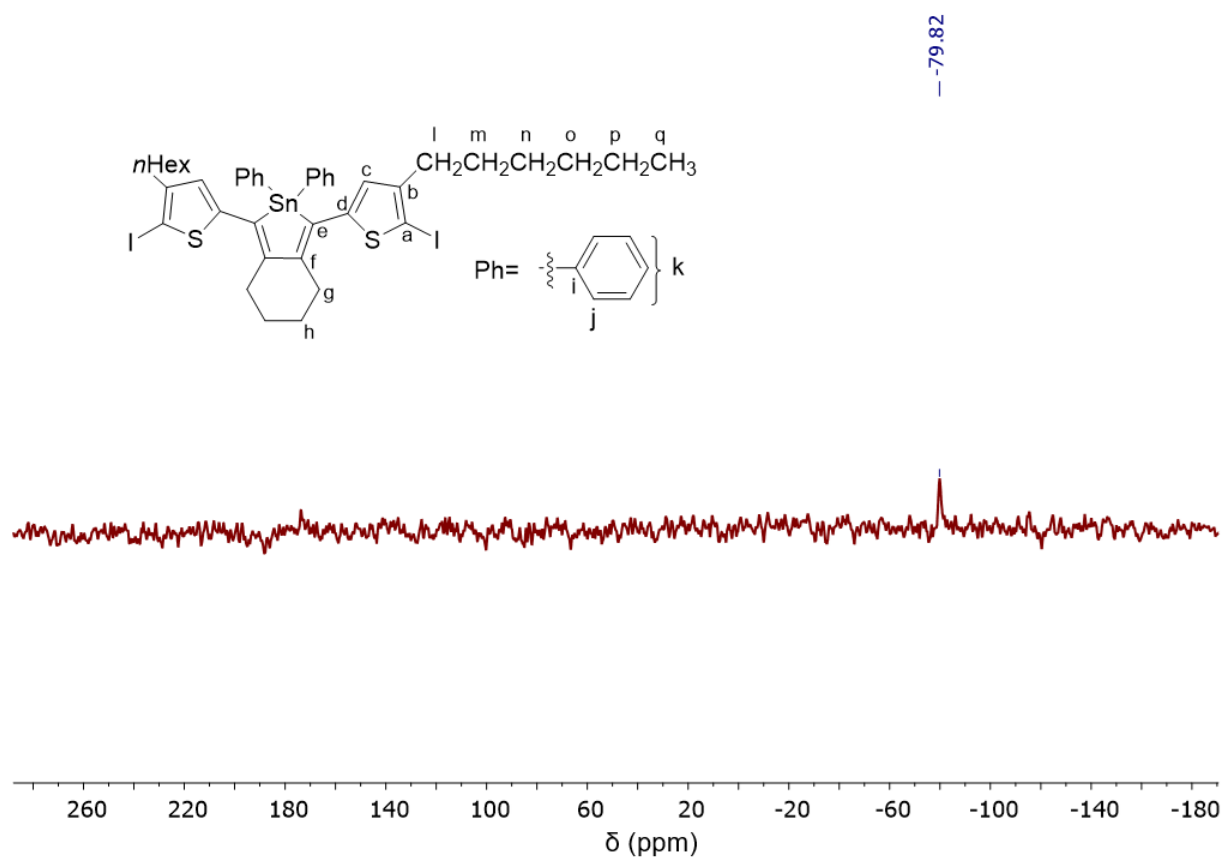


Figure 71. $^{119}\text{Sn}\{^1\text{H}\}$ NMR (160 MHz) spectrum of **70** in C_6D_6 .

1,3-bis(4-Hexyl-5-(trimethylstannyl)thiophen-2-yl)-2,2-diphenyl-4,5,6,7-tetrahydro-2H-benzo[c]stannole (76) in CDCl₃

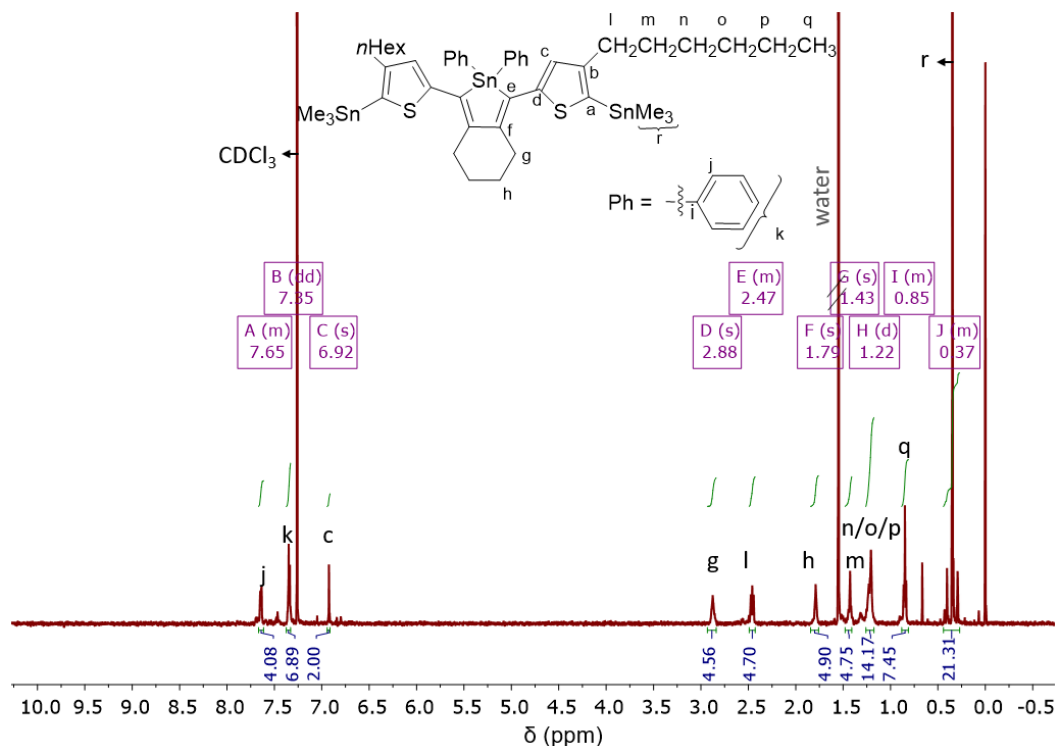


Figure 72. ¹H NMR (600 MHz) spectrum of **76** in CDCl₃.

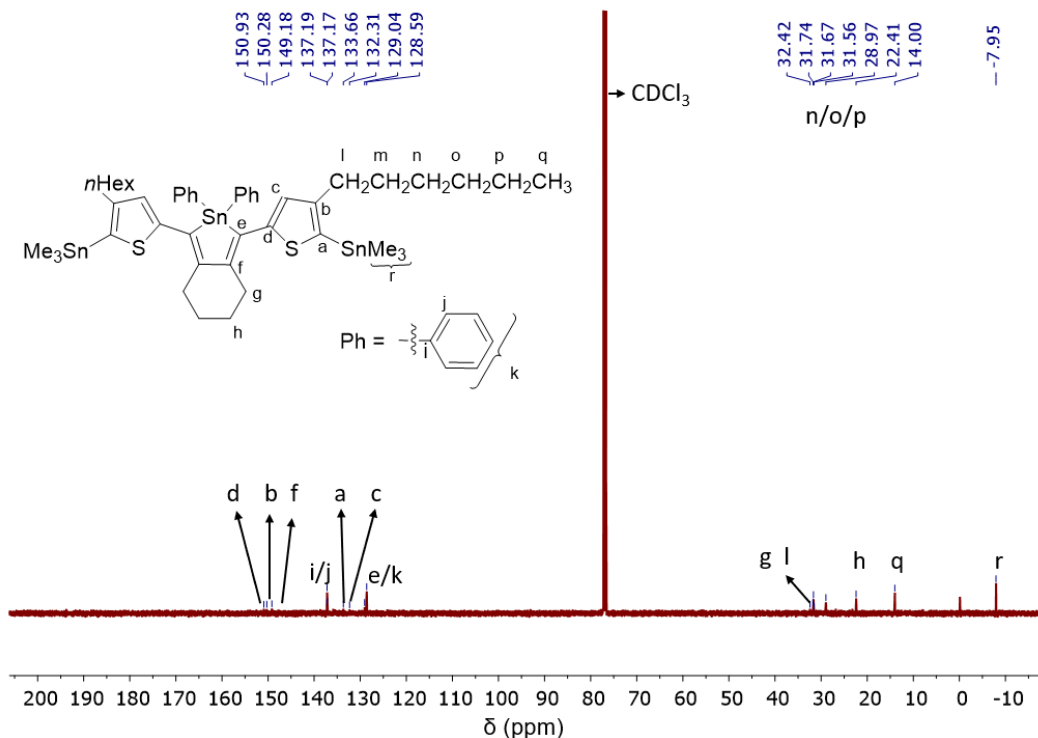


Figure 73. ¹³C{¹H} NMR (126 MHz) spectrum of **76** in CDCl₃.

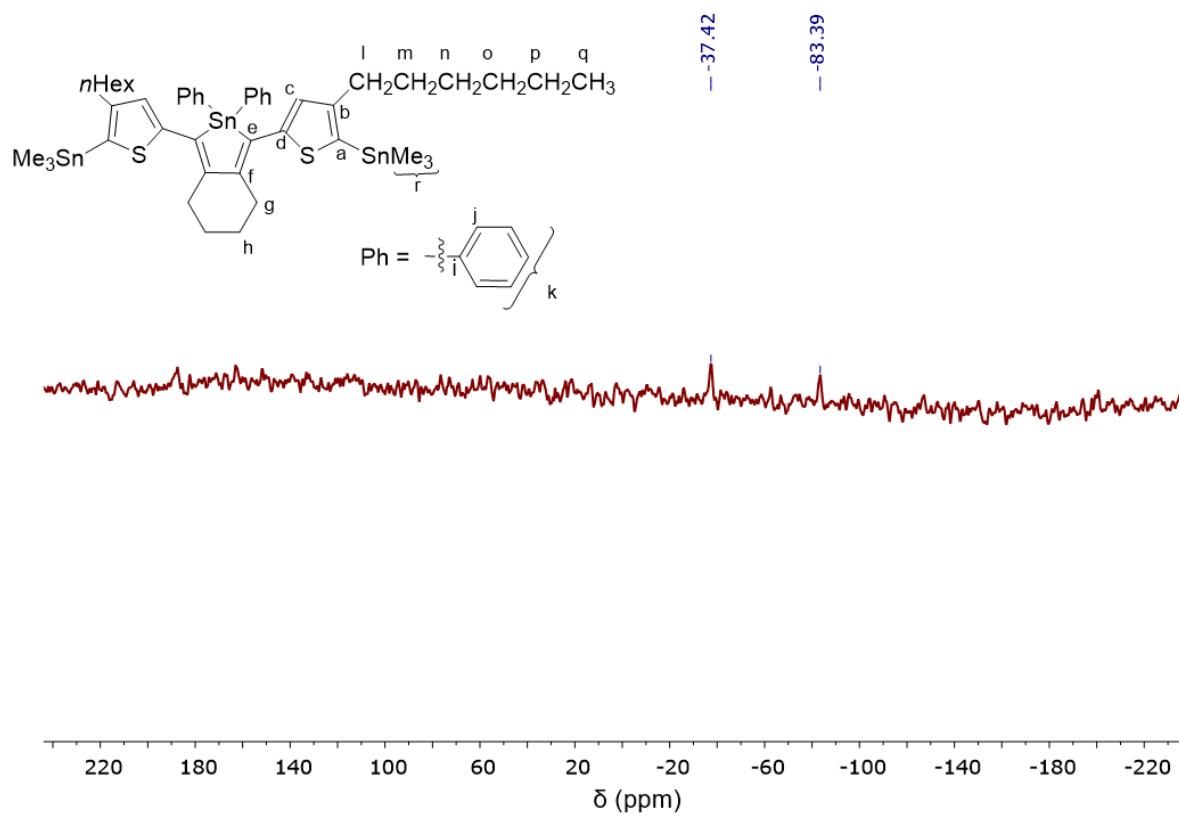
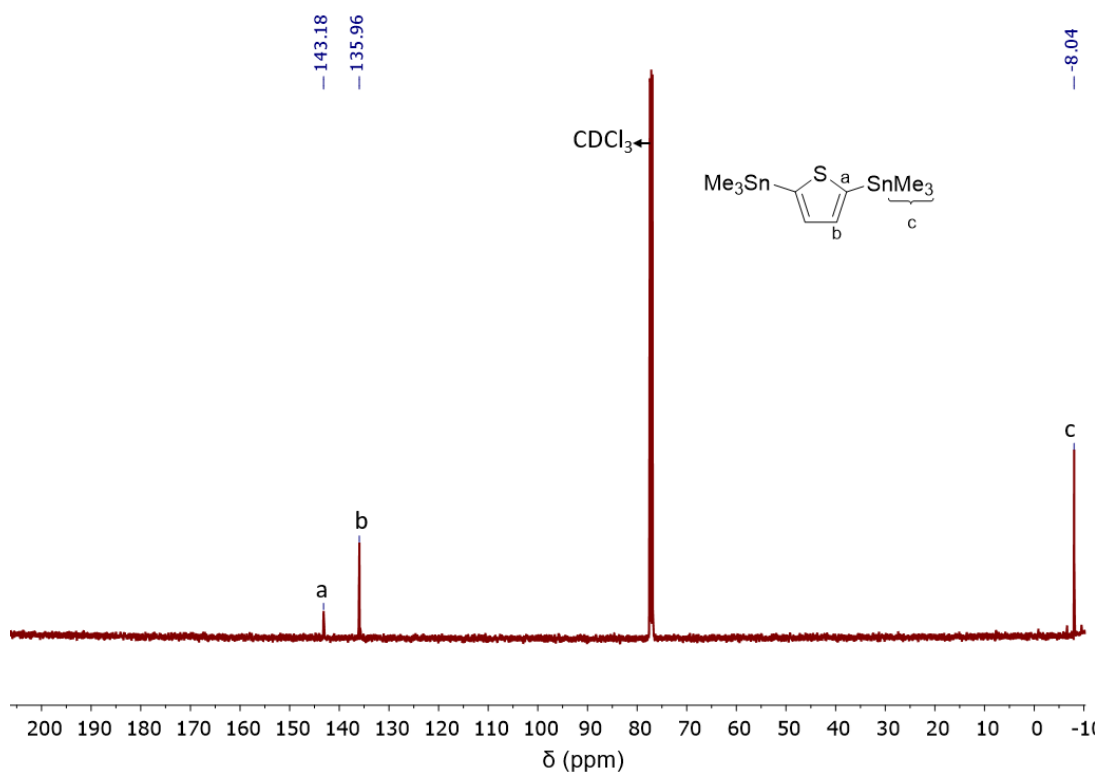
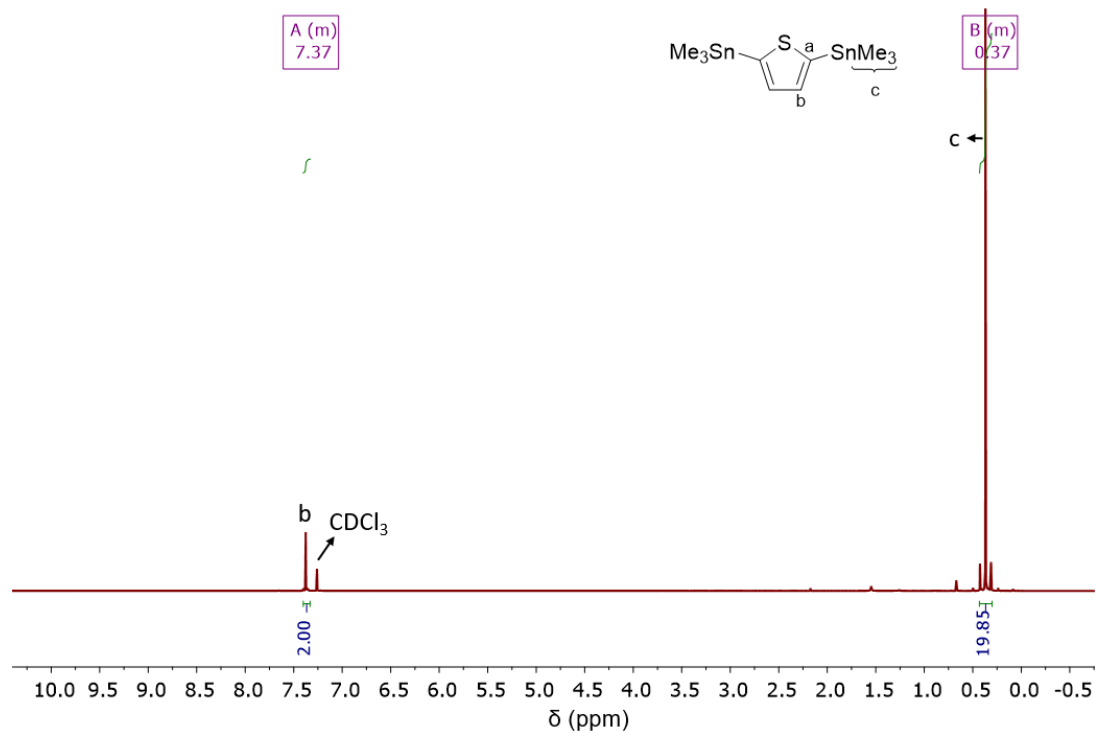


Figure 74. $^{119}\text{Sn}\{^1\text{H}\}$ NMR (160 MHz) spectrum of **76** in C_6D_6 .

2,5-bis(trimethylstannyl)thiophene (71) in CDCl₃^[95]

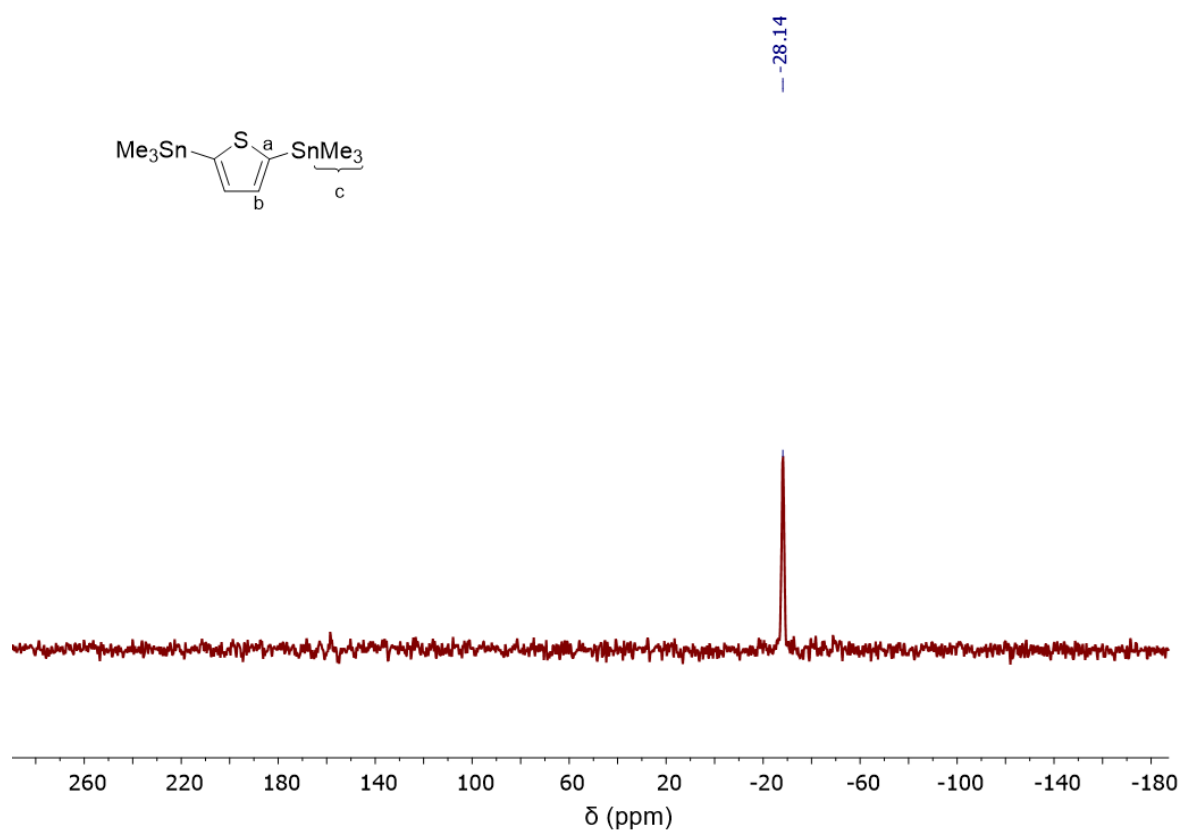


Figure 77. $^{119}\text{Sn}\{^1\text{H}\}$ NMR (160 MHz) spectrum of **71** in C_6D_6 .

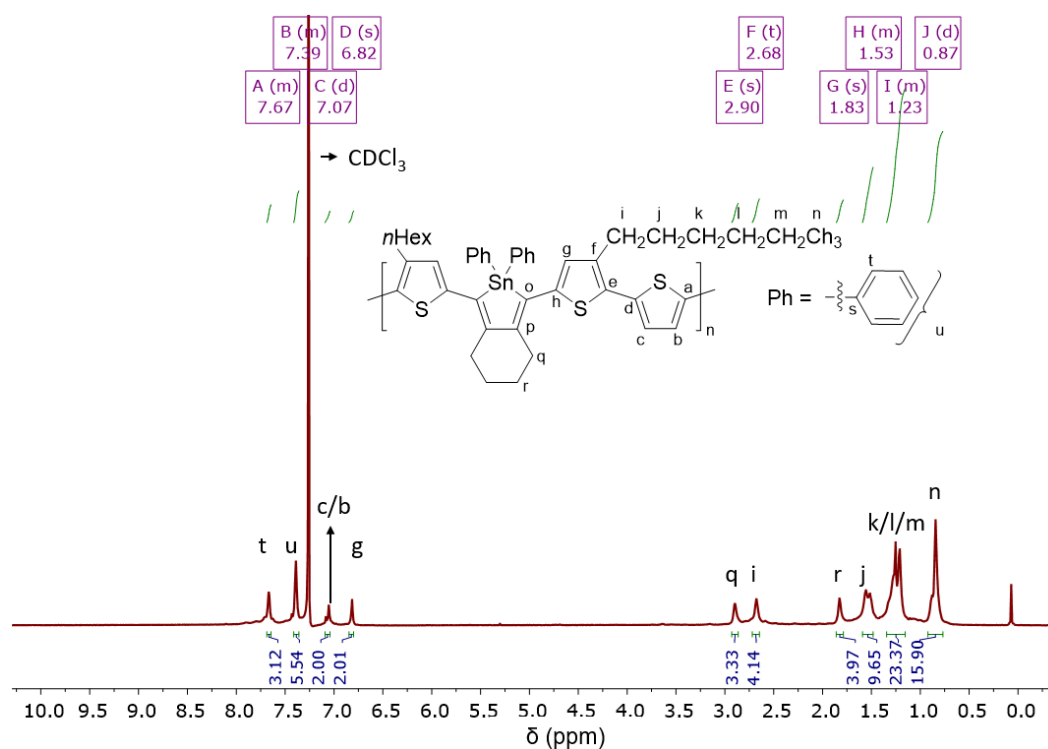
Polymer Containing Thiophene and Thionyl Moieties with a Ratio of 3 : 1 (72)


Figure 78. ^1H NMR (600 MHz) spectrum of **72** in CDCl_3 .

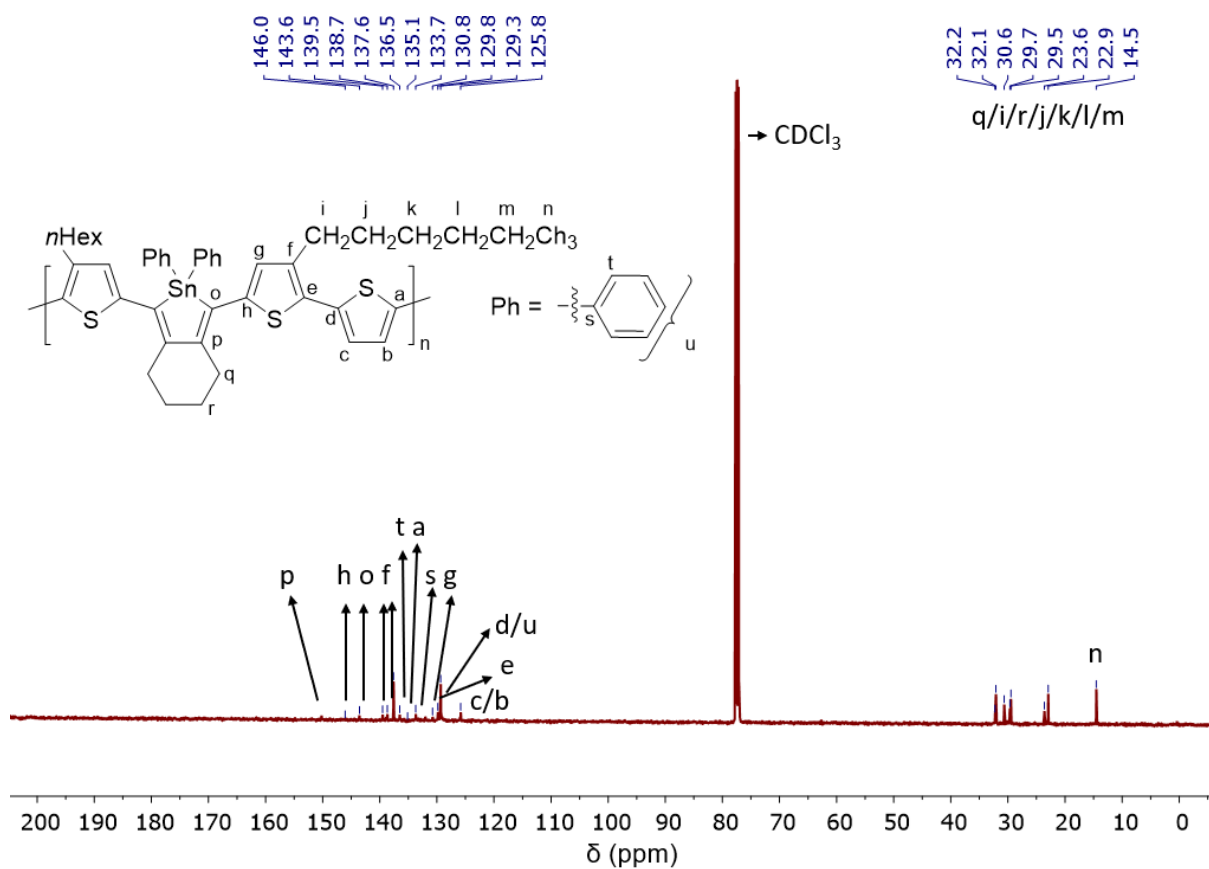


Figure 79. $^{13}\text{C}\{^1\text{H}\}$ NMR (600 MHz) spectrum of **72** in CDCl_3 .

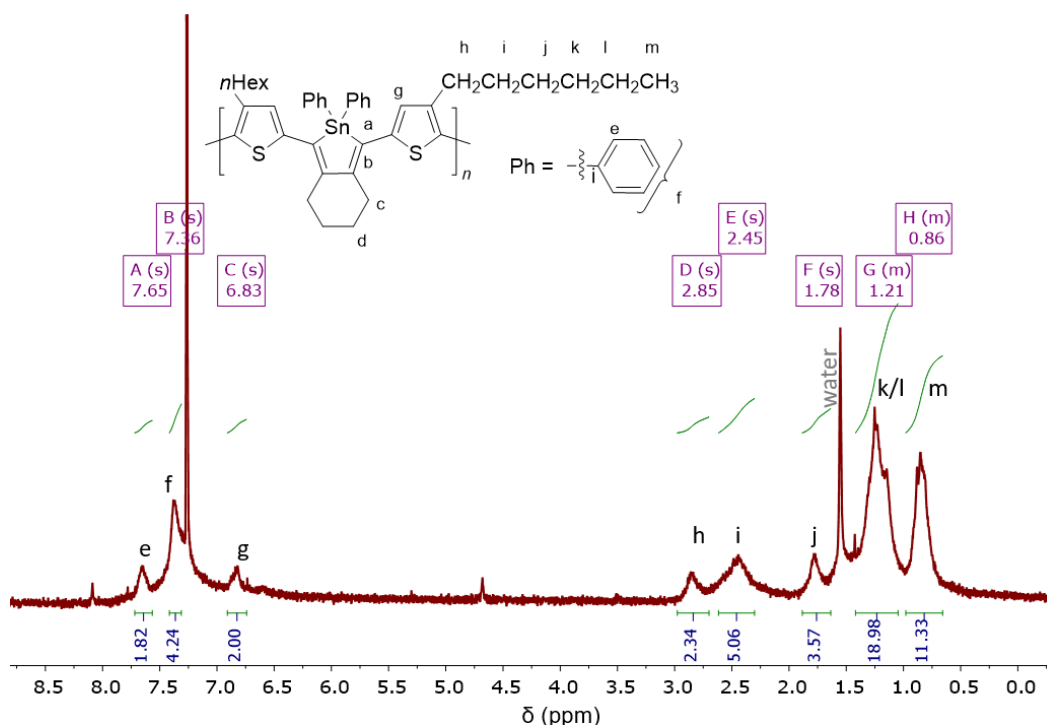
Polymer Containing Thiophene and Thionyl Moieties with a Ratio of 2 : 1 (77)


Figure 80. ¹H NMR (600 MHz) spectrum of **77** in CDCl₃.

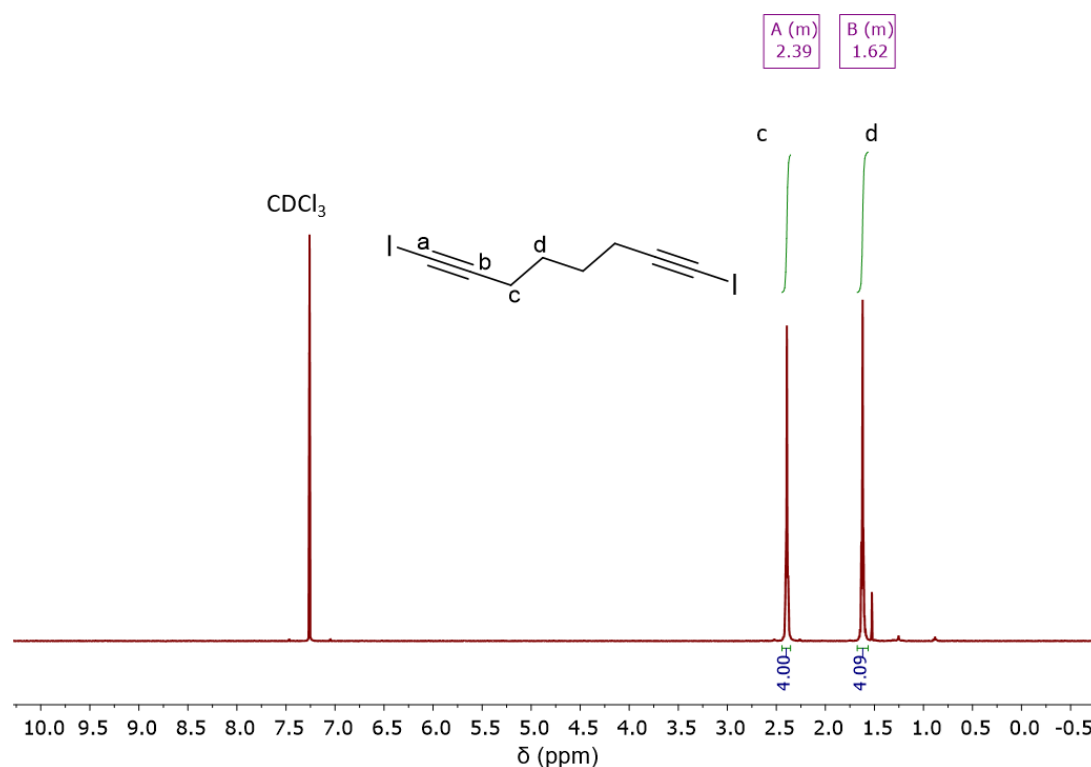
1,8-diiodoocta-1,7-diyne (80) in CDCl₃


Figure 81. ¹H NMR (600 MHz) spectrum of **80** in CDCl₃.

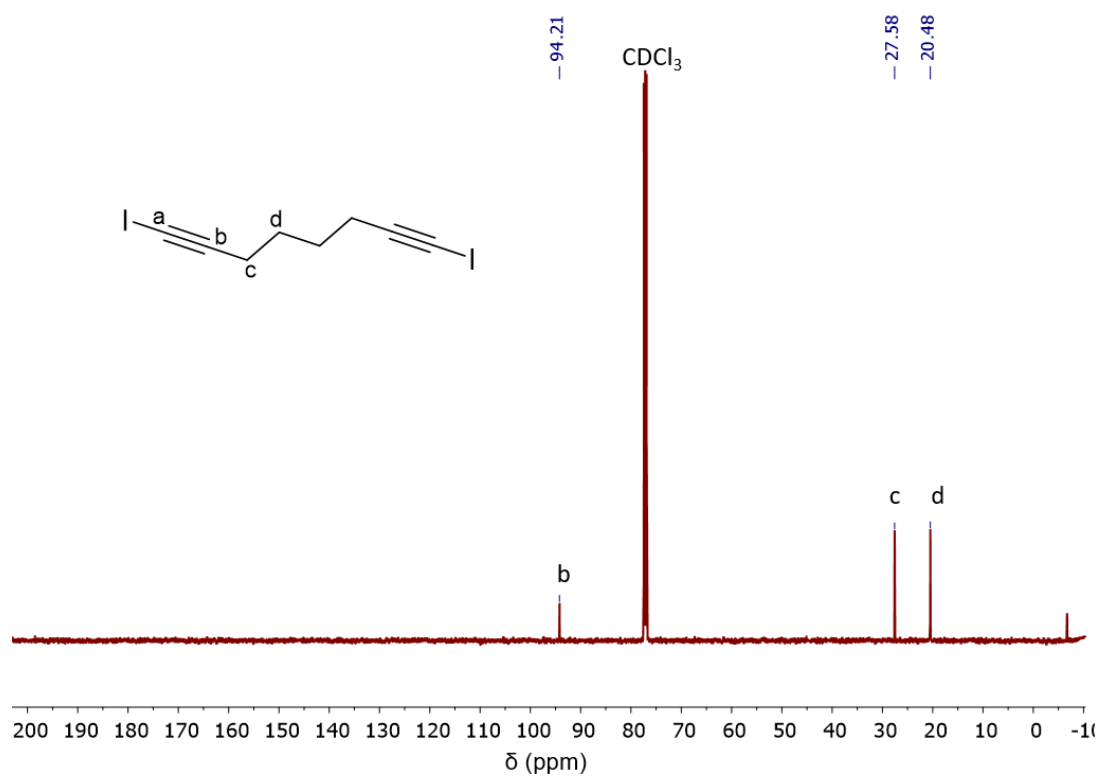
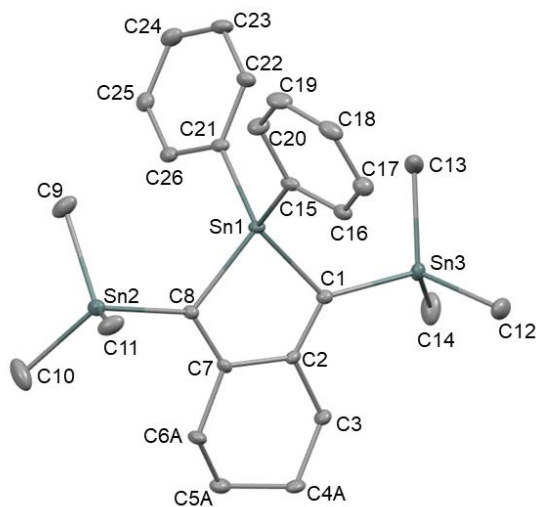


Figure 82. $^{13}\text{C}\{^1\text{H}\}$ NMR (126 MHz) spectrum of **80** in CDCl_3 .

Single Crystal Data

2,2-Diphenyl-1,3-bis(trimethylstannyl)-4,5,6,7-tetrahydro-2H-benzo[*c*]stannole (**48**)



The crystallographic details for the stannole **48** are summarized in Table 8. Some important bond distances and angles are given in Table 8. The bond distances and angles are given in the Table 9 and Table 10 respectively. The intra and intermolecular contacts are listed in the Table 11 Table 12.

CCDC Number	
Empirical Formula	C ₂₆ H ₃₆ Sn ₃
Formula Weight	704.62
Crystal System	Orthorhombic
Space Group	<i>P c a 2</i> ₁
Temperature (K)	100(2)
Wavelength (Å)	0.71073
a(Å)	34.7102(16)
b(Å)	13.4063(6)
c(Å)	17.6034(8)
Volume (Å³)	8191.5(6)
Z	12
D_{calc}(gcm⁻³)	1.714
Abs Coeff. (mm⁻¹)	2.732
F(000)	4104
Crystal Size (mm³)	0.1 × 0.1 × 0.05
θ-range	2.241-31.496

Reflections collected	233292
Uniques reflections	27262
R_{int}	0.0382
R_{obs}[I > 2σ(I)]	0.0262
R_w(all data)	0.0292
Goodness of fit on F²	1.081
Δρ_{max,min} (eÅ⁻³)	1.811/-0.772

Table 8. Crystallographic details.

	Bond Distance(Å)		Bond Distance(Å)
Sn1–C1	2.137(5)	Sn2–C8	2.140(5)
Sn1–C8	2.132(5)	Sn2–C9	2.145(5)
Sn1–C15	2.151(5)	Sn2–C10	2.150(7)
Sn1–C21	2.143(5)	Sn2–C11	2.151(5)
Sn3–C1	2.135(5)	Sn3–C12	2.133(7)
Sn3–C13	2.141(7)	Sn3–C14	2.144(7)
Sn7–C53	2.142(5)	Sn7–C60	2.134(5)
Sn7–C67	2.133(4)	Sn7–C73	2.146(5)
Sn8–C53	2.130(5)	Sn9–C60	2.133(5)
Sn4–C27	2.149(5)	Sn4–C34	2.145(5)
Sn4–C41	2.154(5)	Sn4–C47	2.143(5)
Sn5–C34	2.120(5)	Sn6–C27	2.123(5)
C1–C2	1.355(7)	C2–C7	1.533(7)
C7–C8	1.346(7)	C27–C28	1.348(6)

Table 9. Bond distances for **48**.

	Bond angle(°)		Bond angle(°)
C1–Sn1–C8	85.19(19)	C1–Sn1–C15	117.3(2)
C8–Sn1–C15	116.2(2)	C8–Sn1–C21	115.6(2)
C27–Sn4–C34	85.07(18)	C27–Sn4–C41	115.16(18)
C34–Sn5–C38	111.1(2)	C34–Sn5–C39	102.7(2)
C41–Sn4–C47	106.33(18)	C34–Sn5–C40	114.5(2)

Table 10. Bond angles for **48**.

X–H...Cg	H...Cg (Å)	∠ X–H...Cg (°)	X...Cg (Å)	X–H, Pi(°)	Symmetry
C10–H10B...Cg4	2.97	164	3.917(7)	73	3/2-x,y,-1/2+z
C63–H63B...Cg10	2.99	160	3.932(6)	70	3/2-x,y,1/2+z
C70–H70...Cg11	2.96	127	3.612(6)	38	x,y,z

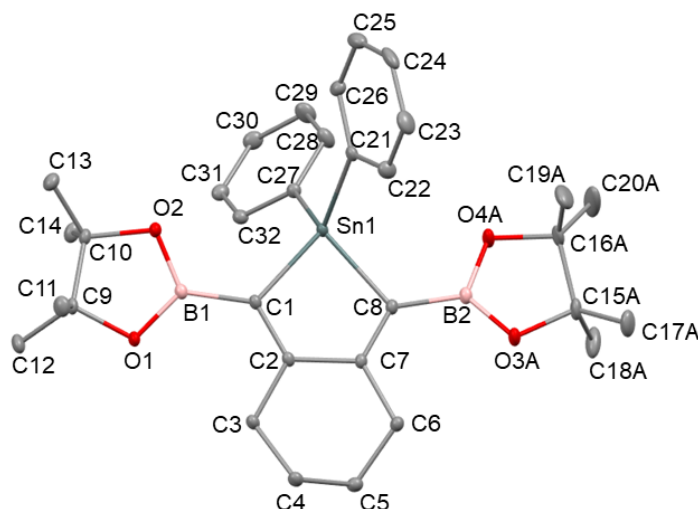
Table 11. Intra and intermolecular C–H... π contacts of **48**.

Cg4 is the centroid of the phenyl ring, C67–C68–C69–C70–C71–C72 ; Cg10 is the centroid of the phenyl ring, C21–C22–C23–C24–C25–C26 ; Cg11 is the centroid of stannole, Sn4–C27– C28–C33–C34.

	Bond Distance(Å)		Bond Distance(Å)
Sn4...H39C	3.3037(1)	Sn5...H32B	3.0529(1)
Sn6...H29B	3.0599(1)	Sn3...H3A	3.0477(1)

Table 12. Short Intramolecular contacts, (C–H...Sn type of interactions) of **48**.

2,2-Diphenyl-1,3-bis(4,4,5,5-tetramethyl-1,3,2-dioxaborolan-2-yl)-4,5,6,7-tetrahydro-2H-benzo[c]stannole (49)



The crystallographic details for the stannole **49** are summarized in Table 13. Some important bond distances and angles are given in Table 14. Bond distances involving Sn and B atoms with directly connected covalent bonds. The bond distances and angles are given in the Table 14 and Table 15 respectively. The intra and intermolecular contacts are listed in the Table 16, Table 17 and Table 18.

CCDC Number	
Empirical Formula	C ₃₂ H ₄₂ B ₂ O ₄ Sn
Formula Weight	630.96
Crystal System	Monoclinic
Space Group	<i>P</i> 2 ₁ / <i>c</i>
Temperature (K)	100(2)
Wavelength (Å)	0.71073
a(Å)	9.7318(2)
b(Å)	11.4264(3)
c(Å)	28.1426(7)
β(°)	96.7990(10)
Volume (Å³)	3107.43(13)
Z	4
D_{calc}(gcm⁻³)	1.349
Abs Coeff. (mm⁻¹)	0.856
F(000)	1304
Crystal Size (mm³)	0.125 x 0.1 x 0.075
θ-range	2.417- 30.603
Reflections collected	109766

Uniques reflections	9546
R_{int}	0.0315
R_{obs}[I>2σ(I)]	0.0194
R_w(all data)	0.0237
Goodness of fit on F²	1.108
Δρ_{max,min} (eÅ⁻³)	0.438/-0.423

Table 13. Crystallographic Table for stannole **49**.

	Bond Distance(Å)		Bond Distance(Å)
B2–O3A	1.3727(18)	Sn1–C1	2.1361(11)
B2–O4A	1.368(2)	Sn1–C8	2.1327(12)
B2–C8	1.5420(16)	Sn1–C21	2.1322(12)
O1–B1	1.3756(14)	Sn1–C27	2.1370(12)
O2–B1	1.3746(14)	B1–C1	1.5450(16)

Table 14. Bond distances involving Sn and B atoms with directly connected covalent bonds.

	Bond angle(°)		Bond angle(°)
C1–Sn1–C8	84.27(4)	C1–Sn1–C21	119.81(4)
C8–Sn1–C21	109.03(5)	C8–Sn1–C27	120.49(4)
C1–Sn1–C27	110.01(4)	C21–Sn1–C27	110.01(4)
O1–B1–O2	112.65(10)	Sn1–C27	2.1370(12)
O1–B1–C1	126.74(10)	O2–B1–C1	120.56(9)
O3A–B2–O4A	113.17(12)	O3A–B2–C8	126.50(11)
O4A–B2–C8	120.20(11)	C9–O1–B1	107.27(9)

Table 15. Bond angles involving Sn and B atoms with directly connected covalent bonds.

D–H...A	D–H (Å)	D...A (Å)	H...A (Å)	D–H...A	Symmetry
C6–H6B...O3B	0.990	3.065(0)	2.382(0)	125.50(0)	x, y, z
C18A–H18C...O2	0.980	3.565(0)	2.745(0)	141.52(0)	x+1, +y, +z
C11–H11B...O3B	0.980	3.597(0)	2.717(0)	149.64(0)	x-1,+y,+z

Table 16. Intra and intermolecular contacts; C–H...O

X–H...Cg	H...Cg (Å)	∠ X–H...Cg (°)	X...Cg (Å)	X–H, Pi(°)	Symmetry
C12–H12A...Cg7	2.93	151	3.8179(14)	61	-x,-1/2+y,1/2-z
C20B–H20D...Cg6	2.86	178	3.844(12)	74	1+x,y,z

Cg7 is the centroid of the phenyl ring C(27)–C(28)–C(29)–C(30)–C(31)–C(32); Cg6 is the centroid of the phenyl ring C(21)–C(22)–C(23)–C(24)–C(25)–C(26).

Table 17. X–H...Cg (Pi-Ring) Interactions

	Bond Distance (Å)		Bond Distance (Å)
Sn1...O2	3.5166(8)	B1...C3	3.0766(16)
Sn1...O4A	3.4598(16)	B2...C6	3.1178(17)
Sn1...O4B	3.510(11)	B2...H6B	2.79
B1...H3B	2.82	Sn1...H22	3.06

Table 18. Short intra and intermolecular distances.

6. Appendix

Glossary

The following terms were used in the thesis :

Band Gap

In organic semiconductors, there are three types of band gaps defined, which represent different properties of the materials (Figure 83). The transport gap or fundamental (ΔE_{fund}) is the difference between the energy of ionization potential (IP) or HOMO and the electron affinity energy (EA) or LUMO. The optical band gap (ΔE_{opt}) is refers to the difference between the ground state S_0 and the first excited state S_1 .^[22b]

The difference between the transport or fundamental gap with the optical gap is called binding energy (E_b), which is referred to the binding energy between holes and electrons in the excited state.^[21a, 97] $E_b = IP - EA - \Delta E_{\text{opt}}$

Finally, the last energy gap is obtained by the difference between the Kohn-Sahn (KS) eigenvalues from the HOMO and LUMO, and it is calculated using KS-DFT calculations. It differs from the fundamental gap by a theoretical derivative discontinuity (Δ_{XC}).

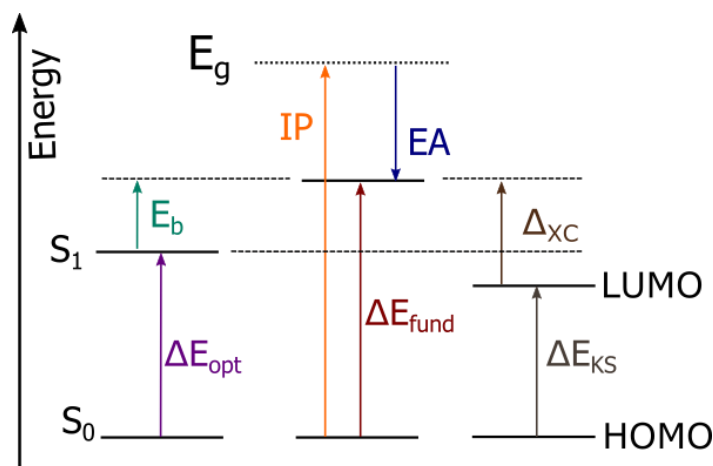


Figure 83. Comparison of the three different energy gaps.

Determination of band gap

Transport or fundamental gap

Method 1: The fundamental gap can be calculated using the combination of direct Valence Band Photoemission Spectroscopy (VB-PES) and inverse photoemission spectroscopy (IPES).^[98] With the VB-PES technique it is possible to measure the energy of electrons emitted after the incidence of

a photon with a synchrotron radiation between 80-150 meV on a material. Under such irradiation, the occupied electronic states of the material below the Fermi energy level (E_F) can be studied (energy level diagram on the top left of the Figure 84). With the VB-PES spectra (left- blue spectrum in Figure 84), the energy from the HOMO (E_{HOMO}) can be calculated and corresponds to the low binding energy under the Fermi level. The position of the vacuum level (E_{VA}) of the sample it is defined as the low kinetic energy edge of the secondary electron peak when a bias of -10 V is applied on the sample. With this technique it is possible as well to calculate the ionization potential defined as $IP = E_{VA} - E_{HOMO}$.

The IPES technique measures the photons emitted after an electron with well-defined energy ($E_i < 20$ eV) couples with states above the vacuum level of the sample from a sample and decay radiatively to lower lying unoccupied electronic with energy E_f (energy level diagram on the top right from Figure 84). The E_f can be calculated following the conservation of energy: $E_i = E_f + h\nu$. The IPES technique is complementary to the VB-PES, therefore study unoccupied electronic states. From the spectrum (Right-red spectrum Figure 84) it is possible calculate the energy from the LUMO and corresponding to the low binding energy above the Fermi level. Using the vacuum level calculated from the VB-PES spectra, it is possible to calculate the electron affinity as $EA = E_{VA} - E_{LUMO}$

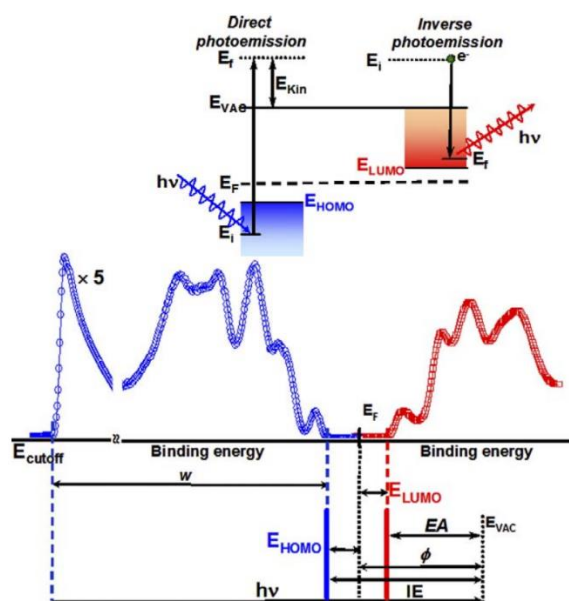


Figure 84. VB-PES (left-blue) and IPES (right-red) spectra of a thin layer of an organic semiconductor. The minimum energy where every spectra cuts represents the HOMO and LUMO energies.^[98] *Reproduced with permission from El Sevier. Copyright El Sevier 2019.*

Method 2: A second way to measure the transport band gap is using electrochemical measurements such as cyclic voltammetry. In the cyclovoltogram of a reversible process, the reduction and oxidation peaks are related to the electron affinity energy and ionization potential respectively. The difference between both peaks represents the ΔE_{fund} .

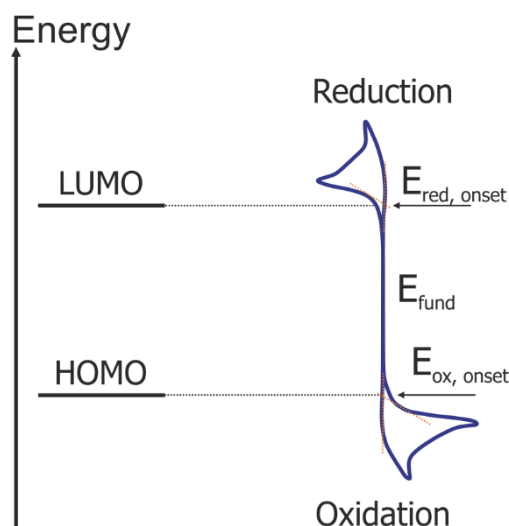


Figure 85. Fundamental band gap calculated from electrochemical measurements. In reversible process the onset potentials of reduction and oxidation are related to electron affinity energy and ionization potential respectively.^[99]

Optical band gap

The optical gap can be determined using the optical absorption spectra. For the calculation of the optical band gap E_g using equation (14), the wavelength λ_{onset} is needed which can be derived from the absorption spectra.

$$E = \frac{hc}{\lambda} = \frac{4.14 \times 10^{-15} \text{ eVs} \cdot 3 \times 10^{17} \text{ nm/s}}{\lambda \text{ (nm)}} = \frac{1240 \text{ eV} \cdot \text{nm}}{\lambda \text{ (nm)}} \quad (14)$$

Like depicted in Figure 86 the edge wavelength is defined as the intersection of the tangent at the most red-shifted curve after the maximum and the one at high wavelength limit in the absorption spectra curve.^[100]

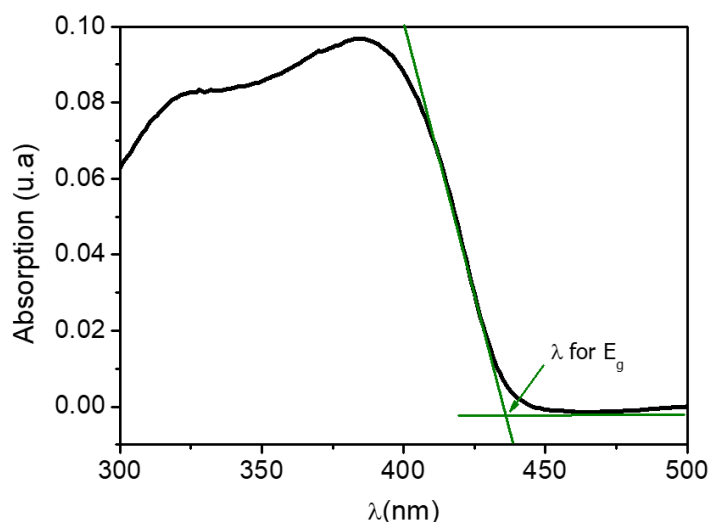


Figure 86. Definition of the edge wavelength for the calculation of E_g .

Molecular Photoluminescence

The process of emission of light can be illustrated in the Jablonski diagram (Figure 87). The ground electronic state (S_0), usually is a singlet state (paired electrons). Excited electronic states are usually singlet (S_1 , S_2) or triplet (unpaired electrons- T_1) states. The absorption of light promotes an electron in a time scale of 10^{-15} s from S_0 to S_1 or S_2 . The radiative and non-radiative processes, that can occur after light absorption are different.^[41] Non-radiative processes are:

- (1) vibrational relaxations are the transitions between higher to lower vibrational levels. Time scale of 10^{-14} - 10^{-12} s.
- (2) Internal conversion is the transition between higher singlet excited state S_2 to lowest-excited state S_1 . Time scale 10^{-12} s.
- (3) Intersystem crossing is the transition between excited states of different spin multiplicity, for example between S_1 to T_1 . These processes are less probable to occur than internal conversion processes and they have a time scale of 10^{-8} s. Molecules containing heavy metals and metals ions, also they have a significant spin-orbital coupling where a change in spin becomes favourable.
- (4) Non-radiative de-excitation is the transition between excited states to the ground state releasing infinitesimal amounts of heat. The quenching of luminescence is the experimental evidence of this type of transition. In solution the energy transfer can be between the molecule and the solvent or in solid state by crystal vibrations (phonons).

Radiative process in which the emission can occur are:

- Fluorescence represented the transition from a singlet excited state (S_1) to the ground state (S_0) with a duration of 10^{-9} – 10^{-7} s. The energy of this transition is not the same as the absorption energy due to the Stokes shift. The Stokes shift is calculated from the difference between the energy of the maximum peaks from the absorption and emission spectra.
- Phosphorescence, which consider that after an intersystem crossing transition occurs a following transition proceed from the state T_1 to the ground state (S_0) releasing a photon. This transition has a longer duration of 10^{-6} – 10^2 s.
- There is a last and less common process which is the thermally assisted delayed fluorescence (TADF). In this process a reverse intersystem crossing can occur by virtual thermal excitation from the triplet excited state T_1 to the singlet S_1 . The photon is released then by delayed fluorescence from the transition of S_1 to S_0 .

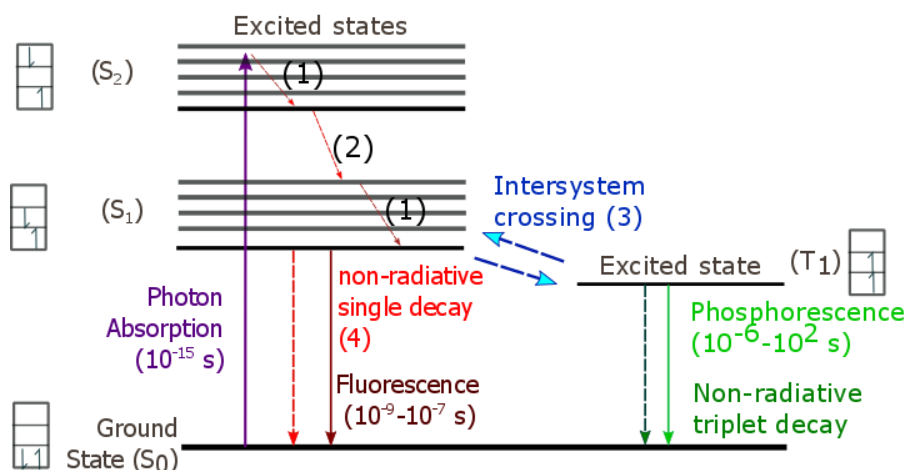


Figure 87. Jalonski diagram. Radiative and non-radiative processes, with their relevant time scales are depicted as solid and dashed lines, respectively.^[101]

Quantum yield (ϕ)

The quantum yield (ϕ) is defined as the number of emitted photons related to the number of absorbed photons of a compound. The comparative method of Williams *et al.* is used to determine the quantum yield.^[102] The idea is that when a solution of a standard (ST) and sample (x) with similar absorbance are excited at the same wavelength, both absorb the same number of photons. If the quantum yield of the standard is known and with a ratio of the fluorescence intensities from the sample and standard, the quantum yield of the sample can be calculated.

Using the area under the curve from the emission spectrum of samples at different concentrations and the absorption of each of them, a linear graph can be drawn where the slope is used for the calculation. Using the refractive index of the solvents (η_x , η_{ST}), the quantum yield is calculated using the equation (15).

$$\phi_x = \phi_{ST} \left(\frac{\text{slope}_x}{\text{slope}_{ST}} \right) \left(\frac{\eta_x^2}{\eta_{ST}^2} \right) \quad (15)$$

The absorption value of the concentrated solution from the standard and sample, should not be higher than 0.1 a.u. (to avoid quenching), which is the maximum value for a cuvette with a path length of 10 mm. As the emission spectra are the result of the transition from the excited state S₁ to the ground state, the excitation wavelength should be suitable for the molecule to reach the state S₁. Kasha's rule explains that the emission spectrum is independent of the excitation wavelength.^[101] That means if the molecules are excited with higher energy, the emission spectrum will not change because the internal conversion inside the molecule is a very fast process and therefore not detectable.

Permissions and licenses

For reprinted content of Figure 1

RE: Copyright permission of one of your images in a thesis document

Subject: RE: Copyright permission of one of your images in a thesis document
From: "Langendijk, E.H.A. (Erno)" <erno.langendijk@tno.nl>
Date: 25/01/2019, 18:55
To: Sara Urrego Riveros <sarita.urrego@gmail.com>, "Tesser, J.J.D. (Judith)" <judith.tesser@tno.nl>

Hi Judith,

Can you help out with the request below?

From my point of view it is fine as long as Lyteus and Holst Centre are mentioned and the copyright is shown in the picture.

Thanks
Erno

E.H.A. (Erno) Langendijk
Business Development &
Program Manager - Flexible OLEDs
Holst Centre
HTC 31, 5656AE, Eindhoven, NL
M +31-6-57511688
E erno.langendijk@tno.nl
Location

This message may contain information that is not intended for you. If you are not the addressee or if this message was sent to you by mistake, you are requested to inform the sender and delete the message. TNO accepts no liability for the content of this e-mail, for the manner in which you use it and for damage of any kind resulting from the risks inherent to the electronic transmission of messages.

-----Original Message-----

From: Sara Urrego Riveros <sarita.urrego@gmail.com>
Sent: maandag 21 januari 2019 19:23
To: Langendijk, E.H.A. (Erno) <erno.langendijk@tno.nl>
Subject: Copyright permission of one of your images in a thesis document

Dear Sir or Madame,

I'm Sara Urrego-Riveros current Chemistry PhD Student from the University of Kiel in Germany.

At the moment I'm writing my PhD thesis based in organic and organometallic monomers to be used in organic electronics. My work was completely synthetic, nevertheless one of the applications that my materials have are OLEDs. Therefore in the introduction part (State of the art) I would like to mention your 15-meter roll-to-roll device in it and use their photo. In order to place the photo that you have in the webpage's gallery in my document, I would need from your company a copyright permission. Do you have a protocol for this kind of requirement?.

I appreciate your help.

Looking forward to hear from you

For reprinted Figure 8

Re: Favor

Subject: Re: Favor
From: <annikaheinrich@aol.com>
Date: 11/29/2018, 4:59 PM
To: sarita.urrego@gmail.com

Hi Sara,

as I do not know what picture exactly you meant, I send all of them to you. Hope it is what you were looking for?!

See you later in the restaurant!

Annika

-----Ursprüngliche Mitteilung-----

Von: Sara Urrego Riveros <sarita.urrego@gmail.com>
An: Annikaheinrich <Annikaheinrich@aol.com>
Verschickt: Mi, 21. Nov. 2018 17:39
Betreff: Favor

Hi Annika,

i wanted to ask a favor related with one of the pictures from your thesis. I wanted to use the photo where you compare the RIR P3HT with the RR P3HT (Figure SI 8 page 260, from your thesis). Anne suggested me to use it in my introduction where i explain the difference between HT , HH, HT etc, and i like the idea too. If you agree i can prepare a document where states that you give me permission and perhaps sign it in our Christmas party . I'm not sure what i should write but i will care about.

I really appreciate your help.

See you next Thursday !

Warm greetings,

Sara

--

Msc. Sara Urrego Riveros
Handy Nr. +49 015770414085

Diese E-Mail wurde von Avast Antivirus-Software auf Viren geprüft.
<https://www.avast.com/antivirus>

— Attachments: —

For Sara P3HT.docx

274 kB

For reprinted content of publication chapter 3.1.3

Rightslink® by Copyright Clearance Center

<https://s100.copyright.com/AppDispatchServlet>

RightsLink®

Home

Account
Info

Help



Title: Synthesis of poly(thiophene-alt-pyrrole) from a difunctionalized thienylpyrrole by Kumada polycondensation

Author: Lu-Ying He, Sara Urrego-Riveros, Paul J. Gates, Christian Näther, Maren Brinkmann, Volker Abetz, Anne Staubitz

Publication: Tetrahedron

Publisher: Elsevier

Date: 19 August 2015

Copyright © 2015 Elsevier Ltd. All rights reserved.

Logged in as:

Sara Urrego Riveros
University of BremenAccount #:
3001173264

LOGOUT

Please note that, as the author of this Elsevier article, you retain the right to include it in a thesis or dissertation, provided it is not published commercially. Permission is not required, but please ensure that you reference the journal as the original source. For more information on this and on your other retained rights, please visit: <https://www.elsevier.com/about/our-business/policies/copyright#Author-rights>

BACK

CLOSE WINDOW

Copyright © 2018 Copyright Clearance Center, Inc. All Rights Reserved. [Privacy statement](#). [Terms and Conditions](#).
Comments? We would like to hear from you. E-mail us at customercare@copyright.com

For reprinted content of publication chapter 3.2.1

**JOHN WILEY AND SONS LICENSE
TERMS AND CONDITIONS**

Sep 19, 2018

This Agreement between University of Bremen -- Sara Urrego Riveros ("You") and John Wiley and Sons ("John Wiley and Sons") consists of your license details and the terms and conditions provided by John Wiley and Sons and Copyright Clearance Center.

License Number	4432520518656
License date	Sep 19, 2018
Licensed Content Publisher	John Wiley and Sons
Licensed Content Publication	Chemistry - A European Journal
Licensed Content Title	Syntheses and Properties of Tin-Containing Conjugated Heterocycles
Licensed Content Author	Sara Urrego-Riveros, Isabel-Maria Ramirez y Medina, Jonas Hoffmann, et al
Licensed Content Date	Jan 31, 2018
Licensed Content Volume	24
Licensed Content Issue	22
Licensed Content Pages	17
Type of use	Dissertation/Thesis
Requestor type	Author of this Wiley article
Format	Print and electronic
Portion	Full article
Will you be translating?	No
Order reference number	102
Title of your thesis / dissertation	Synthesis of new monomers for Semiconductor Polymers and their application in organic optoelectronic devices
Expected completion date	Dec 2018
Expected size (number of pages)	280
Requestor Location	University of Bremen Leobener Str. 7 NW2C , Room 1300 Bremen, Bremen 28359 Germany Attn: University of Bremen
Publisher Tax ID	EU826007151
Total	0.00 EUR
Terms and Conditions	

TERMS AND CONDITIONS

This copyrighted material is owned by or exclusively licensed to John Wiley & Sons, Inc. or one of its group companies (each a "Wiley Company") or handled on behalf of a society with which a Wiley Company has exclusive publishing rights in relation to a particular work (collectively "WILEY"). By clicking "accept" in connection with completing this licensing transaction, you agree that the following terms and conditions apply to this transaction (along with the billing and payment terms and conditions established by the Copyright Clearance Center Inc., ("CCC's Billing and Payment terms and conditions"), at the time that

For reprinted content of publication chapter 3.2.2

Rightslink® by Copyright Clearance Center

https://s100.copyright.com/AppDispatch5

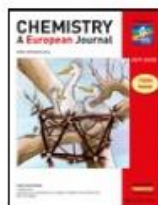


RightsLink®

Home

Account Info

Help



Title: Negishi's Reagent Versus Rosenthal's Reagent in the Formation of Zirconacyclopentadienes

Author: Sara Urrego-Riveros, Isabel-Maria Ramirez y Medina, Daniel Duvinage, et al

Publication: Chemistry - A European Journal

Publisher: John Wiley and Sons

Date: Sep 4, 2019

Logged In as:
Sara Urrego Riveros
University of Bremen
Account #:
3001173264

LOGOUT

© 2019 The Authors. Published by Wiley-VCH Verlag GmbH & Co. KGaA.

Open Access Article

This article is available under the terms of the Creative Commons Attribution Non-Commercial No Derivatives License CC BY-NC-ND (which may be updated from time to time) and permits **non-commercial** use, distribution, and reproduction in any medium, without alteration, provided the original work is properly cited and it is reproduced verbatim.

For an understanding of what is meant by the terms of the Creative Commons License, please refer to [Wiley's Open Access Terms and Conditions](#).

Permission is not required for **non-commercial** reuse. For **commercial** reuse, please hit the "back" button and select the most appropriate **commercial** requestor type before completing your order.

If you wish to adapt, alter, translate or create any other derivative work from this article, permission must be sought from the Publisher. Please email your requirements to RightsLink@wiley.com.

BACK

CLOSE WINDOW

Copyright © 2019 Copyright Clearance Center, Inc. All Rights Reserved. [Privacy statement](#). [Terms and Conditions](#). Comments? We would like to hear from you. E-mail us at customercare@copyright.com

For reprinted content of Figure 84

04/03/2019

RightsLink Printable License

**ELSEVIER LICENSE
TERMS AND CONDITIONS**

Mar 04, 2019

This Agreement between Christian Albrechts Universität zu Kiel -- Sara Urrego-Riveros ("You") and Elsevier ("Elsevier") consists of your license details and the terms and conditions provided by Elsevier and Copyright Clearance Center.

License Number	4541991359574
License date	Mar 04, 2019
Licensed Content Publisher	Elsevier
Licensed Content Publication	Chemical Physics
Licensed Content Title	The transport gap of organic semiconductors studied using the combination of direct and inverse photoemission
Licensed Content Author	Dietrich R.T. Zahn,Gianina N. Gavrilă,Mihaela Gorgol
Licensed Content Date	Jun 9, 2006
Licensed Content Volume	325
Licensed Content Issue	1
Licensed Content Pages	14
Start Page	99
End Page	112
Type of Use	reuse in a thesis/dissertation
Portion	figures/tables/illustrations
Number of figures/tables/illustrations	1
Format	both print and electronic
Are you the author of this Elsevier article?	No
Will you be translating?	No
Order reference number	10032
Original figure numbers	Fig. 3. A VB-PES and IPES spectra of a thin organic film from the HOMO to the low energy cutoff on the left side and unoccupied states with the LUMO on the right side.
Title of your thesis/dissertation	Synthesis of New Monomers for Semiconducting Polymers and Their Application In Organic Optoelectronic Devices
Expected completion date	May 2019
Estimated size (number of pages)	400
Requestor Location	Christian Albrechts Universität zu Kiel Otto-Hahn-Platz 4 Kiel, Schleswig-Holstein 24118 Germany Attn: Christian Albrechts Universität zu Kiel
Publisher Tax ID	GB 494 6272 12
Total	0.00 USD
Terms and Conditions	

INTRODUCTION

7. References

- [1] E. Yablonovitch, *Science* **1989**, *246*, 347.
- [2] H. R. Huff, *Journal of The Electrochemical Society* **2002**, *149*, S35-S58.
- [3] W. Brütting, in *Physics of Organic Semiconductors*, **2006**.
- [4] M. Sano, M. Pope, H. Kallmann, *The Journal of Chemical Physics* **1965**, *43*, 2920-2921.
- [5] H. Shirakawa, E. J. Louis, A. G. Macdiarmid, C. K. Chiang, A. J. Heeger, *Journal of the Chemical Society-Chemical Communications* **1977**, 578-580.
- [6] a) A. J. Heeger, *Reviews of Modern Physics* **2001**, *73*, 681-700; b) A. G. MacDiarmid, *Reviews of Modern Physics* **2001**, *73*, 701-712; c) H. Shirakawa, *Reviews of Modern Physics* **2001**, *73*, 713-718.
- [7] 15-meter roll-to-roll device is world's longest OLED. <https://lyteus.eu/projectnews/15-meter-roll-to-roll-device-is-worlds-longest-oled/> (1.02.2019)
- [8] L. Meng, Y. Zhang, X. Wan, C. Li, X. Zhang, Y. Wang, X. Ke, Z. Xiao, L. Ding, R. Xia, H.-L. Yip, Y. Cao, Y. Chen, *Science* **2018**, *361*, 1094-1098.
- [9] *C&EN Global Enterprise* **2018**, *96*, 8-8.
- [10] F. Wudl, *Faraday Discussions* **2014**, *174*, 9-20.
- [11] A. Köhler, H. Bässler, *Materials Science and Engineering: R: Reports* **2009**, *66*, 71-109.
- [12] D. Braun, A. J. Heeger, *Applied Physics Letters* **1991**, *58*, 1982-1984.
- [13] S. Li, L. Ye, W. Zhao, H. Yan, B. Yang, D. Liu, W. Li, H. Ade, J. Hou, *J. Am. Chem. Soc.* **2018**.
- [14] O. Gidron, A. Dadvand, E. Wei-Hsin Sun, I. Chung, L. J. W. Shimon, M. Bendikov, D. F. Perepichka, *Journal of Materials Chemistry C* **2013**, *1*, 4358-4367.
- [15] M. Hissler, P. W. Dyer, R. Réau, *Coord. Chem. Rev.* **2003**, *244*, 1-44.
- [16] F. So, *Organic Electronics: Materials, Processing, Devices and Applications*, Boca Raton, FL, **2010**.
- [17] B. de Boer, A. Facchetti, *Polymer Reviews* **2008**, *48*, 423-431.
- [18] U. Mitschke, P. Bäuerle, *Journal of Materials Chemistry* **2000**, *10*, 1471-1507.
- [19] a) B. S. Ong, W. Yiliang, L. Ping, *Proceedings of the IEEE* **2005**, *93*, 1412-1419; b) M. R. Andersson, O. Thomas, W. Mammo, M. Svensson, M. Theander, O. Inganäs, *Journal of Materials Chemistry* **1999**, *9*, 1933-1940.
- [20] a) P. Chandrasekhar, *Conducting Polymers, Fundamentals and Applications*, Springer US, **1999**; b) A. Köhler, H. Bässler, *The Electronic Structure of Organic Semiconductors. In Electronic Processes in Organic Semiconductors*, **2015**.
- [21] a) J.-L. Bredas, S. R. Marder, *The WSPC Reference on Organic Electronics: Organic Semiconductors, Vol. Volume 7*, WORLD SCIENTIFIC, **2015**; b) M. Rehahn, *Chemie in unserer Zeit* **2003**, *37*, 18-30.
- [22] a) M. Kertesz, C. H. Choi, S. Yang, *Chem. Rev.* **2005**, *105*, 3448-3481; b) J.-L. Bredas, *Materials Horizons* **2014**, *1*, 17-19.
- [23] a) V. Coropceanu, J. Cornil, D. A. da Silva Filho, Y. Olivier, R. Silbey, J.-L. Brédas, *Chem. Rev.* **2007**, *107*, 926-952; b) J.-L. Brédas, D. Beljonne, V. Coropceanu, J. Cornil, *Chem. Rev.* **2004**, *104*, 4971-5004.
- [24] K. A. McGarry, W. Xie, C. Sutton, C. Risko, Y. Wu, V. G. Young, J.-L. Brédas, C. D. Frisbie, C. J. Douglas, *Chemistry of Materials* **2013**, *25*, 2254-2263.
- [25] T. Thurn-Albrecht, R. Thomann, T. Heinzl, S. Hugger, *Colloid & Polymer Science* **2004**, *282*, 932-938.
- [26] R. Noriega, J. Rivnay, K. Vandewal, F. P. V. Koch, N. Stingelin, P. Smith, M. F. Toney, A. Salleo, *Nature Materials* **2013**, *12*, 1038.

- [27] a) A. Zen, M. Saphiannikova, D. Neher, J. Grenzer, S. Grigorian, U. Pietsch, U. Asawapirom, S. Janietz, U. Scherf, I. Lieberwirth, G. Wegner, *Macromolecules* **2006**, *39*, 2162-2171; b) G. Dennler, M. C. Scharber, C. J. Brabec, *Advanced Materials* **2009**, *21*, 1323-1338.
- [28] Y. Shirota, *Journal of Materials Chemistry* **2000**, *10*, 1-25.
- [29] J. Roncali, *Chem. Rev.* **1997**, *97*, 173-205.
- [30] J. W. Mintmire, C. T. White, M. L. Elert, *Synth. Met.* **1988**, *25*, 109-119.
- [31] I. F. Perepichka, D. F. Perepichka, *Handbook of Thiophene-based Materials: Applications in Organic electronics and Photonics*, Chichester, UK, **2009**.
- [32] a) G. R. Desiraju, V. Nalini, *Journal of Materials Chemistry* **1991**, *1*, 201-203; b) E. A. Marseglia, F. Grepioni, E. Tedesco, D. Braga, *Molecular Crystals and Liquid Crystals Science and Technology. Section A. Molecular Crystals and Liquid Crystals* **2000**, *348*, 137-151.
- [33] a) H. S. O. Chan, S. C. Ng, *Progress in Polymer Science* **1998**, *23*, 1167-1231; b) C. Della-Casa, P. Costa-Bizzarri, M. Lanzi, L. Paganin, F. Bertinelli, R. Pizzoferrato, F. Sarcinelli, M. Casalboni, *Synth. Met.* **2003**, *138*, 409-417; c) M. L. Blohm, J. E. Pickett, P. C. Vandort, *Macromolecules* **1993**, *26*, 2704-2710.
- [34] S. Hotta, K. Ito, *Electronic Properties of Polythiophenes. In Handbook of Oligo- and Polythiophenes*.
- [35] P. J. Skabara, in *Handbook of Thiophene-Based Materials (eds I. F. Perepichka and D. F. Perepichka)*, **2009**.
- [36] L. Zhan, Z. Song, J. Zhang, J. Tang, H. Zhan, Y. Zhou, C. Zhan, *Electrochimica Acta* **2008**, *53*, 8319-8323.
- [37] R. D. McCullough, S. P. Williams, S. Tristram-Nagle, M. Jayaraman, P. C. Ewbank, L. Miller, *Synth. Met.* **1995**, *69*, 279-282.
- [38] a) R. M. S. Maior, K. Hinkelmann, H. Eckert, F. Wudl, *Macromolecules* **1990**, *23*, 1268-1279; b) A. C. J. Heinrich, University of Kiel (Kiel), **2014**; c) P. C. Ewbank, M. C. Stefan, G. Sauvé, R. D. McCullough, in *Handbook of Thiophene-Based Materials* (Ed.: I. F. P. a. D. F. Perepichka), **2009**.
- [39] a) I. F. Perepichka, D. F. Perepichka, H. Meng, F. Wudl, *Advanced Materials* **2005**, *17*, 2281-2305; b) J. Hollinger, A. A. Jahnke, N. Coombs, D. S. Seferos, *J. Am. Chem. Soc.* **2010**, *132*, 8546.
- [40] Q. T. Zhang, J. M. Tour, *J. Am. Chem. Soc.* **1998**, *120*, 5355-5362.
- [41] M. A. Omary, H. H. Patterson, in *Encyclopedia of Spectroscopy and Spectrometry* (Ed.: J. C. Lindon), Elsevier, Oxford, **1999**, pp. 1186-1207.
- [42] a) P. L. Burn, A. B. Holmes, A. Kraft, D. D. C. Bradley, A. R. Brown, R. H. Friend, R. W. Gymer, *Nature* **1992**, *356*, 47; b) T. Yamamoto, Z.-h. Zhou, T. Kanbara, M. Shimura, K. Kizu, T. Maruyama, Y. Nakamura, T. Fukuda, B.-L. Lee, N. Ooba, S. Tomaru, T. Kurihara, T. Kaino, K. Kubota, S. Sasaki, *J. Am. Chem. Soc.* **1996**, *118*, 10389-10399.
- [43] C. E. I. Knappke, A. Jacobi von Wangelin, *Chem. Soc. Rev.* **2011**, *40*, 4948-4962.
- [44] a) Z. Bao, W. K. Chan, L. Yu, *J. Am. Chem. Soc.* **1995**, *117*, 12426-12435; b) B. Carsten, F. He, H. J. Son, T. Xu, L. Yu, *Chem. Rev.* **2011**, *111*, 1493-1528; c) M. P. Bernstein, F. E. Romesberg, D. J. Fuller, A. T. Harrison, D. B. Collum, Q. Y. Liu, P. G. Williard, *J. Am. Chem. Soc.* **1992**, *114*, 5100-5110.
- [45] a) T. A. Chen, X. M. Wu, R. D. Rieke, *J. Am. Chem. Soc.* **1995**, *117*, 233-244; b) T. A. Chen, R. D. Rieke, *J. Am. Chem. Soc.* **1992**, *114*, 10087-10088.
- [46] a) M. Jayakannan, X. Lou, J. L. J. van Dongen, R. A. J. Janssen, *Journal of Polymer Science Part A: Polymer Chemistry* **2005**, *43*, 1454-1462; b) S. Kotha, K. Lahiri, D. Kashinath, *Tetrahedron* **2002**, *58*, 9633-9695.

- [47] a) S. Vandeleene, K. Van den Bergh, T. Verbiest, G. Koeckelberghs, *Macromolecules* **2008**, *41*, 5123-5131; b) S. Wu, L. Huang, H. Tian, Y. Geng, F. Wang, *Macromolecules* **2011**, *44*, 7558-7567.
- [48] L. S. Boffa, in *Applied Polymer Science: 21st Century* (Eds.: C. D. Craver, C. E. Carraher), Pergamon, Oxford, **2000**, pp. 1021-1042.
- [49] G. Odian, *Principles of Polymerization*, John Wiley & Sons, Inc., **2004**.
- [50] a) E. E. Sheina, J. S. Liu, M. C. Iovu, D. W. Laird, R. D. McCullough, *Macromolecules* **2004**, *37*, 3526-3528; b) A. Yokoyama, R. Miyakoshi, T. Yokozawa, *Macromolecules* **2004**, *37*, 1169-1171; c) I. Osaka, R. D. McCullough, *Acc. Chem. Res.* **2008**, *41*, 1202-1214; d) T. Yokozawa, Y. Nanashima, H. Kohno, R. Suzuki, M. Nojima, Y. Ohta, *Pure Appl. Chem* **2013**, *85*, 573-587.
- [51] a) I. A. Liversedge, S. J. Higgins, M. Giles, M. Heeney, I. McCulloch, *Tetrahedron Lett.* **2006**, *47*, 5143-5146; b) S. Guillerez, G. Bidan, *Synth. Met.* **1998**, *93*, 123-126.
- [52] Y. Qiu, J. Mohin, C.-H. Tsai, S. Tristram-Nagle, R. R. Gil, T. Kowalewski, K. J. T. Noonan, *Macromolecular Rapid Communications* **2015**, *36*, 840-844.
- [53] M. C. Iovu, E. E. Sheina, R. R. Gil, R. D. McCullough, *Macromolecules* **2005**, *38*, 8649-8656.
- [54] M. P. Bhatt, H. D. Magurudeniya, P. Sista, E. E. Sheina, M. Jeffries-El, B. G. Janesko, R. D. McCullough, M. C. Stefan, *Journal of Materials Chemistry A* **2013**, *1*, 12841-12849.
- [55] a) T. Beryozkina, V. Senkovskyy, E. Kaul, A. Kiriya, *Macromolecules* **2008**, *41*, 7817-7823; b) C. R. Bridges, D. S. Seferos, in *Semiconducting Polymers: Controlled Synthesis and Microstructure*, The Royal Society of Chemistry, **2017**, pp. 38-84.
- [56] W. Liu, R. Tkachov, H. Komber, V. Senkovskyy, M. Schubert, Z. Wei, A. Facchetti, D. Neher, A. Kiriya, *Polymer Chemistry* **2014**, *5*, 3404-3411.
- [57] a) E. Elmalem, F. Biedermann, K. Johnson, R. H. Friend, W. T. S. Huck, *J. Am. Chem. Soc.* **2012**, *134*, 17769-17777; b) E. Elmalem, A. Kiriya, W. T. S. Huck, *Macromolecules* **2011**, *44*, 9057-9061; c) T. Yokozawa, R. Suzuki, M. Nojima, Y. Ohta, A. Yokoyama, *Macromolecular Rapid Communications* **2011**, *32*, 801-806; d) A. Yokoyama, H. Suzuki, Y. Kubota, K. Ohuchi, H. Higashimura, T. Yokozawa, *J. Am. Chem. Soc.* **2007**, *129*, 7236-+.
- [58] Y. Tokita, M. Katoh, Y. Ohta, T. Yokozawa, *Chem. Eur. J.* **2016**, *22*, 17436-17444.
- [59] A. C. J. Heinrich, B. Thiedemann, P. J. Gates, A. Staubitz, *Org. Lett.* **2013**, *15*, 4666-4669.
- [60] J. Linshoef, A. C. J. Heinrich, S. A. W. Segler, P. J. Gates, A. Staubitz, *Org. Lett.* **2012**, *14*, 5644-5647.
- [61] A. Suzuki, N. Miyauchi, *Chem. Rev.* **1995**, *95*, 2457.
- [62] a) S. Yamaguchi, Y. Itami, K. Tamao, *Organometallics* **1998**, *17*, 4910-4916; b) I.-M. Ramirez y Medina, M. Rohdenburg, F. Mostaghimi, S. Grabowsky, P. Swiderek, J. Beckmann, J. Hoffmann, V. Dorcet, M. Hissler, A. Staubitz, *Inorg. Chem.* **2018**, *57*, 12562-12575.
- [63] a) S. Yamaguchi, K. Tamao, *J. Chem. Soc., Dalton Trans.* **1998**, 3693-3702; b) G. W. Parshall, *Organometallics* **1987**, *6*, 687-692.
- [64] J. Jagur-Grodzinski, *Polymer. Adv. Tech.* **2002**, *13*, 615-625.
- [65] B. L. Lucht, M. A. Buretea, T. D. Tilley, *Organometallics* **2000**, *19*, 3469-3475.
- [66] S. Urrego-Riveros, I. Ramirez y Medina, J. Hoffmann, A. Heitmann, A. Staubitz, *Chem. Eur. J.* **2018**, *24*, 5680-5696.
- [67] X. Yan, C. Xi, *Acc. Chem. Res.* **2015**, *48*, 935-946.

- [68] S.-Y. Liu, J.-H. Chang, I. Wen Wu, C.-I. Wu, **2014**, *4*, 7559.
- [69] K. P. Bhuvana, R. J. Bensingh, M. A. Kader, S. K. Nayak, *Polymer-Plastics Technology and Engineering* **2018**, 1-17.
- [70] P. A. Levermore, R. Jin, X. Wang, L. Chen, D. D. C. Bradley, J. C. de Mello, *Journal of Materials Chemistry* **2008**, *18*, 4414-4420.
- [71] N. Thejo Kalyani, S. J. Dhoble, *Renewable and Sustainable Energy Reviews* **2015**, *44*, 319-347.
- [72] A. Kraft, A. C. Grimsdale, A. B. Holmes, *Angewandte Chemie-International Edition* **1998**, *37*, 402-428.
- [73] S. Gunes, H. Neugebauer, N. S. Sariciftci, *Chem. Rev.* **2007**, *107*, 1324-1338.
- [74] A. Facchetti, (Ed.: I. F. P. a. D. F. Perepichka), **2009**.
- [75] F. Bures, *RSC Advances* **2014**, *4*, 58826-58851.
- [76] L.-Y. He, S. Urrego-Riveros, P. J. Gates, C. Näther, M. Brinkmann, V. Abetz, A. Staubitz, *Tetrahedron* **2015**, *71*, 5399-5406.
- [77] R. Tkachov, V. Senkovskyy, H. Komber, A. Kiriya, *Macromolecules* **2011**, *44*, 2006-2015.
- [78] J. Linshoeft, E. J. Baum, A. Hussain, P. J. Gates, C. Näther, A. Staubitz, *Angew. Chem. Int. Ed.* **2014**, *53*, 12916-12920.
- [79] a) B. Wrackmeyer, *J. Chem. Soc., Chem. Commun.* **1986**, 397-399; b) B. Wrackmeyer, *J. Organomet. Chem.* **1986**, *310*, 151-160.
- [80] G. He, L. Kang, W. Torres Delgado, O. Shynkaruk, M. J. Ferguson, R. McDonald, E. Rivard, *J. Am. Chem. Soc.* **2013**, *135*, 5360-5363.
- [81] a) K. Tamao, S. Yamaguchi, M. Shiro, *J. Am. Chem. Soc.* **1994**, *116*, 11715-11722; b) J. Kurita, M. Ishii, S. Yasuike, T. Tsuchiya, *J. Chem. Soc., Chem. Commun.* **1993**, 1309-1310; c) S. Yamaguchi, K. Tamao, *J. Organomet. Chem.* **2002**, *653*, 223-228.
- [82] N. Miyaura, A. Suzuki, *Chem. Rev.* **1995**, *95*, 2457-2483.
- [83] J. Dubac, C. Guérin, P. Meunier, in *PATAI'S Chemistry of Functional Groups*.
- [84] A. J. Boydston, Y. Yin, B. L. Pagenkopf, *J. Am. Chem. Soc.* **2004**, *126*, 3724-3725.
- [85] J. Dubac, A. Laporterie, G. Manuel, *Chem. Rev.* **1990**, *90*, 215-263.
- [86] J. Linshoeft, University of Kiel (Kiel), **2014**.
- [87] R. C. Coffin, J. Peet, J. Rogers, G. C. Bazan, *Nat Chem* **2009**, *1*, 657-661.
- [88] M. F. Suarez-Herrera, J. M. Feliu, *Journal of Physical Chemistry B* **2009**, *113*, 1899-1905.
- [89] H. Hofmeister, K. Annen, H. Laurent, R. Wiechert, *Angew. Chem. Int. Ed.* **1984**, *23*, 727-729.
- [90] E. Negishi, S. J. Holmes, J. M. Tour, J. A. Miller, F. E. Cederbaum, D. R. Swanson, T. Takahashi, *J. Am. Chem. Soc.* **1989**, *111*, 3336-3346.
- [91] S. Yamaguchi, R.-Z. Jin, Y. Itami, T. Goto, K. Tamao, *J. Am. Chem. Soc.* **1999**, *121*, 10420-10421.
- [92] A. Smeets, K. Van den Bergh, J. De Winter, P. Gerbaux, T. Verbiest, G. Koeckelberghs, *Macromolecules* **2009**, *42*, 7638-7641.
- [93] G. Sheldrick, *Acta Cryst. A* **2008**, *64*, 112-122.
- [94] L. Farrugia, *J. Appl. Cryst.* **1999**, *32*, 837-838.
- [95] D. E. Seitz, S.-H. Lee, R. N. Hanson, J. C. Bottaro, *Synthetic Communications* **1983**, *13*, 121-128.
- [96] L. Iannazzo, N. Kotera, M. Malacria, C. Aubert, V. Gandon, *J. Organomet. Chem.* **2011**, *696*, 3906-3908.
- [97] B. P. Rand, J. Genoe, P. Heremans, J. Poortmans, *Progress in Photovoltaics: Research and Applications* **2007**, *15*, 659-676.
- [98] D. R. T. Zahn, G. N. Gavrila, M. Gorgoi, *Chemical Physics* **2006**, *325*, 99-112.

-
- [99] J. L. Bredas, R. Silbey, D. S. Boudreaux, R. R. Chance, *J. Am. Chem. Soc.* **1983**, *105*, 6555-6559.
- [100] J. C. S. Costa, R. J. S. Taveira, C. F. R. A. C. Lima, A. Mendes, L. M. N. B. F. Santos, *Optical Materials* **2016**, *58*, 51-60.
- [101] J. R. Lakowicz, *Principles of Fluorescence Spectroscopy*, Third ed., Springer, New York, **2006**.
- [102] A Guide to Recording Fluorescence Quantum Yields <http://www.horiba.com/fileadmin/uploads/Scientific/Documents/Fluorescence/quantumyieldstrad.pdf> (16.02.2018)